

**Allosteric modulation of G protein-coupled
receptors: from small molecules to heteromeric
interactions**

Joaquín Botta

University of East Anglia

School of Pharmacy

A thesis submitted for the degree of Doctor of Philosophy

September 2018

©This copy of the thesis has been supplied on condition that anyone who consults it is understood to recognise that its copyright rests with the author and that use of any information derived therefrom must be in accordance with current UK Copyright Law. In addition, any quotation or extract must include full attribution.

To my parents

ACKNOWLEDGEMENTS

First of all, I would like to thank my former primary supervisor Dr Peter J. McCormick for this opportunity. It has been a privilege and an honour learning from you. Being mentored by someone who is as passionate about science as you are has been inspiring. Perhaps the most valuable scientific lesson you taught me has nothing to do with GPCRs, but understanding all the factors involved in science, including the human dimension.

I would like to extend my special thanks to Dr Leanne Stokes. Your support, specially over the last stages of my PhD, has been vital to the realisation of this endeavour. My most sincere gratitude to you and all the members of your lab for treating me as an equal among equals. In addition, thanks to the University of East Anglia and to the School of Pharmacy for the financial support.

I would also like to thank to the past and present colleagues of the lab. Specially to Dr Paola Gasperini, good friend, better person and a wonderful researcher. Problems seem less overwhelming with a spoonful of your Tiramisu, I am still waiting for the protocol...In addition, I would like to extend my gratitude to Julia for all her help and constant positive attitude.

Thanks to the Earlham House plus family; Mahmoud, Hui and Remy (the plus). My friends, you do justice to the etymology of this word. Thanks to you too Gerard, despite more than 4 years abroad, I feel as if nothing had changed when I am back home.

None of this would have been possible without my family. Thanks, Mom and Dad, for being close despite the distance, for your unconditional support and for always having my best interests at heart. You are the unsung heroes of my life! Thanks to my sister and brother, Ana and Juan, for never letting me down. Thanks to my uncles, Tios Juan, Lluís and Blanca, for your constant encouragement. I would also like to thank my Grandparents, “els Iaios”, I miss you!

Last, but certainly not least, thank you Sara! Thank you for finding me along the way, thank you for never failing to surprise me and thank you for your time. After two PhDs, six houses, four different cities and hundreds of miles apart now it is our turn! Thank you, Sara, my partner, confidant and the love of my life.

ABSTRACT

G protein-coupled receptors (GPCRs) exist within a landscape of interconvertible conformations readily influenced by their association with ligands and other GPCRs, formerly known as oligomerisation. Originally thought to function as monomers, the actual challenges encompass understanding the mechanism governing these interactions and their relevance *in vivo*. As for other quaternary arrangements, oligomerisation offers unique allosteric properties. However, unveiling these unappreciated opportunities requires deciphering the molecular basis underlying this phenomenon.

Here, we undertook this challenge focusing on the recently identified heteromers between the serotonin 2A and cannabinoid 1 receptors, which have been recently linked to the cognitive side-effects of cannabis. Our results provide new insights into the structural determinants driving cross-talk within this dimer, organised in a rhombus-shape simultaneously recruiting two G_i proteins. This organisation allows non-canonical downstream signalling pathways, which might account for the cognitive impairment induced by marijuana.

Furthermore, illustrating the significance of heteromerisation *in vivo*, we took advantage of the ability of the histamine H₃ receptor to modulate aberrant D₁R over-activation in Huntington's disease (HD). Using cellular and murine HD models, we identified functional D₁R-H₃R heteromers that are lost over HD progression. In addition, striatal cell death was reverted after the administration of H₃R ligands. This strategy rescued heteromer expression and prevented both cognitive and motor learning deficits in HD mice, providing compelling evidence of a novel heteromer-based target for HD.

Finally, aiming at certain receptor populations through allosteric interactions, we developed 5-HT_{2c}R-selective positive allosteric modulators with anti-obesity properties. For the first time, we identified, validate and delineated a pharmacophore model for the effective targeting of 5-HT_{2c}R allosteric sites, providing an alternative strategy to overcome the often hard to achieve selectivity within receptors subtypes.

Altogether, from small molecules to quaternary interactions, our findings provide important insights into the vast array of pharmacological opportunities arising from GPCR allosteric modulation.

GLOSSARY

2-AG	2-Arachidonoyl Glycerol	CMV	Cytomegalovirus
2PPM	Two-photon Polarization Microscopy	CNS	Central Nervous System
5-HIAA	5-hydroxyindoleacetic acid	Co-IP	Co-Immunoprecipitation
5-HT	Serotonin (5-hydroxytryptamine)	CODA-RET	Complementary Donor-Acceptor RET
5-HT_{2A}R	Serotonin _{2A} receptor	COMT	Catechol-O-methyltransferase
5-HT_{2B}R	Serotonin _{2B} receptor	CPS	Cell Penetrating Sequence
5-HTP	Hydroxyltryptophan	CREB	cAMP Response Element Binding protein
α-MSH	α-Melanocyte-Stimulating Hormone	CTR	Calcitonin receptor
A_{2A}R	Adenosine _{2A} receptor	CXCR4	C-X-C chemokine receptor type 4
AADC	Aromatic L-Amino Acid decarboxylase	D₁R	Dopamine D ₁ receptor
AC	Adenylyl cyclase	DA	Dopamine
Ach	Acetylcholine	DAO	Diamine oxidase
ADHD	Attention-Deficit Hyperactivity Disorder	DAT	Dopamine Active Transporter
AFM	Atomic Force Microscopy	DOI	2,5-dimethoxy-4-iodoamphetamine
AKAPs	A-Kinase Anchor Proteins	eCB	Endocannabinoid
AM	Allosteric Modulator	ECL/ICL	Extracellular/Intracellular Loop
AP-2	Adaptor Protein 2	ECS	Endocannabinoid system
ARTP	Accelerating Rotarod Task Procedure	EES	Early Endosomes
ARC	Arcuate Nuclei	EM	Electron Microscopy
AT₁R	Angiotensin II type 1 receptor	ER	Endoplasmic Reticulum
ATP	Adenosine triphosphate	ERK	Extracellular signal-Regulated Kinases
β₁AR	β ₁ adrenoceptor	ESCRT	Endosomal Sorting Complex Required for Transport
β₂AR	β ₂ adrenoceptor	EYFP	Enhanced Yellow Fluorescent Protein
BAR domain	Bin/amphiphysin/Rvs domain	FAAH	Fatty Acid Amide Hydrolase
BBB	Blood-Brain Barrier	FCS	Fluorescence Correlation Spectroscopy
BMI	Body Mass Index	FDA	Food and Drug Administration
BRET	Bioluminescent Resonance Energy Transfer	FK	Forskolin
CAM	Constitutive Active Mutant	FRAP	Fluorescent Recovery After Photobleaching
cAMP	Cyclic adenosine monophosphate	FRB	FKBP12-rapamycin binding domain of mTOR
CART	Cocaine and Amphetamine Regulated Transcript	FRET	Förster/Fluorescent Resonance Energy Transfer
CaSR	Calcium-Sensing Receptor	FSHR	Follicle Stimulating Hormone Receptor
CB₁R	Cannabinoid type 1 receptor	FZD₆R	Frizzled 6 receptor
CB₂R	Cannabinoid type 2 receptor	GABA	γ-aminobutyric acid
CCPs	Clathrin-Coated Pits	GAPs	GTPase-Accelerating Proteins

GASP-1	GPCR-Associated Binding Protein-1	MAPK	Mitogen-Activated Protein Kinase
GDP	Guanosine diphosphate	MC4R	Melanocortin 4 receptor
GEFs	Guanine nucleotide Exchange Factors	MD	Molecular Dynamics
GI	Gastrointestinal tract	MDL	MDL 100907
GIPC	GAIP Interacting Protein C terminus	mGluR	Metabotropic glutamate receptor
GIPR	Glucose-dependent Insulinotropic Polypeptide Receptor	mHTT	Mutant HTT
GIRKs	G protein-coupled Inwardly-Rectifying K ⁺ Channel	MRAP2	Melanocortin 2 receptor accessory protein 2
GLP-1R	Glucagon-Like Peptide 1 Receptor	MSNs	Medium-Sized spiny Neurons
Gluc	<i>Gaussia princeps</i> luciferase	MVBs	Multivesicular bodies
GPCRs	G Protein-Coupled Receptors	MW	Molecular Weight
Gpe	External globus pallidus	Nac	Nucleus accumbens
Gpi	Internal globus pallidus	NHERF-2	Na ⁺ /H ⁺ Exchanger Regulatory Factor 2
GRK	G protein-coupled receptor kinase	NLuc	Nanoluciferase
GRP	Gastrin Releasing Peptide	NMDARs	N-methyl-D-Aspartate Receptors
GTP	Guanosine triphosphate	NORT	Novel Object Recognition Test
H₃R	Histamine H ₃ Receptor	P2Y12R	Purinergic P2Y12 Receptor
HC	High Content	PALM	Photoactivated Localisation microscopy
HD	Huntington's Disease	PAM	Positive Allosteric Modulator
HDAC	Histone deacetylase	PCR	Polymerase Chain Reaction
HRS	Hepatocyte growth factor Regulated tyrosine kinase Substrate	FCS	Fluorescence Correlation Spectroscopy
HSV-TK	Herpes Simplex Virus Thymidine Kinase	PDEs	Phosphodiesterases
HTRF	Homogeneous Time Resolved Fluorescence	PDS-95	Postsynaptic Density Protein 95
HTT	Huntingtin protein	PDZ	Postsynaptic Density 95/Discs large/Zona occludens-1
IF	Immunofluorescence	PI₃K	Phosphoinositide 3-kinase
ILVs	Intraluminal vesicles	PIP₂	Phosphatidylinositol 4,5 bisphosphate
IP₃	Inositol 1,4,5 trisphosphate	PKA	Protein Kinase A
IP₃R	IP ₃ receptor	PDZ	Postsynaptic density 95/Discs large/Zona occludens-1
IP₆	Inositol hexakisphosphate	PKB	protein kinase A
JAK	Janus Kinase	PLA	Proximity Ligation Assay
JNK	c-Jun N-terminal Kinase	PLC	Phospholipase C
Kir	Inwardly-rectifying K ⁺ channels	PNS	Peripheral Nervous System
L-DOPA	l-3,4-dihydroxyphenylalanine	POMC	pro-opiomelanocortin
LBD	Ligand-Binding Domain	PPAR's	Peroxisome Proliferator Activated Receptors
LPA₂R	Lysophosphatidic acid receptor isoform 2	M71OR	Mouse 71 Olfactory Receptor
LSD	Lysergic acid dimethylamine	PPIs	Protein-Protein Interactions
LTM	Long-Term Memory	PRKACA	PKA catalytic subunit
M₂R	Muscarinic M2 Receptor	PRKAR2A	PKA type 2A regulatory subunit
M71OR	Mouse 71 Olfactory Receptor	PTX	Pertussis Toxin
MAGI-2	Membrane-associated Guanylate kinase Inverted-2 protein	PVH	Paraventricular hypothalamic area
MAOA	Monoamine Oxidase A	RCA	Rolling-Circle Amplification

RET	Resonance Energy Transfer	STORM	Stochastic Optical Reconstruction Microscopy
RGSR	RGS proteins of the R7 family	T-SAT	T-maze Spontaneous Alternation Task
RGSs	Regulators of G protein Signalling	TH	Tyrosine Hydroxylase
RhoA	Ras homology family member A	THC	Δ^9 -tetrahydrocannabinol
RIM	Rimonabant (SR-141716)	TIRF	Total Internal Reflection Fluorescence Microscopy
Rluc	<i>Renilla reniformis</i> luciferase	TM	Transmembrane domain
RMSD	Root-Mean-Dquare deviation	TPH	Tryptophan hydroxylase
SERT	Serotonin transporter	TR-FRET	Time-Resolved FRET
SH	Src protein homology	TRP	Transient Receptor Potential
SMO	Smoothened	V₂R	Vasopressin type 2 receptor
SNe	Substantia Nigra pars compacta	VMAT2	Vesicular Monoamine transporter 2
SNr	Substantia Nigra pars reticulata	VTA	Ventral Tegmental Area
SOD1	Superoxide dismutase 1	WHO	World Health Organisation
SpIDA	Spatial Intensity Distribution Analysis	WIN	(R)-(+)-WIN 55212
SRET	Sequential RET	YFP	Yellow Fluorescent Protein
SSRI	Selective Serotonin Reuptake Inhibitor	α_2C-AR	α_2 C adrenoceptor
SSTR	Somatostatin receptor	δOR	δ Opioid receptor
STAT	Signal Transducer and Activator of Transcription	μOR	μ Opioid receptor
STN	Subthalamic nucleus		

CONTENTS

ABSTRACT	VII
GLOSSARY	IX
CONTENTS	XIII
LIST OF FIGURES	XVII
LIST OF TABLES	XX
1. Chapter 1. General introduction	1
1.1. G protein-coupled receptors.....	3
1.1.1. GPCRs structure and activation.....	5
1.1.2. Heterotrimeric G proteins structure and receptor-mediated activation	7
1.1.3. G protein-dependent signalling.	9
1.1.4. Receptor desensitisation and trafficking	11
1.1.5. Hot topics expanding GPCR functionality.....	14
1.1.5.1. G protein-independent signalling	14
1.1.5.2. Space and time as signalling dimensions.....	16
1.1.5.3. Biased signalling	18
1.2. G protein-coupled receptors oligomerisation.....	20
1.2.1. From early evidence to the establishment of a new paradigm.....	20
1.2.2. Molecular interfaces involved in GPCR oligomerisation.....	24
1.2.3. Minimal functional units.....	28
1.2.4. Methods to study GPCR oligomerisation.....	30
1.2.4.1. Resonance energy transfer-based techniques	30
1.2.4.2. Protein complementation assays (PCAs)	33
1.2.4.3. Fluorescence microscopy-based methods.....	35
1.3. GPCR heteromers form novel signalling entities. Functional consequences.	37
1.3.1. Heteromerisation provides new allosteric opportunities	37
1.3.2. Heteromer-driven biased signalling.....	39
1.3.3. Heteromers modulate receptor biogenesis, arrestin signalling and trafficking.....	42
1.3.4. Switching of coupling selectivity as a mechanism for signal integration by receptor hetero-oligomers.	43
1.4. 5-HT _{2A} -CB ₁ receptor heteromers.....	45
1.4.1. 5-HT and its receptors	45
1.4.2. The endocannabinoid system	47
1.4.3. 5-HT and cannabinoid receptors oligomerisation. Functional interaction between 5-HT _{2A} and CB ₁ receptors.....	51
1.5. Dopamine D ₁ - histamine H ₃ receptor heteromers	53
1.5.1. The dopaminergic system	53
1.5.2. Histamine receptors	57
1.5.3. Dopamine and histamine receptor oligomerisation. Functional interaction between D ₁ and H ₃ receptors.....	61
1.6. Hypothesis and Aims	64
2. Chapter 2. Materials & Methods	67

2.1.	Materials	69
2.1.1.	Antibodies	69
2.1.2.	Buffers and solutions.....	69
2.1.2.1.	PBS and DPBS, pH 7.4	69
2.1.2.2.	Hank's Balanced Salt Solution (HBSS), pH7.4	70
2.1.2.3.	Tris-Acetate-EDTA buffer (TAE), pH~ 8.3-8.6	70
2.1.2.4.	Transformation Buffers (TFB1 and TFB2).....	70
2.1.2.5.	Calcium assay buffers	71
2.1.2.6.	cAMP/NanoBiT assay buffer, pH7.4	71
2.1.2.7.	LB, LB-agar and YT Media.....	71
2.1.2.8.	S.O.C Medium, pH7.....	72
2.1.2.9.	Mammalian cell culture media.....	72
2.1.3.	Enzymes	73
2.1.4.	Ligands.....	73
2.1.5.	Plasmids	74
2.1.5.1.	Plasmids obtained from external sources.....	74
2.1.5.2.	Plasmids generated in this thesis.....	75
2.1.6.	Kits.....	76
2.1.7.	General reagents.....	77
2.1.8.	Cell culture reagents.....	78
2.1.9.	Miscellaneous	79
2.2.	Methods	80
2.2.1.	General molecular biology protocols	80
2.2.1.1.	Generation of chemical competent bacteria cells.....	80
2.2.1.2.	Heat-shock transformation and plasmid amplification.....	80
2.2.1.3.	Site-directed mutagenesis.....	81
2.2.1.4.	Cloning.....	82
2.2.2.	Mammalian cell cultures maintenance	83
2.2.3.	Transient plasmid DNA transfection.....	84
2.2.4.	Calcium mobilization assays.....	85
2.2.5.	Intracellular cAMP accumulation	86
2.2.6.	Determination of ERK1/2 phosphorylation levels	86
2.2.7.	Bimolecular luminescence/fluorescence complementation assays.....	87
2.2.7.1.	GPCR oligomerisation studies.....	87
2.2.7.2.	β -arrestin2 and heterotrimeric G protein recruitment assays	88
2.2.7.3.	NanoBiLC BRET.....	88
2.2.7.4.	Venus YFP Bimolecular Fluorescence complementation assays.....	89
2.2.8.	Cell viability assays.....	89
2.2.8.1.	Label-free Determination of striatal STHdH ^{Q7} and STHdH ^{Q111} cells viability.....	89
2.2.8.2.	Cell death determination with propidium iodide.....	90
2.2.9.	Membrane preparation and radioligand binding.	90
2.2.10.	Peptides stability studies.....	91
2.2.11.	Microscopy methods	92
2.2.11.1.	5-HT _{2A} and CB ₁ receptors surface expression validation.....	92
2.2.11.2.	Internalisation studies.....	92
2.2.11.3.	Two-photon polarization microscopy (2PPM).....	93

2.2.11.4.	In Situ Proximity Ligation Assays (PLA).....	94
2.2.12.	Computational modelling.....	95
2.2.12.1.	5-HT _{2A} and CB ₁ receptors homology modelling.....	95
2.2.12.2.	Orthosteric ligand binding to the 5-HT _{2c} R.....	96
2.2.12.1.	Allosteric ligand binding to the 5-HT _{2c} R.....	97
2.2.13.	<i>In vivo</i> experiments.....	97
2.2.13.1.	Animals.....	97
2.2.13.2.	HD mice Thioperamide treatment.....	98
2.2.13.3.	Acute feeding suppression.....	98
2.2.13.4.	Behaviour assays in HD mice.....	99
2.2.14.	Data analysis, curve fitting and graphing.....	100
3.	Chapter 3. Developing BiLC-based Methods to Study GPCR protein:protein Interactions.....	101
3.1.	Introduction.....	103
3.2.	Results.....	107
3.2.1.	NanoBiT Bimolecular Luminescent Complementation (BiLC) technology provides a versatile tool for the study of GPCR oligomerisation.....	107
3.2.2.	NanoBiT-based β -arrestin assays allow the study of GPCR signalling with kinetic resolution.....	114
3.2.3.	Development of new BiLC NanoBiT-based pairs to investigate GPCRs:G proteins interactions.....	118
3.2.4.	Identification of small-stapled TM peptides targeting 5-HT _{2A} -CB ₁ receptor heteromeric interfaces.....	122
3.3.	Discussion.....	128
3.4.	Acknowledgements.....	132
4.	Chapter 4. Molecular Basis Underlying 5-HT_{2A}-CB₁ Receptor Heteromers.....	133
4.1.	Introduction.....	135
4.2.	Results.....	138
4.2.1.	Functional characterisation of 5-HT _{2A} and CB ₁ receptors mutants.....	138
4.2.2.	Two-photon polarization microscopy (2PPM) reveals heteromer-driven G protein class switch.....	143
4.2.3.	G protein functional coupling to 5-HT _{2A} R is necessary for 5-HT _{2A} R-mediated cAMP release inhibition in 5-HT _{2A} R-CB ₁ R heteromers.....	146
4.2.4.	Heteromer cross-talk is not the same across signalling pathways.....	149
4.2.5.	Heteromer cross-talk and cross-antagonism are driven by different structural arrangements.....	152
4.2.6.	The 5-HT _{2A} R-CB ₁ R heteromer is an heterotetramer.....	154
4.2.7.	Quaternary structure of the 5-HT _{2A} R-CB ₁ R heterotetramer.....	157
4.2.8.	Global proposed mechanism underlying signalling cross-talk in 5-HT _{2A} R-CB ₁ R heteromers.....	158
4.1.	Discussion.....	164
4.1.	Acknowledgements.....	167
5.	Chapter 5. Allosteric D₁-H₃ Hetero-Receptor Interactions Provide a Novel Target for Huntington's Disease.....	169

5.1.	Introduction.....	171
5.2.	Results	174
5.2.1.	Functional D ₁ R-H ₃ R heteromers are expressed in wild type STHdH ^{Q7} and HD model STHdH ^{Q111} striatal cells	174
5.2.2.	Molecular organisation of D ₁ R-H ₃ R heteromers.....	177
5.2.3.	H ₃ R ligands prevent D ₁ R-mediated cell death in STHdH ^{Q7} and STHdH ^{Q111} cells...	179
5.2.4.	H ₃ R ligands revert D ₁ R overstimulation-induced internalisation and heteromer disruption in striatal cells.	183
5.2.5.	D ₁ R-H ₃ R heteromers loss in Hdh ^{Q7/111} mice at early but not late HD stages.	186
5.2.6.	The H ₃ R ligand Thioperamide prevents cognitive and motor learning deficits and loss of D ₁ R-H ₃ R heteromers in Hdh ^{Q7/111} mice.....	189
5.3.	Discussion	192
5.1.	Acknowledgements.....	195
6.	Chapter 6. Serotonin 5-HT_{2C} Receptors positive allosteric Modulation in obesity	197
6.1.	Introduction.....	199
6.2.	Results	202
6.2.1.	Identification of putative 5-HT _{2C} R positive allosteric modulators through high-throughput screening.....	202
6.2.2.	Pharmacological characterisation of compound 11	206
6.2.3.	<i>In vivo</i> evaluation of compound 11	210
6.2.4.	Defining the binding mode of compound 11 by molecular dynamics and site-directed mutagenesis.	211
6.2.5.	SAR-based identification of a G protein biased 5-HT _{2C} R PAM	216
6.3.	Discussion	221
6.1.	Acknowledgements.....	224
7.	Chapter 7. General Discussion.....	225
7.1.	BiLC-based assays to study GPCR interactions	227
7.2.	Allosteric modulation in GPCR dimers: from molecular basis towards disease targeting 228	
7.3.	5-HT _{2C} R PAMs provide a novel target for obesity.....	232
7.4.	Concluding remarks.....	234
7.5.	Future directions	237
	REFERENCES.....	239
	ANNEX I.....	281
	ANNEX II	285
	PUBLICATIONS AND CONFERENCE PRESENTATIONS	294

LIST OF FIGURES

CHAPTER 1

Figure 1.1. Class A GPCRs overall structure and activation	6
Figure 1.2. GPCR-dependent activation of heterotrimeric G proteins	8
Figure 1.3. G proteins-mediated downstream signalling	11
Figure 1.4. GPCR signalling termination and endocytic trafficking	14
Figure 1.5. Representation of the energy landscapes of GPCRs in complex with neutral and biased agonists.....	19
Figure 1.6. Functional consequences of GPCR oligomerisation.....	23
Figure 1.7. Recurrent observed dimeric interfaces in high-resolution GPCR crystal structures	27
Figure 1.8. Current resonance energy transfer strategies for the study of GPCR oligomerisation	32
Figure 1.9. Protein complementation assays to study GPCR oligomers.....	34
Figure 1.10. Proximity ligation assay principle	36
Figure 1.11. Allosteric modulation in GPCR heteromers.....	38
Figure 1.12. GPCR heteromers and ligands operate together to define biased signalling	41
Figure 1.13. The endocannabinoid system and its function in synaptic plasticity	50
Figure 1.14. The basal ganglia in motor control	56

CHAPTER 3

Figure 3.1. Conformational screening of the optimal orientations for CB ₁ , 5-HT _{2A} and 5-HT _{2A} -CB ₁ receptors oligomers. HSV-TK promoter studies	108
Figure 3.2. Functional characterisation of NanoBiT CB ₁ R and 5-HT _{2A} R constructs	109
Figure 3.3. Identification of CB ₁ R, 5-HT _{2A} R and 5-HT _{2A} R-CB ₁ R oligomers using NanoBiT	111
Figure 3.4. Comparative analysis of NanoBiT BiLC and Venus YFP BiFC	113
Figure 3.5. Identification of the optimal receptor:β-arrestin2 pairs to detect agonist-mediated β-arrestin2 activation.....	116
Figure 3.6. Monitoring β-arrestin2 kinetic interactions.....	117
Figure 3.7. Monitoring receptor:G proteins interactions with NanoBiT BiLC.....	120
Figure 3.8. Assay optimisation for the screening of peptides disrupting 5-HT _{2A} R-CB ₁ R heteromers	123
Figure 3.9. Identification of small-stapled TM peptides disrupting 5-HT _{2A} R-CB ₁ R heteromers	125

CHAPTER 4

Figure 4.1. CB ₁ and 5-HT _{2A} receptors mutant proposal	140
Figure 4.2. Cellular distribution of the selected CB ₁ and 5-HT _{2A} receptors mutants and signalling profiling.....	142
Figure 4.3. 5-HT _{2A} R-CB ₁ R heteromers-driven G protein class switch occurs at the plasma membrane.....	145

Figure 4.4. Cross-talk in cAMP signalling requires both functional 5-HT _{2A} and CB ₁ receptors protomers	148
Figure 4.5. Heteromerisation rescues pERK1/2 signalling. Cross-talk requires different conformational changes across signalling pathway	151
Figure 4.6. Cross-talk and cross-antagonism depend on different heteromer domains.....	153
Figure 4.7. 5-HT _{2A} R-CB ₁ R heteromers form higher oligomeric quaternary structures	156
Figure 4.8. Molecular dynamics simulation of the 5-HT _{2A} R-CB ₁ R heterotetramer in complex with two G _i proteins.....	158
Figure 4.9. Proposed mechanism driving cross-talk in 5-HT _{2A} R-CB ₁ R heteromers.....	160
Figure 4.10. The CB ₁ R C-terminal domain controls G protein class-switch and cross-talk in 5-HT _{2A} -CB ₁ receptor heteromers	162

CHAPTER 5

Figure 5.1. Functional characterisation of D ₁ R-H ₃ R heteromers in STHdH ^{Q7} and STHdH ^{Q111} cells	176
Figure 5.2. Molecular architecture of D ₁ R-H ₃ R heteromers	178
Figure 5.3. Proposed mechanism and interacting domains in D ₁ R-H ₃ R heteromers	179
Figure 5.4. H ₃ R ligands revert D ₁ -mediated cell death in STHdH ^{Q7} and STHdH ^{Q111} striatal cells.....	181
Figure 5.5. H ₃ R ligands-mediated cell death recovery depends on functional D ₁ R-H ₃ R heteromers.....	182
Figure 5.6. The H ₃ R antagonist Thioperamide inhibits D ₁ R internalisation.....	184
Figure 5.7. Thioperamide prevents D ₁ R internalisation-driven heteromer loss.....	185
Figure 5.8. Chronic administration of the H ₃ R antagonist Thioperamide prevents loss of D ₁ R-H ₃ R heteromers at late HD stages in HdH ^{Q7/Q111} mice	191

CHAPTER 6

Figure 6.1. High-throughput screening of the Vivia Biotech chemical library.....	203
Figure 6.2. <i>In vitro</i> characterisation of compound 11 PAM profile and selectivity.....	207
Figure 6.3. <i>In vitro</i> characterisation of compound 11-driven β-arrestin2 signalling potentiation.....	209
Figure 6.4. Proposed allosteric binding mode of compound 11	212
Figure 6.5. Homology modelling and site directed mutagenesis defines the allosteric binding pocket of compound 11	215
Figure 6.6. Chemical structure of the analogues targeting the 5-HT _{2C} R.....	217
Figure 6.7. Identification and characterisation of compound WD014 as a biased 5-HT _{2C} R PAM.	218

CHAPTER 7

Figure 7.1. Graphical summary of the main findings of this thesis	236
---	-----

ANNEX I

Supplementary figure 1. 5-HT _{2A} R-CB ₁ R heteromers-driven G protein class switch occurs at the plasma membrane	282
---	-----

Supplementary figure 2. D ₁ R-H ₃ R heteromers are lost in 8-months old HdhQ7/111 HD mice	283
Supplementary figure 3. Chronic administration of the H ₃ R antagonist Thioperamide prevents motor learning and long-term memory deficits in 6-months old HdhQ ^{7/111} HD mice	284
Supplementary figure 4. Compound 11 displays in vivo positive allosteric modulation of 5-HT-induced feeding suppression	285

LIST OF TABLES

CHAPTER 1

Table 1.1. G protein-coupled receptors classification.....	4
Table 1.2. The serotonin receptors family	46
Table 1.3. The dopamine receptors family	54
Table 1.4. The histamine receptors family	58

CHAPTER 3

Table 3.1. PPIs detected using NanoBiT	105
Table 3.2. Comparative studies of different β -arrestin 2 activation assays	118

CHAPTER 4

Table 4.1. 5-HT _{2A} R and CB ₁ R mutants potency and efficacy in ERK1/2 and β -arrestin 2 signalling	143
---	-----

CHAPTER 5

Table 5.1. D ₁ R and H ₃ R expression levels and ligand affinities in STHdH ^{Q7} and STHdH ^{Q111} cells	175
Table 5.2. D ₁ R and H ₃ R expression levels and ligand affinities in striatum, cortex and hippocampus of 4- and 8-months old wild type Hdh ^{Q7/Q7} and HD Hdh ^{Q7/Q111} mice	187

CHAPTER 6

Table 6.1. Analysis of compound 5 and derivatives 6-41 effects on 5-HT-dependent IP accumulation	204
Table 6.2. Compound 11 effect on 5-HT signalling at 5-HT _{2C} WT and mutant receptors	216
Table 6.3. WD014 effects on 5-HT-induced potentiation in Ca ²⁺ and β -arrestin2 signalling at 5-HT _{2C} receptors	220

ANNEX II

Table AII.1. Primer sequences for site-directed mutagenesis	286
Table AII.2. Primer sequences for cloning	288

Chapter 1

General Introduction

1.1. G protein-coupled receptors.

Signal transduction is a crucial process allowing the integration of stimuli from a wide variety of sources into complex coordinated responses. Cell surface membrane proteins are the front line receiving these signals, translating extracellular messages into cascades of intracellular molecular events that ultimately will result in a particular effect. However, minor malfunctions of this tightly regulated process can be detrimental for the homeostatic balance of a given system, leading to pathological conditions^{1,2}. The human genome sequence project predicted that ~20% of all genes account for membrane proteins³, among which the G Protein-Coupled Receptors (GPCRs) superfamily stands out as comprising ~60% of all receptors^{4,5}. Expressed in all tissues, GPCRs diversity is reflected by the extraordinary variety in the physicochemical properties of their ligands, ranging from light photons, protons and ions to hormones, peptides and proteins. Their cell surface expression (exposed binding pockets), together with their participation in a plethora of physiological processes, has favoured GPCR-targeting medicines to account for the majority of best-selling drugs, making up ~30% of the global market share and ~40% of all prescription pharmaceuticals^{6,7}.

Based on sequence homology and structural similarity, Kolakowski originally proposed a classification dividing GPCRs into six classes: Class A (Rhodopsin-like), Class B (secretin receptor family), Class C (metabotropic glutamate/pheromone receptors) Class D (fungi mating pheromone receptors), Class E (cyclic AMP receptors) and Class F (frizzled/smoothened receptors)⁸. However, due to the lack of expression of Class D and E receptors in vertebrates, GPCRs are usually classified into five families following the “GRAFS” classification scheme (**Table 1.1**)⁹.

The common feature that all GPCRs share is the presence of a “central core” domain composed of seven hydrophobic membrane-spanning helices, also known as seven transmembrane (TM) receptors, connected by three intracellular and extracellular loops (ICL1-3 and ECL1-3, respectively). The amino (N)-terminus is located towards the exoplasmic face and the carboxy (C)-terminus extends into the cytoplasm (**Figure 1.1A**). Overall, GPCRs share very little sequence homology between families, even when compared within them. For example, the length of the rhodopsin-like receptors can vary from 413 residues for the prototypical β_2 adrenoceptor (β_2 AR) up to almost 800 amino acids for some glycoprotein hormone receptors. The most conserved features are located within the TM regions, being the ICL3 and both the amino and carboxylic ends highly variable in terms of amino acids number and composition. In fact, the most flexible domain in all GPCRs is the N-terminal domain, which is relatively short for monoaminergic receptors (<50 amino acids),

General Introduction

longer for the Class A glycoprotein hormone receptors or the Class C glutamate receptors (up to 600 amino acids) and up to several thousand residues in the adhesion family¹⁰⁻¹².

Class A GPCRs, the class of receptors most relevant to the focus of this thesis, have been by far the subfamily that has attracted more attention in drug discovery, with most of the solved crystal structures belonging to it (**Table 1.1**). This family contains receptors for small ligands, including odorants, biogenic amine neurotransmitters, peptides and lipids. In addition, it also comprises GPCRs for bigger molecules, such as cytokines or hormones. Even with the low homology between Rhodopsin-like receptors, specific sequence motifs regulating the different receptor conformational states are consistently conserved across this family^{10,13} (further discussed in the next section). Moreover, a relatively common structural determinant among Class A GPCRs is the presence of cysteine residues in the ECLs 1 and 2 and TM3, forming ECL1-ECL2 and ECL2-TM3 disulphide bridges that contribute to the overall receptors stability, their function and membrane expression¹³. In addition, with very few exceptions, most members of the Rhodopsin family experience post-translational modifications, serving the palmitoylation of cysteines located in the receptor C-tail as an anchoring point to the plasma membrane¹⁴.

Table 1.1. G protein-coupled receptors classification.

	Class A Rhodopsin-like	Class B Secretin family	Class C Glutamate family	Adhesion family	Frizzled family
Number	719	15	22	33	11
Orphan	87	-	8	26	-
Sensory	435	-	3	-	-
Unique solves crystal structure	43	4	2	-	1

The GPCRs superfamily distribution across families, classification and available high-resolution structural information. The number of unique crystal structures was last updated in April 2018.

1.1.1. GPCRs structure and activation.

Initial studies led to the two-state equilibrium mode, where, in the absence of ligand, GPCRs alternate between inactive (R) and active (R*) states¹⁵. However, several more complex models, viz. the extended ternary complex and the cubic ternary complex models, were developed and accommodate the fact that different receptor conformations can bind and activate G proteins^{16–18}. In fact, growing experimental evidence has revealed that GPCRs co-exist in multiple states, each with different conformations in regions such as the binding pocket or within the residues exposed to effectively activate G proteins^{10,19}.

Despite each receptor having its unique mode of ligand recognition and activation, several TM conformational changes driving the transition between inactive and active states can be extrapolated across this receptor superfamily. The activation of receptors with affinity for radically different ligands, for example the β_2 AR binding adrenaline and the follicle stimulating hormone receptor (FSHR) binding to the ~36 KDa follicle stimulating hormone glycoprotein, can converge to induce the stimulation of cAMP production through binding the same heterotrimeric G_s proteins, indicating that similar conformational rearrangements are likely to occur in the 7TM bundle and the cytoplasmic loops and/or tails interacting with G proteins. This is supported when comparing the few receptors where both the inactive and active structure has been resolved, revealing agonist-promoted large-scale conformational changes^{20,21}.

The most pronounced common TM rearrangement takes place in TM6. Originally proposed by Schwartz and collaborators as the global toggle-switch model, TM6 experiences a counter clockwise rotation, viewed from the extracellular site, and a pronounced outward movement of its cytoplasmic end, opening the cavity for the G α subunit binding. The TM5, connected to TM6 through the ICL3, “senses” this motion and follows it, moving outward to further enlarge the intracellular cavity (**Figures 1.1A,B**). Although this mechanism has been described in all active-like class A GPCRs x-ray structures, the only available Class B structures obtained in an active state (CTR and GLP-1R) share these features^{22–24}. The helices 3 and 7 also experience substantial agonist-driven reorientations. TM3, a highly bended rod in the 7TM structure, shifts upward its axis with a variable lateral movement and TM7 significantly moves inwards towards TM3. Furthermore, this complex reorientation of the helical domains is accompanied by small conserved changes of local motifs, so-called microswitches²⁵. Thus, Glu/Asp^{3,49} and Arg^{3,50} residues of the D(E)/RY motif, located in the cytoplasmic end of TM3, form a salt bridge with the negatively charged Glu^{6,40} (the “ionic lock”) in the inactive state (superscripts following residue numbers refer to Ballesteros and Weinstein numbering scheme²⁶). This network of polar interactions appears to stabilise the receptor into its closed

General Introduction

conformation and is lost in several agonist-bound crystal structures^{27–29} (**Figure 1.1D**). Natural mutations in the central R^{3.50} of the vasopressin receptor type 2 (V₂R), the gonadotropin-releasing hormone receptor (GnRH-R), and the purinergic P2Y₁₂ receptor (P2Y₁₂R) have been associated with pathological manifestations^{30–32}. An analogous microswitch found in all Class A GPCRs with active and inactive available structures is the TM7 NPxxY motif (**Figure 1.1E**), where a water-bridged hydrogen bond between its Tyr^{7.53} and Tyr^{5.58} has been observed and is suggested to stabilise an energy minimum favouring G protein binding³³. Finally, the binding pocket shows a high degree of heterogeneity between inactive and active-like forms. For example, a significant reduction in the volume of agonist-bound muscarinic M₂ (M₂R) and cannabinoid type 1 (CB₁R) receptors was observed when compared to their respective inactive structures. However, no substantial changes were reported for the β₂AR, μ-opioid (μOR), adenosine 2A (A_{2A}R) or Rhodopsin receptors³⁴.

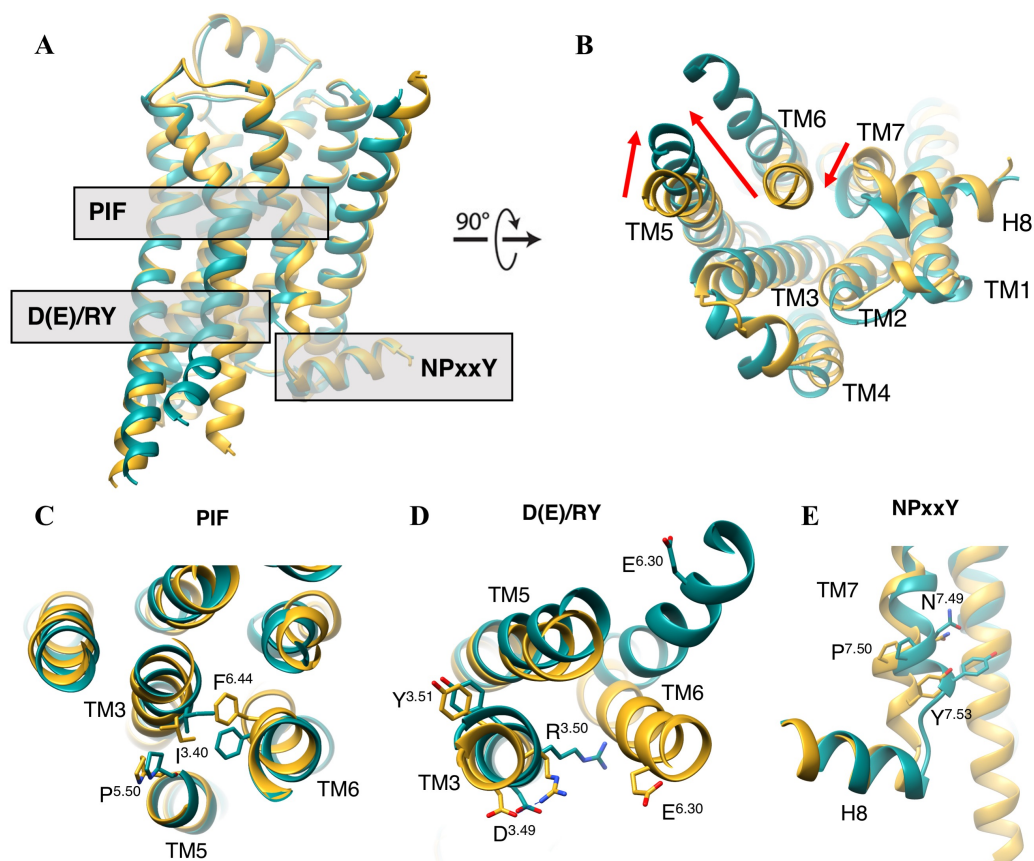


Figure 1.1. Class A GPCRs overall structure and activation. (A) Side view comparison between the inactive (yellow, PDB 3NY8) and active (green, PDB 3SN6) states of the prototypical β₂ adrenergic receptor. (B) Intracellular view illustrating the conserved outward movement of the TM6, the approximation of TMs 5 and 6 enlarging the intracellular cavity and the movement of the TM7 towards the space occupied by TM6 involved in GPCR activation. These rearrangements are integrated by changes in conserved microswitches including the PIF motif at the base of the binding pocket (C), the disruption of the “ionic lock” in the conserved D(E)RY motif (D) and the reorientation of residues in the NPxxY motif (E) stabilising the active conformation.

1.1.2. Heterotrimeric G proteins structure and receptor-mediated activation

As their name implies, heterotrimeric guanine nucleotide-binding proteins are comprised of three subunits; α , β and γ . In humans, 16 genes encode 21 $G\alpha$ subunits, 5 genes encode 6 $G\beta$ subunits and 12 genes encode 12 $G\gamma$ subunits, interacting between them in four main families accounting for $G\alpha$ sequence homology and the effectors modulated ($G\alpha_s$, $G\alpha_{i/o}$, $G\alpha_{q/11}$ and $G\alpha_{12/13}$)^{35,36}.

The $G\alpha$ subunit is formed by two domains: the GTPase or Ras-like domain, highly conserved even across monomeric GTPases, and the helical domain, unique in the $G\alpha$ subunits of heterotrimeric G proteins. The GTPase domain contains three flexible switch regions (SI-SIII) that undergo substantial reorientations between the GDP- and GTP-bound states. The helical domain comprises a six α -helix bundle and its N-terminal helix extends relatively parallel to the plasma membrane, forming a lid over the $G\beta\gamma$ dimer that stabilises this interaction³⁷. In addition, all $G\alpha$ subunits N-terminus, but $G\alpha_t$, undergo post-translational palmitoyl/myristoylations, enhancing membrane trafficking and its interaction with $G\beta\gamma$ ³⁸. $G\beta$ has an α -helix in its N-terminal domain that extends into a β -propeller composed of seven SW40 repeats (common ~ 40 amino acid motifs of 7-8 bladed β -propellers often ending in Trp-Asp). $G\gamma$ is formed by two α -helices connected by an inverting loop. The N-terminus of both $G\beta$ and $G\gamma$ form a coiled-coil interaction and the majority of the remaining $G\gamma$ surface interacts with the external face of the $G\beta$ subunit. In addition, its C-terminus is post-translationally isoprenylated, with the addition of geranylgeranyl or farnesyl groups^{35,39}.

In the basal state, GDP is bound to the binding pocket of the $G\alpha$ subunit, consisting of a crevice formed by amino acids from the GTPase and helical domains. Agonist binding to the receptors allows them to act as guanine nucleotide exchange factors (GEFs) in order to promote the release of GDP and subsequent binding of GTP, which is in higher concentration in the intracellular environment (**Figure 1.2**). The binding of substrate is encompassed by drastic structural rearrangements of all three switches, which subsequently contribute to the displacement and dissociation of the highly stable $G\beta\gamma$ dimer, only dissociable under denaturing conditions. This new configuration allows the GTP-bound $G\alpha$ subunit to interact and further modulate several downstream effectors, including adenylyl cyclase (AC), RhoGEF or phospholipase C β (PLC β). Similarly, the $G\beta\gamma$ dimer can modulate some common effectors (e.g. AC and PLC β) as well as ion channels or some phosphoinositide 3-kinase (PI3K) isoforms (**Figure 1.2**)^{40,41}.

The GTPase domain is highly conserved across $G\alpha$ subunits and crystallographic determinations identified a triad of residues, located in the switches I and II, crucial for its catalytic activity³⁷. However, the original reaction rates, determined with biochemical assays

General Introduction

using purified enzymes, were far slower than observations of downstream signalling activation in more physiological relevant contexts, indicating that the intrinsic activity of the enzyme could not fully describe its kinetics. It was later appreciated that the GTP-bound $G\alpha$ subunit interacts with GTPase-accelerating proteins (GAPs), known as regulators of G protein signalling proteins (RGSs), catalysing the hydrolysis of GTP into GDP and thus synchronising this sophisticated machinery for further cycles (**Figure 2**)⁴². Assuming equal affinities, with 21 $G\alpha$, 6 $G\beta$ and 12 $G\gamma$ subunits there are 72 possible $G\beta\gamma$ dimers that if interacting with all available $G\alpha$ subunits would turn into more than 1.5 thousand different heterotrimeric complexes. However, not all $\beta\gamma$ combinations are favourable and certain $G\alpha$ subunits have preference for specific dimeric compositions, indicating tissue and subcellular expression patterns regulating their signalling³⁵.

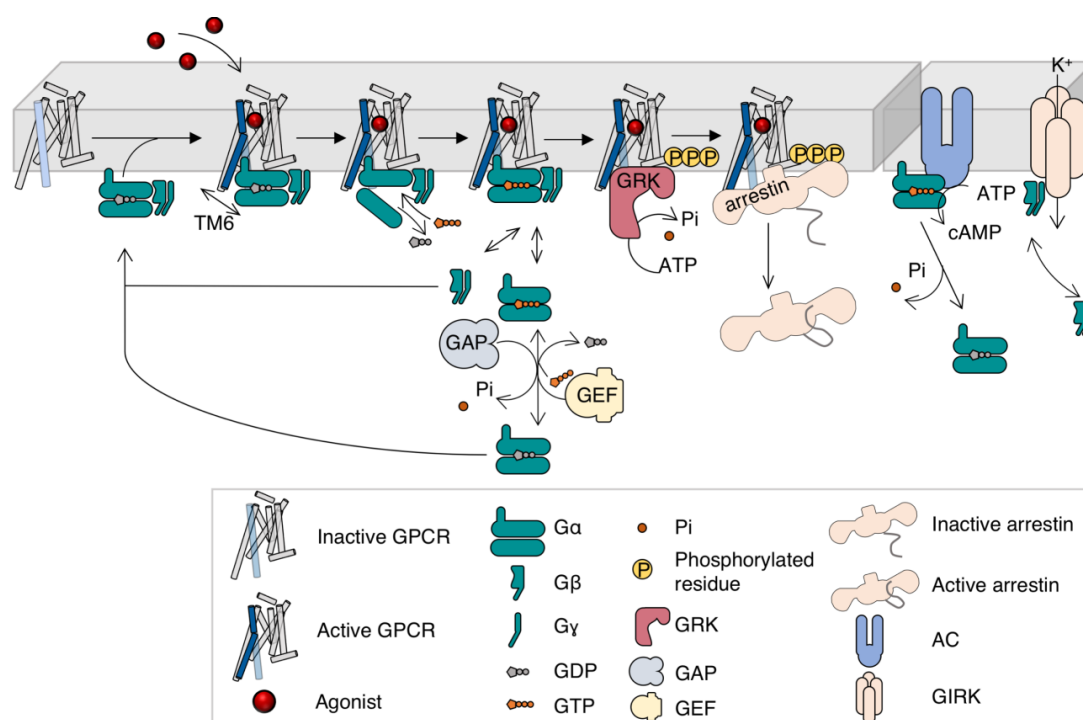


Figure 1.2. GPCR-dependent activation of heterotrimeric G proteins. Agonist binding induces the conformational changes involved in the opening of the intracellular crevice (TM6 outward movement in blue) to accommodate G proteins and other effectors. Agonist-bound receptors act as GEFs, inducing the binding of GDP-bound G proteins, promoting the release of GDP to form the nucleotide-free receptor-G protein complex and dissociating upon GTP exchange. The GTP-bound $G\alpha$ subunit and the $G\beta\gamma$ dimer dissociate from each other to modulate their effectors. G protein-mediated signalling terminates after the hydrolysis of GTP and re-association of the GDP-bound $G\alpha$ and $\beta\gamma$ subunits. Alternatively, GRKs can phosphorylate activated receptors that will bind arrestins to further elicit G protein-independent signalling waves.

Other key aspects that we are just beginning to understand are the mechanism and determinants driving selectivity between GPCRs and G proteins. Even with the elevated number of GPCRs, they couple to four main $G\alpha$ functional subfamilies ($G\alpha_s$, $G\alpha_{i/o}$, $G\alpha_{q/11}$ and $G\alpha_{12/13}$), with some of them being effectors of opposite signalling cascades. Thus, the correct function of this cellular machine requires an exquisite mechanism for the recognition and activation of the right $G\alpha$ proteins upon receptor activation. A pioneer study using all available structures at that time, led to the identification of a barcode in the TM helices interfaces for G protein binding¹³. In particular, comparisons between the active-like β_2 AR and metarhodopsin II showed that the agonist-induced opening of the intracellular TM cavity allows a contact network involving at least eight residues of the TM3, TM5 and TM6 for G protein selective binding^{28,43}. In addition, the ICL2 has a crucial role interacting with the $G\alpha$ N-terminus¹³. Furthermore, a recent study by Flock and collaborators addressed whether a universal allosteric mechanism might drive G protein activation and selectivity. Residues in the helix 5 (H5) of the $G\alpha$ subunit GTPase domain constitute the majority of the receptor-G protein binding surface area (BSA), contacting with the TM3, TM5 and TM6, as well as the ICLs 2 and 3. The authors showed that the highly conserved amino acids across $G\alpha$ types constitute the majority of the BSA, “interaction hotspots”, providing a general mechanism for G protein interaction, while a role in conferring selectivity was proposed to be driven by the less conserved and variable residues⁴⁴. Further analysis of this selectivity determinants led the same group to the identification of a “barcode” of positions in the 16 different $G\alpha$ types that the receptors can selectively “read” using different residues. In their own analogy, different receptors acting as individual keys can open the same lock (G proteins)⁴⁵.

1.1.3. G protein-dependent signalling.

As previously mentioned, G proteins were originally classified into four main classes, each one divided in 2-4 subfamilies: $G\alpha_s$ ($G\alpha_s$ and $G\alpha_{olf}$), $G\alpha_{i/o}$ ($G\alpha_t$, $G\alpha_o$, $G\alpha_i$, and $G\alpha_z$), $G\alpha_{q/11}$ ($G\alpha_q$, $G\alpha_{11}$, $G\alpha_{14}$) and $G\alpha_{12/13}$ ($G\alpha_{12}$ and $G\alpha_{13}$)⁴⁶. Interestingly, a fifth class ($G\alpha_v$) was recently found, expressed in certain species of fishes and lost in tetrapods⁴⁷

Stimulation of 7TM receptors coupled to $G\alpha_s$ or $G\alpha_{i/o}$ proteins activates or inhibits, respectively, adenylyl cyclases (ACs), a family of enzymes heterogeneously expressed across different cell types and tissues composed by nine membrane-bound (ACI-IX) and one single soluble isoform (sAC)⁴⁸. These enzymes catalyse the conversion of adenosine triphosphate (ATP) into cyclic adenosine monophosphate (cAMP). cAMP acts as a second messenger molecule, which binds to the regulatory subunits of the protein kinase A (PKA), composed by

General Introduction

two catalytic and two regulatory subunits, and induces their dissociation, freeing the catalytic subunits to modulate different effector targets, including several ion channels or transcription factors such as the cAMP response element binding (CREB) protein^{49,50} (**Figure 1.3**). The $G\alpha_s$ /AC/PKA signalling axis was the first cAMP-dependent signalling pathway described⁵¹. However, this cyclic nucleotide is associated directly or indirectly to the modulation of hundreds of effectors, including proteins of the mitogen-activated protein kinase pathway (MAPK), Ras GTPases, phosphodiesterases (PDEs) or the Jak/STAT and PI3K/PKB pathways^{40,52,53}.

The prototypical signalling cascade underneath $G\alpha_{q/11}$ coupled GPCRs begins with the activation the β isoform of phospholipase C (PLC β)⁵⁴ (**Figure 1.3**). This enzyme hydrolyses phosphatidylinositol 4,5 bisphosphate (PIP₂) into inositol 1,4,5 trisphosphate (IP₃) and diacylglycerol (DAG), resulting in the opening of IP₃ receptors (IP₃R) located in the membrane of the endoplasmic/sarcoplasmic reticulum and increasing intracellular calcium concentrations ($[Ca^{2+}]_i$), that, by itself, acts as an ubiquitous second messenger involved in many different functions^{55,56}. DAG activates the PKC, allowing it to phosphorylate and thus modulate multiple effectors, including members of the MAPK pathway, RhoGEFs or Akt (PKB).

$G\alpha_{12/13}$ protein function was originally discovered by the ability of certain GTPase-activity deficient mutants to activate actin polymerisation and the assembly of focal adhesions, with both processes being dependent on the Ras homology family member A (RhoA) GTPase⁵⁷. This small protein is activated by members of the RhoGEFs family, directly activated by both $G\alpha_{12}$ and $G\alpha_{13}$ forms (PDZ-RhoGEF, LARG) or only one of them (e.g. $G\alpha_{13}$ activation of p115-RhoGEF) (**Figure 1.3**). As in the case of $G\alpha_s$, $G\alpha_{i/o}$ and $G\alpha_{q/11}$, $G\alpha_{12/13}$ modulates several effectors outside the $G\alpha_{12/13}$ /RhoGEFs/RhoA axis, including cadherins, the protein axin or non-receptor tyrosine kinases^{58,59}.

The downstream signalling pathways described above reflect a small portion of the plethora of proteins that $G\alpha$ subunits are able to modulate. Furthermore, $G\beta\gamma$ not only participates in $G\alpha$ proper folding and orientation, but also constitutes a signalling unit in its own right (**Figure 1.3**)⁶⁰. For example, $G\beta\gamma$, is responsible for the increase in cholinergic-mediated K^+ currents via direct modulation of members of the inwardly-rectifying potassium channels (Kir) family regulated by GPCRs (GIRKs)⁶¹. In addition, novel effectors have been shown to exclusively depend on $G\beta\gamma$, such as the histone deacetylase 5 (HDAC5), Kir3 channels or RGS proteins of the R7 family (RGSR7)^{40,41,62,63}. Therefore, small molecules or peptides with the ability to interact between the $G\alpha$ and $G\beta\gamma$ interacting surface “hotspot” might provide a more selective pharmacological approach than targeting the upstream receptor activating/inhibiting the heterotrimeric G proteins.

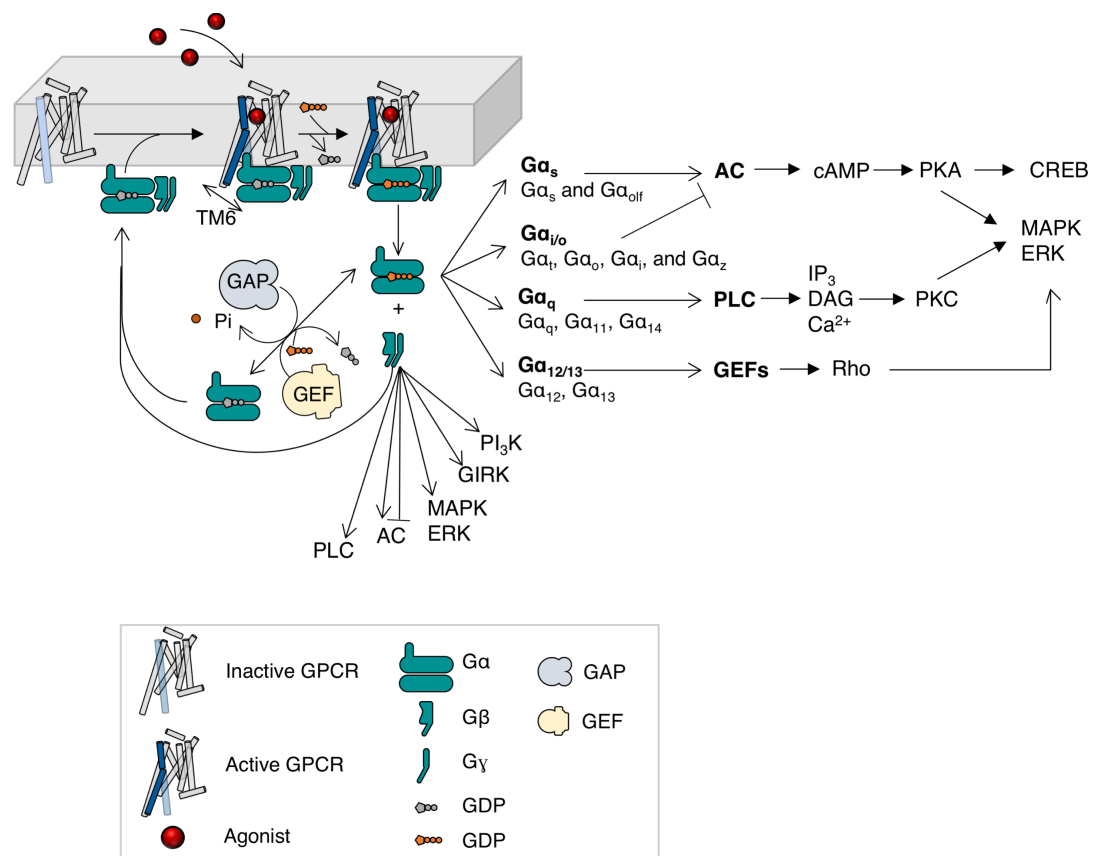


Figure 1.3. G proteins-mediated downstream signalling. Illustration of the canonical signalling pathways downstream the main four G protein classes. Agonist binding-associated receptor conformational rearrangements promote G proteins nucleotide exchange and the dissociation of the $G\alpha$ and $\beta\gamma$ trimer. In their GTP-bound state, the different $G\alpha$ subunits interact with their target effectors. In parallel, the $\beta\gamma$ subunits modulate some common effectors as well as other proteins exclusively depending on its subunits composition. Signalling is terminated after the autocatalytic or GAP-mediated GTP hydrolysis and re-association of the $G\alpha$ and $\beta\gamma$ subunits.

1.1.4. Receptor desensitisation and trafficking.

In parallel to the characteristic cellular responses of each receptor, GPCRs activate regulatory mechanisms to terminate/attenuate the signalling rounds and thus avoid excessive responses. This process is known as desensitisation and allows the receptors to be ready for new waves of stimuli. Genetic mutations, either yielding constitutive active mutants (CAMs) or in accessory proteins involved in this process (e.g. GRKs) have been associated to multiple diseases. This has been extensively documented for Rhodopsin, with 4 CAMs producing congenital night blindness, 10 CAMs causing retinitis pigmentosa and several inactivating mutations in the *GRK1* gene leading to Oguchi disease (a rare form of congenital stationary night blindness)^{64–68}.

General Introduction

Two mechanisms of desensitisation, homologous and heterologous, regulate GPCR surface expression levels and signalling efficacy. Homologous desensitisation is defined by the attenuation of a response driven solely by the agonist acting in a specific receptor, whereas this receptor can activate in parallel downstream effectors, for example the second messenger-dependent PKA or PKC, which are capable of phosphorylating agonist-free nearby receptors and induce their heterologous desensitisation⁶⁹. Homologous desensitisation was originally thought to be a canonical mechanism for signalling attenuation. However, this view was found to be not complete with the Nobel Prize-worthy discovery of GRKs and arrestins as key players⁷⁰⁻⁷².

At the same time that agonist binding promotes structural changes exposing the intracellular cavity and ICLs for G protein recruitment and activation, these conformational rearrangements expose residues, mainly in the receptor C-terminus and the ICL3, that undergo phosphorylation by Ser/Thr kinases of the GRK family (**Figure 1.4**). Importantly, these enzymes only act on agonist-activated receptors. The phosphorylated receptors are then able to interact with multiple effectors, among which arrestins have a fundamental role^{73,74}.

Arrestins 1 and 4, so-called visual arrestins, are exclusively expressed in the rod and cone photoreceptors, whereas the non-visual arrestins 2 and 3 (later renamed β -arrestin1 and β -arrestin2, respectively) have a broader tissue expression pattern. The first effect that arrestins exert upon receptor binding is to sterically hinder further G protein recruitment. In addition, specific arrestin domains allow them to act both as adaptors and scaffolds for the endocytic machinery as well as for G protein-independent signalling (later discussed in this chapter)⁷⁵.

In the Rhodopsin-arrestin 1 complex, the disruption of the “phosphate sensor” by the phosphorylated receptor C-terminus precedes the binding of the “activation sensor” to fully accommodate arrestin 1 into the active-like receptor⁷⁵. However, the molecular basis driving other arrestin-GPCR complexes are less defined. In addition, considering the amino acid heterogeneity across GPCR’s C-terminal and ICL3 domains, defining a “phosphorylation barcode” is substantially challenging. Furthermore, some receptors recruit arrestins in a phosphorylation-independent manner⁷⁶. Interestingly, a recent study led to the identification and experimental validation of two motifs required for high affinity arrestin binding highly conserved between and across GPCRs families and even present in non-GPCRs arrestin binding proteins; PxPxxP/E/D (short code) and PxxPxxP/E/D, where P is a phospho-Ser/Thr and x any residue but proline in the second occurrence⁷⁷. Furthermore, Lefkowitz’s group recently linked two different known receptor-arrestin poses, the “tail” conformation, where arrestin mostly interacts with the phosphorylated receptor C-tail, and the “core” conformation, additionally interacting with the 7TM core, to different functional outputs in terms of desensitisation, signalling and trafficking⁷⁸.

Most GPCRs, but not all, are internalised in an arrestin-dependent fashion, provided by the role of these proteins as adaptors to target receptors to clathrin-coated pits (CCPs). Thus, the internalised GPCRs can be dephosphorylated and recycled back to the membrane or targeted for lysosomal degradation (**Figure 1.4**). Phosphorylated receptor binding promotes the release of the C-terminal from the arrestin polar core, exposing its clathrin and adaptor protein 2 (AP-2) binding motifs^{79,80}. GPCRs do not have a clathrin binding domain, hence, by means of scaffold proteins such as AP-2 or arrestins, the receptors can be incorporated in CCPs. Three clathrin proteins, each one formed by three heavy chains and three light chains, interact together to form the clathrin triskelion, providing a lattice-like structure that will act as a mould in which the vesicles destined for trafficking will form⁸¹⁻⁸³.

Other important molecules for the arrestin-driven receptor internalisation in CPPs are the phosphoinositides, with different members of this family binding both to visual and β -arrestins. β -arrestin 1 has two independent inositol hexakisphosphate (IP₆) binding sites and phosphatidylinositol 4,5-bisphosphate (PIP₂), highly enriched in the plasma membrane, participating in different clathrin-mediated endocytosis steps, including nucleation, cargo selection and coat assembly⁸⁴⁻⁸⁶. Finally, these nascent pits start budding towards the cytosolic space and are pinched off by the GTPase dynamin, whose membrane binding is facilitated by the interaction between PIP₂, its PH domain and the presence of membrane proteins with BAR motifs. Interestingly, some GPCRs can internalise in a dynamin-dependent arrestin-independent way, including caveolae. The nascent vesicles will be directed into early endosomes to further progress through recycling or degradative pathways^{87,88}. Two routes with opposite effects will determine whether receptors are rapidly recycled back to the membrane (resensitisation) or traffic to lysosomes to be down regulated. Regardless of the endocytic itinerary of a given receptor upon acute activation, sustained stimulation generally ends with lysosomal degradation⁸⁹.

GPCRs have been classified into two groups, classes A and B, accounting for the strength and duration of the arrestin-receptor interactions through clathrin-dependent endocytic sorting. With preference towards β -arrestin1, the β_2 AR is the prototypical example of class A receptors, characterised by the dissociation of the complexes near the plasma membrane and a transient pattern of arrestins ubiquitination. By contrast, class B receptors such as the V₂R bind to both non-visual arrestins with equivalent affinities and co-localising over the endocytic system with a sustained ubiquitination mode⁷⁸.

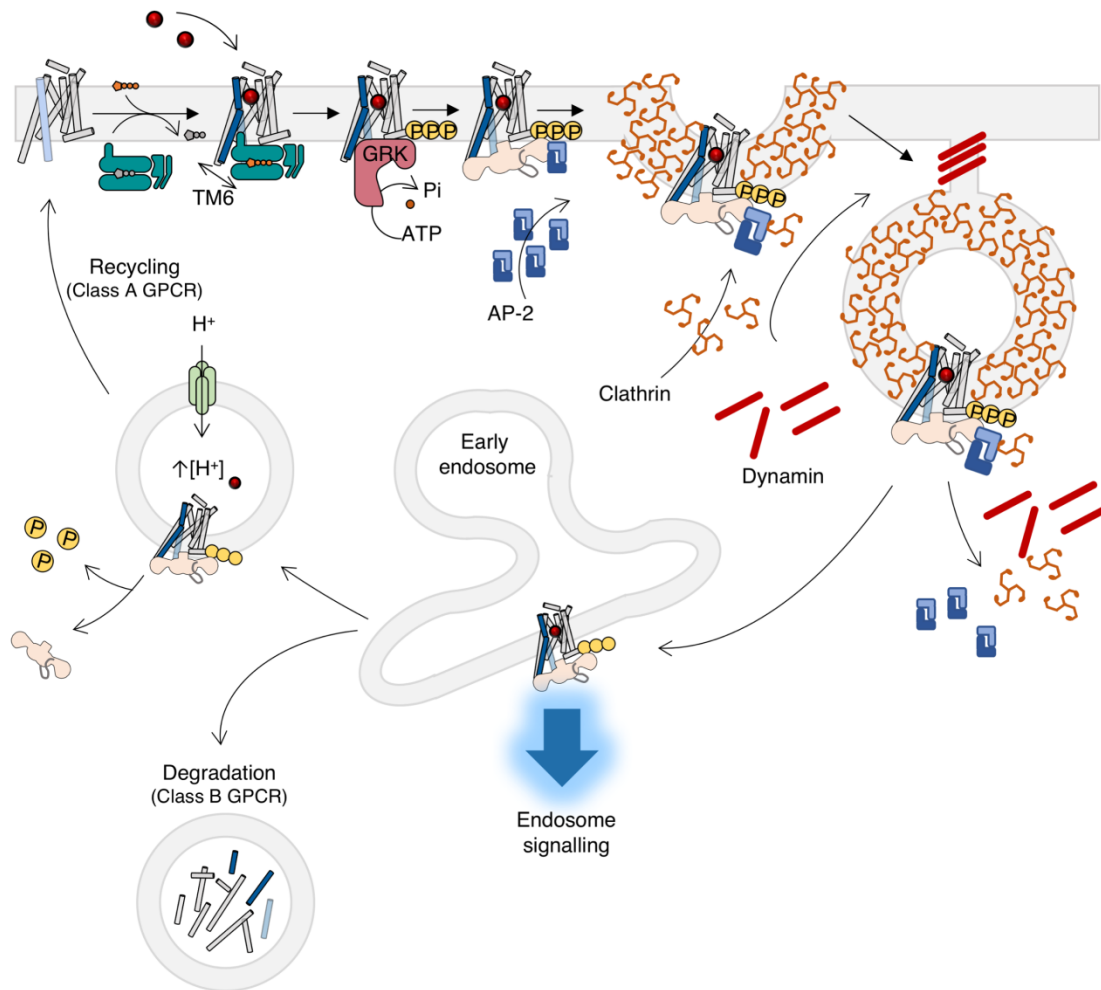


Figure 1.4. GPCR signalling termination and endocytic trafficking. Agonist-mediated activation of the receptors triggers the activation of heterotrimeric G proteins, which in turn activate their downstream effectors. Consequently, the first step in signalling attenuation involves the phosphorylation of the receptors by GRKs and the subsequent arrestin binding, thereby uncoupling GPCRs from G proteins by sterically impeding their interaction. In addition, arrestins direct receptor internalisation into clathrin-coated pits by scaffolding components of the endocytic machinery (AP-2 and clathrin). After the nascent pits are pinched off by the GTPase dynamin, the receptors are internalised into early endosomes for sorting, in which GPCRs can trigger in addition new signalling waves (endosomal signalling). Some receptors (class B) form stable receptor-arrestin interactions and are targeted for degradation into lysosomes. Alternatively, class A GPCRs are directed into acidified endosomal compartments in which receptor undergoes de-phosphorylation and ligands and arrestins dissociate before they are recycled back to the plasma membrane.

1.1.5. Hot topics expanding GPCR functionality.

1.1.5.1. G protein-independent signalling

The classical model of GPCR signalling stated that G proteins must be activated so that signal transduction could occur. However, it is currently accepted that G protein activation is not

categorical for signal transduction^{90,91}. As agonist binding “shapes” GPCRs into G protein receptive units, it also exposes domains for the binding of proteins others than G proteins that, directly or through accessory proteins, direct G protein-independent signalling events. Aside from preventing further G proteins from coupling and direct agonist-mediated trafficking, these scaffolding units can signal per se, regulate the duration/subcellular location of a downstream pathway and bring together GPCRs and effectors into macromolecular signalling complexes. Three major scaffolding proteins regulate GPCR function: arrestins, Postsynaptic density 95/Discs large/Zona occludens-1 (PDZ) domain-containing proteins, and non-PDZ proteins⁹². Their interaction with the receptors is mediated by particular domains, mostly located in the C-terminal tail and the intracellular loops, such as PDZ, Src protein homology 2 (SH2) and 3 (SH3) or arrestin GRK-phosphorylated sites^{86,92}.

Several PDZ proteins have been shown to regulate GPCR signalling through modulating their trafficking. For example, the membrane-associated guanylate kinase inverted-2 protein (MAGI-2) accelerates agonist-induced β_1 AR internalisation, the postsynaptic density protein 95 (PDS-95) retains the β_1 AR in the plasma membrane and the GAIP interacting protein C terminus (GIPC) modulates the endocytic trafficking of the D₂, LH and LPA₁ receptors⁹³⁻⁹⁷. These PDZ proteins not only participate in the post-endocytic sorting in terms of GPCRs recycling or degradation, but also control the spatial context where a signalling event occurs, viz. potentiation/inhibition of endosomal ERK, MAPK, and cAMP signalling⁹⁸⁻¹⁰¹.

A-kinase anchor proteins (AKAPs) are the most studied non-PDZ anchoring proteins regulating GPCR function through direct protein-protein interactions. These scaffolds are characterised by their ability to bind to the regulatory subunits of the PKA, as well as to PKC isoforms, PDEs and phosphatases (e.g. calcineurin)^{92,102}. The discovery of their interaction with GPCRs provided the conceptual basis for understanding cAMP signalling as a spatiotemporal-dependent event. For example, the interaction between the β_2 AR C-terminal domain and AKAP250 enhances PKA-mediated phosphorylation of the receptor. Thus, bringing together members of the cAMP signalling pathway confers obvious advantages, for example in synaptic densities where neurotransmission is controlled by kinases and phosphatases^{103,104}. The AT₁R-dependent activation of the Jak/STAT (just another kinase, JAK, later re-named Janus Kinase, and signal transducer and activator of transcription (STAT) protein, respectively) pathways is another well-known example of G protein independent signalling driven by non-PDZ proteins^{92,98,103}.

With just four players, two of them confined to the visual system, arrestins are the most influential family of scaffolding proteins in diversifying GPCR function. Since Luttrell and collaborators reported the first example of β -arrestin driven signalling, with the

General Introduction

β -arrestin1-dependent recruitment of c-Src upon β_2 AR activation, the list of arrestin interacting partners has followed an exponential growth^{105,106}. Just to name a few (recently reviewed by Peterson and Luttrell⁸⁶) it includes Src family tyrosine kinases, ERK1/2, the c-Jun N-terminal kinase 3 (JNK3), the p38 member of the MAPK pathway, GEFs and GAPs⁸⁶. This variety of interacting proteins is given by the diversity of interacting domains across arrestins structure¹⁰⁵. In addition, whereas G protein-dependent ERK1/2 signalling is translated in nuclear translocation and phosphorylation of transcription factors, arrestins scaffolding allows the formation of signalosomes, confining this pathway in the cytosol¹⁰⁷. This occurs due to the ability of arrestin to confine downstream signalling into different spatiotemporal signalling waves, as in the case of the AT₁, V₂ and PTH₁ receptors, with the MAPK pathway activation being fast when dependent on G proteins and sustained when driven by arrestins¹⁰⁸⁻¹¹⁰.

Overall, the three families of scaffolding proteins described above illustrate how GPCR-mediated downstream signalling involves multiple players that collectively diversify receptors binding to a single molecule type into multiple interrelated responses.

1.1.5.2. Space and time as signalling dimensions

GPCR-mediated outcomes do not only depend on the type of second messengers transducing their information (e.g. cAMP, Ca²⁺, ERKs, etc.). Over the past years, two extra dimensions have been introduced to more accurately depict these intricate signalling networks: space and time¹¹¹. Apart from their role in receptor desensitisation, β -arrestins play a crucial role in the kinetic resolution of GPCR signalling. In the case of cAMP signalling, the development of biosensors capable of being targeted to specific subcellular microdomains in combination with improved faster kinetics explains why the G α_s /AC/PKA axis is perhaps the most well defined downstream signalling pathway in terms of space and time¹¹². A pioneering study by Calebiro et al. showed sustained cAMP signalling in native thyroid follicles after hormone-induced internalisation of the thyroid-stimulation hormone receptor (TSHR), with co-localisation of the internalised labelled agonist, G α_s and ACIII¹¹³. β -arrestins were rapidly added to the equation, as it was reported that they could scaffold the activated TSHR and the G $\beta\gamma$ dimer¹¹³. These observations challenged the classical GPCR signalling paradigm for two obvious reasons. First, they supported the presence of functional signalling units in endosomes, and second, by contradicting mutually exclusive binding of G proteins or arrestins¹¹⁴. However, using single-particle electron microscopy (EM), a quaternary “super-complex” composed by a β_2 AR chimera with the C-tail of the V₂R (β_2 V₂R), the G_s heterotrimer and β -arrestins1 was recently revealed, providing an alternative model that suits well with the aforementioned

observations¹¹⁵. Furthermore, taking advantage Nb37-GFP, a nanobody which specifically binds to the nucleotide-free form of $G\alpha_s$, endosomal GPCR: $G\alpha_s$ complexes have been recently shown for the β_2 and LH receptors^{116,117}.

The nature of a ligand can also modulate the spatiotemporal context of a signalling event. This has been shown for the AT_1R , where the binding of a biased angiotensin II peptide (SII-AngII) resulted in a different compartmentalisation pattern in comparison with AngII¹¹⁸. Similarly, when analysing the intracellular shorting induced by two arrestin biased ligands, AngII analogues, [Sar¹, Ile⁸]-AngII (SI) and [Asp¹, Val⁵, Gly⁸]-AngII (DVG), the half-life of the β -arrestin2- AT_1R complexes in early endosomes (EEs) was lower than the observed by AngII¹¹⁹. Accordingly, using a new set of BRET biosensors, it was shown that, SI and DVG enhance the routing of AT_1R from EEs to shorting and recycling endosomes, whilst AngII is more efficacious in inducing stable β -arrestin2- AT_1R complexes in EEs¹²⁰. Thus, by means of different trafficking patterns, ligands can dictate when and where a signalling event takes place. Similarly, the importance of time in biased signalling (a concept further discussed hereafter) was illustrated in a seminal paper showing how the kinetic context can profoundly impact the apparent bias of different D_2R ligands¹²¹.

Interestingly, a new role of $G\alpha_s$ in controlling GPCRs post-endocytic sorting has recently emerged. Through interacting with the GPCR-associated binding protein-1 (GASP-1) and dysbindin in endosomal membranes, $G\alpha_s$ links them with the hepatocyte growth factor regulated tyrosine kinase substrate (HRS) component of ESCRT (endosomal sorting complex required for transport) machinery as well as with the ESCRT-I-III machinery, promoting the endosomal sorting of the receptors into the intraluminal vesicles (ILVs) of the multivesicular bodies (MVBs) and thus being degraded¹²².

Overall, these examples illustrate how arrestins, G proteins and even different ligands can act synergistically with the endocytic system to define the subcellular location and the duration of downstream signalling. Although a promising field, most limitations are inherent to the limited technologies to study these phenomena and the poor understanding of the spatiotemporal context in pathological conditions. Nevertheless, the incorporation of these two extra dimensions in drug discovery will provide drugs adequately accommodated to the “real” signalling networks occurring in live cells.

General Introduction

1.1.5.3. Biased signalling

The efficacy of certain ligands is not homogeneously distributed across their downstream effectors and some agonists are “functionally selective” towards certain cellular responses, so-called ligand/agonist bias¹²³. Based on incipient observations of GPCR existing in multiple conformations, Kenakin originally proposed this hypothesis under the name of “stimulus trafficking”^{124,125}. Soon after, this was confirmed by the incompatibility of certain dopamine and serotonin receptor agonists-driven responses with single-state receptors^{126,127}. In a context where extensive medicinal chemistry efforts provided potent and selective agonists/antagonists for most therapeutically targeted GPCRs, biased agonism provided new structural opportunities for molecules leading to a particular cellular effect at the expense of others¹²⁸. It is important to distinguish between system bias and ligand/agonist bias. System bias refers to the difference in the observed efficacies of a given pathway conferred by the intrinsic properties of the system. This is the case of β ARs-mediated control of inotropy (contraction) and lusitropy (relaxation) in guinea pig atria, in which the cAMP levels required to induce diastolic relaxation are ~ 4 times lower than the concentration needed to induce contraction¹²⁹. On the other hand, in agonist bias is the molecular structure of the ligand who “biases” the signalling output independently of the cellular context^{128,130,131}.

The two-steps equilibrium models do not accommodate all necessary conformations linked to functional selectivity¹⁵. Instead, GPCR activation is more accurately depicted as an energy landscape in which agonists stabilise several intermediate energy minima, each one with an intrinsic affinity for G proteins, effectors or both of them (**Figure 1.5**)¹³². Thus, several studies have shown that agonists shift the thermodynamic equilibrium of GPCRs existing as ensembles of different conformations¹⁹. At the molecular level, the mechanisms driving bias are poorly understood. However, some reports have linked specific receptor conformations with biased downstream outcomes. For example, Liu et al. showed that β_2 -AR biased ligands preferentially modulate the conformation of the TM7, whereas non-biased agonists alter TM6 position, shifting the equilibrium towards its active-like state¹³³. Similarly, neutral and biased ligands stabilise different V₂R conformations. Accordingly, the TM6 and ICL3 conferred G protein selectivity, while the TM7 and the H8 participated in β -arrestin binding¹³⁴.

The crystal structure of the serotonin (5-HT) type 2B receptor (5-HT_{2B}R) is among the few in complex with a strongly biased drug, the β -arrestin-biased ergotamine. When compared with the closely related ergotamine-bound 5-HT_{1B}R, in which the same drug does not exert bias, the PIF and D(E)RY motifs (**Figure 1.1**) resembled the inactive-like conformation of the β_2 AR, whereas the changes in these conformational switches for the 5-HT_{1B}R were virtually identical of those of the active β_2 AR. Interestingly, both 5-HT receptors showed active-like

conformations of the NPxxY^{27,135}. Recently, Schönege and collaborators identified three clusters of residues with minimal, medium and high perturbations centred around the G protein binding site and the DRY, NPxxY and PIF microswitches. Interestingly, significant alterations across all mutants in the highly perturbed cluster 3 (e.g. loss of the β -arrestin binding) were associated with altered conformations around the NPxxY and PIF motives¹³⁶.

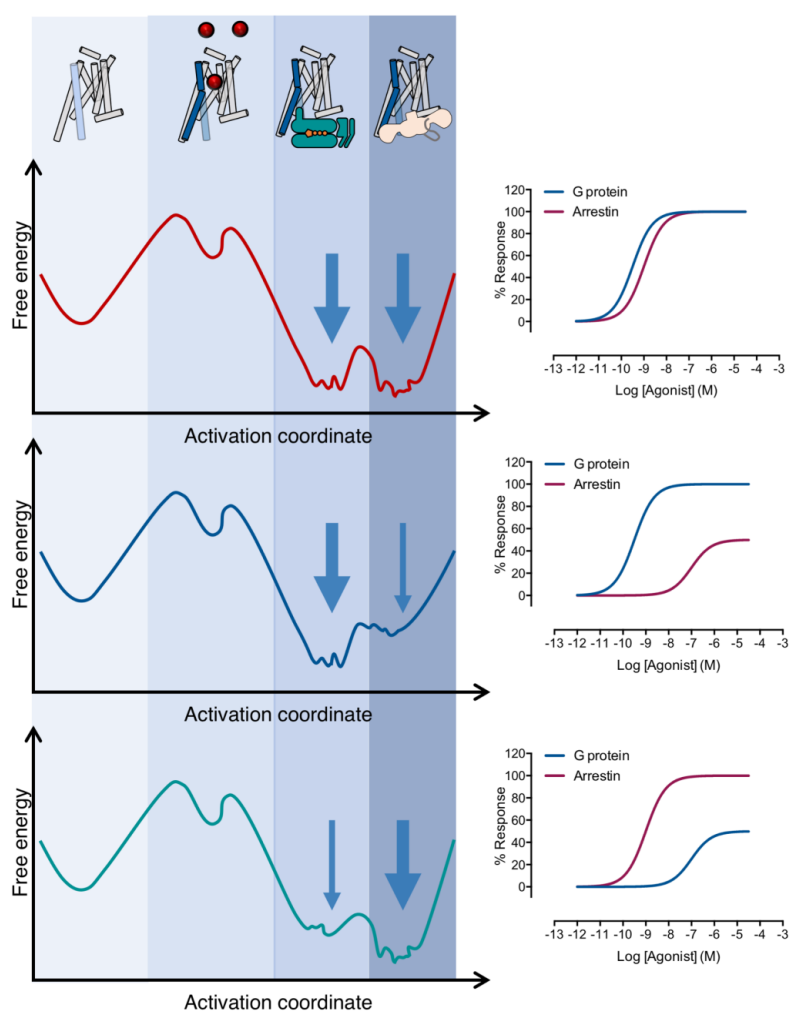


Figure 1.5. Representation of the energy landscapes of GPCRs in complex with neutral and biased agonists.

GPCR activation can be represented as an activation coordinate of its different conformational states and their corresponding free energies. The energy minima correspond to the most stable states in relation to a given downstream signalling pathway. In the presence of balanced agonist (top panels), GPCRs are stabilised into active conformations with similar affinities for G proteins and arrestins. This is translated into similar potencies and/or efficacies across signalling pathways. When bound to biased ligands, GPCRs fall into the energy minima characteristic of singular effectors interactions, therefore displaying preference towards engaging G proteins (middle panels) or arrestins (bottom panels). Accordingly, functional assays reveal differences across signalling pathways.

General Introduction

These studies illustrate conformational differences between balanced and arrestin-biased ligands. However, the rational design of new molecules based on structure-activity relationship is just starting to bloom. An interesting work by McCorvy and colleagues recently revealed that specific ligand interactions in the orthosteric binding pocket accurately predict the biased profile across aminergic receptors, with ECL2 interactions associated to arrestin-biased signalling and TM5 interactions to balanced effector activation¹³⁷.

Ligand bias has been proposed to confer therapeutic advantages over classical drugs in several diseases, including; heart failure, hypertension, diabetes, chronic pain, cancer, schizophrenia, Parkinson's disease and depression¹³⁸⁻¹⁴⁰. An interesting chance discovery of agonist bias therapeutic potential is the case of the β_1 -AR and on β_1 -AR "antagonist" carvedilol, used for the management of congestive heart failure, left ventricular dysfunction and hypertension¹⁴¹. Interestingly, it was recently reported that carvedilol is in fact a β -arrestin biased agonist, inducing GRK/arrestin-mediated signalling and the activation of pro-survival pathways with inverse efficacy for stimulating G protein-dependent signalling¹⁴². Similarly, increasing evidence supports that eliminating the β -arrestin signalling component downstream μ -OR agonism might reduce opioids-associated therapeutic limitations (constipation, respiratory depression and dependence) whilst retaining morphine-like analgesic properties, providing an exciting example of bias translated into improved clinical safety and more favourable outcomes¹⁴²⁻¹⁴⁵.

1.2. G protein-coupled receptors oligomerisation

1.2.1. From early evidence to the establishment of a new paradigm

G protein-coupled receptors were originally thought to operate as monomeric units; thus, one ligand would bind one receptor to couple one G protein. Although this model depicted quite accurately some pharmacological parameters of certain receptors, cumulative evidence suggested that many receptors did not follow the simple mass action law that would be expected from a one-to-one interaction. In these studies, non-linear Scatchard plots were observed, with Hill coefficients different to the unit, indicating simultaneous binding of different molecules to the receptor or to different receptor states, namely cooperativity. One of the earliest, perhaps the first, experimental evidences of interactions between GPCRs was the proposed by Limbird, De Meyts and Lefkowitz, supported by the detected negative cooperativity of [³H](-)alprenolol binding to β ARs in frog erythrocyte membranes¹⁴⁶. It was almost a decade later when Fraser and Venter resolved β_2 ARs from mammalian lung membranes with an apparent molecular weight (MW) of ~109 kDa, that is the arithmetic sum

of two β_2 ARs¹⁴⁷. A year later, Avissar et al. showed muscarinic receptors assembling into higher order quaternary structures via photoaffinity labelling of different brain areas and the heart¹⁴⁸. By means of similar approaches, the dimeric organisation of the α_1 and α_2 adrenergic receptors, AT₂R, D₂R, CaSR and CCR2 was also shown¹⁴⁹⁻¹⁵⁴.

Using chimeric receptors, Maggio and collaborators provided compelling evidence of heteromerisation modulating GPCR function. Domain swapping chimeras were generated by exchanging the M₃R TMs 6 and 7 for the homologous helices from the α_2 AR and vice versa. Although these constructs failed to bind nor signal upon agonist stimulation, ligand binding and downstream effector activation were recovered when co-expressed together^{155,156}. Similarly, function recovery after the co-expression of signalling/binding-deficient mutants attested homo- and hetero-merisation for the AT₁R, somatostatin receptors 1 and 5 (SSTR1 and SSTR5, respectively), D₂R and D₃R¹⁵⁷⁻¹⁵⁹. Based on these observations, two architectonic models were proposed: domain-swapped and contact dimers. In domain-swapping dimers, 2 “new” 7TM bundles are formed as a result of the exchange between helices from both protomers. This organisation would imply a certain degree of TMs unfolding together with spatial flexibility. However, the later appreciation of GPCRs not only organised as dimers, but also being possible multi-oligomeric complexes, strongly suggested that these receptor-receptor interactions might be more readily explained through lateral/contact dimers, a model that, with certain nuances, still prevails^{160,161}. Further data supporting contact dimers arose from two independent studies using peptides mimicking their interacting interfaces, selectively disrupting β_2 AR and D₂R downstream signalling^{152,162}.

In 1996, Romano et al. reported a key finding for the understanding of class C GPCRs biological assembly. For the first time, it was shown that homodimerisation was an intrinsic property of a GPCR, with two mGlu₅R protomers stabilised by inter-molecular disulphide bonds between their VFM motifs¹⁶³. Two years later, three papers revolutionised the GPCR field, demonstrating that oligomerisation was not only possible but compulsory for Class C receptors function¹⁶⁴⁻¹⁶⁶. These seminal works revealed that the interaction between GABA receptors that do not efficiently bind agonists nor signal, GABA_{B2} and GABA_{B1} receptors, is compulsory for their proper membrane sorting and function, providing the first irrefutable evidence of GPCRs heteromerising. GABA_{B1}R contains an ER-retention motif that is masked when interacting with GABA_{B2}R, acting as a quality checkpoint to ensure that only functional complexes can reach the cell surface^{167,168}. Over the following years, it was shown that the CaS, mGlu₁ and mGlu₅ receptors form homodimers stabilised by inter-protomer disulphide bridges¹⁶⁹⁻¹⁷². In addition, the discovery of taste T1R2-T1R3 and T1R1-T1R3 heterodimers as responsible for the sweet and umami tastes, respectively, further aided to establish oligomerisation as a pre-requisite for Class C receptors proper function¹⁷³⁻¹⁷⁵.

General Introduction

Despite Class C receptors homo- and hetero-merisation is accepted¹⁷⁶, the situation concerning Class A and other GPCRs families is more intricate. It is well known that receptors often adopt quaternary structures and the confirmation that this was true for Class C receptors rapidly raised the question whether that could be the case for the Rhodopsin-like family. A turning point in the detection of GPCR homo/hetero-oligomers was the implementation of resonance energy transfer techniques in the field, mostly BRET and FRET. In one of these first studies, Bouvier's group detected constitutive β_2 AR dimers in live cells by BRET¹⁷⁷. RET and its variants, viz. time-resolved FRET (TR-FRET) or complementary donor-acceptor RET (CODA-RET), have profoundly contributed to detect, validate and understand GPCRs interacting between them as well as with their effectors in live cells and native tissues¹⁷⁷⁻¹⁷⁹.

GPCR oligomerisation has been implied in a large number of cellular processes (**Figure 1.6**), including maturation and membrane trafficking, effector efficacy cross-talk, co-internalisation, trans-inhibition and trans-activation¹⁸⁰⁻¹⁸⁵. It should be noted that most of the original RET studies relied on heterologous expression systems in which receptor over-expression might be prone to errors, perhaps precipitating the reported number of GPCR oligomers from these original studies. In fact, the implementation of single-molecule particle tracking suggests that their quaternary structure is dynamic, with the interconversion between monomers, dimers and higher order complexes¹⁸⁶. This appreciation might reconcile the two apparent mutually exclusive pro- and anti-dimer schools. Nowadays, the controversy is not centred on the ability of members of this family to interact, but on what is their relevance *in vivo*. Two major consequences would accrue from this: first, dimerisation would diversify the actions driven by a limited number of encoded proteins, therefore being an evolutionary mechanism to expand the functionality of a given pool of genes and second, from a therapeutic point of view, oligomerisation would provide new opportunities for pharmacological interventions.

For GPCR dimers others than those from the glutamate family, what is a relevant GPCR oligomeric interaction? To answer this legitimate question, Gomes and collaborators recently proposed three criteria that must be fulfilled before labelling a receptor pair as a "true" heterodimer: (1) co-localisation and physical interaction of the heteromer components in native tissues, (2) the heteromers should exhibit pharmacological properties (binding, signalling, trafficking, etc.) different from those of the protomers, often referred to as heteromer biochemical fingerprint¹⁸⁷, and (3) heteromer disruption must result in the loss of heteromer-specific properties¹⁸⁸. Although these rules are meant to define heteromers, this classification can be extended to homodimers.

Heterodimers between the δ and μ opioid receptors are among the few examples fulfilling all requirements. δ OR- μ OR heteromers are co-expressed and interact in native tissues (criterion

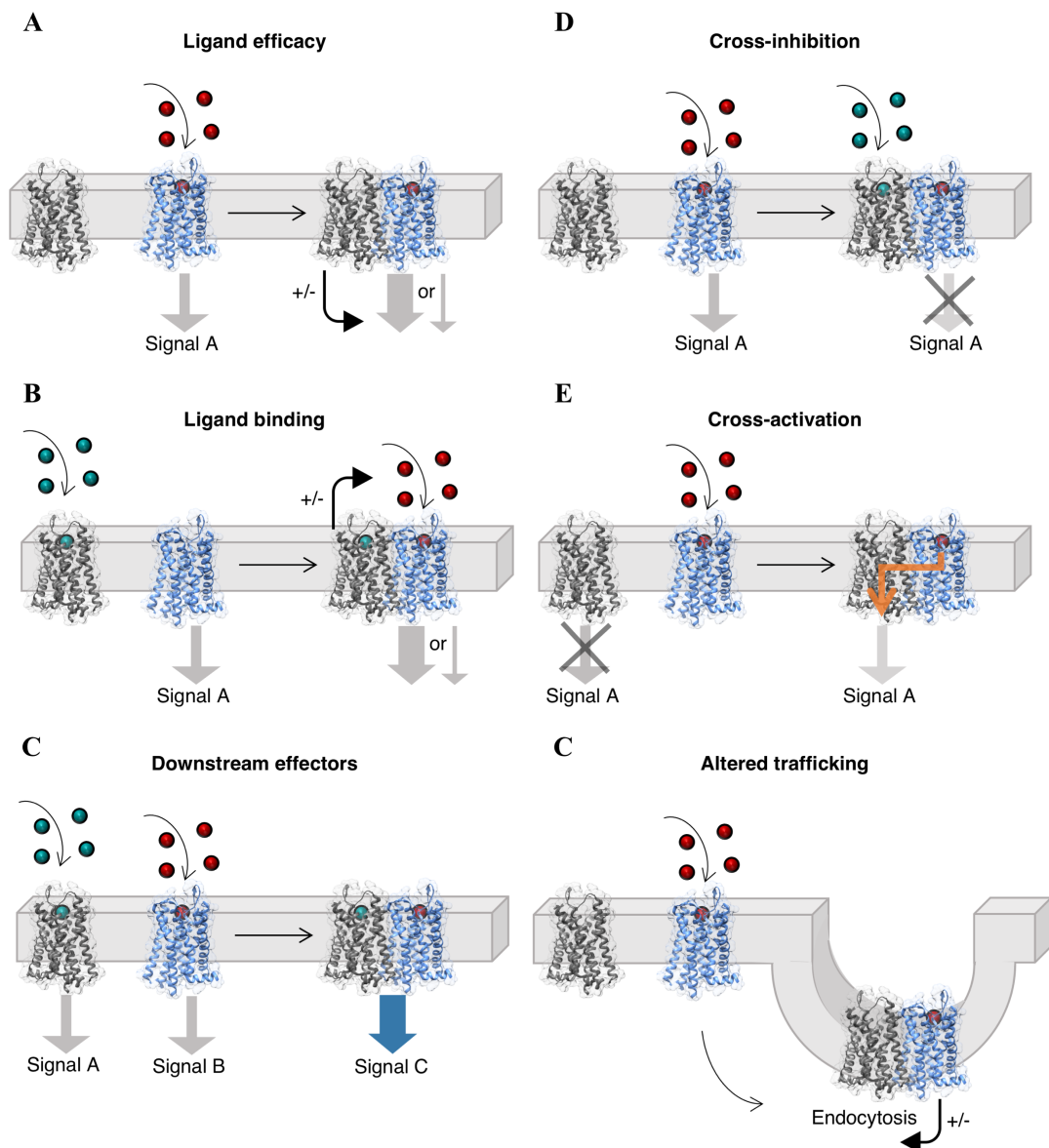


Figure 1.6. Functional consequences of GPCR oligomerisation. Schematic representation of the main cellular effects upon receptor dimerisation. Otherwise stated, the responses after the interaction with the second protomer (in blue) can be extended to both homo- and heteromers. **(A)** The interaction with a second protomer (non-liganded) can lead to increased/reduced efficacy after ligand stimulation. Similarly, cooperativity often takes place at the level of ligand binding **(B)**, when a molecule binding to one protomer increases/decreases the affinity of a second ligand targeting the neighbouring receptor. This is often translated into altered signalling efficacy. Frequently, oligomerisation provides new conformational opportunities to engage different downstream signalling pathways from those of the individual receptors **(C)**. In the case of heteromers, cross-inhibition **(D)** has been extensively reported and refers to the ability of an agonist (negative cross-talk) or antagonist (cross-antagonism) targeting one protomer to inhibit the agonist-driven actions of its interacting partner. Cross-activation **(E)** is another mechanism by which oligomerisation diversify GPCRs. This applies to homomers (e.g. rescue of function after the co-expression of chimeric constructs) and heteromers (e.g. activation of the cognate downstream pathway of one protomer when agonising the other). In addition, oligomerisation can also modulate receptor trafficking **(F)**. Information taken from^{186–188}.

1) and they exhibit a signalling pattern different from the expected from the individual protomers (criterion 2) that can be blocked with heterodimer-specific reagents such as δ OR- μ OR heteromer-selective antibodies, ligands or peptides (criterion 3)¹⁸⁹⁻¹⁹⁴. Similarly, the recently described complexes between the CB₁ and 5-HT_{2A} receptors have shown to physically interact *in vivo* and to constitute new biochemical entities with its particular signalling pattern. Interestingly, disruption of 5-HT_{2A}R-CB₁R heteromers abolished memory impairment after Δ^9 -tetrahydrocannabinol (THC) administration, providing a new pharmacological target to dissociate marijuana side effects¹⁸⁴. In the case of interactions between the same type of receptors, Rivero-Müller provided *in vivo* evidence of LHR inter-molecular complementation using a compelling and elegant approach. Mice co-expressing two mutant LHR forms, signalling-deficient and binding-deficient receptors, restored normal LH actions and gonadal wild type phenotype, demonstrating how receptor-receptor interaction might provide *in vivo* mechanisms to rescue GPCR function¹⁹⁵.

The development of new technologies is progressively allowing to confirm *in vitro* observations in native tissues. However, translating them into the clinic will require answering some fundamental questions that still remain poorly understood: how do protomers talk to each other? What is the minimal functional unit required for downstream signalling? Which domains constitute the interacting interface? How stable are these interactions? Where does oligomerisation begin? In this thesis (see Chapters 3 and 4) we sought to answer some of these questions by providing an exhaustive study on the molecular basis underlying cross-talk in a promising target to dissociate THC's good from the bad, the recently described 5-HT_{2A}-CB₁ receptor heteromers.

1.2.2. Molecular interfaces involved in GPCR oligomerisation

The first high resolution evidence describing the quaternary arrangement of GPCR oligomers *in vivo* came from atomic force microscopy (AFM) studies of mouse rod outer segments disc membranes, revealing that, in rhodopsin and opsin, TMs 4 and 5 stabilise a symmetrical homodimeric interface, whereas contacts within adjacent dimers involve TMs 1 and 2 and the ICL3^{196,197}. Similarly, electron cryomicroscopy of 2-dimension crystal arrays in reconstituted squid membranes showed TM 4 forming inter-molecular contacts between rhodopsin dimers¹⁹⁸. Although both models differ significantly in their overall quaternary structure, these original structures, in combination with experimental validation and molecular modelling, provided the first quaternary structure templates.

The dynamic nature of heteromerisation might be dependent on the receptor pair and on its interacting helices (assuming that several reports have shown alternative TM contacts for a

given oligomeric pair)^{199–201}. For example, while the lateral diffusion of GABA_B receptors increases after agonist stimulation, no effects were observed for both the β_1 and β_2 adrenoceptors using total internal reflection fluorescence microscopy (TIRF)²⁰². Similarly, using fluorescence correlation spectroscopy (FCS), agonists did not induce changes in the oligomeric state of β_2 and M₁ receptors²⁰³. On the other hand, it was recently shown by dual colour fluorescent recovery after photobleaching (dcFRAP) that Frizzled 6 receptors (FZD₆R), forming TM4/TM5 contact homodimers, require agonist-promoted protomer dissociation to effectively activate downstream pathways²⁰⁴. Similar agonist-mediated dynamics were observed in two independent studies of the glutamate receptors family. By single-molecule FRET (smFRET), Vafabakhsh et al. correlated mGlu₂ and mGlu₃ ligands efficacy to three interconvertible states of the receptors' ligand-binding domains (LBD) involved in receptor activation²⁰⁵. These agonist-dependent TM dynamics were well characterised for the mGlu₂R, in which receptor activation depends on an interface switch from TM4-5 to TM6²⁰⁶. Adding an extra layer of complexity, it has been recently shown that the ligand-responsive calcitonin receptor (CTR) species are dimeric, but G protein binding weakens their interaction favouring monomeric receptor:G protein ternary complexes²⁰⁷. Together, these results not only support agonist binding driving dynamic TMs interactions, but the impact of third party proteins (e.g. heterotrimeric G proteins) on their stability.

In most cases, evidence supporting GPCR oligomerisation was obtained using biochemical and biophysical techniques. In 2007, the introduction of improved crystallographic methods led to a boom in the number of high resolution solved GPCRs crystals^{13,208}. Apart from accurately depicting structural determinants in relation to receptor activation, several X-ray structures have captured GPCRs in dimeric states, uncovering some recurrent interacting interfaces (**Figure 1.7**). The crystal structure of the ligand-free turkey β_1 AR revealed two dimeric interfaces formed by TM4/TM5 and TM1/TM2/H8 contacts (**Figure 1.7B**)²⁰⁹. This model is consistent with aforementioned opsin/rhodopsin AFM structures^{196,197}. Similarly, the asymmetric unit of the κ -OR consists of two parallel dimers, with a $\sim 1,100 \text{ \AA}^2$ buried surface area formed through contacts between TM1/TM2 and H8²¹⁰. Furthermore, in a recent study where three M₃R crystallographic variants were generated, all of them showed two interacting modes consisting in antiparallel TM4/TM5 and parallel TM1/TM2 dimeric interfaces²¹¹. Furthermore, the Frizzled class smoothed (SMO) receptor crystallised as parallel dimers with the interface involving TM4/TM5 contacts (**Figure 1.7C**)²¹². The crystal structures of the C-X-C chemokine receptor type 4 (CXCR4) in complex with the small-molecule antagonist IT1t, the cyclic peptide antagonist CVX15 and the viral chemokine antagonist vMIP-II have revealed a conserved homodimeric interface of parallel and symmetric dimers involving TM5/TM6 interactions^{213,214}. Interestingly, CVX15-induced tilt of the extracellular part of

General Introduction

TM5, which approximates this TM to the neighbour protomer, has been involved in ligand binding cooperativity within CXCR4 oligomers²¹³.

Similar to the β_1 AR, two dimeric interfaces were observed in the μ -opioid bound to the morphinan antagonist β -funaltrexamine. TM1/TM2/H8 interactions form an interface with a buried surface area of 650 \AA^2 . The second and most prominent interaction involves TM5/TM6 contacts (**Figure 1.7D**), with a buried surface area of 1492 \AA^2 forming the so-called four-helix bundle motif (a contact network formed by extensive contacts between the TMs 5 and 6)^{209,215}. Furthermore, a parallel dimeric packing involving the TM1/TM2/H8 network was also observed in the agonist-bound μ -OR²¹⁶. Interestingly, the TM5/TM6 dimer surfaces observed in the inactive structure would not be compatible with the conformational changes required to activate both protomers. This steric hindrance imposed by the agonist-driven TM5/TM6 rearrangements might explain the negative cross-talk in signalling after simultaneous stimulation of both protomers in a dimer^{161,184,217}.

Regarding obligate dimers, the mGlu₁R and mGlu₅R crystal structures are the only ones released to date^{11,218,219}. Whilst the mGlu₅R crystallised as antiparallel dimers, the mGlu₁R showed a parallel packing with a cholesterol-facilitated dimer interface through TM1/TM1 contacts^{11,218}. However, although these assemblies accurately depict the overall 7TM structure, they lack their VFT motifs, perhaps not packing in a physiologically relevant conformation. Furthermore, recent cross-linking studies shown TM4/TM5 contacts driving mGluRs interactions, an interface more present in other solved crystal structures²⁰⁶.

Overall, the most prevalent dimeric interface involves TM1/TM2/H8. On the other hand, TM5 is often paired with TM4 (β_1 AR, rhodopsin, opsin, M₃R and SMO receptor) or with TM6 (CXCR4 and μ -OR). Caution must be exercised in assuming GPCR oligomerisation interfaces from crystallography, as represent snapshots of a dynamic process in artificial setups. However, the recurrence of some interfaces in agreement with a large body of experimental strongly supports their functional relevance^{184,220–224}. Hence, the combination of structural information together with biochemical/biophysical approaches and advanced bioinformatics should be used in conjunction to validate the biological relevance of these complexes. An example is the interesting strategy that Jonas et al. recently applied to validate interacting interfaces in live cells. Using dual-colour photoactivated localisation microscopy (PALM) with CAGE photocontrolable dyes (PD-PALM) the authors resolved single GPCRs participating in dimers and/or oligomers with ~ 8 nm resolutions. The combination of spatial organisation from PD-PALM images with molecular modelling allowed the authors to disclose different interacting interfaces driving oligomeric complexes²²⁵.

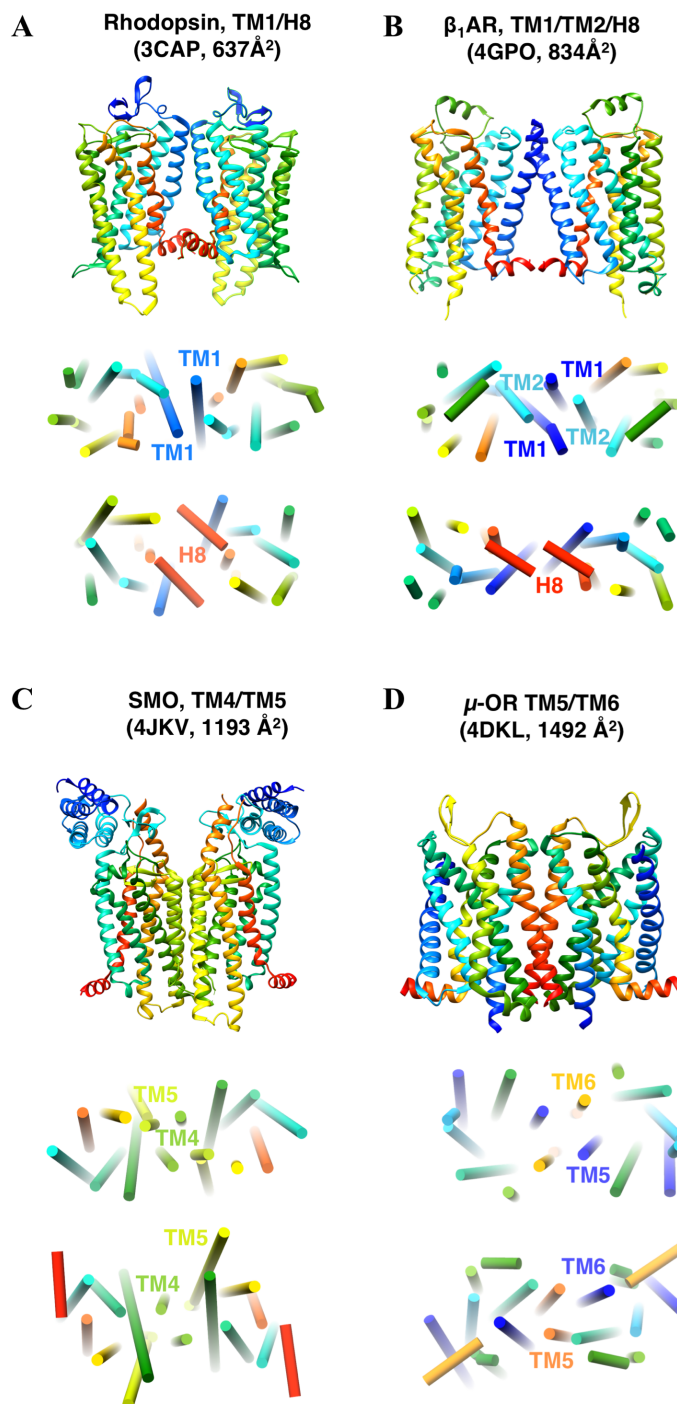


Figure 1.7. Recurrent observed dimeric interfaces in high-resolution GPCR crystal structures. The receptor name and the putative observed interfaces are indicated above the ribbon representation of each GPCR. In brackets, PDB accession number and buried surface area. For each structure, the top, middle and bottom panels correspond to the lateral, extracellular and intracellular views, respectively, of each assembly.

1.2.3. Minimal functional units

Even today, constitutive class A GPCR dimerisation and the minimal stoichiometry required for efficient G protein activation are long debated questions. A brief look at the dynamics of the mGlu receptors activation intuitively raises the question of whether some determinants might be extended to the rhodopsin-like and other GPCRs families²²⁶. For example, glutamate binding cooperatively influences the union of a second agonist molecule in the concomitant protomer^{227,228}. Similarly, cooperativity at the binding site has been reported in several Class A homo/heteromers¹⁷⁶. In addition, cumulative work suggests that ligand binding to both mGluRs subunits is required in order to efficiently activate this receptor^{229,230}. Does the same apply for other GPCR families? Furthermore, in the current view of class C receptor, activation is asymmetric, with the recruitment of a single G protein underneath the dimeric complexes. In the case of GPCR oligomers others than Class C receptors, what is the minimal functional signalling unit?²³¹

Several studies support a symmetric and functional 1:1 receptor:G proteins/arrestins stoichiometry in reconstituted lipid nanodiscs. This has been shown for rhodopsin, the transducin-metarhodopsin II complex and the β_2 and μ -opioid receptors²³²⁻²³⁶. Furthermore, monomeric mGlu2R effectively bind G proteins in response to a positive allosteric modulator (PAM), although orthosteric agonists fail to do so, suggesting the importance of the dimeric organisation in controlling endogenous activation²³⁷. Nevertheless, these studies are not representative of a native environment. In fact, all GPCR oligomers referred to above have been detected as dimers and/or higher order oligomers *in vivo* and/or *in vitro*. Using transgenic rats, Zhang et al. recently demonstrated that dimerisation between S-opsin and R-opsin is required for S-opsin trafficking to the rod outer segments²³⁸. Controversially, the same group supporting the view that monomeric β_2 AR could activate G proteins reported that this receptor mostly forms tetramers when reconstituted into a model lipid bilayer^{233,239}. Moreover, heteromers involving receptors from the opioid receptor family are perhaps the most well validated *in vivo*, including δ -OR- μ -OR, μ -OR-CB₁R and μ -OR-mGlu₅R heteromers (extensively reviewed by Gomes et al.¹⁸⁸).

At the mechanistic levels, few studies have attempted to describe the contribution of each individual protomer to modulate signalling (we will explore this question in Chapter 4). This is partially due to the difficulty to control the individual components of these quaternary complexes. Recently, Han et al. developed an interesting strategy to study cross-talk in D₂R homodimers²⁴⁰. Using a chimeric receptor unable to activate its own fused G protein, co-expression of a WT receptor rescued signalling. This study clearly suggests (1) different conformational states between protomers and (2) that it is the conformation of the second

protomer which modifies signalling. In fact, co-expression of WT D₂R with a non-binding CAM resulted in reduced signalling efficacy²⁴⁰. Using the same system, it was shown that negative cooperativity of the recently re-discovered bitopic D₂R SB269652²⁴¹ depends on a sequential binding mechanism, in which, after binding to the D₂R orthosteric pocket, the allosteric moiety binds to the adjacent protomer²⁴².

These studies support the idea that the state-dependent allosteric communication within protomers is translated into signalling modulation in an asymmetric manner resembling the GABA_{B1}R-GABA_{B2}R, mGluRs, CaSR and taste receptors obligate dimers²⁴³. This is the case of the aforementioned D₂R homodimers²⁴⁰ and, in fact, taking into account all available crystal structures in complex with heterotrimeric G proteins, the interacting surface area is about twice that of the 7TM bundle, being sterically impossible for dual G protein recruitment^{22,23,28}. Where does G protein bind in respect to the agonist bound protomer? In the case of mGluRs homodimers, the current view is consistent with both cis- and trans-activation^{230,244}. Trans-activation in dimeric complexes has been reported for the glycoprotein hormone class A TSH, FSH, LH and TRH receptors²⁴⁵. In addition, trans-activation appears to be predominant in other rhodopsin-like receptors in which the binding site does not comprise a large N-terminal extracellular domain, such as μ -, δ - and γ -ORs and D₂R, whereas cis-activation has only been shown for the leukotriene B₄ receptor BLT1^{240,246,247}. Regardless of the activation route, all these studies support that upon ligand binding to one protomer, the second receptor does not stand indifferent and reacts changing its conformation.

Heterodimerisation and higher order oligomerisation adds an additional level of complexity. Using conformational FRET biosensors, Vilardaga et al. shown a trans-conformational effect in α_{2A} adrenergic and μ -opioid receptor heteromers through which morphine inhibits the active conformation of the norepinephrine-bound α_{2A} AR and, consequently, α_{2A} AR-driven G_i activation²⁴⁸. This negative cross-talk, often observed in several GPCR heterodimers, was proposed to occur through conformational changes across the TM4/TM5 interacting interface. Accordingly, McCormick's group proposed and validated a model in which the reduction in signalling efficacy after dual receptor occupancy can be explained due to a steric clash between the interacting TMs, not allowing to fully open the TMs 5 and 6 to efficiently accommodate G proteins^{184,249}. Finally, few studies attempted to understand the minimal signalling units in higher oligomeric species such as tetramers. Overall, it appears that these macromolecular complexes go back to symmetry, with dimers of dimers, each one potentially interacting with a heterotrimeric G protein, displaying two-fold rotation symmetry, although G protein binding might be asymmetrical^{161,185,217}.

1.2.4. Methods to study GPCR oligomerisation

As previously stated, early evidence suggesting GPCR dimerisation emerged from radioligand binding assays. In addition, the application of biochemical methods, mostly SDS-PAGE, cysteine cross-linking and co-immunoprecipitation (Co-IP), provided the first direct evidences of oligomerisation in membrane preparations from native tissues^{146,147,151,153,250}. However, some of these methods rely on membrane solubilisation using surfactants under denaturing conditions, being prone to artefactual results²⁵¹. Although these biochemical techniques greatly contributed to establishing the concept of dimerisation, the development of new biophysical (RET, protein complementation, etc.) and physiological methods (single-molecule imaging, proximity ligation assays, etc.) have provided useful tools to understand GPCR oligomers in cellular contexts, native tissue and to study their kinetics. The scope of this section is not to extensively cover all methods to study GPCR oligomerisation, excellently reviewed elsewhere^{186,251–253}, but to summarise the main ones within the framework of this thesis.

1.2.4.1. Resonance energy transfer-based techniques

First described by Theodor Förster in 1948, fluorescence/Förster resonance energy transfer (FRET) is a non-radiative energy transfer from a fluorophore in an excited electronic state (donor) to an acceptor chromophore having a similar resonance frequency through a long-range dipole-dipole interaction^{254,255}. Energy transfer efficiency (E_{RET}) is inversely proportional to the sixth potency of the distance between the donor and the acceptor (R). The Förster distance (R_0), distance at which energy transfer efficiency is 50%, is ~5 nm for most fluorophores (with an effective energy transfer range <10 nm), making RET extremely useful to study protein-protein interactions (PPIs) within the range of biological interactions²⁵⁶. Thus, small changes in the distance between fluorochromes, for example doubling the distance between CFP and GFP from 3 to 6 nm (being $R_0=5$ nm for this pair) results in around 75% efficiency reduction (**Figure 1.8A**). In order for RET to occur, the emission spectrum of the donor molecule must overlap the excitation spectrum of the acceptor chromophore. However, energy transfer efficiency depends on different factors, mainly: (1) the extent of donor/acceptor spectral overlap (so-called spectral overlap integral), (2) the relative orientation of the transition dipole moments that must be parallel to each other, (3) the quantum yield of the donor and (4) the donor fluorescence half-life being long enough to allow RET to occur^{251–253}.

The most commonly used donor/acceptor combinations in GPCR FRET studies are the cyan (CFP) and yellow (YFP) fluorescent proteins, respectively (**Figure 1.8B**). This combination was first used by Overton and Blumer to detect dimers of the yeast α -factor receptor in live cells²⁵⁷. Briefly, in FRET experiments, the donor and acceptor proteins are generally fused to the receptor C-terminus after a flexible linker of variable length to avoid orientation constraints. Other donor/acceptor fluorescent protein combinations, including CFP/GFP, GFP/DsRed, GFP/YFP or YFP/RFP, have been successfully applied to detect GPCR dimers^{252,258}.

In BRET, a bioluminescent enzyme such as the *Renilla reniformis* luciferase (Rluc) is used as energy donor (**Figure 1.8C**). The lack of an external excitation light source provides several advantages over FRET because the excitation beam can directly damage the cells, cause autofluorescence and/or photobleaching. In BRET, the luciferase variant catalyses the oxidation of an exogenously added substrate, yielding appropriate energy for the excitation of the acceptor pair^{259,260}. Over the last few years, different BRET configurations have been developed, with BRET¹ (coelenterazine h/Rluc/EYFP) and BRET² (coelenterazine-400a/Rluc/GFP² or GFP10) being the most extensively used when studying receptor oligomers. Yet, their considerable spectral overlap and the low stability/quantum yield of the substrates have urged to develop alternative configurations (BRET³, QD-BRET or NanoBRETTM) through introducing enhanced luciferase variants (Rluc2, Rluc8 and Gaussia, Firefly or Oplophorus luciferases), improved substrates (EndurenTM, furimazine, etc.) and new acceptor proteins (Venus YFP, mOrange, DsRed, etc.)^{261,262}.

One of the main disadvantages of the above described FRET/BRET techniques is their reliance on recombinant proteins expressed in heterologous expression systems. Accordingly, the proper receptor function and membrane shorting must be validated, as “molecular crowding” can lead to false positive RET signals²⁵². In addition, classical dimerisation RET experiments provide information on cell populations, although FRET/BRET microscopy have greatly contributed to overcome this limitation. These restrictions, among others, make imperative the use of a rigorous experimental framework to detect “true” GPCR dimers^{263,264}.

Recently, in order to improve the signal-to-noise ratio, rare-earth lanthanides with long emission half-lives have been incorporated as donor fluorophores, consisting in a macrocycle within which Eu^{3+} or Tb^{2+} cations are embedded (Eu^{3+} and Tb^{2+} cryptates, respectively)²⁶⁵. These fluorophores have several well-defined emission peaks (e.g. Tb^{2+} peak emission at 490, 548, 587 and 621 nm), allowing the pairing with fluorescein-like and allophycocyanin-like acceptors²⁶⁶. In addition, they are not susceptible to photobleaching and their emission is long-lived, allowing a delay between the light pulse and fluorescence acquisition (time resolved; TR) that eliminates the short-lived autofluorescent events. Hence, three main TR-FRET

General Introduction

variants have been used to detect GPCR dimers: (1) antibodies labelled with donor and acceptor compatible pairs²⁶⁷⁻²⁶⁹; (2) covalent labelling of chimeric receptors harbouring self-labelling proteins, enzymes that catalyse the transfer of a fluorescent substrate onto itself (such as the SNAP, CLIP and HaloTag®)^{270,271}; and (3) TR-FRET-compatible labelled ligands (**Figures 1.8D-F**). This last strategy is particularly interesting as allows the it detection of oligomers in native tissues without the need to generate recombinant receptors¹⁷⁸. Overall, TR-FRET time-resolved nature together with the complex emission spectra of the donor molecules and the near-infrared properties of the acceptor dyes provide an excellent homogeneous approach to study GPCR oligomerisation with particularly low signal-to-noise ratios.

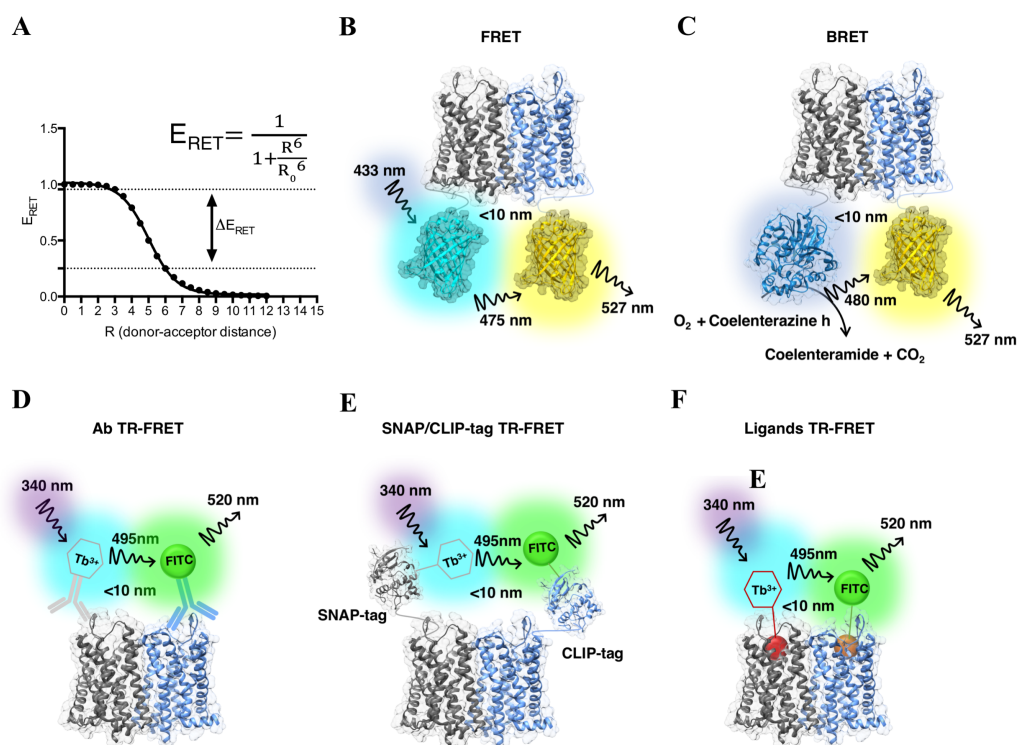


Figure 1.8. Current resonance energy transfer strategies for the study of GPCR oligomerisation. (A) Theoretical simulation of the Förster resonance energy efficiency (E_{RET}) over different distances (R) of a donor-acceptor pair with a Förster distance (R_0) of 5 nm. Dashed lines represent the changes in efficiency (ΔE_{RET}) after doubling the donor-acceptor distance from 3 to 6 nm. (B) FRET principle illustrated using the prototypical CFP and YFP pairs. When oligomerisation drives the positioning of the donor and acceptor molecules within close proximity (<10 nm), the light emitted by CFP (~475 nm) after its excitation with an external source (~433 nm) is within the excitation range of YFP, triggering its fluorescence emission (~527nm). In BRET (C), a luciferase catalyses the oxidation of an exogenous substrate, which results in light within the excitation spectrum of an acceptor fluorophore. The main strategies to detect GPCR oligomers by TR-FRET involve using donor (cryptates) and acceptor RET compatible pairs conjugated to antibodies (D), covalently linked to the receptors by means of self-labelling proteins (E) or conjugated to specific ligands (F).

1.2.4.2. Protein complementation assays (PCAs)

PCAs rely on the functional reconstitution of a protein/enzyme upon the association of their non-fluorescent/enzymatically active split fragments genetically fused to the interacting proteins of interest (**Figure 1.9**). Thus, bimolecular fluorescence and luminescence complementation (BiFC and BiLC, respectively) have been extensively used to study the dimerisation across members of all GPCR families as well as their interaction with effector proteins. It is noteworthy that most BiFC hemiproteins, in contrast to BiLC, remain irreversibly associated, hindering the real-time measurement of the association/dissociation kinetics of the interacting proteins²⁷². Consequently, more than 10 different BiFC pairs, with spectral properties ranging from cyan to far-red emission wavelengths (extensively reviewed elsewhere^{273,274}) have been introduced, mostly aiming to provide reversible complexes, increase their quantum yield, reduce the rate-limiting autocatalytic oxidation of the chromophore (so-called chromophore maturation), the pH/temperature-sensitivity of the reconstituted fluorescent protein and the intrinsic affinity between the interacting partners^{253,275,276}.

Perhaps BiFC's main advantage over BiLC and RET is its inherent simplicity, which allows for the direct visualisation of PPIs by simple fluorescence measurements²⁷⁷. BiFC and BiLC provide low or minimal background signals, as the complementary hemi-halves do not have fluorescent properties nor enzymatic activity by themselves. If something has tipped the balance in favour of BiFC as the first-line PCA is the low quantum yield of most split luciferase variants²⁵³. However, Dixon and collaborators recently managed to split the small and bright NLuc® luciferase into two fragments (MW of 18 kDa and 1.3 kDa; LgBiT and SmBiT, respectively) which display minimal affinity between them and reconstitute NLuc extraordinary brightness upon their association²⁷⁸. Thus, the NLuc® binary interaction technology (NanoBiT®) takes advantage of BiLC benefits (reversibility, low intrinsic affinity between components, kinetic resolution and no maturation steps) whilst overcoming some of its limitations (higher quantum yields and easier detection). In fact, we provided clear evidence of NanoBiT® potential by applying it to the study of GPCR interactions with effector proteins (β -arrestins and heterotrimeric G proteins) and with each other (homo/heterodimerisation) (see Chapters 3, 4 and 6).

By combining PCAs and RET, it is possible to gain insights into the minimal structural components of macromolecular complexes assembled into higher oligomeric architectures²⁷⁹. Therefore, similarly to sequential RET (SRET), in which the emission energy of a typical BRET acceptor excites an additional interacting fluorescent protein²⁸⁰, BiFC can be combined with other BiFC or BiLC allowing the detection of interactions between more than two proteins. For example, Rebois et al. combined constructs in which the N- and C-terminal

General Introduction

fragments from Venus YFP or *Gaussia* luciferase (GLuc) were attached to the carboxy terminal tail of the β_2 AR and performed BRET, revealing homo-tetrameric β_2 AR arrangements²⁸¹. Using an analogous strategy (split Rluc8 and Venus YFP), Guo et al. showed higher order homo-oligomers of the D₂R at the time that validated them via cysteine cross-linking¹⁹⁹. To the best of our knowledge, NanoBiT® is the smallest and brightest reported luciferase, making it an excellent candidate for sequential BiLC-BRET assays while also being spectrally compatible with NanoBRET™. Taking advantage of these two features, we developed a sequential NanoBiT®-NanoBRET™ assay, hereafter referred to as NanoBiLC BRET, providing strong evidence of 5-HT_{2A} and CB₁ receptors forming higher order hetero-oligomers in live cells (see Chapter 3).

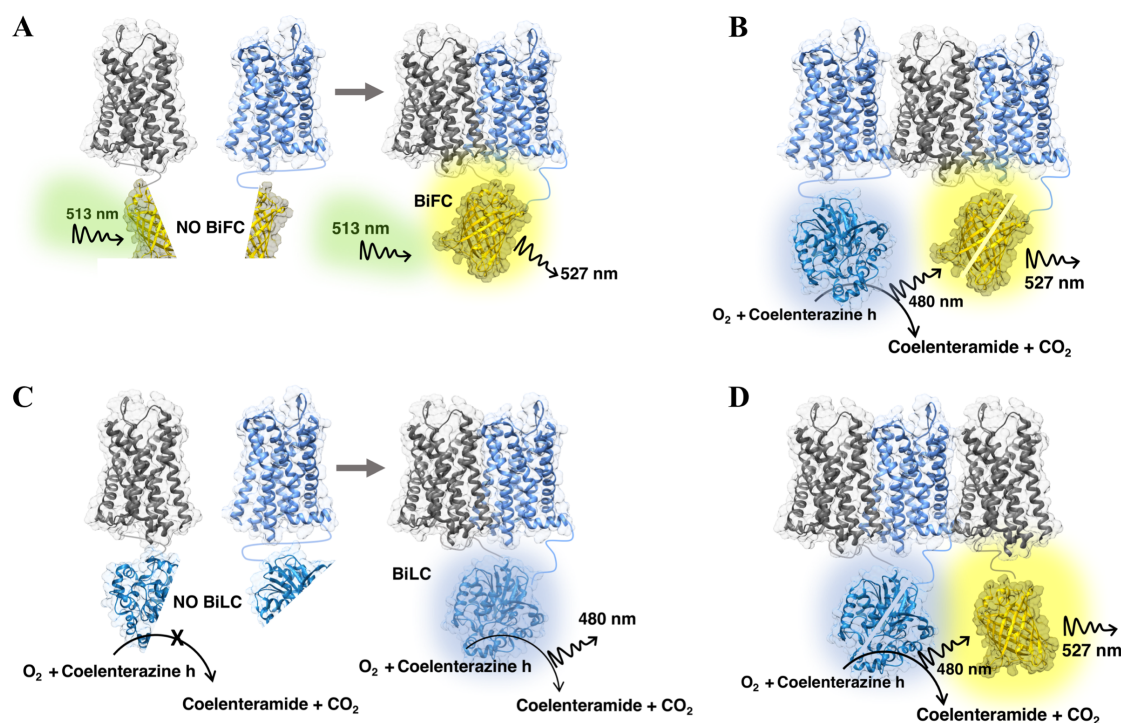


Figure 1.9. Protein complementation assays to study GPCR oligomers. In BiFC (A), two receptors fused to the N-terminal and C-terminal fragments halves of a fluorescent protein, Venus YFP in the example, drive the interaction between the complementary hemiproteins to reconstitute a functional fluorescent complex. (B) Its spectral properties are compatible with a RET acceptor, allowing the detection of higher oligomeric complexes when multiplexed with the appropriate BRET donor (e.g. Rluc). In BiLC (C), the complementary halves of a luminescent protein, Rluc in the example, are fused to the putative interacting receptors. Dimerisation drives both proteins in close proximity so that their functional reconstitution can be assessed after the addition of its substrate. Analogously, its spectral properties allow sequential BiLC BRET (D), in this case being the reconstituted luciferase the donor molecule.

1.2.4.3. Fluorescence microscopy-based methods

Most of the approaches described above fail to describe oligomerisation dynamics, kinetics or receptors distribution across multimeric complexes. Alternatively, methods such as fluorescent recovery after photobleaching (FRAP) or fluorescence correlation spectroscopy (FCS) are useful tools to analyse the diffusional properties/stability of GPCR complexes, but cannot provide information regarding membrane compartmentalisation, subcellular location and receptor stoichiometry¹⁸⁶. With regard to the latter, FRET spectrometry can accurately determine the number and the relative position of receptors within oligomeric complexes. This method allows the generation of apparent FRET efficiency (E_{app}) distribution diagrams (FRET spectrum), rather than averaging the different configurations of a region of interest, that will be compared and matched with a theoretical E_{app} distribution model, providing information of the number and relative position of the receptors²⁸². Alternatively, spatial intensity distribution analysis (SpiDA) was recently introduced by Godin et al. This method is compatible with live cells and fixed tissues and allows the quantification of protein complexes based on the generation of fluorescence intensity histograms obtained from laser scanning microscopy and their posterior fitting to a super-Poissonian distributions²⁸³.

Alternatively, single fluorescent-molecule imaging can answer at once whether GPCRs form dimers or higher oligomers and for how long they do so²⁸⁴. Original studies on the M₁R using total internal reflection fluorescent microscopy (TIRF-M) showed that this receptor alternates between monomeric and dimeric assemblies on timescales of seconds²⁸⁵. Later on, via TIRF-M imaging of covalently labelled receptors, Calebiro et al. confirmed this dynamic equilibrium and, as previously discussed, showed that oligomerisation might be receptor dependent²⁰². The development of super-resolved fluorescence microscopy (2014 chemistry Nobel Prize), has allowed to study protein dynamics at a single-molecule level with extremely high resolution (<10 nm). In the case of GPCR oligomerisation, localisation microscopy techniques such as photo-activated localisation microscopy (PALM) and stochastic optical reconstruction microscopy (STORM) are just starting to be applied, but with promising results²⁸⁶. These methods allow to overcome the diffraction barrier using photoswitchable fluorophores that undergo unmasking/fluorescent emission/photobleaching cycles stochastically and therefore spatial differences in dense populations of molecules can be resolved with super-resolution. To date, few GPCRs have been studied using STORM or PALM. The first attempt was performed by Scarselli and collaborators, in which the authors did not find β_2 AR nor M₃R in clusters of at least five molecules using PALM, although these results did not rule out the presence of smaller oligomers as observed by Calebiro et al.^{202,287}. More recently, Jonas et al. applied dual-colour PALM to study LHR homo-oligomerisation, demonstrating that ~80 of these receptors form oligomers of less than six receptors. An

General Introduction

interesting experimental variation used by the authors consisted in using CAGE photoactivatable dyes, termed PD-PALM²²⁵.

Finally, the proximity ligation assay (PLA) is perhaps the methodology that has provided the most convincing answer to whether GPCR oligomerisation occurs *in vivo*²⁸⁸. PLA is based on the proximal recognition of antibodies that bind to two adjacent target antigens, for example both protomers in a GPCR heterodimer (**Figure 1.10**). In classical PLA (indirect PLA), two primary antibodies, raised in different species, are readily detected by secondary anti-species antibodies covalently linked to complementary ssDNA chains. If both PLA probes are in close proximity (< 40 nm), their intrinsic affinity will join them together and, aided by an extra “connector” oligonucleotide, become capable of undergoing circular DNA amplification. After a local rolling-circle amplification (RCA), the circular ssDNA is detected using fluorescent-labelled complementary oligonucleotide probes, resulting in easily detectable spots using conventional fluorescence microscopy methods. Alternatively, PLA can be performed using primary antibodies directly linked to the short oligonucleotide strands^{289,290}. In addition, by exploiting both antibody and DNA sensitivity, it can even be applied in situations in which receptor expression is low²⁹¹. However, as it is an antibody-based technique, several controls must be performed in parallel to demonstrate the selectivity of the detected interaction^{289,290}. Since Trifilieff et al. applied PLA to confirm adenosine A_{2A}-dopamine D₂ receptor heteromers in mice striatum, increasing “pro-dimer labs” are embracing this approach while multiplexing it with different techniques providing compelling evidence of the functional role of GPCR oligomerisation *in vivo*^{184,288,292,293}.

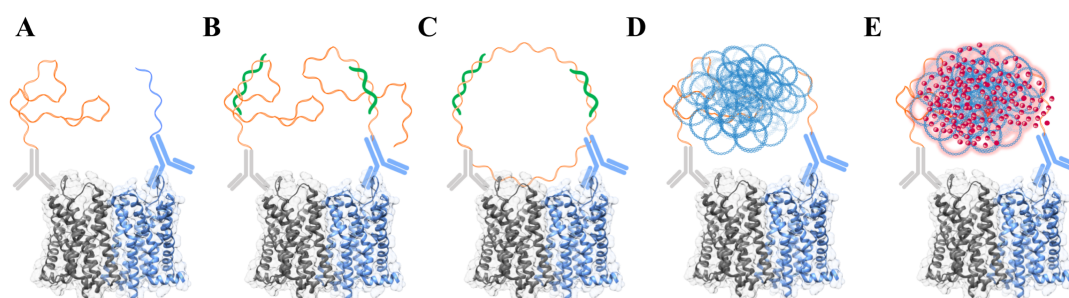


Figure 1.10. Proximity ligation assay principle. (A) Two putative receptors (in grey and blue) are incubated with primary antibodies linked to the PLA PLUS and MIN probes. (B) The connector oligonucleotide (in green) only hybridises if both targets are within 40 nm from each other. After a ligation step (C), the circular DNA can undergo a rolling circle amplification (D) easily detected using fluorescent-labelled complementary oligonucleotide probes (E).

1.3. GPCR heteromers form novel signalling entities. Functional consequences.

1.3.1. Heteromerisation provides new allosteric opportunities

Allosterism is a process through which the binding of a ligand or a protein at one location (the allosteric site), influences the binding or function of the same or a different entity at a topographically distinct site (the orthosteric site)²⁹⁴. Recently, Kenakin and Miller proposed an illustrative analogy involving three main players: the “modulator”, a ligand or protein that binds to a “conduit” (usually a protein) that transduces the thermodynamic allosteric energy to a “guest”²⁹⁵. Therefore, allosterism is a mode of long-distance communicating between topological distinct sites within proteins or macromolecular complexes (**Figure 1.11A**). Allosterism is not exclusive of ligands modulating each other’s properties (affinity and/or efficacy), but drugs stabilising specific receptor conformations can link them to certain intracellular effectors, such as G proteins, GRKs and arrestins, in what is known as “cytosolic allosterism”^{226,295}. Consequently, a situation where the “modulator” orders the “conduit” to send a message to a specific “guest” provides a clear example of allosterism going hand in hand with bias²⁹⁶. This is the case, among others, of the prostaglandin F₂ α (PGF₂ α) receptor AM PDC113.824 or of the CXCR4 allosteric pepducin ATI-2341^{297–299}.

In the case of homo/heteromers, allosterism within oligomers has a dual nature. On the one hand, a ligand (the modulator) alters the conformation of one protomer which then binds and modulates the configuration of the interacting receptor. In this context, the receptor oligomer is the “conduit”, which underlies the often-detected ligand binding cooperativity upon receptor heteromerisation (**Figure 1.11B**). Examples include the reciprocal positive ligand binding cooperativity in δ -OR- μ -OR heteromers^{180,300} or the negative agonist binding cooperativity in A_{2A}-D₂ receptor heteromers^{301–303}. Alternatively, a protomer can be the allosteric modulator (AM) by itself, which, irrespective of binding any ligand, can alter the conformation of the associated receptor, modulating its downstream efficacy and/or ligand affinity (**Figure 1.1.C**). Continuing with the last example, this is the case in A_{2A}-D₂ receptor heteromer, in which the A_{2A}R selective antagonist SCH-442416 binds with much less affinity to its target upon heteromerisation with the D₂R³⁰⁴. The simplest model of heteromerisation involves two receptors. However, higher oligomeric architectures add an extra layer of complexity, as it increases the potential number of “conduits” and/or “modulators”^{185,217}.

Receptors exist in a dynamic equilibrium between closely related conformational (**Figure 1.5**). Importantly, allosteric modulators do not create new conformational ensembles, but by

General Introduction

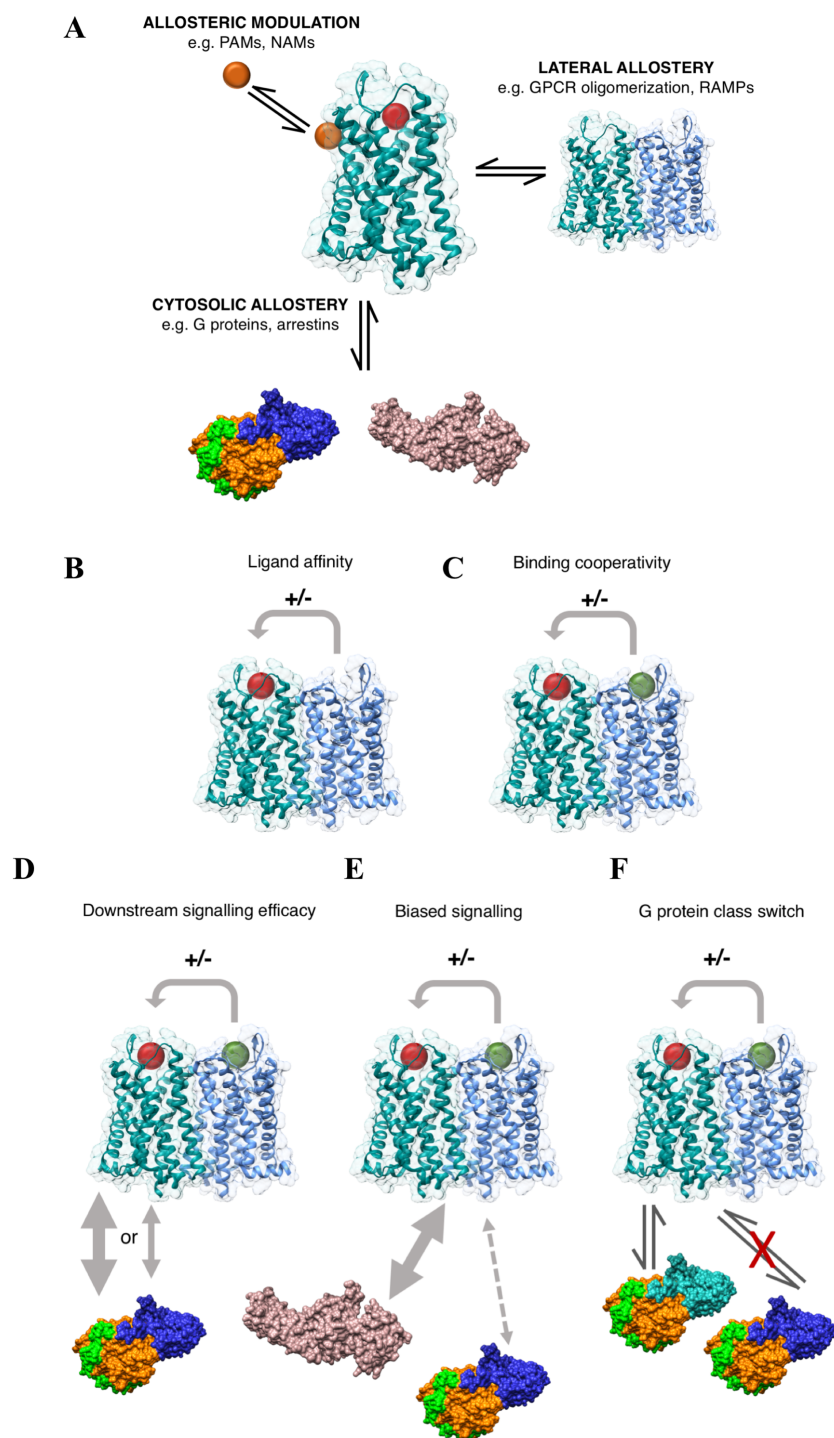


Figure 1.11. Allosteric modulation in GPCR heteromers. (A) Direct interactions between GPCRs and other molecules change the conformational equilibrium of the receptors. This is translated in different reactivity towards effector systems. In addition to the classic allosteric modulation exerted by ligands interacting outside the orthosteric binding pocket, protein-protein interactions at the level of the plasma membrane (lateral allostery) or with cytosolic proteins (cytosolic allostery) alter GPCRs properties. In the case of heteromers, this is often translated into altered ligand affinity after ligand binding to one (B) or both protomers (C). Signalling efficacy is yet another aspect heavily influenced by allostery within heteromers, increasing/decreasing the intensity of a given response (D), driving one cellular effect at the expense of others (E) or promoting the recruitment of non-canonical G proteins (F).

altering the energetic barriers between them, shift their relative distribution. Just as the changes upon receptor binding of a small-molecule AM are a function of its energy minima on a two-dimensional Cartesian coordinate system, the same applies for heteromers. Thus, one function of receptor heteromerisation may be to favour certain receptor conformations, providing an explanation of how cross-talk at the level of intracellular signalling is achieved^{19,305–307}.

Often, cross-talk is a consequence of convergence on effector systems. However, in the case of heteromers, a clear distinction must be drawn, as cross-talk is an unique biochemical signature¹⁸⁷. Cross-talk is not a consequence of changes in the temporal/spatial resolution of a given signalling event, but often is appreciated as a potentiation/inhibition of the efficacy of liganded receptor, usually in the presence of an agonist/antagonist-bound interacting protomer, to trigger a cellular response (**Figure 1.11D**)²⁴⁹. Alternatively, heteromeric interactions might disclose “new” conformations exposing novel surfaces for the binding of atypical effectors. This is often observed at the level of heterotrimeric G protein recruitment, where a protomer recruits a non-canonical G protein in what is known as heteromer-mediated G protein class switch (**Figure 1.11E**). At first glance, this class switch might seem to be incompatible with the definition of allosterism, as allosteric modulators do not create new conformational states but tip the balance towards some of them²⁹⁴. However, through oligomerisation, GPCRs might fall into energy minima virtually unachievable by the individual protomers and therefore diversify their affinity towards alternative effectors. It is important to distinguish between G protein class switch and the often-reported ability of certain receptors to activate more than one G protein pool. While in the first case there is a heteromer-specific signature, receptors’ promiscuity is mainly associated to GPCR overexpression and/or cell context-dependant G protein availability^{308,309}.

1.3.2. Heteromer-driven biased signalling

As just mentioned, heteromerisation often leads to a change in G protein recruitment to the partner receptor (discussed in more detail over the next section). Alternatively, allosterism within protomers is translated into the dominance of the signalling pathway downstream one of the protomers, although the biased nature of the ligands might also play a role in the overall bias of the system (**Figure 1.12**). Thus, the interaction between biased ligands and heteromerisation has been clearly illustrated for 5-HT_{2A}R-D₂R heteromers³¹⁰. Both receptors are targeted by atypical anti-psychotics³¹¹, being their interaction particularly interesting from the point of view of developing new anti-psychotic drugs. On the one hand, the non-biased 5-

General Introduction

HT_{2A}R agonists 5-HT and TCB2 reduced the potency of quinpirole to agonise G_{i/o} signalling downstream of the D₂R (**Figure 1.12A**). In addition to this antagonistic receptor-receptor interaction, quinpirole potentiates 5-HT- and TCB2- mediated PLC and calcium signalling, increasing the efficacy of 5-HT_{2A}R to activate its canonical downstream G_{q/11} signalling³¹². Interestingly, Albizu and collaborators showed that this cross-talk was dependent on the nature of the ligands. Thus, in the presence of agonists known to exert functional selectivity through central 5-HT_{2A}R actions¹²⁶, there is a reduction in IP₃ accumulation when cells expressing 5-HT_{2A}R-D₂R heteromers are co-stimulated with quinpirole³¹³. Alternatively, while assessing these allosteric effects on the other protomer, it was shown that hallucinogenic 5-HT_{2A}R ligands (LSD and DOI) potentiate D₂R-driven G_{i/o} signalling, leading to a facilitatory allosteric interaction^{314,315}. Therefore, endogenous 5-HT and psychedelic ligands stabilise different 5-HT_{2A}R conformations modulating the inter-protomer allosteric communication (**Figure 1.12A**).

Another example of heteromerisation driving bias into higher molecular assemblies applies to 5-HT_{2A}-mGlu₂ receptor heteromers (**Figure 1.12B**). Original studies on this dimer showed that the mGlu₂R protomer had an antagonistic allosteric effect for 5-HT_{2A}R-mediated G_{α_{q/11}} activation, while enhancing its G_{i/o} activity. Furthermore, this G_{i/o} component was associated to hallucinogen-specific signalling pathways and suppressed by the pharmacological activation of the interacting mGlu₂R³¹⁶. Fribourg and collaborators demonstrated that 5-HT_{2A}-mGlu₂ receptor heteromers serve as an integrative switch, modulating the psychoactive behaviour of psychedelic drugs through balancing of the efficacy between G_{i/o} or G_{q/11} signalling³¹⁷. In this sense, while agonism by endogenous ligands favours G_{i/o} signalling, psychedelic 5-HT_{2A}R agonists potentiate G_{q/11} pathways at the expense of G_{i/o}³¹⁷. Recently, Moreno et al. provided new insights into the mechanism driving this cross-talk, showing that mGlu₂R coupling to G_{i/o} was necessary to modulate G_{q/11} signalling downstream 5-HT_{2A}R, providing evidence of an architecture composed of tetramers of mGlu₂R and 5-HT_{2A}R homodimers in complex with G_{i/o} and G_{q/11} proteins, respectively¹⁸⁵.

Heteromerisation might in addition favour arrestin-mediated over G protein-mediated signalling. Rozenfeld et al. showed that, in contrast to when δ-OR and μ-OR are individually expressed, δOR-μOR heteromers constitutively recruit β-arrestins and co-stimulation of both receptors induces a different ERK phosphorylation pattern when compared to that of cells solely expressing each protomer³¹⁸.

In the case of higher order oligomers, mainly tetramers, their architecture is compatible with the presence of two G proteins, although few studies have attempted to experimentally validate dual G protein binding¹⁶¹. One such example are the recently described dimers of dimers of the adenosine A₁ and A_{2A} receptors; A₁-A_{2A} receptor heterotetramers²¹⁷. Oligomerisation

results in a significant reduction in the Brownian motion of each individual receptor. Furthermore, brightness distribution analysis of their stoichiometry revealed that ~75% of the heteromeric species were heterotetramers containing two A_1 and two A_{2A} receptors. Further RET analysis confirmed simultaneous G_i and G_s binding in adenosine A_1 - A_{2A} heterotetramers²¹⁷. However, although both G proteins can be recruited, it seems that the G_s protein, activated by the adenosine A_{2A} receptor, dominates over G_i ^{217,304,319}.

Overall, these examples illustrate how GPCR heteromerisation provides new allosteric opportunities that modulate the conformational landscape of the associated protomers, often leading to biased responses. Furthermore, heteromers might act as integrative units, reacting differently depending on the nature of the ligands. Thus, ligands, heteromers and effectors work together providing novel heteromer-specific responses.

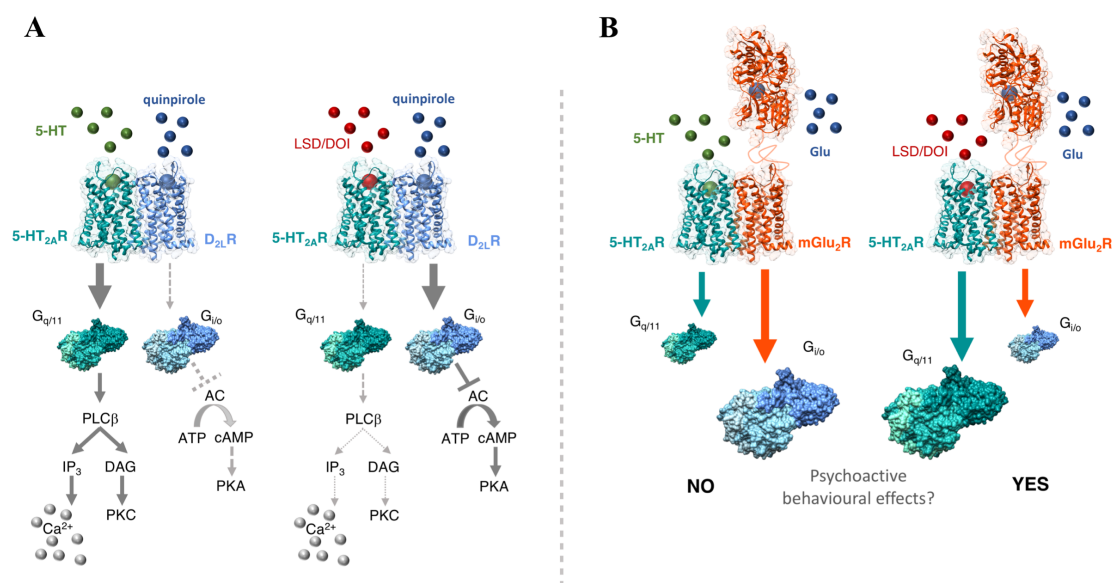


Figure 1.12. GPCR heteromers and ligands operate together to define biased signalling. In 5-HT_{2A}-D_{2R} heteromers (**A**), simultaneous agonist stimulation with non-biased ligands has an inhibitory effect on D_{2R}-mediated $G_{i/o}$ signalling whilst potentiating 5-HT-driven $G_{q/11}$ activation downstream the 5-HT_{2A}R. In contrast, the hallucinogenic 5-HT_{2A}R agonists LSD and DOI differentially modulate the heteromer conformation biasing the system towards D_{2R}-dependent $G_{i/o}$ signalling after quinpirole co-administration. In 5-HT_{2A}-mGlu₂R heteromers (**B**), co-administration of the endogenous 5-HT and glutamate agonists has an inhibitory effect in 5-HT_{2A}R-mediated $G_{q/11}$ signalling whilst maintaining mGlu₂R-driven $G_{i/o}$ signalling. On the other hand, LSD/DOI and glutamate co-administration is integrated by the heteromers in such a way that favours 5-HT_{2A}R effectors. The potentiation of $G_{q/11}$ over $G_{i/o}$ signalling has been linked to the psychedelic effects of hallucinogenic 5-HT_{2A}R agonists.

1.3.3. Heteromers modulate receptor biogenesis, arrestin signalling and trafficking

Most membrane-targeted nascent polypeptides must first insert into the lumen of the endoplasmic reticulum (ER) where folding and oligomerisation take place before the quality-control checkpoint ensures that only properly folded mature proteins reach their final destination³²⁰. Oligomeric integral membrane proteins such as insulin receptors, growth hormone receptors and Type I and Type II transforming growth factor receptors are well known examples of regulated oligomerisation and processing of pro-receptors by the ER quality control machinery^{321–323}. Analogously, dimerisation at the very beginning of the biosynthetic process in the ER has been well documented for many Class C receptors (e.g. GABA_{B1}R-GABA_{B2}R, T1R2-T1R3 and T1R1-T1R3 heteromers)^{167,168,173,174,324–326}.

For the rhodopsin-like family members, it has been shown that removal of a putative dimerisation motif in β_2 AR results in ER retention¹⁸¹. Similarly, using endoplasmic reticulum tapping strategies, evidence of homomerisation occurring at early biogenic stages have been provided for the D₂, V₂ and CXCR1 receptors^{327–329}. In the case of Class A receptor heteromers, several reports suggest similar complementary interactions. For example, heteromerisation between the α_{1D} and α_{1B} adrenoceptors is a pre-requisite for α_{1D} translocation to the cell surface³³⁰. Likewise, that the association between the mouse 71 olfactory receptor (M71OR), difficult to express at the cytoplasmic membrane due to ER retention, with the β_2 AR allows M71OR to reach the cell surface³³¹.

As for G protein signalling, receptor heteromerisation also modulates arrestin responses, which can profoundly affect receptors signalling and trafficking¹⁸⁸. In the case of heteromers between α_{2a} and α_{2c} adrenergic receptors, the α_{2c} AR reduces GRK2-mediated α_{2a} AR phosphorylation and its arrestin recruitment³³². The functional consequences of heteromerisation in arrestin-regulated pathways has been mostly studied from the perspective of agonist-mediated changes in effectors recruitment and/or signalling efficiency. This has been extensively described when the CXCR4 and CXCR7 receptors physically interact. Both receptors are agonised after binding the stromal cell derived factor-1 (SDF-1, also known as C-X-C motive chemokine 12; CXCL12) but elicit different downstream signalling cascades. On one hand, CXCR4 behaves as a prototypical GPCR, that is agonist binding/G protein activation/G protein- or arrestin-dependent signalling. On the other hand, CXCR7 signalling is mainly restricted to β -arrestin-activated downstream pathways³³³. Co-expression of CXCR7 not only modulates CXCR4 ability to recruit its canonical G_{i/o} proteins, but results in constitutive β -arrestin recruitment to CXCR4-CXCR7 heteromers³³⁴.

Recently, Bellot and colleagues provided an exhaustive study illustrating $\alpha_2\text{cAR-AT1R}$ heteromer-specific poses stabilised by dual agonist occupancy³³⁵. Interestingly, single or dual agonist stimulation did not alter the effector recruitment levels, but stabilised three different receptor- β -arrestin2 poses which led to different trafficking pathways. Furthermore, although the $\alpha_2\text{cAR}$ and AT1R are coupled to $G_{i/o}$ and $G_{q/11}$, respectively, dual agonists stabilise a new conformation capable of triggering $G_s/c\text{AMP/PKA}$ signalling pathways³³⁵. Altogether, $\alpha_2\text{cAR-AT1R}$ heteromers provide a clear example of how heteromers form new pharmacological entities that can adopt conformations which differently impact arrestins and/or G protein signalling.

Perhaps closely related to arrestin modulation, heteromers can alter receptors trafficking from the plasma membrane. In some cases, a given protomer can act as a receptor trap for the other, decreasing the extent of agonist-induced internalisation of its interacting protomer. This phenomenon was recently observed for the incretin glucagon-like peptide-1 (GLP-1R), whose agonist-mediated internalisation is blocked when heteromerising with the non-internalising glucose-dependent insulinotropic polypeptide receptor (GIPR)³³⁶. Alternatively, agonist binding to just one of the protomers is enough to promote the internalisation of the full heteroreceptor complex, as for morphine-induced μ -OR-gastrin-releasing peptide (GRP) receptor heteromers internalisation³³⁷.

Finally, one aspect that is expanding GPCR functionality is their ability to signal from internal organelles, with signalling outputs being different from those originated at the cytoplasmic membrane. Thus, based on some observation of heteromer-dependent alterations in post-endocytic sorting, it is tempting to speculate that heteromerisation might also be involved. One such example is the vasopressin V_{1a-V_2} receptor heteromers, where non-selective agonists trigger their internalisation together with β -arrestins, retaining the $V_2\text{R}$ into endosomes and blocking its recycling back to the membrane³³⁸.

1.3.4. Switching of coupling selectivity as a mechanism for signal integration by receptor hetero-oligomers.

GPCR hetero-dimerisation is consistent with a model in which dimers provide scaffolds suitable for the binding of single heterotrimeric G-proteins³³⁹. This implies that the docking interfaces between the receptor and the G-protein could differ in the presence of homo and heterodimers, conferring unique signalling footprints³⁴⁰. For example, the μ and δ -opioid receptors, selectively coupled to the pertussis toxin (PTX) sensitive $G\alpha_{i/o}$ subunits, are insensitive to PTX treatment when co-expressed. This is due to a switch in G protein coupling,

General Introduction

from $G\alpha_{i/o}$ to the PTX insensitive $G\alpha_z$ subunit³⁴¹. Similarly, in cells co-expressing CB_1 and D_2 receptors, dual agonist stimulation results in an increase in cAMP accumulation, although both receptors are canonically coupled to $G_{i/o}$ proteins^{342,343}.

Among the most conclusive works proving heteromer-dependent G protein class switch is the already mentioned study on α_{2C} -AR-AT1R by Galés' group³³⁵. The α_{2C} -AR and AT1R are $G\alpha_{i/o}$ and $G\alpha_{q/11}$ protein-coupled receptors, respectively. However, using a forcing dimerisation strategy, the authors showed that co-stimulation with norepinephrine and angiotensin II directly induces the coupling of $G\alpha_s$ proteins to the hetero-receptor complex. In addition, the relevance of this heteromer-specific G_s /cAMP/PKA signalling pathway was further validated *in vivo*, providing a new mechanism whereby cross-talk between α_{2C} -AR-AT1R heteromers regulate sympathetic activity³³⁵.

Within the framework of this thesis, evidence suggests oligomerisation-mediated G protein class switch for two GPCR oligomers; D_1 - H_3 and 5-HT_{2A}- CB_1 receptor heteromers. In the case of D_1 R- H_3 R complexes, Ferrada et al. described the existence of behaviourally antagonistic postsynaptic interactions while studying the effects of H_3 R ligands on the locomotor activation induced by D_1 and D_2 receptors in reserpinised mice³⁴⁴. Furthermore, in co-transfected SK-N-MC cells, the authors reported that D_1 R agonists do not have any effect on cAMP production but decrease forskolin-induced cAMP accumulation³⁴⁵. In view of these results and taking into account that the H_3 R is coupled to $G\alpha_{i/o}$, D_1 R ligands might bias the complex towards $G_{i/o}$ signalling via a trans-activation of the H_3 R protomer. Alternatively, D_1 R might directly recruit $G_{i/o}$ proteins to the receptor hetero-complex.

For 5-HT_{2A}- CB_1 receptor heteromers the scenario is quite similar, with evidence suggesting that the $G_{q/11}$ -coupled 5-HT_{2A}R protomer might be selectively linked to $G_{i/o}$ pathways when interacting with CB_1 R¹⁸⁴. Furthermore, this cross-talk appears to occur at the cytoplasmic membrane level as disruption with heteromer selective disrupting peptides and PTX-mediated blockage of $G_{i/o}$ abrogates this effect. However, similarly as for D_1 - H_3 receptor heteromers, whether $G_{i/o}$ proteins are binding the “non-canonical” protomer or agonist stimulation induces the trans-activation of the $G_{i/o}$ -coupled concomitant protomer requires further evaluation. Thus, while assessing the molecular basis driving cross-talk in 5-HT_{2A}- CB_1 receptor heteromers we sought to address this question (see Chapter 4), providing strong evidence of a model compatible with the recruitment of two $G_{i/o}$ proteins to both protomers in the heteromer.

1.4. 5-HT_{2A}-CB₁ receptor heteromers

1.4.1. 5-HT and its receptors

Serotonin, 5-hydroxytryptamine (5-HT), belongs to the monoamine neurotransmitters family, who all share a basic structure composed by one amino group connected through a two carbon aliphatic chain to an aromatic ring³⁴⁶. Serotonin is among the most prolific neurotransmitters due in part to the large number of its receptors, with 18 genes encoding for seven transmembrane receptors and ligand-gated ion channels, further increasing this heterogeneity considering the substantial number of splicing variants. Therefore, 5-HT receptors take part in a large number of biological functions, including, among many others, development, memory, cognition, motor control, vascular function, perception, sleep, sex and gastrointestinal function^{347,348}. All 5-HT receptors, with the exception of the 5-HT₃R subtypes, which are ligand-gated ion channels, belong to the Class A GPCRs family and are subdivided in seven groups based on their primary sequence homology/overall structural similarities (**Table 1.2**)³⁴⁹.

G protein-coupled 5-HT receptors share relatively high sequence homology (~35%) when compared to the prototypical Rhodopsin and other aminergic receptors³⁵⁰. Up until now, high resolution crystal structures have only been obtained for four members of this family, the 5-HT_{1B}, 5-HT_{2B} and 5-HT_{2C} GPCRs and the 5-HT₃R ion channel^{27,29,135,351,352}. However, comparative analysis based on primary sequence identity, the available X-ray structures and homology modelling have revealed the presence of conserved domains as well as the role of the previously mentioned conformational microswitches. For example, the disulphide bond between the ultra-conserved Cys^{3,25} at the end of the TM3 and a cysteine residue in the ECL2 has an important role in serotonin receptors stabilisation and ligand recognition²⁷. In addition, disruption of the salt bridge (the “ionic lock”) between the Arg^{3,50} of the D/ERY motif and E^{6,30}, present in all 5-HT receptors but the 5-HT₆R, appears to be a pre-requisite for some members of this family to surmount their ground conformational state. However, some discrepancies might arise if comparing the ERG-bound 5-HT_{1B} and 5-HT_{2B} receptors crystal structures, as it appears intact in the second complex^{27,135,353}. Interestingly, the recently resolved 5-HT_{2B} receptor in complex with LSD shed some light into this apparent discrepancy, showing that ERG and LSD stabilise the receptors in an arrestin-biased pose, which is characterised by fewer activation-related conformational changes in the TM5, TM6 and the DRY motif, whilst active-like changes in the TM7 and the NPxxY²⁹ motif.

Table 1.2. The serotonin receptors family.

Receptors	Subtypes and isoforms	Major G protein coupling	Main effector pathway	Distribution
5-HT1	5-HT _{1A} , 5-HT _{1B} , 5-HT _{1D} , 5-HT _{1E} , 5-HT _{1F}	G _{i/o}	↓cAMP	Blood vessels and CNS
5-HT2	5-HT _{2A} , 5-HT _{2B} , 5-HT _{2C}	G _{q/11}	(+) PLC, ↑IP ₃ , ↑DAG, ↑Ca ²⁺ , PKC	Blood vessels, CNS, PNS, GI, platelets and smooth muscle
5-HT3	5-HT _{3A} , 5-HT _{3B} , 5-HT _{3C} , 5-HT _{3D} , 5-HT _{3E}	Ion channel	3	GI, CNS and PNS
5-HT4	5-HT _{4(ag)} , 5-HT _{4(hb)} , 5-HT _{4(i)} , 5-HT _{4(n)}	G _s	↑cAMP	GI, CNS and PNS
5-HT5	5-HT _{5A} , 5-HT _{5B}	G _{i/o}	↓cAMP	CNS
5-HT6	-	G _s	↑cAMP	CNS
5-HT7	5-HT _{7A} , 5-HT _{7B} , 5-HT _{7C} , 5-HT _{7D}	G _s	↑cAMP	CNS, blood vessels and GI

Serotonin receptors classification, subtypes main signalling pathways and tissue distribution. (+) Stimulation; (↑) concentration increase; (↓) concentration decrease; (CNS) central nervous system; (GI) gastrointestinal tract; (PNS) peripheral nervous system.

5-HT synthesis comprises two enzymatic steps. In the first and rate-limiting step, the L-tryptophan ring is hydroxylated by the tryptophan hydroxylase (TPH), yielding hydroxyltryptophan (5-HTP). Next, 5-HT is generated by side chain decarboxylation of 5-HTP, catalysed by the aromatic L-amino acid decarboxylase (AADC)^{346,354}. Originally, it was thought that TPH1, expressed in the gut (gut neurons and enterochromaffin cells), was the only enzyme responsible for the catalysis of the first step in 5-HT synthesis. However, in 2003 Walther and collaborators isolated a second isoform exclusively expressed in neurons of the raphe nuclei^{355,356}. In the brain, serotonin is synthesised in the terminal axon of serotonergic neurons and stored into synaptic vesicles by the vesicular monoamine transporters (VMAT2) awaiting to be released after an action potential. Non-stored 5-HT is further degraded into 5-hydroxyindoleacetic acid (5-HIAA) by the monoamine oxidase A (MAOA)^{355,357,358}.

Most 5-HT receptors are post-synaptic, with the exception of some 5-HT₁R members (5-HT_{1A}, 5-HT_{1B} and 5-HT_{1D} receptors) and 5-HT_{2B}R that modulate through a negative feedback loop pre-synaptic 5-HT release. Post-synaptic 5-HT1 (5-HT_{1A-B} and 5-HT_{D-F} receptors) and 5-HT₅ receptors activate G_{i/o}-dependent effectors, whereas 5-HT2 receptors (5-HT_{2A} and 5-HT_{2C} receptors) are coupled to G_{q/11} proteins (**Table 1.2**). Activation of 5-HT₃R turns into the

depolarisation of the post-synaptic membrane, further modulating 5-HT₂ receptors activity. In addition, 5-HT binding to 5-HT₄, 5-HT₆ and 5-HT₇ receptors increases the levels of cAMP at the post-synaptic terminals. Importantly, although the above listed receptors distribution appears to be predominant, it is not absolute, as illustrated, for example, by the role of pre-synaptic 5-HT_{2A}R in thalamocortical plasticity and associative learning^{358–362}.

The mammalian serotonergic system originates from the midbrain dorsal and ventral raphe nuclei, located in the midline of the rhombencephalon and in the reticula formation^{363,364}. These 5-HT cell populations are clustered following the B1-B9 scheme originally proposed by Dahlström and Fuxe according to their rostrocaudal distribution³⁶⁵. In addition, these clusters are further subdivided into rostral and caudal sections, where the rostral subdivision projects towards the forebrain and the caudal to the spinal cord and cerebellum. Thus, the dense serotonergic terminals innervate the hippocampus, amygdala, hypothalamus, thalamus, neocortex and the basal ganglia. Moreover, due to the dense collateralisation of the serotonergic efferents, virtually all rostral structures receive serotonin inputs^{355,363,364,366}.

1.4.2. The endocannabinoid system

Over the past 20 years, the endocannabinoid (eCB) system (ECS) has gained importance as a neuromodulatory system regulating the CNS development, synaptic plasticity, food intake, energy metabolism, neuroprotection and reward circuits, among many other processes^{367–369}. The ECS is composed of endocannabinoids (endogenous ligands), the enzymes and transporters responsible of their synthesis/degradation and the eCBs receptors. The cannabinoid type 1 and 2 G protein-coupled receptors are the primary target of endocannabinoid ligands. However, additional targets have shown to respond upon eCBs binding, including some transient receptor potential (TRP) channels, peroxisome proliferator activated receptors (PPAR's) and the orphan class A GPR18, GPR55 and GPR119 GPCRs^{370–374}.

Since endogenous ligands (“endo-opioids”) were identified as molecules targeting the same receptors as the plant-derived morphinans^{375,376}, it was speculated that cannabinoids might operate in similar ways. Soon after cloning the rat and human CB₁ receptors, this hypothesis was confirmed by the isolation of an arachidonic acid derivate, named “anandamide”, as endogenous CB₁R ligand^{377–379}. Since the discovery of anandamide, several endocannabinoids have been isolated, although the best-studied are by far 2-arachidonoyl glycerol (2-AG) and arachidonoyl ethanolamide (anandamide)^{380,381}. Although both ligands contain arachidonic acid, their synthetic/degradative routes involve different enzymes (**Figure 1.13**). Accordingly, several strategies aiming to increase eCBs levels have focussed on inhibiting their catabolism,

General Introduction

as for the notorious case of the fatty acid amide hydrolase (FAAH) inhibitor BIA 10-2574 phase I clinical trial, which was ended prematurely due to the death of one subject and other participants suffering from severe brain damage³⁸². Despite this setback, targeting the endocannabinoid system provides exciting therapeutic opportunities in a plethora of disparate conditions, running from metabolic disorders such as obesity and diabetes, neuropathic pain, multiple sclerosis, cardiac failure, stroke, hypertension, glaucoma and other neurological motor disorders such as Parkinson's, Alzheimer's and Huntington's diseases, to name just a few^{380,383,384}.

Unlike classical neurotransmitters, eCBs are not stored in synaptic vesicles. This is in part due to their lipophilic nature, leading to the current belief that eCBs are synthesised and released "on demand" in response to stimuli³⁸⁵. The current view of eCBs signalling is consistent with them acting as retrograde messengers, modulating the release of neurotransmitters such as GABA, dopamine, noradrenaline, glutamate and serotonin. Thus, eCBs retrograde signalling modulates synaptic plasticity by three mechanisms: the first is the endocannabinoid-mediated regulation of two forms of short-term synaptic plasticity known as depolarisation-induced suppression of inhibition/excitation (DSI/DSE, respectively). DSI/DSE are triggered by the depolarisation of the post-synaptic terminal, that, in a calcium-dependent way, induces the retrograde mobilisation of eCBs to transiently inhibit the afferent synaptic currents upon binding to its receptors (**Figure 1.13E**)^{368,386-388}. Second, eCBs modulate synaptic plasticity through metabotropic-induced suppression of inhibition/excitation (MSI/MSE). This form of short-term synaptic plasticity starts with the activation of a $G_{q/11}$ -coupled post-synaptic receptor which triggers the activation of PLC β , an intermediate enzyme in the synthetic route 2-AG and anandamide. eCBs then diffuse and bind to pre-synaptic CB₁ receptors and inhibit vesicular release (**Figure 1.13.F**)^{387,389}. Finally, eCBs mediate pre-synaptic forms of long-term depression both at inhibitory and excitatory synapses, which is a long-lasting form of inhibition of synaptic strength that can be homosynaptic or, in the case of involving synapses adjacent to the stimulated, heterosynaptic (**Figure 1.13G**)^{387,388}.

Cannabinoid CB₁ and CB₂ receptors inhibit adenylyl cyclase and PKA activity through coupling to heterotrimeric $G_{i/o}$ proteins. In addition, cannabinoid receptors activate several members of the MAPK pathway, arrestins, A-type and inwardly rectifying K⁺ channels and inhibit N- and P/Q-type Ca²⁺ channels and D- and M-type K⁺ channels³⁸⁹⁻³⁹¹.

CB₁R is perhaps the most abundant and extended GPCR in the CNS. Particularly, it is highly expressed in the basal ganglia, olfactory cortex, cerebellum, hippocampus and moderate levels are found in the cortex, olfactory bulb, septum, amygdala, and a few brainstem nuclei^{368,392,393}. Although predominantly present in the brain, CB₁R is expressed to a lesser extent in the periphery such as in adrenal glands, the reproductive system and immune cells^{394,395}. On the

other hand, CB₂R brain levels are, with some exceptions (e.g. microglia and endothelial vascular cells), residual. However, it is expressed in high levels in almost all immune cell types^{368,396}.

CB₁ and CB₂ receptors share 44% of amino acid sequence identity, with the CB₁R ~100 residues longer. In comparison with most GPCRs, cannabinoid receptors lack conserved cysteines in the ECL1 to establish ECL1-ECL2 bridges. Furthermore, CB₁ and CB₂ receptors do not form disulphide bonds between the ECL2 and Cys^{3.25} in TM3. In fact, an ECL2 intra-loop disulphide bond is formed instead^{34,397-399}. Another structural characteristic that differentiates both cannabinoid receptors from most rhodopsin-like GPCRs is the lack of the highly conserved proline in TM5 (Pro^{5.50}), which, acting as a hinge, allows the helical movements required for the activation of many class A GPCRs^{400,401}. The main differences between cannabinoid receptors are contained within the N-terminus and the ICL3, being significantly longer for the CB₁R. However, the TM helices exhibit a substantial degree of homology, being the highest for the TMs 3 and 7 (~80%) and the lowest for TM4 (~35%)⁴⁰².

Recently, three different high-resolution crystal structures have been published illustrating the differences between the agonist- and antagonist-bound human CB₁R^{34,399,403}. Both the AM6538- and taranabant- bound CB₁R crystal structures, stabilised into its inactive conformation, revealed singular structural determinates involved in CB₁R overall organisation and ligand recognition. Thus, its long N-terminus domain is highly organised when compared to the closely related LPA₁ and SIP₁ receptors and forms a lid over the orthosteric binding pocket that shields both inhibitors from solvents. Furthermore, in comparison to other solved class A receptors structures, both ligands are deeply inserted into the binding pocket^{399,403}. The recent active CB₁R structures in complex with tetra (AM11542) and hexa (AM841) hydrocannabinols revealed interesting changes in its activation dynamics. First, as previously discussed, it appears that the disruption of the “ionic lock” between Arg^{3.50} and Asp^{6.30} is a pre-requisite for the inactive-to-active transition. Interestingly, agonist binding induces a substantial (53%) reduction in the volume of the orthosteric pocket which is accompanied by a significant increase in the G protein interacting cavity³⁴. Finally, in comparison to the inactive CB₁R structure, the V-shaped N-terminal lid is not observed in the agonist-bound CB₁R, although as discussed in the study, the use of a N-terminal truncated receptor cannot preclude this arrangement in a full-length receptor^{34,399,403}.

General Introduction

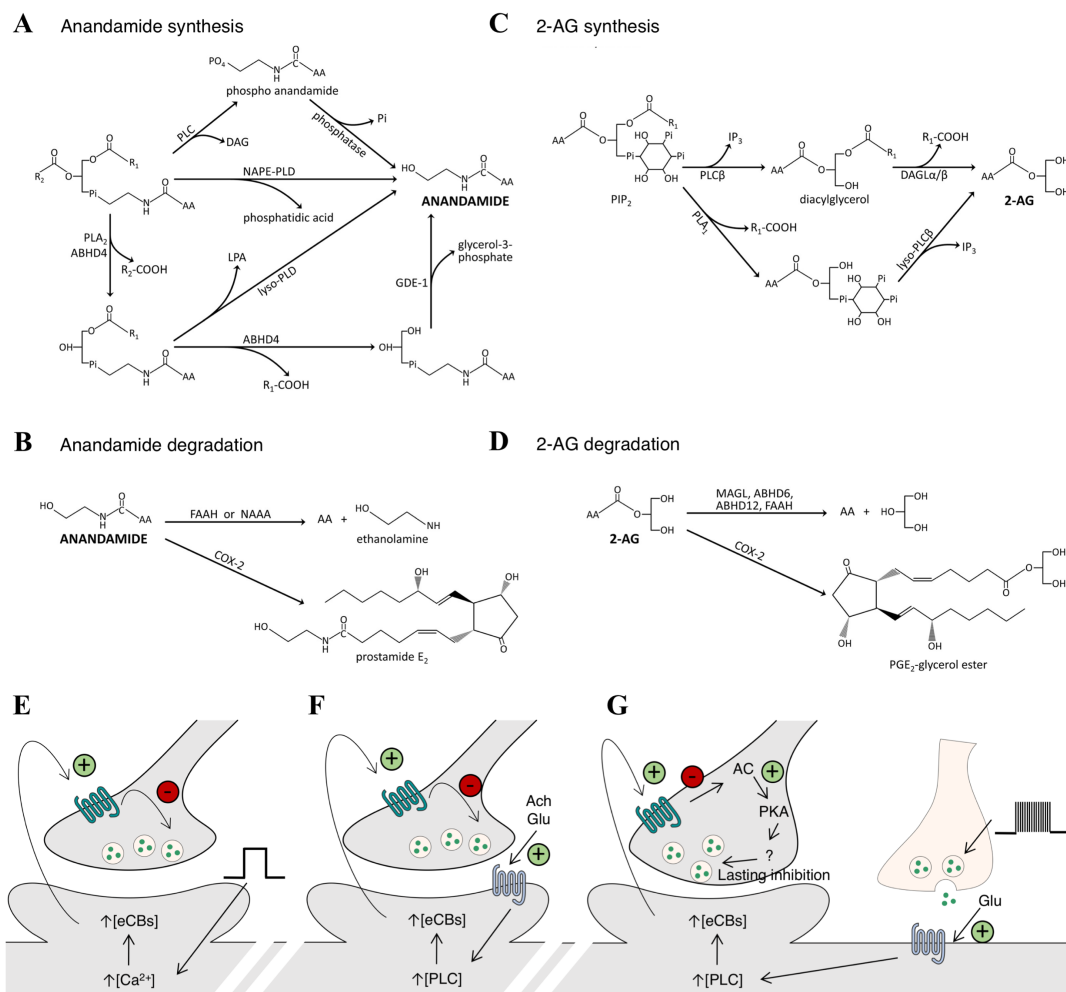


Figure 1.13. The endocannabinoid system and its function in synaptic plasticity. Primary biosynthetic and degradative pathways for anandamide (A-B) and 2-arachidonoyl glycerol (2-AG) (C-D). ECs retrograde signalling modulates two forms short-term synaptic plasticity; depolarisation-induced suppression of excitation/inhibition (E) and metabotropic-induced suppression of excitation/inhibition (F). In addition, pre-synaptic receptors modulate eCBs-mediated long-term depression at homo/heterosynapses (G). (AA) arachidonic acid; (ABH4) alpha/beta domain-containing hydrolase 4; (ABHD6) alpha/beta domain-containing hydrolase 6; (ABHD12) alpha/beta domain-containing hydrolase 12; (COX-2) cyclooxygenase-2; (DAG) diacylglycerol; (DAGL) diacylglycerol lipase; (FAAH) fatty acid aminohydrolase; (GDE-1) glycerophosphodiester phosphodiesterase I; (LPA) lysophosphatidic acid; (lyso-PLC) lyso-phospholipid-preferring phospholipase C; (MAGL) monoacyl glycerol lipase; (NAAA) N-acyl ethanolamine amino hydrolase; (NAPE-PLD) N-arachidonoyl phosphatidyl ethanol-preferring phospholipase D; (PLA2) phospholipase A2; (PLC) phospholipase C. Adapted from Lu and Mackie³⁸⁷.

1.4.3. 5-HT and cannabinoid receptors oligomerisation. Functional interaction between 5-HT_{2A} and CB₁ receptors.

Serotonin receptors are one of the class A GPCRs family subgroups within which their ability to self-assemble or heteromerise has been more explored, extensively reviewed elsewhere^{347,404–407}. Accordingly, to date, of the 14 different 5-HT receptors, only for the 5-HT_{1E/F}, 5-HT_{2B}, 5-HT_{5A/B} and 5-HT₆ receptors there is no available data supporting their homomerisation. However, due to the high degree of homology between 5-HT₁ and 5-HT₂ members, it is likely that they can assemble into similar multi-receptor complexes. The case of 5-HT_{5B} is particularly interesting, as it does not code a functional protein due to the presence of stop codons in its coding sequence but its mRNA has been detected in different brain structures^{350,408}. Therefore, it is tempting to speculate that similarly to the α_{1D} AR or GABA_{B1}R and additional GPCR might be required for its proper folding and membrane trafficking^{167,168,330}.

With regards to homomerisation of CB₁ and CB₂ receptors, several studies have shown their ability to form oligomeric complexes *in vivo* and in heterologous expression systems⁴⁰⁹. Among the most conclusive evidences of CB₁R homomers in native tissue was provided by Wager-Miller and collaborators, who developed a polyclonal rat antibody with preference for CB₁R homodimers⁴¹⁰. Interestingly, brain immunochemical studies showed a similar CB₁R distribution pattern to that seen using conventional antibodies, suggesting that perhaps this might be the constitutive native architecture of CB₁ receptors^{409,410}. In addition, CB₁R *in vivo* homodimerisation has also been explored with bivalent ligands, showing a reduction in food intake or attenuation of cannabinoid-induced antinociception^{411,412}. However, the functional consequences of CB₁R homodimerisation have not been determined. In contrast, evidence suggesting CB₂R homodimers is sparser and mostly relies on observations from electrophoretic analysis of purified receptors^{413,414}.

Heteromers comprising 5-HT receptors are among the most well established. Applying the strict criteria for the recognition of G protein-coupled receptor heteromultimers established by IUPHAR¹⁷⁶, the functional *in vivo* relevance of 5-HT_{1A}R-5-HT₇R, 5-HT_{1A}R-EGFR1, 5-HT_{2A}R-5-HT_{2c}R, 5-HT_{2A}R-CB₁R, as well as the previously discussed 5-HT_{2A}R-D₂R and 5-HT_{2A}R-mGlu₂R heteromers has been extensively studied -an excellently detailed review of the above mentioned examples has been recently published by Grinde and Herrick-Davis³⁴⁷. Similarly, and not surprisingly due to the heterogeneous distribution of CB₁R across the brain and CB₂R in the immune system, heteromerisation involving cannabinoid receptors has been extensively confirmed. Examples include the role in analgesia mediated by μ and δ opioid receptor heteromerising with CB₁R, CB₁R-A_{2A}R heteromers-mediated modulation of the

General Introduction

indirect striatal pathway (fulfilling all IUPHAR criteria), the potential reduction of CXCR4-driven tumour progression through cross-talk in CB₂R-CXCR4 or the proposed targeting of AT₁R-CB₁R complexes for the development of heteromer-specific anti-fibrotic drugs, just to name a few examples^{293,415-417}.

Due to the promising potential of 5-HT_{2A}-CB₁ receptor heteromers as an alternative target to dissociate the side-effects of synthetic cannabinoids¹⁸⁴, one of the objectives of this thesis is to provide an exhaustive study of the molecular basis driving cross-talk between these receptors (see Chapter 4). Both receptors are expressed in brain areas involved in emotions, learning and memory and compelling literature supports the functional interaction between the serotonergic and endocannabinoid systems^{418,419}. In addition, it has been recently shown that some behavioural effects classically associated to 5-HT_{2A}R activity are modulated by cannabinoids^{420,421}. Using PLA, Viñals et al. showed that 5-HT_{2A}R-CB₁R heteromers are found in the striatum, cortex and hippocampus (brain regions participating in memory processing, rewards processing and effective disorders including anxiety)^{184,422-424}. At the signalling level, their interaction has an antagonistic effect, resulting in decreased cAMP levels, β -arrestin 2, ERK1/2 and PKB upon dual agonist stimulation. In addition, bi-directional cross-antagonism was reported and the heteromer has a biased preference to signal towards G_{i/o}-dependent pathways¹⁸⁴. With regard to the later, we addressed whether 5-HT_{2A}R trans-activates G_{i/o} proteins binding to the CB₁R interacting protomer or if this phenomenon is due to a G protein class switch underneath 5-HT_{2A}R (see Chapter 4). Importantly, THC-induced memory deficits, anxiolytic-like effects and withdrawal were abrogated or attenuated in 5-HT_{2A}R KO mice. Surprisingly, THC's Anxiogenic and analgesic properties were intact in these animal models, pointing out a 5-HT_{2A}R-dependent component in THC's side effects. Furthermore, pharmacological inhibition (5-HT_{2A}R antagonism) or disruption of 5-HT_{2A}R-CB₁R heteromers with acute administration of TM disrupting peptides dissociated THC's "bad effects" while maintaining its antinociceptive properties¹⁸⁴. Accordingly, targeting this heterodimer with specific agents that block or disrupt 5-HT_{2A}R-CB₁R heteromers is an attractive strategy to take advantage of the potential of synthetic cannabinoids. This requires the development of heteromer-specific compounds (e.g. TM mimicking peptides) with improved physicochemical properties and robust screening platforms to identify hits (see Chapter 3). Likewise, an exhaustive study of the architecture and the ongoing "conversation" between protomers might provide a better depiction of these druggable units while enabling us to extrapolate it to other GPCR heteromers with similar characteristics (see Chapter 4).

1.5. Dopamine D₁- histamine H₃ receptor heteromers

1.5.1. The dopaminergic system

DA is the main catecholamine in the brain, regulating neuronal signalling networks involved in motor control, cognition, emotions, reward, motivation as well as endocrine modulation^{425,426}. In addition, almost half of the dopamine produced in the body is synthesised in the mesenteric organs⁴²⁷. Consequently, DA exerts its central and peripheral physiological effects through binding to five class A GPCR sparsely distributed across the full body, grouped into two major groups accounting for their ability to engage G_{i/o} or G_{s/olf} signalling pathways (**Table 1.3**). Thus, the D₁-class DA receptors (D₁ and D₅) stimulate the synthesis of cAMP and its downstream associated pathways, whereas the D₂-class (D₂, D₃, and D₄) receptors have the opposite effect⁴²⁸. However, as for most GPCRs, DA signalling is more complex and involves additional receptor forms generated by alternative splicing, Gβγ-dependent signalling or G proteins-independent signalling^{426,429-431}.

In the brain, the first step into DA biosynthesis is the conversion of L-tyrosine into l-3,4-dihydroxyphenylalanine (L-DOPA, levodopa). This is the rate-limiting step and is catalysed by the tyrosine hydroxylase (TH)^{426,432}. The next step comprises L-DOPA decarboxylation to DA by the AADC⁴³³. Alternatively, tyrosinase can catalyse the formation of L-DOPA from L-tyrosine or DA can be directly synthesised from tyramine by the cytochrome P450 2D6 (CYP2D6), although the contribution of this alternative pathway to the total DA brain levels is poorly understood^{434,435}. Free cytosolic DA is highly prone to oxidation, which is avoided by its rapid uptake into synaptic vesicles via the VMAT2⁴³⁶.

After an action potential, DA is released into the synaptic cleft to bind post-synaptic receptors in dopamine targeting cells (e.g. striatal GABAergic MSNs) as well as pre-synaptic autoreceptors in dopaminergic neurons. D₁-like DA receptors are mostly post-synaptic, whereas it is currently accepted that the D₂, D₃ and D₄ receptors are expressed both in post-synaptic dopamine target cells as well as pre-synaptically in dopaminergic neurons⁴²⁶. To avoid over-stimulation, free DA is cleared from the synaptic space by recycling it back via the sequential action of the dopamine active transporter (DAT) pump and the VMAT2. In parallel, DA is uptaken into glial cells via DAT and further degraded by the monoamine oxidase (MAO) and the catechol-O-methyltransferase (COMT). Similarly, cytosolic DA non-incorporated into vesicles undergoes a degradative process in dopaminergic neurons, although that is mostly dependent on the MAO^{433,436}.

Table 1.3. The dopamine receptors family.

Receptor subtype	D ₁ -like		D ₂ -like		
	D ₁ R	D ₅ R	D ₂ R	D ₃ R	D ₄ R
Isoforms	None	None	D _{2L} , D _{2S}	Yes	Yes
Canonical G protein coupling	G _{s/olf}	G _{s/olf}	G _{i/o}	G _{i/o}	G _{i/o}
DA affinity pK_i	4.3 – 5.6	6.6	5.3 – 6.4	6.4 – 7.3	7.4 – 7.6
Distribution	Cerebral cortex, hippocampus, striatum, hypothalamus, brainstem, retina and white adipose tissue	Cerebral cortex, hippocampus, striatum, hypothalamus, brainstem, olfactory bulb, retina and testes	Cerebral cortex, hippocampus, striatum, hypothalamus, pituitary gland, brainstem, olfactory epithelium, retina, heart ad testes	Cerebral cortex, hippocampus, striatum, hypothalamus, pituitary gland, brainstem, olfactory bulb and stomach	Pituitary gland, retina, ovary and testes

Serotonin receptors classification, subtypes, canonical heterotrimeric G proteins coupling, endogenous ligand affinity and tissue distribution. pK_i: $-\log_{10}$ of the equilibrium inhibitory dissociation constant in M. Affinity data extracted from ⁴³⁷.

Most dopaminergic neurons develop from a single embryological cell group that originates from the mesencephalic-diencephalic junction. The long-axons of these cell groups project to different forebrain areas, divided into four major systems or pathways: the nigrostriatal, mesolimbic, mesocortical and tuberoinfundibular pathways^{433,438,439}. The most extensively studied and more relevant within the context of this thesis is the nigrostriatal pathway (**Figure 1.14**), which plays a major role in motor control and the learning of new motor skills. Alterations in components of this system are underlying the pathophysiology of severe motor disorders, including Parkinson’s and Huntington’s diseases^{440–442}. The nigrostriatal pathway originates in the substantia nigra pars compacta (SNc), from which DA neurons project to the striatum, formed by the caudate nucleus and the putamen in primates (**Figure 1.14A**). The striatum is a major afferent nucleus in the basal ganglia, also receiving glutamatergic inputs from the motor and somatosensory cortex as well as from other cortical areas. The classical view of motor control distinguishes between two routes integrating dopaminergic and glutamatergic neurotransmission: the direct and indirect pathways (**Figure 1.14B**)^{443,444}. According to this model, glutamate release into the striatum from cortical projections activates GABAergic MSNs. These GABAergic cells, of inhibitory nature, comprise ~90% of all striatal neurons and project to the substantia nigra pars reticulata (SNpr) and the internal face

of the globus pallidus (GPi), output nuclei of the nigrostriatal direct pathway. Thalamic glutamatergic neurons, projecting to the motor cortex, receive inhibitory afferents from the SNpr and GPi GABAergic neurons. Thus, activation of striatal MSNs is translated into the inhibition of the SNpr and GPi and the subsequent disinhibition of the thalamus, therefore initiating locomotor activity^{445,446}. Alternatively, via the external part of the globus pallidus (GPe) and the subthalamic nucleus (STN), activated striatonigral MSNs can indirectly project to the SNpr. MSNs-driven inhibition of the GPe leads to the disinhibition of the glutamatergic STN neurons, which project and activate the SNpr GABAergic neurons, ultimately inhibiting locomotor activity^{445,446}.

Striatal MSNs are characterised by their differential expression pattern of dopaminergic receptors. MSNs of the direct pathway express the D₁R, substance P and dynorphin, whereas “indirect” striatopallidal neurons are enriched in D₂R and enkephalin. Dopamine, through the different biochemical responses driven by both receptors, exerts a dichotomous effect. Whereas DA binding to D₁R-expressing MSNs potentiates the direct pathway, activation of D₂R has an inhibitory effect in the GABAergic striatopallidal MSNs of the indirect pathway. Thus, by simultaneously activating and inhibiting “pro-kinetic” (direct) and “anti-kinetic” (indirect) pathways, DA regulates the transmission of coordinated locomotor responses from the motor cortex^{445,446}. The role of the striatum in motor control is clearly evidenced in pathologies whose ethology directly (destruction of MSNs in Huntington’s disease) or indirectly (nigral cell death in Parkinson’s disease) involves it^{447,448}.

Apart from the motor function, the striatum participates in multitude of fundamental processes. For example, almost all cortical areas project to different striatal regions. Thus, the putamen and caudate nucleus receive projections from the sensorimotor and associative cortex, respectively. Similarly, limbic cortical areas project to ventral striatum (nucleus accumbens; NAc)⁴⁴⁹. The dopaminergic system provides a link to systems as varied as emotions, reward/addiction, motivational and emotional responses as well as the hormonal release through its additional dopaminergic pathways. Thus, DA neurons in the ventral tegmental area (VTA) give rise to the mesolimbic and mesocortical pathways, regulating “pleasure” and emotions, respectively, by projecting to different brain nuclei. The mesolimbic extends to the NAc, amygdala, the olfactory tubercle innervating the septum, pyriform cortex and hippocampus. On the other hand, the mesocortical pathway projects to the prefrontal, cingulate and perirhinal cortex. Due to the extensive overlapping between both systems and their implication in the emotion-reward process, they are often referred to as the mesocorticolimbic system^{433,450}.

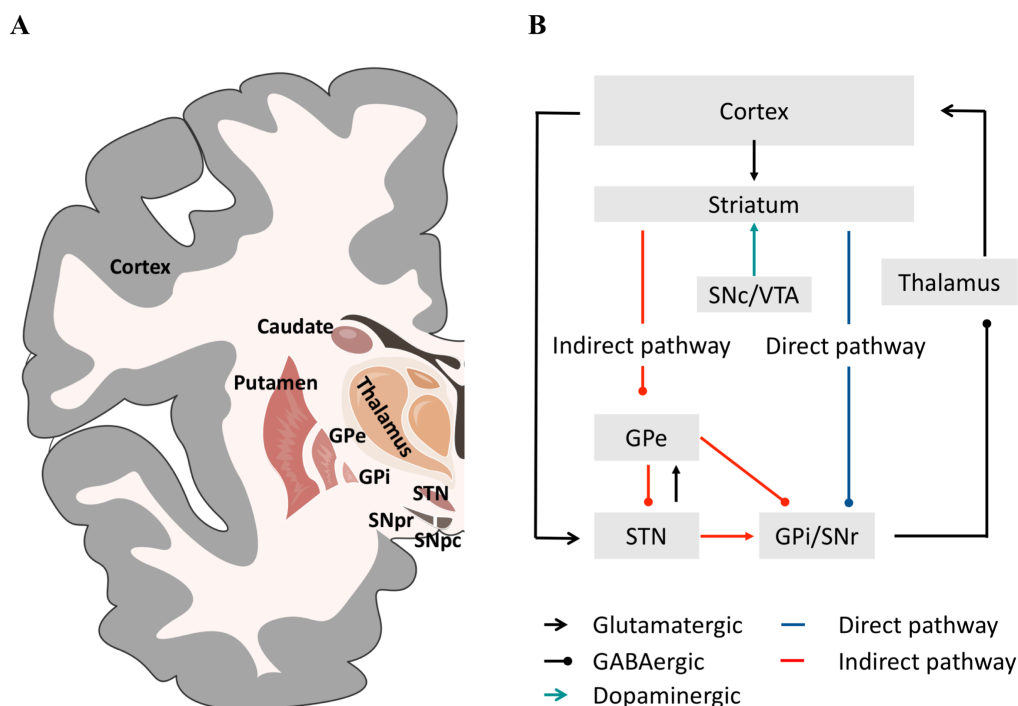


Figure 1.14. The basal ganglia in motor control. (A) Representation of the anatomical distribution of the basal ganglia nuclei and associated brain structures involved in voluntary motor function: dorsal striatum (caudate and putamen), globus pallidus, substantia nigra and subthalamic nucleus. (B) Dopaminergic transmission from the SNc activates D₁R-expressing MSNs of the striatonigral (direct) pathway at the same time as inhibiting D₂R-expressing MSNs of the striatopallidar (indirect) pathway. Consequently, the inhibition of thalamic activity, exerted by the GPi/SNr output nuclei, is abrogated, which in turn sends afferents to the motor cortex. (GPe) globus pallidus pars externa; (GPi) globus pallidus pars interna; (SNc) substantia nigra pars compacta; (SNr) substantia nigra pars reticulata; (STN) subthalamic nucleus; (VTA) ventral tegmental area.

From a structural point of view, high resolution crystallographic information is only available for the D₂, D₃ and D₄ receptors, all captured in their inactive conformations^{451–453}. However, several differential characteristics are well defined between D₁-and D₂-like receptors. D₁ and D₅ receptors share significant similarities, mostly centred around their helical regions, with an 80% identity in TM domains. Similarly, D₃ and D₄ receptors are 75% and 53% homologous to the dopamine D₂ receptor, respectively⁴²⁶. A distinctive feature of D₁-like receptors is the length of their C-terminal tail, significantly longer (~100 amino acids) in comparison with D₂-class receptors (~1-20 amino acids). In addition, whilst the ICL3 is relatively short in the D₁ and D₅ receptors (~20-30 residues), this region extends from ~130 amino acids in the D₂R to up to ~150 residues in D₄R. Differences between these domains are heavily involved in G protein coupling and subtype selectivity^{454–456}.

Similar to other resolved class A receptors, the ECL2 participates in the ligand binding pocket, although lacks helical secondary structure. In addition, sequence alignment comparisons predicting the canonical cysteine bonding between the ultra-conserved Cys in the TM3 (Cys^{3.25}) and the ECL2 was confirmed in all available X-ray structures^{451–453}. In addition, the ECL3 intra-loop disulphide bridge was also observed in both the D₃ and D₄ receptor high-resolution structures^{451,452}. Furthermore, all DA receptors share Arg^{3.50} in the DRY/F motif as well as a glutamic acid residue in the TM6 (Glu^{6.30}) potentially forming the “ionic lock” in the ground-state. This interaction was observed in the antagonist-bound state of the D₂ and D₃ receptors, strongly suggesting that this microswitch might be an activation sensor across dopamine receptors. However, this feature is not observed in the recent nemonapride-D₄R X-ray crystals, although as hypothesised for other receptors, this might be due to the insertion of thermostabilising fusions in the ICL3^{451–453}. In addition, combination of structural/computational biology and medicinal chemistry led to the identification of highly selective molecules against the D₄R. This provided the first steps towards the design of safe drug candidates against a family of receptors which, despite being extensively targeted in many pathological conditions (Parkinson’s, Alzheimer’s, schizophrenia, bipolar disorders, depression, etc.), is often associated to selectivity-related side effects.

1.5.2. Histamine receptors

Outside the brain, histamine is synthesised by multiple cell types, including mast cells, basophils gastric enterochromaffin-like cells, dendritic cells and T cells⁴⁵⁷. In the immune system, mast cells and basophils are the primary source of histamine, where it is stored in cytoplasmic granules together with other amines, cytokines and proteases. After degranulation, histamine elicits different biological functions through binding to its receptors, four class A GPCRs: the histamine H₁, H₂, H₃ and H₄ receptors (**Table 1.4**)^{458,459}.

The histamine H₁ and H₂ receptors have been the most extensively studied members of this family, yielding several blockbuster drugs⁴⁶⁰. The H₁R is expressed in vascular and airway smooth muscle cells, chondrocytes, hepatocytes, endothelial cell, dendritic cells, monocytes, neutrophils and T and B lymphocytes. In particular, its presence in endothelial cells and bronchial smooth muscle cells as well as its implication in allergic disorders has been extensively exploited with anti-histaminergic (colloquial name usually restricted to H₁R antagonising drugs)^{459,461}. The H₂R is widely distributed across the full body as well, including smooth muscle cells, T and B lymphocytes, dendritic cells, cardiac tissue and gastric parietal cells. From a functional point of view, it participates in many processes, including mast cells

General Introduction

degranulation and the relaxation of smooth muscle cells in the blood vessels, airways and the uterus. However, due to its ability to stimulate acid release from the parietal cells in the gastric mucosa, H₂R antagonists have been an extremely profitable target, extensively used to treat dyspepsia, acid reflux and gastric/duodenal ulcers^{459,462}. The H₃ and H₄ receptors have been the last additions to the histamine receptors family. The existence and physiological relevance of the H₃R arose from studies in rat cerebral cortex showing that histamine regulates its own synthesis and release by means of an “autoreceptor” other than the H₁ and H₂ receptors^{463,464}. Later studies confirmed its pre-synaptic function and ability to control the release of other neurotransmitters, including dopamine, serotonin, acetylcholine and noradrenalin. Although the H₃R is widely distributed in the body (e.g. gastrointestinal and cardiovascular systems), it is mostly expressed in the CNS, especially at high densities within several nuclei in the basal ganglia⁴⁶⁵.

Table 1.4. The histamine receptors family.

Receptor subtype	H ₁ R	H ₂ R	H ₃ R	H ₄ R
Best characterised physiological function	Allergic reactions	Gastric acid secretion	CNS neuromodulation	Allergic reactions
Canonical G protein coupling	G _{q/11}	G _s	G _{i/o}	G _{i/o}
Main effector pathway	+PLC, ↑IP ₃ , ↑DAG, ↑Ca ²⁺ , PKC	↑cAMP	↓cAMP, ↑Ca ²⁺	↓cAMP, ↑Ca ²⁺
Histamine affinity pK_i	4.7 – 5.9	3.8	7.1 – 8.3	7.2 – 8.3
Distribution	Ubiquitous, including CNS, smooth muscle (airways, blood vessels), epithelial cells, endothelial cells and immune cells.	Ubiquitous, including gastric mucosa parietal cells, smooth muscle, heart, epithelial cells, endothelial cells and immune cells.	High expression in histaminergic neurons (CNS and PNS)	Bone marrow and hematopoietic cells

Histamine receptors classification, function, main signalling pathways, endogenous ligand affinity and tissue distribution. (+) Stimulation; (↑) concentration increase; (↓) concentration decrease; (CNS) central nervous system; (PNS) peripheral nervous system. (pK_i) –log₁₀ of the equilibrium inhibitory dissociation constant in M. Affinity data extracted from Chazot et al.⁴⁶⁶

In agreement, the H₃R is a recognised target for several neurological disorders, including alterations in the sleep-wake cycle such as narcolepsy, cognitive and memory disorders (attention-deficit hyperactivity disorder, schizophrenia, Alzheimer's and Huntington's diseases), epilepsy and food disorders⁴⁶⁷⁻⁴⁷⁰. The H₄R cloning was relatively recent⁴⁷¹. This receptor shares little sequence homology with members of this family and its expression is mostly restricted to hematopoietic cells, suggesting its role in the modulation of the immune system, namely T-cells, natural killer cells, dendritic cells, eosinophils, basophils and mast cells^{468,472}. In fact, the first *in vivo* evidence strongly supporting H₄R's role in inflammation had to wait until the development of selective ligands, such as the JNJ 7777120 antagonist^{473,474}. Thus, several lines of investigation propose H₄R antagonists as strong candidates for the treatment of some inflammatory and immune disorders, including T_H2 allergic responses, pruritus-associated diseases and cancer^{472,475-477}.

Overall, histamine receptors share ~35% sequence identity, mostly conserved within the TM regions. For example, while the H₁R and H₂R are 37% homologous at the amino acid level, the H₁R is ~25% homologous to the H₃ and H₄. In fact, some members have greater sequence identities when compared to other aminergic receptors and within the same family the maximal identity scores are for the H₃ and H₄ TM regions (~58%)^{478,479}. High-resolution structural information is only available for the histamine H₁ receptor, crystallised into its inactive conformation in complex with doxepin, a first-generation antihistaminergic⁴⁸⁰. Similar to other aminergic receptors, it shares common structural features, such as the ECL2-TM3-connecting disulphide bond between Cys^{3,25} and Cys 180^{ECL2}. These residues are conserved across all four histamine receptors, presumably playing a similar role in structure stabilisation and ligand recognition. Interestingly, the H₁R lacks the palmitoylation site in its C-terminus found in several GPCRs, although putative sites are present in the H₂, H₃ and H₄ receptors^{481,482}. Most histamine receptors have the DRY motif, with the exception of the H₃R in which the third residue is a phenylalanine. In addition, the presence of conserved Glu/Asp^{6,30} residues in all but the H₄R suggests the potential formation of the "ionic lock". Interestingly, in the inactive doxepin-H₁R complex, R^{3,50} presents an alternative orientation in respect to other closely related class A GPCRs, establishing hydrogen bonds with the G^{6,36}, although as previously mentioned for other crystals, ICL3 insertions might alter the overall architecture surrounding this motif^{27,33,124,480}. In addition, the NPxxY motif connecting the TM7 and the helix 8 is present in all histaminergic receptors. Histamine displays a broad range of affinities towards its receptors. While the equilibrium dissociation constants for the H₁ and H₂ receptors within the micromolar range, histamine affinity for the H₃ and H₄ receptors is ~10-100 fold higher^{459,466,483}. An important aspect of the histamine receptors family is the diversification of its receptors due to polymorphisms and alternative splicing variants. Thus,

General Introduction

H₃R genomic organisation allows the generation of almost 20 different isoforms through alternative splicing, with some of the detected forms rendering non-ligand binding mutants, truncated receptors or forms with variable ICL3 lengths⁴⁸¹.

In the brain, histamine acts as a neurotransmitter synthesised by a particularly limited (~64,000 cells) and localised pool of neurons located in the tuberomammillary nucleus of the posterior hypothalamus^{484,485}. Histamine biosynthesis occurs through the oxidative decarboxylation of L-histidine, exclusively catalysed by the L-histidine decarboxylase (HDC). Histamine can barely cross the blood-brain barrier (BBB) and, unlike other biogenic amines, its limiting synthetic step does not comprise enzymatic activity but the availability of its precursor. L-histidine circulating in the cerebrospinal fluid is rapidly uptaken by L-amino acid transporters, converted into histamine and stored in vesicles by VMAT2-mediated active transport. In comparison with other biogenic amines, histamine levels in the brain are relatively low, although are subject to unimportant turnover. Furthermore, its biosynthesis and the firing rate of TMN neurons display circadian rhythms, with maximal activities reached over the state of vigilance⁴⁸⁶. After an action potential, histamine is released into the synaptic cleft where it binds to the histamine H₁, H₂ and H₃ receptors. H₁R and H₂R are located post-synaptically in neurons and glial cells, whereas the expression of H₃R is restricted to neurons. The H₃R acts both as a pre- and post-synaptic receptor, with its autoreceptor function being crucial for the control of histamine synthesis as well as tonically inhibiting neuronal activity by modulation of inward Ca²⁺ currents^{459,470,481}. In the extracellular space, histamine is inactivated through the action of the histamine-N-methyltransferase (HNMT), yielding telemethylhistamine that is further transformed into telemethyl-imidazolacetic acid by the MAO B. In the peripheral tissues, histamine is primarily catabolised by the diamine oxidase enzyme (DAO) directly producing imidazoleacetic acid⁴⁸⁷. Consequently, HNMT blockers to increase histamine levels in the brain have been proposed as drug candidates for neurological disorders such as Alzheimer's disease^{488,489}.

In the CNS, histaminergic TMN neurons project their fibres to virtually all the different brain regions. Although their diffuse pattern, three major pathways can be delineated, two ascending bundles projecting to different forebrain structures (hypothalamus, septum, thalamus, hippocampus and amygdala) and one descending bundle towards the cerebellum and spinal cord^{481,485}. The cerebral cortex, amygdala, substantia nigra, striatum and spinal cord receive dense innervations from the TMN, whereas this pattern appears more diffuse in the hippocampus and thalamus^{490,491}. This widespread distribution of the histaminergic system all over the brain is in accordance with its participation in the above-mentioned plethora of biological functions. The most well studied process regulated by histamine in the CNS is the sleep/wakefulness cycles. In addition, hypothalamic H₁ and H₃ receptors regulate feeding

behaviours⁴⁹². H₁R activation in the hypothalamic paraventricular and ventromedial nucleus induces satiety by a mechanism involving leptin and GLP1 as well as histamine H₃ autoreceptors^{492,493}. Indeed, betahistidine (Betaserc®), a H₁R agonist/H₃R antagonist has been clinically explored and diminishes the metabolic side-effects associated with antipsychotics^{494,494,495}.

Over the last years, the third histaminergic receptor has attracted interest for its implication in cognitive and motor disorders. Thus, in AD patients, there is a loss of TMN neurons and reduced histamine levels in memory-related areas (cortex, hippocampus and hypothalamus)⁴⁹¹. In addition, through its control over adrenergic and cholinergic transmission, H₃R activity might account for the reduction in the concentration of these neurotransmitters in the prefrontal cortex. Consequently, selective H₃R antagonists have been explored in several AD clinical trials, although no improvements in memory decline have been reported so far^{496,497}. Similarly, because of H₃R-driven inhibition of dopaminergic and cholinergic transmission, H₃R antagonists might provide potential drug candidates for the treatment of attention-deficit hyperactivity disorder (ADHD) and schizophrenia^{469,491}. Finally, the H₂ and H₃ receptors play a fundamental role in motor control. The histaminergic system controls the nigrostriatal and corticostriatal pathways at multiple levels (extensively reviewed by Panula and Nuutien⁴⁷⁰). Thus, H₃ autoreceptors in striatal afferents from the cortex, thalamus and hypothalamus inhibit glutamate release in MSNs synapses. In addition, through different intracellular signalling mechanisms (including heteromerisation), H₂ and H₃ receptors modulate the activity of striatal MSNs. Considering the promising array opportunities, several H₃R antagonists have been and are at different stages in clinical trials for diverse CNS-related disorders, mainly sleep disorders, AD and dementia, schizophrenia and ADHD (reviewed by Sadek et al.⁴⁹⁶)

1.5.3. Dopamine and histamine receptor oligomerisation. Functional interaction between D₁ and H₃ receptors

Oligomerisation between members of the dopamine receptor family has been extensively studied, including oligomers within the same type of receptors (homomers) as well as within different dopaminergic receptor subtypes (heteromers). In fact, using different biophysical approaches, homodimers of the D₁, D₂, D₃ and D₄ dopamine receptors have been reported^{203,498,499}. Similarly, heterodimers composed of distinct dopamine receptors have been repeatedly shown (D₁-D₂, D₁-D₃, D₂-D₅, D₂-D₄, D₂-D₃, and D₁-D₅)⁵⁰⁰⁻⁵⁰⁵, with some of them, viz. D₁-D₂ heteromers, well validated *in vivo* and with compelling evidence suggesting their

General Introduction

role in pathology of schizophrenia and depression⁵⁰⁶. Dopamine receptors can also interact with other Class A GPCR families (e.g. D₂R-5-HT_{2A}R, D₂R-A_{2A}R, D₁R-H₃R) as well as with members belonging to the metabotropic glutamate family (e.g. D₂R-mGlu₅R, D₂R-mGlu₅R-A_{2A}R)⁵⁰⁷. In addition, several non-GPCR partners have been identified, including the N-methyl-D-aspartate receptor (NMDA)-mediated regulation of D₁R through interaction with the NR2A subunit of this Ca²⁺ channel or the interaction with chaperoning proteins in D₁-σ₁ heteroreceptor complexes⁵⁰⁸⁻⁵¹⁰. An excellent revision on the dopamine receptor heteromers identified to date has been recently put together by Asher and colleagues⁵⁰⁷.

Similar to dopaminergic receptors, oligomerisation involving histamine receptors appears to be a common phenomenon. While its functional relevance has been explored in less detail, evidence supporting homomerisation has been provided for all four receptors⁵¹¹⁻⁵¹⁵. Interestingly, supporting the biological role of H₁R homomeric assemblies, Bakker and collaborators restored ligand binding after the co-expression of two binding-deficient mutants⁵¹⁴. In addition, heteromerisation between histaminergic receptors has also been reported⁵¹⁶. This is the case of H₁R-H₂R heteromers, in which one protomer cross-desensitises the functional responses driven by the other receptor⁵¹⁷. Thus, H₁R-mediated cell proliferation and signalling was blocked after co-stimulation with selective H₂R agonists. Furthermore, heteromerisation was confirmed by FRET microscopy and both receptors co-internalised together after stimulation with either selective agonist⁵¹⁷.

Histamine receptors are also able to dimerise with other Class A GPCRs, with evidence supporting the interaction between the H₃R and the A_{2A}, D₁ and D₂ receptors^{344,345,518}. In the case of A_{2A}-H₃ heteroreceptor complexes, Morales-Figueroa recently showed in isolated globus pallidus rat terminals (synaptosomes) an antagonistic effect of H₃R agonists on A_{2A}R-mediated depolarisation-evoked [3H]-GABA release, suggesting a mechanism involving direct protein-protein interactions⁵¹⁸. For D₂-H₃ receptor heteromers, Ferrada and collaborators showed by BRET that both receptors can interact in heterologous HEK293 cells. In addition, H₃R antagonists potentiate D₂-dependent potentiation of locomotor activity in reserpinised mice, indicating functional behaviour interactions³⁴⁴. However, although these authors reported that H₃R agonists decreased D₂ agonists affinity in sheep striatal membranes, that is negative cooperativity at the binding sites, Humbert-Claude et al. showed no interaction between D₂ and H₃ receptor ligands on [³⁵S]GTPγ[S] binding to rat striatal membranes⁵¹⁹. Thus, whether ligand cooperativity does not impact G protein binding and/or the potential heteromerisation of these receptors *in vivo* requires further studies.

Opposite to the above-mentioned cases, heteromerisation between D₁ and H₃ receptors is well supported *in vitro* and *in vivo*. Both receptors are expressed, co-localise and interact in striatonigral GABAergic neurons of the direct pathway^{345,520,521}. The functional relevance of

their interaction was proposed two decades ago by measuring [^3H]GABA release in rat slices of the SNpr⁵²¹. In these studies, selective H₃R agonists inhibited the fraction of [^3H]GABA release controlled by D₁R activity⁵²¹. Similarly, Arias-Montaño showed that K⁺-induced release of [^3H]GABA in reserpinised rat striatal slices required D₁R agonism and that this effect could be attenuated in the presence of the H₃R antagonist Thioperamide, suggesting functional cross-talk in striatal MSNs⁵²². Using BRET, Ferrada et al. provided the first direct evidence of direct interactions between the D₁ and H₃ receptors in heterologous cells. In addition, the biphasic binding of D₁R agonists was abolished in the presence of H₃R agonists, indicative of cooperativity at the plasma membrane level³⁴⁵. Interestingly, H₃R stimulation only triggered ERK1/2 phosphorylation when co-expressed with the D₁ receptor and H₃ ligands blocked D₁R-mediated signalling, and vice versa³⁴⁵. D₁R-dependent H₃R ERK1/2 signalling and the bidirectional cross-antagonism was further confirmed in brain striatal slices of mice exclusively expressing D₁ receptors⁵²³. Importantly, ERK1/2 phosphorylation upon H₃R stimulation was restricted to MSN of the direct pathway, suggesting a new mechanism to regulate dopaminergic transmission in the direct striatal pathway⁵²³.

Using PLA, Moreno and collaborators confirmed the expression of D₁R-H₃R heteromers in mouse and rat striatum⁵²⁴. Intriguingly, in this work, the authors detected a novel interacting partner, the σ_1 receptor, forming σ_1 R-D₁R-H₃R heterotrimers. Furthermore, cocaine was able to alter the D₁R-H₃R heteromer-specific G protein signalling and abrogated the bidirectional cross-antagonism in ERK1/2 phosphorylation. This last effect was further confirmed in striatal mice slices as was absent in σ_1 R K.O. animals, although D₁R-H₃R heteromers expression was unaltered, indicating the σ_1 R-dependent component for cocaine to alter D₁R-H₃R heteromers properties⁵²⁴. The σ_1 receptor is an orphan endoplasmic-reticulum-resident transmembrane chaperone. Although its biological function is poorly understood, it modulates several neurotransmitter systems and has been implicated in a variety of neurologic disorders, including depression, anxiety, schizophrenia and drug addiction^{525,526}.

Finally, a recent work from Rodríguez-Ruiz confirmed by PLA rat cortical D₁R-H₃R heteromers in complex with the NR1A and NR2B NMDA and the ability of H₃R ligands, via negative cross-talk, to reduce NMDA and D₁R overstimulation-induced cell death and β_{1-42} -amyloid peptide toxicity⁵²⁷. In light of the above, compelling evidence supports that H₃R ligands might act as a “molecular brake” for D₁ signalling via heteromerisation with the D₁R. Accordingly, in this thesis (see Chapter 5) we will explore the potential of this interaction in the context of Huntington’s disease, in which altered striatal dopaminergic transmission is a major player over its progression^{442,528}.

1.6. Hypothesis and Aims

As discussed in this chapter, GPCRs are dynamic proteins existing as ensembles of ephemeral conformations moulded by their ligands and/or interacting proteins. This conformational flexibility is reflected by allostery, allowing 7TM receptors to control the intracellular machinery by means of integrating signals alternative to “endogenous” orthosteric ligands, including small molecules and proteins. With regard to the foregoing, the functional consequences arising from the ability of GPCRs, particularly Class A receptors, to interact with themselves or with members belonging to different subfamilies has been one of the most controversial topics since the mid-90s. GPCR organisation as dimers or higher order oligomers is well established, yet it is also acknowledged that this might not be always required for proper receptor function. Therefore, integrating this diversity into the development of the next generation of medicines involves understanding how GPCRs communicate both with their external and internal environments.

GPCR oligomerisation raises key outstanding questions typically falling into two main categories. The first encompasses understanding the rules governing these interactions from a mechanistic perspective, including their stability, architecture/interfaces, conformational arrangements driving cross-talk and the reciprocal effects of G protein binding. Accordingly, due to the compelling evidence supporting 5-HT_{2A}R-CB₁R receptor heteromers as a novel target to dissociate THC's detrimental side effects, the first general aim of this thesis was to provide a model accounting for the molecular basis underlying cross-talk in this well validated heteromer. Thus, the specific aims were to:

- a) Develop BiLC-based assays to study homo/heteromerisation, and effector binding (arrestins and G proteins).
- b) Apply the above-mentioned technology to identify small-stapled TM peptides targeting this heteromer.
- c) Generate 5-HT_{2A} and CB₁ receptor mutants to control their active conformation/G protein binding.
- d) Take advantage of these mutants to delineate the determinants driving cross-communication across different downstream signalling pathways.
- e) Delineate 5-HT_{2A}R-CB₁R architecture in relation to G proteins.

The second challenge that receptor oligomerisation presents is to understand the significance of these complexes into the native *in vivo* environment. Thus, we hypothesised that the functional consequences arising from the interaction between the D₁ and H₃ receptors could

indeed be used to slow down or halt Huntington's disease. Accordingly, the increasing body of evidence supporting aberrant D₁R overactivation in HD neurodegeneration together with the co-localisation of both receptors in striatonigral MSNs and the well validated inhibitory effect of H₃R ligands over D₁R signalling through D₁R-H₃R heteromers provide the ideal scenario to explore class A GPCR heteromers in relation to disease. According to this second main objective, the specific aims were to:

- a) Identify and characterise the pharmacological properties (signalling and trafficking) of D₁R-H₃R heteromers in a HD striatal cellular model (STHdH^{Q7} and STHdH^{Q111} cells).
- b) Define the oligomeric interfaces of D₁R-H₃R heteromers.
- c) Study the feasibility of H₃R ligands to revert D₁R-mediated cell death.
- d) Evaluate the effect of H₃R ligands for the treatment of cognitive and motor deficits in a HD murine model (Hdh^{Q7/111}).

Finally, the above mentioned GPCR conformational flexibility was exploited to identify small-molecule PAMs. As will be discussed further below, 5-HT_{2C} receptors are a well validated target for anti-obesity drugs. However, the extraordinary extent of homology within the 5-HT₂ family makes their selective agonism uniquely challenging. Our hypothesis was that targeting the presumably less conserved allosteric sites of 5-HT_{2C}R would allow us to circumvent off-target-related side effects. Thus, the specific aims of this third main objective were to:

- a) Identify putative 5-HT_{2C}R PAMs to use as hit to lead from a proprietary chemical library.
- b) Develop improved PAMs via structure-activity-aided optimisation of the initial hits.
- c) Evaluate *in vivo* the potential candidates.
- d) Identify and validate a pharmacophore model via site-directed mutagenesis and homology modelling.
- e) Explore the proposed model for the development of enhanced PAMs.

Chapter 2

Materials & Methods

2.1. Materials

2.1.1. Antibodies

Antibody	Host	Application (dilution; v:v)	Supplier	Product no.
Alexa Fluor® 488 Goat Anti-Guinea Pig IgG	Goat	IF (1:100)	Jackson ImmunoResearch	106-545-006
AlphaLISA® CaptSure™ Acceptor Beads	N.A.	1:100	Perkin Elmer®	ALSU-PERK-A10K
AlphaScreen® Streptavidin Donor Beads	N.A.	1:100	Perkin Elmer®	ALSU-PERK-A10K
Cy™3 Goat Anti-Rabbit IgG	Goat	IF (1:500)	Jackson ImmunoResearch	111-166-003
D₁R	Guinea pig	IF (1:100); PLA (1:200)	Frontier institute	D1R-GP-Af500
H₃R	Rabbit	PLA (1:200)	Alpha Diagnostics	H3R31-A
HA-Tag	Rabbit	IF (1:1600)	Cell Signalling	3724S
PLA probe anti-Guinea Pig IgG MINUS	Donkey	PLA (1:5)	Olink Biosciences	90206
PLA probe anti-Rabbit Pig PLUS	Donkey	PLA (1:5)	Olink Biosciences	90302

IF: immunofluorescence; N.A.: non-applicable; PLA: Proximity Ligation Assay

2.1.2. Buffers and solutions

2.1.2.1. PBS and DPBS, pH 7.4

Phosphate-Buffer Saline (PBS), pH 7.4		Dulbecco's PBS (DPBS), pH 7.4 (Ca ²⁺ and Mg ²⁺ free)	
Inorganic salts	[] (mM)	Inorganic salts	[] (mM)
Na ₂ HPO ₄ ·7H ₂ O	3.0	Na ₂ HPO ₄ ·7H ₂ O	8.1
NaCl	155.2	NaCl	137.9
KH ₂ PO ₄	1.1	KCl	2.7
		KH ₂ PO ₄	1.5

Materials & Methods

2.1.2.2. Hank's Balanced Salt Solution (HBSS), pH 7.4

Inorganic salts and other components	(mM)
CaCl ₂	1.3
MgCl ₂	0.5
MgSO ₄	0.4
KCl	5.3
KH ₂ PO ₄	0.4
NaHCO ₃	4.2
NaCl	137.9
Na ₂ HPO ₄	0.3
D-Glucose	5.5

2.1.2.3. Tris-Acetate-EDTA buffer (TAE), pH~ 8.3-8.6

Inorganic salts	(mM)
Tris Base	40
EDTA	1
Acetic acid	20

2.1.2.4. Transformation Buffers (TFB1 and TFB2)

Transformation Buffer 1 (TFB1), pH5.8		Transformation Buffer 2 (TFB2), pH 6.5	
Inorganic salts and other components	Concentration	Inorganic salts and other components	Concentration
CaCl ₂	10 mM	CaCl ₂	75 mM
CH ₃ CO ₂ K	30 mM	MOPS	10 mM
Glycerol	15% (v:v)	Glycerol	15% (v:v)
MnCl ₂ -4H ₂ O	50 mM	RbCl	100 mM
RbCl	100 mM		

* Adjust to pH 5.8 with acetic acid (2N)

* Adjust to pH 6.5 with KOH (1N)

2.1.2.5. Calcium assay buffers

Calcium assay buffer, pH7.4 (HEK293 cells)		Calcium assay buffer, pH7.4 (STHdH cells)	
Inorganic salts and other components	(mM)	Inorganic salts and other components	(mM)
CaCl ₂	2	CaCl ₂	2.3
D-Glucose	10	D-Glucose	5.6
HEPES	10	Glycine	0.01
KCl	2.5	HEPES	5
MgCl ₂	1	KCl	5.6
NaCl	145	NaHCO ₃	3.6
		NaCl	154

2.1.2.6. cAMP/NanoBiT assay buffer, pH 7.4

Inorganic salts and other components	Concentration
HBSS	1X
CaCl ₂	1.3 mM
HEPES	20 mM
MgSO ₄	1 mM
NaHCO ₃	3.3 mM
BSA	0.1% (w:v)

2.1.2.7. LB, LB-agar and YT Media

	Luria-Bertani (LB) broth, pH 7.5	LB-agar, pH 7.5	2X YT Media, pH 7
Inorganic salts and other components	Concentration	Concentration	Concentration
Bacto-tryptone	1% (w:v)	1% (w:v)	1.6% (w:v)
NaCl	1% (w:v)	1% (w:v)	0.5% (w:v)
Yeast extract	0.5% (w:v)	0.5% (w:v)	1% (w:v)
Agar	-	2% (w:v)	-

Materials & Methods

2.1.2.8. S.O.C Medium, pH 7

Inorganic salts and other components	Concentration
Bacto-tryptone	2% (w:v)
NaCl	10 mM
Yeast extract	0.5% (w:v)
KCl	2.5 mM
MgCl ₂	10 mM
MgSO ₄	10 mM
D-Glucose	20 mM

2.1.2.9. Mammalian cell culture media

HEK 293 cells culture media		STHdH cells culture media	
Base media	Supplements	Base media	Supplements
DMEM	D-Glucose (4.5 g/L) FBS 10% (v:v) L-Glutamine (2 mM) Penicillin (100 U/mL) Sodium pyruvate (1 mM) Streptomycin (100 µg/mL)	DMEM	D-Glucose (4.5 g/L) FBS 10% (v:v) L-Glutamine (2 mM) G418 (400 µg/mL) Penicillin (100 U/mL) Sodium pyruvate (1 mM) Streptomycin (100 µg/mL)

Cell starvation media

Base media	Supplements
DMEM	BSA (0.1% w:v) D-Glucose (4.5 g/L) L-Glutamine (2 mM) Sodium pyruvate (1 mM)

2.1.3. Enzymes

Enzyme	Supplier	Product no.
DpnI	Thermo Scientific™	ER1705
DreamTaq DNA Polymerase	Thermo Scientific™	K1071
Phusion® High-Fidelity DNA Polymerase	Thermo Scientific™	FZF-530L

2.1.4. Ligands

Name	Biological activity	Supplier	Product no.
(±)-2,5-Dimethoxy-4-iodoamphetamine hydrochloride (DOI)	5-HT _{2A} /5-HT _{2C} receptor agonist (Ki 5-HT _{2A} R/5-HT _{2C} R < Ki 5-HT _{2B} R)	Tocris®	2643
(R)-(+)-WIN 55212 (WIN)	CB ₁ /CB ₂ receptor agonist (Ki CB ₂ R < Ki CB ₁ R)	Tocris®	1038
(R)-N-α-[methyl-3H]-methylhistamine dihydrochloride ([3H]RAMH)	Selective histamine H ₃ receptor agonist	Perkin Elmer®	NET1027250UC
[N-Methyl-3H]-SCH 23390 ([3H]SCH 23390)	Dopamine D ₁ -like receptor antagonist	Perkin Elmer®	NET930025UC
5-Hydroxytryptamine (5-HT, serotonin)	Endogenous 5-HT receptors and 5-HT transporters agonist	Tocris®	3547
Forskolin	Cell-permeable activator of adenylyl cyclases	Hello Bio	HB1348
Imetit dihydrobromide (Imetit)	H ₃ and H ₄ receptors agonist (Ki H ₃ R < Ki H ₄ R)	Tocris®	0729
MDL 100907 (MDL)	Selective 5-HT _{2A} receptor antagonist	Tocris®	4173
Rimonabant hydrochloride/ SR-141716 (RIM)	Selective CB ₁ R inverse agonist	Sigma-Aldrich	SML0800
Sertraline hydrochloride	Selective serotonin reuptake inhibitor	Tocris®	2395
SCH 23390 hydrochloride (SCH 23390)	Dopamine D ₁ -like receptor antagonist	Tocris®	0925

Materials & Methods

SKF 81297 hydrobromide (SKF81297)	Dopamine D ₁ -like receptor agonist	Tocris®	1447
Thioperamide	H ₃ and H ₄ receptors inverse agonist	Tocris®	0644

Ki: inhibition dissociation equilibrium constant.

2.1.5. Plasmids

2.1.5.1. Plasmids obtained from external sources

Name	Source	Product no.
pGP-CMV-GCaMP6s	Addgene	40753
LgBiT-PRKAR2A	Promega	N203A
pBiFC-bFosVC155	Addgene	22013
pBiFC-bJunVN173	Addgene	22012
pBiT1.1-C [TK/LgBiT]	Promega	N196A
pBiT1.1-N [TK/LgBiT]	Promega	N198A
pBiT2.1-C [TK/SmBiT]	Promega	N197A
pBiT2.1-N [TK/SmBiT]	Promega	N199A
pcDNA3.1-3xHA-5-HT _{2A} R	cDNA resource center	HTR02A0001
pcDNA3.1-3xHA-CB ₁ R	cDNA resource center	CNR01LTN00
pcDNA3.1-CB ₁ R-YFP	Dr. Josef Lazar	-
pcDNA3.1-3xHA-CB ₂ R	cDNA resource center	CNR0200000
pcDNA3.1-5-HT _{2C} R	cDNA resource center	HTR02C0000
pcDNA3.1-ARRB2	cDNA resource center	ARRB200001
pcDNA3.1-D ₁ R	cDNA resource center	DRD0100000
pEYFP-N1-D ₁ R	In-house	-
pcDNA3.1-Galphi1	Dr. Andy Chevigné	-
pcDNA3.1-Galphi3	Dr. Andy Chevigné	-
pcDNA3.1-Galphiq	Dr. Andy Chevigné	-
pGAP43-CFP-Goi1	Dr. Josef Lazar	-
pGβ1	Dr. Josef Lazar	-
pGγ2	Dr. Josef Lazar	-
pcDNA3.1-H ₃ R	cDNA resource center	HRH0300000
pFN21A HaloTag® CMV Flexi® Vector	Promega	G2821
pGloSensor™-22F cAMP Plasmid	Promega	E2301
SmBiT-PRKACA	Promega	N204A

2.1.5.2. Plasmids generated in this thesis

Name	Backbone
CMV-5-HT _{2A} R-LgBiT	pcDNA3.1-3xHA-5-HT _{2A} R
CMV-5-HT _{2A} R-SmBiT	pcDNA3.1-3xHA-5-HT _{2A} R
CMV-5-HT _{2C} R-LgBiT	pcDNA3.1-5-HT _{2C} R
CMV-5-HT _{2C} R-SmBiT	pcDNA3.1-5-HT _{2C} R
CMV-5-HT _{2A} R-VC155	pcDNA3.1-3xHA-5-HT _{2A} R
CMV-5-HT _{2A} R-VN173	pcDNA3.1-3xHA-5-HT _{2A} R
CMV-5-HT _{2A} R(I163A)-LgBiT	CMV-5-HT _{2A} R-LgBiT
CMV-5-HT _{2A} R(I181A)-LgBiT	CMV-5-HT _{2A} R-LgBiT
CMV-CB ₁ R-LgBiT	pcDNA3.1-3xHA-CB ₁ R
CMV-CB ₁ R ^{Δ23}	pcDNA3.1-3xHA-CB ₁ R
CMV-CB ₁ R ^{Δ23} -LgBiT	pcDNA3.1-3xHA-CB ₁ R
CMV-CB ₁ R-SmBiT	pcDNA3.1-3xHA-CB ₁ R
CMV-CB ₁ R-VC155	pcDNA3.1-3xHA-CB ₁ R
CMV-CB ₁ R-VN173	pcDNA3.1-3xHA-CB ₁ R
CMV-CB ₁ R(L341A)-LgBiT	CMV-CB ₁ R-LgBiT
CMV-CB ₁ R(L341A)-SmBiT	CMV-CB ₁ R-SmBiT
CMV-CB ₁ R(L345A)-LgBiT	CMV-CB ₁ R-LgBiT
CMV-CB ₁ R(L345A)-SmBiT	CMV-CB ₁ R-SmBiT
CMV-CB ₂ R-LgBiT	pcDNA3.1-3xHA-CB ₂ R
CMV-CB ₂ R-SmBiT	pcDNA3.1-3xHA-CB ₂ R
CMV-HaloTag®-5-HT _{2A} R	pcDNA3.1-3xHA-5-HT _{2A} R
CMV-HaloTag®-CB ₁ R	pcDNA3.1-3xHA-CB ₁ R
CMV-LgBiT-5-HT _{2A} R	pcDNA3.1-3xHA-5-HT _{2A} R
CMV-LgBiT-CB ₁ R	pcDNA3.1-3xHA-CB ₁ R
CMV-LgBiT-β-arrestin2	pcDNA3.1-ARRB2
CMV-SmBiT-5-HT _{2A} R	pcDNA3.1-3xHA-5-HT _{2A} R
CMV-SmBiT-CB ₁ R	pcDNA3.1-3xHA-CB ₁ R
CMV-SmBiT-Gai1	pcDNA3.1-Galphi1
CMV-SmBiT-Gai3	pcDNA3.1-Galphi3
CMV-SmBiT-Gaq	pcDNA3.1-Galphaq
CMV-SmBiT-β-arrestin 2	pcDNA3.1-ARRB2
CMV-SmBiT ₁₂₄ -Gaq	pcDNA3.1-Galphaq
HSV-TK-5-HT _{2A} R-LgBiT	pBiT1.1-C [TK/LgBiT]
HSV-TK-5-HT _{2A} R-SmBiT	pBiT2.1-C [TK/SmBiT]
HSV-TK-CB ₁ R-LgBiT	pBiT1.1-C [TK/LgBiT]
HSV-TK-CB ₁ R-SmBiT	pBiT2.1-C [TK/SmBiT]
pcDNA3.1-3xHA-5-HT _{2A} R(I163A)	pcDNA3.1-3xHA-5-HT _{2A} R
pcDNA3.1-3xHA-5-HT _{2A} R(I181A)	pcDNA3.1-3xHA-5-HT _{2A} R

Materials & Methods

pcDNA3.1-3xHA-5-HT_{2A}R(L325A)	pcDNA3.1-3xHA-5-HT _{2A} R
pcDNA3.1-3xHA-5-HT_{2A}R(T275A)	pcDNA3.1-3xHA-5-HT _{2A} R
pcDNA3.1-3xHA-CB₁R(I297A)	pcDNA3.1-3xHA-CB ₁ R
pcDNA3.1-3xHA-CB₁R(L222A)	pcDNA3.1-3xHA-CB ₁ R
pcDNA3.1-3xHA-CB₁R(L222A/I297A)	pcDNA3.1-3xHA-CB ₁ R
pcDNA3.1-3xHA-CB₁R(L222A/L345A)	pcDNA3.1-3xHA-CB ₁ R
pcDNA3.1-3xHA-CB₁R(L341A)	pcDNA3.1-3xHA-CB ₁ R
pcDNA3.1-3xHA-CB₁R(L345A)	pcDNA3.1-3xHA-CB ₁ R
pcDNA3.1-3xHA-CB₁R(T210A)	pcDNA3.1-3xHA-CB ₁ R
pcDNA3.1-3xHA-CB₁R(V204A)	pcDNA3.1-3xHA-CB ₁ R
pcDNA3.1-3xHA-CB₁R(V204A/L222A)	pcDNA3.1-3xHA-CB ₁ R
pcDNA3.1-3xHA-CB₁R(V204A/L345A)	pcDNA3.1-3xHA-CB ₁ R
pcDNA3.1-5-HT_{2C}R (K348A)	pcDNA3.1-5-HT _{2C} R
pcDNA3.1-5-HT_{2C}R(E347A)	pcDNA3.1-5-HT _{2C} R
pcDNA3.1-5-HT_{2C}R(L209A)	pcDNA3.1-5-HT _{2C} R
pcDNA3.1-5-HT_{2C}R(N331A)	pcDNA3.1-5-HT _{2C} R
pcDNA3.1-5-HT_{2C}R(N351A)	pcDNA3.1-5-HT _{2C} R
pcDNA3.1-5-HT_{2C}R(S334A)	pcDNA3.1-5-HT _{2C} R
pcDNA3.1-5-HT_{2C}R(V208A)	pcDNA3.1-5-HT _{2C} R

2.1.6. Kits

Name	Supplier	Product no.
AlphaLISA SureFire Ultra p-ERK1/2 (Thr202/Tyr204) Assay Kit	Perkin Elmer®	ALSU-PERK
DreamTaq PCR Master Mix (2X)	Fisher Scientific	K1071
Duolink® In Situ Detection Reagents Green	Sigma-Aldrich	DUO92014
Duolink® In Situ Detection Reagents Red	Sigma-Aldrich	DUO92008
Macherey-Nagel™ NucleoSpin™ Gel and PCR Clean-up Kit	Fisher Scientific	11992242
Macherey-Nagel™ NucleoSpin™ Plasmid Kit	Fisher Scientific	11932392
NanoBiT® PPI MCS Starter System	Promega	N2014
NanoBRET™ PPI Flexi® Starter System	Promega	N1821
NEBuilder® HiFi DNA Assembly Master Mix	New England Biolabs	E2621S
Pierce™ BCA Protein Assay Kit	Thermo Scientific™	23225
PureYield™ Plasmid Maxiprep System	Promega	A2393

2.1.7. General reagents

Name	Supplier	Product no.	Name	Supplier	Product no.
Acetic acid glacial	Fisher Scientific	12686657	Methanol	Fisher Scientific	10499560
Agar	Fisher Scientific	10572775	MgCl₂-6H₂O	Fisher Scientific	10647032
Agarose	Fisher Scientific	10366603	MgSO₄-7H₂O	Fisher Scientific	10346190
Ampicillin Sodium Salt	Fisher Scientific	10193433	MnCl₂-4H₂O	Fisher Scientific	11452844
Bacto-tryptone	Fisher Scientific	11365982	MOPS	Sigma-Aldrich	M3183
Bovine Serum Albumin (BSA)	Sigma-Aldrich	A7906	NaCl	Fisher Scientific	10616082
CaCl₂-2H₂O	Fisher Scientific	10316313	NaHCO₃	Fisher Scientific	10244683
CH₃CO₂K	Fisher Scientific	10522955	NaOH	Fisher Scientific	10396240
Dimethyl sulfoxide (DMSO)	Sigma-Aldrich	D8418	Paraformaldehyde	Sigma-Aldrich	P6148
dNTPs (10mM each)	Fisher Scientific	BP25652	Paraformaldehyde (32% Solution)	VWR	15714
DPBS	Fisher Scientific	14190144	PBS (10X)	Fisher Scientific	10051163
EDTA	Sigma-Aldrich	324503	Polyethylenimine	Sigma-Aldrich	408727
Ethanol Absolute	Fisher Scientific	10000652	RbCl	Fisher Scientific	10549390
Glycerol (99.5%)	Fisher Scientific	10692372	Sodium Dodecyl Sulphate (SDS)	Fisher Scientific	10090490
Glycine	Fisher Scientific	10061073	Sodium Bicarbonate (7.5% solution)	Fisher Scientific	12529089
KOH	Fisher Scientific	10366240			

Materials & Methods

HBSS	Fisher Scientific	HBSS (10X)	Tris base	Fisher Scientific 10376743
HEPES (10X)	Fisher Scientific	10397023	Tris HCl	Fisher Scientific 10316893
Isopropanol	Fisher Scientific	11388461	Triton™ X-100	Fisher Scientific BP151
Kanamycin sulphate	Fisher Scientific	10031553	Tween(R) 20	Fisher Scientific 10113103
KCl	Fisher Scientific	10375810	Yeast extract	Fisher Scientific 11385992

2.1.8. Cell culture reagents

Name	Supplier	Product no.	Name	Supplier	Product no.
Corning® 96 Well plate, black and clear	Corning®	10530753	Opti-MEM™ I Reduced Serum Medium, No Phenol Red	Fisher Scientific	11520386
Corning® 96 Well plate, white and clear	Corning®	10517742	PBS (1X)	Fisher Scientific	11530546
Lipofectamine™ 3000 Transfection Reagent	Fisher Scientific	15292465	Penicillin-Streptomycin (10,000 U/mL)	PAN-Biotech	15140122
Cell Counting Slides	Bio Rad	1450011	Poly-D-lysine	Sigma-Aldrich	P0899
DMEM, High Glucose	Fisher Scientific	11500416	Sodium Pyruvate	Fisher Scientific	11360070
DPBS (10X), no calcium, no magnesium	Fisher Scientific	11530486	Tissue culture plastic (flasks and plates)	Triplered	TCF012250, TCF011050, TCP011006, TCP011096
FBS Good	PAN-Biotech	P40-39500	Tissue culture plastic (serological pipettes and tubes)	Triplered	CFT011150, CFT011500, CFT001015
Geneticin™	Fisher Scientific	10131035	Trypan Blue Solution (0.4%)	Fisher Scientific	11538886

(G418 Sulphate)					
L-Glutamine	Fisher Scientific	25030081	Trypsin-EDTA (0.05%)	Fisher Scientific	25300054
			Versene Solution	Fisher Scientific	15040033

2.1.9. Miscellaneous

Name	Supplier	Product no.	Name	Supplier	Product no.
20 mm round coverslips	VWR	631-1581	Microscope Slides	Fisher Scientific	10170301
16 mm round coverslips	VWR	631-1579	Nuclease-free water	Qiagen	129114
Agarose Gel-Loading Dye (6X)	Fisher Scientific	10205023	Primers	Integrated DNA technologies	-
D- Luciferin	Nanolight®	2591-17-5	ProLong Gold antifade reagent with DAPI	Fisher Scientific	11569306
E-Plate L8 PET	Cambridge Bioscience	300 600 860	Protease Inhibitors cocktail III	Sigma-Aldrich	539134
Ecoscint H	National Diagnostics	LS-275	ProxiPlate-384 Plus	Perkin-Elmer	6008280
Gblock	Integrated DNA technologies		Sterile PES Syringe Filter 0.2 um	Fisher Scientific	15206869
GeneRuler 1 kb DNA Ladder	Fisher Scientific	10809360	SYBR™ Safe™ DNA Gel Stain	Fisher Scientific	10328162
HyperLadder™ 25bp	Bioline	BIO-33031	Thermowell™ Sealing plates	Corning®	6570
LVis Plate	BMG Labtech	680-101	Whatman® glass microfiber filters	Sigma-Aldrich	WHA1822024

2.2. Methods

2.2.1. General molecular biology protocols

2.2.1.1. Generation of chemical competent bacteria cells

Escherichia coli (DH5 α strain) chemical competent cells were generated by the rubidium chloride method. Bacteria stocks were thawed on ice, streaked into LB agar plates and grown at 37°C overnight (O/N). The day after, a single colony was inoculated into a starter culture of 20 mL of S.O.C. media and amplified under constant shaking conditions (200 rpm) at 37°C O/N. The next morning, the starter culture was transferred into 2X YT media (1:1000 v:v starter culture/2X YT media), under the same shaking and temperature conditions, and the OD₆₀₀ was continuously monitored. When the OD₆₀₀ reached 0.4-0.6, the cultures were chilled on ice and subsequently centrifuged at 5000 x g for 10 min at 4°C (after this point, all steps were performed on ice and with pre-chilled buffers). After discarding the supernatant, the cell pellets were rinsed with a small aliquot of TFB1 (~20 mL), resuspended in TFB1 (1:2.5 v:v TFB1/growth culture) and incubated on ice for 5 min. Cells were further spin down (5000 x g, 4°C and 5 mins), the supernatant was discarded and the pellets were gently resuspended in TFB2 (1:25 v:v TFB2/growth culture). The cells were then incubated on ice for 30 min, aliquoted and snap-frozen with liquid nitrogen.

2.2.1.2. Heat-shock transformation and plasmid amplification

E. coli DH5 α competent cells were thawed on ice and an aliquot (25 μ L) was transferred into round bottom 15 mL tubes. 2 μ L (~5-100 ng) of DNA (for plasmid amplification, PCR product for mutagenesis or Gibson assembly reaction for cloning), were added to the cells and gently mixed by tapping the tubes. After 30 min on ice, cells were heat-shocked on a water bath pre-heated at 42°C for 30 secs and incubated on ice for 2 min. 475 μ L of LB media or S.O.C. media (for mutagenesis and cloning) were added and the mix was incubated for 1 hour at 37°C under constant shaking (250 rpm). 50-100 μ L of cells were immediately spread into LB-agar plates with the corresponding antibiotic resistance (100 μ g/mL and 50 μ g/mL for ampicillin and kanamycin selection, respectively) and incubated at 37°C O/N. The day after, colonies were processed according to the downstream application.

For small plasmid preparation (miniprep), a single colony was picked, inoculated into 10 mL of LB media with antibiotics and grown O/N (200 rpm at 37°C). The day after, the samples

were processed following the miniprep manufacturer's instructions (Macherey-Nalgen™, Germany). For larger-scale DNA isolation (maxiprep), a single colony was picked, inoculated into 5 mL of LB media with antibiotics and grown (200 rpm at 37°C) until turbidity was visually appreciable. The starter culture was then transferred into 250 mL of LB media with antibiotics and grown O/N (200 rpm at 37°C). The day after, maxipreps were performed as per instructed in the kit manual (Promega, UK).

For cloning experiments, colonies were processed as described for miniprep with an additional colony PCR step. Briefly, the same tip used to inoculate the growth culture was placed in 20 µL of nuclease-free H₂O and the solution was pipette up and down several times to induce hypo-osmotic shock. Cultures were further processed based on the expected length of the PCR product after agarose gel electrophoresis.

DNA purity (A_{260}/A_{280}) and concentration (A_{260} , $\epsilon_{dsDNA} = 0.020 \text{ (}\mu\text{g/mL}\cdot\text{cm}^{-1}\text{)}$) were quantified using the LVis Plate (BMG Labtech, Germany) in the CLARIOstar multi-mode microplate reader (BMG Labtech, Germany).

2.2.1.3. Site-directed mutagenesis

For site-directed mutagenesis, two primer design strategies were applied. The first was according to the Quick Change™ site-directed mutagenesis protocol, in which the desired mutation was introduced in the middle of complementary primers (25-45 bases in length) with a melting temperature (T_m) $\geq 78^\circ\text{C}$. These constrains might often be inadequate for genomic regions in which the intrinsic sequence (e.g. low GC content) impedes to fulfil these criteria, and thus primer dimer formation becomes more favourable. Alternatively, primers were designed according to the protocol described by Liu and Naismith⁵²⁹. Briefly, this method combines primers with 5' complementary sequences harbouring the point mutation but with extended non-overlapping 3' ends. Thus, the newly synthesised DNA is not "nicked", allowing it to be used in subsequent amplification cycles, increasing the reaction efficiency at the time that provides greater primer design flexibility. All primer sequences and cDNA templates are detailed in **Annex I**.

50 µL of the reaction mix contained 25 ng of DNA template, dNTP mix at a final concentration of 200 µM each nucleotide, 0.5 µM primer pairs, 1X Phusion® HF buffer and 1U of Phusion® High-Fidelity DNA Polymerase. PCR cycling was carried out using a Veriti thermal cycler (Applied Biosystems, UK), initiated at 98°C for 3 min followed by 25 amplification cycles. Each cycle consisted of 98°C for 1 min, an annealing gradient of 60/65/70°C for 30s and extension at 72°C (20s/Kb). The PCR cycles were terminated with a final 1 min annealing

Materials & Methods

step followed by 30 min extension. To digest parental methylated DNA, the PCR product was treated at 37°C for ≥ 2 hours with 5U of DpnI restriction enzyme and 10 μ L of each PCR product was subsequently analysed by agarose gel (1% w:v) electrophoresis. *E. coli* DH5 α competent cells (50 μ L) were transformed with 2 μ L of positive PCR products following the heat-shock method (see above). Similarly, DNA amplification and isolation (miniprep) were performed as previously detailed using the NucleoSpin® Plasmid kit (Macherey-Nalgen™, Germany). To verify the mutations, DNA Sanger sequencing was carried out by Source Biosciences, UK, using universal T7 forward (5' TAA TACGACTCACTATAGGG 3') and BGH reverse (5' TAGAAGGCACAGTCGAGG 3') primers.

2.2.1.4. Cloning

All constructs encoding fusion proteins were generated by the Gibson assembly method⁵³⁰. Detailed information regarding the backbone vectors, inserts and cloning primers is provided **in Annex II**. This strategy allows the assembly of several DNA fragments in a single step without the necessity of restriction digestion of the DNA fragments/PCR products. Briefly, the different fragments are amplified with primers harbouring two features: a gene-specific sequence required for gene priming and a 5' non-priming overlapping sequence (15-25 bp) homologous to the 5' end of the adjacent fragment. The linearised PCR products are further incubated in a reaction mix containing 5' exonuclease, DNA polymerase and DNA ligase. The exonuclease chews the 5' ends generating single-stranded 3' overhang that facilitate the hybridisation of the overlap regions. The PCR polymerase extends the 3' ends filling in the gaps and the DNA ligase seals the nicks yielding a fully closed dsDNA product⁵³⁰.

The PCR mix and cycling conditions were performed as described for site-directed mutagenesis. Similarly, to avoid parental DNA transformation, the PCR products were digested with DpnI restriction enzyme following the same conditions. The correct size of the vector/inserts was validated by agarose gel (1-2% w:v) electrophoresis and the DNA from the positive bands was purified using the NucleoSpin™ Gel and PCR Clean-up Kit (Macherey-Nalgen™, Germany).

For the Gibson assembly reaction, 100 ng of linearized vector were incubated with the corresponding insert at a 1:3 or 1:5 (for insert sizes less than 200 bp) molar ratios on ice in a final volume of 20 μ L of HiFi DNA Assembly Master Mix (New England Biolabs, UK) and rapidly transferred to a 50°C preheated Veriti thermal cycler (Applied Biosystems, UK). After 15 min, *E. coli* DH5 α competent cells (50 μ L) were transformed with 2 μ L of the assembly reaction by the heat shock method (see above). The day after, single isolated colonies were

picked and processed as previously described for colony PCR. The reaction mix contained 25 μL of DreamTaq PCR Master Mix (2X), primers flanking the insert region (1 μM each) and H_2O to a final volume of 50 μL . PCR cycling was carried out using a Veriti thermal cycler (Applied Biosystems, UK), initiated at 95°C for 3 min followed by 30 amplification cycles. Each cycle consisted of 95°C for 30 sec, annealing for 30s at the primers melting temperature (T_m) minus 5°C and extension for 1 min at 72°C. After a final extension for 15 min at 72°C, the PCR products (50 μL) were analysed by agarose gel (1-2% w:v) electrophoresis. Inoculated cultures yielding the right molecular size band were further processed and the DNA was purified (miniprep) as previously described. To verify the correct cloning, DNA Sanger sequencing was carried out by Source Biosciences, UK. The primers used for sequencing and for colony PCR were the same: universal T7 forward (5' TAATACGACTCACTATAGGG 3') and BGH reverse (5' TAGAAGGCACAGTCGAGG 3') for constructs in pcDNA3.1 backbone, 5' TTGGCAATCCGGTACTGTGG 3' forward and 5' GCAATAGCATCACAAATTTC 3' reverse primers for pBiT1.1-C [TK/LgBiT] and pBiT1.1-N [TK/LgBiT] and 5' TTGGCAATCCGGTACTGTGG 3' forward and 5' GCAATAGCATCACAAATTTC 3' reverse primers for constructs in pBiT2.1-C [TK/SmBiT] and pBiT2.1-N [TK/SmBiT].

2.2.2. Mammalian cell cultures maintenance

Human embryonic kidney 293 (HEK293) cells (ATCC® CRL-1573™) were grown in Dulbecco's modified Eagle's medium supplemented with 2 mM L-glutamine, 4.5 g/L D-glucose, 100 $\mu\text{g}/\text{mL}$ sodium pyruvate, 100 U/mL penicillin, 100 $\mu\text{g}/\text{mL}$ streptomycin and 10% (v:v) heat inactivated fetal bovine serum (Pan Biotech, Germany) at 37°C in a 5% CO_2 humidified atmosphere. Striatal STHdH^{Q7} and STHdH^{Q111} cells (obtained from Silvia Gines' lab) were grown in the same complete media supplemented with 400 $\mu\text{g}/\text{mL}$ G418 (Geneticin®) at 33°C in a 5% CO_2 humidified atmosphere. These striatal-derived progenitor cell lines were originally derived from HdH^{Q111} knock-in and wild-type mice and immortalised using defective retrovirus transducing the tsA58/U19 SV40 large T antigen⁵³¹.

The general maintenance/passage of both HEK293 and striatal cell lines was performed following the same conditions, usually grown in T-75 cm^2 flasks, when the cell cultures reached ~80% confluence. Briefly, the medium was removed and the cell monolayer was rinsed once with ~4 mL of DPBS without Ca^{2+} and Mg^{2+} before the addition of 2.5 mL of Trypsin-EDTA solution. The cells were incubated at 33/37°C for 5-15 min and periodically observed under an inverted microscope until the full dispersion of the cell monolayer. Trypsin

Materials & Methods

activity was neutralised by the addition of 8 mL of complete cell culture media and the cell suspension was centrifuged at 300 x g for 5 min at RT. The supernatant was carefully removed and the cells were gently resuspended in complete cell culture media at different densities depending on their end use.

2.2.3. Transient plasmid DNA transfection

HEK293, STHdH^{Q7} and STHdH^{Q111} cells were transfected with Lipofectamine™ 3000 (Invitrogen, UK) following the standard and reverse transfection strategies. For standard transfection of attached cells, the cell cultures were split the day before so that cell confluence was ~80% on the day of transfection. The following protocol describes the general methods used for transfection in 6 well plates, although, depending on the downstream applications, the volumes were scaled up or down according to the manufacturer's instructions.

2 hours before the transfection, the cell culture media was replaced with 1 mL/well of Opti-MEM® I reduced-serum medium. In a 1.5 mL tube, 1-2 µg of plasmidic DNA and 2-4 µL of P3000™ reagent (1:2 w:v DNA:P3000/Lipofectamine™ ratio) were added to 125 µL of Opti-MEM® media. In a separate tube, 2-4 µL of Lipofectamine™ were added to 125 µL of Opti-MEM® media. Both reaction mixes were vortexed (2-5 sec) and incubated at RT for 5 min. After this time, the diluted DNA was added dropwise to the Lipofectamine™-containing tube and gently mixed by pipetting up and down. After 15 min incubation at RT, the transfection mix was dispensed dropwise to the cells and the plates returned back to the incubator at 33/37°C in a 5% CO₂ humidified atmosphere for six hours. The medium was replaced with complete cell culture media and the cells were further incubated for 48 hours prior to the experiments.

Reverse transfection of HEK293 cells was performed in 96 well plate format. For each well, two transfection mixes were prepared as described above. Briefly, in a 1.5 mL tube, 100-200 ng of plasmidic DNA and 0.2-0.4 µL of P3000™ reagent (1:2 w:v DNA:P3000/Lipofectamine™ ratio) were added to 25 µL of Opti-MEM® media. In a separate tube, 0.2-0.4 µL of Lipofectamine™ were added to 25 µL of Opti-MEM® media. Both reaction mixes were vortexed (2-5 sec) and incubated at RT for 5 min. After this time, the diluted DNA was added dropwise to the Lipofectamine™-containing tube, gently mixed by pipetting up and down and incubated for 15 min at RT. In parallel, cells were trypsinised as described above and resuspended in complete cell culture media to 5 x 10⁵ viable cells/mL. 100 µL of the cell suspension were distributed in each well and 50 µL of the transfection mix

were added on top of the cells. The plates were incubated at 37°C in a 5% CO₂ humidified atmosphere for 24 hours before performing the experiments.

2.2.4. Calcium mobilization assays.

For [Ca²⁺]_i release experiments in HEK293 cells, 50,000 cells/well were seeded in poly-D-lysine coated black clear bottom 96 well plates and reverse transfected with 50 ng/well of GCaMP6s calcium sensor vector and 100 ng/well of receptor (5-HT_{2A,2C} WT receptors, 5-HT_{2A,2C} receptors mutants and 5-HT_{2A,2C} receptors fusion proteins constructs) or 100 ng/well of each CB₁ and 5-HT_{2A} receptors forms when studies required the co-expression of both them. To study the CB₁R/5-HT_{2A}R stoichiometry, a fix amount of 5-HT_{2A}R (100ng/well) was co-transfected with increasing concentrations of the different CB₁R constructs (from 0 to 300 ng/well) in the presence of empty vector (pcDNA3.1) to keep constant the total amount of DNA/well. 24 h after transfection, the cell culture medium was removed and the cells were starved in FBS-free DMEM cell culture media for 4 hours at 37°C in a 5% CO₂ humidified atmosphere. After this time, the cells were rinsed once with calcium assay buffer and the plates were pre-equilibrated for 1 hour with 180 µL of the same solution at 37°C in the dark. When pre-treatment with 5-HT_{2C}R compounds was required, the cells were pre-incubated with 160 µL of assay buffer and 20 µL of the allosteric modulator were added 20 min before the addition of the receptor ligands at the desired concentrations (see figure legends).

To determine calcium release in striatal STHdH^{Q7} and STHdH^{Q111} cells, cells growing at ~80% confluence in T25 flasks were transfected using the standard Lipofectamine™ 3000 method with 4 µg of GCaMP6s calcium sensor according to the protocol described above. After 48 hours, cells were non-enzymatically dissociated using Versene solution and resuspended in calcium assay buffer to yield 1 x 10⁵ cells/well in a final volume of 100 µL. The plates (black clear bottom 96 well plates) were pre-equilibrated for 1 hour at 33°C in the dark and, when TAT-TM peptides treatment was performed, peptides were added over this pre-equilibration step.

Immediately following agonists addition, fluorescence emission intensity was recorded at 515 nm upon excitation at 488 nm in a CLARIOstar Multimode Plate Reader (BMG Labtech, Germany) for 330 secs every 5 sec and 40 flashes per well at 33/37°C. To account for differences in expression/cell density, the average of 5 pre-readings was used to normalise each well's response.

2.2.5. Intracellular cAMP accumulation

HEK293 cells, 50,000 cells/well, were seeded in poly-D-lysine coated white clear bottom 96 well plates and reverse transfected with 50 ng/well of pGloSensorTM-22F cAMP sensor plasmid and 100 ng/well of receptor (CB₁ and CB₂ WT receptors, CB₁ receptor mutants and CB₁ and CB₂ receptors fusion proteins constructs) or 100 ng/well of each CB₁ and 5-HT_{2A} receptors forms when studies required the co-expression of both them. 24 h after transfection, the cell culture medium was removed and the cells were starved in FBS-free DMEM cell culture media for 4 hours at 37°C in a 5% CO₂ humidified atmosphere. After this time, the cells were rinsed once with cAMP assay buffer and the plates were pre-equilibrated in the dark for 2 hours at 28°C with 100 µL of cAMP assay buffer supplemented with 0.45 mg/mL of D-Luciferin. When required, antagonists were pre-incubated for 20 min prior to agonist stimulation. Bioluminescence was quantified over 40 min every 2 min at 28°C in a CLARIOstar® Multimode Plate Reader (BMG Labtech, Germany) with 1s integration time and no lens. Prior to the treatment, 5 measures were taken (2 min intervals), to determine the basal luminescence levels. To account for differences in expression/cell density, the average of these 5 pre-readings was used to normalise each well's response.

2.2.6. Determination of ERK1/2 phosphorylation levels

To measure ERK1/2 (Thr202/Tyr204) phosphorylation in HEK293 cells, 50,000 cells/well were seeded in poly-D-lysine coated clear 96 well plates and reverse transfected with 100 ng/well of receptor (5-HT_{2A} and CB₁ WT or mutant receptors) or 100 ng/well of each CB₁ and 5-HT_{2A} receptors forms when studies required the co-expression of both them. 24 hours after transfection, the cell culture medium was removed and the cells were starved in FBS-free DMEM supplemented with 0.1% (w/v) BSA (hereafter ERK media) for 4 h at 37°C in a 5% CO₂ humidified atmosphere. ERK1/2 phosphorylation levels were measured using the AlphaLISA SureFire UltraTM ERK1/2 cellular assay kit according to the manufacturer's instructions. Briefly, after the starvation period, the cell media was replaced with 50 µL of ERK media containing vehicle or, when necessary, the required antagonist and the plates were incubated for 20 min at 37°C. After agonist stimulation (7.5 min), the media was quickly aspirated, replaced with 50 µL of the proprietary lysis buffer and the plates were agitated (350 rpm) for 30 min at RT. Lysates (10 µL) were transferred to low volume round bottom white 384 well/plates (ProxiPlate-384 Plus) and 5 µL of each donor/acceptor mix beads were sequentially added. Plates were sealed, protected from light and incubated for 24 h at RT before the readings were taken. Fluorescence at 615 nm was analysed on a CLARIOstar

Multimode Plate Reader (BMG Labtech, Germany) equipped with an Alpha Technology optical module.

To determine ERK 1/2 phosphorylation in striatal STHdH^{Q7} and STHdH^{Q111} cells, 35,000 cells/well were cultured with non-supplemented medium ON before. Then, cells were pre-treated at 25°C for 20 min with antagonists/vehicle and subsequently stimulated for an additional period of 7 min with agonists (see figure legends). All further steps were performed as described above.

2.2.7. Bimolecular luminescence/fluorescence complementation assays

2.2.7.1. GPCR oligomerisation studies

To assess GPCR protein:protein interactions with the NanoBiT technology, HEK293 cells (50,000 cells/well) were seeded in poly-D-lysine coated white clear bottom 96 well plates and reverse transfected with the plasmids encoding the complementary NanoBiT hemiprotein fragments. For orientation screenings, cells were transfected with two different concentrations (50 and 100 ng/well) of each receptor alone or in combination with the investigated partner (see figure legends) in the presence of empty vector (pcDNA3.1) to normalise the total amount of DNA/well. For studies in the presence of increasing non-tagged receptor competitors, 100 ng of each receptor pair (CB₁R LgBiT + CB₁R SmBiT, 5-HT_{2A}R LgBiT + 5-HT_{2A}R SmBiT and 5-HT_{2A}R LgBiT + CB₁R SmBiT) were co-transfected with increasing concentrations of the different non-tagged constructs (from 0 to 300 ng/well) and the total amounts of DNA/well were normalised with empty vector (pcDNA3.1). For the screening of stapled peptides, 50 ng/well of both LgBiT CB₁R and SmBiT 5-HT_{2A}R were reverse transfected as previously detailed.

24 hours after transfection, the cell culture medium was removed and the cells were starved in FBS-free DMEM for 4 h at 37°C in a 5% CO₂ humidified atmosphere. The cell culture media was replaced by 100 µL of NanoBiT assay buffer and the plates were pre-equilibrated for 1 hour at RT in the dark. When TAT-TM peptides treatment was performed, peptides were added over this pre-equilibration step, unless when studying inhibition kinetics, in which the peptides were administered immediately after the first luminescence recording. 25 µL/well of a 5X solution of the Nano-Glo® Live cell reagent containing the cell-permeable furimazine substrate dissolved in Nano-Glo® LCS Dilution buffer were added and the luminescence was

Materials & Methods

immediately monitored over 1 hour every 60s at 25°C in a CLARIOstar® Multimode Plate Reader (BMG Labtech, Germany) with 1s integration time and no lens.

2.2.7.2. β -arrestin2 and heterotrimeric G protein recruitment assays

To establish the optimal receptor:arrestin or receptor:G protein pairs, HEK293 cells (50,000 cells/well) were seeded in poly-D-lysine coated white clear bottom 96 well plates reverse co-transfected with the plasmids encoding the receptor (100 ng/well) and the complementary G protein or β -arrestin2 fusions at increasing concentrations (see figure legends) in the presence of empty vector (pcDNA3.1) to account for differences in the total amount of DNA/well. On the basis of these results, 10 ng/well of SmBiT β -arrestin 2 were co-transfected with either 100 ng/well of CB₁R LgBiT or 5-HT_{2A}R LgBiT and 10 or 2.5 ng/well of LgBiT β -arrestin 2 were co-transfected with 100 ng/well of CB₂R SmBiT or 5-HT_{2C}R SmBiT, respectively.

Until the addition of the NanoBiT substrate, cells were processed as detailed in the previous section. 25 μ L/well of a 5X solution of the Nano-Glo® Live cell reagent were added and luminescence readings were taken every minute at 37°C until the signals were stable (20-30 min). When necessary, antagonist pre-treatments were performed over this step. Immediately after, 10 μ L of agonists/vehicle were added and the luminescence was further recorded for 60 min (1s integration time and 1 min intervals for arrestins) or for 30 minutes (0.5 sec integration time and 5s intervals for G proteins) at 37°C using a CLARIOstar® Multimode Plate Reader (BMG Labtech, Germany). To account for differences in expression/cell density, the average of at least 5 stable pre-readings was used to normalise each well response.

2.2.7.3. NanoBiLC BRET

To study the potential higher oligomeric organisation of 5-HT_{2A}R-CB₁R heteromers, we developed a BRET assay based on resonance energy transfer between the functionally reconstituted NanoLuc pairs (donor) and a fluorescently labelled receptor (acceptor). Thus, HEK293 cells (50,000 cells/well) were seeded in poly-D-lysine coated white clear bottom 96 well plates and reverse co-transfected with 50 ng/well of both the N-terminally tagged NanoBiT donor pairs (LgBiT CB₁R and SmBiT 5-HT_{2A}R) and 100 ng/well of either the HaloTag® 5-HT_{2A}R or the HaloTag® CB₁R constructs. 24 hours after transfection, the cell media was removed and replaced with 100 μ L of assay medium (Phenol red-free Opti-MEM® I reduced-serum medium with 4% (w:v) FBS) supplemented with 100 nM HaloTag® NanoBRET™ 618 ligand and the plates were incubated in the dark for 12-16 hours at 37°C in

a 5% CO₂ humidified atmosphere. On the day of the experiment, the plates were equilibrated at 25°C inside the plate reader (15-20 min) before the addition of substrate. 25 µL/well of a 5X solution of the Nano-Glo® Live cell reagent prepared in phenol red-free Opti-MEM® I Reduced Serum Medium were added and BRET measurements were taken every minute at 25°C for 1 hour in a CLARIOstar® Multimode Plate Reader (BMG Labtech, Germany) using the monochromator optic settings (460-60 nm for NanoBiT and 660-100 nm for the HaloTag® ligand, 3600 gain for both wavelengths).

2.2.7.4. Venus YFP Bimolecular Fluorescence complementation assays

HEK293 cells growing at ~80% confluence in 6 well/plates were transfected using the standard Lipofectamine™ 3000 method (see section 2.2.3) with 1.5 µg/well of both Venus YFP complementary plasmids or the corresponding individual receptor constructs. The total amounts of DNA/well were normalised with empty vector (pcDNA3.1). 24 hours after transfection, the cells were detached as described above (see section 2.2.2), 50,000 cells/well were seeded in poly-D-lysine coated black clear bottom 96 well plates and incubated at 37°C in a 5% CO₂ humidified atmosphere O/N. On the day of the experiment (48 hours after transfection), the cell culture media was replaced by 100 µL of NanoBiT assay buffer and the plates were pre-equilibrated for 1 hour at RT in the dark. Venus YFP fluorescence was measured at 530 nm (550-50 nm and 517.2 nm dichroic filter) upon excitation (40 flashes/well) at 489 nm (497-15 nm) in a CLARIOstar Multimode Plate Reader (BMG Labtech, Germany) at 25°C.

2.2.8. Cell viability assays

2.2.8.1. Label-free Determination of striatal STHdH^{Q7} and STHdH^{Q11} cells viability.

The non-invasive label-free technology, xCELLigence Real-Time Cell Analyser (RTCA) instrument (Roche Diagnostics GmbH and ACEA Biosciences), was used to measure cell viability based on changes in electrical impedance over time, which is defined as the cell index (CI) variable⁵³². Prior to the assay, the background CI levels of each well of the 8-well E plate (ACEA Biosciences, USA) were measured after the addition of 200 µL/well of pre-warmed (33°C) striatal complete cell culture media. This background reading was subtracted from all

Materials & Methods

subsequent CI measurements. In parallel, striatal STHdh^{Q7} and STHdh^{Q111} cells growing in tissue culture flasks (<80% confluence) were trypsinised as previously described and resuspended in complete cell culture media to 2.5×10^5 viable cells/mL. 200 μ L of the cell suspension were distributed in each well (50,000 cells/well) and the E plates were left in the tissue culture hood at room temperature for 30 min. After this time, the E-plates were put back in the instrument and cell growth was continuously monitored every 30 min at 33°C in a 5% CO₂ humidified atmosphere. After 24 hours, the E-plates were removed from the device, the cells were treated with 20 μ L of ligands (see figure legends) and returned back to the RTCA analyser. Impedance changes were monitored for the next 72 hours every hour at 33°C in a 5% CO₂ humidified atmosphere. Normalised cell index refers to the ratio between the CI values and CI from the time point immediately prior to ligand addition.

2.2.8.2. Cell death determination with propidium iodide.

Striatal STHdh^{Q7} or STHdh^{Q111} cells were grown at 50% of confluence in 12-well plates containing 3 cm² glass coverslips. The cell culture media was replaced with STHdh cell culture media containing 0.5% (v:v) FBS. When antagonist pre-treatments were required, vehicle, SCH 23390 or Thioperamide were administered and pre-incubated for 1 hour before agonist administration. When TAT-TM peptides were applied, these were added 4 hours before the addition of the D₁R agonist. After SKF 81297 treatment, the cells were incubated for 24 hours at 33°C in a 5% CO₂ humidified atmosphere. Then, the coverslips were covered with a 10 μ M propidium iodide (PI) solution prepared in PBS and the plates were incubated at 37°C for 1 h in the dark. Then cells were washed twice (5 min each) in ice-cold PBS and fixed with 4% (w:v) paraformaldehyde/PBS for 1 hour at 4°C. After two additional washing steps, sample nuclei were stained with Hoechst (0.01mg/mL) for 10 min at RT in the dark, rinsed twice with PBS and mounted with Mowiol. A minimum of 10 fields were taken from each coverslip using a Leica SP2 confocal microscope (20x; UV, 561 lasers) and the Image-based Tool for Counting Nuclei (ITCN) plugin for ImageJ was used to quantify the total nuclei. Cell death is expressed as the percentage of PI positive cells in the total Hoechst-stained nuclei.

2.2.9. Membrane preparation and radioligand binding.

Striatal cells grown in cell culture flasks were rinsed once with ice-cold 50 mM Tris-HCl buffer (pH 7.4), scrapped in the same buffer containing a protease inhibitor mixture (1:1000,

v:v) and the cells were pelleted by centrifugation at 300 x g for 5 min at 4°C. Mouse striatal, cortical or hippocampal tissue and the cell pellets were homogenised in 50 mM Tris-HCl buffer (pH 7.4), containing protease inhibitors, with an Ultra-Turrax homogeniser (~20,000 rpm, 3 times for 5s each). The cellular debris was removed by centrifugation at 13,000 x g for 5 min at 4°C and the membranes were obtained by ultracentrifugation at 105,000 x g for 30 min at 4°C. Membranes were subjected to two additional rounds of homogenisation-centrifugation under the same conditions to ensure thorough homogenisation and the removal of endogenous ligands. The final pellet was resuspended by homogenisation one last time and the protein concentration was quantified using the Pierce™ BCA Protein Assay Kit. Briefly, 25 µL of the samples or albumin standards (5-2000 µg/mL working range) were mixed with 200 µL of the BCA working reagent (50:1 ratio BCA Reagent A/ BCA Reagent B) in clear 96 well plates and incubated at 37°C for 30 min under constant shaking conditions (300 rpm). The absorbance was measured at 562 nm in the CLARIOstar multi-mode microplate reader (BMG Labtech, Germany). After protein quantification, the fresh membrane preparations were subsequently used or stored at -80°C.

Ligand binding was performed with membrane suspension (0.2 mg of protein/mL) in 50 mM Tris-HCl buffer (pH 7.4) containing 10 mM MgCl₂, at 25°C. For the saturation curves, membranes were incubated with increasing concentrations of the D₁R antagonist [³H] SCH 23390 (0.02 nM to 10 nM) or the H₃R agonist [³H]RAMH (0.1 nM to 20 nM) for 2 hours to achieve stable equilibrium. Nonspecific binding was determined in the presence of 30 µM of non-labelled ligands. Free and membrane bound ligand were separated by filtration of 500 µl aliquots in a cell harvester (Brandel, USA) through Whatman glass fibre grade GF/C filters embedded in 0.3% (w:v) polyethylenimine and subsequently washed with 5 mL of ice-cold 50 mM Tris-HCl buffer (pH 7.4). The filters were incubated overnight with 10 mL of Ecoscint H scintillation cocktail at RT under constant shaking. Radioactivity counts were determined using a Tri-Carb 1600 scintillation counter (PerkinElmer, USA) with an efficiency of 62%.

2.2.10. Peptides stability studies

For stability in trypsin and chymotrypsin, to 100 µL of peptide solution (100 µM, dissolved in ammonium bicarbonate buffer, pH7.5), 60 µL ammonium bicarbonate buffer (pH7.5) were added, together with 20 µL of temperature-equilibrated (37°C) trypsin from porcine pancreas or α-chymotrypsin from bovine pancreas (5 µg/mL each; 13,000-20,000 BAEE units/mg protein and > 40 units/mg protein, respectively). Peptides were incubated for 15, 30, 60, 120, 240 and 480min and then MeOH (HPLC Grade) + 0.05% TFA was added. The samples were

Materials & Methods

then centrifuged (15 000 rpm) and supernatant analysed, using Fmoc-Gly (10 μ l, 0.2mM) as an internal standard. The amount of intact peptide remained in the mixture was quantified by RP-HPLC.

For stability in mouse serum, to 200 μ L of fresh non-sterile mouse serum 25 μ l of peptide solution (100 μ M, dissolved in ammonium bicarbonate buffer, pH7.5, containing 10% DMSO) were added, and the mixture was incubated at 37 °C. At the specified time (see figure legends), an aliquot of incubation mixture was withdrawn and quenched by addition of equal volume of 15% trichloroacetic acid in acetonitrile to precipitate out serum proteins (30 min at 4 °C). The mixture was then centrifuged at 13,500 rpm for 10 min and the supernatant was collected and analysed by HPLC as described above.

2.2.11. Microscopy methods

2.2.11.1. 5-HT_{2A} and CB₁ receptors surface expression validation

HEK293 cells growing in poly-D-lysine coated 16 mm coverslips placed in a six well plate, two per well at ~60% confluence, were transiently transfected using the standard Lipofectamine™ 3000 method (see section 2.2.3) with 1 μ g/well of the constructs encoding the wild type CB₁ and 5-HT_{2A} receptors and their corresponding mutants. 48 hours after transfection, the cells were rinsed twice with ice-cold PBS and fixed with 4% (w:v) paraformaldehyde/PBS for 15 min at RT. After three washes with PBS with 20 mM glycine (5 min each), the coverslips were incubated for 60 min at RT with the blocking/permeabilisation solution (PBS with 1% w:v BSA and 0.3% v:v Triton™ X-100). After this time, the blocking/permeabilisation solution was gently aspirated and the primary antibody (anti HA-Tag, 1:1600 v:v diluted in blocking/permeabilisation solution) was applied and incubated overnight at 4°C. The coverslips were rinsed three times with PBS (5 min each) and the cells were incubated for 1 hour at RT in the dark with the secondary antibody (Cy™3 Goat Anti-Rabbit, 1:500 v:v diluted in blocking/permeabilisation solution). The coverslips were rinsed three times with PBS (5 min each) and mounted using ProLong® Gold antifade reagent with DAPI. Images were acquired in a Nikon Eclipse 50i fluorescence microscope using a 100x oil objective (Hg lamp, DAPI and Tx-Red excitation filter cubes).

2.2.11.2. Internalisation studies

For internalisation studies in HEK293 cells, cells growing in poly-D-lysine coated 16 mm coverslips placed in a six well plate at ~60% confluence were transiently transfected using the

standard Lipofectamine™ 3000 method with 1 µg/well of both the H₃R and the D₁R-YFP encoding plasmids. 48 hours after transfection, the cell culture medium was removed and the cells were starved in FBS-free DMEM cell culture media for 4 hours at 37°C in a 5% CO₂ humidified atmosphere. After this time, the cells were pre-incubated for 1 hour under the same conditions with vehicle or the H₃R antagonist Thioperamide (10 µM) prior to agonist administration (30 µM SKF 81297) for the indicated times. To stop internalisation, the cells were rapidly place on ice, washed twice with ice-cold PBS and fixed with 4% (w:v) paraformaldehyde/PBS for 15 min at RT. The coverslips were rinsed twice with PBS containing 20 mM glycine (5 min each) followed by an additional washing step in PBS and mounded using ProLong® Gold antifade reagent with DAPI.

For agonists-mediated D₁R internalisation in striatal cells, STHdH^{Q7} and STHdH^{Q111} cells (~60% confluence) growing in poly-D-lysine coated 16 mm were starved with FBS-free striatal cell culture media for 4 hours at 33°C in a 5% CO₂ humidified atmosphere. After this time, the cells were treated with vehicle or the D₁R agonists SKF 81297 (30 µM) and subsequently place on ice to stop the internalisation. After this point, the protocol was analogous as described above (see section 2.2.11.1) using primary guinea pig anti-D₁R (1:100 v:v) and secondary goat anti guinea pig Alexa Fluor® 488 (1:100 v:v) antibodies. Nuclei were stained with Hoechst (0.01mg/mL) for 10 min at RT in the dark, rinsed twice with PBS and mounted with Mowiol. Images were acquired in a Zeiss LSM510 META confocal using a 63x oil objective (Ar 364 nm and 488 nm lasers).

2.2.11.3. Two-photon polarization microscopy (2PPM)

HEK293 cells growing in 8-well microscopy slides (~80% confluence) were transiently transfected using the Lipofectamine™ 2000 according to the manufacturer protocol. Equimolar amounts of all constructs were used in co-transfections and the cells were incubated for 24-48 hours at 37°C in a 5% CO₂ humidified atmosphere. Prior to imaging, DMEM cell culture media was replaced with HEPES-buffered HBSS (20 mM HEPES, pH 7.4) and the 5-HT_{2A}R and CB₁R agonists (100 nM and 10 µM, respectively) were applied at room temperature.

The 2PPM technique and image analysis procedures have been described in detail previously^{533,534}. Briefly, 2PPM observations were carried out on a customised laser scanning microscope (FV1200, Olympus, Japan) equipped with a titanium:sapphire laser (Mai Tai, Spectraphysics, USA), using a UApon340 40x water-immersion objective lens (Olympus, Japan). A long-pass dichroic mirror and an emission filter (BF460-500) separated

Materials & Methods

fluorescence from the excitation laser beam. Fluorescence was detected in a non-descanned arrangement, by a photomultiplier (FV10 MPIXDZCH) equipped with an IR-reflecting dichroic mirror (NRDM690). Excitation light polarization was alternated between horizontal and vertical by a polarization modulator (RPM-2P, Innovative Bioimaging, USA) synchronised with the microscope and operating at 100 kHz. Images were typically acquired at 100 nm x 100 nm pixel size and 10 μ s pixel dwell time. Raw images were deinterleaved into pairs of images, showing fluorescence excited with light polarized horizontally and vertically, respectively. Images were processed and quantitatively analysed as described previously^{533,534}. Linear dichroism was quantitatively expressed as a logarithm of the dichroic ratio ($\log_2(r_{\max})$) observed in sections of the cell outline oriented horizontally or vertically. At least 12 cells were quantitatively analysed for each experimental condition.

2.2.11.4. In Situ Proximity Ligation Assays (PLA)

For PLA experiments, 4-, 6- and 8-month-old Hdh^{Q7/Q7} and Hdh^{Q7/Q111} mice were deeply anaesthetised and immediately perfused transcardially with saline (PBS) followed by 4% (w:v) paraformaldehyde/PBS. Brains were removed and post-fixed overnight in the same solution, cryoprotected by immersion in 10, 20, 30% (w:v) gradient sucrose (24 hours for each sucrose gradient) at 4°C and then frozen in dry ice-cooled methylbutane. Serial coronal cryostat sections (30 μ m) through the whole brain were collected in PBS-0.025% azide as free-floating sections and stored at 4°C until PLA experiments were performed. Striatal STHdH^{Q7} and STHdH^{Q111} cells were seeded in glass coverslips and fixed following the same conditions previously detailed (see section 2.2.11.2).

Cells or mouse brain slices mounted on glass slides were washed on time with TBS buffer (50 mM Tris-HCl, 150 mM NaCl, pH 7.5), permeabilised with TBS containing 0.01% (v:v) Triton™ X-100 (TBS-T) for 10 min at RT and successively washed with TBS. Heteromers were detected using the Duolink II in situ PLA detection Kit following the instructions of the supplier. Briefly, the samples were blocked with Duolink® blocking solution for 30 min at 37°C in a pre-heated humidity chamber prior to overnight incubation with the primary guinea pig anti-D₁R (1:200 v:v) and rabbit anti H₃R (1:200 v:v) antibodies at 4°C in a humidity chamber. The slides were washed one time for 5 min with TBS-T and incubated with a mix containing both the Duolink® PLA probes anti-guinea pig minus and anti-rabbit plus (1:5 v:v in Duolink® antibody diluent) for 1 hour at 37°C in a pre-heated humidity chamber. After this time, two washing steps with TBS-T, 5 min each, were performed before proceeding to the ligation and amplification steps using the Duolink® detection reagent red. Thus, the samples were incubated with the Duolink® hybridisation solution (1:5 v:v diluted in nuclease-free

water) in a pre-heated humidity chamber for 15 min at 37°C. The slides were rinsed on time with TBS-T and a 1:40 (v:v) dilution of Duolink® ligase in Duolink® ligation solution was applied for 15 min at 37°C in a pre-heated humidity chamber. For the amplification step, the samples were washed with TBS-T, twice 1 minute each, and incubated with the Duolink® Polymerase (1:80 v:v diluted in Duolink® amplification solution) for 100 min at 37°C in a pre-heated humidity chamber. The final washing steps were performed with serial dilutions of the Duolink® wash buffer (twice 10 minute each with 1X wash buffer and 1 minute with 0.01X wash buffer), the slides were dried at RT in the dark and mounted with Doulink® mounting medium with DAPI.

The samples were observed in a Leica SP2 confocal microscope (Leica Microsystems, Germany) using a 63x oil objective (UV 405 nm and DPSS 561nm lasers). For each field of view a stack of two channels (one per staining) and 9 to 15 Z stacks with a step size of 1 µm were acquired. For PLA with brain slices, after image processing, the red channel was depicted in green colour to facilitate detection on the blue stained nucleus and maintaining the colour intensity constant for all images. A quantification of cells containing one or more spots versus total cells (blue nucleus) and, in cells containing spots, the ratio r (number of red spots/cell containing spots) were determined, using the Fiji package (<http://pacific.mpi-cbg.de/>), considering a total of 600-800 cells from 4-10 different fields within each brain region from 3 different mice per group.

2.2.12. Computational modelling

2.2.12.1. 5-HT_{2A} and CB₁ receptors homology modelling

5-HT_{2A}R protomers were modelled based on the homology with the 5-HT_{2B}R using the crystal structures of the inactive (PDB:4IB4, for the protomer that does not bind G_i) or active (PDB:5TUD, for the protomer that does bind G_i) 5-HT_{2B}R^{135,535}. CB₁R protomers were modelled based on the inactive (PDB:5U09, for the protomer that does not bind G_i) or active (PDB:5XRA, for the protomer that does bind G_i) crystal structures^{34,403}. Both active models incorporate the large movement of TM6 as it appears in the crystal structure of the β₂-AR in complex with G_s (PDB:3SN6)²⁸. Both inactive protomers, which from the heteromeric interface, incorporate the orientation of TMs 5 and 6 present in the crystal structure of the µ-opioid receptor (PDB:4DKL)²¹⁵. All protomeric models lack the N-terminus and the C-terminus just after helix 8; the long third intracellular loops could not be modelled and were

Materials & Methods

replaced by 8 glycines each. G_i was modelled using a multi-template alignment combining the structure of G_i in the closed conformation (PDB:1AGR)⁵³⁶ and G_s in the β_2 -AR- G_s complex with (PDB:3SN6)²⁸. Modeller 9.18 was used to build all protomeric models⁵³⁷.

The model of the 5-HT_{2A}R-CB₁R heterotetramer bound to two G_i (closed α_i AH domains) was build following the protocol recently used for the A₁R A_{2A}R tetramer⁵³⁸, except that the TM4/5 interface was modelled using the recent crystal structure of the A₁R (PDB:5UEN)⁵³⁹. The molecular models of the 5-HT_{2A}R-CB₁R heterotetramer bound to two G_i were embedded in a pre-equilibrated box containing a lipid bilayer (~800 POPC molecules) with explicit solvent (~110,000 waters) and 0.15 M concentration of Na⁺ and Cl⁻ (~1,800 ions). These initial complexes were energy-minimised and subsequently subjected to a 21 ns Molecular Dynamic (MD) equilibration, with positional restraints on protein coordinates. The production (unrestrained) run lasted 750 ns. MD simulations were produced at constant pressure and temperature using the GROMACS 2016 simulation package⁵⁴⁰. The force field employed combines AMBER99SB force field and Berger parameters for POPC lipids as previously described⁵⁴¹. PyMOL2.0 [The PyMOL Molecular Graphics System, Version 2.0 Schrödinger, LLC.] was used to generate all molecular figures and to compute the electrostatic potential surface of G_i and G_q .

2.2.12.2. Orthosteric ligand binding to the 5-HT_{2C}R

The crystal structure of the active 5-HT_{2c} receptor in complex with the agonist ergotamine (ERG) at 3.0Å resolution (PDB:6BQG)⁵⁴² was used to estimate the molecular interactions of the endogenous serotonin (5-HT) and the positive allosteric modulator VIVIA012 (Compound 11) to the 5-HT_{2c}R. First, 5-HT was docked into the 5-HT_{2c}R structure using the Molecular Operating Environment (MOE)⁵⁴³. One hundred flexible docking poses were produced by the triangle matcher algorithm into the orthosteric site of the receptor and the high score solution was energy minimised. The resulting 5-HT_{2c}R-5-HT complex was embedded in pre-equilibrated lipid bilayer containing 170 POPC molecules, 16.000 (TIP3P) waters and 258 monoatomic Na⁺ and Cl⁻ ions (0.2 M). Taking into account that agonists alone are not able to preserve a fully active conformation of the receptor in the absence of the G protein, the 5-HT_{2c}R-5-HT complex was further stabilised by the inclusion of the G protein mimic nanobody particle towards the cytoplasmic region⁵⁴⁴. The resulting molecular system was subject to a 10.000 steps of energy minimisation, followed by 20.0 ns of gradual relaxation of positional restraints in receptor backbone coordinates using the GROMACS software v4.5⁵⁴⁰. After equilibration, 1.0 μ s unrestrained MD simulation was produced. Analysis of the MD trajectory revealed that the protonated amine and the hydroxyl groups of SRT where in close contact

with Asp134(3.32) and Ser219(5.43) residues throughout all the simulation, in a similar orientation as the related catecholamines adrenaline and isoprenaline in adrenergic receptors (PDB:4LDO and 2Y03).

2.2.12.1. Allosteric ligand binding to the 5-HT_{2c}R

Ten evenly spaced snapshots were extracted from the MD trajectory of the 5-HT_{2c}R-5-HT molecular complex and used in molecular docking experiments of the VIVIA012 allosteric modulator. The Site Finder application in MOE was used to localise the binding cavities from the 3D atomic coordinates of selected structures and one hundred flexible docking poses were produced. The five top-ranking solutions were further studied during 100ns MD simulations with the GROMACS MD simulation package. All simulations were run at a constant temperature of 300 K by using separate v-rescale thermostats for the protein, ligands and solvent molecules. Lennard–Jones interactions were computed by using a cut-off of 10.0 Å, and electrostatic interactions were treated by using PME with the same real-space cut-off. A time step of 2.0 fs was used. The Amberff99SB-ILDN force field was used to describe protein atoms, whereas the general Amber force field (GAFF) and HF/6-31G*-derived RESP atomic charges were used for the ligands.

2.2.13. *In vivo* experiments

All procedures were conducted in adherence to the European Communities Council Directive (86/609/ECC) and Spanish regulations (BOE 252/34367-91, 2005) for the use of laboratory animals. They were reviewed and approved by the local animal care committee of the Universitat de Barcelona (99/01) and the Generalitat de Catalunya (00/1094) (Barcelona, Spain) and by the Comisión de ética e Investigación, Hospital Carlos Haya (Malaga, Spain).

2.2.13.1. Animals

Knock-in mice models of Huntington's disease, with targeted insertion of 109 CAG repeats that extends the glutamine segment in murine huntingtin to 111 residues, and the corresponding littermates having 7 glutamine residues were maintained on a C57BL/6 genetic background⁵⁴⁵. Hdh^{Q7/Q111} heterozygous males and females were intercrossed to generate age-matched Hdh^{Q7/Q111} heterozygous and Hdh^{Q7/Q7} wild-type littermates. Only males were used for all experiments. Animals were housed in a humidity- and temperature-controlled (22 °C)

Materials & Methods

vivarium on a 12 h light/dark cycle (lights off at 9 PM) with water and standard laboratory chow available *ad libitum*.

For *in vivo* evaluation of the 5-HT_{2C}R allosteric modulator, male Wistar rats (Charles Rivers Laboratories, Spain) weighing 200-250 g and aged 10-12 weeks at the beginning of the experiments were used. Rats were made obese after 8 weeks treatment with high fat diet (HFD, 60% fat diet-D12492, Brogaarden, Denmark) containing 5.24 kcal/g (20% of the metabolisable energy content was protein, 20% carbohydrates and 60% fat). Animals were housed in a humidity- and temperature-controlled (22 °C) vivarium on a 12 h light/dark cycle (lights off at 8 PM) with HFD and water available *ad libitum*.

2.2.13.2. HD mice Thioperamide treatment

Thioperamide maleate salt was prepared fresh daily being dissolved in sterile saline (0,9% w:v NaCl) in order to deliver a final dose of 10 mg/kg in a final volume of 0.01 mL/g of body weight⁵⁴⁵. The vehicle treatment consisted of an equal volume of saline solution. All injections were given via the intra-peritoneal route (*i.p.*). Three *i.p.* injections per week were administered to wild-type Hdh^{Q7/Q7} and mutant knock-in Hdh^{Q7/Q111} mice from 5 months of age until 6 months of age (when one cohort of animals was perfused to analyze PLA after behavioral assessment) or until 8 months of age (when a second cohort of animals were perfused to analyze PLA at this more advanced disease stage). A total of 11 saline-Hdh^{Q7/Q7} mice, 10 thioperamide-Hdh^{Q7/Q7} mice, 7 saline-Hdh^{Q7/Q111} mice and 9 thioperamide-Hdh^{Q7/Q111} mice were treated. All treatments were performed in the afternoon to avoid the stress caused by the treatments during the behavioral assessment. Thus, during behavioral analysis treatments were performed after the evaluation of motor learning or cognitive tasks.

2.2.13.3. Acute feeding suppression

Adult rats were food deprived for 16 h prior to refeeding, to habituate the animals to the procedure. On the testing day, and after food deprivation, the animals were pre-treated with the inhibitor of the serotonin re-uptake system sertraline (doses of 2 and 5 mg/kg dissolved in sterile saline) by *i.p.* injection 30 min prior to compound 11 administration. 11 was *i.p.* injected at the doses of 0.5, 2 and 10 mg/kg dissolved in sterile saline and food and water intake were then measured at 30, 60, 20 and 240 min after the presentation of food.

2.2.13.4. Behaviour assays in HD mice

For the accelerating rotarod performance test, the animals were placed on a motorised rod (30mm diameter) and the rotation speed gradually increased from 4 to 40 rpm over the course of 5 min. The time latency was recorded when the animal was unable to keep up on the rotarod with the increasing speed and fell. Rotarod training/testing was performed as 4 trials per day during 3 consecutive days. A resting period of one hour was left between trials and rotarod apparatus was rigorously cleaned with ethanol between animal trials in order to avoid odours.

The novel object recognition test (NORT) consisted in a white circular arena of 40 cm diameter and 40 cm high. Mice were first habituated to the open field arena in the absence of objects (2 days, 15 min/day) whilst several parameters were measured to ensure the proper habituation of all animals in the new ambient. As a measure of anxiety or motivation behaviours, the distance that each mice rove in the periphery or in the center of the open field arena was measured as the rove distance in the periphery or in the center x 100/the total distance. The same analysis was performed by counting the number of entries in the periphery and in the center as well as the time that each mouse spent exploring the periphery or the center. The total distance that each mouse rove during these two days of habituation was also recorded as a measure to evaluate spontaneous locomotor activity. On the third day, two similar objects were presented to each mouse during 10 min (A, A' condition) after which the mice were returned to their home cage. Twenty-four hours later (LTM), the same animals were re-tested for 5 min in the arena with a familiar and a new object (A, B condition). The object preference was measured as the time exploring each object x 100/time exploring both objects. The arena was rigorously cleaned with ethanol between animal trials in order to avoid odors. Animals were tracked and recorded with SMART junior software (Panlab, Spain).

For T-maze spontaneous alternation task (T-SAT), the T-maze apparatus used was a wooden maze consisting of three arms, two of them situated at 180° from each other, and the third, representing the stem arm of the T, situated at 90° with respect to the other two. All arms were 45 cm long, 8 cm wide and enclosed by a 20-cm wall. Two identical guillotine doors were placed in the entry of the arms situated at 180°. In the training trial, one arm was closed (new arm) and mice were placed in the stem arm of the T (home arm) and allowed to explore this arm and the other available arm (old arm) for 10 min, after which they were returned to the home cage. After 5 h (LTM), mice were placed in the stem arm of the T-maze and allowed to freely explore all three arms for 5 min. The arm preference was determined by calculating the time spent in each arm x 100/time spent in both arms (old and new arm). The T-maze was rigorously cleaned with ethanol between animal trials in order to avoid odours.

2.2.14. Data analysis, curve fitting and graphing

Data were analysed using unpaired two-tailed t-tests (between groups) followed by Holk-Sidak corrections, Wilcoxon signed rank test in 2PPM experiments and by one-way (1 factor, >2 levels) or two-way (2 factors, >2 levels) analysis of variance (ANOVA) with Bonferroni post hoc tests.

Dose-response curves were fitted using a four-parameter logistic nonlinear regression mode (Eq.1) where Y is the expected response at dosage X, a is the minimum asymptote when X=0, b is the maximum asymptote when X→∞, EC/IC₅₀ is the concentration at which 50% of the response is achieved and the Hill Slope is the slope at the steepest part of the curve.

Saturation response curves were fitted using a logistic nonlinear regression mode accounting for the specific (Y_{esp}) and non-specific binding (Y_{ns}), Eq. 2 and 3, respectively. Where X is the ligand concentration, B_{max} is the maximum specific binding when X→∞, K_D is the equilibrium dissociation constant, NS is the slope of the non-specific binding and background is the Y_{ns} when X=0.

Peptide stability data were fitted using a nonlinear regression mode for dissociation kinetics (Eq. 4) where Y is the expected intact fraction at time X, Y₀ is the intact fraction at time 0, K is the rate constant, and NS is Y when t → ∞.

$$\text{Eq. 1} \quad Y = a \frac{b-a}{1 + \left(\frac{EC_{50}}{X}\right)^{\text{Hill Slope}}}$$

$$\text{Eq. 2} \quad Y_{\text{esp}} = \frac{B_{\text{max}} \cdot X}{K_D + X}$$

$$\text{Eq. 3} \quad Y_{\text{ns}} = NS \cdot X + \text{Background}$$

$$\text{Eq. 4} \quad Y = (Y_0 - NS)^{-K \cdot X} + NS$$

All statistical test, curve fitting and graphing were performed using GraphPad Prism 6.0h (GraphPad Software, La Jolla, CA). Information on the statistical test, significance and experimental replicates are provided in the figure legends. Microscopy images were assembled using ImageJ 1.51u (NIH) and the final figures were generated in Microsoft Power Point 15.41 (Microsoft corporation, Redmond, Washington).

Chapter 3

Developing BiLC-based Methods to Study GPCR protein:protein Interactions

3.1. Introduction

Protein-protein interactions (PPIs) regulate a plethora of biological processes, including the cell cycle, signal transduction and homeostatic balance. Accordingly, PPIs are intimately linked to the development of pathological states⁵⁴⁶. Except in isolated cases, proteins do not act alone, making up bigger molecular complexes to execute multiple biological functions. Over the last decades, advances in structural biology, the expansion of computational tools and the development of more reliable high-throughput screening assays have contributed to progressively unravelling the map of PPIs occurring in living organisms, also known as “the interactome”. Thus, today PPIs are proving successful in drug discovery^{547,548}.

One family of proteins where PPIs are less exploited is the family of GPCRs. For the past 20 years, it has been known that GPCRs can expand their functionality through homo/heteromerisation^{188,249,549}. As discussed above (see section 1.2.4), a wide variety of biochemical and biophysical techniques have been essential for the identification and characterisation of these receptor complexes. Among them are the RET-based approaches and protein complementation assays, which provide information in a non-destructive way of the cellular events occurring in living cells⁵⁵⁰. To date, FRET and BRET methods are still the most widely used strategies to identify GPCR oligomers. This is partially due to the inherent limitations of the earlier developed BiFC and BiLC protein pairs, including time for the maturation of the fluorophore, irreversibility of the bimolecular complexes under some conditions and the finite affinity between the protein fragments^{276,551}.

Recently, Dixon and collaborators took advantage of the small and bright NanoLuc luciferase to develop a new complementation reporter assay known as NanoLuc binary technology (NanoBiT)²⁷⁸. This BiLC assay is based on the functional reconstitution of NLuc after the interaction between LgBiT (18kDa subunit) and SmBiT (11 amino acid peptide). Importantly, the low intrinsic affinity between the split pairs (~190 μ M), NLuc high quantum yield, the specificity of its substrate and performance over different temperature ranges (20-37°C) provide an exciting tool to monitor dynamic processes at the subcellular level²⁷⁸.

We hypothesised that this technology might provide a more sensitive complementation approach than the widely used Venus-YFP BiFC for the study of GPCR oligomers. Using NanoBiT complementation, we validate the presence of the recently described heteromeric complexes between CB₁ and the 5-HT_{2A} receptors as well as the homodimeric arrangements between CB₁ and 5-HT_{2A} receptors, supporting a better performance of NanoLuc complementation in terms of sensitivity, assay window and hands-on time^{184,410,552}.

Developing BiLC-based Methods to Study GPCR protein:protein Interactions

As illustrated in **Table 3.1**, several authors successfully implemented this technology to monitor arrestin recruitment to GPCRs upon receptor activation. Since its discovery in the late 1980s, different unappreciated properties of β -arrestins have come to light. Arrestins are not just steric inhibitors of GPCR signalling, but also take part in a wide range of biological processes, scaffolding effector proteins of a given signalling pathway (e.g. Raf-1, JNK3 and Akt) and components of the endocytic machinery⁵⁵³. In addition, the ability of certain agonists to preferentially activate some but not all signalling pathways through bias (reviewed in more detail in section 1.3.2) has motivated the development of better β -arrestin recruitment assays^{86,554}. In this regard, three approaches all of them requiring the generation of fusion proteins have been extensively used: (1) high-content (HC) imaging-based redistributions assays, (2) enzyme fragment complementation or gene reporter assays (e.g. PathHunter® and Tango™) and (3) BRET-based approaches. Although HC-based assays provide temporal and spatial resolution of the GPCR:arrestin interaction, their main disadvantage is the inherent need of HC analysis systems. On the other hand, fragment complementation/gene reporter strategies can be performed in most standard benchtop plate readers, although fail to depict the dynamic nature of this interaction. Alternatively, arrestin BRET assays allow to follow arrestin kinetics, but can often be hindered by the dipole orientation and large size of the complementary RET pairs^{555,556}. Therefore, NanoBiT pairs' small size and its fast association/dissociation kinetics provide an alternative strategy to overcome most of these limitations.

Accordingly, we developed a NanoBiT-based assay to monitor 5-HT_{2A}R: β -arrestin2 interactions as well as to quantify β -arrestin2 binding to both the cannabinoid type 1 and 2 receptors. Our results on CB₁ and CB₂ receptors are in agreement with those recently published by Cannaert et al., whilst, for the first time, we have applied this technology for the 5-HT_{2A}R⁵⁵⁷. Importantly, this receptor has been extensively studied at the level of bias or functional selectivity, as some of its ligands such as lysergic acid dimethylamine (LSD) or the 2,5-dimethoxy-4-iodoamphetamine (DOI) exert hallucinogenic effects. However, the mechanism underlying the absence of psychedelic effects in response to the endogenous ligand, serotonin (5-HT), remains elusive^{29,558-560}.

Based on the versatility of NanoBiT to address GPCR oligomerisation and arrestin dynamics, we addressed a more challenging interaction from the point of view of its fast kinetics and dynamic nature; heterotrimeric G protein binding. G protein activation is the first and characteristic hallmark following agonist binding. However, although it has a central role in signal transduction, the rules governing receptor:G protein interactions remain among the most elusive challenges in GPCR pharmacology and only recently we have begun to understand their association/dissociation kinetics, confinement in the plasma membrane and

Table 3.1. PPIs detected using NanoBiT.

Cells type	Interaction tested	Reference
HEK 293T	FRB:FKBP β_2 AR: β -arrestin2 V ₂ R: β -arrestin2 PRKACA:PRKR2A	278
COS7 Neuro2a	SOD1:SOD1	561
HEK 293T	CB ₁ R: β -arrestin2 CB ₂ R: β -arrestin2	557
HEK 293T	RGS: G α	562
HEK 293	GPR27V2R: β -arrestin2	563
COS-7 LNCaP	PHB:E2F1	564
HEK 293T	ER:ER ER:PELP1	565
CHO	GHSR1a:MRAP2	566

Recently validated PPI interactions using NanoBiT technology. β_2 AR, β_2 adrenergic receptor; CB₁R, cannabinoid type 1 receptor; CB₂R, cannabinoid type 2 receptor; E2F1, transcription factor E2F1; ESR1, estrogen receptor 1; FKBP, FK506-binding proteins; FRB, FKBP12-rapamycin binding domain of mTOR; G α , heterotrimeric G protein α subunit; GHSR1, growth hormone secretagogue receptor type 1; GPR27V2R, GPR27 vasopressin receptor 2 chimera; MRAP2, melanocortin 2 receptor accessory protein 2; PELP1, proline, glutamate and leucine rich protein 1; PHB, prohibitin; PRKACA, protein kinase A catalytic subunit; PRKR2A, protein kinase A type 2A regulatory subunit; RGS, regulator of G protein signalling; SOD1, superoxide dismutase 1; V₂R, vasopressin receptor 2.

the structural motifs driving their specificity^{21,44,45,307,567}. In fact, most of our understanding comes from the pharmacological blockage of G proteins with toxins, biochemical assays in the presence of non-hydrolysable G protein substrates analogues or measuring downstream activated pathways. However, recent advances in plasmon waveguide resonance (PWR) spectroscopy, single-molecule imaging, fluorescent polarization microscopy and new resonance energy transfer protein pairs have contributed to provide some answers to this complex process^{307,335,533,567-569}. Thus, the development of new biophysical techniques with increased sensitivity and spatiotemporal resolution still remains a challenging task. Accordingly, we sought to apply the NanoBiT technology to monitor the direct coupling between 5-HT_{2A} and CB₁ receptors to its cognate heterotrimeric G proteins, showing that, although significant interactions were detected in the basal state, this approach fails to provide kinetic resolution after agonist binding.

Developing BiLC-based Methods to Study GPCR protein:protein Interactions

Overall, our data strongly supports that NanoBiT minimal steric burden, high sensitivity and adequacy within the dynamics of protein-protein interactions provides an excellent tool for investigating GPCRs interacting between them at the plasma membrane as well as their transient interactions with cytosolic effectors. In addition, illustrating the versatility of NanoBiT BiLC in PPIs drug discovery, we developed a sensitive assay for the identification of peptides disrupting GPCR oligomerisation. Specifically, we screened a small library of synthetic peptides that lead us to the identification of a small synthetic stapled peptide with improved stability and selectivity towards 5-HT_{2A}-CB₁ receptor heteromers.

3.2. Results

3.2.1. NanoBiT Bimolecular Luminescent Complementation (BiLC) technology provides a versatile tool for the study of GPCR oligomerisation

In order to assess whether NanoBiT BiLC may be a suitable system to study GPCR oligomerisation, we generated CB₁R and 5-HT_{2A}R constructs with the small and large BiT pairs (SmBiT and LgBiT, respectively) attached to the C-terminus end of both receptors. Thus, a total of four fusion proteins were generated, with Sm/LgBiT fused after the Gly/Ser rich flexible linker and under the control of the herpes simplex virus thymidine kinase gene promoter (HSV-TK) (**Figure 3.1A**). Next, we performed conformational screenings to assess the optimal configuration for all receptor pairs. Accordingly, when analysing 5-HT_{2A}R-CB₁R heteromers, HEK293 cells were transiently transfected with all possible combinations of 5-HT_{2A}R-Lg/SmBiT and CB₁R-Lg/SmBiT at two different DNA ratios (**Figure 3.1B**). Surprisingly, none of the analysed configurations yielded a positive interaction. This heteromer has been recently characterised both *in vivo* and in heterologous expression systems using a broad range of biochemical approaches¹⁸⁴. Similarly, when addressing the formation of CB₁R and 5-HT_{2A}R homodimers, none of the examined orientations nor DNA ratios exhibit significant differences in comparison with the individual receptors when expressed by themselves (**Figures 3.1C-D**). Importantly, to rule out whether these negative results might reflect the unsuitability of the NanoBiT system for the analysis of GPCR oligomerisation rather than any kind of experimental hindrance, we analysed the known interaction between the protein kinase A catalytic (PRKACA) and type 2A regulatory (PRKAR2A) subunits. This protein pair positive control has been previously optimised, being LgBiT-PRKAR2A and SmBiT-PRKACA the optimal configuration²⁷⁸. In agreement, co-transfection of both proteins resulted in a significant increase in the luminescence recorded over the different receptor ratios. Furthermore, co-transfection of LgBiT-PRKAR2A with a non-interacting fusion protein (HaloTag®-SmBiT) did not yield any increase in luminescence (**Figure 3.1E**), supporting the specificity of the detected interaction and the suitability of this system under our assay conditions. However, our results do not rule out whether the complementary fusions restrict 5-HT_{2A}R or CB₁R functionality or if the lack of complementation is in fact the actual scenario. In addition, it should be noted that to minimise potential non-specific interactions all generated constructs were under the control of the HSV-TK promoter.

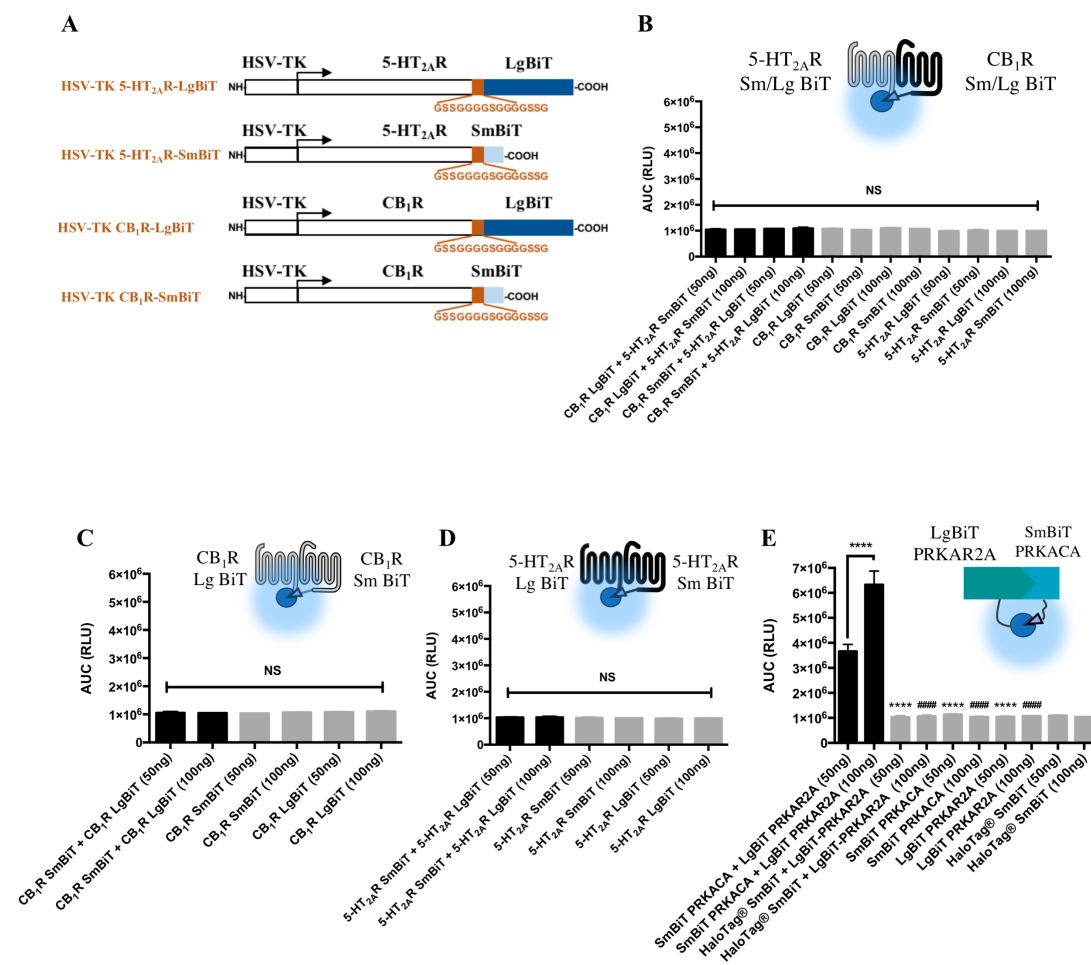


Figure 3.1. Conformational screening of the optimal orientations for CB₁, 5-HT_{2A} and 5-HT_{2A}-CB₁ receptors oligomers. HSV-TK promoter studies. (A) Schematic representation of the NanoLuc fusion proteins. HEK 293 cells were transiently transfected with all possible fusions of LgBiT and SmBiT to the C-terminal domain of the 5-HT_{2A} and CB₁ receptors at two different DNA ratios (50 or 100 ng receptor/well) to assess 5-HT_{2A}-CB₁R heteromers **(B)**, CB₁R homodimers **(C)** and 5-HT_{2A}R homodimers. In **(E)**, the SmBiT-PRKACA and LgBiT-PRKAR2A positive controls were transfected under the same conditions and compared to the non-interacting LgBiT-PRKAR2A and HaloTag®-SmBiT negative controls. Grey bars represent the RLU of each individual construct expressed alone. Data are mean AUC (RLU) ± SEM (n = 3). Statistical significance was evaluated by one-way analysis of variance (ANOVA) followed by Bonferroni post hoc tests showing significant effects for SmBiT PRKACA + LgBiT PRKAR2A (50 ng) over SmBiT PRKACA + LgBiT PRKAR2A (100 ng), HaloTag®SmBiT + LgBiT PRKAR2A (50ng) or each individual equivalent construct (****p ≤0.0001) and SmBiT PRKACA + LgBiT PRKAR2A (100 ng) over HaloTag®SmBiT + LgBiT PRKAR2A (100 ng) or each individual equivalent construct (####p ≤0.0001). HSV-TK, herpes simplex virus thymidine kinase promoter; NS, non-statistical significant.

Thus, in order to address these options, we performed second messenger signalling experiments and re-cloned all four receptors configurations under the control of the high-level

expression cytomegalovirus (CMV) promoter. Interestingly, all 5-HT_{2A}R constructs in an HSV-TK context failed to elicit intracellular calcium release (canonical signalling pathway downstream the the G_{q/11}- coupled 5-HT_{2A}R) after agonist stimulation⁵⁷⁰. However, both 5-HT_{2A}R-LgBiT and 5-HT_{2A}R-SmBiT displayed similar efficacies and potencies in comparison to the wild type (WT) receptor when expressed under the control of the CMV promoter (**Figure 3.2A**). Similarly, we assessed CB₁R-driven adenylate cyclase (AC) inhibition with analogous results. Both CMV-regulated CB₁R constructs inhibited the Forskolin (FK)-induced cAMP release with equivalent potencies and efficacies to the WT CB₁R receptor. However, under the HVS-TK promoter, CB₁R-LgBiT failed to signal through heterotrimeric G_{i/o} proteins and CB₁R-SmBiT exhibited a reduced AC inhibitory activity (~20%) when compared to WT CB₁R receptor (**Figure 3.2B**). These results indicate that the NanoBiT fusions do not adversely affect 5-HT_{2A} nor CB₁ receptor functionality, as the ligands potencies and maximal efficacies are within the wild type receptors ranges. Thus, the absence of luciferase complementation between HSV-TK regulated constructs might reflect low levels of receptor expression, rather than steric hindrance of the interacting pairs.

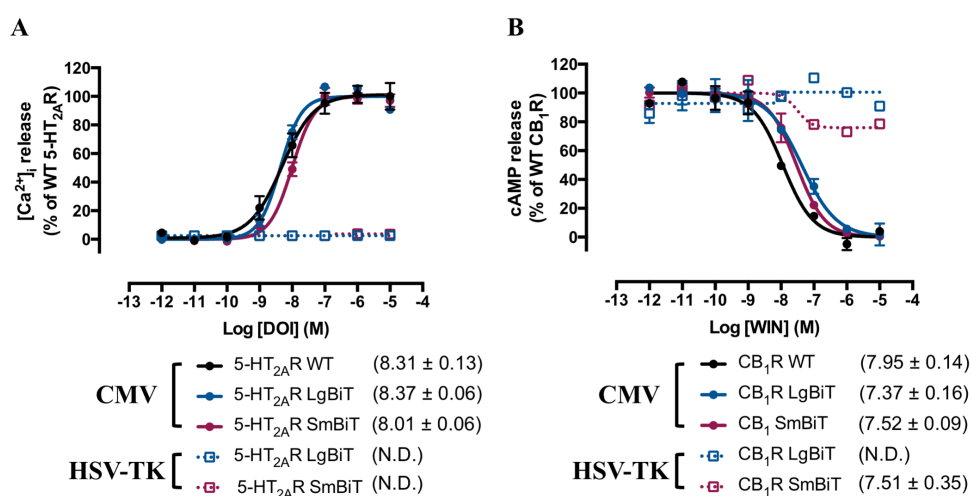


Figure 3.2. Functional characterisation of NanoBiT CB₁R and 5-HT_{2A}R constructs. In (A), dose-response intracellular Ca²⁺ release curves for 5-HT_{2A}R constructs under the CMV and HSV-TK promoters. In (B), forskolin-induced (7.5 μM) cAMP release inhibition dose-response curves for CB₁R constructs under the CMV and HSV-TK promoters. Data are mean ± SEM percentage of activation normalised to wild type receptors maximal response of three individual experiments each performed in duplicates. Values in brackets represent the mean pEC₅₀/pIC₅₀ ± SEM (n=3). Statistical significance of pEC₅₀/pIC₅₀ was evaluated by one-way analysis of variance (ANOVA) followed by Bonferroni post hoc tests, indicating no significant effects between groups. ND: non-determined, indicate non-convergent curve fits; CMV: human cytomegalovirus immediate-early promoter; HSV-TK: herpes simplex virus thymidine kinase gene promoter.

Accordingly, as in the previous studies illustrated in **Figure 3.1**, we repeated the conformational screenings with the new set of constructs under the CMV promoter. When analysing 5-HT_{2A}R-CB₁R heteromerisation, we detected a significant increase in the luminescence for all receptor combinations, with 5-HT_{2A}R-LgBiT:CB₁R-SmBiT being the optimal pair in terms of assay window (**Figure 3.3B**). To validate the specificity of the interaction, increasing amounts of untagged 5-HT_{2A}R and CB₁R receptors were transfected in the presence of a fixed 5-HT_{2A}R-LgBiT:CB₁R-SmBiT ratio. Accordingly, we observed a decreased luminescence with increasing levels of both untagged proteins (**Figures 3.3G,H**), indicating that the detected interaction was not driven by the finite affinity between the NanoLuc subunits. In parallel, we assessed CB₁R and 5-HT_{2A}R homomerisation with similar results. Co-transfection of both CB₁R interacting pairs resulted in a significant increase in luminescence that could be reverted over increasing untagged CB₁R concentrations (**Figures 3.3C,E**). Similarly, the specific interaction between 5-HT_{2A}R-LgBiT and 5-HT_{2A}R-SmBiT was hindered when titrating increasing concentrations of untagged 5-HT_{2A}R (**Figures 3.3D,F**). Importantly, when comparing the relative intensities of these interactions, we found that 5-HT_{2A}R homodimers displayed the highest luminescent signals, followed by 5-HT_{2A}R-CB₁R heteromers and CB₁R homodimers (RLU for 5-HT_{2A}R:5-HT_{2A}R > 5-HT_{2A}R:CB₁R > CB₁R: CB₁R). In addition, higher non-tagged 5-HT_{2A}R concentrations were necessary to displace 5-HT_{2A}R homodimers (**Figure 3.3F**). However, our results cannot discriminate whether it reflects the relative affinities between the interacting receptors or a more favourable orientation of the NanoBiT pairs in the N-terminus of the receptors. Altogether, our data strongly supports NanoBiT BiLC as a non-destructive and powerful tool to study GPCR oligomerisation, providing a specific and sensitive assay to detect these receptor complexes in live cells. In addition, in order to obtain a more comprehensive understanding of bimolecular complementation assays to study GPCR oligomerisation, we sought to address whether NanoBiT could provide better results in comparison to bimolecular fluorescent complementation. To this end, we developed a Venus BiFC assay to study CB₁R and 5-HT_{2A}R homo/heteromerisation. Specifically, fragments derived from the truncated Venus fluorescent protein at either position D155 (VC155; residues 155 to 238) or D173 (VN173; residues 1 to 173) were fused after the Gly/Ser rich flexible linker to the C-terminus of both CB₁ and 5-HT_{2A} receptors (**Figure 3.4A**). This strategy has been extensively applied to the study of PPIs and takes advantage of Venus, a variant of the enhanced yellow fluorescent protein (eYFP) with improved sensitivity to chromophore maturation under physiological temperatures²⁷⁵. In fact, several authors have used this approach to study GPCR

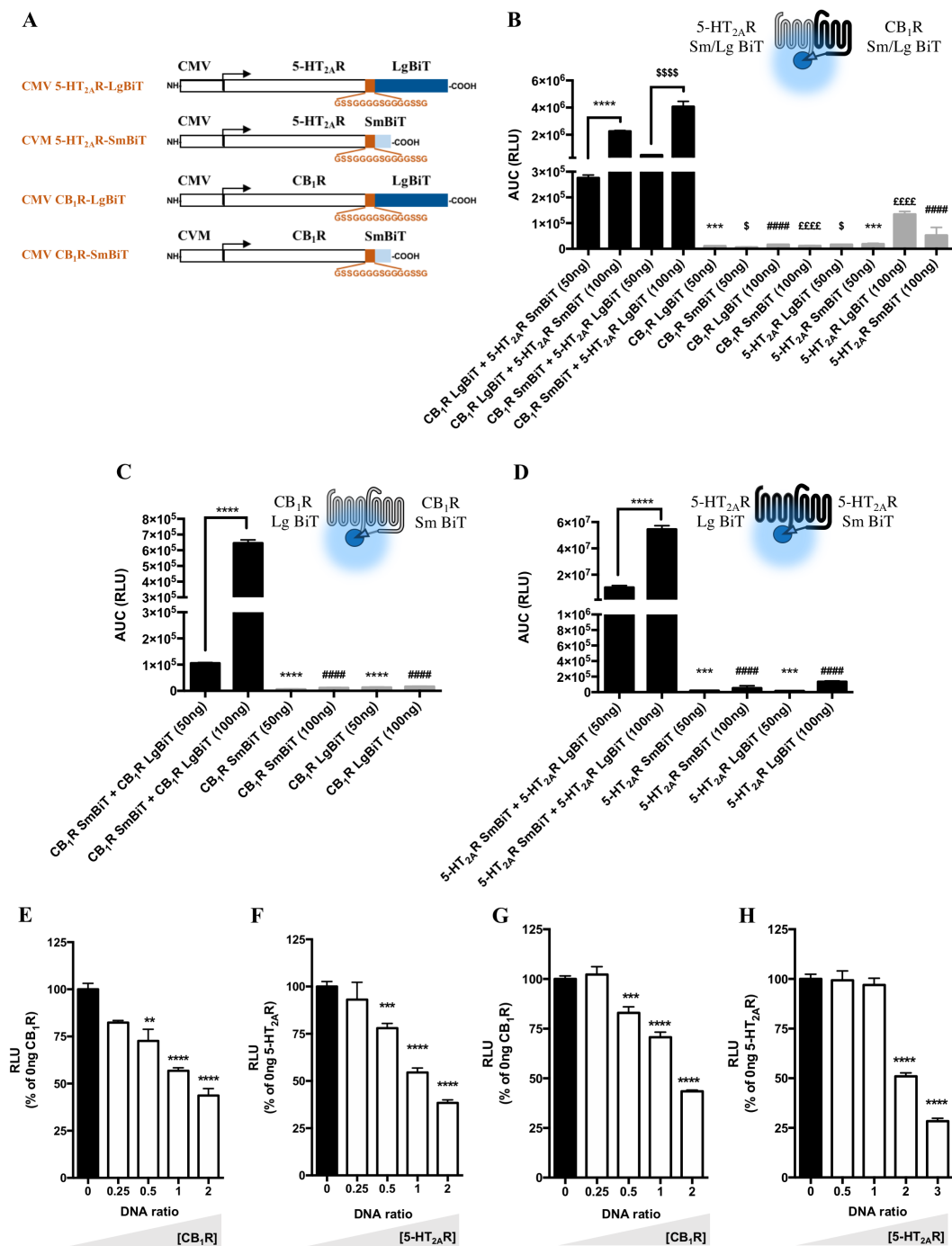


Figure 3.3. Identification of CB₁R, 5-HT_{2A}R and 5-HT_{2A}R-CB₁R oligomers using NanoBiT. (A) Schematic representation of the NanoLuc fusion proteins. HEK 293 cells were transiently transfected with all possible fusions of LgBiT and SmBiT to the C-terminal domain of the 5-HT_{2A} and CB₁ receptors at two different DNA ratios (50 or 100 ng receptor/well) to assess 5-HT_{2A}R-CB₁R heteromers (B), CB₁R homodimers (C) and 5-HT_{2A}R homodimers. The optimal receptor pairs were transfected with increasing no-tagged receptor concentrations to disrupt CB₁R homodimers (E), 5-HT_{2A}R homodimers (F) and 5-HT_{2A}R-CB₁R heteromers (G and H). In B-D, data are mean AUC (RLU) ± SEM (n = 3). In (B), statistical significance was evaluated by one-way analysis of variance (ANOVA) followed by Bonferroni post hoc tests showing significant effects for CB₁R LgBiT + 5-HT_{2A}R SmBiT (50ng) against the same configuration at 100 ng/well or each equivalent individual construct (***p ≤ 0.001, ****p ≤ 0.0001), for CB₁R LgBiT + 5-HT_{2A}R SmBiT (100ng) over each equivalent individual construct (#####p ≤ 0.0001),

Developing BiLC-based Methods to Study GPCR protein:protein Interactions

for CB₁R SmBiT + 5-HT_{2A}R LgBiT (50ng) over the same configuration at 100 ng/well or each equivalent individual construct ($^{\$}p \leq 0.05$, $^{SSSS}p \leq 0.0001$) and for CB₁R SmBiT + 5-HT_{2A}R LgBiT (100ng) over each equivalent individual construct ($^{EEEE}p \leq 0.0001$). In B and C, statistical significance was evaluated as in A, showing significant effects for CB₁ SmBiT + CB₁R LgBiT (50) or 5-HT_{2A}R SmBiT + 5-HT_{2A}R LgBiT (50) over the same configuration at 100 ng/well or each equivalent individual construct ($^{***}p \leq 0.001$, $^{****}p \leq 0.0001$) and for CB₁ SmBiT + CB₁R LgBiT (100) or 5-HT_{2A}R SmBiT + 5-HT_{2A}R LgBiT (100) over each individual construct ($^{####}p \leq 0.0001$). In E-H, values are mean \pm SEM (n = 3) of percentage of luminescence normalised to 0 ng of non-tagged competitor. For each condition, statistical significance was evaluated by one-way analysis of variance (ANOVA) followed by Bonferroni post hoc tests showing significant effects over 0 ng of non-tagged competitor ($^{**}p \leq 0.01$, $^{***}p \leq 0.001$, $^{****}p \leq 0.001$). CMV, human cytomegalovirus immediate-early promoter.

oligomerisation, including heteromers between the adenosine A_{2A} (A_{2A}R) and the dopamine D₂ (D₂R) receptors, D₂R oligomers or neuropeptide Y Y₁/Y₅ receptor heterodimers^{199,571,572}. Attachment of both Venus hemiprotein fragments to the 5-HT_{2A}R C-terminal tail (5-HT_{2A}R-VN173 and 5-HT_{2A}R-VC155 constructs) did not impact receptor function, with equivalent [Ca²⁺]_i release dose-response curves in comparison to the wild type receptor (**Figure 3.4B**). Similarly, the VC155 fragments fused to CB₁R (CB₁R-VC155) did not affect CB₁R-mediated cAMP release inhibition. However, although its maximal efficacy remained unaltered, VN1733 fusion to CB₁R (CB₁R-VN173) resulted in ~10-fold reduction in WIN 55212-2 (WIN) potency (**Figure 3.4C**). Next, we proceeded to compare both protein complementation assays. For CB₁R and 5-HT_{2A}R homomers, BiFC experiments were performed under the same conditions that yielded the optimal assay windows in the NanoBiT BiLC experiments (**Figures 3.3**). When assessing 5-HT_{2A}R-CB₁R heteromers, both possible receptor configurations (5-HT_{2A}R-VN173:CB₁R-VC155 or 5-HT_{2A}R-VC155:CB₁R-VN173) were taken into account. Surprisingly, 24 hours after transfection, none of the analysed BiFC combinations yielded significant fluorescent levels (data not shown), suggesting time-dependent protein maturation and/or folding. Therefore, the following BiFC experiments were performed 48 hours after transfection, although BiLC assays remained under the same setup (24 hours post-transfection). In comparison to Venus BiFC, NanoBiT complementation provided higher assay windows over all the oligomeric configurations (**Figure 3.4D**). Specifically, we observed a 20-fold increase for CB₁R homodimers, 130-fold increase for 5-HT_{2A}R homodimers and 9-18-fold increase for 5-HT_{2A}R-CB₁R heteromers. Interestingly, the relative fluorescent/luminescent intensities for the different receptor pairs followed the same trend across both methods (RFU/RLU for 5-HT_{2A}R:5-HT_{2A}R > 5-HT_{2A}R:CB₁R > CB₁R:CB₁R), suggesting that this could reflect the affinity between these oligomeric arrangements.

Together, our results support that NanoBiT BiLC is a suitable approach to detect GPCR homo/heteroreceptor complexes in the plasma membrane of live cells. Furthermore, when compared to Venus BiFC, NanoBiT showed a significant improvement in signal-to-noise ratio and assay time, thereby reducing the likelihood of overexpression-driven associations or the time-dependant irreversibility of the complementation between the hemiproteins pairs. In addition, NanoBiT benefits from the small size of its components, minimising the steric interference on appended target proteins.

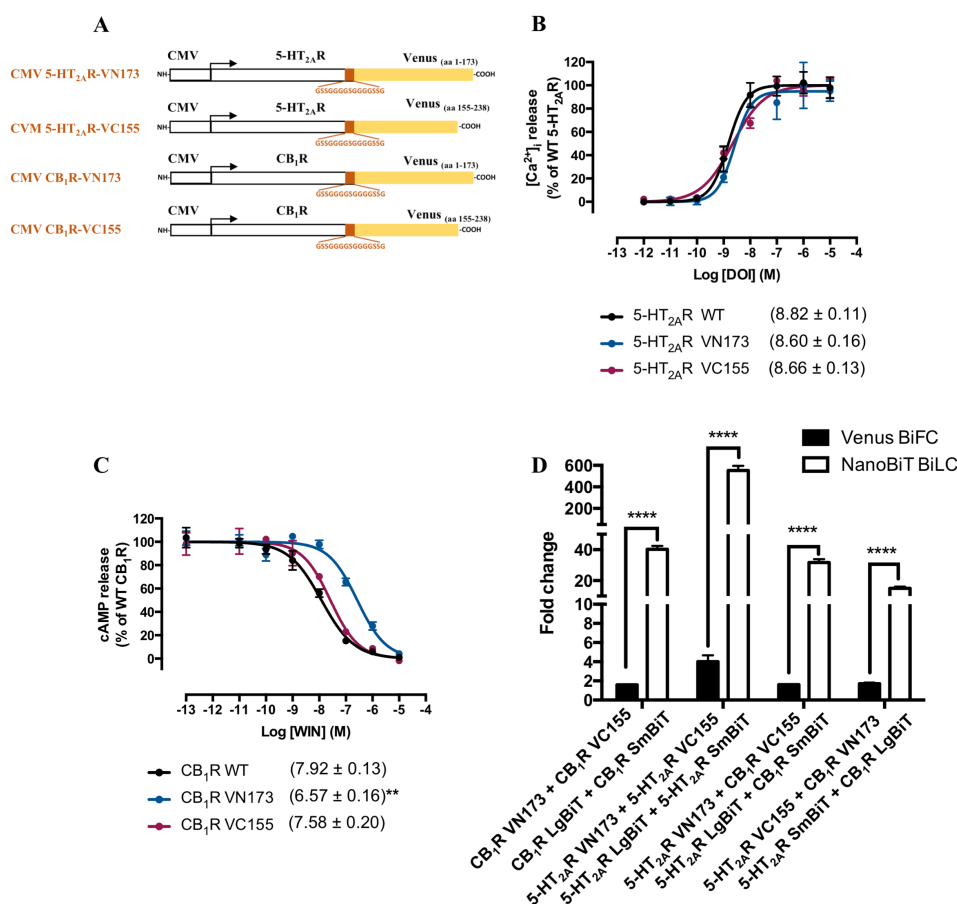


Figure 3.4. Comparative analysis of NanoBiT BiLC and Venus YFP BiFC. (A) Schematic representation of the Venus YFP BiFC fusion proteins. In (B), dose-response intracellular Ca²⁺ release curves for 5-HT_{2A}R constructs. In (C), forskolin-induced (7.5μM) cAMP release inhibition dose-response curves for CB₁R. Data are mean ± SEM percentage of activation normalised to wild type receptors maximal response of three individual experiments each performed in duplicates. Values in brackets represent the mean pEC₅₀/pIC₅₀ ± SEM (n=3). Statistical significance of pEC₅₀/pIC₅₀ was evaluated by one-way analysis of variance (ANOVA) followed by Bonferroni post hoc tests, indicating significance over wild type receptors (**p ≤ 0.01). In (D), HEK293 cells were transiently transfected with all possible Venus YFP fusions and compared to the equivalent NanoBiT BiLC pairs to assess CB₁R homodimers, 5-HT_{2A}R homodimers and 5-HT_{2A}R-CB₁R heteromers. Data are mean ± SEM (n ≥ 3) of fold change, calculated as ratio between each condition and the individual receptor construct with the highest luminescence/fluorescence values. Statistical significance was evaluated by unpaired t-tests between groups followed by Holk-Sidak corrections for multiple comparison (****p ≤ 0.0001). CMV: human cytomegalovirus immediate-early promoter.

3.2.2. NanoBiT-based β -arrestin assays allow the study of GPCR signalling with kinetic resolution

In the classical view of GPCR signalling transduction, agonists promote the association between receptors and G proteins to form the so called ternary complex. However, it is well established that GPCR signalling is not restricted to this ternary complex model and receptor activation often leads to G protein-independent signalling pathways. Of these, β -arrestins have drawn particular attention, leading to new approaches in GPCR drug discovery, such as biased ligands screenings^{128,573}. As previously discussed, NanoBiT provides an excellent alternative to overcome the main limitations of the currently available arrestin recruitment assays (HC, enzyme fragment complementation, gene reporter and BRET) by: (1) allowing real-time monitoring of β -arrestins recruitment, (2) taking advantage of NLuc brightness and furimazine stability and (3) lessening the possibility of artefactual receptor: β -arrestin interactions due to its enzyme fragment complementation nature. Therefore, we sought to take advantage of the previously characterised Sm/LgBiT C-terminal tagged CB₁ and 5-HT_{2A} receptors (**Figure 3.2A,B**) to develop an arrestin recruitment assay. In addition, to further explore its potential, we set out to study the closely related cannabinoid type 2 receptor (CB_{2R}).

Recent structural information indicates a biphasic interaction between arrestins and GPCRs. Hence, the C-terminal tail, by establishing hydrophobic interactions with the N-domain and a salt bridge with the polar core, has a crucial role in stabilising arrestins in the basal state. After receptors undergo activation, the phosphorylated receptor C-tail displaces the arrestin C-terminus, allowing the formation of the GPCR:arrestin “pre-complex”. This induces a series of conformational rearrangements, allowing additional interactions with various loops in the arrestin (including the finger loop) to form the “high affinity complex”^{74,115,574,575}. Accordingly, we hypothesised that fusing the small and large NLuc complementary pairs to the N-terminal domain of the human β -arrestin2 (SmBiT- β -arrestin2 and LgBiT- β -arrestin2, respectively) would be less disruptive for arrestin function (**Figure 3.5A**).

Next, we analysed which configuration would provide the optimal receptor:arrestin pair. It should be noted that, although Sm/LgBiT did not impact 5-HT_{2A} nor CB₁ receptor function when cloned on its C-tail (**Figure 3.2A,B**), LgBiT negatively affected CB_{2R} signalling (**Figure 3.5E**). Importantly, the CB_{2R}-SmBiT construct displayed signalling properties equivalent to those of the wild type CB_{2R}. Thus, a fixed amount of each receptor was transiently co-expressed in HEK293 cells with increasing concentrations of β -arrestin2, covering all possible interacting configurations. For 5-HT_{2A}R and CB₁R, the optimal combinations consisted in the LgBiT-tagged receptors in combination with SmBiT-tagged β -arrestin2 (**Figure 3.5 B,C**). For CB_{2R}, the CB_{2R}-SmBiT:LgBiT- β -arrestin2 pair yielded the

best assay window, presumably due to the negative impact of LgBiT in CB₂R function (**Figure 3.5D**). Interestingly, all titration experiments displayed an inverted U-shaped profile, with the intermediate arrestin DNA concentrations being the optimal to monitor agonist-induced arrestin binding. Hence, all further experiments were performed in HEK293 cells transiently transfected with either the 5-HT_{2A}R-LgBiT:SmBiT- β -arrestin2, the CB₁R-LgBiT:SmBiT- β -arrestin2 or the CB₂RSmBiT:LgBiT- β -arrestin2 combinations.

Stimulation of cells with the selective 5-HT_{2A}R agonist DOI, induced arrestin recruitment in a dose-dependent manner. Importantly, the effect of a semi-saturating concentration (EC₈₀) of DOI was reverted in the presence of increasing concentrations of the selective 5-HT_{2A}R antagonist MDL 100907 (MDL) (**Table 3.2 and Figure 3.6B**). Similarly, WIN induced a dose-dependent interaction between β -arrestin2 and both cannabinoid receptors. In addition, pre-incubation with increasing concentrations of either Rimobabant or AM630, selective CB₁R and CB₂R inverse agonists, respectively, abrogated agonist-induced arrestin recruitment (**Table 3.2 and Figure 3.6D-F**). The relative potencies obtained in our assay are in line with those reported by others (**Table 3.2**), indicating that NanoBiT is a reliable method to quantitatively assess arrestin binding to these receptors. In addition, the fact that the agonist-induced β -arrestin2 recruitment to all three GPCRs was blocked by their selective antagonist in a concentration-dependent manner, illustrates the specificity of the assay. Furthermore, this strategy allowed us to obtain information on the dynamic nature of this PPI. Thus, stimulation of both CB₁ and CB₂ receptors induced a fast and transient interaction with β -arrestin2 (**Figure 3.6C,E**). Interestingly, although the association for all three receptors occurred within the same timeframe (~100% arrestin bound after 5 min stimulation), the association between 5-HT_{2A}R and β -arrestin2 was more stable, with ~50% still complexed after 1 hour (**Figure 3.6A**). Together, our results illustrate how the application of the NanoBiT technology provides a sensitive and accurate platform to study the dynamic interaction between GPCRs and β -arrestins.

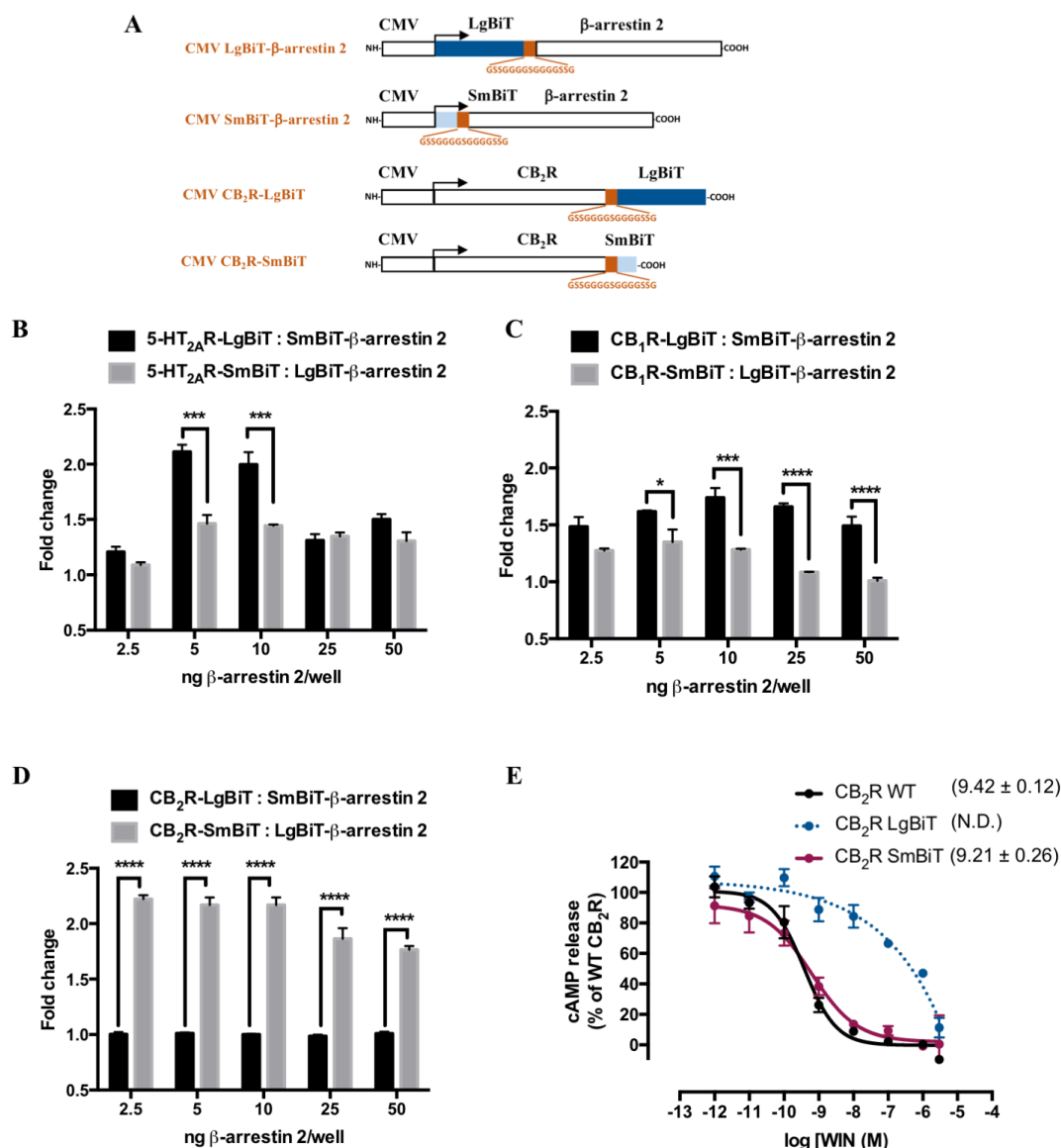


Figure 3.5. Identification of the optimal receptor:β-arrestin 2 pairs to detect agonist-mediated β-arrestin2 activation. (A) Schematic representation of the NanoLuc β-arrestin2 and CB₂R fusion proteins. HEK 293 cells were transiently co-transfected with a fixed amount (100 ng/well) of the 5-HT_{2A}R (B), CB₁R (C) and CB₂R (D) and increasing concentrations (see figure legends) of β-arrestin2 N-terminally tagged either with SmBiT or LgBiT. Data are mean ± SEM (n = 3) fold change, calculated as the ratio between agonist (1 μM DOI or WIN for 5-HT_{2A}R and CB_{1/2}R, respectively) and vehicle-treated cells. Statistical significance was evaluated by two-way analysis of variance (ANOVA) followed by Bonferroni post hoc tests showing significant effects (*p ≤ 0.05, ***p ≤ 0.001, ****p ≤ 0.0001). In (E) forskolin-induced (7.5 μM) cAMP release inhibition dose-response curves for CB₂R. Data are mean ± SEM percentage of activation normalised to wild type receptors maximal response of three individual experiments each performed in duplicates. Values in brackets represent the mean pEC₅₀/pIC₅₀ ± SEM (n=3). One-way analysis of variance (ANOVA) followed by Bonferroni post hoc tests revealed no significant differences between groups. N.D., non-determined, indicate non-convergent curve fits. CMV, human cytomegalovirus immediate-early promoter.

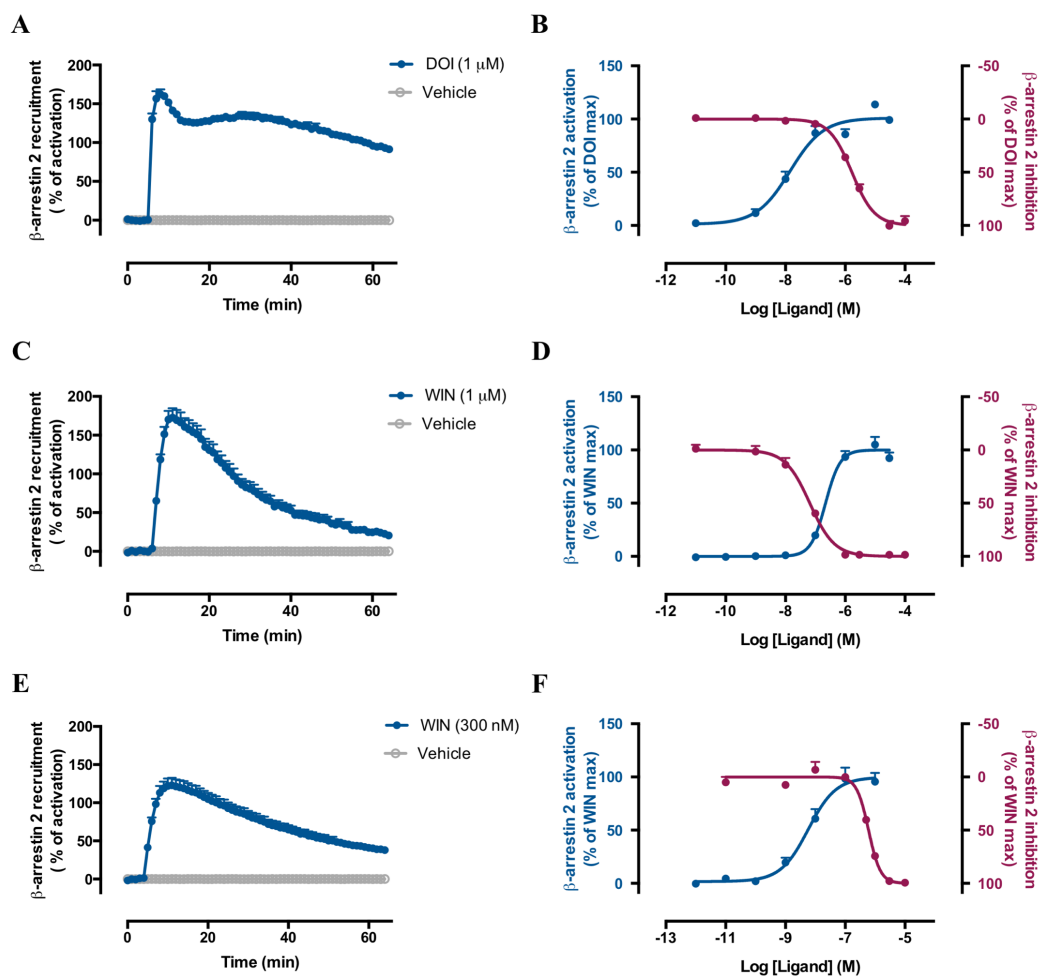


Figure 3.6. Monitoring β -arrestin2 kinetic interactions. Representative traces of agonist-mediated β -arrestin2 recruitment followed over time for 5-HT_{2A} (A), CB₁ (C) and CB₂ (E) receptors. Data are mean \pm SEM percentage of activation normalised to vehicle-treated cells of a representative experiment performed in triplicates. Dose-dependent activation (blue) or inhibition (red) of β -arrestin 2 binding to 5-HT_{2A} (B), CB₁ (D) and CB₂ (F) receptors. For inhibition dose-response, cells were pre-incubated with different concentrations (see figure legends) of the selective 5-HT_{2A}R and CB₁R antagonist, MDL 100907 and Rimonabant, respectively, before agonist stimulation (1 μ M DOI or WIN) or with the selective CB₂R antagonist AM630 prior to stimulation with WIN (100 nM). Data are mean + SEM percentage of activation normalised to agonist-induced maximal response of three individual experiments each performed in duplicates.

Table 3.2. Comparative studies of different β -arrestin 2 activation assays.

Receptor	Ligand	NanoBiT pEC ₅₀ /pIC ₅₀	Reported pEC ₅₀ /pIC ₅₀	Assay	References
CB ₁ R	WIN 55212-2	6.66 ± 0.08	6.74 ± 0.21	PathHunter®	576
	Rimonabant	7.19 ± 0.06	8.25 ± 0.04 ^{*,b}	PathHunter®	576
CB ₂ R	WIN 55212-2	8.24 ± 0.13	7.93 ± 0.42	PathHunter®	576
	AM630	6.22 ± 0.03	6.15 ± 0.08	PathHunter®	576
5-HT _{2A} R	5-HT	7.01 ± 0.15	6.89 ± 0.07	Tango™	29
	DOI	7.85 ± 0.14	N.A.		
	MDL100907	5.78 ± 0.04	N.A.		

Recently reported β -arrestin2 signalling efficacies of CB₁, CB₂ and 5-HT_{2A} receptors agonists (WIN 55212-2, 5-HT and DOI) and antagonists (Rimonabant, AM630 and MDL 100907). For NanoBiT arrestin assays, values represent the mean pEC₅₀/pIC₅₀ ± SEM (n=3). Statistical significance was evaluated by unpaired t-tests between groups followed by Holk-Sidak corrections for multiple comparison (^{*}p ≤ 0.0001). ^bPerformed in the presence of the EC₈₀ of CP 55940 (K_i CP55940 < K_i WIN 55212-2; ⁵⁷⁷).

3.2.3. Development of new BiLC NanoBiT-based pairs to investigate GPCRs:G proteins interactions

Based on our previous results illustrating how NanoBiT provides an excellent approach to understand the dynamic interaction between GPCRs and arrestins, we sought to explore whether a similar strategy could be applied to monitor the recruitment of heterotrimeric G proteins to their cognate receptors. Classical assays (e.g. [³⁵S]GTPγS binding, second messenger signalling, Gα subunit blockage with toxins, etc.) have deeply contributed to establishing the foundations of modern GPCR pharmacology, yet they are indirect measures of G protein activation. More recently, the introduction of RET and single-molecule imaging approaches has facilitated real-time monitoring of G protein activation kinetics in live cells^{567,578}. Thus, C-terminal labelled GPCRs with either the donor or acceptor RET pairs are combined with Gα, Gβ or Gγ subunits fused to their complementary RET probes. A similar, but indirect, strategy consists in monitoring the changes in energy transfer efficacy after the dissociation of the Gα subunit and the Gβγ dimer, each labelled with BRET/FRET compatible reporters^{569,579}. However, labelling the Gα subunit is non-trivial as both the amino and carboxy terminal ends participate in G proteins structure stability, receptor recognition and activation^{44,45}.

Accordingly, we hypothesised that the small size of SmBiT (1.3 kDa) in comparison with eYFP or RLuc (27 and 36 kDa, respectively), would minimise steric hindrance where spatial

constraints may be critical. In addition, owing to the disorder-to-order transition of the $G\alpha$ subunit C-terminal tail interface when accommodated into the intracellular receptor cavity after ligand activation⁴⁴, we selected the $G\alpha$ subunit N-terminal tail of $G\alpha_q$, $G\alpha_{i1}$ and $G\alpha_{i3}$ as anchoring point for the 11 amino acids SmBiT pair (**Figure 3.7A**). The above characterised CB₁R-LgBiT and 5-HT_{2A}-LgBiT constructs (**Figure 3.2**), well established G_{i/o} and G_{q/11} proteins-coupled receptors, respectively, were selected as complementary fusion^{346,580}. First, we assessed CB₁R ability to couple to $G\alpha_i$ proteins. For that purpose, a fixed CB₁R-LgBiT DNA concentration shown to inhibit Forskolin-induced cAMP release (**Figure 3.3**), was co-expressed in HEK293 cells with increasing amounts of either the $G\alpha_{i1}$ or $G\alpha_{i3}$ heterotrimeric G proteins subunits tagged with SmBiT in their N-terminus. $G\alpha_{i1}$ and $G\alpha_{i2}$ association has been shown to be regulated by residues in the 3rd intracellular loop (IL3) of CB₁R, whilst $G\alpha_{i3}$ binding is highly controlled by the juxtamembrane C-terminal domain⁵⁸¹. Accounting for these options, we observed an increment in the luminescence readout over increasing $G\alpha$ concentrations in cells expressing the CB₁R-LgBiT:SmBiT- $G\alpha_{i1}$ combination. However, we did not detect significant differences upon agonist stimulation (**Figure 3.7B**). A similar trend applied for the CB₁R-LgBiT:SmBiT- $G\alpha_{i3}$ combination, without significant changes between vehicle or WIN-treated cells (**Figure 3.7C**). Interestingly, in both CB₁R co-transfected cells with $G\alpha_{i1}$ or $G\alpha_{i3}$, the luminescence readouts were relatively high at low $G\alpha_{i1}$ and $G\alpha_{i3}$ ratios. These results may be in line with recent studies from Bondar and Lazar, demonstrating that CB₁R exhibits constitutive binding to $G\alpha_{i1}$ proteins⁵³⁴. In fact, when measuring $G\alpha_q$ binding to 5-HT_{2A}R this effect was not observed (**Figure 3.7D**). However, although the overall luminescence intensity was higher in comparison with CB₁R-LgBiT:SmBiT- $G\alpha_{i1}$ and CB₁R-LgBiT:SmBiT- $G\alpha_{i3}$, no differences between vehicle or DOI treatment were observed. Taking into account these results in all the combinations tested, the DNA concentration-dependent increase in luminescence might result from the non-specific interaction between receptors and G proteins. In addition, the intrinsic affinity between both NanoBiT fragments might drive their interaction and stabilise these complexes. To rule out these options, we explored whether non-canonical G proteins might bind 5-HT_{2A} or CB₁ receptors. Accordingly, in cells transfected with 5-HT_{2A}R, over-expression of $G\alpha_{i1}$ or $G\alpha_{i3}$ yielded significantly lower luminescence levels in comparison to its cognate $G\alpha_q$ protein, showing 5-HT_{2A}R preference towards binding its canonical G proteins in the basal state (**Figure 3.7E**). Similarly, when comparing the interaction between CB₁R and $G\alpha_q$, the basal recruitment was significantly lower in comparison when co-expressed with the $G\alpha_{i1}$ subunit (**Figure 3.7F**), indicating that, despite lacking temporal resolution, NanoBiT complementation can discriminate the natural coupling between receptors and their cognate G proteins.

Developing BiLC-based Methods to Study GPCR protein:protein Interactions

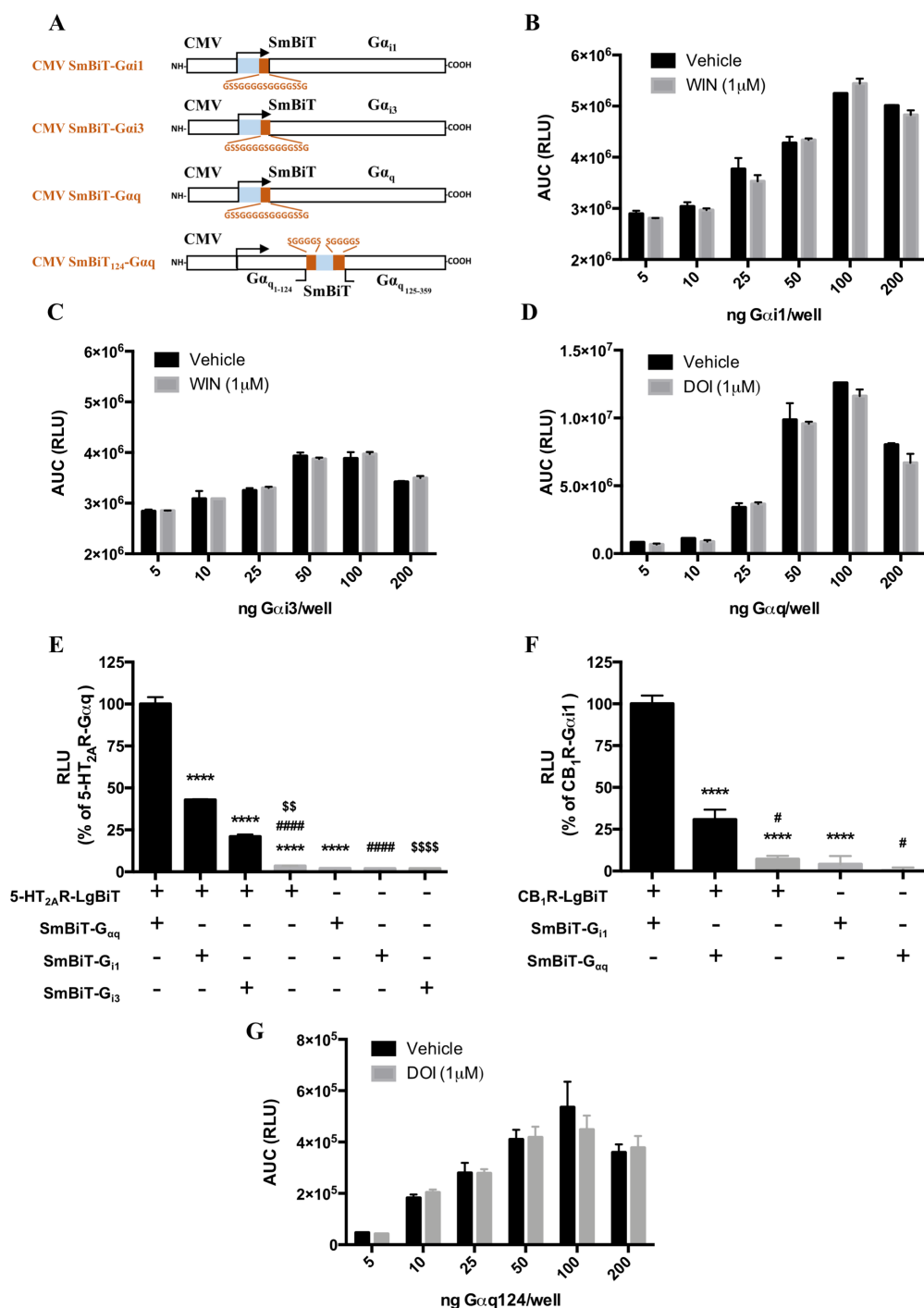


Figure 3.7. Monitoring receptor:G proteins interactions with NanoBiT BiLC. (A) Schematic representation of the $G\alpha$ subunits NanoLuc fusions. HEK293 cells were transiently co-transfected with a fixed amount (100 ng/well) of the CB₁R and increasing concentrations (see figure legends) of SmBiT $G\alpha_{i1}$ (B) or SmBiT $G\alpha_{i3}$ (C). Similarly, 5-HT_{2A}R (100 ng/well) was co-transfected with increasing SmBiT $G\alpha_q$ concentrations (D). Luminescence recordings were continuously recorded 5s after agonist addition. Data are mean AUC (RLU) \pm SEM (n = 3). Statistical significance was evaluated by two-way analysis of variance (ANOVA) followed by Bonferroni post hoc tests showing no significance between vehicle or agonist-treated cells. In (E) and (F), 100 ng of 5-HT_{2A}R or CB₁R, respectively, were co-transfected with different $G\alpha$ subunits (1:1 receptor: $G\alpha_x$ DNA ratio). Data are mean RLU \pm SEM (n = 3) percentage normalised to each receptor plus its canonical $G\alpha$ subunit, see figure axis. In E, statistical significance was evaluated by one-way analysis of variance (ANOVA) followed by Bonferroni post hoc

tests showing significant effects for 5-HT_{2A}R-LgBiT + SmBiT-G α_q vs 5-HT_{2A}R-LgBiT + SmBiT-G α_{i1} , 5HT_{2A}R-LgBiT + SmBiT-G α_{i3} , 5HT_{2A}R-LgBiT and SmBiT-G α_q (****p \leq 0.0001), for 5-HT_{2A}R-LgBiT + SmBiT-G α_{i1} vs 5-HT_{2A}R-LgBiT and SmBiT-G α_{i1} (####p \leq 0.0001) and for 5-HT_{2A}R-LgBiT + SmBiT-G α_{i3} vs 5-HT_{2A}R-LgBiT and SmBiT-G α_{i3} (##p \leq 0.01, ####p \leq 0.0001). In F, statistical significance was evaluated as in E showing differences for CB₁R-LgBiT + SmBiT-G α_{i1} vs CB₁R-LgBiT + SmBiT-G α_q , CB₁R-LgBiT and SmBiT-G α_{i1} (****p \leq 0.0001) and for CB₁R-LgBiT + SmBiT-G α_q vs CB₁R-LgBiT and SmBiT-G α_q (#p \leq 0.05). In (G), the 5-HT_{2A}R (100 ng/well) was co-transfected with increasing concentrations (see figure legends) of the intramolecular SmBiT₂₂₄-G α_q . Data are mean AUC (RLU) \pm SEM (n = 3), showing no significant differences between treatments after one-way analysis of variance (ANOVA) followed by Bonferroni post hoc tests. CMV: human cytomegalovirus immediate-early promoter.

Whilst our results indicate selective GPCRs-G protein interactions, they fail to depict agonist-promoted recruitment. Even if the SmBiT size is considerably small, minor alterations in G α N-terminus might impact its myristoylation and/or palmitoylation or the association with the the G $\beta\gamma$ dimer. Hence, we considered intramolecular insertion of SmBiT and selected the 5-HT_{2A}R as prototypical example for G α_q coupling. SmBiT was inserted in between the human G α_q Ser124 and the Glu125 (SmBiT₁₂₄-G α_q), residues located in the loop connecting the helices α B and α C in the helical domain, with a flexible linker (SGGGGS) flanking SmBiT (**Figure 3.7A**). Importantly, GFP and YFP insertions at this position have shown preserved G α_q function and plasma membrane distribution^{582,583}. Next, increasing SmBiT₁₂₄-G α_q concentrations were co-expressed in the presence of a fixed amount of 5-HT_{2A}R-LgBiT (**Figure 3.7G**). In the basal state, the relative luminescence values were lower in comparison when the SmBiT was fused to G α_q N-terminus, suggesting that under this new configuration non-specific encounters are less likely to occur. However, agonist stimulation did not elicit NanoBiT complementation, indicating that neither intramolecular nor N-terminal insertions provide suitable NanoBiT pairs to study GPCR-driven G protein activation. It is important to highlight that the lack of agonist-driven changes in luminescence might reflect limitations in our setup, rather than steric and/or functional hindrances. Recent studies have added new light to the kinetics of receptor-G protein interactions, revealing that agonists mostly regulate receptor-G proteins interactions at the level of their association constant (K_{on})^{307,567}. Together, with half-lives of ~hundreds of milliseconds, the kinetics of heterotrimeric G proteins activation are fast and compatible with NanoBiT rate constants, with similar off rates (0.2 s⁻¹ for NanoBiT versus 0.1-0.2 s⁻¹ or 0.8 s⁻¹ for the β_2 AR-G α_s or α_{2A} ARs-G α_i complexes, respectively) but substantially faster on rates (~500 M⁻¹s⁻¹ for NanoBiT versus ~50 mM⁻¹ s⁻¹ for β_2 AR-G α_s). However, due to the speed of G protein activation and the bioluminescent nature of our assay, our microtiter setup might not provide enough sensitivity

(number of detected photons per integration time) nor speed (time delay after agonist injection) and thereby obviating these events.

3.2.4. Identification of small-stapled TM peptides targeting 5-HT_{2A}-CB₁ receptor heteromeric interfaces

Several X-ray resolved GPCRs crystal structures have revealed common dimeric interfaces stabilising oligomeric arrangements within the Rhodopsin-like family receptors (reviewed in more detail in section 1.2.2.) The selective disruption of these dimers using synthetic peptides harbouring the same sequence as the interacting TMs, has helped to validate and understand the functional consequences derived from these quaternary receptors organisation, including the β_2 adrenergic, CXCR4, oxytocin and apelin receptors homo-oligomers^{220,223,584,585}. Thus, considering heterodimers as new pharmacological entities with unique properties, TM peptides allow one to discriminate between those effects driven by the interacting receptors and those derived from the individual protomers⁵⁸⁶. In addition, TM peptides are likely to be not only tools, but rather drug-like entities in a context where a given undesired effect is driven by homo/hetero-oligomerisation. This is the case of the recently described CB₁ and 5-HT_{2A} receptor heteromers, where the cognitive impairment induced by trans- Δ^9 -tetrahydrocannabinol (THC) was abrogated after treatment with CB₁R TM5/6 peptides, although its antinociceptive properties remained intact¹⁸⁴. Therefore, being a promising target to dissociate marijuana's "good from the bad", we sought to develop a NanoBiT-based assay for the screening of a small library of hydrocarbon stapled CB₁R TM5 and TM6 mimicking peptides (**Figure 3.9A**). Our previous results validate how the fusion of the NanoBiT pairs to the CB₁R and 5-HT_{2A}R C-terminus provides a sensitive and specific approach to detect homo/heteromers (**Figure 3.3**). Importantly, this configuration was selected based on the idea to expand their potential in β -arrestin and G protein recruitment assays. However, before proceeding to screen peptides targeting the 5-HT_{2A}R-CB₁R heteromeric interface, we assessed whether N-terminal tagging could yield better assay windows (**Figure 3.8A**). SmBiT and LgBiT fusion to the 5-HT_{2A}R extracellular end did not impact DOI-induced maximal calcium release efficacy, although a small reduction in DOI potency was observed in the LgBiT-5-HT_{2A}R construct (**Figure 3.8B**). The homologous CB₁R constructs remained unaltered, with virtually the exact potencies and maximal responses as the WT receptor (**Figure 3.8C**). Next, we compared N- or C-terminal NanoBiT-tagged receptors accounting for their ability to reveal CB₁R and 5-HT_{2A}R homo/heteromers. When measuring the

interaction between receptors from the same type, NanoBiT attachment to the C-terminal domain provided the optimal orientation for CB₁R homomers (**Figure 3.8C**). In the case of 5-HT_{2A}R homomers, N-terminally tagging resulted in a discrete but significant improvement in the assay window at high DNA concentrations (**Figure 3.8D**). Interestingly, the biggest difference was observed when assessing the optimal 5-HT_{2A}R-CB₁R heteromeric conformation, providing the N-terminal fusions the best results (**Figure 3.8E**). Importantly, a ~200-fold increase was achieved at low DNA transfected concentrations, therefore reducing the probability of stochastic non-specific interactions as it would occur under physiological expression levels. Thus, the LgBiT-CB₁R and SmBiT-5-HT_{2A}R combination was used in all further experiments. In previous studies, Viñals and collaborators demonstrated that 5-HT_{2A}R-CB₁R heteromers could be selectively disrupted using peptides mimicking CB₁R TM5 and TM6¹⁸⁴, fused to the HIV-TAT (GRKKRRQRRR) cell penetrating sequence (CPS)⁵⁸⁷. Accordingly, using these structures as a starting point, we hypothesised that shortening their length, in combination with hydrocarbon peptide stapling, would result in improved peptides with small molecule-like properties (**Figure 3.9A**). This strategy, through the incorporation of α -methyl- α -alkenyl amino acids, combines the methylation of the α -carbon atom together with the introduction of a covalent side chain to side chain cross-link, resulting in peptides with increased α -helicity and improved proteolytic resistance^{588,589}. In addition, several studies support the ability of the CPPs to enhance cargo transport across the blood-brain barrier^{590,591}. Pre-incubation of HEK293 cells transiently co-expressing LgBiT-CB₁R and SmBiT-5-HT_{2A}R with the TM5-TAT and TM6-TAT, but not the TM7-TAT (negative control) peptides resulted in a decrease in the luminescence readout (**Figure 3.9B**), corroborating the previously reported results demonstrating the involvement of TM5 and TM6, but not TM7, in the heteromeric interface¹⁸⁴. In addition, these results demonstrate the suitability of our NanoBiT-based peptide screening assay and the specificity of the detected interaction. Next, we analysed the s6 and s6-TAT peptides, short-stapled versions of TM6-TAT with or without, respectively, the HIV-TAT cell penetrating sequence. Interestingly, we only detected a luminescence reduction in the TM6 peptide carrying the HIV-TAT sequence (s6-TAT). However, the non-stapled control of s6 (non-s6) displayed a similar effect (**Figure 3.9B**). Thus, whether non-s6 provides a conformation more likely to disrupt 5-HT_{2A}R-CB₁R heteromers than s6 requires a more in-depth characterisation. When analysing the TM5-TAT-derived peptides, s5-TAT exerted a significant decrease in NanoBiT complementation. Interestingly, neither the version lacking the HIV-TAT CPS (s5) nor the non-staple non-s5 peptides induced any change when compared to vehicle or TM7-TAT treated cells. In addition, the luminescence reduction was higher in comparison to the full-length TM5-TAT control peptide, appointing s5-TAT as a hit

for a more detailed characterisation (**Figure 3.9B**). Accordingly, we sought to further investigate s5-TAT disruption efficacy and the temporal-resolution of its interaction.

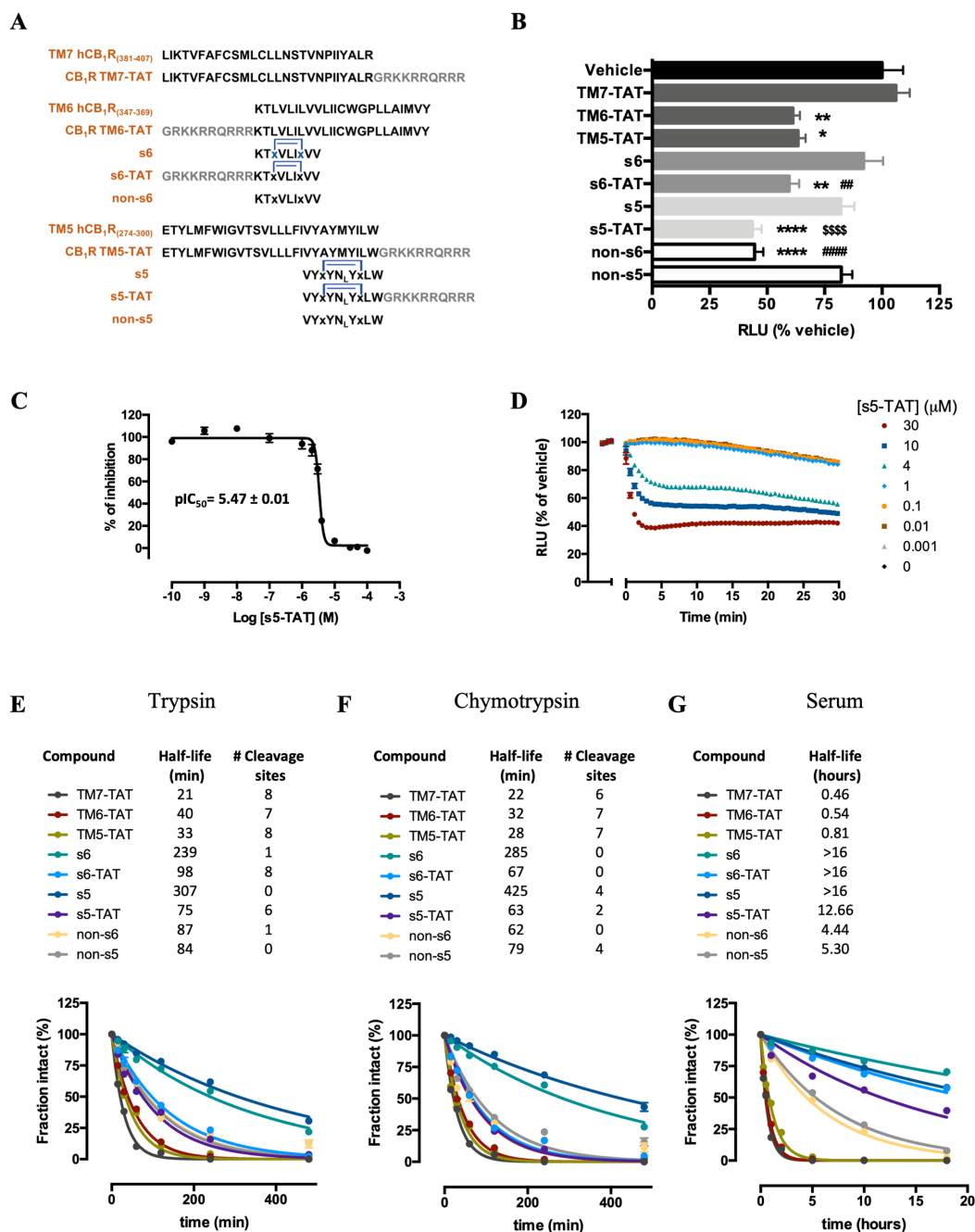


Figure 3.9. Identification of small-stapled TM peptides disrupting 5-HT_{2A}R-CB₁R heteromers. (A) Sequence alignment of the targeted TM regions their mimicking peptides. Blue bridges indicate the stapled residues and the HIV-TAT sequence is displayed in grey. In (B), HEK 293 cells transiently expressing the LgBT-CB₁R and SmBiT-5-HT_{2A}R complementary pairs were pre-incubated for 1h at 37°C with the indicated peptides (4 μM) or vehicle prior to luminescence recording. Data are mean ± SEM (n ≥ 5) percentage of activation normalised to vehicle treated cells. Statistical significance was evaluated by one-way analysis of variance (ANOVA) followed by Bonferroni post hoc tests, indicating significant differences over vehicle-treated cells (*p ≤ 0.05, **p ≤ 0.01, ****p

Developing BiLC-based Methods to Study GPCR protein:protein Interactions

≤ 0.0001), for s6 over its non-stapled (non-s6) and TAT-fused (TAT-s6) versions ($^{##}p \leq 0.01$, $^{####}p \leq 0.0001$) and for s5 over its non-stapled (non-s5) and TAT-fused (TAT-s5) versions ($^{ssss}p \leq 0.0001$). Cells transfected as in (A) were incubated with increasing concentrations (see figure legends) of the s5-TAT peptide for 1h at 37°C prior to substrate addition and luminescence recording (C). Alternatively, to assess the kinetics of the s5-TAT peptide-driven heteromer disruption (D), prior to s5-TAT administration at different concentrations (see figure legends), the cells were pre-incubated with substrate and the luminescence was recorded over the following 30 min. Data are mean \pm SEM ($n \geq 3$) percentage of activation normalised to vehicle treated cells. Values in brackets represent the mean $pIC_{50} \pm$ SEM ($n=3$). For proteolytic stability studies, the peptides solution (55.5 μ M for trypsin and chymotrypsin and 11.1 μ M for serum) were incubated in the presence of 0.55 μ g/mL of trypsin from porcine pancreas (E), α -chymotrypsin (F) or mouse serum (G) at 37 °C for the indicated times (see figure legends). Quantification of intact peptide remaining in the mixture was performed by HPLC. Data are mean \pm SEM ($n = 3$) percentage of intact peptides respect normalised to $t=0$. Proteolytic half-lives and putative cleavage sites (predicted using ExPASy server's model with the 50% cleavage possibility) are indicated in the upper panels of each figure.

Treatment with increasing s5-TAT concentrations induced a dose-dependent luminescence decrease, with a potency in the low micromolar range ($pIC_{50} = 5.47 \pm 0.01$) (Figure 3.9C). Surprisingly, the ability of s5-TAT to disrupt 5-HT_{2A}R-CB₁R heteromers was rather fast, almost reaching its maximal inhibitory response five minutes after administration (Figure 3.9D). Together, by combining hydrocarbon peptide stapling with the HIV-TAT CPS, we were able to identify an exciting candidate to selectively disrupt 5-HT_{2A}-CB₁ receptors complexes. However, the administration of peptides to disrupt GPCR interactions is a relatively new, with no available information regarding their pharmacokinetics and/or pharmacodynamics. In fact, proteolytic degradation is one of the main challenges facing protein/peptide therapies. Consequently, we subjected our peptide library to *in vitro* trypsin, chymotrypsin and serum proteolytic stability. When monitoring trypsin (0.5 mg/mL) degradation kinetics (Figure 3.9E), a rapid proteolysis was observed for the TM7-TAT, TM6-TAT and TM5-TAT control peptides (55 μ M each), with half-lives ranging from 20-40 minutes. Interestingly, their respective short-stapled versions harbouring the HIV-TAT CPS (s5-TAT and s6-TAT peptides) displayed longer half-lives, with a 2-3-fold enhancement in trypsin resistance, following the same trend the non-stapled non-s5 and non-s6 peptide controls. Furthermore, removal of the HIV-TAT CPS in the stapled s-5 and s-6 peptides yielded the longest half-lives (~5 hours), as neither lysine nor arginine residues were available for the trypsin to cleave. Chymotrypsin proteolytic kinetics showed similar results (Figure 3.9F), being the full length TM7-TAT, TM6-TAT and TM5-TAT peptides more susceptible to cleavage (half-lives ranging from 20 to 30 min). Again, a ~2-fold resistance improvement was detected for the stapled HIV-TAT-fused (s5-TAT and s6-TAT) and non-fused (non-s5

and non-s6) peptides. Likewise, s5 and s6 were the peptides with longer half-lives (5-6 hours) (**Figure 3.9F**). In mouse serum, a more physiologically relevant context, the TM7-TAT, TM6-TAT and TM5-TAT peptides were rapidly degraded, with 1-hour incubation being enough to breakdown 50% of them (**Figure 3.9G**). Hydrocarbon stapling was translated in an even higher serum stability in comparison with trypsin and chymotrypsin, ranging from half-lives of 4-6 hours for the non-s5 and non-s6 peptides to up to more than 10 hours for the rest of the stapled peptides. These results positively correlate with the respective helicity of each peptide, as the reinforcement of α -helical structure limits the peptides to adopt the extended conformation required by proteases to hydrolyse the amide bonds⁵⁸⁸. Altogether, by developing a sensitive and specific bimolecular luminescent complementation assay we were able to screen a library of small peptides targeting 5-HT_{2A}R-CB₁R heteromers. In addition, covalent side chain to chain cross-linking through hydrocarbon peptide stapling lead us to the identification of a small TM peptide mimetic, s5-TAT, with improved stability, helicity and efficacy.

3.3. Discussion

G protein-coupled receptor signalling is allosterically modulated by other proteins, including β -arrestins, heterotrimeric G proteins and receptors from the same or different classes. Understanding their pharmacology requires the development of non-destructive techniques capable of monitoring these interactions at the molecular level, with improved sensitivity and spatiotemporal resolution. Here, we illustrated how a new bimolecular luminescent complementation assay, NanoBiT, is a versatile solution to study GPCR signalling. By sequentially developing and applying different NanoBiT-based constructs, we were able to study a series of events ranging from PPIs in the plasma membrane, ligand-mediated G proteins/ β -arrestins activation and the screening of peptides disrupting 5-HT_{2A}-CB₁ receptor heteromers.

Non-invasive RET (BRET and FRET) techniques has been the most widely adopted methods to detect GPCR oligomerisation^{252,258}. However, distinguishing real interactions from chance proximity RET (bystander RET) can be challenging under some conditions. Assuming a “true” specific interaction, RET should be finite when all donor pairs are interacting with their acceptors. Thus, increasing the acceptor-to-donor ratio (A:D) should yield saturable hyperbolic curves. Importantly, situations where non-interacting proteins display hyperbolic A:D titration curves, or “real” oligomers fail to achieve RET saturation, can often lead to the misinterpretation of the results^{592,593}. Conclusions are often mistakenly drawn only taking into account the A:D ratios. However, when over-expressing heterologous receptors in cells, the acceptor density might better reflect the relevance of the detected interaction, as increasing the amount of donor has been shown to decrease the expression levels of the acceptor protein and thereby result in artefactual hyperbolic BRET/FRET saturation curves⁵⁰⁷. Unlike RET, where the strength of the signal depends on the inverse eighth power of the donor-acceptor distance, bimolecular fluorescence/luminescence complementation is not affected by the relative orientation of the interacting pairs.

Thus, one of the main attractions of BiFC is the inherent simplicity of the assay principle, allowing the detection of PPIs using relatively standard microscopy setups, providing, unlike most RET biochemical assays, spatial information of the ongoing interaction. However, the main inconvenience that often tips the balance in favour of BRET/FRET is the fact that BiFC does not reflect an equilibrium between the complexes. There is a time delay between the interaction of the fusion proteins and the functional reconstitution of the fluorescent reporter. Accordingly, reconstitution of all GFP variants requires an autocatalytic oxidation step ($t_{1/2} \sim 1h$), process known as maturation, followed by the formation of irreversible

complexes^{275,594,595}. In contrast, BiLC is reversible and protein complementation does not trap the complexes, so association and dissociation events are able to occur. Split fragments derived from the humanised forms of *Renilla reniformis* (RLuc), *Photinus pyralis* (firefly: FLuc) and *Gaussia princeps* (GLuc) luciferases have been successfully used to detect several PPIs^{596,597}. However, in comparison to RET and BiFC, the number of studies using BiLC as a favoured choice to investigate GPCR oligomerisation are rather few. In fact, BiLC has mostly been used when the analysis of higher order GPCR oligomeric structures (trimers and tetramers) or the assessment of dimer-mediated recruitment of G proteins and β -arrestin required the multiplexing of different biophysical techniques for example, using complemented donor-acceptor energy transfer (CODA-RET) or BRET between BiLC and BiFC compatible pairs^{179,199,253,281,598}.

Here, we successfully applied the recently developed NanoLuc binary technology (NanoBiT) to study GPCR oligomerisation. Using this system, we validated the previously demonstrated constitutive association of CB₁R and 5-HT_{2A} receptors as homodimers and their ability to form heteromers^{184,410,599}. To the best of our knowledge, this is the first report describing its implementation to identify GPCR dimers. We predicted that the small size of the complementary fragments (18 kDa and 1.3 kDa for LgBiT and SmBiT, respectively), would minimise steric conflicts. In fact, agonist potencies and maximal efficacies were equivalent to their matched wild type receptors under the same promoters. Apart from GLuc (19 kDa), NLuc (19 kDa) is significantly smaller in comparison to other fluorescent/luminescent proteins used in RET or protein complementation assays (ranging from 26 kDa for YFP up to 61 kDa for FLuc). In addition, no post-translational modifications have been reported in mammalian cells, resulting in lower energetic costs in terms of translation, shorting and proper polypeptide folding. Accordingly, our initial studies were performed under the control of the low copy number herpes simplex virus thymidine kinase gene promoter (HSV-TK)⁶⁰⁰. However, under this configuration, we were not able to quantitatively assess agonist-induced downstream signalling pathways. Importantly, most DNA constructs for FRET/BRET and BiFC assays use transient expression systems such as pcDNA3.1 vectors, with the cDNA expressed under the control human cytomegalovirus (CMV) immediate-early enhancer and promoter^{252,258}. Using this strategy, we developed a microtiter-based homogeneous assay that allowed the identification of GPCR oligomers in just 24 hours, reducing the chance of over-expression-related artefactual interactions. For all receptor pairs, the intensity of the luminescent readout was significantly reduced when co-expressed alongside increasing concentrations of non-tagged receptors. Although indicative of the specificity of the interaction, conclusions regarding the reversibility/stability of the receptors complexes (discussed further on) cannot be drawn from titration experiments, as the equilibrium is diverted towards certain species.

Developing BiLC-based Methods to Study GPCR protein:protein Interactions

Furthermore, when comparing our NanoBiT-based dimerisation assay with Venus YFP BiFC, an approach used to visualise more than 200 PPIs, including many GPCR homo/heteromers²⁵³, NanoBiT BiLC proved far more sensitive at detecting CB₁R and 5-HT_{2A}R homodimers and 5-HT_{2A}R-CB₁R heteromers. Presumably, the small size of the fused fragments, NanoLuc high quantum yield and the lack of BiFC maturation step act synergistically to allow us to detect PPIs 24 hours after transfection under physiological conditions.

Perhaps the most notable weakness of BiLC methods is the difficulty in obtaining spatial information, as standard luciferases low quantum yield requires intensified charge-coupled devices (CCD) and longer exposure times for their imaging. However, the natural brightness of NanoLuc in combination with an improved substrate (furimazine) has shown to be compatible with relatively simple luminescence imaging setups²⁷⁸. Thus, whether our approach allows the direct visualisation of GPCR complexes requires further studies.

We developed NanoBiT-based assays that reflect the dynamic character of the β -arrestin2 interaction with the CB₁, CB₂ and the 5-HT_{2A} receptors. Importantly, when compared to other commercially available assays (PathHunter® and Tango™), the potencies of their selective agonists and antagonist (EC₅₀/IC₅₀) were within the same ranges^{29,576}. Furthermore, our results for the CB₁ and CB₂ receptors are in line with those reported by Caninaert et al., demonstrating that the CB₁R-LgBiT:SmBiT- β -arrestin2 and the CB₂R-SmBiT:LgBiT- β -arrestin2 provide the best protein pairs⁵⁵⁷.

Early studies on the 5-HT_{2A}R contributed to laying the foundations of the concept known as “functional selectivity” or “ligand bias”¹²⁶. However, despite many efforts, the basis underlying why certain 5-HT_{2A}R agonist (LSD, DOI, mescaline, psilocybin) exert hallucinogenic effects remain elusive. β -arrestin-dependent signalling has been closely interlinked, while 5-HT-induced head twitch responses, ERK1/2 phosphorylation and receptor internalisation are β -arrestin2-dependent processes, the hallucinogenic 5-HT_{2A}R agonist DOI is able to trigger these responses regardless of β -arrestin2 expression⁵⁶⁰. Consequently, 5-HT_{2A}R drug discovery requires new reliable approaches to cover the different signalling events downstream of receptor activation. Notably, our NanoBiT β -arrestin2 recruitment assay provided information of the kinetic context in which the interactions are taking place, leading us to observe a more sustained receptor:arrestin interaction for 5-HT_{2A}R in comparison with the related rhodopsin-like CB₁ and CB₂ receptors. So far, only BRET-based assays allow to measure the time frame and duration of this G protein-independent signalling pathway. Here we provide an alternative approach using smaller fusion proteins and a more stable substrate. Time is an extra dimension that should be taken into account in drug discovery, as elegantly illustrated by Lane, Christopoulos and collaborators, who showed that the direction of certain D₂ biased ligands is profoundly influenced by the kinetic context¹²¹

More challenging, from the kinetic perspective, is the interaction between receptors and G proteins. Similarly, Bodle et. al successfully developed a NanoBiT assay to study the interaction between 15 different regulators of G protein signalling (RGS) proteins with their cognate heterotrimeric G proteins. However, the elapsed time between the direct pharmacological activation of the G proteins and the formation of 50% of the RGS:G proteins complexes ranged from 15 to 20 minutes. In addition, not depending on receptor-induced G protein conformational rearrangements might allow a more flexible choice when designing the anchoring points of the NanoBiT subunit⁵⁶². Our results, although not revealing changes after agonist stimulation, show CB₁R and 5-HT_{2A}R preference to interact with their respective cognate G $\alpha_{i/3}$ and G α_q G protein subunits in the basal state, as illustrated when non-canonical G α subunits were co-expressed in the presence of either CB₁ or 5-HT_{2A} receptors. These observations are in line with those from Galés and collaborators, which suggest a constitutive α_{2A} AR-G $\alpha\beta\gamma$ pre-association⁵⁷⁸. However, intramolecular insertion of SmBiT into G α_q (SmBiT₁₂₄-G α_q) strongly suggests that, even in an allegedly fully functional configuration, our NanoBiT setup cannot provide real-time information about G protein activation. BRET studies revealed that receptor-G protein complexes are stable just over a few seconds^{569,578}. In addition, recent single-molecule analysis has shown that agonist binding mostly accelerates the on rates of the receptor:G protein complexation, whereas the K_{off} is only marginally affected^{307,567}. Interestingly, using single-molecule imaging in live cells, Calebiro and collaborators shown that α_{2A} -ARs:G α_i and β_2 -ARs:G α_s interactions take place in particular domains of the plasma membrane, termed “hot spots” and that only a small fraction of agonist-bound membrane receptors (~5%) are in complex with G α subunits at any given time⁵⁶⁷. Taking together the kinetics of these interactions and the low populations forming them might account for not detecting agonist-driven G protein recruitment with our NanoBiT setup.

The use of TM peptides to disrupt the interfaces interacting in homo/hetero-receptors complexes is two-fold. First, allowing to dissect specific events driven by these complexes, TM peptides may help to answer to which extent oligomerisation is functionally relevant. Second, in a pathophysiological context where receptor complexes drive undesired outcomes, TM peptides can become a therapeutically agent. Whereas in the recent years increasing number of *in vitro* studies illustrate their potential, just few authors report their use in animal models. For example, disrupting D₁-D₂ receptor heteromers with TAT fused D₂R IL3 or D₁R C-tail mimetic peptide resulted in antidepressant-like effects^{601,602}. These interactions are previously mapped in heterologous expression systems, thereby the development of robust screening platforms that as far as it is possible reflect a physiological context is the first step to identify successful candidates⁶⁰³. Using NanoBiT, we established an assay to screen a small library of hydrocarbon-stapled peptides. Importantly, although for some particular receptors

Developing BiLC-based Methods to Study GPCR protein:protein Interactions

it has been shown to affect surface expression, fusing NanoLuc pairs to the N-terminus of CB₁ and 5-HT_{2A} receptors rendered constructs with wild type-like properties. In addition, the LgBiT-CB₁R:SmBiT-5-HT_{2A}R pair yielded the best assay window under relatively low levels of transfections. The former is an important concept as an optimal BRET-based approach often requires higher levels of receptor expression. This strategy led us to the identification of a small CB₁R TM5-derived peptide, s5-TAT, which combines two important structural features: the HIV-TAT cell penetrating sequence and hydrocarbon-stapling with improved α -helical stability. Importantly, kinetic studies reveal that the s5-TAT peptide was able to disrupt 5-HT_{2A}R-CB₁R heteromers in a time-dependent manner, demonstrating the reversibility of our BiLC assay. For the first time, we provided GPCR disrupting peptides stability data. Hydrocarbon stapling resulted in 2-fold trypsin and chymotrypsin proteolytic resistance and 10-fold stability increase in serum. This correlates with the reduction of putative proteolytic cleavage sites and the reported decreased rate of proteolysis due to α -helical structure confinement⁵⁸⁸.

Most *in vivo* studies on GPCR oligomers targeting with peptides have applied intracerebroventricular or intraperitoneal administration routes. Although highly specific and well tolerated, the hydrophobicity, low membrane permeability and stability of these therapies are limiting factors for the clinical development. It is even more challenging if we consider the case of CNS disorders where the blood-brain barrier confers an extra impediment. We hypothesise that favourable pharmacokinetics might be achieved by combining the improved peptide stability with the cell penetrating HIV-TAT sequence, as illustrated by the c-Jun N-terminal kinase (JNK) TAT-fused inhibitor D-JNKI-1, having central effects after chronic intraperitoneal administration⁵⁹⁰.

Overall, from signalling to receptor:receptor complexes, we provided a comprehensive study illustrating how a new BiLC-based assay can be successfully applied to study different aspects of GPCR pharmacology. Using NanoBiT, we developed useful tools that will be further explored in future sections of this thesis (See Chapters 4 and 6).

3.4. Acknowledgements

We thank Andy Cheigné for plasmids encoding the G α_{i1} , G α_{i3} and G α_q proteins in pcDNA3.1 backbone and Dr Lesley Howell and Lucka Bibic for peptide synthesis and stability studies.

Chapter 4

Molecular Basis Underlying 5-HT_{2A}-CB₁ Receptor Heteromers

4.1. Introduction

As previously discussed (see section 1.2), the ability of GPCRs to form quaternary macromolecular structures brings together a whole new set of allosteric possibilities²⁴⁹. Despite over fifteen years of research on homo and heteromers, there is still little understanding of how these interactions occur. In Chapter 3, we developed a series of tools allowing us to monitor GPCR interacting with each other and with effector proteins. Accordingly, in the present section we will take advantage of them, together with other complementary techniques, to tackle Class A oligomerisation from a mechanistic perspective, that is, understanding the allosteric communication within GPCR heteromers.

Allosterism is usually referred to by the ability of certain modulators to alter the conformation of their target protein through binding to a topologically distinct binding site from the orthosteric ligand²⁹⁴. Perhaps the most common form of this way of communication is through protein-protein interactions, where long range conformational changes can be transmitted within the different subunits resulting in their activation/inhibition, ligand cooperativity, or the recruitment of new effectors^{604,605}. This is clearly illustrated by the bi-directional allosteric influence between GPCRs and G proteins. While agonist binding to the receptors promotes conformations capable of binding heterotrimeric G proteins, this coupling also influences ligand affinity to the orthosteric site⁶⁰⁵. Similarly, the perturbation generated after a conformational rearrangement of a protomer will be transmitted to the concomitant receptor within a dimer.

The functional outcome of heteromer formation has been generally appreciated to be in the form of signalling and/or ligand binding cross-talk. Early studies reported this through cooperativity between orthosteric ligands binding to the different protomers, including homomeric M₂R, D₂R, and TSHR or A_{2A}R-D₂R, CCR2-CCR5 heteromeric complexes⁶⁰⁶⁻⁶¹⁰. In addition, oligomerisation consequences can be appreciated from pharmacological observations in terms of altered signalling, for example, increased morphine efficacy in α_{2A} AR- μ OR heteromers but decreased response when co-administrated together with an α_{2A} AR agonist^{248,611}. The application of resonance energy transfer (RET) to the study of GPCR oligomerisation has been crucial for the identification of homo- and hetero-oligomeric complexes in live cells⁶¹². However, although this strategy has provided strong support for their stoichiometry and the structural assembly, these findings have been buttressed by recent advances in super resolution and single-molecule microscopy, which, in conjunction with crystallographic information, have revealed a complex diversity of assemblies (dimers, trimers, etc.) and conserved interfaces stabilising them^{186,209,213,215}.

Molecular Basis Underlying 5-HT_{2A}-CB₁ Receptor Heteromers

As is the case for many heteromers, one central question remains to be addressed, that is the mechanism driving cross-talk. Moreno et al. recently showed that mGlu2-driven 5-HT_{2A}R signalling in mGlu2-5-HT_{2A}R heteromers requires both protomers capable of binding G proteins. In addition, the authors proposed a tetrameric assembly formed by dimers of homodimers¹⁸⁵. A similar mechanism was found with the adenosine A₁ and A_{2A} receptor heteromers, where they form heterotetramers of homodimers, capable of simultaneously binding their respective G_i and G_s proteins but efficiently activating only one of them²¹⁷.

Cross-talk appears to be uniform, that is if, a heteromer enhances signalling, then this increased signalling is seen on all downstream pathways. This suggests that what drives the cross-talk is inherent to the complex itself. This can be observed, for example, in the dopamine D₁-D₃ receptor heteromers, where D₃R agonist enhances agonist binding to D₁R in a non-reciprocal way, potentiating D₁R-mediated cAMP stimulation and synergistically promoting locomotor activity in reserpinised mice^{613,614}. Similarly, antagonism in δ OR potentiates μ OR agonists binding, signalling and antinociception through δ OR- μ OR heteromers¹⁸⁰. While the opposite is also true, when an interaction leads to a reduction or blocking of a signalling pathway, this is seen on all the pathways. This phenomenon is perhaps the most reported consequence of oligomerisation, with most studies reporting negative cooperativity at the binding sites, agonist-driven negative cross-talk and cross-antagonism. However, it is not clear if the regions responsible for this across the board cross-communication between receptors are conserved. In addition, to what extent is a functional receptor required for the observed cross-talk? In the case of homodimers, using signalling and/or binding-deficient mutants, evidence was provided unequivocally that through intermolecular cooperation dimerisation provides a mechanism to rescue function, including the class A D₂, TSH, FSH and LH receptors^{240,242,615}. These studies suggest asymmetrical intermolecular trans-activation with one G protein. However, whether G proteins are required for heteromer cross-talk has not been explored, but suggestions that G proteins may be involved have been shown for the A₁-A_{2A} and the 5-HT_{2A}-mGlu₂ receptor heteromers^{185,217}. In addition, several studies have looked at the architecture of heteromers, with the general consensus that they can function as either dimers of dimers or as dimers alone¹⁶¹. In the case of higher order oligomeric structures, are more than one G protein bound? In the case of the A₁-A_{2A} heteromers it appeared that both G proteins could associate but activation was limited to only one G protein at a time. For other heteromers, such as the 5-HT_{2A}R-CB₁R oligomers, a G protein class switch has been suggested, but it was never demonstrated how many G proteins were actually bound and to which protomer they were coupled.

In view of the above, does the agonistic/antagonist nature of heteromers cross-talk determine the activation/inhibition of all downstream signalling pathways or, on the contrary, does it

depend on each individual effector system? If the second is true, which are the minimal structural determinants driving that? In addition, whereas in some cases cross-talk occurs in the presence of a ligand-free protomer (e.g. A_{2A}-D₂ receptor heteromer)³⁰⁴, dual ligand binding is often required. Intuitively, this raises the issue about to what extent the functionality or conformational state of the receptors influences their “dialog”. Furthermore, as for monomeric receptors, what role do G proteins play and how many are involved in heteromer function and communication?

In the present study, we sought to answer some of these questions by studying the recently identified heteromers between 5HT_{2A}R and CB₁R to understand what drives functional crosstalk. This heteromer is responsible for the cognitive side effects of Δ⁹-tetrahydrocannabinol (THC), the psychoactive ingredient of marijuana¹⁸⁴. Importantly, CB₁R-5-HT_{2A}R complexes are among the few oligomers wherein their expression in native tissues and physiological relevance has been demonstrated, meeting all the recently proposed criteria to define genuine GPCR heteromers: (1) co-localisation and physical interaction, (2) constitute a new pharmacological entity with different properties from those of the protomers and (3) selective disruption of the complexes leads to the loss of the heteromer-specific outcomes¹⁸⁸. On the basis of their promising implications as alternative pain treatments and in the safe use of cannabinoid-based therapies, we sought to provide an exhaustive study from a mechanistic perspective as there are still basic questions remaining on how such complexes function.

4.2. Results

4.2.1. Functional characterisation of 5-HT_{2A} and CB₁ receptors mutants

In order to uncover the mechanism and key motifs driving CB₁-5-HT_{2A} receptor heteromer function, we first rationally designed a series of 5-HT_{2A}R and CB₁R mutants. Our goal was to create receptors that were either unable to undergo ligand-induced activation or to efficiently couple G proteins (**Figures 4.1A, B**) with unaltered ligand affinity.

Upon receptor activation, the cytoplasmic end of TM6 moves away from TM3 and towards TM5 to contact the C-terminal $\alpha 5$ helix of the G α subunits^{43,616,617}. The sequence of events following ligand binding starts with the transmission switch and end with the stable binding of the G protein at the cavity generated by the TM6 movement^{618,619}. Comparative studies between the human β_2 adrenoceptor (β_2 -AR) bound to a G protein-like nanobody and the metarhodopsin II in complex with a C-terminal 11-aminoacid peptide derived from G_t led to the identification of positions in TM3, TM5 and TM6 forming a consensus network for receptor-G protein interaction^{13,43,620}. Accordingly, we designed alanine substitutions in both the 5-HT_{2A}R and the CB₁R aiming to impede receptor activation via (i) the transmission switch (mutants 5-HT_{2A}R I163^{3,40} and CB₁R V204^{3,40}; superscripts following residue numbers refer to Ballesteros and Weinstein numbering scheme²⁶), (ii) an intermediate switch that involves Thr210^{3,46} (CB₁R only; mutant CB₁R T210^{3,46}), and (iii) residues involved in the receptor-G protein binding interface (mutants I181A^{ICL2}, T257A^{5,61} and L325A^{6,37} in 5-HT_{2A}R and I297A^{5,61}, L341A^{6,33} and L345A^{6,37} in CB₁R).

We tested 5-HT_{2A}R mutants for their ability to mobilise intracellular calcium [Ca²⁺]_i, a canonical second messenger downstream the G_{q/11}-coupled 5-HT_{2A}R⁶²¹. 5-HT_{2A}R I163A^{3,40} failed to mobilise [Ca²⁺]_i after 2,5-Dimethoxy-4-iodoamphetamine (DOI) administration in transiently transfected HEK293 cells (**Figure 4.1C**), confirming the importance of the transmission switch in aminergic receptors⁶²². 5-HT_{2A}R I181A^{ICL2} impaired both potency and receptor maximal response (E_{max}) (**Figure 4.1C**), nearly abolishing DOI-induced [Ca²⁺]_i release (~25% E_{max}, 5-HT_{2A}R WT Vs 5-HT_{2A}R I181A^{ICL2}) and decreasing ~100 fold DOI's half maximal effective concentration (EC₅₀) (pEC₅₀= 9.9 and 7.8 for WT Vs 5-HT_{2A}R I181A^{ICL2}, respectively). Similar results have been recently observed for the 5-HT_{2A}R I181D mutant¹⁸⁵. In addition, previous studies on the α_{1B} -adrenergic and histamine H₁ receptors identified conserved hydrophobic residues in their second intracellular loop (ICL2) required for the efficient coupling of G_{q/11} without impairing ligand binding⁶²³. Mutants T257A^{5,61} and

L325A^{6,37} impaired 5-HT_{2A}R signalling (**Figure 4.1C**), with a rightward shift in DOI-induced potency and nearly reaching half E_{max} in comparison to the wild type (WT) receptor.

5-HT_{2A} receptors were among the first GPCRs identified to exhibit functional selectivity¹²⁶. As previously discussed (see section 1.1.5.3), some of their ligands induce psychedelic LSD-like effects, while others, such as the endogenous serotonin (5-HT) monoaminergic neurotransmitter does not⁵⁷³. To verify that the above mentioned 5-HT_{2A}R mutants do not display “ligand-bias”, we assessed the effect of the endogenous non-hallucinogenic 5-HT ligand in calcium signalling (**Figure 4.1E**). In agreement with our previous results, 5-HT_{2A}R I163A^{3,40} and I181A^{ICL2} did not elicit $[Ca^{2+}]_i$ release under saturating 5-HT concentrations and 5-HT efficacy was significantly reduced in 5-HT_{2A}R T257A^{5,51} and L325A^{6,37} mutants. In addition, we did not observe differences between both ligands, indicating that the proposed mutations are not ligand/mutant-specific.

We tested the CB₁R mutants for their ability to reduce the production of cAMP⁶²⁴. Interestingly, the V204A^{3,40} substitution had no impact on CB₁R, as cAMP levels were still reduced after WIN 55212-2 (WIN) stimulation (**Figure 4.1D**). This result argues against the existence of a transmission switch in the CB₁R (and related receptors) that lack Pro^{5,50}. Next, we analysed the effects of the CB₁R T210A^{3,46} mutant, as this position has been linked to conformational rearrangements in the transition between the inactive and active CB₁R structures⁶²⁵. In agreement, we found a discrete but significant decrease in CB₁R-mediated cAMP release inhibition (**Figure 4.1D**). L341A^{6,33} and L345A^{6,37} mutants significantly impacted CB₁R function, with the alanine substitution at position 341 sufficient to banish receptor signalling (**Figure 4.1D**). Likewise, using a different non-classical CB₁R agonist (CP55940), it was recently shown that alanine substitution in CB₁R L341^{6,33} retained ligand binding but prevented G_{i/o} recruitment and activation, identifying a series of crucial residues in the juxtamembrane regions of the ICL2 and ICL3 for productive receptor:G protein interactions⁶²⁶. By contrast, the CB₁R L222A^{ICL2}, homologous to the 5-HT_{2A}R I181^{ICL2} substitution, had no effect in CB₁R function (**Figure 4.1D**). We thus assessed whether double substitutions could fully block CB₁R by designing double mutants that combined positions involved in receptor activation and G protein recruitment (V204A^{3,40}/L222A^{ICL2} and V204A^{3,40}/L345A^{6,37} double mutants) or looking for synergic effects of substitutions in residues presumably driving CB₁R-G_{i/o} interaction (L222A^{ICL2}/L297A^{5,61} and L222A^{ICL2}/L345A^{6,37} double mutants). Unfortunately, none of the constructs were more effective than the single mutants L345A^{6,37} or T210A^{3,46} alone (**Figure 4.1D**). Together, our mutational data indicate different structural determinants between 5-HT_{2A} and CB₁ receptors driving receptor activation and/or G protein coupling.

Molecular Basis Underlying 5-HT_{2A}-CB₁ Receptor Heteromers

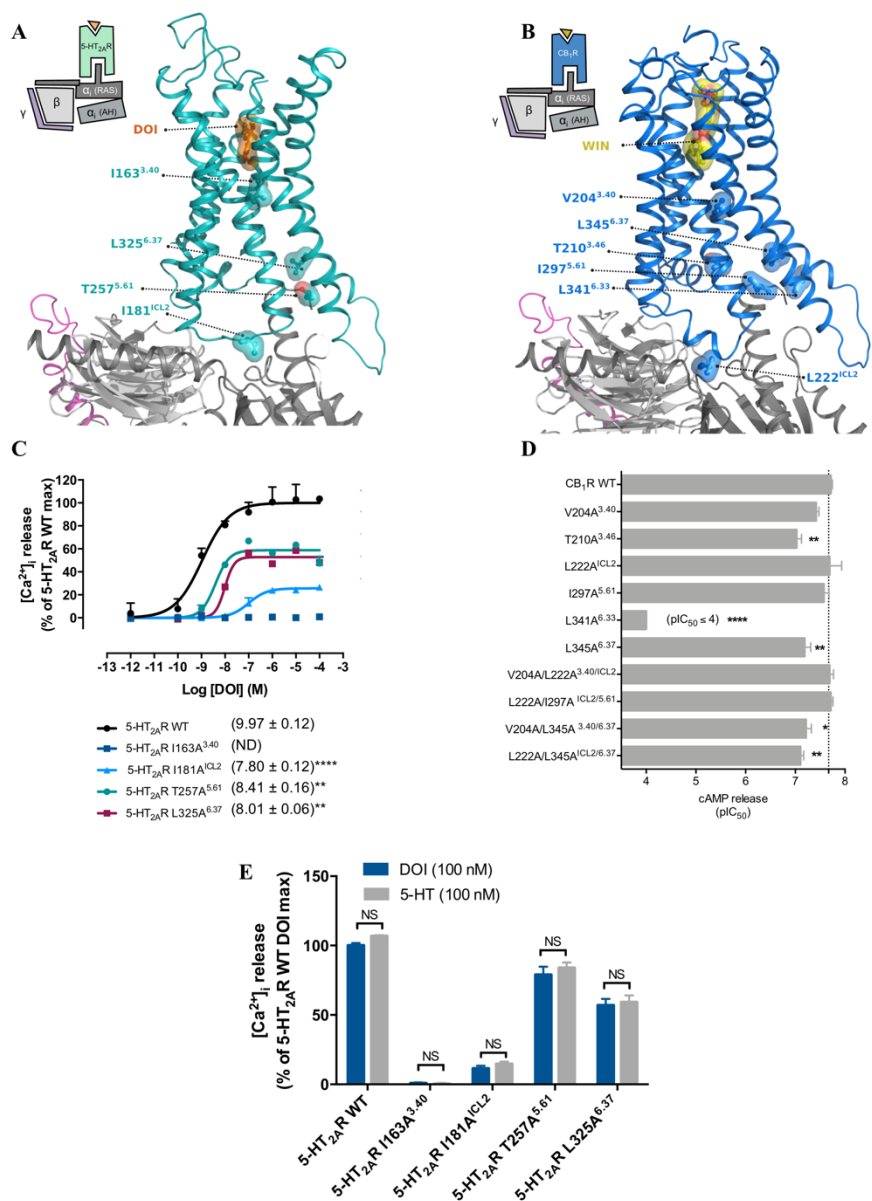


Figure 4.1. CB₁ and 5-HT_{2A} receptors mutant proposal. Molecular models of the CB₁R-5HT_{2A}R heteromers in complex with G_i (A) or G_q (B) proteins (grey) illustrating the location of the mutated residues after simultaneous agonist activation. The CB₁R (PDB:5TGZ) and 5-HT_{2B}R (PDB:4IB4) crystal structures were used as template for CB₁R and 5-HT_{2A}R, respectively, incorporating features (cytoplasmic ends of TMs 5 and 6) from the active β_2 AR-G_s complex (PDB:3SN6) to model G protein binding. In (C), representative dose-response intracellular Ca²⁺ release curves for the 5-HT_{2A}R mutants. Values in brackets represent the mean pEC₅₀ ± SD (n=2) indicating significant differences over WT 5-HT_{2A}R evaluated by one-way analysis of variance (ANOVA) followed by Bonferroni post hoc tests (**p ≤ 0.01, ****p ≤ 0.0001). In (D), mean pIC₅₀ ± SEM (n=3) forskolin-induced (7.5 μM) cAMP release inhibition for the CB₁R mutants. Statistical significance was evaluated as in C, indicating significant differences over WT CB₁R (*p ≤ 0.05, **p ≤ 0.01 and ****p ≤ 0.0001). (E) Intracellular Ca²⁺ release was measured to assess the non-ligand-dependent profile of the 5-HT_{2A}R mutants after administration of a saturating concentration (100 nM) of the endogenous non-hallucinogenic 5-HT and the psychedelic DOI agonists. Data are mean ± SEM (n=3-4) of percentage of activation normalised to WT 5-HT_{2A}R maximal response. Unpaired t-tests analysis between groups followed by Holk-Sidak corrections for multiple comparison showed no statistical significance.

On the basis of these findings, we selected 5-HT_{2A}R single mutants I163A^{3.40} and I181A^{ICL2} (gave complete or 100-fold Ca²⁺ signal inhibition, respectively) and CB₁R single mutants L341A^{6.33} and L345A^{6.37} (gave a complete or partial cAMP release inhibition, respectively).

In order to provide a more detailed characterisation, first we validated their correct surface expression by immunofluorescence. All 5-HT_{2A}R and CB₁R constructs displayed a homogeneous distribution across the cell-surface, with similar fluorescence intensities and no appreciable signs of neither endoplasmic reticulum nor export/retention impairments (**Figure 4.2A**). Next, we studied their effect in two well know signalling events downstream of most GPCRs' activation; β -arrestin2 recruitment and extracellular regulates kinases 1 and 2 (ERK1/2) phosphorylation (**summarised in Table 4.1**). To monitor β -arrestin 2-receptor interactions, we applied the previously optimised NanoBiT technology (see Chapter 3).

In agreement with the calcium flux assays, I163A^{3.40} and I181A^{ICL2} substitutions in 5-HT_{2A}R abolished DOI-induced ERK1/2 phosphorylation (**Figure 4.2B**). Interestingly, while we did not detect any levels of β -arrestin2 binding to 5-HT_{2A}R I163A^{3.40}, I181A^{ICL2} replacement had no impact on β -arrestin2 recruitment (**figure 4.1D**), although its signalling through intracellular calcium and ERK1/2 pathways was highly impaired (**Figures 4.1C and 4.2B**). Regarding CB₁R, L341A^{6.33} inhibited WIN-induced ERK1/2 and β -arrestin2 signalling (**Figure 4.2C,E**), showing that a single alanine substitution in this position is able to completely block G_{i/o}, ERK1/2 and arrestin signalling. In addition, CB₁R L345A^{6.37} displayed a similar trend as in cAMP assays (**Figure 4.2C,E**), with discrete activation of both pathways (E_{max} ~40% and 20% in ERK1/2 and β -arrestin2, respectively).

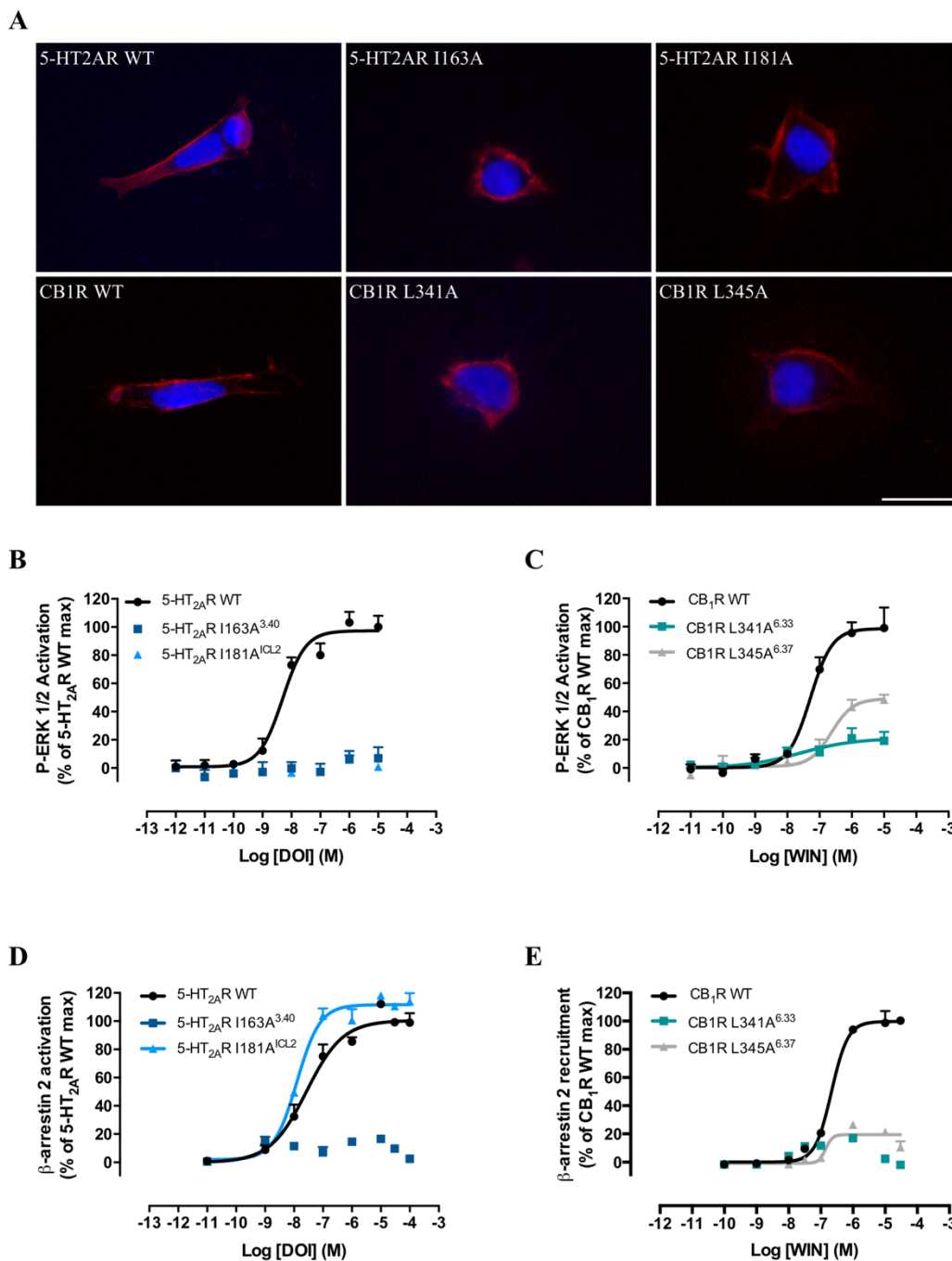


Figure 4.2. Cellular distribution of the selected CB₁ and 5-HT_{2A} receptors mutants and signalling profiling.

(A) representative immunofluorescence microscopy images of HEK293 cells transiently transfected with HA-tagged wild type or mutant receptor forms (see figure legends) illustrating cell surface receptor expression (red) surrounding the DAPI stained nucleus (blue). Scale bars: 10 μ m. Representative dose-dependent pERK1/2 activation curves upon 5-HT_{2A} (B) and CB₁ (C) stimulation ($n \geq 4$) or agonist-driven β -arrestin 2 recruitment to 5-HT_{2A}R (D) and CB₁R (E) ($n \geq 2$). Data are mean + SEM (B and C) or SD (D and E) percentage normalised to WT maximal response.

Table 4.1. 5-HT_{2A}R and CB₁R mutants potency and efficacy in ERK1/2 and β -arrestin 2 signalling.

Receptor	pERK1/2		β -arrestin 2	
	pEC ₅₀	E _{max} (% of WT)	pEC ₅₀	E _{max} (% of WT)
5-HT _{2A} R				
WT	8.31 ± 0.15	100 ± 5	7.57 ± 0.15	100 ± 5
I163A	ND	ND	ND	ND
I181A	ND	ND	7.91 ± 0.09	111 ± 4
CB ₁ R				
WT	7.23 ± 0.16	100 ± 6	6.67 ± 0.07	100 ± 3
L341A	7.60 ± 0.93	21 ± 8 ^{***}	ND	ND
L345A	6.63 ± 0.23	50 ± 6 ^{**}	6.84 ± 0.01	21 ± 2 ^{**}

Agonist-induced β -arrestin2 signalling and ERK1/2 phosphorylation in response to the 5-HT_{2A}R and CB₁R agonists DOI and WIN, respectively. Values represent the mean pEC₅₀/pIC₅₀ ± SEM or the mean E_{max} ± SEM percentage normalised to WT receptor maximal activation (n=3). Statistical significance was evaluated by two-tailed unpaired t-test when comparing two groups or by one-way ANOVA followed by Bonferroni post hoc tests for three groups. (**p ≤ 0.01, ***p ≤ 0.001). ND, non-determined, indicate non-convergent curve fits.

4.2.2. Two-photon polarization microscopy (2PPM) reveals heteromer-driven G protein class switch

Heteromerisation can lead to a switch in G protein recruitment of the interacting protomer, termed “class switch”. This is the case of the dopamine D₁-D₂ heterooligomers-specific coupling to G_{q/11} heterotrimeric G proteins⁶²⁷. In addition, it can enable the partner receptor to signal through its G protein, as reflected by the ability of the G_{i/o}-coupled metabotropic glutamate 2 (mGlu₂) receptor to activate G_{q/11}-dependent signalling through 5-HT_{2A}-mGlu₂ receptor heteromers, termed “trans-activation”^{185,317}. CB₁R and 5-HT_{2A}R are well-established G_{i/o}- and G_{q/11}-coupled receptors^{628,629}. Previous studies found that co-expression of both receptors led to 5-HT_{2A}R signalling through G_{i/o} proteins, as cells expressing only 5-HT_{2A}R retain their canonical G_{q/11} coupling signature¹⁸⁴. These results suggest two different scenarios: first, the conformational change upon agonist binding to the 5-HT_{2A}R protomer allosterically shifts the CB₁R state into an active-like conformation capable of binding G_{i/o} subunits (receptor trans-activation) or, second, heteromerisation offers 5-HT_{2A}R new conformational options allowing non-canonical G_{i/o} protein binding (G protein class switch).

To examine the heteromer-driven non-canonical binding of heterotrimeric G_{i/o} proteins after 5-HT_{2A}R stimulation, we employed a recently developed two-photon polarization microscopy (2PPM) technique to directly visualise receptor:G protein interactions^{533,534}. 2PPM allows

Molecular Basis Underlying 5-HT_{2A}-CB₁ Receptor Heteromers

visualisation of G protein activation, due to the accompanying changes in orientation freedom of fluorescent labels attached to the investigated G α subunits. Fluorescent labels in non-activated G α subunits (present in heterotrimeric complexes with G β and G γ subunits) generally display higher values of linear dichroism (LD; differences between images acquired with two distinct linear polarizations of excitation light) than in activated, monomeric G α subunits. Thus, we transfected HEK293 cells with constructs encoding the G α_{i1} protein subunits (GAP43-eCFP-G α_{i1} , G β 1, G γ 2) and the investigated receptors (5-HT_{2A}R, and/or CB₁R-eYFP) (**Figures S1A-E**). In the presence of only 5-HT_{2A}R, the GAP43-eCFP-G α_{i1} construct exhibited log₂(r_{max}) values of 0.249 (0.183/0.371) (median (25% percentile/75% percentile)). Importantly, no change in LD of the G α_{i1} protein could be observed upon stimulation of the receptor with DOI (100 nM) (**Figure S1A**), showing the lack of G_i coupling to 5-HT_{2A}R in our experimental setup. In the presence of only CB₁R-eYFP, the eCFP-tagged G α_{i1} subunit showed lower LD (0.131 (0.107/0.182)) than in the presence of 5-HT_{2A}R. This is likely due to the baseline constitutive activity of the CB₁R receptor⁵³⁴. As expected from its canonical G_{i/o} coupling, a pronounced decrease in LD was observed upon CB₁R stimulation with WIN (10 μ M) (**Figure S1B**). Furthermore, stimulation of cells expressing CB₁R-eYFP with DOI (100 nM) did not lead to any change in LD of the G α_{i1} construct, thus precluding potential ligand selectivity (**Figure S1C**). However, in cells expressing both 5-HT_{2A}R and CB₁R-eYFP, DOI application led to a significant decrease in LD from 0.181 (0.145/0.279) to 0.136 (0.073/0.183) of the eCFP-tagged G α_{i1} subunit, consistent with 5-HT_{2A}R-mediated non-canonical G_i proteins activation through 5-HT_{2A}R-CB₁R heteromers (**Figure S1D**). Finally, we sought to test whether there was a trans-activation of G protein occurring. We repeated our experiments using the above characterised 5-HT_{2A}R I181A^{ICL2} mutant, designed to avoid G protein recruitment. Accordingly, cells co-transfected with CB₁R-eYFP and the 5-HT_{2A}R mutant I181A^{ICL2} did not show any change in LD of the G α_{i1} construct upon DOI application (**Figure S1E**). These data indicate that (i) the G α_{i1} protein can be activated by stimulating 5-HT_{2A}R, but only in the presence of CB₁R, (ii) the efficiency of 5-HT_{2A}R-mediated activation appears lower than the efficiency of direct G α_{i1} activation through CB₁R and (iii) that heteromerisation provides new opportunities to switch 5-HT_{2A}R G protein preferential coupling.

According to this scenario, we would expect that increasing the number of CB₁R:5-HT_{2A}R complexes by altering the cDNA ratio would enhance the ability of 5-HT_{2A}R to dimerise with CB₁R, and hence its classical G_{q/11}-dependant [Ca²⁺]_i release would be hampered. Accordingly, a 1:1 CB₁R:5-HT_{2A}R ratio nearly halved 5-HT_{2A}R-triggered calcium signalling, with and almost completely blockage of this pathway at higher ratios (**Figure 4.3B**).

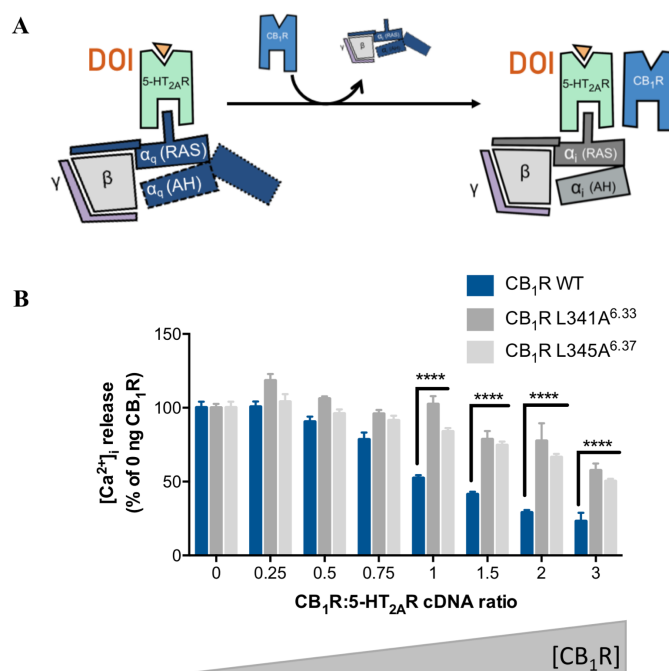


Figure 4.3. 5-HT_{2A}R-CB₁R heteromers-driven G protein class switch occurs at the plasma membrane. (A) Schematic representation of G protein class switch over increasing CB₁R concentrations. **(B)** HEK293 cells co-transfected with a fixed amount of 5-HT_{2A}R and increasing WT CB₁R, CB₁R L341A and CB₁R L45A (see figure legend) ratios were stimulated with a saturating concentration (100 nM) of the 5-HT_{2A}R agonist DOI. Values are mean ± SEM percentage [Ca²⁺]_i release normalised to 0 ng CB₁R transfected cells (n ≥ 4). Statistical significance was evaluated by two-way ANOVA followed by Bonferroni post hoc tests showing significance over WT CB₁R (****p ≤ 0.0001)

Interestingly, this effect was only observed in the presence of WT CB₁R. By contrast, co-expression of WT 5-HT_{2A}R with either the CB₁R L341A^{6.33} or L345A^{6.37} non-functional mutants retained DOI-mediated [Ca²⁺]_i release at a 1:1 cDNA ratio. In addition, this effect was maintained over higher receptor ratios, with the ability of CB₁R mutants to uncouple 5-HT_{2A}R from its canonical G_{q/11} downstream signalling pathway significantly lower (**Figure 4.3B**). It is important to note that the above mentioned decrease in [Ca²⁺]_i signalling was not observed as a result of altering 5-HT_{2A}R expression levels, as the [Ca²⁺]_i release levels were upregulated over increasing CB₁R mutant concentrations. Altogether, our 2PPM and Ca²⁺ results indicate that CB₁R can modulate 5-HT_{2A}R independently of its ligand-bound state. However, confining CB₁R into an inactive-like conformation through L341A^{6.33} and L345A^{6.37} suffices to banish its allosteric effect on 5-HT_{2A}R. Our results strongly support that, in the presence of CB₁R, 5-HT_{2A}R uncouples from G_{q/11} heterotrimeric G proteins and switches towards the binding of

G_{i/o} subunits. In addition, this phenomenon requires two functional protomers capable of undergoing ligand activation and to bind G proteins.

4.2.3. G protein functional coupling to 5-HT_{2A}R is necessary for 5-HT_{2A}R-mediated cAMP release inhibition in 5-HT_{2A}R-CB₁R heteromers.

Previous studies have shown how 5-HT_{2A}-CB₁ receptor heteromers display negative cross-talk and cross-antagonism both *in vivo* and *in vitro*¹⁸⁴. Cross-antagonism defines the action of a selective antagonist of one receptor to not only block its expected target function but, in addition, allosterically inhibiting the partner protomer in the heteromer. Likewise, agonists can act in a similar manner, influencing the activation of the concomitant receptor and often restricting its signalling, termed, negative cross-talk. In agreement with our 2PPM results (**Figures S1A-E**), DOI stimulation resulted in a reduction in forskolin (FK)-induced cAMP accumulation in cells co-expressing CB₁R and 5-HT_{2A}R (**Figure 4.4A**), showing functional 5-HT_{2A}R-mediated G_{i/o} signalling. In addition, simultaneous addition of both agonists did not evoke an additive effect, confirming the above stated negative cross-talk. It is important to note the specificity of DOI and WIN effects, as both were blocked by their corresponding selective antagonist, MDL 100907 (MDL) and Rimonabant (RIM), respectively (**Figure 4.4A-3F**). Of note, it was previously reported the selectivity of all ligands used in this study in cells only expressing CB₁ or 5-HT_{2A} receptors and the lack of G_{i/o} coupling in HEK293 cells expressing only 5-HT_{2A}R¹⁸⁴. This is further supported by our 2PPM results (**Figures 3A-F**). On the basis of the above ratio experiments, all experiments were performed in a 1:1 CB₁R:5-HT_{2A}R ratio.

Next, we sought to address whether this pharmacological fingerprint depends on the presence of a functional 5-HT_{2A}R. To this end, we assessed the effect in cross-talk of the non-functional (**Figures 4.1C, 4.2B and 4.2D**) 5-HT_{2A}R I161A^{3,40} mutant. Although CB₁R signalling properties remained unaltered (**Figure 4.4B**), co-transfection of WT CB₁R with 5-HT_{2A}R I161A^{3,40} abolished DOI-induced cAMP inhibition, thus negative cross-talk was virtually impossible. These results point again towards the necessity of two functional protomers so that cross-communication between protomers takes place. However, this configuration could fail to depict a scenario where trans-activation from 5-HT_{2A}R towards CB₁R involves residues close to the binding pocket, as 5-HT_{2A}R I161A^{3,40} could be stabilised into a conformationally restricted state and therefore allosteric modulation within protomers would not take place.

To address this option, we took advantage of the 5-HT_{2A}R I181A^{ICL2} mutant (**Figures 4.1C, 4.2B and 4.2C**), designed to keep its ligand binding unaffected but unable to interact with G_{q/11} proteins¹⁸⁵. Co-expression with WT CB₁R resulted in the loss of cross-talk, as can be seen by the absence of cAMP release inhibition when cells were treated with DOI (**Figure 4.4C**). Again, CB₁R signalling properties remained intact. These results indicate that rather than receptor trans-activation, allosteric communication from 5-HT_{2A}R towards CB₁R does not occur through the conformational rearrangement of residues in TM3 after agonist-induced 5-HT_{2A}R activation, as shown for the WT CB₁R-5HT_{2A}R I181A^{ICL2} heteromers combination, nor does it involve residues in the G protein-receptor interaction, as illustrated by the WT CB₁R-5HT_{2A}R I163A^{3,40} combination. Instead, DOI-induced cAMP signalling inhibition is a linear process starting with agonist binding to 5-HT_{2A}R and translated into the coupling of non-canonical G_{i/o} proteins when heteromerising with CB₁R.

With the aim of understanding the rules underlying this functional interaction, we performed similar experiments, but this time in the presence of CB₁R mutants (**Figures 4.4D and 4.4E**). In line with our previous results (**Figures 4.1D, 4.2C and 4.2E**), stimulation with WIN had no effect on cAMP accumulation for CB₁R L341A^{6,33} and a small inhibition in comparison with the WT receptor was observed for CB₁R L345A^{6,67}, supporting CB₁R's inability to trans-activate 5-HT_{2A}R (**Figures 4.4D,E**). Interestingly, DOI stimulation did not induce signalling when WT 5-HT_{2A}R was co-transfected with either CB₁R L341A^{6,33} or L345A^{6,37} mutants (**Figure 4.4D,E**), denoting that 5-HT_{2A}R-driven AC inhibition requires a fully functional interacting CB₁R protomer and that this non-canonical signalling it is not achieved through 5-HT_{2A}R trans-activating CB₁R. This is in line with the CB₁R titration experiments (**Figure 4.3F**), where 5-HT_{2A}R only loses its coupling to G_{q/11} and therefore its calcium signalling efficiency is narrowed when interacting with WT CB₁R.

Altogether, these results indicate that for DOI-induced cAMP release inhibition in cells expressing 5-HT_{2A}R-CB₁R heteromers it is required the presence of two functional protomers capable of undergoing ligand-mediate activated and to bind G proteins. In addition, our results point against trans-activation in either direction, providing evidence of a G_{i/o} class switch underneath 5-HT_{2A}R and raising the possibility of simultaneous recruitment of heterotrimeric G_{i/o} proteins to the hetero-receptor complexes after dual stimulation.

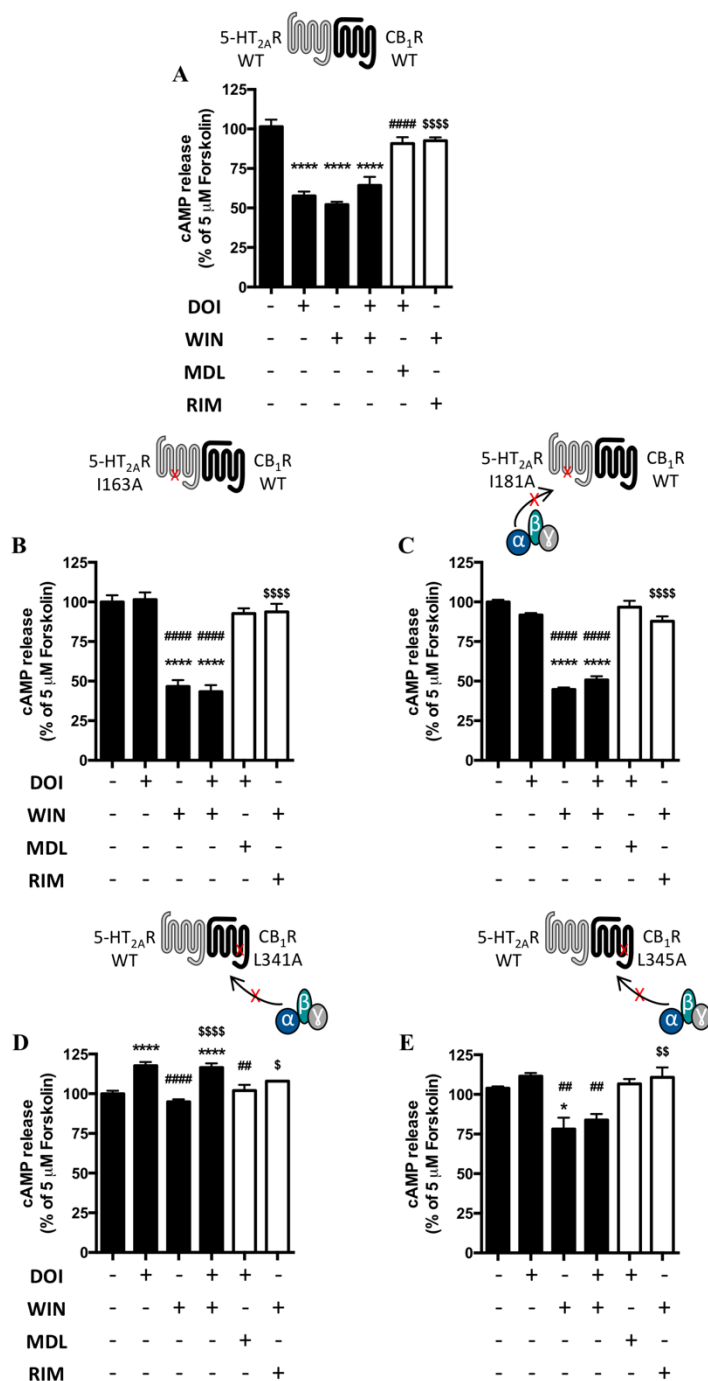


Figure 4.4. Cross-talk in cAMP signalling requires both functional 5-HT_{2A} and CB₁ receptors protomers. HEK293 cells co-expressing WT CB₁R with either WT 5-HT_{2A}R (A), 5-HT_{2A}R I163A (B) or 5-HT_{2A}R I181A (C) or cells expressing the WT 5-HT_{2A}R together with CB₁R L341A (D) or CB₁R L345A (E) were pre-incubated for 20 minutes with vehicle, the 5-HT_{2A}R antagonist MDL 100907 (MDL; 1 μM) or the CB₁R antagonist Rimonabant (RIM; 1 μM) prior to the stimulation with the 5-HT_{2A}R agonist 5-Dimethoxy-4-iodoamphetamine (DOI; 100 nM), the CB₁R agonist WIN 55212-2 (WIN; 100 nM) or both 5-HT_{2A}R and CB₁R agonist (100 nM each). The pGloSensor™-22F cAMP biosensor luminescence changes were monitored for 1 hour after agonist addition and the area under the curve was integrated. Values are mean ± SEM (n ≥ 6) of percentage of activation normalised to vehicle treated cells. Statistical significance was evaluated by one-way analysis of variance (ANOVA) followed by Bonferroni post hoc test showing significant effects over basal activation levels (*p ≤ 0.05, ****p ≤ 0.0001), over DOI (##p ≤ 0.01, ####p ≤ 0.0001) or over WIN (§p ≤ 0.05, §§p ≤ 0.01, §§§§p ≤ 0.0001).

4.2.4. Heteromer cross-talk is not the same across signalling pathways

As previously shown, heteromer formation often leads to altered downstream signalling, engaging intracellular effectors different from those expected after the activation of the individual receptors. This phenomenon is not unique to ligand-binding or G protein interactions. Downstream signalling can also be affected. We thus examined one such pathway, the MAP kinase ERK1/2. This pathway has drawn attention because of its implication in a plethora of processes, including schizophrenia and other psychoses, both linked to 5-HT_{2A} and CB₁ receptors⁶³⁰⁻⁶³². Thus, we explored the basis underlying cross-talk in this pathway. As previously reported¹⁸⁴, co-stimulation with DOI and WIN had an inhibitory effect in cells co-expressing 5-HT_{2A} and CB₁ receptors, simultaneous agonist treatment did not increase the phosphorylation levels reached by each agonist separately (**Figure 4.5A**). This negative cross-talk was in line with the results obtained at the level of cAMP (**Figure 4.4A**). Next, we explored the effect of the 5-HT_{2A}R I163A^{3,40} and I181A^{ICL2} mutants in cross-talk. Surprisingly, although 5-HT_{2A}R I163A^{3,40} did not signal through either Ca²⁺, β-arrestin2 nor ERK1/2 pathways when expressed alone (**Figures 4.1C and 4.2B,D**), heteromerisation resulted in a functional recovery. Albeit lower, in comparison to the wild type 5-HT_{2A}R, a significant increase in phospho-ERK1/2 levels was observed after DOI stimulation (**Figures 4.5B**). In addition, co-expression of CB₁R with 5-HT_{2A}R I163A^{3,40} retained the negative cross-talk. This rescue in function when transduction-deficient mutants dimerise represents another example of how receptor-receptor interactions can provide new/compensatory mechanisms^{195,335}. This is the case of the luteinising hormone receptor (LHR), were transgenic mice co-expressing binding and signalling mutant forms of LHR restored LH function through intermolecular function complementation¹⁹⁵.

These results indicate that, at the level of ERK1/2 signalling, allosteric communication between receptors may occur independently of the activation state or G protein/β-arrestin 2 potential binding to 5-HT_{2A}R. To better explore these options, we studied the influence of G protein binding to the 5-HT_{2A}R. Unexpectedly, in cells co-expressing 5-HT_{2A}R I181A^{ICL2} and WT CB₁R, DOI was able again to elicit ERK1/2 phosphorylation, although residual Ca²⁺ mobilisation and not ERK1/2 signalling were detected when expressed alone (**Figure 4.5C**). In addition to this heteromer-driven 5-HT_{2A}R functional recovery, DOI and WIN co-administration did not impair ERK1/2 signalling. Instead, we observed an additive effect equal to the sum of the signal when both receptors are individually activated by their respective agonist (**Figure 4.5C**). This loss of cross-talk illustrates how different transduction-deficient mutants can allosterically influence in a different way the interacting protomer so that a given signalling event can be dissociated, in this case cross-talk at the level of ERK1/2 signalling.

Molecular Basis Underlying 5-HT_{2A}-CB₁ Receptor Heteromers

Next, we sought to address the mirror experiments studying the influence of the CB₁R protomer towards 5-HT_{2A}R (**Figures 4.5D,E**). Co-expression of CB₁R L345A^{6.37} and WT 5-HT_{2A}R restored CB₁R function, as we did not observe differences between the levels of ERK1/2 phosphorylation after WIN addition in comparison to the WT receptor (**Figure 4.5E**). In a similar way as we observed with the 5-HT_{2A}R I181A^{ICL2} mutant, co-stimulation with DOI and WIN in cells expressing CB₁R L345A^{6.37} and WT 5-HT_{2A}R did not exhibit negative cross-talk, but an additive effect in the ERK1/2 phosphorylation levels was observed. Again, a single alanine substitution in one of the protomers had a major impact in the allosteric communication taking place between receptors, allowing us to dissociate the negative cross-talk in this particular pathway. Next, we explored the effect of the CB₁R L341A^{6.33} mutant, located one helical turn below CB₁R L345^{6.37} and pointing towards TM 3^{34,399,403}. As previously shown, removal of the hydrophobic side chain by alanine replacement (CB₁R L341A^{6.33}) resulted into a cAMP, ERK1/2 phosphorylation and β -arrestin2 signalling deficient receptor (**Figures 4.1D, 4.2C,E**). However, co-expression with WT 5-HT_{2A}R rescued CB₁R driven ERK1/2 signalling, with WIN capable of increasing ERK1/2 phosphorylation levels (**Figure 4.5D**). Surprisingly, despite the relatively close position and orientation of the leucine residues 341 and 345 in CB₁R, co-transfection with WT 5-HT_{2A}R resulted in different signalling responses in terms of cross-talk. Thus, in cells expressing CB₁R L341A^{6.33} and WT 5-HT_{2A}R, simultaneous stimulation with DOI and WIN had an inhibitory effect retaining the negative cross-talk, as can be appreciated by the lack of additive ERK1/2 phosphorylation levels in comparison to the values obtained after each receptor was individually activated (**Figure 4.5D**). However, as stated above, the WT 5-HT_{2A}R-CB₁R L345A^{6.37} combination abrogated the negative cross-talk (**Figure 5.4E**). Thus, by limiting either protomer allosteric communicating capability through rational designed receptor mutants, we were able to abrogate the negative cross-talk. Our results indicate different rules driving receptor-receptor communication across signalling pathways. At the level of cAMP release inhibition (**Figures 4.4A-E**), cross-talk requires two functional protomers capable of undergoing ligand-mediated activated and to recruit G proteins. However, when studying ERK1/2 signalling (**Figures 4.5A-E**), heteromerisation restores transduction-deficient mutants function and cross-talk is impeded in the presence of certain mutant combinations. At the level of ERK1/2 phosphorylation, allosteric communication may take place between residues involved in G protein/ β -arrestin coupling, as the WT CB₁R-5-HT_{2A}R I181A^{ICL2} and CB₁R L345A^{6.33}-5-HT_{2A}R receptor combinations did not display cross-talk.

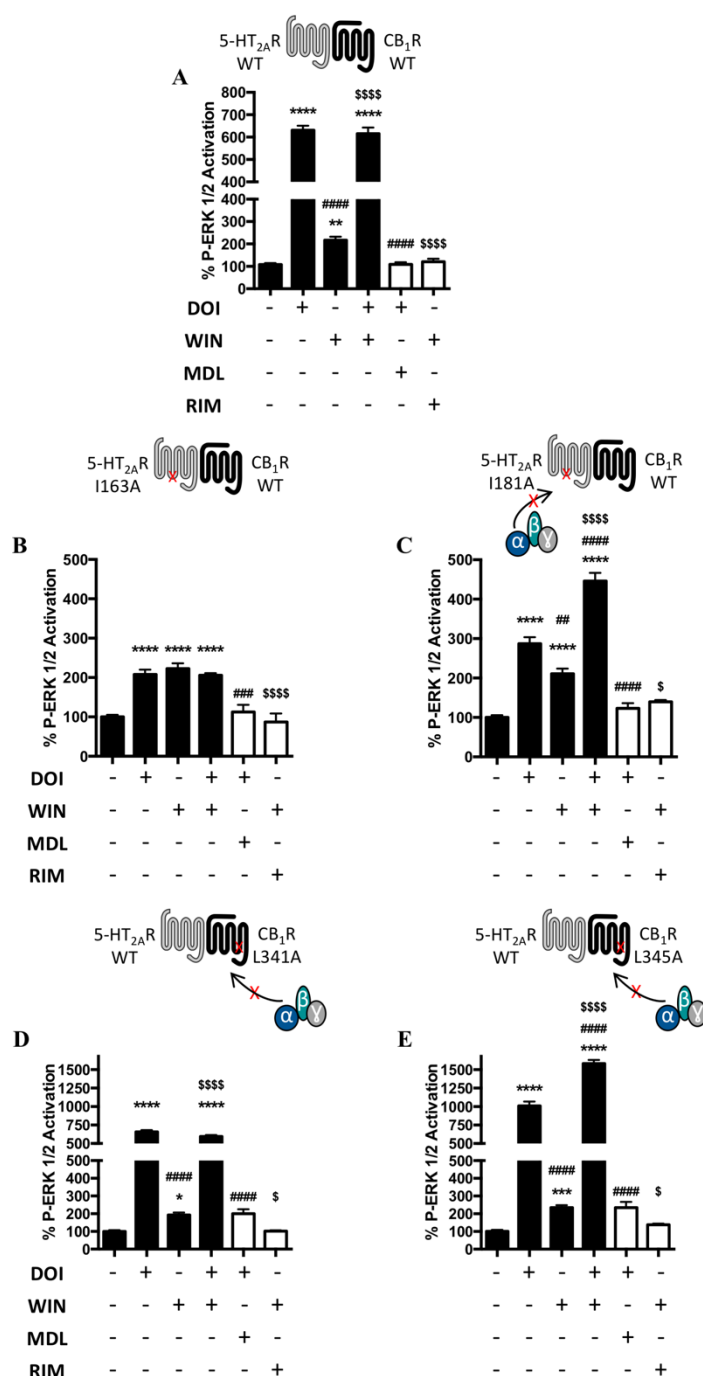


Figure 4.5. Heteromerisation rescues pERK1/2 signalling. Cross-talk requires different conformational changes across signalling pathways. HEK293 cells co-expressing WT CB₁R with either WT 5-HT_{2A}R (A), 5-HT_{2A}R I163A (B) or 5-HT_{2A}R (C) or cells expressing the WT 5-HT_{2A}R together with CB₁R L341A (D) or CB₁R L345A (E) were pre-incubated for 20 minutes with vehicle, the 5-HT_{2A}R antagonist MDL 100907 (MDL; 1 μ M) or the CB₁R antagonist Rimonabant (RIM; 1 μ M) prior to the stimulation with the 5-HT_{2A}R agonist 5-Dimethoxy-4-iodoamphetamine (DOI; 100 nM), the CB₁R agonist WIN 55212-2 (WIN; 10 μ M) or both 5-HT_{2A}R and CB₁R agonist (100 nM and 10 μ M, respectively) for 5 minutes and ERK1/2 phosphorylation levels were measured. Values are mean \pm SEM (n \geq 3) percentage of activation normalised to vehicle treated cells. Statistical significance was evaluated by one-way analysis of variance (ANOVA) followed by Bonferroni post hoc test showing significant effects over basal activation levels (*p \leq 0.05, **p \leq 0.01, ***p \leq 0.001, ****p \leq 0.0001), over DOI (###p \leq 0.001, ####p \leq 0.0001) or over WIN (\$p \leq 0.05, \$\$\$\$p \leq 0.0001).

4.2.5. Heteromer cross-talk and cross-antagonism are driven by different structural arrangements

The fact that 5-HT_{2A}R-mediated AC inhibition was lost when co-expressing WT CB₁R with 5-HT_{2A}R mutants (I163A^{3,40}, I181^{ICL2}) but transduction deficient mutants partially recovered ERK1/2 signalling, strongly supports different subsets of conformational rearrangements within 5-HT_{2A}R-CB₁R heteromers. Indeed, while some mutants negatively impact the conduit driving the G protein class switch, the structural determinants responsible of engaging ERK1/2 signalling remained partially unaltered. Noteworthy, it was recently shown that cross-talk in this pathway is a direct consequence of CB₁ and 5-HT_{2A} receptors directly interacting at the plasma membrane, rather than signalling converging in downstream effectors¹⁸⁴. Agonistic or antagonistic cooperativity might depend on the eye of the beholder, that is, the analysed signalling pathway. For example, while the neurotensin receptor agonist JMV 449 reduces D₂R-mediated cAMP release inhibition efficacy in NTS1R-dopamine D₂ receptor heteromers, it has a synergic effect in terms of ERK1/2 activation⁶³³.

We have shown that 5-HT_{2A}R-CB₁R heteromers display negative cross-talk in cAMP and ERK1/2 signalling (**Figures 4.4,4.5**). However, bi-directional cross-antagonism has also been reported¹⁸⁴. In agreement, pre-incubation of HEK293 cells expressing both wild type receptor forms with the antagonist of either 5-HT_{2A}R or CB₁R, MDL and RIM, respectively, decreased the ERK1/2 phosphorylation levels induced by the agonist of the partner protomer (**Figure 4.6A**). Importantly, the antagonists had no effect by themselves. In line with the functional ERK1/2 signalling recovery and the presence of cross-talk under certain receptor configuration of transduction deficient mutant, we sought to explore whether a similar mechanism could drive cross-antagonism. Noteworthy, since no 5-HT_{2A}R-mediated AC inhibition was observed for any CB₁R nor 5-HT_{2A}R mutants, being bi-directional cross-antagonism virtually impossible in this pathway, we assessed cross-antagonism in ERK1/2 signalling. In cells co-expressing WT CB₁R and 5-HT_{2A}R I163A^{3,40}, MDL was able to block agonist-induced CB₁R activation. Likewise, pre-incubation with the CB₁R antagonist Rimonabant blocked ERK1/2 phosphorylation after DOI stimulation (**Figure 4.6B**). Interestingly, although the negative cross-talk was lost in the CB₁R-5-HT_{2A}R I181A^{ICL2} combination, we observed bi-directional cross-antagonism in this receptors pair, as illustrated by the reduction in ERK1/2 phosphorylation in cells pre-treated with the antagonist of one receptor and stimulated with the agonist of the other (**Figure 4.6C**). These results suggest that mechanism underlying cross-talk and cross-antagonism might differ and involve different residues or receptor conformational rearrangements. In fact, when

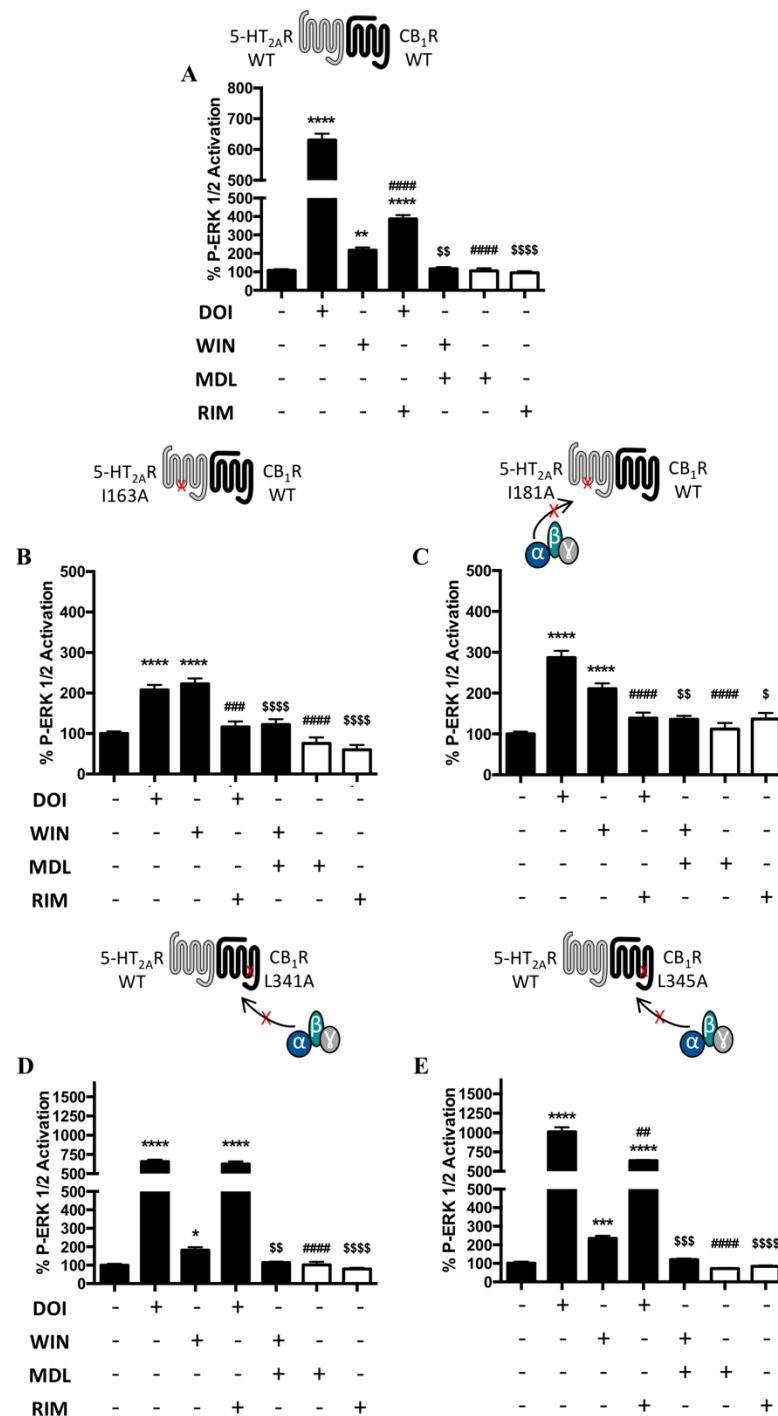


Figure 4.6. Cross-talk and cross-antagonism depend on different heteromer domains. HEK293 cells co-expressing WT CB₁R with either WT 5-HT_{2A}R (A), 5-HT_{2A}R I163A (B) or 5-HT_{2A}R (C) or cells expressing the WT 5-HT_{2A}R together with CB₁R L341A (D) or CB₁R L345A (E) were pre-incubated for 20 minutes with vehicle, the 5-HT_{2A}R antagonist MDL 100907 (MDL; 1 μ M) or the CB₁R antagonist Rimobant (RIM; 1 μ M) prior to the stimulation with the 5-HT_{2A}R agonist 5-Dimethoxy-4-iodoamphetamine (DOI; 100 nM) or the CB₁R agonist WIN 55212-2 (WIN; 10 μ M) for 5 minutes and ERK1/2 phosphorylation levels were measured. Values are mean \pm SEM ($n \geq 3$) percentage of activation normalised to vehicle treated cells. Statistical significance was evaluated by one-way analysis of variance (ANOVA) followed by Bonferroni post hoc test showing significant effects over basal activation levels (* $p \leq 0.05$, ** $p \leq 0.01$, *** $p \leq 0.001$, **** $p \leq 0.0001$), over DOI (## $p \leq 0.01$, ### $p \leq 0.001$, #### $p \leq 0.0001$) or over WIN (\$ $p \leq 0.05$, \$\$ $p \leq 0.01$, \$\$\$ $p \leq 0.001$, SSSS $p \leq 0.0001$).

analysing cross-antagonism in CB₁R mutants, we observed that cross-antagonism from CB₁R towards 5-HT_{2A} was impaired, being Rimonabant unable to dampen DOI-induced ERK1/2 activation when the WT 5-HT_{2A}R was co-expressed with the non-functional CB₁R L341A^{6.33} mutant. Interestingly, cross-antagonism remained unaltered in the opposite direction, with MDL blocking agonist-mediated CB₁R stimulation (**Figure 4.6D**). Further supporting the idea of a non-convergent mechanism driving cross-talk/antagonism is the fact that for the 5-HT_{2A}R-CB₁R L345^{6.37} combination, where the negative cross-talk was abrogated, cross-antagonism was a two-way process (**Figure 4.6E**). Together, our results indicate that allostereism within protomers is a complex process depending on multiple and different heteromeric states. For example, albeit through mutagenesis in two very different domains (5-HT_{2A}R I181A^{ICL2} and CB₁R L345A^{6.37} mutants) we were able to selectively disrupt the cross-talk, cross-antagonism remained unaltered in these configurations.

4.2.6. The 5-HT_{2A}R-CB₁R heteromer is an heterotetramer

Using a wide range of biochemical approaches, it was recently shown that 5-HT_{2A} and CB₁ receptors oligomerise both *in vitro* and *in vivo*¹⁸⁴. In order to assess whether the aforementioned mutations did not adversely affect 5-HT_{2A}R-CB₁R dimerisation, we applied the NanoBiT technology (see Chapter 3). Thus, we used the fully functional previously characterised 5-HT_{2A}R and CB₁R constructs, encoding NanoBiT long and small hemiproteins, respectively, in their C-terminus tail. Pre-incubation of cells co-expressing 5-HT_{2A}R-LgBiT and CB₁R-SmBiT with the TM5-TAT peptide inhibited NanoLuc complementation, whereas the TM7-TAT peptide, mimicking the TM7 predicted to be outside the helical interacting core, had no effect in the luminescent readout (**Figure 4.7A**). Next, we introduced the I163A^{3.40} and I181A^{ICL2} substitutions in 5-HT_{2A}R-LgBiT and the L341A^{6.33} and L345A^{6.37} in CB₁R-SmBiT. None of the mutations affected receptor oligomerisation, with the luminescence values significantly higher in comparison when each construct was expressed alone. Furthermore, we did not observe significant differences between the different combinations of WT and mutant receptors (**Figure 4.7B**).

By 2PPM and [Ca²⁺]_i signalling we have shown that the 5-HT_{2A}R G protein class switch only occurs when interacting with a fully functional CB₁R (**Figure S1F**). In addition, in cells expressing 5-HT_{2A}R-CB₁R heteromers, DOI-mediated cAMP release inhibition (cross-talk) requires two protomers both them capable of adopting an active conformation and to bind G proteins (**Figure 4.4A-E**). These results gave rise to the question whether a higher oligomeric

quaternary structure may take place, as simultaneous recruitment of two G proteins to a GPCR homo/hetero-dimer cannot occur due to steric clashes¹⁶¹. Dimers of dimers (tetramers) have been identified at the plasma membrane of different cell types^{185,199,217}. Consequently, in order to identify the molecular architecture used by CB₁R-5-HT_{2A}R we sought to combine NanoLuc bimolecular luminescence complementation (BiLC) with bioluminescence resonance energy transfer (BRET). First, we used the previously characterised CB₁R and 5-HT_{2A}R, with SmBiT and LgBiT attached to their N-terminus (see Chapter 3). Thus, the combination that yielded the best assay window, consisting in LgBiT-CB₁R and SmBiT-5-HT_{2A}R, was chosen as BRET donor. In agreement with the above results, when the hemi-NanoLuc halves were attached to the C-terminus of the receptors (**Figure 4.7A**), pre-treatment with the disrupting HIV-TAT TM5 peptide reduced the luminescence readout, with no effect in the presence of the HIV-TAT TM7 negative control peptide (**Figure 4.7C**), validating the specificity of the detected interaction. Although BRET assays have been extensively applied in the study of protein:protein interactions, its applicability has been hindered due to the limited sensitivity and dynamic range of the available donor/acceptor pairs (discussed in detail in section 1.2.4.1). To improve BRET dynamic range and sensitivity, we applied a variant of the recently developed NanoBRET, which combines the extremely bright NLuc and a red-shifted fluorophore for attachment into the haloalkane dehalogenase linker (HaloTag®)²⁶². Thus, we used the LgBiT-CB₁R and SmBiT-5-HT_{2A}R interacting proteins as BRET donor (NanoBiLC BRET donor) and the acceptor was generated by cloning the HaloTag® enzyme to the N-terminal domain of both CB₁ (Halo-CB₁R) and 5-HT_{2A} (Halo-5-HT_{2A}R) receptors. Incorporation of the HaloTag® enzyme in both constructs slightly decreased agonists potency to induce downstream signalling in both the CB₁R and 5-HT_{2A}R constructs. However, the maximal responses remained equivalent to their respective WT receptors and even with this potency impairment the EC₅₀/IC₅₀ values remained in the low (5-HT_{2A}R) or medium (CB₁R) nanomolar range (**Figure 4.7D**). Cells co-expressing the NanoBiLC BRET donor and Halo-CB₁R or Halo-5-HT_{2A}R were incubated in the presence of the HaloTag®NanoBRET™ 618Ligand (590 and 618 nm excitation and emission peaks, respectively) before performing the NanoBiLC BRET assays. As predicted, a robust and sustained increase in energy transfer was detected from the 5-HT_{2A}R-CB₁R heterodimers towards both CB₁ and 5-HT_{2A} acceptor pairs (**Figure 4.7E,F**), indicating constitutive higher order oligomers and an architecture composed of at least three receptors; CB₁R:CB₁R:5-HT_{2A}R and 5-HT_{2A}R:5-HT_{2A}R:CB₁R. Importantly, the detected BRET was not due to random collision, as the acceptor HaloTag®NanoBRET™ 618Ligand was present in excess over the different conditions.

Molecular Basis Underlying 5-HT_{2A}-CB₁ Receptor Heteromers

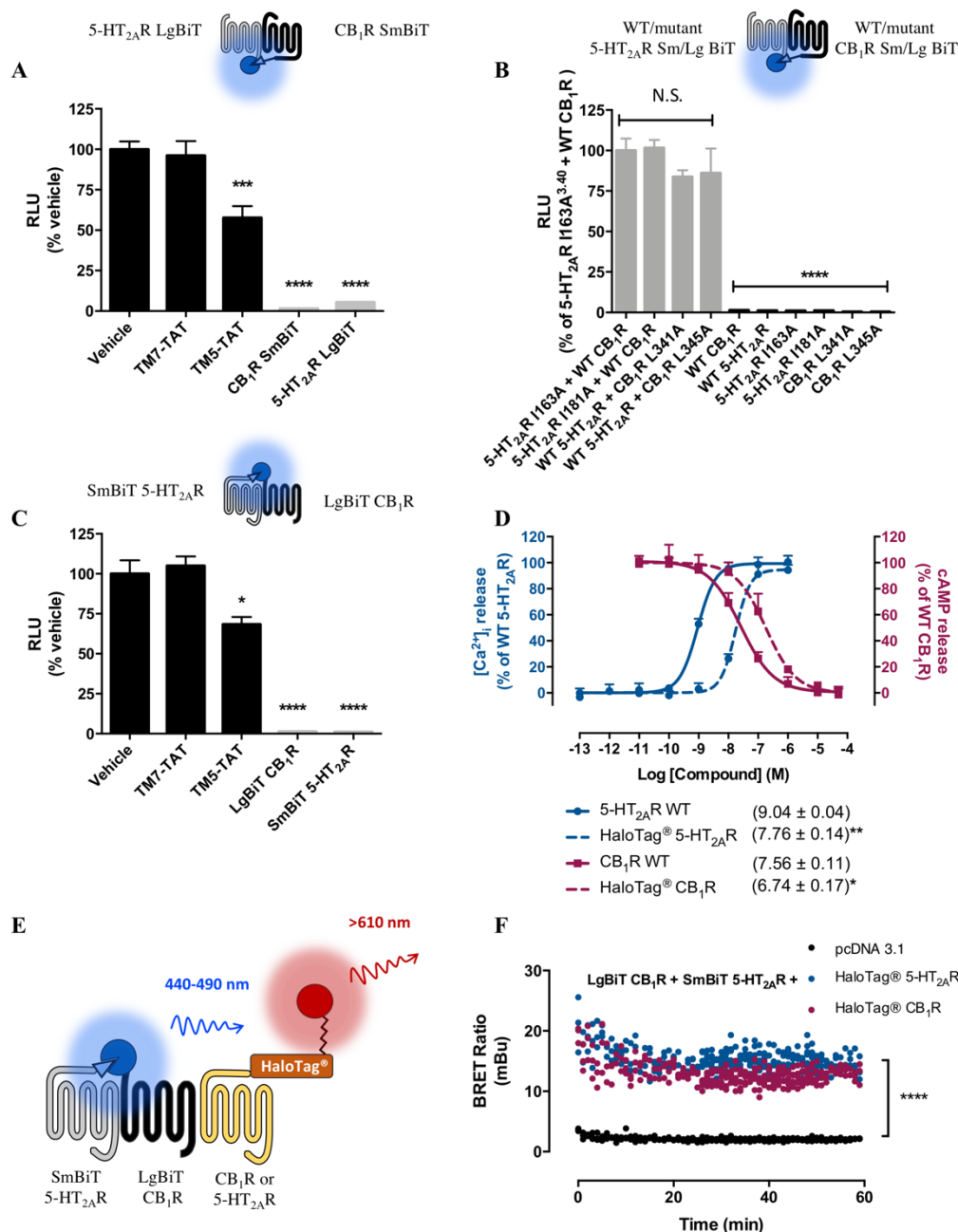


Figure 4.7. 5-HT_{2A}R-CB₁R heteromers form higher oligomeric quaternary structures. In (A), HEK293 cells co-transfected with 5-HT_{2A}R LgBiT and CB₁R SmBiT (black columns) or the individual receptor pairs (grey columns) were pre-incubated with vehicle, TM7-TAT or TM5-TAT (4 μM peptide) for 1 hour prior to the luminescence reading. Data are mean ± SEM (n ≥ 3) percentage of activation normalised to vehicle treated cells indicating significant differences over vehicle treated cells assessed by one-way analysis of variance (ANOVA) followed by Bonferroni post hoc test (***)p ≤ 0.01, ****p ≤ 0.0001). In (B), HEK293 cells were co-transfected with the different combinations of mutant and WT receptors or the individual receptor pairs (see figure legends), showing no statistically significant differences (N.S.) between the different CB₁R and 5-HT_{2A}R combinations and significance when the receptor pairs were compared against cells transfected with each single receptor. Data are mean ± SEM (n ≥ 3) percentage of activation normalised to 5-HT_{2A}R I163A + CB₁R WT mean luminescence. One-way analysis of variance (ANOVA) followed by Bonferroni post hoc test (*p ≤ 0.05, ****p ≤ 0.0001). In (C), cells transfected with the N-terminally tagged SmBiT-5-HT_{2A}R and LgBiT-CB₁R or the individual receptor pairs were treated as in A. Data are mean ± SEM (n ≥ 3) percentage of activation normalised to vehicle treated cells.

Statistical analysis was performed as in A. In **(D)**, functional characterisation of the HaloTag® 5-HT_{2A}R and CB₁R constructs. Representative [Ca²⁺]_i release (blue) and forskolin (7.5µM)-induced cAMP accumulation inhibition dose-response curves. Data are mean + SEM (n=3) percentage of activation normalised to 5-HT_{2A}R or CB₁R maximal response. Values in brackets represent the mean pEC₅₀/IC₅₀ ± SD (n=2 performed in triplicates) indicating significant differences over WT 5-HT_{2A}R or WT CB₁R evaluated by two-tailed unpaired t-test (*p ≤0.05, **p ≤0.01). **(E)** Schematic representation of the NanoBiLC BRET assay. In **(F)**, cells expressing LgBiT-CB₁R and SmbiT-5-HT_{2A}R were transfected with HaloTag®-CB₁R, HaloTag®-5-HT_{2A}R or empty plasmid and incubated overnight with the HaloTag®NanoBRET™ 618Ligand. BRET was monitored over time immediately after furimazine addition. One-way analysis of variance (ANOVA) with repeated measures followed by Bonferroni post hoc test indicates significant differences over BRET donor expressing cells (****p ≤0.0001).

4.2.7. Quaternary structure of the 5-HT_{2A}R-CB₁R heterotetramer

Our HaloTag®NanoBRET™ experiments point to a quaternary tetrameric structure composed of interacting CB₁R and 5-HT_{2A}R homodimers in complex with two G proteins. In addition, the requirement of simultaneous G protein recruitment to both protomers for cross-talk in cAMP signalling and 5-HT_{2A}R G protein-coupling class switch supports that. Furthermore, in agreement with previous studies which showed that heteromerisation between 5-HT_{2A} and CB₁R occurs via TM5 and TM6¹⁸⁴, our complementation experiments using NanoBiT technology and synthetic peptides revealed that TM5 is part of the heteromeric interfaces. This is precisely the same (heteromeric) interface recently observed in the adenosine A₁R-A_{2A}R heteromer, where the minimal functional unit was a compact rhombus-shaped heterotetramer composed of A₁R and A_{2A}R homodimers bound to two different interacting heterotrimeric G proteins (G_s and G_i)^{217,538}. Consistently, here we hypothesised that the intriguing functional behaviour of the 5-HT_{2A}-CB₁ heteromer could be due to a similar mechanism (with two G_i proteins instead). We therefore constructed a computational model assuming TM4/5 (homomeric) and TM5/6 (heteromeric) interfaces (**Figure 4.8**). We used molecular dynamics (MD) simulations of the 5-HT_{2A}-CB₁ heterotetramer in complex with two G_i in the GDP-bound closed conformations to both refine and evaluate the plausibility of the model. After some structural rearrangements during the first 400 ns of simulations, we obtained a compact and stable tetramer (**Figures 4.8**). The distances between protomers all decrease by ~10 Å relative to the initial model, while the distance between both G_i increases by ~10 Å as well because larger heteromer compactation at the extracellular half than in the intracellular half.

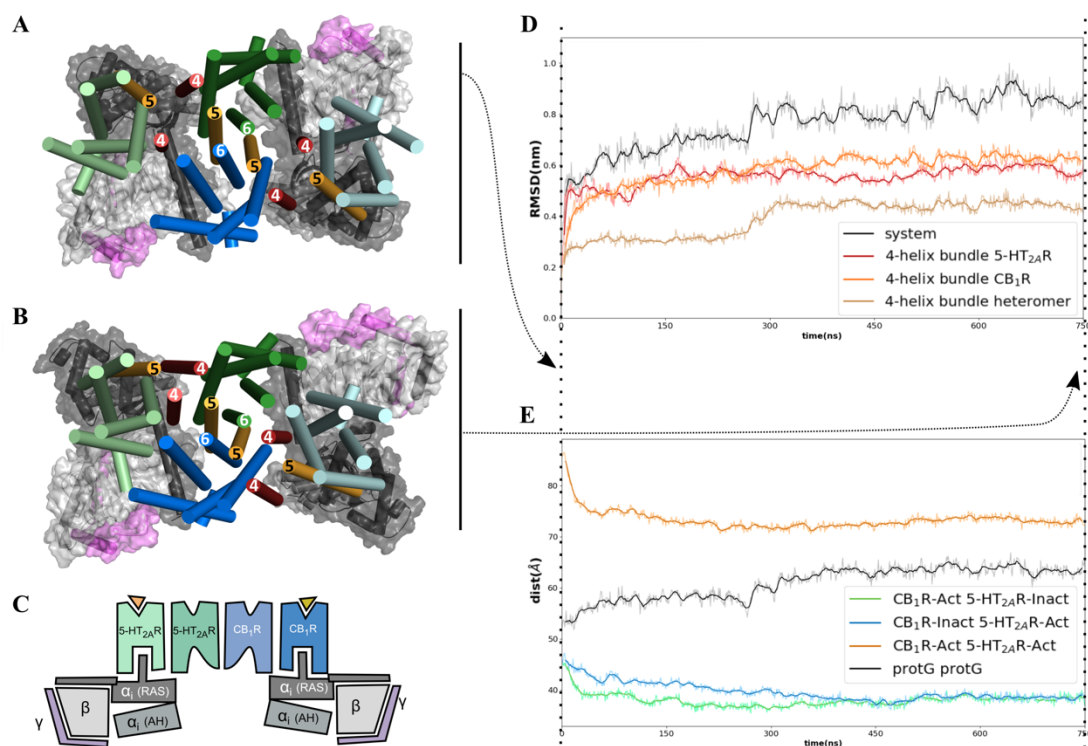


Figure 4.8. Molecular dynamics simulation of the 5-HT_{2A}R-CB₁R heterotetramer in complex with two G_i proteins. Computational-based model of the 5-HT_{2A}R-CB₁R heterotetramer in complex with two GDP-bound G_i proteins at the beginning (B) and end of the MD (750 ns) simulation illustrating the compaction of the four-helix TM5/6 bundle. The colour of the proteins is depicted in (C). (D) Root-mean-square deviations (RMSD) on protein α-carbons of the four-helix bundles forming the TM5/6 interface (clear brown line), TM4/5 interface of the 5-HT_{2A}R homodimer (red line), the TM4/5 interface of the CB₁R homodimer (orange line) and the system (black line) through the MD simulation. (E) Intermolecular distances between the centre of masses of the TM5/6 interacting protomers in single or dual activation states and between the G proteins obtained from the MD simulations.

4.2.8. Global proposed mechanism underlying signalling cross-talk in 5-HT_{2A}R-CB₁R heteromers

The proposed molecular model of the heterotetramer permits to suggest a global mechanism for the cAMP and ERK signalling above, which is shown schematically in **Figure 4.9**. The mechanism for receptor-catalysed nucleotide exchange in G proteins involves a large-scale opening of the α-helical domain (αAH) of the α-subunit, from the Ras domain, allowing GDP to freely dissociate^{19,567}. Although our final model obtained at the end of the simulation clearly shows that the heterotetramer tolerates two bound G_i in the closed conformation, the model also predicts that it is only possible to activate one single G_i protein at a time because of steric

hindrance between the α AH domains (**Figure 4.9A top panel**). When we impair G_i binding on the 5-HT_{2A}R by (I181^{ICL2} or I163^{3,40} mutants), the heteromer loses 5-HT_{2A}R-mediated but keeps normal CB₁R-mediated signalling (**Figure 4.9A middle panel**). Conversely, impaired G_i binding on CB₁R blocks both CB₁R- and 5-HT_{2A}R-mediated G_i signalling (**Figure 4.9A bottom panel**). This could suggest interaction at the level of the two G proteins as a trigger for the G_q to G_i switch on the 5-HT_{2A}R. The fact that 5-HT_{2A}R-mediated G_i signalling can occur without activating CB₁R is compatible with pre-coupling of the G_i to the CB₁R, as recently reported for the CB₁R/dopamine D₂ receptor heteromer⁶³⁴. However, even in this scenario the distance between both G_i is too large when only one G_i activates, making unlikely the possibility of direct interaction. On the search for an alternative explanation we computed potential energy surfaces of G_i and G_q (**Figure 4.9C-F**). The comparison shows that the faces of 5-HT_{2A}R-bound G proteins exposed towards CB₁R are more positive in G_i than in G_q . (**Figures 4.9D,E**) This is compatible with the presence of negatively charged and phosphorylatable serines and threonines in the C-terminus and in the ICL3 of CB₁R (**Figure 4.9F**). We propose that the favourable interactions between the C-terminus and in the ICL3 of CB₁R with 5-HT_{2A}R-bound G_i are responsible for the G_i switch (**Figure 4.9C**). Still, this requires an optimal conformation of the C-terminus and/or the ICL3 of the CB₁R that is enabled by the CB₁R-bound G_i only. Without G_i bound to CB₁R the stabilising interactions with the 5-HT_{2A}R-bound G_i do not occur and 5-HT_{2A}R keeps the normal G_q signalling.

ERK signalling also supports the concept of pre-coupling of G_i to CB₁R. This would explain that without any mutation only 5-HT_{2A}R in the heteromer preferentially recruits β -arrestin, as the G protein/ β -arrestin binding pocket is already occupied by the G_i (**Figure 4.9B**). Interestingly, the 5-HT_{2A}R I163^{3,40} strongly impairs ERK signalling due to deficient β -arrestin recruitment in the heteromer (**Figure 4.9B middle panel**). By contrast CB₁R mutants L341^{6,33} and L345^{6,37} disrupt the CB₁R- G_i complex but still permit β -arrestin binding. In this situation both 5-HT_{2A}R and CB₁R are capable to signal through β -arrestin (**Figure 4.9B middle panel**). In fact, cross-talk in ERK signalling is exclusively lost when combining two receptors capable of recruit β -arrestin (**Figure 4.5 A and E**). Accordingly, under the 5-HT_{2A}R I181A^{ICL2} plus WT CB₁R and WT 5-HT_{2A}R plus CB₁R L345A^{6,37} configurations, simultaneous agonist stimulation yields an additive effect. On the other hand, cross-talk is maintained under the 5-HT_{2A}R I163A^{3,40} plus WT CB₁R and WT 5-HT_{2A}R plus CB₁R L341A^{6,33}, where now only one protomer is capable of binding arrestins (**Figure 4.5 B and D**). Overall, these results suggest that cross-talk in ERK signalling is driven by an antagonistic interaction at the level of simultaneous G protein and arrestin binding.

Molecular Basis Underlying 5-HT_{2A}-CB₁ Receptor Heteromers

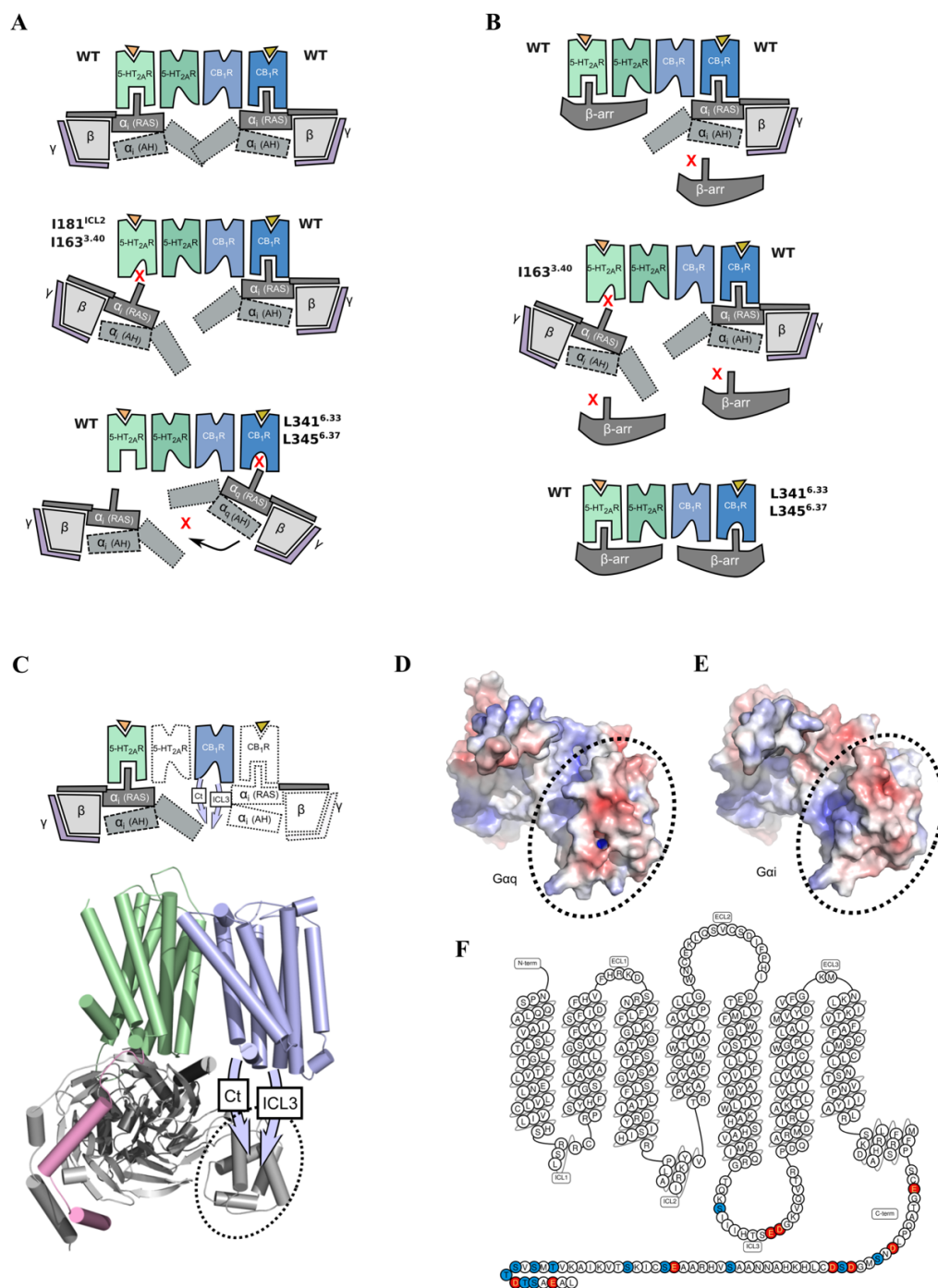


Figure 4.9. Proposed mechanism driving cross-talk in 5-HT_{2A}-CB₁R heteromers. (A) Schematic cartoon representations of the rules governing simultaneous G_i binding to 5-HT_{2A}-CB₁R heterotetramer. After dual agonist stimulation, our mode supports two GDP-bound G_i proteins. Due to a steric clash, only one α-helical domain (αAH) of the α-subunit can open at each time (top panel). Impairing G_i binding to 5-HT_{2A}R (middle panel), allows the opening of the αAH of the Gα_i subunit bound to CB₁ and thereby downstream signalling. Similarly, the high constitutive activity of CB₁R favors the coupling of G_i and thus arrestin is only available for 5-HT_{2A}R (B, top panel). Impeding G protein binding to 5-HT_{2A}R (B, middle panel) and the G_i pre-coupling to CB₁R significantly impairs ERK signalling after dual protomer stimulation. Inhibiting G protein binding to CB₁R allows arrestin binding to both receptors (B, bottom panel). G_i binding to the CB₁R protomer stabilises a conformation in which residues in the ICL2 and C-terminus favour the interaction between a second G_i molecule and 5-HT_{2A}R (C). Comparing the potential energy surfaces of the Gα subunits between the G_i-bound (D) and the G_q-bound (E) 5-

HT_{2A}R, the more positive surface in the G_i-bound 5-HT_{2A}R facilitates its interaction with putative phosphorylable electronegative Ser/Thr residues in the ICL3 and C-terminus of the CB₁R concomitant to the G_i-bound CB₁R protomer (**F**).

According to our proposed mechanism, 5-HT_{2A}R G protein class switch is facilitated by the conformation and exposure of negative charged residues within the C-terminus and ICL3 of the G_i protein-bound CB₁R protomer. In order to validate our model, we hypothesised that the removal of the negatively charged Asp/Glu and phosphorylable Ser/Thr residues via the truncation of the last 23 amino acids of the CB₁R C-tail (CB₁R^{Δ23} and CB₁R^{Δ23}-LgBit, for β-arrestin2 signalling) would abrogate this effect (**Figure 4.10A**). In comparison to the WT CB₁R, deleting these amino acids resulted in a 10-fold potency reduction in WIN-mediated cAMP release inhibition (**Figure 4.10B**). No significant differences were observed when analysing the ability of the same ligand to elicit ERK1/2 phosphorylation after 5 min stimulation (**Figure 4.10C**), although the CB₁R^{Δ23}-LgBit construct failed to recruit β-arrestin2 (**Figure 4.10D**). These results are in line with previous observations where alanine substitution of all Ser/Thr within the last 13 amino acids of the CB₁R C-terminus retained ERK signalling in a β-arrestin2-independent manner⁶³⁵. It is noteworthy to highlight the adequacy of the CB₁R^{Δ23} construct to assess our proposed mechanism both at the level of cAMP and ERK signalling, as retains G protein binding (G_i protein class switch requires simultaneous G_i proteins binding) without coupling β-arrestin2 (cross-talk in ERK signalling is lost when both receptors are capable of binding arrestins).

First, we measured [Ca²⁺]_i release over increasing CB₁R:5-HT_{2A}R ratios expecting to “force” G_{i/o} coupling to the 5-HT_{2A}R at the expense of its canonical G_{q/11} binding. Similar as we observed for the CB₁R L341A^{6.33} and L345A^{6.37} mutants (**Figure 4.3B**), co-expression of WT 5-HT_{2A}R and CB₁R^{Δ23} retained canonical G_{q/11}-dependant Ca²⁺ release upon 5-HT_{2A}R activation (**Figure 4.10E**). Under this combination, unlike when 5-HT_{2A}R dimerises with transduction deficient CB₁R mutants (CB₁R L341A^{6.33} and L345A^{6.37}), this effect does not result from the lack of two G_i proteins being recruited to the heterotetramer (CB₁R^{Δ23} displays G_{i/o} signalling, **Figure 4.10B**). Instead, and according to our aforementioned model, this is due to CB₁R^{Δ23} failing to achieve the optimal conformation of its C-tail and ICL3 and thus precluding G_{i/o} binding to the agonist-bound 5-HT_{2A}R protomer. Accordingly, when directly assessing this pathway, DOI did not inhibit forskolin-induced cAMP release in cells expressing both WT 5-HT_{2A} and CB₁R^{Δ23} receptors (**Figure 4.10F**). Next, we evaluated the adequacy of our proposed mechanism at the level of the ERK1/2 pathway.

Molecular Basis Underlying 5-HT_{2A}-CB₁ Receptor Heteromers

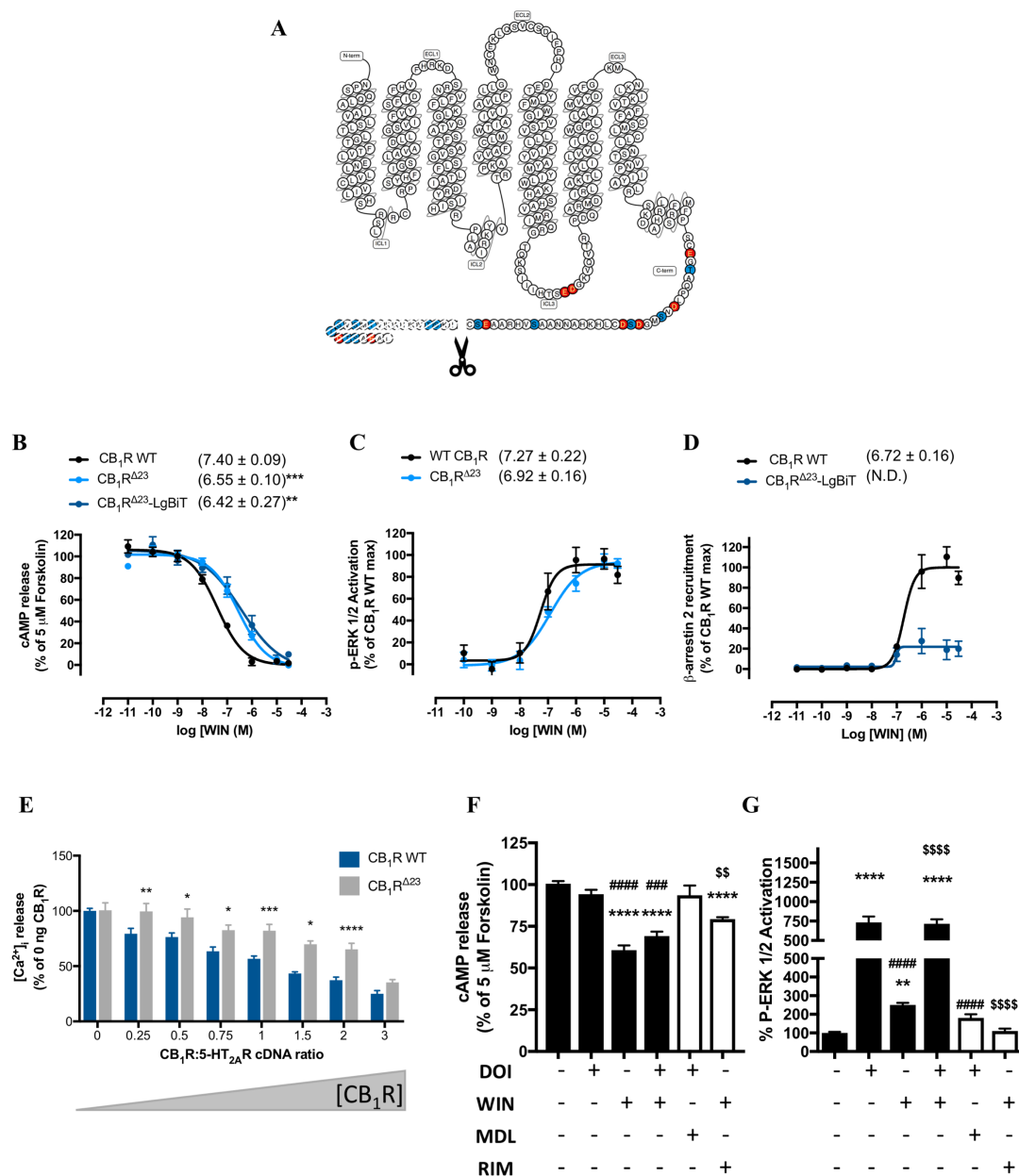


Figure 4.10. The CB₁R C-terminal domain controls G protein class-switch and cross-talk in 5-HT_{2A}-CB₁ receptor heteromers. (A) CB₁R^{Δ23} snake plot illustrating putative phosphorylatable Ser/Thr (blue) and negatively charged (red) residues within its ICL3 and C-tail. Dashed lines indicate truncated amino acids. Summary WIN dose-dependent cAMP accumulation (B), ERK1/2 phosphorylation (C) and β-arrestin2 recruitment (D) curves for the WT CB₁R and CB₁R^{Δ23} receptors. Values in brackets represent the mean pEC₅₀/pIC₅₀ ± SD (n=3) indicating significant differences over WT CB₁R evaluated by one-way analysis of variance (ANOVA) followed by Bonferroni post hoc tests (**p ≤ 0.01, ****p ≤ 0.0001). ND: non-determined, indicate non-convergent curve fits. In (E), HEK293 cells co-transfected with a fix amount of 5-HT_{2A}R and increasing WT CB₁R or CB₁R^{Δ23} (see figure legend) ratios were stimulated as in figure 4.3B. Sample size and statistical significance were evaluated as previously described (see figure 4.3B). HEK293 cells co-expressing WT 5-HT_{2A}R and CB₁R^{Δ23}R were treated as in figures 4.4. and 4.5 for cAMP release (F) and ERK1/2 phosphorylation (G), respectively with the exception that for cAMP experiments WIN was applied at 1 μM. Sample size and statistical significance were evaluated as previously described (see figures 4.4 and 4.5).

Considering the signalling profile of the CB₁R^{Δ23} (β-arrestin2-independent ERK activation), we would expect that co-expression with WT 5-HT_{2A}R would retain this heteromer characteristic negative cross-talk. Accordingly, no additive effect in signalling was observed upon dual receptor activation (**Figure 4.10G**), supporting the recurring observation that cross-talk is only lost when both receptors are able to bind β-arrestins. With regard to the later, we cannot preclude that the additive effect observed for the 5-HT_{2A}R I181A^{ICL2} plus WT CB₁R, WT 5-HT_{2A}R plus CB₁R L345A^{6.37} and WT 5-HT_{2A}R plus CB₁R^{Δ23} combinations is due to β-arrestin-dependent ERK1/2 activation arising from monomeric species.

4.1. Discussion

Most of the mechanistic insights into allosteric cross-communication in GPCR oligomers come from studies on homomeric Rhodopsin-like and homo/heteromeric Class C family receptors^{206,228,242}. There has been tremendous interest in GPCR heteromers over the years yet detailed studies of how they actually function are sparse, including 5-HT_{2A}-mGlu2, α_{2C} -AR-AT1 and A₁-A_{2A} receptor heteromers^{185,217,636,637}. Recent findings shown that THC's detrimental amnesic properties result from 5-HT_{2A}R interacting with CB₁R, whilst its antinociceptive properties remain unaltered upon the disruption of these complexes¹⁸⁴. Here, we have probed the molecular mechanisms behind this model GPCR heteromer in the hopes to gain insight into how these allosteric interactions influence receptor function. Our results reveal that (1) G proteins seem to be a key component behind the allosteric interactions, (2) the interactions controlling signalling cross-talk are not the same for every signalling pathway, and that (3) in heteromers where a G protein class switch occurs, the most likely conformation is a tetramer as this is more amenable to any potential G protein class switch.

By means of rationally designing a series of mutants to control the contribution of each protomer in the signalling profile of 5-HT_{2A}R-CB₁R heteromers, we show different mechanisms driving cross-talk across signalling pathways and the dependence on the receptors' conformational states. In addition, using two-photon polarization microscopy to visualise G proteins activation, we provide direct evidence of a G protein class switch binding 5-HT_{2A}R in 5-HT_{2A}R-CB₁R heteromers. Finally, using a new developed RET strategy, in conjunction with advance molecular dynamics, we demonstrate that 5-HT_{2A}R-CB₁R heteromers are consistent with a higher order oligomeric architecture composed of tetramers of homodimers in complex with two G_i proteins.

Our cAMP accumulation data argues against 5-HT_{2A} trans-activating CB₁R. Thus, neither co-expressing WT CB₁R with 5-HT_{2A}R mutants distributed across the transmission switch (5-HT_{2A}R I163A^{3,40}) nor the G protein binding interface (5-HT_{2A}R I181A^{ICL2}) altered cAMP levels. This G_{i/o} protein class switch binding the 5-HT_{2A}R protomer in the heteromer is further supported by 2PPM and Ca²⁺ titration experiments. Moreover, mirror experiments in the presence of CB₁R signalling-deficient mutants indicate that the functional coupling of G_{i/o} to CB₁R is a pre-requisite for 5-HT_{2A}R agonists to directly stimulate G_{i/o} signalling through this receptor. Importantly, the fully active CB₁R-G_{i/o} complex enabling cross-talk in the ligand free-state it is compatible with our 2PPM data and previous observations highlighting CB₁R's high baseline constitutive activity^{534,638}. A similar mechanism (although compatible with receptor trans-activation) supporting dual G protein binding to each hetero-oligomeric species

for cross-talk to occur was recently delineated in 5-HT_{2A}-mGlu2 dimers, also consisting of G_{q/11} and G_{i/o} protein-coupled receptor heteromers, respectively¹⁸⁵. Specifically, the binding of the mGlu2/3R agonist LY379268 to the G_{i/o}-bound mGlu2R begins a series of conformational rearrangements that are translated into the functional coupling of G_{q/11} proteins to the concomitant 5-HT_{2A}R protomer¹⁸⁵. Other examples supporting the aforementioned include the cross-communication between G_{i/o} and G_s in A₁-A_{2A}R receptor heteromers^{217,637}.

The first conclusion arising from our p-ERK1/2 is the ability of certain mutants to restore their function upon heteromerisation. Although this is the first report showing complementation of function for CB₁R, this phenomenon has been extensively documented in other class A GPCR homo- and hetero-meric complexes^{195,240,639}. More intriguing is the finding that the interactions influencing p-ERK1/2 and cAMP pathways between the protomers of 5-HT_{2A}R-CB₁R heteromers are not the same, showing that different mechanisms drive cross-talk across signalling pathways. These results are somewhat surprising as classically “cross-talk” was considered to be reciprocal and equal. However, considering the concept of allosterism and in line of what is known of the complexity of temporal and spatial signalling associated with GPCRs, they support a view where different regions of a receptor influence each signalling pathway differently^{77,121,136}. These differential effects are reminiscent of what is observed with biased compounds, where different conformations of a receptor are stabilised over others^{128,132}. This conformational flexibility is further supported when comparing cross-talk and cross-antagonism in p-ERK1/2 signalling, where constraining specific conformation through mutagenesis abrogates cross-talk but not cross-antagonism, or vice versa.

Our experimental data and proposed model suggest that the loss of cross-talk (additive effect after dual agonist occupancy) in p-ERK1/2 signalling results from simultaneous β -arrestin binding to the heterotetramer. Our MD simulations of 5-HT_{2A}R-CB₁R heteromers in complex with two G_i subunits are in agreement with other studies analysing the feasibility of similar higher oligomeric quaternary arrangements, which predict that, due to steric hindrance between the α AH domains, it is only possible to activate one single G protein at a time¹⁶¹. On the other hand, our model tolerates the binding without steric clashes of two arrestin molecules to the distal protomers of the tetramer. Emerging structural information agrees with different receptor conformations/surfaces governing G protein or arrestin recruitment^{640,641}. Accordingly, analogously as for monomeric GPCRs, the conformational differences between arrestin-dependent or G protein-dependent arrangements might differentially influence allosterism across protomers in a dimer. Further experiments monitoring the direct recruitment of arrestins to the dimer and whether they bind sequentially will be required. In addition, forced dimerisation assays might provide a strategy to rule out the contribution of non-dimerising species.

Molecular Basis Underlying 5-HT_{2A}-CB₁ Receptor Heteromers

Although what determines G protein binding to a receptor is unclear, a recent bioinformatics study supported a complex lock and key mechanism with multiple determinants influencing binding of the G protein⁴⁵. For a heteromer, it thus is reasonable to propose that the introduction of additional surfaces available for binding might influence the lock and key combination presented to a given G protein. Our results, when altering helix 8 by shortening the tail of the CB₁R (CB₁R^{Δ23}), support the idea that such an arrangement in the heteromer could influence G protein specificity. In fact, when computing the potential energy surfaces of G_q and G_i proteins bound to 5-HT_{2A}R, we found that the G_i-bound CB₁R homomer exposes C-terminal and ICL3 negatively charged residues which might favour 5-HT_{2A}R-G_i interactions. By cAMP and [Ca²⁺]_i signalling we support this hypothesis. In addition, our results with the CB₁R^{Δ23} mutant agree with the previously-stated dependence on dual arrestins binding for cross-talk in p-ERK1/2 signalling to be lost. In cells co-expressing CB₁R^{Δ23} (drives ERK1/2 phosphorylation in a G protein-dependent β-arrestin2-independent manner⁶³⁵) and 5-HT_{2A}R, cross-talk remains unaltered.

The concept of GPCR oligomers influencing the conformational state of a receptor may be one of the key functions of GPCR heteromers *in vivo*. This has been well described in Class C receptors^{642,643}. One such interesting case in relation to G proteins is the adenosine A₁R-A_{2A}R heteromers. Particularly, allostery across dimers it is not only controlled by the re-orientation of the helical domains, but the C-terminus of the G_s-bound A_{2A}R hinders G_i activity bound to A₁R⁶³⁷. Further support for this was seen with heteromers involving the CRF receptor, where a constitutive CRF receptor was still able to influence its partner receptor in a heteromer⁶⁴⁴. Indeed, the stabilisation of conformations is one of the ways we believe GPCR heteromers and allostery work in general receptor function. Thus, the oligomerisation of a receptor alters the energy landscape to either lower or raise the activation energy barrier for R*. Our finding here that G proteins can also influence this is in line with the observations of reciprocal allosteric interactions between G protein and receptor^{605,645}.

Recent structural studies comparing G_i-receptor vs G_s-receptor X-ray and cryoEM structures propose that for G_i specificity there is a smaller separation of TM5 and TM6 as well as a closer proximity of the α5 helix of the G protein to TM7 and helix 8⁶⁴⁶⁻⁶⁴⁹. Our demonstration that there is a change from G_q to G_i binding to 5-HT_{2A}R in the 5-HT_{2A}R-CB₁R heteromer suggests that CB₁R allosteric interactions with 5-HT_{2A}R might influence the distance between TM5 and TM6 and potentially have a knock-on effect on the G protein alpha subunit to TM7. Accordingly, it would be interesting to measure the evolution of TM5-TM6 distances over advanced MD simulations using our computational-based model as template.

Finally, although our results indicate an overall receptor architecture in homogenous cell populations, we did not assess the dynamics of 5-HT_{2A}R-CB₁R heteromers. Thus, recent findings indicate alternating contacting interfaces in response to ligands or their role in the stabilisation/destabilisation of certain dimer populations^{201,204,206}. In addition, single-molecule tracking analysis might provide important insights on whether these complexes are constitutive/transient and the prevalence of each oligomeric species.

In conclusion, the data presented here on 5-HT_{2A}-CB₁ receptor heteromers, along with previous studies on adenosine receptor heteromers, dopamine heteromers, serotonin homomers and sex hormone receptor, support that the architecture of oligomers are key to their functional significance of heteromers *in vivo*^{225,293,303,404}.

4.1. Acknowledgements

We are very grateful to Dr Javier Salguero and Dr Paul Thomas for access to their respective microscopy facilities and expert technical assistance. 2PPM and MD were performed in collaboration with Dr Joseph Lazar's and Dr Leonardo Pardo's labs, respectively.

Chapter 5

Allosteric D₁-H₃ Hetero-receptor Interactions Provide a Novel Target for Huntington's Disease

5.1. Introduction

First described in 1872 by George Huntington, Huntington's disease (HD) is an inherited autosomal dominant progressive neurodegenerative disorder with severe motor, cognitive and psychiatric disturbances⁶⁵⁰. This monogenic and fully penetrant disease is caused by the expansion of CAG repeats within exon 1 of the huntingtin gene (*HTT*) and, similarly to other neurodegenerative diseases, leads to protein misfolding associated with aggregation and gain-of-function toxicity⁶⁵¹. Genetic confirmation of the polyQ repeats (≥ 36 CAG triplets) near the N-terminal segment of the huntingtin protein (HTT) is the hallmark of modern HD diagnosis^{447,652}. Although HD is endemic of all populations, its prevalence varies more than tenfold across geographic regions, with an estimated occurrence of 4-10 individuals per 100,000 people. The length of the CAG repeats accounts for 50-70% of the variation in the age of earlier motor onset, with the remaining variance attributed to genetic and/or environmental factors. In addition, a weaker association between the number of polyQ repeats and the rate of progression has been described^{447,653}.

The normal function of HTT is still unclear, with 23 CAG repeats and encoding for 3144 amino acids, it participates in the development of the central nervous system, cell adhesion and the physiological synthesis and traffic of the brain-derived neurotrophic factor (BDNF)⁶⁵⁴. Mutant HTT (mHTT) is highly prone to form aggregates and one of the distinguishing features of HD is the appearance of cytoplasmic aggregates and nuclear inclusions in different brain areas. Although the formation of large inclusions has been proposed as a mechanism to cope against the high toxicity of small soluble oligomeric species, little is known about the mechanism underlying this process^{655,656}. mHTT negatively influence several molecular pathways leading to neuronal dysfunction and cell loss, including glutamatergic excitotoxicity, mitochondrial dysfunction, transcriptional dysregulation, protein homeostasis and degradation and stress responses^{657,658}.

The major neuropathological feature of HD is the death of striatal motor neurons, with up to 95% cell loss of GABAergic medium-sized spiny neurons (MSNs). In addition, throughout HD progression, there is atrophy of other non-striatal regions including the globus pallidus (GP), the cerebral cortex, subcortical white matter, thalamus, specific hypothalamic nuclei, substantia nigra and cerebellum⁶⁵³. Chorea (ancient Greek for "dance"), defined as involuntary movements that are abrupt, unpredictable and non-rhythmic, is one of the most common clinical phenotypes in HD patients, particularly in early stages⁶⁵⁹. However, cognitive deficits, depression and personality changes can appear at early stages long before the onset of motor disturbances⁴⁴⁷.

Allosteric D₁-H₃ hetero-receptor interactions provide a novel target for HD

MSNs in the striatum receive glutamatergic cortical afferents. Among other processes, glutamate neurotransmission homeostasis depends on (a) the fine tuning of the *N*-methyl-d-aspartate (NMDA), the α -amino-3-hydroxy-5-methyl-4-isoxazolepropionic acid (AMPA) and the kainic acid (KA) receptors, (b) the regulation of extracellular glutamate concentrations by high affinity transporters expressed in neurons and glial cells, and (c) the glutamate/glutamine metabolism to replenish the vesicles pools. Alterations of this equilibrium lead to aberrant glutamate-mediated excitotoxicity, involved in HD cell pathology as well as its motor and cognitive symptoms⁶⁵⁷. In addition to glutamatergic efferents, the striatum receives dense dopaminergic innervations from ventral midbrain neurons; from the ventral tegmental area (VTA) and the substantia nigra compacta (SNC). Given the role of dopamine (DA) in motor control (see section 1.5.1), it has been shown that alterations in the dopaminergic system contribute to HD neuropathology. Indeed, DA balance in the striatum is not only altered in HD, but in Parkinson's disease (PD) as well. Thus, DA levels and signalling are increased in the early hyperkinetic HD phase. However, similar to what occurs through PD, DA levels are decreased in the late akinetic stage⁶⁶⁰. Neurotoxicity and increased free radicals levels have been reported after DA over-stimulation in rat primary striatal neurons⁶⁶¹. In fact, the only drugs specially licenced by the FDA to treat HD patients are tetrabenazine and deutetabenazine, which are vesicular monoamine transporter inhibitors used for the management of chorea symptoms^{447,662,663}. These results are in line with observations where pharmacological blockage of dopamine receptors reduces HD-associated motor symptoms, while agonists exacerbate them^{664,665}.

One characteristic hallmark in HD is the differential vulnerability of GABAergic MSNs within the striatum. Based on their projection targets and neurochemical content, MSNs in the striatum can be classified in two groups (see Chapter 1 figure 1.14): (a) MSNs forming the direct/striatonigral pathway characterised by the differential expression of dopamine D₁ receptors, substance P and dynorphin and (b) MSNs forming the indirect/striatopallidal pathway expressing enkephalin and dopamine D₂ receptors (D₂R). MSNs of the indirect pathway are affected in earlier HD stages and are believed to be the most vulnerable. Dysfunctions in the indirect pathway are linked to the advent of chorea-like movements in the early hyperkinetic HD phase, whilst degeneration of the direct pathway occur later on and correlates with the appearance of akinesia and dystonia^{666,667}. After the initial loss of MSN from the indirect pathway, there is an imbalance between both circuits, leading to the over-activation of D₁R-expressing striatonigral MSNs. Thus, strategies that might reduce D₁R signalling have been proposed to prevent HD. In fact, early studies found increased DA and tyrosine hydroxylase (enzyme in the DA synthesis pathway) levels in the striatum of post-mortem HD brains⁶⁶⁸. Using YAC128 and BACHD mouse models of HD, it has been shown

that both the inhibitory and excitatory transmission in direct pathway neurons can be normalised via D₁R antagonist or DA depleting agents^{669,670}. In addition, it has been reported that DA, acting through D₁R, potentiates glutamate-induced apoptosis in Hdh^{Q7/111} HD mice derived striatal cell lines and striatal neurons from YAC128^{441,528}. Overall, targeting D₁R may be a promising strategy to treat HD. However, its pharmacological blockage might have many inherent problems. For example, D₁R is the most widely expressed DA receptor in the brain and is localised within different brain areas. In addition, it is not limited to the CNS and spreads across different tissues⁴²⁶. Furthermore, chronic administration of D₁R antagonists has been linked to several side effects in HD patients, including locomotor impairments, depression, drug-induced parkinsonism and sedation^{663,671,672}.

In light of the foregoing, we hypothesised that indirectly targeting D₁R through interacting proteins expressed in brain areas affected in HD might overcome the inherent problems of D₁R antagonists, providing a selective and provocative strategy that might slow down or halt HD progression. The interacting partner should follow the following criteria: (a) be expressed in MSNs of the direct pathway, (b) exert an antagonistic effect through direct or indirect modulation of D₁R, and (c) have low peripheral distribution to reduce the possibility of non-CNS related side effects. Thus, this could be achieved via the well validated receptor heterocomplexes between the D₁R and the histamine H₃ receptor (H₃R) (further discussed in section 1.5.3)^{345,470,523,673}. Unlike the type 1 and 2 members of this family, H₃R expression is restricted to neurons. Originally categorised as histaminergic neurons auto-receptor, H₃R also acts as hetero-receptor regulating GABA, glutamate, acetylcholine (ACh) and noradrenaline (NA) in non-histaminergic neurons. In addition, H₃R post-synaptically modulates other systems, for example, it participates in the regulation of dopaminergic signalling in the striatum^{459,470}. Importantly, both D₁ and H₃ receptors are co-expressed in GABAergic dynorphinergic MSNs and interact to form receptor heterocomplexes called heteromers. Furthermore, it has been shown that this interaction has an inhibitory effect for D₁R signalling.

While in the previous chapters we explored GPCR dimers from a mechanistic point of view, in the present chapter we sought to take advantage of the new opportunities provided by these complexes in the context of a disease. Accordingly, our hypothesis is that modulating D₁R through D₁R-H₃R heteromers might provide a provocative strategy to mitigate or slow down the progression of HD.

5.2. Results

5.2.1. Functional D₁R-H₃R heteromers are expressed in wild type STHdH^{Q7} and HD model STHdH^{Q111} striatal cells

To test whether D₁R-H₃R heteromers could regulate the increased dopaminergic signalling in HD, our first approach was to assess the expression levels of both receptors in immortalised striatal cells expressing the normal (STHdH^{Q7}) or mutant (STHdH^{Q111}) huntingtin forms. This HD model has been previously validated and expresses wild type or mutant huntingtin with 7 or 111 CAG repeats, respectively, under the control of the endogenous promoter. In addition, the lack of amino-terminal inclusions reflects better the changes involved in early HD pathogenesis⁵³¹.

Using saturation ligand binding, we confirmed that D₁ and H₃ receptors are endogenously expressed in similar levels in both cell lines (**Table 5.1**). In addition, STHdH^{Q111} mutant cells displayed higher affinities for both D₁ and H₃ receptors ligands (~two-fold K_D reduction for the D₁R/D₅ antagonist [³H]SCH 23390 and the H₃R agonist [³H]R- α -methyl histamine; [³H]RAMH). Nevertheless, despite these differences, their affinities were in the low/sub-nanomolar range. Next, using Proximity Ligation Assays (PLAs) (see section 1.2.4.3), we validated the existence of D₁R-H₃R heteromers in both STHdH^{Q7} and STHdH^{Q111} cells, as can be appreciated by the presence of fluorescent spots surrounding the nucleus (**Figure 5.1A,B**).

Functional D₁R-H₃R heteromers have been previously identified in human neuroblastoma cells and rat GABAergic striatal neurons of the direct pathway. At the level of cell signalling, activation of H₃R has an inhibitory effect for D₁R. Thus, selective H₃R agonists and antagonists have shown to decrease agonist-induced D₁R signalling via negative cross-talk and cross-antagonism, respectively^{345,523}. Therefore, we sought to investigate this pharmacological fingerprint in both STHdH^{Q7} and STHdH^{Q111} cells. Stimulations with the D₁R agonist SKF 81297 and the H₃R agonist Imetit induced an increase in the phosphorylation levels of ERK1/2 in STHdH^{Q7} and STHdH^{Q111} cells (**Figure 5.1C,D**), whereas simultaneous administration of both agonists did not induce an additive effect. Instead, we observed a complete blockage of ERK1/2 phosphorylation, validating the existence of negative cross-talk in this HD model. Furthermore, pre-incubation of both cell lines with the D₁R antagonist SCH 23390 or the H₃R antagonist Thioperamide inhibited the SKF 81297-induced ERK1/2 pathway activation, indicating the ability of H₃R to block D₁R signalling via cross-antagonism. It should be noted the small differences in ERK phosphorylation levels and that potential changes in protein levels due to cell loss were not taken into account. Further

experiments (e.g. total protein quantification via Western blot) might provide complementary information to take this factor into consideration.

Next, we studied the influence of D₁R-H₃R dimerisation in D₁-mediated [Ca²⁺]_i release, an additional signalling pathway downstream D₁R apart from its canonical G_{α_{s/olf}}-mediated stimulation of cAMP production⁶⁷⁴. First, we assessed D₁R ability to induce Ca²⁺ release in STHdH^{Q7} and STHdH^{Q111} cells. In agreement, stimulation with the D₁R agonist SKF 81297 produced a rapid dose-dependent [Ca²⁺]_i increase that could be prevented after pre-incubation with the D₁R antagonist SCH 23390 (**Figure 5.1E,F**). In a similar way as we observed when analysing the ERK1/2 pathway, D₁ and H₃ receptors co-activation had an inhibitory effect at the level of cell signalling. Simultaneous administration of the D₁R and H₃R agonists inhibited SKF 81297-mediated [Ca²⁺]_i release (negative cross-talk) in both STHdH^{Q7} and STHdH^{Q111} cells (**Figure 5.1G,H**). Furthermore, pre-incubation with the H₃R antagonist Thioperamide, via cross-antagonism, was also able to block D₁-triggered calcium signalling (**Figure 5.1G,H**).

Altogether, our data not only strongly supports the presence of D₁-H₃ receptor heteromers in these HD model cells, but also their ability to form functional pharmacological entities. These results suggest that H₃R, more likely through a direct receptor-receptor interaction, is able to allosterically influence D₁R behaviour, reducing its downstream ERK1/2 and [Ca²⁺]_i pathways and thus acting as a molecular brake for D₁ signalling in these HD striatal cells.

Table 5.1. D₁R and H₃R expression levels and ligand affinities in STHdH^{Q7} and STHdH^{Q111} cells.

Receptor	STHdH ^{Q7}	STHdH ^{Q7}	STHdH ^{Q111}	STHdH ^{Q111}
	B _{max} (fmol/mg protein)	K _D (nM)	B _{max} (fmol/mg protein)	K _D (nM)
H ₃ R	160 ± 2	1.92 ± 0.07	160 ± 34	0.71 ± 0.25
D ₁ R	200 ± 20	0.3 ± 0.1	220 ± 40	0.16 ± 0.08

Binding affinities of [³H]RAMH and [³H]SCH 23390 to H₃ and D₁ receptors, respectively, in STHdH^{Q7} and STHdH^{Q111} striatal cells membrane suspensions. Data are mean ± SEM (n=3). K_D, equilibrium dissociation constant; B_{max}, maximum receptor densities.

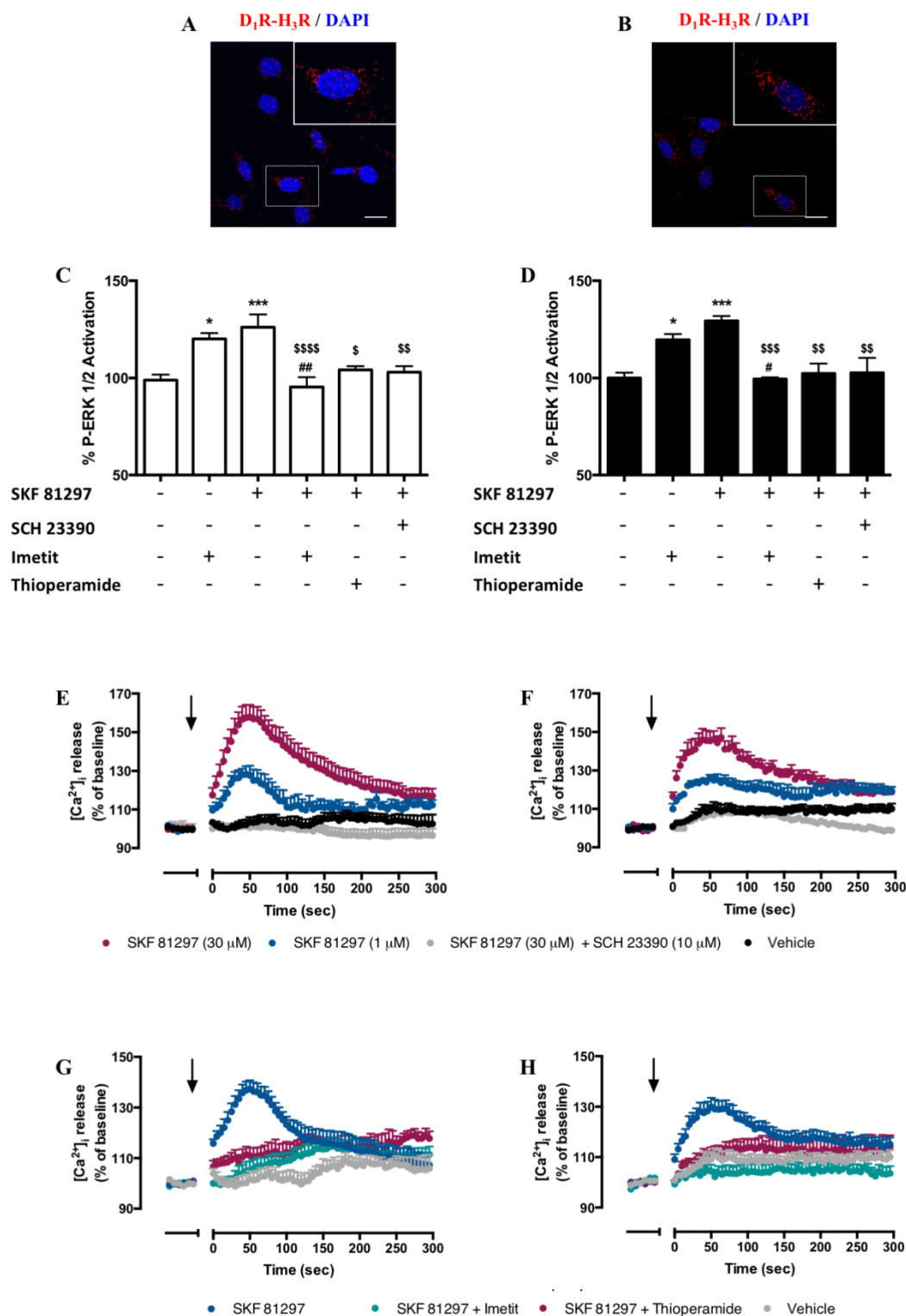


Figure 5.1. Functional characterisation of D₁R-H₃R heteromers in STHdH^{Q7} and STHdH^{Q111} cells. Representative Proximity Ligation Assays (PLAs) performed in striatal wild type STHdH^{Q7} (A) and HD STHdH^{Q111} cells (B). Heteromers are visualised as red puncta surrounding the blue nucleus stained with DAPI. Scale bars: 20 μm. In (C and D), STHdH^{Q7} and HD STHdH^{Q111} cells, respectively, we pre-incubated for 20 minutes with vehicle, the D₁R antagonist SCH 23390 (1 μM), the H₃R agonist Imetit (100 nM) or the H₃R antagonist Thioperamide (1 μM) prior to the stimulation with the D₁R agonist SKF 81297 or Imetit (100 nM) for 10 minutes and ERK1/2 phosphorylation levels were measured. Values are mean ± SEM (n ≥ 3) of percentage of activation

normalised to vehicle treated cells. Statistical significance was evaluated by one-way analysis of variance (ANOVA) followed by Bonferroni post hoc tests showing significant effects over basal phosphorylation levels (* $p \leq 0.05$, *** $p \leq 0.001$), over SKF 81297 ($^{\$}p \leq 0.05$, $^{ss}p \leq 0.01$, $^{sss}p \leq 0.001$, $^{ssss}p \leq 0.0001$) or over Imetit ($^{\#}p \leq 0.05$, $^{##}p \leq 0.01$). In (E and F), STHdH^{Q7} and HD STHdH^{Q111} cells, respectively, were pre-incubated for 20 minutes with vehicle or SCH 23390 prior to the stimulation (arrows) with SFK 81297 (30 and 1 μ M). Intracellular calcium release was monitored over time using the GCaMP6s biosensor. Data are mean + SEM (n=3-9) of the percentage of activation normalised to the average basal signal prior to stimulation. In (G and H), STHdH^{Q7} and HD STHdH^{Q111} cells, respectively, were pre-incubated for 20 minutes with vehicle, Imetit (10 μ M) or Thioperamide (10 μ M) before stimulation (arrows) with SFK 81297 (1 μ M). Intracellular calcium release was measured as in G and H. Data are mean + SEM (n \geq 7) of percentage of activation normalised to the average basal signal prior to stimulation.

5.2.2. Molecular organisation of D₁R-H₃R heteromers

Our results point towards H₃R allosterically inhibiting D₁R activation through D₁R-H₃R heteromers. However, this raised the question of whether the above observed negative cross-talk and cross-antagonism resulted from a direct receptor-receptor interaction at the membrane level or, on the other hand, reflect a post-receptor downstream signalling cross-talk. As previously discussed (see section 1.2.1), several class A GPCRs crystal structures have revealed recurrent oligomeric interfaces^{161,209,215}. In addition, recent studies of heterodimers between the dopamine D₁ and D₃ receptors have shown that TM5 and TM6 but not TM7 are part of the conduit of the allosteric interaction between these receptors⁶⁷⁵. Therefore, we hypothesised that D₁R-H₃R heteromers could interact between TM5/6. To test it, we used the same strategy previously applied to disrupt 5-HT_{2A}R-CB₁R heteromers (see Chapter 4). In this case, using synthetic peptides consisting of the sequence of D₁R TM5 or TM7 (positive and negative controls, respectively) fused to the HIV-TAT cell penetrating sequence. As we predicted, pre-incubation of STHdH^{Q7} and STHdH^{Q111} cells with the TM5 peptide resulted in a near complete loss of the characteristic PLA positive fluorescent dots surrounding the blue-stained nucleus (**Figure 5.2A,C**). Importantly, we did not observe any fluorescence reduction for the negative TM7 peptide control (**Figure 5.2B,2D**). These results support our original hypothesis that heteromerisation occurs via TMs 5 and 6. However, to explore whether the negative cross-talk and cross-antagonism reflect allosterism at the cell membrane, we performed calcium mobilisation experiments in the presence of TM peptides. Pre-treatment of both cell lines with the TM5 peptide inhibited both negative cross-talk and cross-antagonism. Thus, we observed an increase in Ca²⁺ release after D₁R stimulation without regard to whether SKF81297 was co-administrated with the H₃R agonist or antagonist (**Figure**

Allosteric D₁-H₃ hetero-receptor interactions provide a novel target for HD

5.2E,F). Importantly, the ability of both Imetit and Thioperamide to block D₁-mediated [Ca²⁺]_i remained unaltered in the presence of the negative control TM7 peptide (**Figure 5.2G,H**). These results not only validate the presence of D₁R-H₃R heteromers in these HD cells but, in agreement with the oligomeric arrangement of the μ-OR crystal structure²¹⁵, our data supports an architecture where the TMs 5/6 form the interacting interface between protomers and TM7 face each other outside the four helix bundle (detailed in **Fig 5.3**). Furthermore, we demonstrated that negative cross-talk and cross-antagonism are consequence of the allosteric communication between receptors.

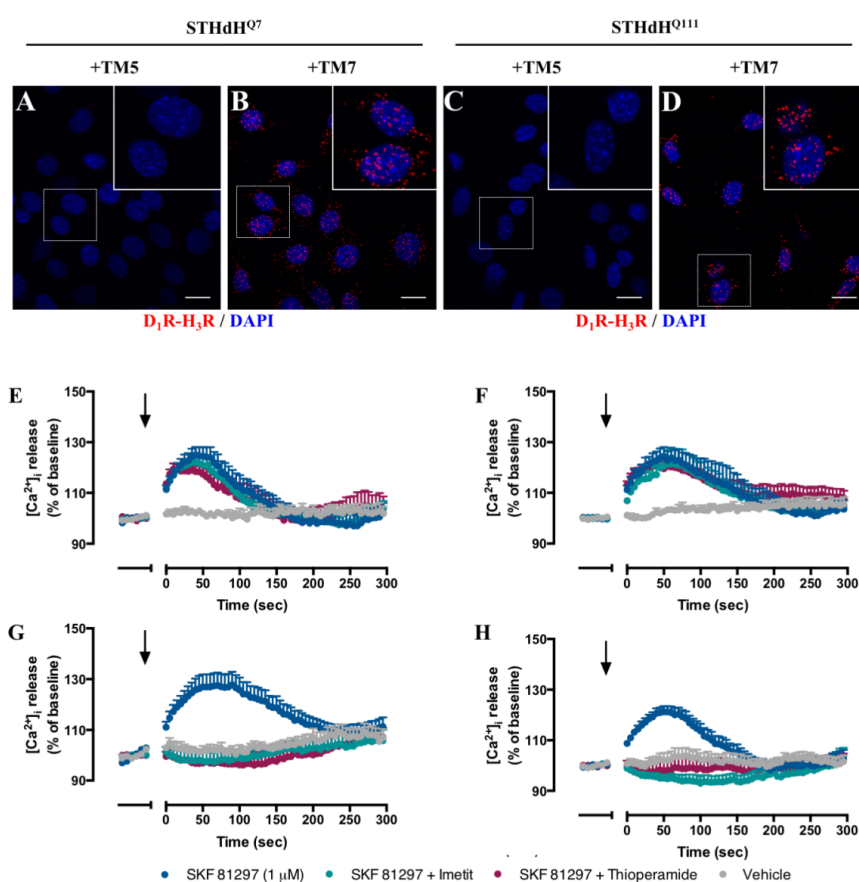


Figure 5.2. Molecular architecture of D₁R-H₃R heteromers. In PLAs experiments, STHdH^{Q7} (**A and B**) or STHdH^{Q111} (**C and D**) cells were pre-treated for 60 minutes with synthetic peptides (4 μM) with the sequences of the D₁R TM5 or TM7 fused to the HIV-TAT cell-penetrating sequence. Representative PLAs showing heteromers as red stained puncta surrounding the blue nucleus stained with DAPI. Scale bars: 20 μm. In calcium experiments, STHdH^{Q7} (**E and G**) or STHdH^{Q111} (**F and H**) cells were pre-incubated for 60 minutes with the D₁R TM5 (**E and F**) or TM7 (**G and H**) peptides prior to cross-talk assessment. 20 minutes prior to the calcium recordings, cells were incubated with vehicle, the H₃R agonist Imetit (10 μM) or the H₃R antagonist Thioperamide (10 μM) before stimulation (arrows) with the D₁R agonist SKF 81297 (1 μM). Intracellular calcium release was monitored over time using the GCaMP6s biosensor. Data are mean + SEM (n ≥ 4) of the percentage of activation normalised to the average basal signal prior to stimulation.

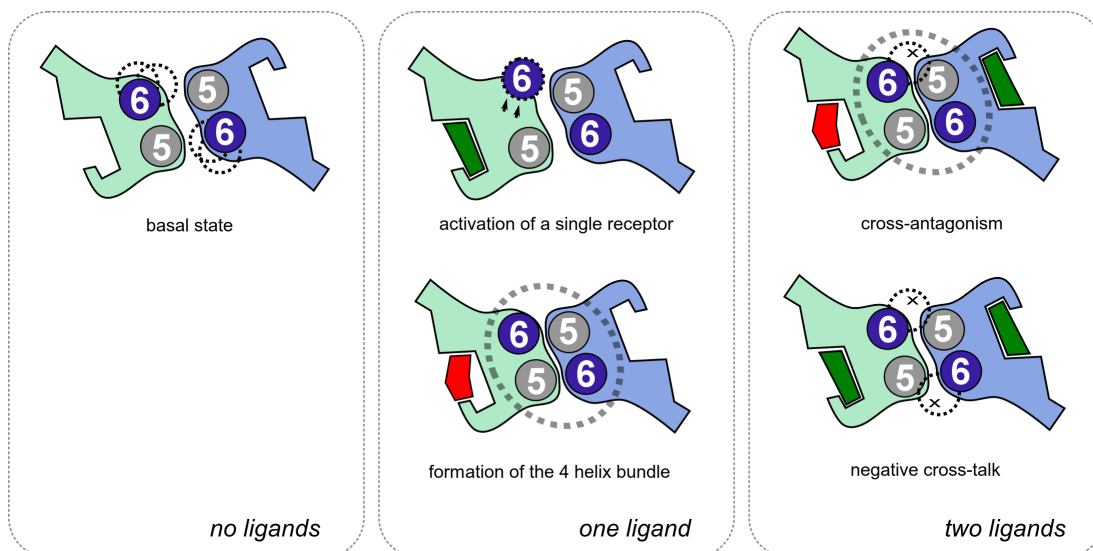


Figure 5.3. Proposed mechanism and interacting domains in D₁R-H₃R heteromers. Agonist binding at the extracellular pocket of GPCRs leads to local conformational changes that increase signalling by opening an intracellular cavity via the movement of transmembrane helices 5 and 6. In the ligand-free basal state, D₁R-H₃R heteromerisation occurs via TMs 5 and 6 (**left panel**). Ligand binding slightly modifies this dimerisation interface (**middle panel**), relative to the unliganded form, in such a manner that antagonists/inverse agonist binding (in red) to any protomer stabilises the inactive conformation of the receptor and the four-helix TMs 5 and 6 bundle observed in the crystal structure of the μ -OR²¹⁵, whereas agonist binding (green) allows the movement of the cytoplasmic end of TM6 for G protein or arrestin binding (green). Bidirectional cross-antagonism (**right panel**) is due to the fact that agonist binding to the unliganded protomer cannot surmount the very stable four-helix bundle for receptor activation (right panel). Negative cross-talk occurs as the simultaneous movement of TM6 in both protomers is not feasible due to steric clash (right panel).

5.2.3. H₃R ligands prevent D₁R-mediated cell death in STHdH^{Q7} and STHdH^{Q111} cells

Over the last decades, an increasing body of evidence have supported the role of altered function of both glutamatergic and dopaminergic transmission to the induction of striatal MSNs death. MSNs receive glutamatergic inputs from the cortex and dopaminergic inputs from the striatum and recent studies have linked the activation of glutamate receptors with an aberrant cytosolic Ca²⁺ signalling and consequent MSN apoptosis in yeast artificial chromosome transgenic (YAC128) HD mouse^{676,677}. Using the same HD model it has been shown that dopamine, though dopamine D₁-class but not D₂-class receptors, acts synergistically with glutamate inducing aberrant Ca²⁺ signalling and apoptosis in YAC128 MSNs⁴⁴¹. However, the molecular mechanism underlying HD striatal cells vulnerability to glutamine and dopamine still remains unclear. In addition, Paoletti et al. recently demonstrated

Allosteric D₁-H₃ hetero-receptor interactions provide a novel target for HD

that dopaminergic stimulation with the D₁ receptor SKF 38393 partial agonist induces cell death in striatal STHdH^{Q7} and STHdH^{Q111} cells⁵²⁸. Taking into account H₃R inhibitory effect over D₁R-mediated ERK1/2 phosphorylation and [Ca²⁺]_i signalling through D₁R-H₃R heteromers, we explored whether H₃R ligands could prevent striatal cell death. Using label-free technology we monitored in real time D₁R-mediated striatal cell toxicity (**Figure 5.4A, B**). In agreement with previous results using the D₁R partial agonist SKF 38393⁵²⁸, we observed a dose-dependent reduction in viability in both STHdH^{Q7} and STHdH^{Q111} cells (**Figure 5.4A, B ;top panes**). Importantly, significant cell death did not occur until 30 μM SKF 81297 was administrated (pIC₅₀= 4.8± 0.06 and 4.9± 0.03 for STHdH^{Q7} and STHdH^{Q111}, respectively). Thus, this D₁R agonist concentration was used in all future studies. However, our results showing H₃R ligands ability to modulate D₁R signalling through negative cross-talk and cross-antagonism were performed at a lower SKF 81297 dose (1 μM) (**Figures 5.1G,H and 5.2E-H**). Therefore, we repeated [Ca²⁺]_i signalling experiments under this new concentration. In line with our previous results, 30 μM SKF 81297-induced cytosolic calcium release was blocked by Imetit (negative cross-talk) and Thioperamide (cross- antagonism) (**Figure 5.4C, D**) in both cell lines, showing H₃R-mediated inhibition of D₁R signalling across a broader concentration range. Next, we explored H₃R ligands potential to rescue D₁R-induced cell death through D₁R-H₃R heteromers. Pre-treatment of both STHdH^{Q7} and STHdH^{Q111} cells with the H₃R antagonist Thioperamide had a protective effect, reducing in a dose-response manner SKF 81297-mediated striatal cell death (**Figure 5.4E**). Likewise, Imetit increased the number of surviving cells (~2-fold cell viability increase) in the presence of SKF 81297 (**Figure 5.4F**). Interestingly, both Thioperamide (pEC₅₀= 5.4± 0.10 and 5.5± 0.08 for STHdH^{Q7} and STHdH^{Q111}, respectively) and Imetit potencies (pEC₅₀= 5.4± 0.10 and 5.5± 0.08 for STHdH^{Q7} and STHdH^{Q111}, respectively) to revert D₁R-mediated cell death were within the same concentration ranges, being 30 μM the concentration of H₃R ligands chosen for further studies.

These results strongly support D₁-triggered striatal cell death and the potential of H₃R as a new target which, through heteromerisation, can prevent this effect. Therefore, we sought to assess whether the recovery in cell viability was in fact due to heteromerisation between D₁ and H₃ receptors. First, we validated the specificity of all ligands employed in viability experiments. As expected, pre-incubation with the D₁R antagonist SCH 23390 prevented STHdH^{Q7} and STHdH^{Q111} cell death after D₁R over-stimulation. In addition, neither the H₃R agonist Imetit nor the antagonist Thioperamide had an effect in cell viability by themselves (**Figure 5.5A**). In order to validate that the recovery in viability induced by the H₃R Imetit and Thioperamide was an heteromer-specific biochemical property, we used cell penetrating peptides. Pre-incubation of both STHdH^{Q7} and STHdH^{Q111} cells with the TM 7 peptide did not influence

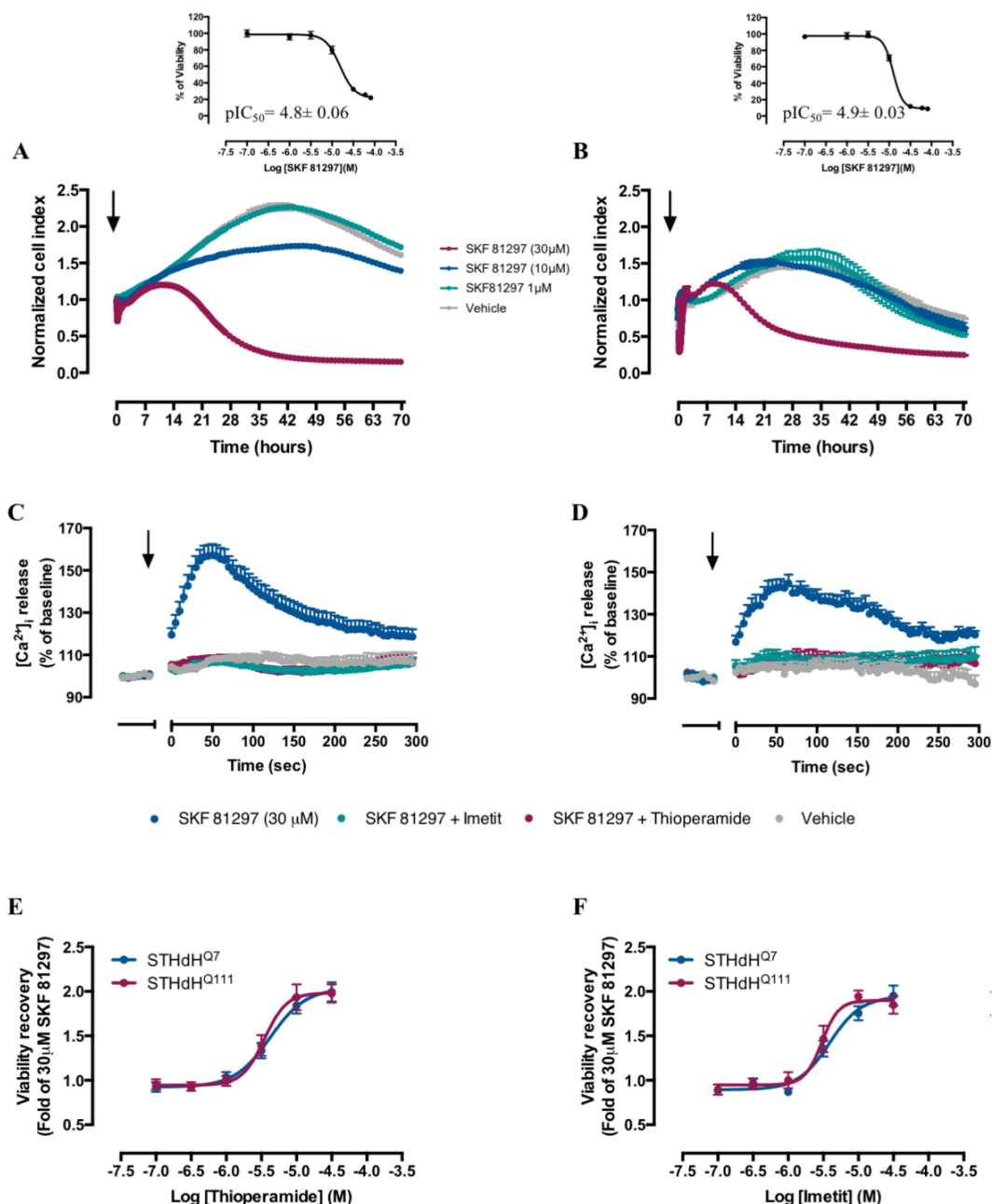


Figure 5.4. H₃R ligands revert D₁-mediated cell death in STHdH^{Q7} and STHdH^{Q111} striatal cells. Using the label free Real Time Cell Analyser (RTCA) technology, cell death was assessed over 72 hours in STHdH^{Q7} (A) and STHdH^{Q111} (B) striatal cells after administration (arrows) of vehicle or the D₁R agonist SKF 81297 (1, 10 and 30 μM). Data are mean ± SD (n=2). Top inserts correspond to SKF 81297 dose-response dependent effects in cell viability expressed as mean ± SEM (n=24-30) of percentage of viable cells respect to vehicle-treated cells. For more details, refer to Materials and Methods section. In (C and D), STHdH^{Q7} and HD STHdH^{Q111} cells, respectively, were pre-incubated for 20 minutes with vehicle, the H₃R agonist Imetit (10 μM) or the H₃R antagonist Thioperamide (10 μM) before stimulation (arrows) with a cytotoxic concentration of SFK 81297 (30 μM). Intracellular calcium release was monitored over time using the GCaMP6s biosensor. Data are mean + SEM (n ≥ 9) of the percentage of activation normalised to the average basal signal prior to stimulation. In (E and F), cell viability was determined in STHdH^{Q7} and STHdH^{Q111} cells pre-treated for 1 hour with increasing concentrations of the H₃R ligands Thioperamide (E) or Imetit (F) prior to the over-stimulation with SFK 81297 (30 μM). Values represent mean ± SEM (n=19) of viable cells normalised to 30 μM SFK 81297 treated cells.

Allosteric D₁-H₃ hetero-receptor interactions provide a novel target for HD

H₃R ligands ability to rescue D₁R-mediated decrease in viability (**Figure 5B,C**), supporting our previous results where the TM 7 of D₁ and H₃ receptor are facing outside the 4-helix bundle. In agreement, neither Imetit nor Thioperamide were able to rescue striatal viability in the presence of the TM 5 peptide, with no differences in comparison with cells treated with SKF 81297 alone (**Figure 5.5 B,C**). Together, our data indicate that H₃R ligands, through allosteric communication between D₁R-H₃R heteromers, constitute a new and alternative pharmacological entity to target striatal cell death.

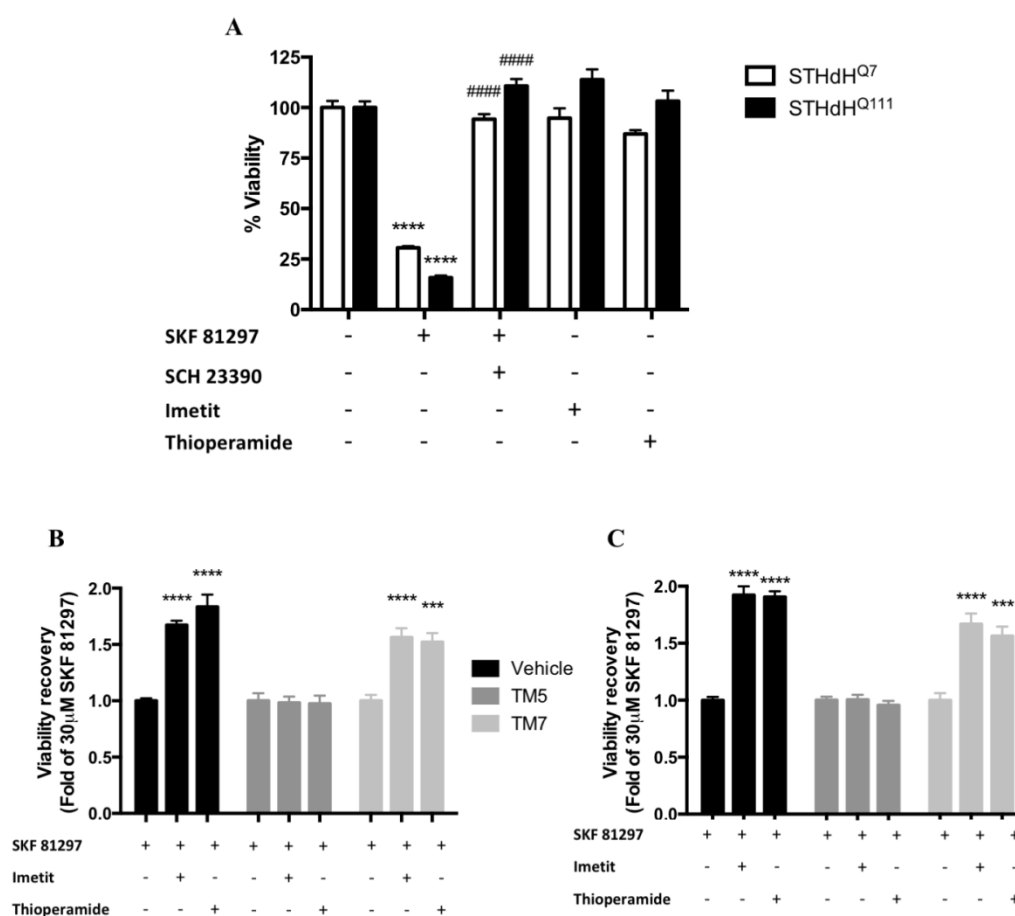


Figure 5.5. H₃R ligands-mediated cell death recovery depends on functional D₁R-H₃R heteromers. In (A), STHdH^{Q7} and STHdH^{Q111} cells were pre-treated for 1 hour with vehicle, the D₁R antagonist SCH 23390 (10 μM), the H₃R agonist Imetit (10 μM) or the H₃R antagonist Thioperamide (10 μM) prior over-stimulation with the D₁R agonist SKF 81297 (30 μM). Cell viability is expressed as mean ± SEM (n=7-22) of percentage of viable cells respect to vehicle-treated cells. Statistical significance was evaluated by two-way ANOVA followed by Bonferroni post hoc tests showing significant effects over vehicle treated cells (****p ≤ 0.0001) and over SKF 81297 versus SKF 81297 plus SCH 23390 (####p ≤ 0.0001). In (B and C), STHdH^{Q7} and STHdH^{Q111} cells, respectively, were pre-incubated for 1 hour with the D₁R TMs 5 and 7 (4 μM) prior to vehicle or D₁R over stimulation with SKF 81297 (30 μM). Values represent mean ± SEM (n ≥ 15) of viable cells normalised to 30 μM SKF 81297 treated cells. Statistical significance was evaluated by one-way ANOVA followed by Bonferroni post hoc tests showing significant effects over 30 μM SKF 81297 treated cells (***p ≤ 0.001, ****p ≤ 0.0001).

5.2.4. H₃R ligands revert D₁R overstimulation-induced internalisation and heteromer disruption in striatal cells.

GPCR signalling is not confined to the plasma membrane and the recent discovery that receptors can signal in internal organelles, with different cellular consequences from those originated at the membrane, raised the question whether homo/heterodimers may operate in similar manner²⁴⁹. In fact, numerous reports have shown oligomerisation-dependent alterations in receptor trafficking^{336,678}. In the case of the dopaminergic receptors, several studies have described a functional and direct interaction between N-methyl-D-aspartate receptors (NMDARs) and D₁R in MSNs and recombinant cells^{679,680}. D₁R forms oligomeric complexes directly interacting with the NR1 subunit of the NMDAR channel. In the absence of NR2, D₁R-NR1 hetero-complexes are retained in the endoplasmic reticulum. However, co-expression with the NR2 subunit translocates D₁R-NR1 heteromers to the plasma membrane. Interestingly, besides modulating D₁R trafficking, co-transfection of NR1 and NR2 abolishes agonist-induced D₁R internalisation⁶⁸⁰. Thus, to better understand the mechanism driving D₁R-H₃R heteromerisation and the protective effect of H₃R ligands against D₁R-mediated cell death, we set ourselves to investigate whether a similar mechanism might be taking place. Over-stimulation of most GPCRs induces receptor internalisation and the D₁R is no exception^{681,682}. In addition, decreased levels of D₁ and D₂ receptors in human post-mortem HD brains and diminished expression of D₁R in various HD mouse models have been reported^{528,683–686}. To explore the molecular mechanism of the D₁R-H₃R interaction, first we investigated the effect of the cytotoxic SFK 81297 (30 μM) concentration in STHdH^{Q7} and STHdH^{Q111} cells. Using immunocytochemistry and confocal microscopy, we observed that receptor over-stimulation induced D₁R internalisation in both cell lines, as can be appreciated by the redistribution and consequent confinement of fluorescently stained D₁ receptors into the cytosolic space (**Figure 5.6A**). Next, we validated this result in HEK293 cells (**Figure 5.6B**). We moved to this different heterologous cell line to assess whether H₃R-mediated D₁R sequestration to the plasma membrane could be a general mechanism through which D₁R-H₃R heteromers may operate. In agreement with the results in striatal cells, 30 μM SFK 81297 treatment induced a rapid and continuous over time internalisation of the YFP labelled D₁R (**Figure 5.6B**). Importantly, pre-treatment with Thioperamide prior to D₁R stimulation prevented SKF 81297-mediated internalisation, supporting our hypothesis that H₃R can act as a “receptor trap” when heteromerising with D₁R and that D₁R-H₃R complexes are not sorted together to endosomal compartments upon D₁R over-activation.

Next, we explored this characteristic in striatal cells. In both STHdH^{Q7} and STHdH^{Q111} cells treated with vehicle, we observed the characteristic positive fluorescent PLA staining surrounding the nucleus (**Figure 5.7**). In agreement with the results in HEK293 cells, D₁R

Allosteric D₁-H₃ hetero-receptor interactions provide a novel target for HD

over-stimulation with 30 μ M SKF 81297 resulted in heteromer disruption, as evidenced by the lack of PLA staining either in STHdH^{Q7} or STHdH^{Q111} (**Figure 5.7**). Thus, D₁R-H₃R heteromers do not traffic together and are disrupted after D₁R internalisation. Thereupon, we

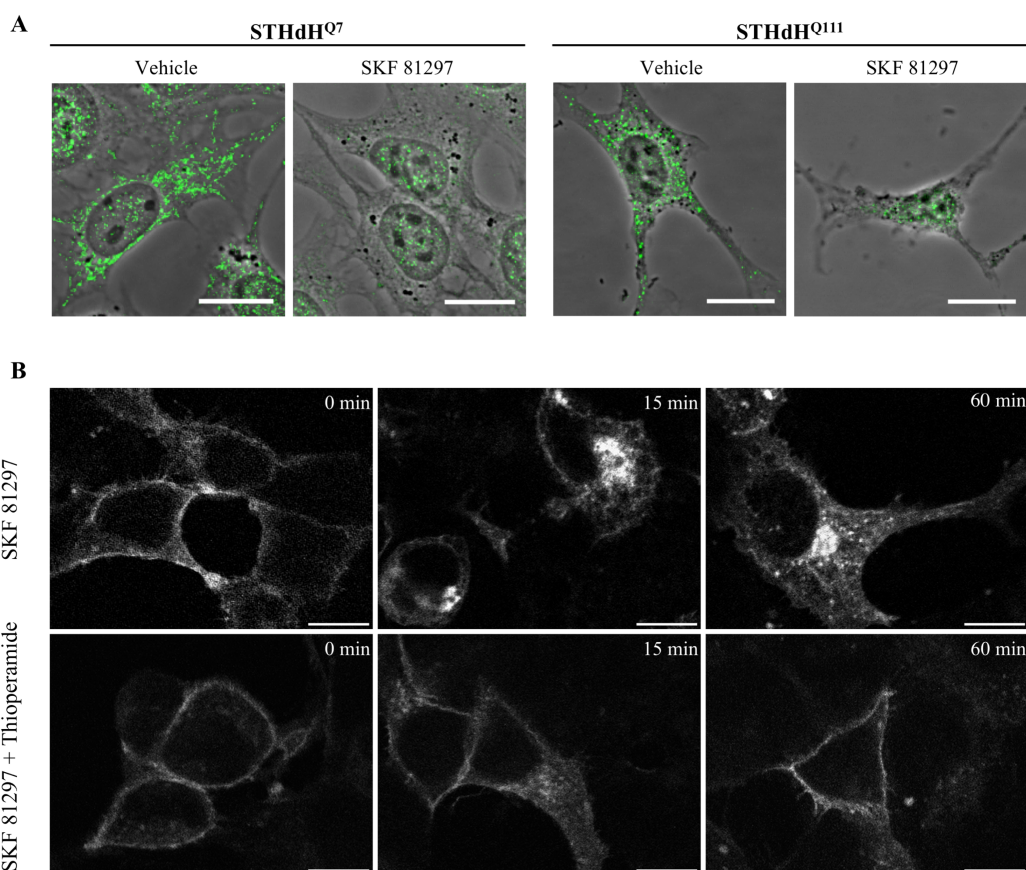


Figure 5.6. The H₃R antagonist Thioperamide inhibits D₁R internalisation. In (A), STHdH^{Q7} and STHdH^{Q111} cells were treated with vehicle or the D₁R agonist SKF 81297 (30 μ M) for 45 minutes. Representative superposition of phase contrast and confocal microscopy (superimposed Z stacks) for immunostained D₁R (green). In (B), representative confocal microscopy images of HEK 293 cells transiently expressing the yellow fluorescent protein tagged D₁R (white) and the H₃R were pre-incubated with vehicle or the H₃R antagonist Thioperamide (10 μ M) for 1 hour prior to the stimulation with SKF 81297 (30 μ M) for the indicated times. Scale bars: 10 μ m.

assessed the effect of pre-treatment with the H₃R agonist and antagonist prior to D₁R stimulation. Interestingly, both Imetit and Thioperamide restored the punctate PLA spots decreased after 30 μ M SKF 81297-induced D₁R internalisation (**Figure 5.7**). Together, these

results indicate that H₃R can block D₁R internalisation and its signalling pathways (e.g. [Ca²⁺]_i release), contributing to reverse striatal cell death induced by aberrant D₁R activation.

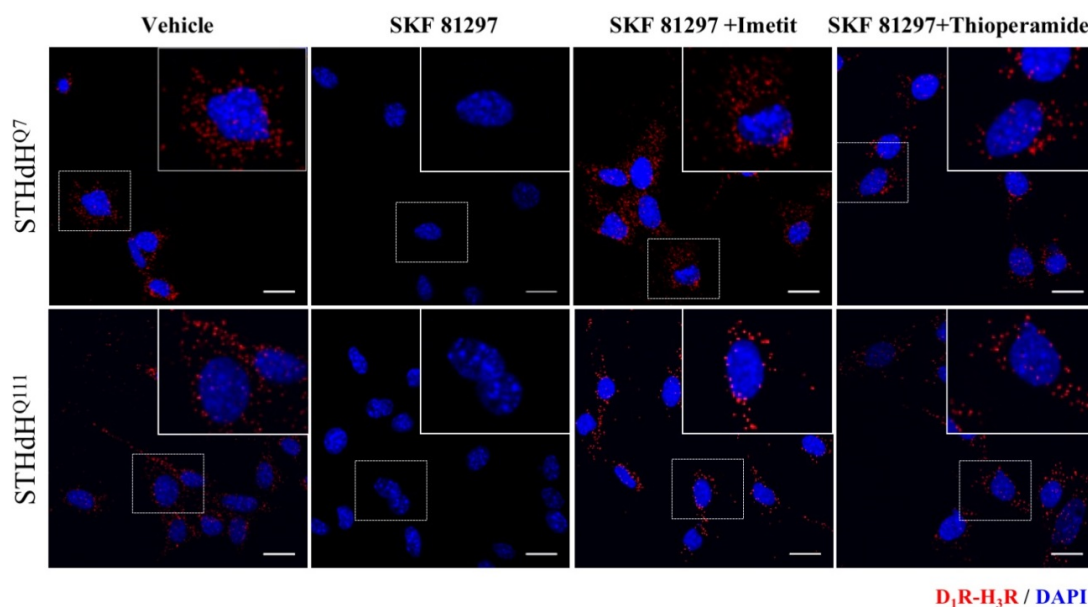


Figure 5.7. Thioperamide prevents D₁R internalisation-driven heteromer loss. STHdH^{Q7} and STHdH^{Q11} cells were pre-incubated for 1 hour with vehicle or the H₃R antagonist Thioperamide (10 μM) before D₁R overstimulation for 45 minutes with SKF 81297 (30 μM). Representative PLA confocal microscopy images illustrating D₁R-H₃R heteromers (red puncta) surrounding the blue nucleus stained with DAPI. Scale bars: 20 μm.

5.2.5. D₁R-H₃R heteromers loss in Hdh^{Q7/Q111} mice at early but not late HD stages.

To explore if D₁-H₃R heteromers could be indeed a therapeutic target for Huntington's disease, we sought to investigate the expression levels of D₁ and H₃ receptors and the presence of the heterocomplexes in the striatum, cortex and hippocampus of heterozygous mutant knock-in (KI) Hdh^{Q7/Q111} and wild type Hdh^{Q7/Q7} HD mice. In this murine model, the exon 1 of the mutant huntingtin gene (*HTT*) has been replaced by the mutated gene carrying 111 CAG repeats⁶⁸⁷. Because the mutation is under the control of the *HTT* endogenous promoter, provides an appropriate genomic and protein context, being the one of the most reliable and widely accepted preclinical model of HD⁶⁸⁸. In early stages, Hdh^{Q7/Q111} mice show somatic HD CAG repeat instability and nuclear accumulation of the full-length mutant huntingtin protein (2.5 months), preceding the appearance of N-terminal huntingtin inclusions in the nucleus (10 months)⁶⁸⁹. Importantly, none of the KI HD models exhibit striatal death, although reactive astrogliosis appears in the striatum of 24-months-old Hdh^{Q7/Q111} mice⁶⁹⁰.

The striatum is the primary site of neuronal loss throughout HD pathology, with up to 95% loss of GABAergic MSNs in later stages of HD. Furthermore, atrophy of the cerebral cortex and the hippocampus, although less severe than in the striatum, are highly implicated in the pathology of HD⁶⁵³. Thus, first we analysed D₁R and H₃R expression levels/affinities and the presence of heteromers in these brain structures in both wild type Hdh^{Q7/Q7} and mutant HD Hdh^{Q7/Q111} mice at 4 and 8-months of age (**detailed in Table 5.2**). In 4-month old mice, we did not observe H₃R expression/affinity differences in any of the analysed tissues. In agreement with the course of HD, at this early stage, we already detected a significant reduction in the levels of D₁R in Hdh^{Q7/Q111} cortex. Interestingly, hippocampal D₁R expression and [³H]SCH 23390 affinity were increased in 4-months old Hdh^{Q7/Q111} mice. These results correlate with recent data from Dallérac et al., where using immunofluorescent labelling they detect increased D₁R levels in 3-months old but not 7-months old R6/1 HD mice. These effects may reflect an up-regulation in receptor number due to decreased dopaminergic innervation⁶⁹¹. In 8-months old mice, we observed a discrete reduction in H₃R levels in Hdh^{Q7/Q111} mice. The most marked changes occurred at the D₁R level, with almost 50% [³H]SCH 23390 B_{max} reduction in the HD model. Next, we compared the affinities and receptor densities between 4- and 8-months old mice. In wild type animals, H₃R levels remained stable over time, with only minor changes in receptor affinity in 8-months old striatum and cortex. In agreement with early positron emission tomography (PET) studies in healthy volunteers assessing D₁R age-related decline in caudate and putamen⁶⁹², we observed a significant reduction in 8-months old Hdh^{Q7/Q7} mice striatal D₁R. Interestingly, similarly to [³H]SCH 23390 autoradiography studies in CA1, CA3 and CA4 rat hippocampal areas, D₁R levels were upregulated in 8 months wild type mice hippocampus⁶⁹³. When comparing 4 and 8 months-

old Hdh^{Q7/Q111} mice, the main changes occurred for D₁R. However, it should be noted a small decrease in H₃R levels in 8 months-old striatum and a significant reduction in [³H]RAMH affinity at the same age in the hippocampus. As expected, a dramatic change in D₁R density occurred in 8 months-old Hdh^{Q7/Q111} mice in the striatum.

Table 5.2. D₁R and H₃R expression levels and ligand affinities in striatum, cortex and hippocampus of 4- and 8-months old wild type Hdh^{Q7/Q7} and HD Hdh^{Q7/Q111} mice.

Receptor	Brain region	Hdh ^{Q7/Q7}	Hdh ^{Q7/Q7}	Hdh ^{Q7/Q111}	Hdh ^{Q7/Q111}
		B _{max} (fmol/mg protein)	K _D (nM)	B _{max} (fmol/mg protein)	K _D (nM)
H ₃ R 4months	Striatum	197 ± 3	0.16 ± 0.02	187 ± 9	0.20 ± 0.03
	Cortex	157 ± 8	0.17 ± 0.03	160 ± 7	0.18 ± 0.03
	Hippocampus	110 ± 1	0.02 ± 0.02	92 ± 6	0.08 ± 0.03
D ₁ R 4months	Striatum	1219 ± 40	0.27 ± 0.02	776 ± 30 ^a	0.15 ± 0.01
	Cortex	46 ± 5	0.16 ± 0.05	67 ± 4	0.01 ± 0.006
	Hippocampus	77 ± 8	0.39 ± 0.09	177 ± 21 ^a	0.03 ± 0.02 ^{aaaa}
H ₃ R 8months	Striatum	193 ± 6	0.27 ± 0.03 ^b	155 ± 6 ^{aaa,b}	0.26 ± 0.03
	Cortex	146 ± 4	0.22 ± 0.02	152 ± 8	0.24 ± 0.04
	Hippocampus	92 ± 1	0.20 ± 0.01 ^{bb}	88 ± 3	0.37 ± 0.1 ^{bb}
D ₁ R 8months	Striatum	1088 ± 50 ^b	0.17 ± 0.02	529 ± 32 ^{aaaa,bbbb}	0.11 ± 0.01
	Cortex	99 ± 5	0.05 ± 0.01	73 ± 4	0.01 ± 0.01
	Hippocampus	257 ± 10 ^{bb}	0.03 ± 0.02 ^{bbb}	187 ± 19	0.09 ± 0.07

Binding affinities of [³H]RAMH and [³H]SCH 23390 to H₃ and D₁ receptors, respectively, in Hdh^{Q7/Q7} and HD Hdh^{Q7/Q111} mice striatal, cortical and hippocampal tissue homogenates. Data are mean ± SEM (n=3) performed in triplicates (6, and 5 animals for Hdh^{Q7/Q7} and Hdh^{Q7/Q111} mice, respectively). Statistical significance was evaluated by two-way ANOVA followed by Bonferroni post hoc tests comparing the K_D and B_{max} values at a given age between genotypes (^ap ≤ 0.05, ^{aa}p ≤ 0.01, ^{aaa}p ≤ 0.001, ^{aaaa}p ≤ 0.0001) or by comparison of the K_D and B_{max} values within genotypes over 4 and 8 months (^bp ≤ 0.05, ^{bb}p ≤ 0.01, ^{bbb}p ≤ 0.001, ^{bbbb}p ≤ 0.0001). K_D: equilibrium dissociation constant; B_{max}: maximum receptor densities.

Allosteric D₁-H₃ hetero-receptor interactions provide a novel target for HD

Our next strategy was to investigate the presence of D₁R-H₃R heteromers in brain slices of Hdh^{Q7/Q7} and Hdh^{Q7/Q111} mice sacrificed at 4 and 8 months. We detected positive PLA staining in both 4 months-old wild type and KI animals in all brain structures analysed, as evidenced by the presence of green fluorescent puncta surrounding the blue stained nucleus (**Figure S2A**). Importantly, no PLA signal was detected in negative controls missing the primary antibodies, indicating that the stochastic recognition and amplification of the PLA probes does not occur (**Figure S2E**). Although we observed some differences between genotypes in the expression levels of receptors in cortex (**Table 5.2**), the number of positive PLA stained cells was homogenous across all three analysed regions at 4 months of age (**Figure S2C**). These results indicate that D₁-H₃ heteromers are present at early pre-symptomatic stages in both wild type and HD animals, providing a timeframe for targeting D₁-mediated cell death through H₃R modulation of D₁R-H₃R heteromers. To test this hypothesis, we assessed if the appearance of HD phenotype (8 months-old) in KI Hdh^{Q7/Q111} mice could affect heteromerisation (**Figure S2B**). In wild type Hdh^{Q7/Q7}, we detected positive PLA staining in striatum, cortex and hippocampus, indicating that the minor changes in receptor expression do not alter oligomerisation and that D₁R-H₃R heteromers levels are maintained over time in healthy wild type animals. In addition, PLA quantification revealed no differences in the number of complexes across tissues (**Figure S2D**). Surprisingly, in 8-months old KI Hdh^{Q7/Q111} animals, we observed an almost complete loss of D₁R-H₃R heteromers in striatum, cortex and hippocampus. Although using ligand binding we detected a significant reduction in D₁R levels in Hdh^{Q7/Q111} animals in comparison with Hdh^{Q7/Q7} mice, this heteromer loss is not likely to occur due to a lack of receptor expression. Indeed, D₁ and H₃ receptors levels in hippocampus and cortex were not altered in HD animals, even though PLA staining disappeared after 8 months. Furthermore, although D₁R density in cortex decreases by around 50% in 8-months old KI animals, its levels were highly superior in comparison with other analysed tissues. Our results corroborate the presence of D₁R-H₃R heteromers in early but not late HD stages, suggesting H₃R ligands as a strategy to prevent D₁R-mediate cell death in early stages of the illness.

5.2.6. The H₃R ligand Thioperamide prevents cognitive and motor learning deficits and loss of D₁R-H₃R heteromers in Hdh^{Q7/111} mice.

Considering the role of H₃R in preventing striatal cell death and the progressive loss of D₁R-H₃R heteromers in KI Hdh^{Q7/111} mice, we assessed whether early treatment with the H₃R antagonist Thioperamide may exert a therapeutic opportunity to prevent HD associated motor and learning deficits. Exhaustive studies in this HD model have recently described spatial, recognition and associative memory deficits in 6-months old but not 4 months-old mice^{694,695}. Therefore, we selected 5-months old animals for chronic treatment with Thioperamide over one month (for behaviour experiments in 6-months old mice) or continued with the treatment until the 8th month.

The acquisition of new motor skills is impaired in disorders affecting corticostriatal circuits, such as AD and HD. Thus, using the accelerating rotarod task procedure (ARTP), corticostriatal function was assessed⁶⁹⁶. In saline and Thioperamide-treated Hdh^{Q7/Q7} mice, the latency to fall from the rotarod incremented over each trial, indicating that Thioperamide by itself does not affect the ability to acquire a new motor skill (**Figure S3A**). As previously reported, saline-treated Hdh^{Q7/Q111} mice were unable to maintain their balance on the rod^{694,695}. Surprisingly, chronic treatment with Thioperamide rescued Hdh^{Q7/Q111} mice ARTP performance to wild type levels, as can be appreciated by the lack of significant differences in the latency to fall between saline-treated Hdh^{Q7/Q7} and Thioperamide-treated Hdh^{Q7/Q111} mice (**Figure S3A**).

Next, we tested recognition long-term memory (LTM) using the novel object recognition test (NORT). Before performing the experiments, the animals were habituated in the open field arena for two days, without alterations in motivation, anxiety and locomotor activity between genotypes and/or treatments. After habituation, the littermates were placed in the open-field arena containing two similar objects (A and A') for the familiarisation phase, with any genotype nor treatment displaying significant differences in the amount of time exploring both objects (**Figure S3B**). 24 hours after training, the NORT was performed by exchanging one of the previous objects by a novel one (B). Hdh^{Q7/Q7} saline and Thioperamide-treated mice spent more time exploring B, reflecting the natural preference for novel objects displayed by rodents (**Figure S3B**). As expected, saline-treated in Hdh^{Q7/Q111} mice exhibited recognition LTM deficits, with no preference for the novel object with respect to the familiar one. However, chronic Thioperamide administration completely recovered LTM deficits in Hdh^{Q7/111} mice.

Spatial LTM was assessed using the T-maze spontaneous alternation task (T-SAT) (**Figure S3C**). No differences between genotypes and/or treatments were observed during the training

Allosteric D₁-H₃ hetero-receptor interactions provide a novel target for HD

phase, with analogous exploration time and number of arm entries in all groups. After 5 hours, during the testing session, saline-treated Hdh^{Q7/Q111} mice exhibited spatial LTM deficits, with no preference between both arms. Saline and Thioperamide-treated Hdh^{Q7/Q7} mice showed preference for the new arm. However, Thioperamide-treated Hdh^{Q7/Q111} littermates exhibited the same tendency, indicating that the chronic pharmacological blockage the H₃R reverts spatial LTM deficits.

Together, our data demonstrate that motor learning and spatial/recognition LTM deficits can be prevented by Thioperamide in Hdh^{Q7/111}. Accordingly, we sought to investigate if these effects correlate with preservation of D₁R-H₃R heteromers in striatum, cortex and hippocampus. Similarly to what we observed by PLA in 8-months old Hdh^{Q7/111} mice (**Figure S2B,D**), the number of hetero-receptor complexes were significantly reduced in saline-treated 6-months old Hdh^{Q7/111} mice, indicating that D₁-H₃ heteromers already disappear at this early stage of the disease (**Figure 5.8A**). Importantly, Thioperamide treatment reverted this effect in all analysed brain regions not only in 6-months old HD mice (**Figure 5.8A**), but also in 8-months old in Hdh^{Q7/111} mice (**Figure 5.8B**). Overall, these results demonstrate that targeting D₁R-H₃R heteromers through antagonising H₃R with Thioperamide is an effective treatment for restoring motor learning and preventing spatial and recognition LTM deficits in Hdh^{Q7/Q111} mice. In addition, our results suggest that the altered trafficking observed in cells may also occur *in vivo* and that the effect of Thioperamide in learning and memory requires the expression of functional D₁-H₃ receptor heteromers.

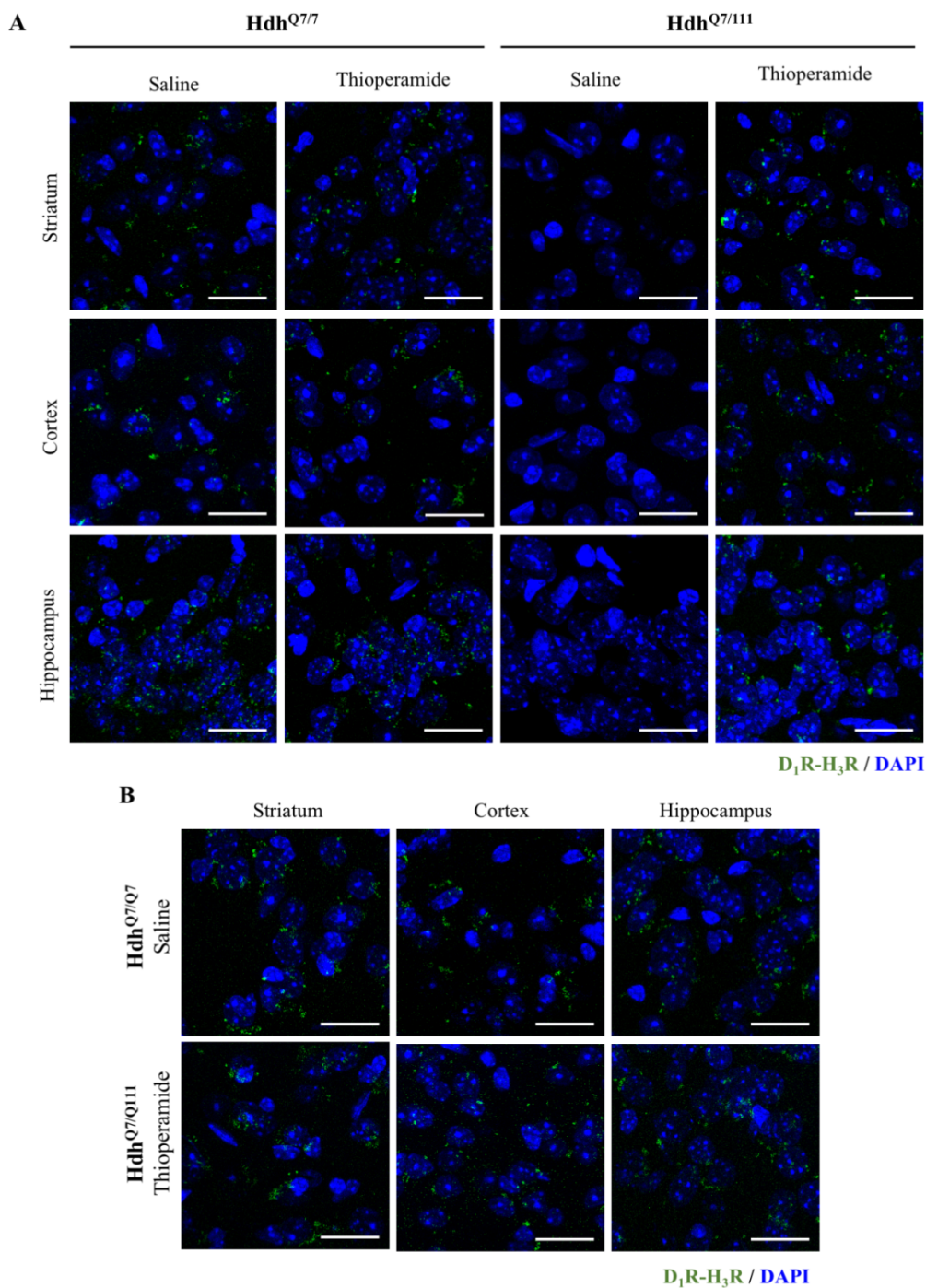


Figure 5.8. Chronic administration of the H₃R antagonist Thioperamide prevents loss of D₁R-H₃R heteromers at late HD stages in Hdh^{Q7/Q111} mice. In (A), Representative striatal, cortical and hippocampal Proximity Ligation Assays (PLAs) confocal microscopy images of 6-months old wild type Hdh^{Q7/7} and HD Hdh^{Q7/111} mice chronically treated with vehicle or the H₃R antagonist Thioperamide. D₁R-H₃R heteromers (green puncta) were not visualised in 6-months Hdh^{Q7/Q111} mice treated with vehicle. In (B), D₁R-H₃R heteromers expression was restored in 8-months old Thioperamide-treated Hdh^{Q7/Q111} mice to similar levels as in wild type Hdh^{Q7/7}. Scale bars: 20 μ m.

5.3. Discussion

Alterations in the dopaminergic system have major consequences in several motor disorders, such as Parkinson's and Huntington's diseases. Over HD progression, the imbalance in dopamine inputs plays a key role leading to substantial neuronal dysfunction and cell death^{653,669,670}. Here, we propose a strategy to dampen D₁R signalling by means of taking advantage of the biochemical properties of D₁R-H₃R heteromers, demonstrating for the first time the potential of GPCR heteromers as a target for HD. Our results support that (1) H₃R ligands can modulate D₁R downstream signalling in striatal cells, (2) this effect is due to the formation of hetero-receptor complexes interacting through TMs 5 and 6, (3) D₁-mediated cell death can be reduced targeting its interacting H₃R protomer, (4) D₁R-H₃R heteromers are expressed in the striatum, cortex and hippocampus of wild type and HD mice at early but not late HD stages, and (5) H₃R ligands can revert motor and learning deficits in HD mice while the heteromers are still expressed.

MSNs appear to be the preferential source of degeneration and death in HD. Increasing evidence suggest the role of glutamate and DA-mediated excitotoxicity, with both systems intimately linked. In fact, several studies show how DA increases MSNs sensitivity to glutamate stimuli, synergistically leading to striatal neurodegeneration. This effect has been shown to be D₁R-dependant, as selective D₂R agonist or specific D₁R antagonists abrogate this cross-talk⁵²⁸. Thus, reducing D₁R signalling using pharmacological tools may provide a therapeutic opportunity to tackle striatal cell death. Controversially, the exclusive role of D₁R over-activation in MSNs cell death is contradicted by studies showing that antagonising D₂R activation reduces mHTT toxicity in cultured striatal neurons transiently expressing the GFP-tagged-exon 1 of mHTT⁶⁹⁷. Moreover, pharmacological blockage of D₂R has been extensively used to treat chorea symptoms and psychiatric disturbances in HD patients. Although its ability to improve motor skills, their effectiveness in terms of cognitive deterioration improvement are contradictory, most likely due to the biphasic nature of HD progression^{698,699}.

Even if it is clear the role of both D₁ and D₂ receptors in striatal neurodegeneration, our results in both STHdH^{Q7} and STHdH^{Q111} striatal cell lines point towards D₁R having the main role in striatal cell death. We have demonstrated that toxic concentrations (30 μ M) of the selective D₁R agonist SFK 81297 induces intracellular Ca²⁺ overload, starting signalling pathways that ultimately will result in cell death⁷⁰⁰. Thus, considering the increased DA levels in the striatum at early HD stages and the excess of D₁ over D₂ receptors in the striatum, modulation of D₁R signalling might be beneficial to treat HD⁷⁰¹. However, as previously stated, D₁R direct targeting entails serious adverse effects. In this frame, we propose an alternative strategy to

modify D₁R via the previously characterised D₁R-H₃R heteromers, in which the H₃R acts as a “molecular brake” for D₁R signalling^{523,524}. In this frame, we hypothesised that striatal cell death might be prevented targeting D₁R-H₃R heteromers with H₃R ligands. Accordingly, we found that agonists and antagonists of the H₃R, via negative cross-talk and cross-antagonism, completely blocked striatal cell death upon D₁R over-stimulation. This effect was heteromer-driver, as pre-incubation of both STHdH^{Q7} and STHdH^{Q111} striatal cells with the TM5 (positive control) but not the TM7 (negative control) peptides abrogated H₃R ligands ability to revert cell death.

Allosteric communication between protomers is often observed in terms of altered signalling. In the case of D₁R-H₃R complexes, this is supported by our Ca²⁺ mobilisation experiments and the disruption of the negative cross-talk and cross-antagonism with peptides. However, another mechanism through which heteromers can expand its functionality is by altering receptor trafficking²⁴⁹. Indeed, when exploring the molecular basis underlying D₁R-H₃R heteromerisation, we found that the H₃R acts as a membrane trap for D₁R in heterologous expression systems. In addition, Imetit and Thioperamide pre-incubation in STHdH^{Q7} and STHdH^{Q111} cells restored the PLA positive staining after D₁R over-stimulation. Thus, the signalling effects that we observed appear to occur over different timescales. The former is an important concept, as one of the main criticisms concerning GPCR oligomers targeting with therapeutic purposes is the limited information regarding their stability and kinetics. Our results show that D₁R-H₃R heteromers are stable over fast (Ca²⁺ release), medium (ERK1/2 phosphorylation) and longer (D₁R internalisation) signalling events.

Provided the potential role of D₁R-H₃R heteromers to reduce striatal cell loss in HD, we investigated whether these complexes are present *in vivo* in brain regions known to be susceptible to mHTT toxicity⁷⁰². Importantly, we detected them at early stages in the striatum, cortex and hippocampus of wild type and knock-in Hdh^{Q7/Q111} mice. However, D₁R-H₃R heteromers were lost in all analysed brain areas at late HD stages (6 and 8-months old). These results do not reflect the progressive reduction in D₁R striatal expression over HD course, as its levels were significantly higher in comparison with other brain areas where both D₁ and H₃ receptors densities remained unchanged (cortex and hippocampus).

Growing evidence suggests that neuronal dysfunction is the earliest disturbance in HD, leading to cognitive and behavioural changes well before the appearance of the motor symptoms associated with striatal and cortical cell death⁷⁰³. In addition, exhaustive studies both in humans and HD animal models have illustrated more complex mechanisms underlying these cognitive deficits, not just involving the basal ganglia and cortical dysfunction but also other brain structures like the hippocampus^{704,705}. Thus, given that memory and learning processes involve intricate brain circuits, most neurodegenerative disorders' treatments do not

Allosteric D₁-H₃ hetero-receptor interactions provide a novel target for HD

cover the cognitive decline. Moreover, the timing of the intervention is a key factor to take into account. HD pathophysiology is dynamic and brain atrophy and dysfunction progress over time. Considering the role of dopamine and histamine in synaptic plasticity and memory, the therapeutically potential of H₃R ligands through D₁R-H₃R heteromers might not be limited to HD motor dysfunctions but also improve cognitive decline and learning impairments^{706,707}. Supporting this hypothesis, we found that starting the chronic treatment with the H₃R antagonist Thioperamide in 5-months old Hdh^{Q7/Q111} HD mice improved motor learning and spatial/recognition long term memory deficits. Interestingly, emphasising the central role of D₁R-H₃R complexes as responsible of these effects, Thioperamide retained the presence of the heteromers over 6 and 8 months of age.

Our results do not rule out the possibility that Thioperamide may be targeting another recently described heteromeric complex between the dopamine D₂ and the histamine H₃ receptors. In fact, using reserpinised mice, it has been reported a post-synaptic antagonistic interaction in locomotor activation mediated by H₃R-D₂R heteromers³⁴⁴. However, first, our results showing how D₁R over activation elicits cell death related pathways and heteromer disruption; second, the fact that pre-treatment with H₃R ligands revert these effects; and third, our data illustrating how synthetic peptides analogues of D₁R TM5 abrogate D₁R-H₃R heteromer-specific effects strongly support our hypothesis that the observed outcomes are dependent of functional D₁R-H₃R heteromers. Another option, although striking, is that pre-synaptic H₃R blockage increases the local histamine concentration in the synaptic cleft, thus binding to post-synaptic H₃ receptors and hence decreasing D₁R signalling. Our *in vivo* results do not count this option out and the exact mechanism whereby Thioperamide improves cognitive function through D₁R-H₃R heteromers is yet to be unveiled.

The early hyperkinetic HD phase is characterised by increased DA levels and activity⁷⁰⁸. DA depleting agents/stabilisers such as tetrabenazine, deutetrabenazine and pridopidine have successfully shown in the clinical and preclinical models neuroprotection and motor coordination improvement^{660,709–711}. However, none of these agents have shown improvements in cognitive function. Although the concept of GPCR heteromers has been going on over the last decades, only recently are beginning to emerge as potential druggable entities, with just few examples illustrating their physiological relevance in relation to disease^{184,317,712,713}. Our results open up a new scenario of opportunities to fight against HD, providing a new drug target in a hopeless disease.

5.1. Acknowledgements

We thank Dr Silvia Gines' lab for mice *in vivo* behavioural experiments and for providing Hdh^{Q7/Q7} and Hdh^{Q7/Q111} mice samples. We are very grateful to Dr Estefania Moreno for tissue PLA experiments.

Allosteric D₁-H₃ hetero-receptor interactions provide a novel target for HD

Chapter 6

Serotonin 5-HT_{2C} Receptors Positive Allosteric Modulation in Obesity

6.1. Introduction

With an estimated worldwide prevalence of ~2 billion overweighted adults, within which 640 million are obese, its health- and economic-associated concerns have led the World Health Organisation (WHO) to incorporate increased body mass index (BMI) among the global non-communicable diseases targets^{714,715}. Obesity is a major risk factor for the development of some of the comorbidities associated with metabolic syndrome, cardiovascular and kidney diseases, type II diabetes mellitus and musculoskeletal disorders⁷¹⁶. In addition, several studies have shown a positive correlation between increased BMI and the prevalence and/or mortality of certain types of cancer (e.g. endometrial, colorectal, breast and prostate cancers), with obesity-triggered chronic subclinical inflammatory states emerging as key players in this process^{717,718}. Moreover, obesity is associated with increased odds for developing psychiatric disorders, such as anxiety and depression, and impaired cognitive function⁷¹⁹.

Obesity aetiology is a complex combination between genetic, environmental, psychologic, social and economic factors. Thus, the energy balance will depend on the coordinated interaction between these elements and the effector systems responsible for food intake and energy expenditure⁷²⁰. The complexity and multifactorial nature of this disease makes its clinical management especially challenging. In fact, lifestyle interventions (e.g. dietary restrictions and physical activity), the “obvious” cornerstone for weight loss, have shown little long-term success, with most subjects regaining the initial body weight reduction (~5-10%) within 5 years⁷²¹. Hence, with an estimated global prevalence of ~20% by 2025, the development of more “aggressive” pharmacological therapies appear to be necessary⁷¹⁵.

Although different targets have been explored to treat obesity, most of the efforts have been fruitless, resulting in the withdrawn from both the US and European administrations of most of these medicines due to adverse side effects⁷²². Currently approved anti-obesity drugs target different systems, including GLP1R agonists (Liraglutide) and pancreatic lipase inhibitors (Orlistat). In addition, increasing monoamine neurotransmitters levels via sympathomimetic drugs (Phentermine, Diethylpropion and Naltrexone) or the direct activation of their receptors (Lorcaserin) underlie the rationale behind the last generation of approved anti-obesity drugs. In particular, activation of the 5-HT_{2C}R with the selective agonists Lorcaserin (FDA approval 2012) is the most advanced strategy for the long-term management of food intake and body weight reduction^{723,724}.

The relationship between increased serotonergic activity and the attenuation of food intake began to be delineated in the late 80s, highlighting the hypothalamus as a key structure for 5-HT-mediated anorectic properties^{725,726}. Recent advances in molecular biology and genetics

Serotonin 5-HT_{2C} Receptors Positive Allosteric Modulation in Obesity

have narrowed the anorectic properties of 5-HT receptor ligands to the 5-HT_{1B}R, 5-HT_{2C}R and 5-HT₆R subtypes. Whilst 5-HT_{1B}R and 5-HT_{2C}R actions depend on integratory hypothalamic peptidergic circuits within the arcuate (ARC) and paraventricular (PVH) nuclei and the lateral hypothalamic area (LHA), the mechanism underlying 5-HT₆R blockage-dependent food intake attenuation is not clear, although its expression in the ARC has led to the current model in which 5-HT₆R antagonism increases the α -melanocyte-stimulating hormone (α -MSH) levels via the blockage of GABAergic afferents to pro-opiomelanocortin (POMC) neurons⁷²⁷⁻⁷²⁹.

5-HT_{2C} receptors expression is mainly confined to the CNS, where they are sparsely allocated virtually in all brain structures. Therefore, alterations in 5-HT_{2C}R function have been associated to several major mental disorders (schizophrenia, depression and bipolar disorders) as well as to obesity^{725,730,731}. With respect to the later condition, activation of post-synaptic 5-HT_{2C}R receptors in POMC neurons of the ARC nucleus stimulate the releases of α -MSH, which binds to melanocortin 4 receptors (MC4R) in the PVN to induce satiety⁷³². Although this was postulated as the main mechanism whereby 5-HT_{2C}R modulates feeding behaviour, recent pre-clinical and clinical data supports the role of this 5-HT receptor subtype in motivation and reward circuits, such as its inhibitory effect on the dopaminergic mesolimbic pathway⁷³³⁻⁷³⁵. Accordingly, activation of 5-HT_{2C} receptors might provide a two-edged sword by inducing satiety and attenuating the reinforcing properties of feeding behaviours. In addition, Lorcaserin has shown positive outcomes in smoking cessation⁷³⁵, decreases alcohol intake in murine alcohol consumption models⁷³⁶ and is currently undergoing Phase II clinical trials for cocaine use disorders⁷³⁷.

Although the 5-HT_{2C}R receptor is a well validated target for obesity, the extraordinary high homology between 5-HT₂ receptors (~50% overall sequence identity) and the residues conserved within the orthosteric binding pockets makes their selective targeting extraordinary challenging^{29,135,352}. In addition, taking into account the potential hallucinogenic effects exerted by non-selective binding to 5-HT_{2A} and 5-HT_{2B} receptors and the involvement of 5-HT_{2B}R agonists in valvulopathy and cardiopulmonary diseases, specifically targeting subtypes within the 5-HT₂ family is an intrinsically risky endeavour^{29,738,739}. In fact, the first-generation anti-obesity drugs Sibutramine (non-selective serotonin reuptake inhibitor) and Dexfenfluramine (“selective” serotonin transporter inhibitor) were withdrawn by the European and American drug agencies due to severe cardiac and pulmonary off-target effects associated with their high affinity binding to 5-HT_{2B} receptors⁷⁴⁰.

In light of the validated effective strategy of directly (agonism) or indirectly (monoamine transporters/reuptake inhibitors) targeting 5-HT_{2C}R for obesity, we thought to circumvent potential off-target issues by exploring allosteric drug candidates. Allosteric modulators

provide several advantages over classical agonists/antagonists. In the case of neutral modulators (ligands without intrinsic activity), the spatial and temporal context of the endogenous ligand is retained. Importantly, the allosteric binding pockets are less conserved than the orthosteric sites, facilitating the selective targeting across receptor subtypes^{741,742}. Another important advantage of allosteric modulators arises from the saturability of their effects. Thus, under high dosage administration, finite responses limit on-target-associated toxicity⁷⁴².

To date, PNU-69176E and CYD-1-79 are the only 5-HT_{2C}R selective positive allosteric modulators (PAMs) whose chemical structures have been reported. Interestingly, a recent study has shown CYD-1-79 *in vivo* PAM efficacy attenuating cocaine cue reactivity in rats⁷⁴³⁻⁷⁴⁶. While this study strongly supports 5-HT_{2C}R allosteric modulation as an alternative target for the management of cocaine use disorders, the effect of such molecules as anti-obesity drugs remains to be explored⁷⁴⁶.

Here, we explored allosteric modulation of GPCRs from a “more conventional” perspective. That is, targeting these elusive alternative binding pockets with small-molecule compounds. The screening of a proprietary chemical library allowed us to identify a selective 5-HT_{2C}R PAM (compound 5). A series of analogues were developed based on its chemical structure, leading to a 5-HT_{2C}R-specific PAM with enhanced efficacy: compound 11 (*N*-[(1-benzyl-1*H*-indol-3-yl)methyl]pyridin-3-amine). Furthermore, supporting the potential of 5-HT_{2C} PAMs as anti-obesity drugs candidates, compounds 11 displayed anorectic properties and enhanced the effect of serotonin reuptake inhibitors in rodent feeding models. These promising results led us to explore its binding mechanism in order to develop further SAR-based analogues. By homology modelling and site-directed mutagenesis we delineated the 5-HT_{2C}R allosteric binding pocket, providing structural insights for the design of a new series of derivatives. Interestingly, one such analogue, WD014 (*N*-((1-([1,1'-biphenyl]-3-ylmethyl)-1*H*-indol-3-yl)methyl)pyridin-3-amine) exhibited PAM activity in a β -arrestin2-independent way, providing the first example, to the best of our knowledge, of a G protein-biased 5-HT_{2C}R PAM.

6.2. Results

6.2.1. Identification of putative 5-HT_{2C}R positive allosteric modulators through high-throughput screening

The ExviTech® platform of Vivia Biotech was used to screen a proprietary library of ~1600 small molecule compounds in order to identify potential 5-HT_{2C}R positive allosteric modulators (PAMs). This screening platform allows the sensitive detection by flow cytometry of whole cell changes in calcium mobilisation, canonical second messenger downstream the G_{q/11} protein-coupled 5-HT_{2C}R⁷⁴⁷. Accordingly, HEK293 cells stably expressing the 5-HT_{2C} receptor were pre-incubated for 20 min with tested compounds (10 μM) prior to the stimulation with a concentration of 5-HT that yields 25% of the maximal effective response (EC₂₅). Simultaneously, using multiparametric flow cytometry and cell tracking dyes, receptor-subtype specificity was assessed in cells expressing the closely related 5-HT_{2A} and 5-HT_{2B} receptors. Three putative PAMs displayed enhanced calcium responses (~20% E_{max} potentiation) in comparison with cells only treated with an EC₂₅ concentration of 5-HT, with a 5-HT_{2C}R subtype specific profile suggesting an allosteric mechanism of action.

To validate the potentiation in signalling of the three potential PAMs, we measured inositol monophosphate (IP₁) accumulation, which is a well-established downstream metabolite of inositol 1,4,5-trisphosphate after 5-HT_{2C}R activation⁷⁴⁷, by homogeneous time resolved fluorescence (HTRF). Chinese hamster ovary-K1 (CHO-K1) cells stably expressing the 5-HT_{2C}R were incubated with a fixed concentration of each putative modulator (10 μM) prior to the stimulation with increasing concentrations of 5-HT. Using this approach, we detected a potentiation in 5-HT E_{max} (~20%) for one of the compounds (hereafter compound 5) (**Figure 6.1** and **table 6.1**), supporting the allosteric nature of this initial hit. Accordingly, compound 5 was chosen as “hit-to-lead” with the objective to develop 5-HT_{2C}R PAMs with improved efficacy.

Based on the chemical structure of compound 5, two series of analogues were synthesised by modification of either the pyrimidine (compounds 6-14) or the phenyl rings (compounds 15-41) attached to the indole scaffold (**Table 6.1 top scheme**). For compounds 6-14, the phenyl ring was maintained and the pyrimidine ring was substituted by different nitrogen-containing heterocycles (**Table 6.1**). Next, we assessed the potential positive allosteric effect of this first series of analogues. Accordingly, 5-HT_{2C}R-induced IP₁ release was measured after stimulation with increasing concentrations of 5-HT in the presence of the tested compounds (10 μM) in CHO-K1 cells stably expressing the 5-HT_{2C} receptor. Comparing the E_{max} of

vehicle- vs compound-treated cells (**Table 6.1**), potentiation was almost confined to analogues harbouring pyridyl derivatives (compounds 11, 12 and 14). In particular, compound 11 (3-pyridyl analogue) displayed the maximal E_{\max} potentiation, increasing by $\sim 35\%$ IP_1 accumulation in response to saturating 5-HT concentrations.

On the basis of the above findings, a second series of analogues (**Table 6.1**) was designed around the phenyl ring (compounds 15-41). To explore the impact of substituents of different size and the electronic effect, F, Cl, Br, Me, OMe, CF₃ and CN groups were introduced at different positions in the benzene ring (compounds 15-37). In addition, in compounds 38-40, we assessed the effect of replacing the phenyl ring with pyridines. Furthermore, in order to investigate whether aromatic groups at 1-position of the indole scaffold are required and/or confer selectivity, the benzene ring was substituted by a cyclopropane ring (compound 41).

Compounds 15-41 effect was assessed as described above. Thus, IP_1 accumulation after dose-response stimulation with 5-HT was evaluated in the presence of vehicle or 10 μM of the tested ligands (**Table 6.1**). In comparison to compound 11, none of the analogues yielded enhanced signalling potentiation. However, several aryl derivatives (compounds 16, 19, 26 and 27) retained substantial potentiation of the endogenous agonist effect (20-30% E_{\max} potentiation). In addition, either the substitution of the benzene ring with pyridyl derivatives nor the non-aromatic cyclopropane improved allosteric potentiation, with 3-pyridyl insertion (compound 39) in 1-position of the indole scaffold being the only derivative retaining 5-HT potentiation ($\sim 25\%$). These results suggest the role of aromatic groups attached to the pyrrole ring stabilising ligand binding to the 5-HT_{2C}R allosteric pocket. Therefore, compound 11 was chosen for further pharmacological characterisation in order to validate its positive allosteric modulator nature, specificity towards 5-HT_{2C} receptors and key residues involved in its binding mechanism.

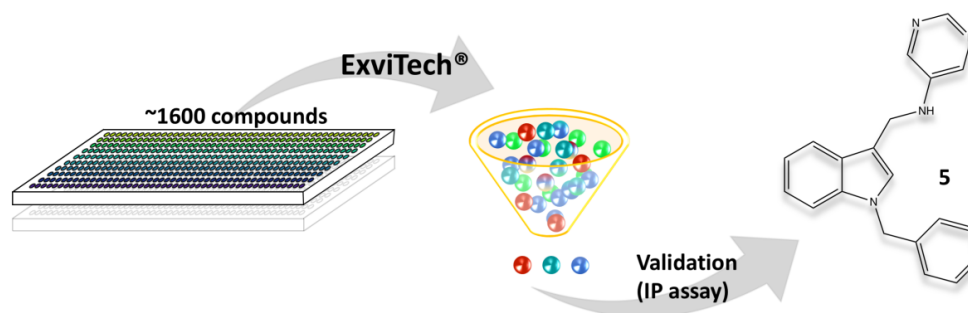
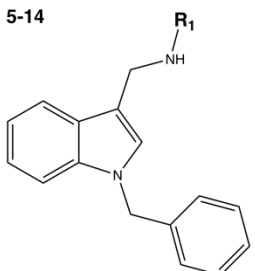
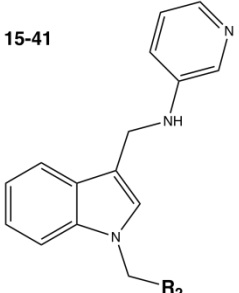
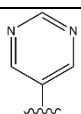
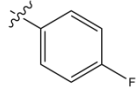
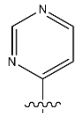
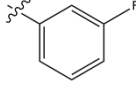
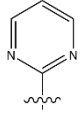
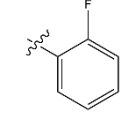
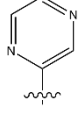
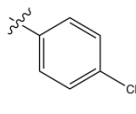
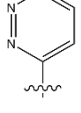
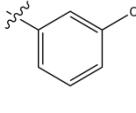
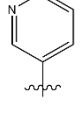
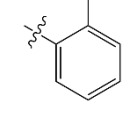
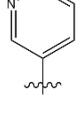
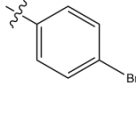
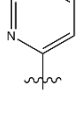
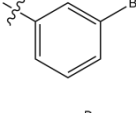
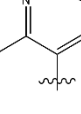
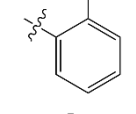
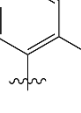
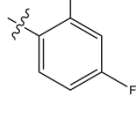


Figure 6.1. High-throughput screening of the Vivia Biotech chemical library. Schematic diagram illustrating the workflow for the identification of 5-HT_{2C}R positive allosteric modulators. A total of ~ 1600 compounds were screened using the ExviTech® platform of Vivia Biotech. Three initial hits were functionally validated (IP_1) among which compound 5 (VA240) was selected as starting scaffold for a medicinal chemistry program.

Serotonin 5-HT_{2C} Receptors Positive Allosteric Modulation in Obesity

Table 6.1. Analysis of compound 5 and derivatives 6-41 effects on 5-HT-dependent IP accumulation.

					
Compound	R ₁	Potentiation	Compound	R ₂	Potentiation
5		20 ± 4	15		9 ± 2
6		0	16		22 ± 3
7		0	17		6 ± 1
8		0	18		13 ± 3
9		9 ± 3	19		9 ± 3
10		0	20		7 ± 2
11		35 ± 5	21		6 ± 2
12		25 ± 3	22		7 ± 3
13		0	23		0
14		21 ± 4	24		9 ± 1

Compound	R ₂	Potentialiation	Compound	R ₂	Potentialiation
25		9 ± 2	34		0
26		9 ± 2	35		7 ± 2
27		24 ± 2	36		22 ± 2
28		27 ± 3	37		7 ± 4
29		7 ± 3	38		9 ± 3
30		6 ± 2	39		25 ± 3
31		0	40		0
32		0	41		0
33		8 ± 4			

Potentialiation of 5-HT-induced IP₁ maximal accumulation (E_{max}) in CHO-K1 cells stably expressing the 5-HT_{2C}R after pre-incubation (10 μM, 20 min) with the tested compound prior to stimulation with saturating 5-HT doses. Values are the percentage of potentialiation ± SEM (n=3), each experiment performed in duplicates, normalised to vehicle treated cells.

6.2.2. Pharmacological characterisation of compound 11

These results suggest that compound 11-mediated intracellular signalling potentiation occurs through binding to the 5-HT_{2C}R in a topologically distinct domain other than orthosteric pocket. Thus, to validate its positive allosteric effect, we evaluated the influence of increasing concentrations of compound 11 over dose-response stimulation with the endogenous 5-HT_{2C}R agonist serotonin. Due to its higher sensitivity (amplification step) and kinetic resolution, the *in vitro* characterisation of compound 11 was performed by measuring changes in calcium mobilisation⁷⁴⁸. Importantly, measuring this alternative signalling pathway is not a factor to take into account in terms of agonist bias, as both IP₁ and Ca²⁺ levels directly depend on the upstream G_q-mediated activation of the phospholipase C by the 5-HT_{2C}R⁷⁴⁷.

As shown in **Figure 6.2**, administration of compound 11 at 10 μM potentiated the effect of saturating concentrations of 5-HT with similar results as observed by IP₁ accumulation (57% vs 35% E_{max} increase for Ca²⁺ vs IP₁ accumulation, respectively). Importantly, the potentiation of the compound displayed a dose-dependent profile, as can be appreciated by the proportional increase in [Ca²⁺]_i over its different tested concentrations (**Figure 6.2A**), with a maximal effect of ~95% potentiation at 30 μM. It should be noted that, as expected from an allosteric modulator, higher doses of compound 1 (100 μM) did not induce further potentiation in [Ca²⁺]_i release. However, significant levels of toxicity were observed after visual inspection of the cells most likely due to the elevated concentration of DMSO (1% v:v) required to achieve this concentration. Therefore, in order to avoid false conclusions, these results were obviated (data not shown).

Interestingly, compound 11 did not modify 5-HT potency. Thus, no statistically significant differences were observed when comparing 5-HT pEC₅₀ between vehicle- or compound-treated cells (**Figure 6.2A,B**). While these results strongly suggest that compound 11 has no intrinsic agonist activity, we validated it by showing that this ligand does not increase Ca²⁺ levels in the absence of 5-HT (**Figure 6.2E**). Moreover, we confirmed the subtype selectivity of compound 11 in functional assays by measuring [Ca²⁺]_i release in cells expressing the closely related 5-HT_{2A} and 5-HT_{2B} receptors (**Figure 6.2C and D, respectively**). Pre-treatment with compound 11 had no impact in the maximal efficacy nor potency of 5-HT in both cell types. In agreement, administration of compound 11 alone had no effect in calcium mobilisation (**Figure 6.2CD**). In addition to 5-HT_{2C}R selectivity, potential off-target binders (including GPCRs, ion channels and enzymes and transporters involved in neurotransmitter and lipid metabolism) were externally evaluated with the SafetyScreen™ Functional Panel (CEREP, Eurofins) showing no significant agonist/antagonist activity over this broad range of targets. In order to confirm that compound 11 acts via positive allosteric modulation of the

5-HT_{2C}R we performed radioligand competition binding assays with different well-established orthosteric ligands (**Figure 6.2F**). In the presence of 10 μ M compound 11, [³H]serotonin, [³H]mesulergine and [³H]clozapine displacement was moderate. However, compound 11 significantly displaced [³H]LSD.

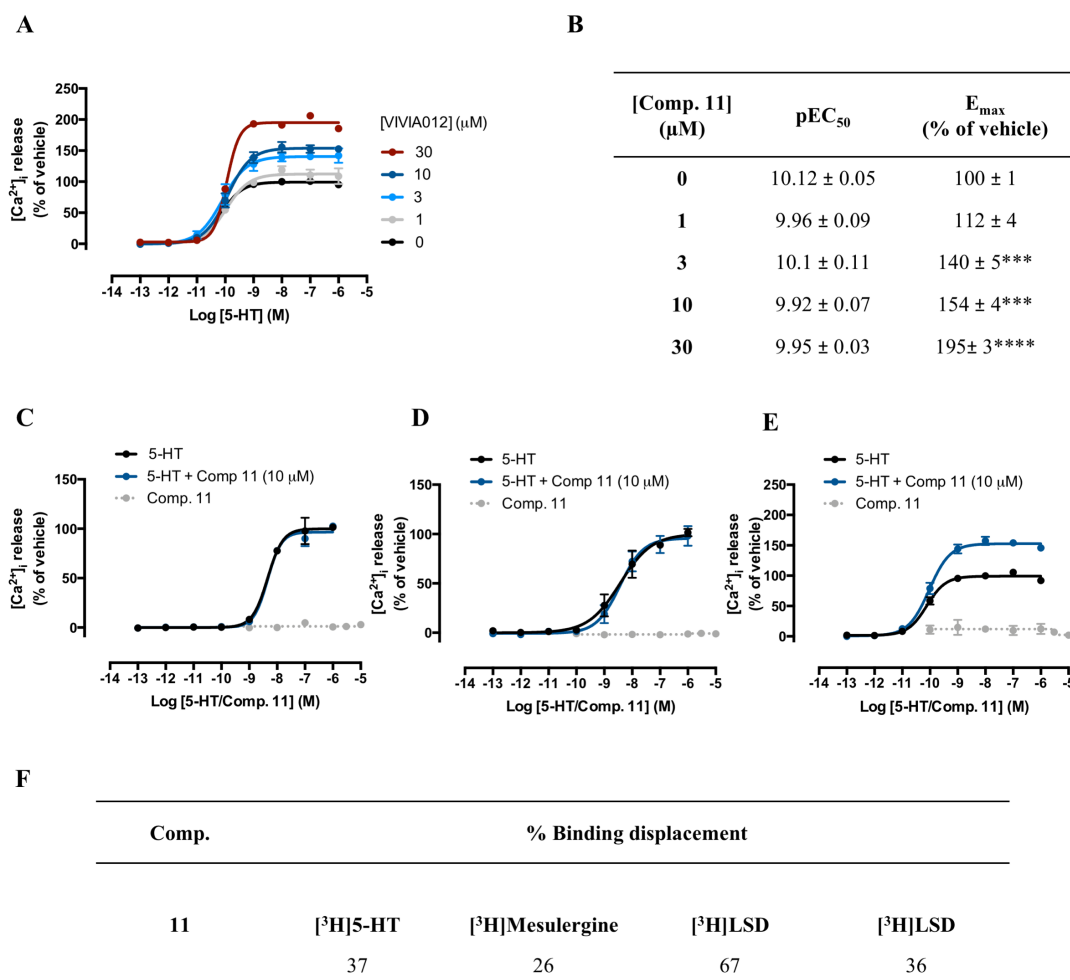


Figure 6.2. *In vitro* characterisation of compound 11 PAM profile and selectivity. (A) Summary 5-HT dose-dependent [Ca^{2+}]_i release curves in the presence of increasing comp. 11 concentrations. 5-HT potency (pEC₅₀) and maximal efficacy (E_{max}) are summarised in (B). Data are mean pEC₅₀/E_{max} \pm SD of two individual experiments each performed at least in duplicates. Statistical significance was evaluated by one-way analysis of variance (ANOVA) followed by Bonferroni post hoc tests, indicating significant differences over vehicle-treated cells (**p \leq 0.001, ****p \leq 0.0001). Evaluation of potential intrinsic agonist activity (grey lines) and allosteric potentiation (blue lines) in cells expressing the 5-HT_{2A} (C), 5-HT_{2B} (D) and 5-HT_{2C} (E) receptors. Data are mean \pm SEM (n=3) percentage of activation normalised to vehicle-treated cells. (F) Mean percentage binding displacement of different 5-HT_{2C}R radioligands by 10 μ M comp. 11 performed in triplicates.

At first glance, the moderate (serotonin, mesulergine and clozapine) and high (LSD) affinities for 5-HT_{2C}R might suggest interactions at the level of the orthosteric pocket. However, the proposed binding mode of compound 11 (discussed further on), resting on top of 5-HT close to the extracellular juxtamembrane space (a common binding site of aminergic allosteric modulators), might account for this displacement by limiting the access of orthosteric ligands to their binding pocket^{749,750}. In addition, the particular binding pose of LSD in the close related 5-HT_{2B}R crystal structure, with an extended position close to the ECL2 and the extracellular space, is in agreement with the observed moderate displacement²⁹.

Agonist bias is an emerging concept already showing important advantages in order to achieve pathway-specific and safer drugs (see section 1.1.5.3)²⁴⁹. In this sense, functional selectivity (G protein Vs β -arrestin preference) has been extensively explored for some 5-HT₂ receptor subtypes, mostly 5-HT_{2A} and 5-HT_{2B} receptors, due to its pivotal role in the hallucinogenic actions of some its agonists and their implication in valvular heart diseases^{128,751}. In fact, the 5-HT_{2B}R bound to ergotamine and the recent 5-HT_{2B}R-LSD complexes are among the few structures crystallised in association with well-established biased ligands^{29,135}. On the other hand, few reports explored this concept in 5-HT_{2C}R. In a recent study, particularly addressing G_{q/11} over β -arrestin2 functional selectivity, Cheng et al. recently developed a series of benzofuran derivatives exhibiting strong G protein signalling bias⁷⁵². Accordingly, we sought to investigate whether compound 11 retains its PAM activity in β -arrestin2 functional assays. To this end, we first developed an arrestin recruitment assay by taking advantage of the NanoBiT technology²⁷⁸. As previously shown, this strategy allowed us the sensitive monitoring of this protein:protein interaction for the CB₁, CB₂ and 5-HT_{2A} receptors (see Chapters 3 and 4). Thus, first we cloned the small (5-HT_{2C}R-SmBiT) and large (5-HT_{2C}R-LgBiT) hemiprotein halves of NanoLuc in the C-terminus of the 5-HT_{2C}R and assessed their impact in 5-HT_{2C}R functionality. In comparison with the WT receptor, none of the constructs affected 5-HT-driven calcium release maximal efficacy (**Figure 6.3A**). At the level of agonist potency, we observed a minimal but statistically significant reduction in 5-HT EC₅₀ (see **figure 6.3A** inserts). However, 5-HT-driven Ca²⁺ still remained within the low nanomolar range for all constructs, thus being unlikely to affect 5-HT_{2C}R function. Next, we assessed which configuration of arrestin and receptor pairs yielded the optimal combination to monitor arrestin binding. Therefore, the same concentration of both the 5-HT_{2C}R-LgBiT and 5-HT_{2C}R-SmBiT constructs used for [Ca²⁺]_i release experiments (100 ng/well) were co-transfected with the complementary arrestin plasmids harbouring the SmBiT and LgBiT fused to β -arrestin2 N-terminus (**Figure 6.3B**). Surprisingly, most cDNA ratios and combinations yielded significant levels of activation after stimulation with 5-HT (1 μ M), with the 5-HT_{2A}R-LgBiT plus SmBiT- β -arrestin2 pair displaying higher assay windows in comparison to the reciprocal

combination. Particularly, low (2.5 and 5 ng/well) SmBiT- β -arrestin2 transfection levels provided excellent assay windows (~9- and 6-fold change, respectively), thus all further arrestin recruitment experiments were performed in cells co-transfected with 100 ng/well of 5-HT_{2A}R-LgBiT and 2.5 ng/well of SmBiT- β -arrestin2 (**Figure 6.3B**).

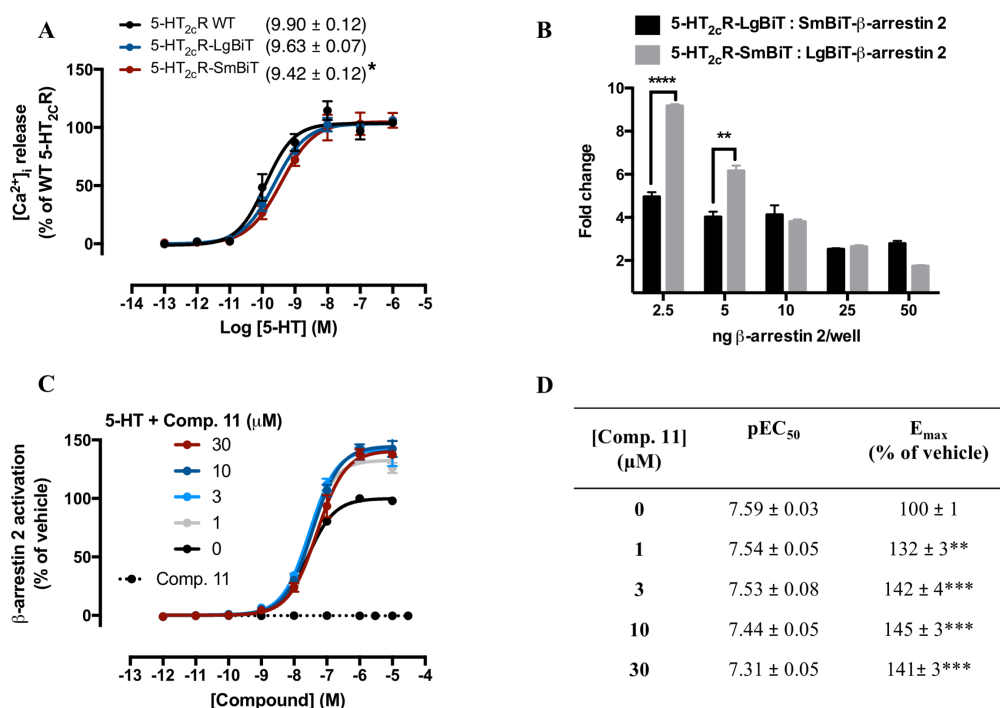


Figure 6.3. *In vitro* characterisation of compound 11-driven β -arrestin2 signalling potentiation. In (A), dose-response intracellular Ca²⁺ release curves for 5-HT_{2c}R constructs. Data are mean \pm SEM percentage of activation normalised to wild type receptors maximal response of three individual experiments each performed in duplicates. Values in brackets represent the mean pEC₅₀ \pm SEM (n=3). Statistical significance was evaluated by one-way analysis of variance (ANOVA) followed by Bonferroni post hoc tests, indicating significant differences over wild type receptors (*p \leq 0.05). In (B), cells were transiently co-transfected with a fixed amount (100 ng/well) of the 5-HT_{2c}R and increasing concentrations (see figure legends) of the complementary β -arrestin2 NanoBiT pair. Data are mean \pm SD (n=2) fold change, calculated as the ratio between agonist (1 μ M 5-HT) and vehicle-treated cells. Statistical significance was evaluated by two-way analysis of variance (ANOVA) followed by Bonferroni post hoc tests showing significant effects between groups (**p \leq 0.01, ***p \leq 0.0001). (C) Summary 5-HT dose-dependent β -arrestin2 recruitment curves in the presence of increasing comp. 11 concentrations. 5-HT potency (pEC₅₀) and maximal efficacy (E_{max}) are summarised in (D). Data are mean pEC₅₀/ E_{max} \pm SD of two individual experiments each performed at least in duplicates. Statistical significance was evaluated by one-way analysis of variance (ANOVA) followed by Bonferroni post hoc tests, indicating significant differences over vehicle-treated (**p \leq 0.01, ***p \leq 0.001).

The efficacy measured after dose-response stimulation with 5-HT was virtually identical to the recently reported by Cheng et al. using Tango β -arrestin-2 recruitment technology (pEC_{50} = 7.66 ± 0.02 vs 7.58 ± 0.03 for Tango and NanoBiT, respectively), validating the suitability of our assay to measure this PPI (**Figures 6.3C,D**). In addition, our assay provides temporal resolution^{278,752}. To assess compound 11 PAM potential of arrestin signalling, 5-HT dose-response curves were performed in the presence of increasing concentrations of the analogue. As shown in **Figures 6.3C,D**, co-administration of compound 11 enhanced 5-HT-driven maximal β -arrestin2 binding by ~50%, almost inducing maximal potentiation at the lowest assayed concentration (1 μ M). In addition, no potentiation was observed in the absence of 5-HT (**Figure 6.3C**), indicating that compound 11 is a pure PAM. When analysing 5-HT potency (EC_{50}), the only difference occurred at the highest tested dose of compound 11 (pEC_{50} = 7.58 ± 0.03 vs. 7.31 ± 0.06 for 30 μ M vs. 0 μ M treatments, respectively; p -value = 0.016), although it is questionable whether this small difference might be functionally relevant. The increase in agonist efficacy, the saturability of its effect and the lack of intrinsic agonist activity strongly supports that compound 11 is a pure positive allosteric modulator of β -arrestin2 signalling downstream 5-HT_{2C}R activation. In addition, this analogue is a neutral PAM, as it does not alter 5-HT's natural bias towards G_{q/11} signalling in 5-HT_{2C}R. Altogether, the *in vitro* profiling of compound 11 and the lack of off-target effects supports its safe *in vivo* evaluation.

6.2.3. *In vivo* evaluation of compound 11

In order to validate the allosteric effect of compound 11 *in vivo*, we evaluated the potentiation serotonin-induced feeding suppression when co-administered with the selective serotonin reuptake inhibitor (SSRI) sertraline. This class of drugs, via the blockage of pre-synaptic serotonin transporters (SERT), increase 5-HT bioavailability in the synapse to activate post-synaptic serotonin receptors. Particularly, 5-HT-mediated activation of 5-HT_{2C}R in POMC/CART (pro-opiomelanocortin/cocaine and amphetamine regulated transcript, respectively) neurons in the arcuate nucleus of the hypothalamus has been shown to play a key role in the serotonergic pathways regulating appetite control^{753,754}. In fact, several SSRI prescribed for the treatment of depression have shown anorectic properties both in animal models and in humans, including Prozac®, fluvoxamine, paroxetine and sertraline^{755,756}. Accordingly, we hypothesised that if compound 11 exerts its effects via allosteric potentiation of 5-HT binding to 5-HT_{2C} receptors, increasing the endogenous 5-HT via the blockage of

serotonin re-uptake in combination with compound 11 would result in enhanced feeding suppression over animals treated exclusively with sertraline.

In agreement with previously published data⁷⁵⁷, administration of sertraline results in a mild suppression of food intake (**Figure S4A**). Thus, different sertraline doses (0.4–10 mg/kg) induced feeding suppression over the different times points after intraperitoneal injection of obese rats ($F(3.112) = 29.1, P < 0.01$). Next, we evaluated whether compound 11 might enhance sertraline effects at the time that evaluating its efficacy per se, without pharmacologically increasing synaptic 5-HT levels. To this end, we assessed two concentrations of compound 11 (0.5 and 2 mg/kg) in combination, or not, with sertraline at 2 and 5 mg/kg (**Figures S4B,C**). In animals treated with both configurations comprising the SSRI and compound 11 (0.5 mg/kg compound 11 plus 2 mg/kg sertraline and 2 mg/kg compound 11 plus 5 mg/kg sertraline, **Figures S4B and C**, respectively), the anorectic effect of sertraline was potentiated (interaction compound 11-sertraline ($F(9.111) = 4.6, P < 0.01$), indicating *in vivo* positive allosteric modulation of the 5-HT_{2c}R. Furthermore, compound 11 was able to reduce food intake when administered alone, with more marked effects at the highest administrated dose, supporting its efficacy under physiological 5-HT levels.

Altogether, this compound displays an active PAM profile in active feeding rat models, reducing food intake and potentiating the anorectic effect of antidepressants when administered subchronically. The latter is particularly interesting as the strong prevalence of depression in obese individuals^{758,759}, suggesting a combined therapeutic regimen in obese patients.

6.2.4. Defining the binding mode of compound 11 by molecular dynamics and site-directed mutagenesis.

The pharmacological characterisation of compound 11 indicates that this analogue is a selective 5-HT_{2c}R PAM capable of exerting anorectic effects via potentiating the efficacy of endogenous 5-HT. To rationalise these results and identify the key motives driving its affinity we sought to combine three-dimensional molecular docking and alanine scanning mutagenesis of the ligand-receptor complexes. Thus, based in the recent 5-HT_{2c}R crystal structure in complex with ergotamine, we built an active-like model of the human 5-HT_{2c}R binding both to the endogenous ligand (5-HT), and compound 11 (VIVIA012). In our model, D134^{3.32} (superscript refers to the Ballesteros-Weinstein nomenclature system)²⁶ forms a salt bridge with the 5-HT protonated primary amine site (**Figure 6.4B**). This is in agreement with the

Serotonin 5-HT_{2C} Receptors Positive Allosteric Modulation in Obesity

canonical interaction between the protonated nitrogen of many biogenic amines forming a salt bridge with the conserved D134^{3,32}. In fact, this was the only common ligand contact observed in the recently released ergotamine- and ritanserin-bound 5-HT_{2C}R crystal structures, agonist and inverse agonists, respectively, at this receptor³⁵². In addition, the hydroxyl substituent in the indole ring hydrogen bonds S219^{5,43}.

As shown in **Figures 6.4A and B**, compound 11 lays above the orthosteric binding pocket forming extensive contacts within the extracellular vestibule embed by the TMs 5 and 6 and the ECL2. The 3-pyridiyl moiety of compound 11 is orientated towards the TM6, stabilised by hydrogen bonding with the side chains of asparagine and serine residues N331^{6,55} and S334^{6,58}. The indole scaffolding ring is perpendicularly positioned with respect to the pyridyl ring inserted deeper into the TM bundle potentially establishing hydrophobic contacts with V208 in the ECL2. The phenyl group appears slightly tilted, orientated towards the TM3 stacked above the serotonin molecule.

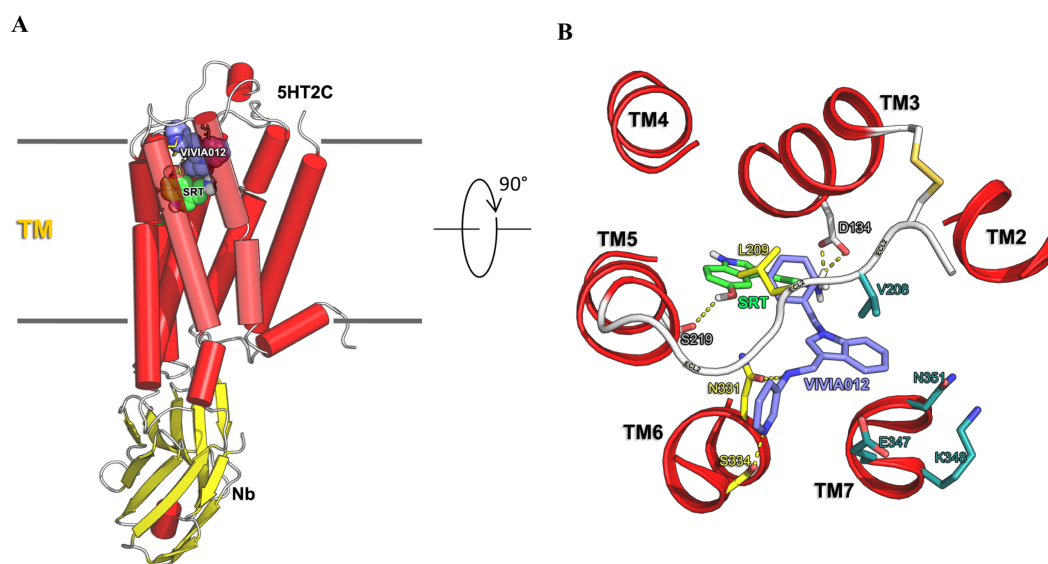


Figure 6.4. Proposed allosteric binding mode of compound 11. Lateral (A) and extracellular view (B) of the binding modes of 5-HT (green sticks) and compound 11 (VIVIA012; blue sticks) in the energy-minimised model of the active 5-HT_{2C}R. Mutate residues are labelled in the top view. The 5-HT_{2C}R (PDB:6BQG) crystal structure was used as template for the 5-HT_{2C}R, incorporating features (G protein mimic nanobody) of the active muscarinic M₂R-Nb9-8 complex (PDB:4MQS) to achieve a fully active conformation.

To validate the binding mode of compound 11 and the contribution of the identified 5-HT_{2C}R residues to the affinity/efficacy of this allosteric modulator we mutated all the amino acids predicted to form the allosteric binding pocket (displayed as sticks in figure **6.4B**). For this purpose, the TM6 residues N331^{6.55}, S334^{6.58} and V206 and L209 in the ECL2 were replaced by alanine. In addition, recent studies on Class A receptors allosteric modulators support putative binding pockets in the extracellular vestibule surrounded by the TM1, TM2 and TM7 helices. After visual inspection of our model, we investigated this option by alanine substitution of the TM7 E347^{7.32}, E348^{7.33} and N351^{7.36} residues.

As previously shown, we used [Ca²⁺]_i calcium release as a measure of 5-HT_{2C}R activation. Precisely, concentration dose-response curves of the endogenous orthosteric 5-HT agonist were performed in the absence or presence of the compound 11 PAM (10 μM). 5-HT potency (EC₅₀) and maximal responses (E_{max}) for WT and all mutant receptor forms are detailed in **Table 6.2**. None of the mutants located close to the extracellular space of TM7 (E347^{7.32}, E348^{7.33} and N351^{7.36}) experienced changes in affinity nor efficacy. In comparison with the WT 5-HT_{2C}R, 5-HT EC₅₀ and E_{max} values remained virtually identical in the presence or absence of compound 11 (**Table 6.2** and **Figures 6.5F-I**). On the basis of these results, the possibility of a potential putative allosteric pocket involving the TM7, TM2 and TM1 helices was excluded according to our initially proposed model.

Next, we explored the hydrogen bonding network between the 3-pyridyl moiety of compound 11 and the TM6 (**Figure 6.4B**). Ala substitution of N331^{6.55} induced a ~10-fold decrease in 5-HT-driven Ca²⁺ potency. Importantly, this effect was more pronounced when co-administrated with compound 11 (**Table 6.2** and **Figure 6.5D**), suggesting an antagonistic effect over the orthosteric binding pocket when non-stabilised by N331^{6.55} hydrogen bonding. In addition, the N331A^{6.55} mutant showed a significant decrease in compound 11-driven allosteric potentiation, indicating the participation of this residue in the binding pocket. Notably, as shown by Peng et al., the impact of Ala substitution on 5-HT potency is not due to changes in ligand affinity, suggesting the contribution of this TM6 position in the overall motion towards an active receptor conformation³⁵². The S334A^{6.58} mutant displayed a similar signalling profile, with reduction in 5-HT potency in the presence of the compound 11 (**Table 6.2** and **Figure 6.5E**). However, we did not detect changes in E_{max}, probably due the compensatory effect of the interaction with N331^{6.55} (**Figure 6.4B**).

In our model, the side chain of L209^{ECL2} points into the extracellular cavity towards the phenyl moiety of compound 11. This residue is conserved in all but the 5-HT₄R serotonin receptors, recently identified as a key determinant of ligand residence time and biased signalling in 5-HT_{2A} (L229^{ECL2}) and 5-HT_{2B} (L209^{ECL2}) receptors²⁹. Accordingly, L209^{ECL2} interacts with the tripeptide moiety of ergotamine (ERG) in the ERG-5-HT_{2C}R crystal structure. In the LSD-

bound 5-HT_{2B}R crystal structure, the ECL2 forms a lid over the LSD binding pocket, where L209^{ECL2} forms hydrophobic contacts with the psychedelic ligand. Removal of the bulky side chain by alanine substitution and molecular dynamics revealed that L209^{ECL2} acts as a latch, decreasing LSD residence time, increasing its on-rate but without affecting its affinity in the equilibrium²⁹. In our system, the L209A^{ECL2} mutant retained WT-like potency in Ca²⁺ release in the presence or absence of compound 11. Intriguingly, we observed a complete loss in allosteric potentiation, suggesting a lid-like mechanism governing the access and egress of the PAM (**Table 6.2** and **figure 6.5C**). In agreement, the neighbouring L208A^{ECL2} mutant had similar effects, with no changes in 5-HT EC₅₀ and a tendency (although not statistically significant) to reduced maximal efficacy (**Table 6.2** and **figure 6.5B**).

Altogether, these results allowed us to validate a pharmacophore model for the binding of the PAM compound 11 to the 5-HT_{2C}R, embedded within the TMs 3, 5, 6 and the ECL2 forming a lid over it. In addition, based on the experimental validation of the involvement of L209 in the ECL2, we propose that compound 11 might be exerting allosteric modulation over 5-HT by controlling the association/dissociation of the orthosteric ligand to its pocket, a recurrent feature observed in muscarinic allosteric modulators^{760,761}.

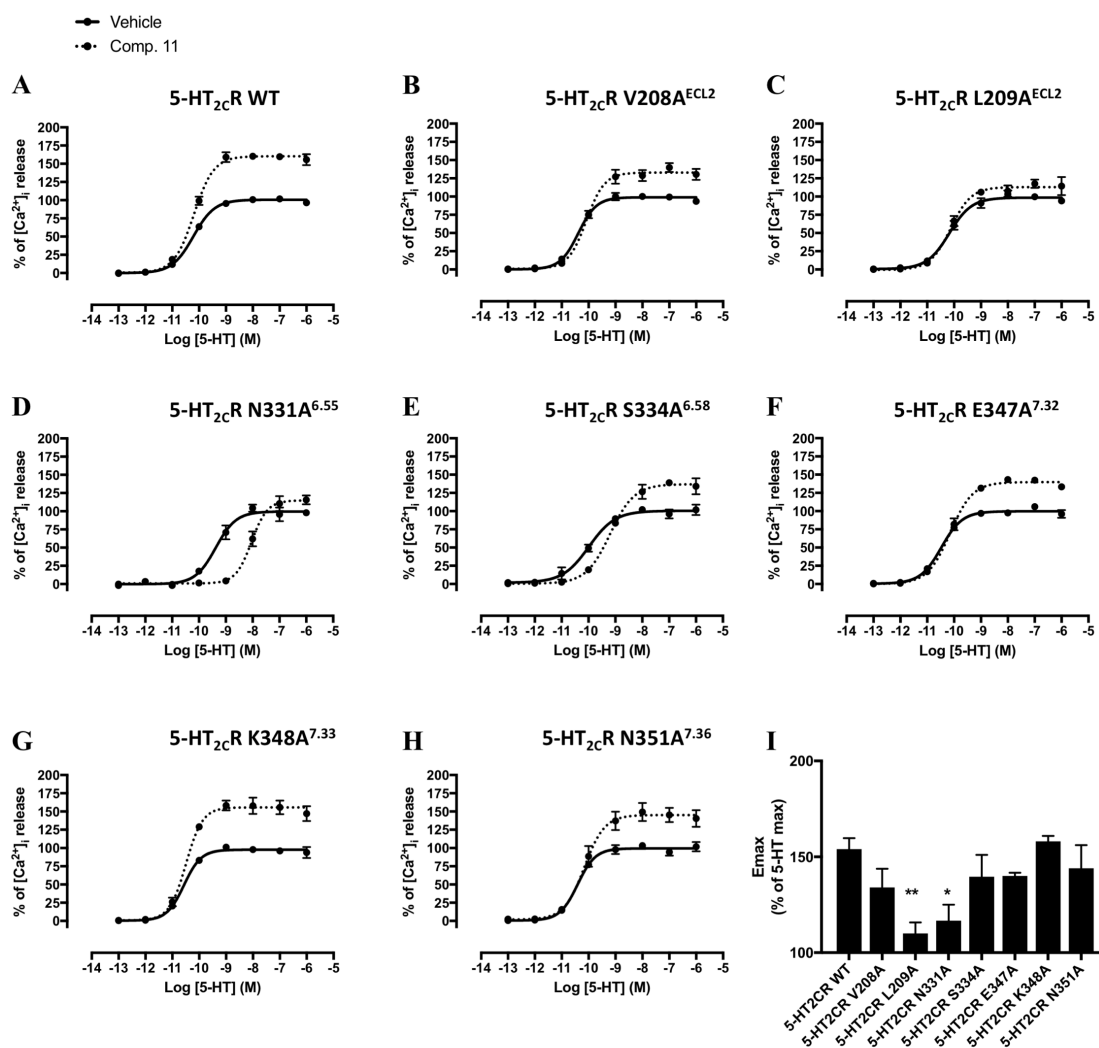


Figure 6.5. Homology modelling and site directed mutagenesis defines the allosteric binding pocket of compound 11. (A-H) Summary 5-HT dose-dependent $[Ca^{2+}]_i$ release curves in HEK293 cells transiently expressing the WT and 5-HT_{2c}R mutants in the presence of 10 μ M comp. 11. Residues replaced by alanine are indicated above each panel. Data are mean \pm SEM percentage of activation normalised to vehicle-treated cells of 3-4 individual experiments each preformed at least in duplicates. (I) Comparison of comp. 11-induced maximal efficacy (E_{max}) over WT and mutant receptors obtained from A. Statistical significance was evaluated by one-way analysis of variance (ANOVA) followed by Bonferroni post hoc tests showing significant effects over WT 5-HT_{2c}R (* $p \leq 0.05$, ** $p \leq 0.01$).

Table 6.2. Compound 11 effect on 5-HT signalling at 5-HT_{2C} WT and mutant receptors.

	pEC ₅₀		E _{max}
	- Comp. 11	+ Comp. 11	+ Comp. 11
5-HT _{2C} R WT	10.22± 0.09	10.13± 0.11	154± 6
5-HT _{2C} R V208A ^{ECL2}	10.38±0.1	10.06± 0.03	134± 10
5-HT _{2C} R L209A ^{ECL2}	10.11± 0.16	10.13± 0.16	110± 6 **
5-HT _{2C} R N331A ^{6.55}	9.32± 0.29****	7.94± 0.26 ***	117± 8 *
5-HT _{2C} R S334A ^{6.58}	10.2± 0.34	9.19± 0.11 ****	140± 11
5-HT _{2C} R E347A ^{7.32}	10.48± 0.06	10.14± 0.16	140± 2
5-HT _{2C} R K348A ^{7.33}	10.54± 0.08	10.25± 0.28	158± 3
5-HT _{2C} R N351A ^{7.36}	10.40± 0.07	10.17± 0.14	144± 12

5-HT-induced Ca²⁺ release in the presence of 10 μM comp. 11. pEC₅₀ and E_{max} represent the mean ± SEM values obtained from **Figures 6 A-H**. Statistical significance was evaluated by one-way analysis of variance (ANOVA) followed by Bonferroni post hoc tests showing significant effects over WT 5-HT_{2C}R (*p ≤0.05, **p ≤0.01, ***p ≤0.001, ****p ≤0.0001).

6.2.5. SAR-based identification of a G protein biased 5-HT_{2C}R PAM

By molecular modelling and site directed mutagenesis we defined a binding mechanism in which hydrogen bonding between Asn and Ser (N331^{6.55} and S334^{6.58}) and the pyrimidine ring of compound 11 is necessary to retain its PAM activity. However, the *N*-benzylic position is further inserted towards the TM bundle without establishing any apparent interaction with it nor with 5-HT (**Figures 6.5A,B**). Accordingly, we sought to explore the flexibility of the large hydrophobic cavity flanked by the TMs 3 and 5 by exploiting the *N*-benzylic position of compound 11. Thus, we synthesised *o*-, *m*- and *p*-biphenyl analogues (comp. WD013, WD014 and WD015, respectively) in order to determine putative large hydrophobic binding pockets or cationic side chains in the allosteric binding site (**Figure 6.6**). Similarly, since nitrobenzyl analogues can provide important SAR information due to its electron withdrawing properties and consequent involvement in non-covalent interactions (hydrogen bond acceptors), we studied the effects of nitrobenzyl substitution (comp. WD020 and WD024) in the 1-position of the indole scaffold (**Figure 6.6**). Furthermore, although the lack of allosteric potentiation after substitution of the benzene ring by cyclopropane in compound 41 suggests the requirement of aromaticity in this position (**Table 6.1**), we sought to validate the need of π bonding by replacing the phenyl group by a cyclohexane derivative (comp. WD027) (**Figure 6.6**).

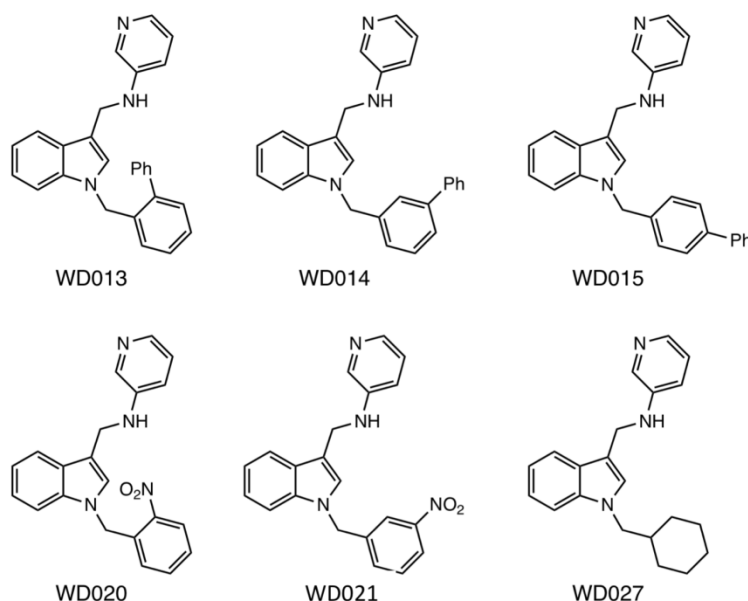


Figure 6.6. Chemical structure of the analogues targeting the 5-HT_{2c}R. In WD derivatives the 3-pyridyl moiety of compound 11 was maintained as *N*-heterocycle and the phenyl ring attached to the indole scaffold was modified.

To evaluate the allosteric potentiation of the new synthesised analogues, we assessed $[Ca^{2+}]_i$ release and β -arrestin2 recruitment in HEK293 cells transiently expressing the 5-HT_{2c}R. In comparison with the initial hit identification experiments (**Table 6.1**), in which IP₁ release was measured in CHO-K1 cells, we opted for this strategy due to the improved sensitivity and assay window under these experimental conditions. To account for differences between assays, we selected the *o*-, *m*- and *p*-fluorophenyl derivatives (comp. 15-17), which displayed low, high and low IP₁ accumulation potentiation, respectively, comp. 30 (no allosteric potentiation) and the reference comp. 11 to be assayed in parallel to the newly synthesised molecules.

Signalling potentiation in $[Ca^{2+}]_i$ and β -arrestin2 signalling was measured after stimulation with a saturating concentration of 5-HT (0.1 and 1 μ M, respectively; see **Figures 6.7B,D**) in the presence of a fixed concentration (10 μ M) of the tested compounds. In agreement with our previous IP₁ accumulation experiments (**Table 6.1**), comps. 15, 17 and 30 displayed low or no Ca^{2+} release potentiation. Similarly, comp. 16-driven potentiation was within the same range as for the comp. 11 PAM, indicating the reproducibility across both downstream signalling readouts (**Figure 6.7A**).

Serotonin 5-HT_{2C} Receptors Positive Allosteric Modulation in Obesity

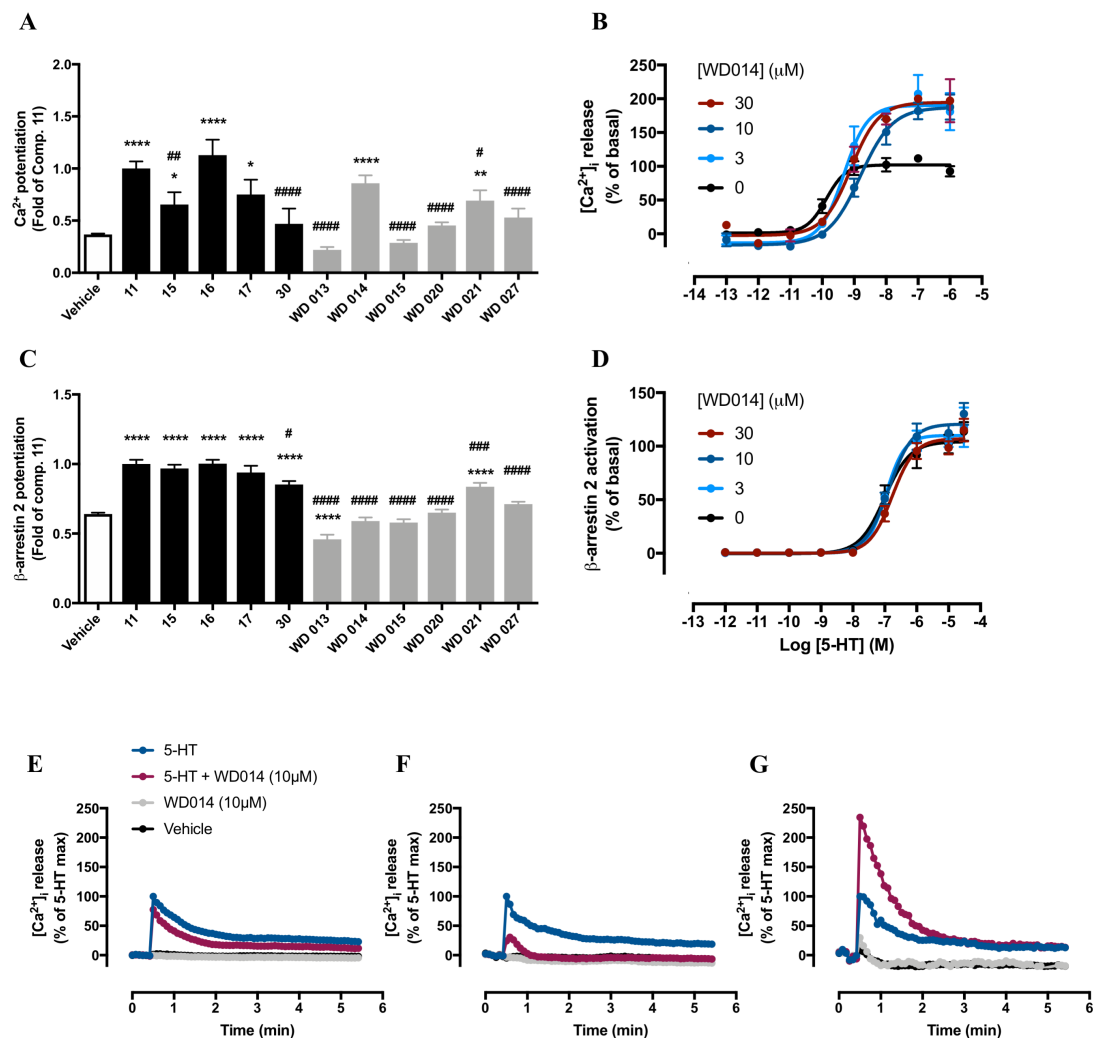


Figure 6.7. Identification and characterisation of compound WD014 as a biased 5-HT_{2C}R PAM. Potentiation of 5-HT-induced [Ca²⁺]_i release (**A**) and β-arrestin2 recruitment (**C**) in HEK293 cells transiently expressing the 5-HT_{2C}R. Cells were pre-incubated with the tested compounds (10 μM for 20 min) prior to stimulation with a saturating concentration 5-HT (100 nM or 1 μM for Ca²⁺ or β-arrestin2 signalling, respectively). Data are mean ± SEM (n ≥ 4) fold change normalised to comp. 11-treated cells. Statistical significance was evaluated by one-way analysis of variance (ANOVA) followed by Bonferroni post hoc tests, indicating significant differences over vehicle-treated cells (*p ≤ 0.05, **p ≤ 0.01, ****p ≤ 0.0001) or comp. 11-treated cells (#p ≤ 0.05, ##p ≤ 0.01, ###p ≤ 0.001, ####p ≤ 0.0001). Summary 5-HT dose-dependent [Ca²⁺]_i release (**B**) and β-arrestin2 recruitment (**D**) curves in the presence of increasing comp. 11 concentrations. Data are mean ± SD percentage of activation normalised to vehicle cells from two individual experiments each performed at least in duplicates. Evaluation of potential intrinsic agonist activity (grey lines) and allosteric potentiation (blue lines) in HEK293 cells transiently expressing the 5-HT_{2A} (**E**), 5-HT_{2B} (**F**) and 5-HT_{2C} (**G**) receptors. Data are mean ± SEM (n ≥ 4) percentage of activation normalised to vehicle-treated cells.

Surprisingly, compound 30 (exhibiting no potentiation over vehicle treated cells in Ca^{2+} signalling) significantly enhanced 5-HT-mediated β -arrestin2 binding to the 5-HT_{2C}R (**Figure 6.7B**). Similarly, comps. 15 and 17 induced similar levels of β -arrestin2 recruitment as the reference comp. 11, although significantly lower when analysing calcium releases, indicating higher efficacy in eliciting arrestin signalling. Furthermore, the lack of homogeneity across signalling pathways suggest that compound 30 might be a β -arrestin biased 5-HT_{2C}R PAM.

Next, we evaluated the newly synthesised biphenyl analogues (WD013-015). Ortho- and para-substitution (WD013 and WD015, respectively) did not yield compounds with enhanced Ca^{2+} nor β -arrestin2 potentiation (**Figure 6.7A-B**). In fact, arrestin recruitment after WD013 pre-treatment was significantly lower than in vehicle-treated cells, suggesting an antagonistic interaction. Interestingly, WD014 enhanced 5-HT-dependent $[\text{Ca}^{2+}]_i$ accumulation to the same extend as comp. 11 in a β -arrestin2-independent manner (**Figures 6.7A,B**), strongly suggesting its G protein-biased nature. For the nitrobenzyl analogues, WD020 had no effect in any of the analysed effector pathways and WD021 potentiated both Ca^{2+} and β -arrestin2 signalling, although to a lesser extend in comparison with comp. 11 and/or WD014 (**Figure 6.7A,B**). Moreover, supporting our original hypothesis of a pharmacophore model in which our 5-HT_{2C}R PAMs require electron-rich π system rings in the 1-position of the indole scaffold, substitution of the benzene ring by cyclopropane (SW027) had no effects in Ca^{2+} nor β -arrestin2 activity (**Figure 6.7A,B**).

Considering that WD014 displayed similar Ca^{2+} potentiation as compound 11 without altering β -arrestin2 signalling, we sought to confirm both its allosteric and biased mechanism of action. As it can be appreciated in **Figure 8.8C** and **Table 8.3**, all the assayed WD014 concentrations potentiated 5-HT_{2C}R-dependent $[\text{Ca}^{2+}]_i$ release in a finite manner, indicating (a) its allosteric action and (b) suggesting improved affinity and/or efficacy in comparison with comp. 11. It should be noted that this *m*-biphenyl derivative induced a slight but significant rightward shift on 5-HT potency (**Figure 8.8C** and **Table 8.3**), potentially due to steric hindrance of the orthosteric binding pocket as a result of the extended pose of the biphenyl ring above 5-HT (see **Figure 8.5**). Interestingly, when analysing β -arrestin2 signalling, none of the WD014 tested concentrations altered 5-HT potency nor efficacy (**Fig. 8.8C** and **Table 8.3**), thereby confirming WD014 G protein-biased positive allosteric modulation. Remarkably, to the best of our knowledge, this is the first report describing a biased 5-HT_{2C}R PAM. Finally, we explored potential WD014 off-target effects by analysing 5-HT₂ receptors (5-HT_{2A}R, 5-HT_{2B}R and 5-HT_{2C}R) subtype selectivity. Importantly, WD014 had no intrinsic agonistic effect (ago-PAM) in any of these receptors (**Figure 8.8E-G**). For the 5-HT_{2A}R, pre-incubation of cells with a saturating (10 μM) concentration of this analogue

Serotonin 5-HT_{2C} Receptors Positive Allosteric Modulation in Obesity

had a small inhibitory effect on serotonin-induced calcium release (**Figure 8.8E**). This effect was more pronounced for the 5-HT_{2B}R, with an almost complete blockage of agonist-induced [Ca²⁺]_i release (**Figure 8.8F**). Despite this antagonistic activity on 5-HT_{2A} and 5-HT_{2B} receptors, its selective potentiation of 5-HT_{2C}R signalling might limit potential off-target hallucinogenic effects. In addition, the lack of agonistic activity on 5-HT_{2B} receptors is a good predictor to assure no cardiopulmonary side effects^{29,352,740}. Furthermore, it should be noted the high concentration of WD014 assayed, thus, whether lower doses of this molecule retain its selective 5-HT_{2C}R positive allosteric modulation without altering 5-HT_{2A} and 5-HT_{2B} receptors signalling remains to be addressed.

Overall, a second round of SAR based on the validated binding mechanism of comp. 11 lead us to design a small series of derivatives around its phenyl group. For the first time, we provide evidence of a 5-HT_{2C}R PAM biased towards G_{q/11}-dependent downstream signalling. WD014 provides a promising tool to dissociate between G protein and β -arrestin2 effectors in order to delineate the contribution of each other in the control of 5-HT_{2C} receptors activity in relation to obesity.

Table 6.3. WD014 effects on 5-HT-induced potentiation in Ca²⁺ and β -arrestin2 signalling at 5-HT_{2C} receptors.

[WD014] (μ M)	[Ca ²⁺] _i		β -arrestin2	
	pEC ₅₀	E _{max}	pEC ₅₀	E _{max}
0	9.9 \pm 0.11	100 \pm 4	7.0 \pm 0.1	100 \pm 5
3	9.3 \pm 0.13*	187 \pm 11**	7.1 \pm 0.06	106 \pm 2
10	8.8 \pm 0.12**	184 \pm 10**	6.9 \pm 0.08	116 \pm 5
30	9.1 \pm 0.13**	192 \pm 12**	6.8 \pm 0.08	103 \pm 4

5-HT-induced Ca²⁺ release and β -arrestin2 signalling in the presence of increasing concentrations of WD014. pEC₅₀ and E_{max} represent the mean \pm SD values obtained from **Figures 8.8 C and D**. Statistical significance was evaluated by one-way analysis of variance (ANOVA) followed by Bonferroni post hoc tests showing significant effects over vehicle-treated cells (*p \leq 0.05, **p \leq 0.01).

6.3. Discussion

An initial screening of ~1600 compounds followed by activity-based chemical modification led to the development of compound 11 (*N*-[(1-benzyl-1*H*-indol-3-yl)methyl]pyridin-3-amine), which behaves as a selective 5-HT_{2C}R PAM *in vitro*. Furthermore, in active feeding rat models, administration of this compound had anorectic properties, suggesting its efficacy under endogenous 5-HT levels. In addition, compound 11-mediated potentiation of the reduction in food intake when co-administered with the SSRI sertraline further supports (a) its *in vivo* PAM effect and (b) the potential of developing 5-HT_{2C}R PAMs as anti-obesity drugs. In view of the above, we set ourselves to delineate compound's 11 allosteric pocket. By molecular modelling and site-directed mutagenesis we defined a pharmacophore model in which comp. 11 binds to the 5-HT_{2C}R extracellular vestibule underneath a lid-like structure formed by the ECL2. The 3-pyridyl group interact with residues in the TM6, whereas the indole scaffold and phenyl ring appear to have more conformational freedom, being orientated deeper towards the orthosteric site between the TMs 3 and 5. We further explored this large hydrophobic pocket by synthesising a new series of compound 11 derivatives, leading to the identification of WD014 (*N*-((1-([1,1'-biphenyl]-3-ylmethyl)-1*H*-indol-3-yl)methyl)pyridin-3-amine) which, to the best of our knowledge, is the first reported G protein biased 5-HT_{2C}R PAM.

The rationale behind modulating the serotonergic system, and particularly the 5-HT_{2C}R, to develop anti-obesity therapies is not new, as neither is the potential fatality associated with off-targeting close related 5-HT₂ receptor subtypes^{740,762}. Examples include the striking withdrawal of the anti-obesity drug fenfluramine and the antiparkinsonians pergolide and cabergoline due to valvular heart disease associated with the activation of the 5-HT_{2B}R^{740,763,764}. To date, lorcaserin is the only FDA-approved selective 5-HT_{2C}R agonist for the treatment of obesity (~20 and ~100-fold selectivity over 5-HT_{2A} and 5-HT_{2B} receptors, respectively). Despite it is classified as a safe drug in terms of valvulopathy, a closer look at the FDA Lorcaserin Medical Review⁷³⁷ rises reasonable concerns about its safety, particularly the significant increased incidence of moderate or greater mitral regurgitation at week 52 and the association between lorcaserin and depression, a condition already prevalent by ~19% in severe obese patients^{758,765}. Our *in vitro* profiling of compound 11 revealed no effect at 5-HT_{2A} and 5-HT_{2B} sites even under the relatively high assayed concentration (10 μM). The former might provide an important advantage over lorcaserin as, despite its relative selectivity and high affinity towards 5-HT_{2C} receptors, it still retains sub-micromolar agonist activity at 5-HT_{2A} and 5-HT_{2B} receptors (K_i= 15 ±1, 112 ±7 and 174 ±32 nM for the human 5-HT_{2C}R, 5-HT_{2A}R and 5-HT_{2B}R, respectively)⁷⁶⁶. In fact, major neuropsychiatric disturbances have

Serotonin 5-HT_{2C} Receptors Positive Allosteric Modulation in Obesity

been reported in subjects exceeding the recommended lorcaserin dose (>20 mg/day), including euphoria, hallucinations and suicidal ideation⁷⁶⁷. In addition, unlike classic orthosteric agonists, PAMs are less likely to induce receptor desensitisation as a result of constant over-exposure to agonists and retain the physiological spatiotemporal resolution of the endogenous ligands^{768,769}.

Another important opportunity arising from our study is the possibility of a combinatory therapy to reduce the feeding behaviour in depressed patients⁷⁵⁹. Our *in vivo* results support the idea that in a context where 5-HT levels are increased via SSRIs, administration of a 5-HT_{2C}R PAM potentiates its anorectic effects. Therefore, activation of hypothalamic (ARC nucleolus) and mesolimbic (VTA) 5-HT_{2C} receptors might act synergistically to reduce food intake. Importantly, increasing evidence supports the inhibitory effect of activating 5-HT_{2C} receptors over the mesoaccumbens dopamine system, providing a full set of opportunities in the treatment of drug addiction^{733–735,746}.

A few limitations of our study should be noted. Although compound 11 appeared after activity-base optimisation of compound 5, we did not fully explore the SAR around the indole scaffold. The same applies for the second series of derivatives (WD compounds) at 1-position of the indole ring. Docking and virtual screening strategies have proven successful in identifying high affinity and/or selective orthosteric ligands^{770,771}. However, allosteric pockets are less defined and their highly solvent exposed surface often undergoes a substantial reduction in volume upon receptor activation⁷⁵⁰. In addition, although recent high-resolution crystal structures in complex with allosteric modulators have provided crucial information, they also emphasise the topographical heterogeneity of allosteric sites^{750,772–776}. Thus, a common limitation in the search for allosteric modulators is the difficulty to find surfaces with the psychochemical properties capable of leading structure-informed design of new molecules, which is often results in low efficacy compounds¹⁴⁰. However, recent structure-guided drug discovery attempts have successfully allowed the identification of selective and potent GPCR allosteric modulators, being particularly interesting its fruitfully implementation in orphan GPCRs^{749,777}. Therefore, taking into account that our results allowed us to identify and validate a putative 5-HT_{2C}R allosteric pocket, screening a larger chemical library against this surface and subsequent docking-based refinement is an exciting direction to pursue.

As observed in the 5-HT_{2B}-ERG complex, ERG adopts a shallower binding pose in the 5-HT_{2C}R reassembling a bitopic ligand (namely a molecule interacting with both the allosteric and orthosteric pockets)¹⁴⁰. Thus, whereas the ergoline ring is deeper inserted into the TM within the TMs 3, 5 and 6, the tripeptide and benzyl groups extend toward the extracellular vestibule where it tolerates a high degree of flexibility. In this cavity, the tripeptide and benzyl substituents establish van der Waals contacts with residues in the TMs 5, 6 and 7 as well as a

hydrogen bond with the backbone of L209^{ECL352}. This pocket is compatible with our proposed putative allosteric pocket and the binding mechanism of compound 11. To validate this model, we mutated several of the residues involved, showing a reduction in allosteric potentiation after L209A^{ECL2} and N331A^{6.55} substitutions. Furthermore, the fact that increasing the size (WD014) and electronic density (WD021) at 1-position of the indole scaffold yielded two 5-HT_{2C}R PAMs strongly supports an extended allosteric pocket involving the extracellular vestibule of the TMs 3 and 5.

Leu/Val/Ile residues in homologous positions as the L209^{ECL2} in the 5-HT_{2C}R are conserved in all receptors displaying high affinity ERG binding. Furthermore, it has been shown that this position deeply impacts the residence time of LSD via the formation of an ECL2 lid-like structure over it, a feature on which β -arrestin recruitment to 5-HT_{2A} and 5-HT_{2B} receptors depends²⁹. Accordingly, although speculative, a possible mechanism whereby compound 11 increases 5-HT signalling might be by decreasing 5-HT off-rate by means of stabilising this ECL2 lid-like structure. Alternatively, another mechanism through which comp. 11 might potentiate 5-HT mediated [Ca²⁺]_i release is enhancing sustained G_{q/11} signalling from endosomal compartments.

Unlike in compound 11 studies, where selectivity was assessed across a broad panel of GPCRs and kinases, WD014 off-target effects were only assayed for the closely related 5-HT_{2A} and 5-HT_{2B} receptor subtypes. Thus, to ensure an unbiased interpretation of its activity *in vivo*, we must first assay this compound against side-effect target panels. It should be also pointed out WD014 significant inhibitory effect on 5-HT_{2B}R function. However, even within the lowest assayed concentration (3 μ M), WD014 induced maximal potentiation. Hence, titrating lower concentrations might still retain its PAM activity whilst reducing side off-targeting.

Surprisingly, whilst WD014 induced a robust potentiation in Ca²⁺ release, this effect was absent when assessing β -arrestin 2 signalling. In other words, WD014 is a G protein biased PAM. However, although functional selectivity has been extensively studied in the close related 5-HT_{2A} and 5-HT_{2B} receptors, little is known about biased agonism at the 5-HT_{2C} receptor. The combination of allosterism and bias under the same molecule provides an exciting opportunity to develop safer drugs. For instance, the selective engagement of some signalling pathways at the expense of others via biased mGlu5R PAMs is showing promising pre-clinical results for the treatment of schizophrenia^{741,778,779}.

In summary, our results support the hypothesis that allosteric modulation of GPCRs, and especially those whose high homology within subtypes often leads to intra-family off-target effects, can be successfully applied to target receptors otherwise elusive with conventional orthosteric ligands. Our results defined a putative 5-HT_{2C}R allosteric pocket, which, together

with recent high-resolution structural information and the provided chemical scaffolds, might guide future structure-based screenings to identify potent and selective 5-HT_{2C}R PAMs. Finally, the effectivity of compound 11 in pre-clinical obesity models provides an exciting alternative strategy to tackle this pandemic disorder.

6.1. Acknowledgements

We thank María L. López-Rodríguez and Lesley Howell labs for synthesis of compounds 5-41 and WD, respectively, and Fernando Rodríguez Fonseca's lab for *in vivo* experiments. MD were performed in collaboration with Leonardo Pardo's lab.

Chapter 7

General discussion

7.1. BiLC-based assays to study GPCR interactions

Understanding the basis governing allosteric homo/hetero-receptor interactions requires the development of suitable tools to delineate the contribution of each of the individual components in the overall system responses. Our first objective was to implement a technology flexible enough to readily answer whether GPCRs interact between them whilst could be multiplexed to monitor the direct recruitment of downstream effectors (G proteins and arrestins) (**Figure 7.1**). We thus chose the recently developed NanoBiT assay, which, as discussed in detail in Chapter I, provides a PCA more in tune with GPCR dynamics^{266,278}.

For the first time, we reported the potential of NanoBiT for the detection of GPCR homo- (CB₁R and 5-HT_{2A}) and heterodimers (5-HT_{2A}R-CB₁R). The specificity and reversibility of the detected interactions (two properties often absent in other PCAs) were validated via titrating unlabelled receptors and using TM disrupting peptides. Furthermore, comparative studies against Venus YFP BiFC, the “gold standard” PCA for GPCR dimers, showed that our assay displays a superior dynamic range (10-125-fold increase in assay window) whilst reducing by half the hands-on time (Venus YFP BiFC was only detected 48 hours post-transfection). The same strategy was applied to monitor receptor-arrestin interactions, obtaining results in line with those reported in the literature^{29,557,576}. The temporal overlap between the formation of the arrestin-receptor complexes and the luminescent output, together with furimazine’s improved stability, allow to follow up in real-time and over longer time periods these transient complexes²⁶¹. This is particularly important as recently illustrated by the influence of the kinetic context in apparent biased agonism¹²¹. Therefore, the simplicity, sensitivity and minimum hands-on time (24 hours assay format and easy data processing) provides an excellent complementary/alternative approach to monitor GPCR PPIs.

Next, we sought to develop a NanoBiT-based G protein activation assay for G α_{i1} , G α_{i3} and G α_q . Although this strategy allowed us to distinguish the receptors’ preference towards its canonical G proteins, neither G α constructs in which SmBiT was fused to its N-terminus (for SmBiT-G α_{i1} , SmBiT-G α_{i3} and SmBiT-G α_q) nor internally (for SmBiT₁₂₄-G α_q) allowed us to detect changes after agonist stimulation. Using an alternative approach, Laschet et al. recently illustrated the suitability of NanoLuc binary technology to detect GPCR-G protein complexes in living cells⁷⁸⁰. On the contrary of our strategy, SmBiT was fused to the receptor C-tail and LgBiT was introduced in the loop connecting the helices α B and α C. In addition, using the natural peptide (NP) as an alternative for SmBiT, allowed the detection transient complexes with improved signal-to-noise ratios. Although we originally hypothesised that the intrinsic low affinity between SmBiT and LgBiT would minimize potential perturbations introduced by the complementary pairs, these result stress the importance of the affinity between the interacting partners⁷⁸⁰. Alternatively, recently unpublished studies took advantage of mini-G

General discussion

proteins to quantify agonist-promoted G protein recruitment. These chimeric G proteins consist of only the GTPase domain of the $G\alpha$ subunit⁷⁸¹. Similar to our approach, this strategy combines LgBiT in the receptor C-terminus and SmBiT in the mini-G protein N-terminus. Against this background, we are currently assessing the above-mentioned mini-G proteins.

An important caveat to add is the lack of spatial resolution of NanoBiT's applications described above. GPCR signalling is not only confined to the plasma membrane and increasing evidence illustrate sustained activation across endocytic compartments^{113,117,782}. NanoBiT's quantum yield make it compatible with bioluminescence imaging, although with limited resolution at the subcellular level²⁷⁸. Alternatively, as discussed below (see section 7.5), whether NanoLuc spectral properties can be exploited in RET systems to improve its resolution is currently assessed.

“Stapling” peptides harbouring cell penetrating sequences offers unique alternatives to retain α -helical structures, overcome proteasomal degradation, increase bioavailability and cross the blood-brain barrier^{590,783–785}. Although several studies describe the use of GPCR TM-mimicking peptides, to the best of our knowledge, this is the first time that combining both features for such purpose has been reported. Importantly, we provided extensive data of its stability *in vitro*, a common limiting factor of peptide therapeutics often overlooked when studying GPCR dimerisation. We identified the s5-TAT peptide as a promising candidate with improved efficacy over its parental full length TM5-TAT peptide. s5-TAT displayed enhanced proteolytic resistance with a remarkably high half-life in serum when compared to TM5-TAT ($t_{1/2}$ > 16 hours vs. ~ 30 min, respectively). It should be noted that none of the studies on GPCR TM disrupting peptides for CNS-related disorders explored an administration route other than intraventricular, with most behavioural test performed after acute treatments^{184,644}. This is both because of plasmatic instability and low BBB permeability. Our data suggests that improving stability (hydrocarbon stapling) and permeability (incorporation of cell penetrating sequences) might allow chronic treatments through alternative administration routes. Together, s5-TAT is a promising candidate to test 5-HT_{2A}R-CB₁R heteromers disruption *in vivo*.

7.2. Allosteric modulation in GPCR dimers: from molecular basis towards disease targeting

In Chapter 3, we tailored an assay in order to obtain adequate tools to be applied across this thesis. Specially, to answer a central question in the field of GPCR oligomers: the molecular determinants and the mechanism driving heteromerisation. In Chapter 4, we undertook this challenge focusing on 5-HT_{2A}R-CB₁R heteromers. Thus, understanding the alternative signalling events arisen from the formation of these complexes, their stoichiometry and

architecture are the necessary first steps towards taking advantage of the promising opportunities arising from the pharmacological manipulation of this and other hetero-receptor complexes (**Figure 7.1**).

We hypothesised that controlling the state (activation and/or effector coupling) of the “building blocks” of these multiprotein complexes would allow us to disaggregate the number and contribution of each of its elements. At the single receptor level, our extensive mutagenesis characterisation indicates different molecular determinants driving activation across both class A receptors. Next, taking advantage of the recently developed 2PMM^{533,534}, we assessed whether heteromerisation-driven 5-HT_{2A}R G_{i/o} signalling was due to trans-activation or G protein class switch. This strategy not only allowed us to quantitatively assess direct receptor:G_{i/o} binding, but to visualise it. Our results clearly support an heteromer-dependent G_{i/o} coupling to 5-HT_{2A}R, arguing against receptor trans-activation. In addition, 2PPM experiments suggested that this alternative G_{i/o} signalling might be dependent on a fully functional CB₁R interacting protomer, which was later confirmed by Ca²⁺ and cAMP release experiments in the presence of non-functional 5-HT_{2A}R and CB₁R mutants. Our data not only argues against trans-activation in either direction but stresses the necessity of two functional protomers each capable of recruiting G proteins so that class switch can occur, raising the possibility of higher order oligomeric structures. This is further supported by the recurrent observation of tetrameric arrangements in hetero-receptor complexes where a G protein class switch occurs^{316,317,637}.

Next, we explored whether the same mechanism might be consistent across signalling pathways. Surprisingly, as reported in other GPCR oligomers, heteromerisation restored ERK1/2 signalling function^{195,335}. Intriguingly, cross-talk was not homogeneous across signalling pathways. This suggests that, upon ligand binding, different structural rearrangements drive cAMP and p-ERK1/2 signalling. These results somewhat challenge the classical view of cross-talk in GPCR dimers, considered to be bidirectional and reciprocal. However, this is more in line with the current view of receptors existing as ensembles of conformations allowing biased agonism.^{136,137,786}

As previously discussed (see Chapter 4), a mechanism involving two fully functional protomers capable of recruiting G proteins would imply a quaternary structure other than heterodimers. For the first time, we multiplexed NanoBiT with BRET (termed NanoBiLC BRET) to detect constitutive higher oligomeric states, which, together with the data confirming the presence of homodimers of each species and the disruption of the heteromeric complexes with TM peptides, support the presence of constitutive 5-HT_{2A}R-CB₁R heterotetramers. It is noteworthy that our NanoBiLC BRET assay reflects heteromers in whole cellular populations. However, it is increasingly accepted that the formation of these

General discussion

complexes is dynamic and involves transitions between monomeric, dimeric and oligomeric forms^{286,787}. In addition, ligand binding to certain receptors has shown to alter this monomer-oligomer equilibrium^{788,789}. Furthermore, recent advances in single-molecule microscopy allow lifetime quantification of each species^{186,790}. Thus, similar studies are needed in order to determine the dynamics of 5-HT_{2A}R-CB₁R heteromers and the influence of ligands.

In order to rationalise the intriguing behaviour of 5-HT_{2A}-CB₁ oligomers, we explored whether four receptors and two G proteins could be accommodated. Thus, based on our experimental observations, we build a computational model assuming TM4/5 (homomeric) and TM5/6 (heteromeric) interfaces and two heterotrimeric G_i proteins in the GDP-bound closed conformations. Our molecular dynamics simulations clearly show a compact and stable heterotetramer that tolerates two bound G_i proteins, although only one G protein can be activated at each time. The fact that when blocking CB₁R G protein coupling hinders 5-HT_{2A}R G protein class switch, but not in the other way around, might suggest contacts between both G_i proteins. However, their distance is too large when only one is in its active open conformation. Alternatively, we observed that in the G_i-bound state, the CB₁R homomer exposes negatively charged residues (ICL3 and C-term Ser/Thr) towards the 5-HT_{2A}R-G_i bound, which is more electropositive than the 5-HT_{2A}R-G_q bound face. Expanding the lock (signalling pathway) and key (receptor) analogy for GPCR-G-protein selectivity to dimers⁴⁵, the CB₁-G_i bound receptor constitutes a new key that facilitates to unlock 5-HT_{2A}R's ability to bind G_i proteins, thus acting at the same time as an allosteric modulator and a facilitatory scaffold.

On the basis of the aforementioned model, we proposed a global mechanism driving cross-talk in 5-HT_{2A}R-CB₁R heteromers that reconciles our experimental observations and that might be applied to other heteromeric pairs where similar observations have been reported. For example, in the case of the 5-HT_{2A}R-mGluR2 and 5-HT_{2A}-D_{2L}R heterodimers (both consisting of G_q and G_i coupled receptors), simultaneous stimulation of the mGluR2/D_{2L}R protomers with hallucinogenic 5-HT_{2A}R agonists (LSD and/or DOI) has shown to shift the signalling signature of 5-HT_{2A}-D_{2L}R towards G_i-dependent pathways^{312,314} and, in the case of 5-HT_{2A}R-mGluR2 heteromers, to enhance 5-HT_{2A}R-mediated G_q signalling^{316,317}.

Despite the existence of GPCR homo/hetero-oligomeric species has become increasingly accepted, just few studies, including our proposed model driving crosstalk in 5-HT_{2A}R-CB₁R heteromers, have approached this matter at the mechanistic level. Even less frequent are the investigations attesting their physiological relevance, with only a handful of Class A GPCR heteromers having shown their relevance *in vivo*¹⁸⁸. “True” GPCR heteromers must display singular fingerprints^{187,791}. Analogously as in biased agonism, through which receptors are directed towards specific downstream pathways, allosterism within protomers can be

exploited to potentiate/inhibit certain effectors activity. Accordingly, in Chapter 5, we explored allosteric communication between GPCRs in relation to disease (**Figure 7.1**).

The D₁ and H₃ hetero-receptor complexes provide an excellent example of how taking advantage of these “new signatures” arising from oligomerisation might allow to bypass the detrimental effects associated to the scattered anatomical distribution of a therapeutic target (in this case, heterogeneous D₁R expression across the brain and PNS). Thus, we hypothesised that targeting D₁R through its association with H₃R might unveil a new target against Huntington’s disease (HD) due to: (i) the overlapping expression of both receptors in striatonigral MSSNs, (ii) over activation of these D₁R-expressing neurons as a pathological hallmark in HD, (iii) H₃R expression being restricted to histaminergic neurons and (iv) the antagonistic effects of H₃R ligands over D₁R activity^{345,523,673}.

First, using WT STHdH^{Q7} and mutant knock-in HD STHdH^{Q111} cells, we have shown that D₁ and H₃ receptors form functional heteromers where H₃R agonists (negative cross-talk) and antagonist (cross-antagonism) have an inhibitory effect over D₁R signalling. Importantly, the control of the H₃R over D₁R activity has been reported in different neuronal-derived cell lines and organotypic striatal slice, suggesting a general mechanism through which D₁R-H₃R heteromers control neuronal activity^{345,523}. Using a similar strategy as in Chapters 3 and 4, we confirmed that the negative cross-talk and cross-antagonism were due to a direct PPI. Accordingly, a D₁R TM5-mimicking peptide, but not a TM7-mimicking peptide, abrogated the unique biochemical properties of D₁R-H₃R heteromers. These results not only validated the presence of functional complexes in this HD striatal cell model, but also, based on their architecture, allowed us to propose a mechanism that might explain the functional consequences arising from allostery within protomers interacting through TMs 5 and 6 (further detailed in Chapter 5). In fact, negative cross-talk appears to be recurrent in heteromers involving TM5/6 interfaces, which might be explained by a steric clash in the attempt of simultaneous TM6 movement in both protomers^{184,293,675}.

Next, we explored D₁R-H₃R heteromers regulatory effect over D₁R-mediated cell death. In agreement with our hypothesis, regardless of the agonistic or antagonistic nature of the H₃R ligands, stimulation/inhibition of this protomer reverted D₁-overstimulation induced cell death. Furthermore, as clearly illustrated when applying TM-disrupting peptides, this is a heteromer-dependent signature, therefore presenting a provocative target to be explored in Huntington’s disease. Much in the same way as the NMDAR blocks agonist-induced D₁R internalisation, we hypothesised that the H₃R might revert D₁R overstimulation-mediated cell death via a similar mechanism. Accordingly, the H₃R antagonist Thioperamide blocked SKF 81297-induced D₁R internalization, as indicated by its cytosolic confinement by immunofluorescence and the loss of PLA staining in HD cells. These results are consistent

General discussion

with well-reported examples of GPCR oligomerisation-dependent alterations in receptor trafficking (e.g. GLP1R-GIPR, GLP1R-GCGR and CXCR4-CXCR7 heteromers)^{336,678}. Therefore, the antagonist-bound H₃R might act as a “membrane trap” preventing D₁R internalisation and downstream signalling, contributing to revert the cytotoxic effects upon aberrant D₁R over-activation.

In view of the above, we explored whether this hetero-receptor complexes might be indeed a therapeutic target for HD by taking advantage of an extensively characterised murine pre-clinical model of HD: heterozygous mutant knock-in (KI) Hdh^{Q7/Q111} and wild type Hdh^{Q7/Q7} HD mice⁶⁸⁸. Surprisingly, we observed a near disappearance of the complexes in 8-months old HD Hdh^{Q7/Q111} mice.. Thus, provided this timeframe for therapeutic intervention and cumulative evidence of H₃R attenuation of D₁R function, we explored whether chronic Thioperamide administration might prevent HD-associated motor and cognitive dysfunction. To this end, we performed a battery of behavioural tests assessing the acquisition of new motor skills (ARTP), recognition long-term memory (NORT) and spatial long-term memory (T-SAT). Remarkably, chronic Thioperamide administration from 5 months of age restored all motor and cognitive deficits, without significant differences between saline-treated Hdh^{Q7/Q7} and Thioperamide-treated Hdh^{Q7/Q111} mice. In addition, heteromer expression was restored in 8-months old Hdh^{Q7/Q111} mice, unambiguously legitimating this new heteromeric target in HD.

Overall, in Chapter 5, we provided compelling evidence of GPCR oligomerisation *in vivo* and how, through taking advantage of the allosteric opportunities arising from it, new drugable entities emerge. Therefore, cross-antagonism from H₃R ligands towards the D₁R act as a “molecular brake” that can be effectively used to dampen aberrant striatonigral D₁R over activation leading to cell death, motor and cognitive deficits in Huntington’s disease.

7.3. 5-HT_{2c}R PAMs provide a novel target for obesity

Whilst in the Chapters 3 to 5 we explored GPCR allosterism from the perspective of their interaction with other proteins, that is both the allosteric “modulator” and the “conduit” were GPCRs, in the Chapter 6 we explored allosterism within 7TM through a more classical concept already represented in the pharmacopoeia: small molecule allosteric modulators of GPCRs⁶. Targeting unique allosteric pockets with small drugs holds promise for developing safer compounds capable of circumventing the high degree of homology within orthosteric sites (**Figure 7.1**). However, the identification of these “hot spots” and the paths used in this way of long-distance communication continue to be challenging. Accordingly, we sought to

identify allosteric 5-HT_{2C}R pockets and to develop selective PAMs with the objective of overcoming selectivity-related issues associated with classical anti-obesity drugs^{738,740}.

Starting from a proprietary library of ~1600 we identified compound 5 (VA240), which selectively enhanced 5-HT efficacy (~20%) at 5-HT_{2C} receptors. Based on its chemical structure, a first round of analogues was generated around its pyrimidine ring (compounds 6-14). Interestingly, improvements (enhanced efficacy) were only observed in analogues harbouring pyridyl derivatives at 3-position of the indole scaffold, with compound 11 (*N*-[(1-benzyl-1*H*-indol-3-yl)methyl]pyridin-3-amine) displaying enhanced activity over compound 5. Accordingly, the 3-pyridyl moiety of compound 11 was maintained and a second series of analogues was generated around its phenyl ring (compounds 15-41). Although any of these derivatives improved compound 11 potentiation, our extensive coverage of size, electronic effect and aromaticity at this position suggests the importance of aromatic groups stabilising ligand binding to this putative 5-HT_{2C}R allosteric site, thereby providing the initial hints to delineate a pharmacophore model.

Prior to the *in vivo* evaluation of compound 11, we validated that this analogue is indeed a specific and pure 5-HT_{2C}R PAM. Next, we evaluated whether allosteric 5-HT_{2C}R potentiation has anorectic properties. As previously discussed in Results Chapter 6, the appetite-suppressant effects of 5-HT_{2C}R stimulation in POMC/CART neurons in the hypothalamic ARC nucleus has been extensively documented^{753,754}. For the first time, we investigated the potential of 5-HT_{2C}R PAMs as anti-obesity drugs. In agreement with our hypothesis, compound 11 enhanced sertraline anorectic properties. Furthermore, compound 11 reduced food intake when administered alone, supporting its PAM effect under endogenous 5-HT levels. The latter is a significant advantage over conventional orthosteric ligands, particularly important if taking into account that most anti-obesity therapies require a sub-chronic treatment regime. Therefore, PAMs such as compound 11 allow to keep the spatiotemporal context of the endogenous ligands whilst reducing the likelihood of receptor desensitisation³⁰⁶.

An increasing body of evidence indicates 5-HT_{2C}R-mediated suppression of mesolimbic dopaminergic reward circuits. Altogether, this not only increases the interest of agonism at 5-HT_{2C}R sites for its dualistic anti-obesity and suppression of feeding behaviours properties, but also for its application in addiction disorders^{733-735,746}. In fact, recent pre-clinical data have shown the suppressive effect of a 5-HT_{2C}R PAM in relapse vulnerability in cocaine use disorders. Accordingly, it is tempting to speculate that modulating compound 11 might exert similar effects in this DA-dependent behaviour⁷⁴⁶.

The development of selective 5-HT_{2C}R PAMs has been largely unsuccessful, with only a few of such molecules reported in the literature⁷⁴⁴⁻⁷⁴⁶. Therefore, we sought to define this 5-HT_{2C}R

General discussion

allosteric pocket in order to provide a structural template for future compound development. By molecular docking we predicted a putative allosteric pocket in the extracellular vestibule above the 5-HT occupied orthosteric site in which compound 11 is stabilised within the TMs 5 and 6 and the ECL2. The proposed binding mode was later confirmed by site-directed mutagenesis, resembling the binding pose of the tripeptide and benzyl groups of ERG in the ERG-bound 5-HT_{2B}R and 5-HT_{2C}R crystal structures^{140,352}. Interestingly, in the recently reported 5-HT_{2C}R PAM CYD-1-79, the authors proposed a similar binding pocket and fitting mode, although their predictions were only supported by docking studies^{542,746}. Furthermore, our mutagenesis studies and recent crystallographic information allow us to speculate that the basis whereby compound 11 enhances 5-HT efficacy might be by retaining 5-HT in its binding pocket in a mechanism aided by the stabilisation of a ECL2 lid-like structure²⁹.

Our model suggested that a larger hydrophobic cavity surrounding the *N*-benzylic position of compound 11 might be further explored. We investigated this cavity by synthesising a third series of analogues. WD014 (*m*-biphenyl derivative) potentiated Ca²⁺ to a similar extent as compound 11. Surprisingly, no effect was observed in β -arrestin2 recruitment, yielding, to the best of our knowledge, the first G protein biased 5-HT_{2C}R PAM. Accordingly, WD014 might be a useful tool to unveil the contribution of arrestin signalling in 5-HT_{2C}R-mediated feeding suppression. Although WD014 displayed antagonism in 5-HT_{2B} receptors, preliminary data suggest that WD014 might be, in fact, more potent than compound 11. This might allow to decrease WD014 dosage and, consequently, reduce potential subtype selectivity issues. Furthermore, this candidate must be assayed against a broader panel of targets before further *in vivo* investigations.

Overall, in this last experimental chapter, we provided a comprehensive study illustrating how allosterism provides alternatives to surpass off-target effects derived from the conservation within orthosteric binding pockets. This rationale was contextualised within developing and validating 5-HT_{2C} receptor PAMs as promising anti-obesity drugs. Finally, by defining a putative 5-HT_{2C}R allosteric binding pocket and a pharmacophore model we provided important insight for the development of further improved 5-HT_{2C}R PAMs.

7.4. Concluding remarks

Over the last 100 years, even before the concept of membrane receptor was generally acknowledged, seven transmembrane receptors have been the most widely studied drug targets. One century later, this fascinating family of plasma membrane proteins still hold many secrets, with new questions appearing as we endeavour to delve into their basis^{792,793}. Modern challenges involve translating the continuing boom in structural information to decode the

molecular underpinnings of these dynamic proteins or to incorporate emerging textures (e.g. allostery, bias and spatiotemporal signalling) into drug discovery. However, among the questions still pending, Class A GPCRs minimal functional units is one of the most controversial. Accordingly, even if our knowledge of GPCR homo/hetero-merisation has developed extensively over the past decades, little is known about why, how, when and where these quaternary structures exist. Therefore, in order to take advantage of the new pharmacological opportunities arising from this form of allostery, two of the main objectives of this thesis were to investigate the mechanistic basis for GPCR heteromerisation and to explore its *in vivo* relevance in the context of disease.

First, by tailoring signalling assays (NanoBiT) and receptors (site-mutagenesis), we provided new insights into the structural determinants, composition and conformational states of 5-HT_{2A}R-CB₁R oligomers. Our results revealed a global mechanism which might account for the similar signalling signatures observed in other heteromer pairs and provide the first insights to understand how CB₁-5-HT_{2A} receptor heteromers control THC's cognitive deficits^{312,316}. Going one step further, we undertook one of the most elusive challenges in the field: identify functional heteromers which might be targeted with a therapeutic perspective. Here, we identified functional D₁-H₃ receptor heteromers expressed in different brain areas affected in HD. Furthermore, we have shown how these receptor complexes gradually disappear over the course of the disease. Taking advantage of the vast array of opportunities that heteromerisation brings, we shown how H₃R ligands allosterically inhibit D₁R activity, which was exploited to revert motor and learning deficits in HD mice while retaining heteromer expression. Therefore, our work provides a clear example of heteromers as “true” drugable entities, suggesting a provocative strategy to reduce or mitigate HD progression.

Finally, applying some of the assays and techniques developed over this thesis, we sought to study allostery within 7TM through the perspective of identifying and characterising the binding mode of 5-HT_{2C}R small-molecule modulators. Our results emphasise the potential of allosteric modulation to overcome the limitations associated with classic orthosteric agonists, highlighting the potential of 5-HT_{2C}R PAMs as new anti-obesity treatment and providing structural insights for future drug design.

Overall, by investigating GPCRs interacting between them or with small drugs we have provided an extra layer to our understanding of the diversity of opportunities arising from allosterically modulating this receptor family (**Figure 7.1**).

General discussion

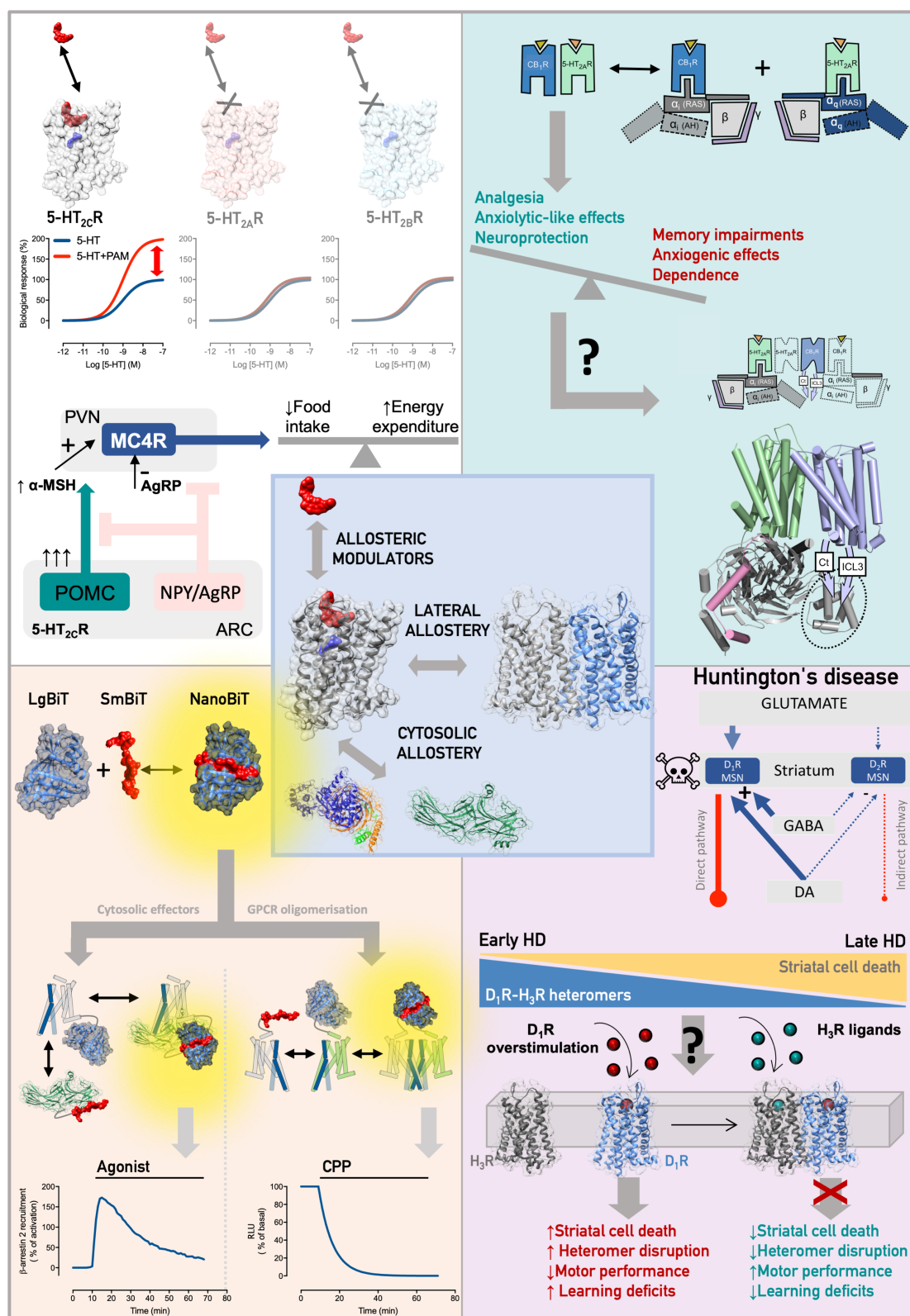


Figure 7.1. Graphical summary of the main findings of this thesis. GPCRs conformational flexibility is illustrated by the wide variety of allosteric interactors influencing its function (middle panel), including small molecules (e.g. allosteric ligands, PAMs and NAMs), cytosolic proteins (e.g. G proteins and arrestins) and membrane proteins (e.g. GPCR oligomerisation). This thesis explored GPCR allosterism at all the above-mentioned levels. We provided compelling evidence of how 5-HT_{2c}R PAMs are a safe and selective strategy for obesity treatment (top left panel). In addition, cytosolic allosterism (bottom left panel) was investigated developing

bimolecular luminescent complementation assays based on NanoLuc® Binary Technology (NanoBiT™) to study receptor:effector interactions. The same assay principle was developed to assess homo/hetero-receptor interactions and to identify hydrocarbon-stapled cell penetrating peptides disrupting 5-HT_{2A}R-CB₁R heteromers. Furthermore, lateral allostery (top and bottom right panels) was extensively investigated in 5-HT_{2A}R-CB₁R and D₁R-H₃R heteromers. An exhaustive study on the molecular basis driving allosteric communication in 5-HT_{2A}R-CB₁R heteromers (top right panel) provided a global mechanism and stoichiometry that might account for the intriguing behaviour of this heteromer *in vivo*. Finally, taking advantage of H₃R's ability to modulate D₁R signalling through D₁R-H₃R heteromers (bottom right panel), we showed that the unique biochemical properties of these complexes can be exploited to selectively prevent striatal cell death and motor and learning deficits in Huntington's' disease. Overall, this thesis provides new insights into the allosteric modulation of G protein-coupled receptors from small molecules to heteromeric interactions.

7.5. Future directions

Aim 1: develop NanoBiT-based assays to monitor GPCR oligomerisation/signalling in real time and space.

Hypothesis: recent findings illustrate how different ligands can alter the manner in which receptors traffic and signal, having a profound effect in cellular responsiveness^{115,117}. In fact, given that endosomal trafficking is no longer considered just as a mechanism of receptor attenuation, there is an increasing need for new methods to keep track of where receptors are, with whom they interact and how stable are these complexes. NanoBiT high quantum yield recently allowed the detection by bioluminescence imaging of temporal differences in arrestin binding between the arginine vasopressin receptor 2 and the β 2 adrenergic receptors, although with poor resolution at the level of subcellular compartments²⁷⁸. Alternatively, as recently shown by Bouvier's group, it is not unreasonable to assume that, nominally, NanoBiT spectral properties might allow one to follow GPCR dimerisation and β -arrestin trafficking via bystander BRET¹²⁰.

Experimental approach: to achieve this, our interacting partners (SmBiT and LgBiT fusions) would behave as the donor in a BRET system in which the acceptor is a fluorescent protein compatible with NanoLuc spectral properties (e.g., GFP from *Renilla reniformis*; rGFP) fused to a plasma membrane- or endosomal-targeting sequence. For plasma membrane targeting, we would generate rGFP constructs harbouring the fatty acylation motif of the Lyn-kinase (MGCIKSKGKDS) in its N-terminus. For early endosomes targeting, the FYVE domain of the human endofin would be attached to the C-terminus of rGFP¹²⁰. In addition, to follow up signalling across endocytic compartments we would generate rGFP constructs C-terminally tagged with Rab5a (early endosomes marker), Rab7 (late endosomal marker) and Rab11a (recycling endosomes marker)⁷⁹⁴. The experiments would be performed using standard BRET

General discussion

microplate reader setting, although it would be interesting to further explore its suitability for BRET imaging. In the case of arrestin:receptor interactions, in which this strategy was recently applied via labelling arrestins and endosomal markers with compatible BRET pairs, our strategy goes one step further as the BRET donor is the dimeric complex itself.

Aim 2: structure-based docking and optimisation of 5-HT_{2C}R PAMs.

Hypothesis: in Chapter 6 we provided strong evidence supporting the anti-obesity properties of a newly synthesised (compound 11) 5-HT_{2C}R PAMs and defined its allosteric binding pocket. However, although several derivatives were generated based on this structure, we did not explore its full SAR. In addition, the relative potency and efficacy of our PAMs were reasonably modest. In order to develop 5-HT_{2C}R PAMs with improved potency and efficacy, we would like to take advantage of the recently resolved high-resolution 5-HT_{2C}R crystal structure⁵⁴². Accordingly, our hypothesis is that the combination of molecular docking and SAR-guided optimisation might lead to the development of improved molecules.

Experimental approach: our proposed pharmacophore model defined an allosteric site against where molecular docking can be performed. We would like to generate a virtual library of drug-like compounds based on compound 11 and on identity/similarity searches in databases of commercially available compounds (e.g. ZINC database)⁷⁹⁵. Each of these molecules will be docket against 5-HT_{2C}R allosteric pocket and the best-ranking molecules will be purchased. The initial hits will be assessed for their biological activity and receptor subtype specificity using a multigene delivery system (MultiBacMamTM)⁷⁹⁶. Unlike classical viral delivery systems (e.g. retrovirus and adenovirus), which offer a limited cargo size, we are currently developing baculovirus based on the *Autographa californica* multiple nuclear polyhedrovirus (AcMNPV) genome, which allows the efficient transduction of ~100 kbp cargos in a wide variety of cell types^{796,797}. Briefly, baculovirus harbouring two independent expression cassettes encoding for the GCaMP6s calcium biosensor⁷⁴⁸ and the GPCR of interest (initially the 5-HT_{2C}, 5-HT_{2A} and 5-HT_{2B} receptors) will be used to transduce HEK293 cells prior to the evaluation of the PAM effect of the selected compounds. The same strategy could be applied if a round of SAR-guided optimisation of the initial hits is required. Finally, taking advantage of this efficient transduction system, the optimised compounds will be assayed in primary neuronal cultures or induced-pluripotent stem cells (iPS), which provide a more physiologically relevant cellular background.

REFERENCES

1. Ferrari, S. *et al.* Retinitis pigmentosa: genes and disease mechanisms. *Curr. Genomics* **12**, 238–49 (2011).
2. Insel, P. A., Tang, C.-M., Hahntow, I. & Michel, M. C. Impact of GPCRs in clinical medicine: monogenic diseases, genetic variants and drug targets. *Biochim. Biophys. Acta* **1768**, 994–1005 (2007).
3. Lander, E. S. *et al.* Initial sequencing and analysis of the human genome. *Nature* **409**, 860–921 (2001).
4. Dunham, I. *et al.* An integrated encyclopedia of DNA elements in the human genome. *Nature* **489**, 57–74 (2012).
5. Almén, M. S., Nordström, K. J. V., Fredriksson, R. & Schiöth, H. B. Mapping the human membrane proteome: a majority of the human membrane proteins can be classified according to function and evolutionary origin. *BMC Biol.* **7**, 50 (2009).
6. Hauser, A. S., Attwood, M. M., Rask-Andersen, M., Schiöth, H. B. & Gloriam, D. E. Trends in GPCR drug discovery: new agents, targets and indications. *Nat. Rev. Drug Discov.* **16**, 829–842 (2017).
7. Oprea, T. I. *et al.* Unexplored therapeutic opportunities in the human genome. *Nat. Rev. Drug Discov.* **17**, 317–332 (2018).
8. Kolakowski, L. F. GCRDb: a G-protein-coupled receptor database. *Receptors Channels* **2**, 1–7 (1994).
9. Schiöth, H. B. & Fredriksson, R. The GRAFS classification system of G-protein coupled receptors in comparative perspective. *Gen. Comp. Endocrinol.* **142**, 94–101 (2005).
10. Kobilka, B. K. G protein coupled receptor structure and activation. *Biochim. Biophys. Acta* **1768**, 794–807 (2007).
11. Doré, A. S. *et al.* Structure of class C GPCR metabotropic glutamate receptor 5 transmembrane domain. *Nature* **511**, 557–562 (2014).
12. Rosenbaum, D. M., Rasmussen, S. G. F. & Kobilka, B. K. The structure and function of G-protein-coupled receptors. *Nature* **459**, 356–363 (2009).
13. Venkatakrisnan, A. J. *et al.* Molecular signatures of G-protein-coupled receptors. *Nature* **494**, 185–194 (2013).
14. Chini, B. & Parenti, M. G-protein-coupled receptors, cholesterol and palmitoylation: facts about fats. *J. Mol. Endocrinol.* **42**, 371–9 (2009).
15. Pallotta, B. S. Single ion channel's view of classical receptor theory. *FASEB J.* **5**, 2035–43 (1991).
16. Samama, P., Cotecchia, S., Costa, T. & Lefkowitz, R. J. A mutation-induced activated state of the beta 2-adrenergic receptor. Extending the ternary complex model. *J. Biol. Chem.* **268**, 4625–36 (1993).
17. Weiss, J. M., Morgan, P. H., Lutz, M. W. & Kenakin, T. P. The Cubic Ternary Complex Receptor-Occupancy Model III. Resurrecting Efficacy. *J. Theor. Biol.* **181**, 381–397 (1996).
18. Kenakin, T. Ligand-selective receptor conformations revisited: the promise and the problem. *Trends Pharmacol. Sci.* **24**, 346–354 (2003).
19. Nygaard, R. *et al.* The dynamic process of β 2-adrenergic receptor activation. *Cell* **152**,

References

- 532–42 (2013).
20. Zhang, D., Zhao, Q. & Wu, B. Structural Studies of G Protein-Coupled Receptors. *Mol. Cells* **38**, 836–42 (2015).
 21. Venkatakrisnan, A. J. *et al.* Diverse activation pathways in class A GPCRs converge near the G-protein-coupling region. *Nature* **536**, 484–7 (2016).
 22. Zhang, Y. *et al.* Cryo-EM structure of the activated GLP-1 receptor in complex with a G protein. *Nature* **546**, 248–253 (2017).
 23. Liang, Y.-L. *et al.* Phase-plate cryo-EM structure of a class B GPCR–G-protein complex. *Nature* **546**, 118–123 (2017).
 24. Jazayeri, A. *et al.* Crystal structure of the GLP-1 receptor bound to a peptide agonist. *Nature* **546**, 254–258 (2017).
 25. Katritch, V., Cherezov, V. & Stevens, R. C. Structure-function of the G protein-coupled receptor superfamily. *Annu. Rev. Pharmacol. Toxicol.* **53**, 531–56 (2013).
 26. Ballesteros, J. A. & Weinstein, H. Integrated methods for the construction of three dimensional models and computational probing of structure-function relations in G-protein coupled receptors. *Methods Neurosci* **25**, 366–428 (1995).
 27. Wang, C. *et al.* Structural basis for molecular recognition at serotonin receptors. *Science* **340**, 610–4 (2013).
 28. Rasmussen, S. G. F. *et al.* Crystal structure of the β 2 adrenergic receptor–Gs protein complex. *Nature* **477**, 549–555 (2011).
 29. Wacker, D. *et al.* Crystal Structure of an LSD-Bound Human Serotonin Receptor. *Cell* **168**, 377–389.e12 (2017).
 30. Costa, E. M. F. *et al.* Two Novel Mutations in the Gonadotropin-Releasing Hormone Receptor Gene in Brazilian Patients with Hypogonadotropic Hypogonadism and Normal Olfaction¹. *J. Clin. Endocrinol. Metab.* **86**, 2680–2686 (2001).
 31. Feldman, B. J. *et al.* Nephrogenic Syndrome of Inappropriate Antidiuresis. *N. Engl. J. Med.* **352**, 1884–1890 (2005).
 32. Patel, Y. M. *et al.* A novel mutation in the P2Y₁₂ receptor and a function-reducing polymorphism in protease-activated receptor 1 in a patient with chronic bleeding. *J. Thromb. Haemost.* **12**, 716–725 (2014).
 33. Manglik, A. & Kruse, A. C. Structural Basis for G Protein-Coupled Receptor Activation. *Biochemistry* **56**, 5628–5634 (2017).
 34. Hua, T. *et al.* Crystal structures of agonist-bound human cannabinoid receptor CB1. *Nature* **547**, 468–471 (2017).
 35. Oldham, W. M. & Hamm, H. E. Heterotrimeric G protein activation by G-protein-coupled receptors. *Nat. Rev. Mol. Cell Biol.* **9**, 60–71 (2008).
 36. Downes, G. B. & Gautam, N. The G Protein Subunit Gene Families. *Genomics* **62**, 544–552 (1999).
 37. Coleman, D. E. *et al.* Structures of active conformations of Gi alpha 1 and the mechanism of GTP hydrolysis. *Science* **265**, 1405–12 (1994).
 38. Wedegaertner, P. B. Lipid modifications and membrane targeting of G alpha. *Biol. Signals Recept.* **7**, 125–35 (1998).
 39. Kimple, A. J., Bosch, D. E., Giguère, P. M. & Siderovski, D. P. Regulators of G-protein signaling and their G α substrates: promises and challenges in their use as drug discovery targets. *Pharmacol. Rev.* **63**, 728–49 (2011).
 40. Milligan, G. & Kostenis, E. Heterotrimeric G-proteins: a short history. *Br. J.*

- Pharmacol.* **147**, S46–S55 (2009).
41. Dupré, D. J., Robitaille, M., Rebois, R. V. & Hébert, T. E. The role of Gbetagamma subunits in the organization, assembly, and function of GPCR signaling complexes. *Annu. Rev. Pharmacol. Toxicol.* **49**, 31–56 (2009).
 42. Soundararajan, M. *et al.* Structural diversity in the RGS domain and its interaction with heterotrimeric G protein alpha-subunits. *Proc. Natl. Acad. Sci. U. S. A.* **105**, 6457–62 (2008).
 43. Choe, H.-W. *et al.* Crystal structure of metarhodopsin II. *Nature* **471**, 651–5 (2011).
 44. Flock, T. *et al.* Universal allosteric mechanism for G α activation by GPCRs. *Nature* **524**, 173–179 (2015).
 45. Flock, T. *et al.* Selectivity determinants of GPCR–G-protein binding. *Nature* **545**, 317–322 (2017).
 46. Wilkie, T. M. *et al.* Evolution of the mammalian G protein α subunit multigene family. *Nat. Genet.* **1**, 85–91 (1992).
 47. Oka, Y., Saraiva, L. R., Kwan, Y. Y. & Korsching, S. I. The fifth class of G proteins. *Proc. Natl. Acad. Sci.* **106**, 1484–1489 (2009).
 48. Kamenetsky, M. *et al.* Molecular Details of cAMP Generation in Mammalian Cells: A Tale of Two Systems. *J. Mol. Biol.* **362**, 623–639 (2006).
 49. Knighton, D. R. *et al.* Crystal structure of the catalytic subunit of cyclic adenosine monophosphate-dependent protein kinase. *Science* **253**, 407–14 (1991).
 50. Taylor, S. S., Ilouz, R., Zhang, P. & Kornev, A. P. Assembly of allosteric macromolecular switches: lessons from PKA. *Nat. Rev. Mol. Cell Biol.* **13**, 646–658 (2012).
 51. Walsh, D. A., Perkins, J. P. & Krebs, E. G. An adenosine 3',5'-monophosphate-dependant protein kinase from rabbit skeletal muscle. *J. Biol. Chem.* **243**, 3763–5 (1968).
 52. Cheng, X., Ji, Z., Tsalkova, T. & Mei, F. Epac and PKA: a tale of two intracellular cAMP receptors. *Acta Biochim. Biophys. Sin. (Shanghai)*. **40**, 651–62 (2008).
 53. Pierre, S., Eschenhagen, T., Geisslinger, G. & Scholich, K. Capturing adenylyl cyclases as potential drug targets. *Nat. Rev. Drug Discov.* **8**, 321–335 (2009).
 54. Waldo, G. L., Boyer, J. L., Morris, A. J. & Harden, T. K. Purification of an AIF4- and G-protein beta gamma-subunit-regulated phospholipase C-activating protein. *J. Biol. Chem.* **266**, 14217–25 (1991).
 55. Mikoshiba, K. IP $_3$ receptor/Ca $^{2+}$ channel: from discovery to new signaling concepts. *J. Neurochem.* **102**, 1426–1446 (2007).
 56. Jacoby, E., Bouhelal, R., Gerspacher, M. & Seuwen, K. The 7 TM G-Protein-Coupled Receptor Target Family. *ChemMedChem* **1**, 760–782 (2006).
 57. Buhl, A. M., Johnson, N. L., Dhanasekaran, N. & Johnson, G. L. G alpha 12 and G alpha 13 stimulate Rho-dependent stress fiber formation and focal adhesion assembly. *J. Biol. Chem.* **270**, 24631–4 (1995).
 58. Kelly, P., Casey, P. J. & Meigs, T. E. Biologic functions of the G12 subfamily of heterotrimeric g proteins: growth, migration, and metastasis. *Biochemistry* **46**, 6677–87 (2007).
 59. Worzfeld, T., Wettschureck, N. & Offermanns, S. G(12)/G(13)-mediated signalling in mammalian physiology and disease. *Trends Pharmacol. Sci.* **29**, 582–9 (2008).
 60. Smrcka, A. V. G protein $\beta\gamma$ subunits: Central mediators of G protein-coupled receptor signaling. *Cell. Mol. Life Sci.* **65**, 2191–2214 (2008).

References

61. Logothetis, D. E., Kurachi, Y., Galper, J., Neer, E. J. & Clapham, D. E. The $\beta\gamma$ subunits of GTP-binding proteins activate the muscarinic K⁺ channel in heart. *Nature* **325**, 321–326 (1987).
62. Smrcka, A. V. G protein $\beta\gamma$ subunits: central mediators of G protein-coupled receptor signaling. *Cell. Mol. life Sci. C.* **65**, 2191–2214 (2008).
63. Khan, S. M. *et al.* The expanding roles of G $\beta\gamma$ subunits in G protein-coupled receptor signaling and drug action. *Pharmacol. Rev.* **65**, 545–577 (2013).
64. Sieving, P. A. *et al.* Dark-light: model for nightblindness from the human rhodopsin Gly-90-->Asp mutation. *Proc. Natl. Acad. Sci. U. S. A.* **92**, 880–4 (1995).
65. al-Jandal, N. *et al.* A novel mutation within the rhodopsin gene (Thr-94-Ile) causing autosomal dominant congenital stationary night blindness. *Hum. Mutat.* **13**, 75–81 (1999).
66. Dryja, T. P., Berson, E. L., Rao, V. R. & Oprian, D. D. Heterozygous missense mutation in the rhodopsin gene as a cause of congenital stationary night blindness. *Nat. Genet.* **4**, 280–283 (1993).
67. Zeitz, C. *et al.* Identification and Functional Characterization of a Novel Rhodopsin Mutation Associated with Autosomal Dominant CSNB. *Investig. Ophthalmology Vis. Sci.* **49**, 4105 (2008).
68. Thompson, M. D., Percy, M. E., Burnham, W. M. & Cole, D. E. C. in *Methods in molecular biology (Clifton, N.J.)* **448**, 109–137 (2008).
69. Kelly, E., Bailey, C. P. & Henderson, G. Agonist-selective mechanisms of GPCR desensitization. *Br. J. Pharmacol.* **153 Suppl 1**, S379-88 (2008).
70. Strasser, R. H., Sibley, D. R. & Lefkowitz, R. J. A novel catecholamine-activated adenosine cyclic 3',5'-phosphate independent pathway for beta-adrenergic receptor phosphorylation in wild-type and mutant S49 lymphoma cells: mechanism of homologous desensitization of adenylate cyclase. *Biochemistry* **25**, 1371–7 (1986).
71. Benovic, J. L., Strasser, R. H., Caron, M. G. & Lefkowitz, R. J. Beta-adrenergic receptor kinase: identification of a novel protein kinase that phosphorylates the agonist-occupied form of the receptor. *Proc. Natl. Acad. Sci. U. S. A.* **83**, 2797–801 (1986).
72. Lohse, M. J., Benovic, J. L., Codina, J., Caron, M. G. & Lefkowitz, R. J. beta-Arrestin: a protein that regulates beta-adrenergic receptor function. *Science* **248**, 1547–50 (1990).
73. Moore, C. A. C., Milano, S. K. & Benovic, J. L. Regulation of Receptor Trafficking by GRKs and Arrestins. *Annu. Rev. Physiol.* **69**, 451–482 (2007).
74. Scheerer, P. & Sommer, M. E. Structural mechanism of arrestin activation. *Curr. Opin. Struct. Biol.* **45**, 160–169 (2017).
75. Shukla, A. K., Xiao, K. & Lefkowitz, R. J. Emerging paradigms of β -arrestin-dependent seven transmembrane receptor signaling. *Trends Biochem. Sci.* **36**, 457–469 (2011).
76. Jala, V. R., Shao, W.-H. & Haribabu, B. Phosphorylation-independent beta-arrestin translocation and internalization of leukotriene B₄ receptors. *J. Biol. Chem.* **280**, 4880–7 (2005).
77. Zhou, X. E. *et al.* Identification of Phosphorylation Codes for Arrestin Recruitment by G Protein-Coupled Receptors. *Cell* **170**, 457–469.e13 (2017).
78. Cahill, T. J. *et al.* Distinct conformations of GPCR- β -arrestin complexes mediate desensitization, signaling, and endocytosis. *Proc. Natl. Acad. Sci. U. S. A.* **114**, 2562–2567 (2017).

79. Goodman, O. B. *et al.* β -Arrestin acts as a clathrin adaptor in endocytosis of the β 2-adrenergic receptor. *Nature* **383**, 447–450 (1996).
80. Lefkowitz, R. J. & Shenoy, S. K. Transduction of Receptor Signals by beta-Arrestins. *Science* (80-.). **308**, 512–517 (2005).
81. Paczkowski, J. E., Richardson, B. C. & Fromme, J. C. Cargo adaptors: structures illuminate mechanisms regulating vesicle biogenesis. *Trends Cell Biol.* **25**, 408–16 (2015).
82. Laporte, S. A., Oakley, R. H., Holt, J. A., Barak, L. S. & Caron, M. G. The interaction of beta-arrestin with the AP-2 adaptor is required for the clustering of beta 2-adrenergic receptor into clathrin-coated pits. *J. Biol. Chem.* **275**, 23120–6 (2000).
83. Schmid, E. M. *et al.* Role of the AP2 β -Appendage Hub in Recruiting Partners for Clathrin-Coated Vesicle Assembly. *PLoS Biol.* **4**, e262 (2006).
84. McMahon, H. T. & Boucrot, E. Molecular mechanism and physiological functions of clathrin-mediated endocytosis. *Nat. Rev. Mol. Cell Biol.* **12**, 517–533 (2011).
85. Tian, X., Kang, D. S. & Benovic, J. L. β -arrestins and G protein-coupled receptor trafficking. *Handb. Exp. Pharmacol.* **219**, 173–86 (2014).
86. Peterson, Y. K. & Luttrell, L. M. The Diverse Roles of Arrestin Scaffolds in G Protein-Coupled Receptor Signaling. *Pharmacol. Rev.* **69**, 256–297 (2017).
87. Bhatnagar, A. *et al.* The Dynamin-dependent, Arrestin-independent Internalization of 5-Hydroxytryptamine 2A (5-HT_{2A}) Serotonin Receptors Reveals Differential Sorting of Arrestins and 5-HT_{2A} Receptors during Endocytosis. *J. Biol. Chem.* **276**, 8269–8277 (2001).
88. Morlot, S. & Roux, A. Mechanics of dynamin-mediated membrane fission. *Annu. Rev. Biophys.* **42**, 629–49 (2013).
89. Hanyaloglu, A. C. & Zastrow, M. von. Regulation of GPCRs by Endocytic Membrane Trafficking and Its Potential Implications. *Annu. Rev. Pharmacol. Toxicol.* **48**, 537–568 (2008).
90. Tilley, D. G. G protein-dependent and G protein-independent signaling pathways and their impact on cardiac function. *Circ. Res.* **109**, 217–30 (2011).
91. Heuss, C. & Gerber, U. G-protein-independent signaling by G-protein-coupled receptors. *Trends Neurosci.* **23**, 469–75 (2000).
92. Walther, C. & Ferguson, S. S. G. Minireview: Role of Intracellular Scaffolding Proteins in the Regulation of Endocrine G Protein-Coupled Receptor Signaling. *Mol. Endocrinol.* **29**, 814–830 (2015).
93. Jeanneteau, F., Diaz, J., Sokoloff, P. & Griffon, N. Interactions of GIPC with dopamine D2, D3 but not D4 receptors define a novel mode of regulation of G protein-coupled receptors. *Mol. Biol. Cell* **15**, 696–705 (2004).
94. Hirakawa, T., Galet, C., Kishi, M. & Ascoli, M. GIPC binds to the human lutropin receptor (hLHR) through an unusual PDZ domain binding motif, and it regulates the sorting of the internalized human choriogonadotropin and the density of cell surface hLHR. *J. Biol. Chem.* **278**, 49348–57 (2003).
95. Varsano, T., Taupin, V., Guo, L., Bateria, O. Y. & Farquhar, M. G. The PDZ Protein GIPC Regulates Trafficking of the LPA1 Receptor from APPL Signaling Endosomes and Attenuates the Cell's Response to LPA. *PLoS One* **7**, e49227 (2012).
96. Xu, J. *et al.* beta 1-adrenergic receptor association with the synaptic scaffolding protein membrane-associated guanylate kinase inverted-2 (MAGI-2). Differential regulation of receptor internalization by MAGI-2 and PSD-95. *J. Biol. Chem.* **276**, 41310–7 (2001).

References

97. Jean-Alphonse, F. *et al.* Spatially Restricted G Protein-coupled Receptor Activity via Divergent Endocytic Compartments. *J. Biol. Chem.* **289**, 3960–3977 (2014).
98. Magalhaes, A. C., Dunn, H. & Ferguson, S. S. Regulation of GPCR activity, trafficking and localization by GPCR-interacting proteins. *Br. J. Pharmacol.* **165**, 1717–1736 (2012).
99. Oh, Y.-S. *et al.* NHERF2 Specifically Interacts with LPA2 Receptor and Defines the Specificity and Efficiency of Receptor-Mediated Phospholipase C-3 Activation. *Mol. Cell. Biol.* **24**, 5069–5079 (2004).
100. Capuano, P. *et al.* Defective coupling of apical PTH receptors to phospholipase C prevents internalization of the Na⁺-phosphate cotransporter NaPi-IIa in Nherf1-deficient mice. *AJP Cell Physiol.* **292**, C927–C934 (2006).
101. Fam, S. R. *et al.* P2Y1 receptor signaling is controlled by interaction with the PDZ scaffold NHERF-2. *Proc. Natl. Acad. Sci. U. S. A.* **102**, 8042–7 (2005).
102. Malbon, C. C., Tao, J. & Wang, H.-Y. AKAPs (A-kinase anchoring proteins) and molecules that compose their G-protein-coupled receptor signalling complexes. *Biochem. J* **379**, 1–9 (2004).
103. Fraser, I. D. *et al.* Assembly of an A kinase-anchoring protein-beta(2)-adrenergic receptor complex facilitates receptor phosphorylation and signaling. *Curr. Biol.* **10**, 409–12 (2000).
104. Fan, G., Shumay, E., Wang, H. & Malbon, C. C. The Scaffold Protein Gravin (cAMP-dependent Protein Kinase-anchoring Protein 250) Binds the β_2 -Adrenergic Receptor via the Receptor Cytoplasmic Arg-329 to Leu-413 Domain and Provides a Mobile Scaffold during Desensitization. *J. Biol. Chem.* **276**, 24005–24014 (2001).
105. Luttrell, L. M. *et al.* Beta-arrestin-dependent formation of beta2 adrenergic receptor-Src protein kinase complexes. *Science* **283**, 655–61 (1999).
106. Xiao, K. *et al.* Functional specialization of beta-arrestin interactions revealed by proteomic analysis. *Proc. Natl. Acad. Sci. U. S. A.* **104**, 12011–6 (2007).
107. Tohgo, A., Pierce, K. L., Choy, E. W., Lefkowitz, R. J. & Luttrell, L. M. beta-Arrestin scaffolding of the ERK cascade enhances cytosolic ERK activity but inhibits ERK-mediated transcription following angiotensin AT1a receptor stimulation. *J. Biol. Chem.* **277**, 9429–36 (2002).
108. Feinstein, T. N. *et al.* Retromer terminates the generation of cAMP by internalized PTH receptors. *Nat. Chem. Biol.* **7**, 278–284 (2011).
109. Ahn, S., Shenoy, S. K., Wei, H. & Lefkowitz, R. J. Differential Kinetic and Spatial Patterns of β -Arrestin and G Protein-mediated ERK Activation by the Angiotensin II Receptor. *J. Biol. Chem.* **279**, 35518–35525 (2004).
110. Tohgo, A. *et al.* The Stability of the G Protein-coupled Receptor- β -Arrestin Interaction Determines the Mechanism and Functional Consequence of ERK Activation. *J. Biol. Chem.* **278**, 6258–6267 (2003).
111. Kholodenko, B. N., Hancock, J. F. & Kolch, W. Signalling ballet in space and time. *Nat. Rev. Mol. Cell Biol.* **11**, 414–426 (2010).
112. Willoughby, D. & Cooper, D. M. F. Live-cell imaging of cAMP dynamics. *Nat. Methods* **5**, 29–36 (2007).
113. Calebiro, D. *et al.* Persistent cAMP-signals triggered by internalized G-protein-coupled receptors. *PLoS Biol.* **7**, e1000172 (2009).
114. Grundmann, M. & Kostenis, E. Temporal Bias: Time-Encoded Dynamic GPCR Signaling. *Trends Pharmacol. Sci.* **38**, 1110–1124 (2017).
115. Thomsen, A. R. B. *et al.* GPCR-G Protein- β -Arrestin Super-Complex Mediates

- Sustained G Protein Signaling. *Cell* **166**, 907–919 (2016).
116. Irannejad, R. *et al.* Conformational biosensors reveal GPCR signalling from endosomes. *Nature* **495**, 534–538 (2013).
 117. Sposini, S. *et al.* Integration of GPCR Signaling and Sorting from Very Early Endosomes via Opposing APPL1 Mechanisms. *Cell Rep.* **21**, 2855–2867 (2017).
 118. Balla, A. *et al.* Mapping of the localization of type 1 angiotensin receptor in membrane microdomains using bioluminescence resonance energy transfer-based sensors. *J. Biol. Chem.* **287**, 9090–9 (2012).
 119. Zimmerman, B. *et al.* Differential β -arrestin-dependent conformational signaling and cellular responses revealed by angiotensin analogs. *Sci. Signal.* **5**, ra33 (2012).
 120. Namkung, Y. *et al.* Monitoring G protein-coupled receptor and β -arrestin trafficking in live cells using enhanced bystander BRET. *Nat. Commun.* **7**, 12178 (2016).
 121. Klein Herenbrink, C. *et al.* The role of kinetic context in apparent biased agonism at GPCRs. *Nat. Commun.* **7**, 10842 (2016).
 122. Rosciglione, S., Thériault, C., Boily, M.-O., Paquette, M. & Lavoie, C. Gas regulates the post-endocytic sorting of G protein-coupled receptors. *Nat. Commun.* **5**, 4556 (2014).
 123. Kenakin, T. Functional Selectivity and Biased Receptor Signaling. *J. Pharmacol. Exp. Ther.* **336**, 296–302 (2011).
 124. Palczewski, K. *et al.* Crystal structure of rhodopsin: A G protein-coupled receptor. *Science* **289**, 739–45 (2000).
 125. Kenakin, T. Agonist-receptor efficacy II: agonist trafficking of receptor signals. *Trends Pharmacol. Sci.* **16**, 232–238 (1995).
 126. Berg, K. A. *et al.* Effector pathway-dependent relative efficacy at serotonin type 2A and 2C receptors: evidence for agonist-directed trafficking of receptor stimulus. *Mol. Pharmacol.* **54**, 94–104 (1998).
 127. Lawler, C. *et al.* Interactions of the Novel Antipsychotic Aripiprazole (OPC-14597) with Dopamine and Serotonin Receptor Subtypes. *Neuropsychopharmacology* **20**, 612–627 (1999).
 128. Kenakin, T. Signaling bias in drug discovery. *Expert Opin. Drug Discov.* **12**, 321–333 (2017).
 129. Kenakin, T. P., Ambrose, J. R. & Irving, P. E. The relative efficiency of beta adrenoceptor coupling to myocardial inotropy and diastolic relaxation: organ-selective treatment for diastolic dysfunction. *J. Pharmacol. Exp. Ther.* **257**, (1991).
 130. Rajagopal, S., Rajagopal, K. & Lefkowitz, R. J. Teaching old receptors new tricks: biasing seven-transmembrane receptors. *Nat. Rev. Drug Discov.* **9**, 373–86 (2010).
 131. Winpenny, D., Clark, M. & Cawkill, D. Biased ligand quantification in drug discovery: from theory to high throughput screening to identify new biased μ opioid receptor agonists. *Br. J. Pharmacol.* **173**, 1393–1403 (2016).
 132. Costa-Neto, C. M., Parreiras-E-Silva, L. T. & Bouvier, M. A Pluridimensional View of Biased Agonism. *Mol. Pharmacol.* **90**, 587–595 (2016).
 133. Liu, J. J., Horst, R., Katritch, V., Stevens, R. C. & Wüthrich, K. Biased signaling pathways in β 2-adrenergic receptor characterized by 19F-NMR. *Science* **335**, 1106–10 (2012).
 134. Rahmeh, R. *et al.* Structural insights into biased G protein-coupled receptor signaling revealed by fluorescence spectroscopy. *Proc. Natl. Acad. Sci. U. S. A.* **109**, 6733–8 (2012).

References

135. Wacker, D. *et al.* Structural features for functional selectivity at serotonin receptors. *Science* **340**, 615–9 (2013).
136. Schönege, A.-M. *et al.* Evolutionary action and structural basis of the allosteric switch controlling β 2AR functional selectivity. *Nat. Commun.* **8**, 2169 (2017).
137. McCorvy, J. D. *et al.* Structure-inspired design of β -arrestin-biased ligands for aminergic GPCRs. *Nat. Chem. Biol.* **14**, 126–134 (2018).
138. Rankovic, Z., Brust, T. F. & Bohn, L. M. Biased agonism: An emerging paradigm in GPCR drug discovery. *Bioorg. Med. Chem. Lett.* **26**, 241–250 (2016).
139. Bologna, Z., Teoh, J.-P., Bayoumi, A. S., Tang, Y. & Kim, I.-M. Biased G Protein-Coupled Receptor Signaling: New Player in Modulating Physiology and Pathology. *Biomol. Ther. (Seoul)*. **25**, 12–25 (2017).
140. Wacker, D., Stevens, R. C. & Roth, B. L. How Ligands Illuminate GPCR Molecular Pharmacology. *Cell* **170**, 414–427 (2017).
141. Schwarz, E. R. *et al.* Cardioprotection by Carvedilol: Antiapoptosis is Independent of β -Adrenoceptor Blockage in the Rat Heart. *J. Cardiovasc. Pharmacol. Ther.* **8**, 207–215 (2003).
142. Wisler, J. W. *et al.* A unique mechanism of beta-blocker action: carvedilol stimulates beta-arrestin signaling. *Proc. Natl. Acad. Sci. U. S. A.* **104**, 16657–62 (2007).
143. Viscusi, E. R. *et al.* A randomized, phase 2 study investigating TRV130, a biased ligand of the μ -opioid receptor, for the intravenous treatment of acute pain. *Pain* **157**, 264–272 (2016).
144. Koch, W. J. *et al.* Cardiac function in mice overexpressing the beta-adrenergic receptor kinase or a beta ARK inhibitor. *Science* **268**, 1350–3 (1995).
145. Caron, M. G., Bohn, L. M., Gainetdinov, R. R., Lin, F.-T. & Lefkowitz, R. J. Mu-opioid receptor desensitization by beta-arrestin-2 determines morphine tolerance but not dependence. *Nature* **408**, 720–723 (2000).
146. Limbird, L. E., Meyts, P. D. & Lefkowitz, R. J. Beta-adrenergic receptors: evidence for negative cooperativity. *Biochem. Biophys. Res. Commun.* **64**, 1160–8 (1975).
147. Fraser, C. M. & Venter, J. C. The size of the mammalian lung β 2-adrenergic receptor as determined by target size analysis and immunoaffinity chromatography. *Biochem. Biophys. Res. Commun.* **109**, 21–29 (1982).
148. Avissar, S., Amitai, G. & Sokolovsky, M. Oligomeric structure of muscarinic receptors is shown by photoaffinity labeling: subunit assembly may explain high- and low-affinity agonist states. *Proc. Natl. Acad. Sci. U. S. A.* **80**, 156–9 (1983).
149. Venter, J. C., Schaber, J. S., U'Prichard, D. C. & Fraser, C. M. Molecular size of the human platelet alpha 2-adrenergic receptor as determined by radiation inactivation. *Biochem. Biophys. Res. Commun.* **116**, 1070–5 (1983).
150. Venter, J. C., Horne, P., Eddy, B., Greguski, R. & Fraser, C. M. Alpha 1-adrenergic receptor structure. *Mol. Pharmacol.* **26**, 196–205 (1984).
151. Rogers, T. B. High affinity angiotensin II receptors in myocardial sarcolemmal membranes. Characterization of receptors and covalent linkage of 125I-angiotensin II to a membrane component of 116,000 daltons. *J. Biol. Chem.* **259**, 8106–14 (1984).
152. Ng, G. Y. K. *et al.* Dopamine D2 Receptor Dimers and Receptor-Blocking Peptides. *Biochem. Biophys. Res. Commun.* **227**, 200–204 (1996).
153. Bai, M., Trivedi, S. & Brown, E. M. Dimerization of the extracellular calcium-sensing receptor (CaR) on the cell surface of CaR-transfected HEK293 cells. *J. Biol. Chem.* **273**, 23605–10 (1998).

154. Rodríguez-Frade, J. M. *et al.* The chemokine monocyte chemoattractant protein-1 induces functional responses through dimerization of its receptor CCR2. *Proc. Natl. Acad. Sci. U. S. A.* **96**, 3628–33 (1999).
155. Maggio, R., Vogel, Z. & Wess, J. Coexpression studies with mutant muscarinic/adrenergic receptors provide evidence for intermolecular ‘cross-talk’ between G-protein-linked receptors. *Proc. Natl. Acad. Sci. U. S. A.* **90**, 3103–3107 (1993).
156. Maggio, R., Barbier, P., Fornai, F. & Corsini, G. U. Functional role of the third cytoplasmic loop in muscarinic receptor dimerization. *J. Biol. Chem.* **271**, 31055–60 (1996).
157. Monnot, C. *et al.* Polar residues in the transmembrane domains of the type 1 angiotensin II receptor are required for binding and coupling. Reconstitution of the binding site by co-expression of two deficient mutants. *J. Biol. Chem.* **271**, 1507–13 (1996).
158. Rocheville, M. *et al.* Subtypes of the somatostatin receptor assemble as functional homo- and heterodimers. *J. Biol. Chem.* **275**, 7862–9 (2000).
159. Scarselli, M. *et al.* D2/D3 dopamine receptor heterodimers exhibit unique functional properties. *J. Biol. Chem.* **276**, 30308–14 (2001).
160. Bouvier, M. Oligomerization of G-protein-coupled transmitter receptors. *Nat. Rev. Neurosci.* **2**, 274–286 (2001).
161. Cordero, A., Navarro, G., Aymerich, M. S. & Franco, R. Structures for G-Protein-Coupled Receptor Tetramers in Complex with G Proteins. *Trends Biochem. Sci.* **40**, 548–51 (2015).
162. Hebert, T. E. *et al.* A peptide derived from a beta2-adrenergic receptor transmembrane domain inhibits both receptor dimerization and activation. *J. Biol. Chem.* **271**, 16384–92 (1996).
163. Romano, C., Yang, W. L. & O’Malley, K. L. Metabotropic glutamate receptor 5 is a disulfide-linked dimer. *J. Biol. Chem.* **271**, 28612–28616 (1996).
164. Kaupmann, K. *et al.* GABAB-receptor subtypes assemble into functional heteromeric complexes. *Nature* **396**, 683–687 (1998).
165. Jones, K. A. *et al.* GABAB receptors function as a heteromeric assembly of the subunits GABABR1 and GABABR2. *Nature* **396**, 674–679 (1998).
166. White, J. H. *et al.* Heterodimerization is required for the formation of a functional GABAB receptor. *Nature* **396**, 679–682 (1998).
167. Couve, A. *et al.* Intracellular Retention of Recombinant GABABReceptors. *J. Biol. Chem.* **273**, 26361–26367 (1998).
168. Margeta-Mitrovic, M., Jan, Y. N. & Jan, L. Y. A trafficking checkpoint controls GABA(B) receptor heterodimerization. *Neuron* **27**, 97–106 (2000).
169. Ward, D. T., Brown, E. M. & Harris, H. W. Disulfide Bonds in the Extracellular Calcium-Polyvalent Cation-sensing Receptor Correlate with Dimer Formation and Its Response to Divalent Cations in Vitro. *J. Biol. Chem.* **273**, 14476–14483 (1998).
170. Fan, G.-F., Ray, K., Zhao, X., Goldsmith, P. K. & Spiegel, A. M. Mutational analysis of the cysteines in the extracellular domain of the human Ca²⁺ receptor: effects on cell surface expression, dimerization and signal transduction. *FEBS Lett.* **436**, 353–356 (1998).
171. Ray, K. & Hauschild, B. C. Cys-140 Is Critical for Metabotropic Glutamate Receptor-1 Dimerization. *J. Biol. Chem.* **275**, 34245–34251 (2000).
172. Romano, C. *et al.* Covalent and noncovalent interactions mediate metabotropic

References

- glutamate receptor mGlu5 dimerization. *Mol. Pharmacol.* **59**, 46–53 (2001).
173. Nelson, G. *et al.* Mammalian Sweet Taste Receptors. *Cell* **106**, 381–390 (2001).
174. Nelson, G. *et al.* An amino-acid taste receptor. *Nature* **416**, 199–202 (2002).
175. Li, X. *et al.* Human receptors for sweet and umami taste. *Proc. Natl. Acad. Sci. U. S. A.* **99**, 4692–6 (2002).
176. Pin, J.-P. *et al.* International Union of Basic and Clinical Pharmacology. LXVII. Recommendations for the Recognition and Nomenclature of G Protein-Coupled Receptor Heteromultimers. *Pharmacol. Rev.* **59**, 5–13 (2007).
177. Angers, S. *et al.* Detection of beta 2-adrenergic receptor dimerization in living cells using bioluminescence resonance energy transfer (BRET). *Proc. Natl. Acad. Sci.* **97**, 3684–3689 (2000).
178. Albizu, L. *et al.* Time-resolved FRET between GPCR ligands reveals oligomers in native tissues. *Nat. Chem. Biol.* **6**, 587–94 (2010).
179. Urizar, E. *et al.* CODA-RET reveals functional selectivity as a result of GPCR heteromerization. *Nat. Chem. Biol.* **7**, 624–630 (2011).
180. Gomes, I. *et al.* A role for heterodimerization of μ and δ opiate receptors in enhancing morphine analgesia. *Proc. Natl. Acad. Sci.* **101**, 5135–5139 (2004).
181. Salahpour, A. *et al.* Homodimerization of the β 2-Adrenergic Receptor as a Prerequisite for Cell Surface Targeting. *J. Biol. Chem.* **279**, 33390–33397 (2004).
182. Waldhoer, M. *et al.* A heterodimer-selective agonist shows in vivo relevance of G protein-coupled receptor dimers. *Proc. Natl. Acad. Sci.* **102**, 9050–9055 (2005).
183. Terrillon, S., Barberis, C. & Bouvier, M. Heterodimerization of V1a and V2 vasopressin receptors determines the interaction with β -arrestin and their trafficking patterns. *Proc. Natl. Acad. Sci. U. S. A.* **101**, 1548–1553 (2004).
184. Viñals, X. *et al.* Cognitive Impairment Induced by Delta9-tetrahydrocannabinol Occurs through Heteromers between Cannabinoid CB1 and Serotonin 5-HT2A Receptors. *PLoS Biol.* **13**, e1002194 (2015).
185. Moreno, J. L. *et al.* Allosteric signaling through an mGlu2 and 5-HT2A heteromeric receptor complex and its potential contribution to schizophrenia. *Sci. Signal.* **9**, ra5 (2016).
186. Scarselli, M. *et al.* Revealing G-protein-coupled receptor oligomerization at the single-molecule level through a nanoscopic lens: methods, dynamics and biological function. *FEBS J.* **283**, 1197–1217 (2016).
187. Ferré, S. *et al.* Building a new conceptual framework for receptor heteromers. *Nat. Chem. Biol.* **5**, 131–134 (2009).
188. Gomes, I. *et al.* G Protein-Coupled Receptor Heteromers. *Annu. Rev. Pharmacol. Toxicol.* **56**, 403–425 (2016).
189. Gomes, I. *et al.* Heterodimerization of μ and δ opioid receptors: A role in opiate synergy. *J. Neurosci.* **20**, RC110 (2000).
190. George, S. R. *et al.* Oligomerization of μ - and δ -Opioid Receptors. *J. Biol. Chem.* **275**, 26128–26135 (2000).
191. Gomes, I. *et al.* A role for heterodimerization of μ and δ opiate receptors in enhancing morphine analgesia. *Proc. Natl. Acad. Sci.* **101**, 5135–5139 (2004).
192. Zhang, P. *et al.* Novel nanostructured lipid-dextran sulfate hybrid carriers overcome tumor multidrug resistance of mitoxantrone hydrochloride. *Nanomedicine* **8**, 185–193 (2012).

193. Berg, K. A. *et al.* Allosteric interactions between δ and κ opioid receptors in peripheral sensory neurons. *Mol. Pharmacol.* **81**, 264–72 (2012).
194. Gomes, I. *et al.* Identification of a μ - δ opioid receptor heteromer-biased agonist with antinociceptive activity. *Proc. Natl. Acad. Sci. U. S. A.* **110**, 12072–7 (2013).
195. Rivero-Müller, A. *et al.* Rescue of defective G protein-coupled receptor function in vivo by intermolecular cooperation. *Proc. Natl. Acad. Sci. U. S. A.* **107**, 2319–24 (2010).
196. Liang, Y. *et al.* Organization of the G Protein-coupled Receptors Rhodopsin and Opsin in Native Membranes. *J. Biol. Chem.* **278**, 21655–21662 (2003).
197. Fotiadis, D. *et al.* Atomic-force microscopy: Rhodopsin dimers in native disc membranes. *Nature* **421**, 127–128 (2003).
198. Davies, A., Gowen, B. E., Krebs, A. M., Schertler, G. F. X. & Saibil, H. R. Three-dimensional structure of an invertebrate rhodopsin and basis for ordered alignment in the photoreceptor membrane1. *J. Mol. Biol.* **314**, 455–463 (2001).
199. Guo, W. *et al.* Dopamine D2 receptors form higher order oligomers at physiological expression levels. *EMBO J.* **27**, 2293–2304 (2008).
200. Mancía, F., Assur, Z., Herman, A. G., Siegel, R. & Hendrickson, W. A. Ligand sensitivity in dimeric associations of the serotonin 5HT2c receptor. *EMBO Rep.* **9**, 363–369 (2008).
201. Dijkman, P. M. *et al.* Dynamic tuneable G protein-coupled receptor monomer-dimer populations. *Nat. Commun.* **9**, 1710 (2018).
202. Calebiro, D. *et al.* Single-molecule analysis of fluorescently labeled G-protein-coupled receptors reveals complexes with distinct dynamics and organization. *Proc. Natl. Acad. Sci. U. S. A.* **110**, 743–8 (2013).
203. Herrick-Davis, K., Grinde, E., Cowan, A. & Mazurkiewicz, J. E. Fluorescence correlation spectroscopy analysis of serotonin, adrenergic, muscarinic, and dopamine receptor dimerization: the oligomer number puzzle. *Mol. Pharmacol.* **84**, 630–42 (2013).
204. Petersen, J. *et al.* Agonist-induced dimer dissociation as a macromolecular step in G protein-coupled receptor signaling. *Nat. Commun.* **8**, 226 (2017).
205. Vafabakhsh, R., Levitz, J. & Isacoff, E. Y. Conformational dynamics of a class C G-protein-coupled receptor. *Nature* **524**, 497–501 (2015).
206. Xue, L. *et al.* Major ligand-induced rearrangement of the heptahelical domain interface in a GPCR dimer. *Nat. Chem. Biol.* **11**, 134–140 (2014).
207. Furness, S. G. B. *et al.* Ligand-Dependent Modulation of G Protein Conformation Alters Drug Efficacy. *Cell* **167**, 739–749.e11 (2016).
208. Tate, C. G. & Schertler, G. F. Engineering G protein-coupled receptors to facilitate their structure determination. *Curr. Opin. Struct. Biol.* **19**, 386–395 (2009).
209. Huang, J., Chen, S., Zhang, J. J. & Huang, X.-Y. Crystal structure of oligomeric β 1-adrenergic G protein-coupled receptors in ligand-free basal state. *Nat. Struct. Mol. Biol.* **20**, 419–425 (2013).
210. Wu, H. *et al.* Structure of the human κ -opioid receptor in complex with JDTic. *Nature* **485**, 327–332 (2012).
211. Thorsen, T. S., Matt, R., Weis, W. I. & Kobilka, B. K. Modified T4 Lysozyme Fusion Proteins Facilitate G Protein-Coupled Receptor Crystallography. *Structure* **22**, 1657–64 (2014).
212. Wang, C. *et al.* Structure of the human smoothed receptor bound to an antitumour

References

- agent. *Nature* **497**, 338–343 (2013).
213. Wu, B. *et al.* Structures of the CXCR4 chemokine GPCR with small-molecule and cyclic peptide antagonists. *Science* **330**, 1066–71 (2010).
214. Qin, L. *et al.* Crystal structure of the chemokine receptor CXCR4 in complex with a viral chemokine. *Science* **347**, 1117–22 (2015).
215. Manglik, A. *et al.* Crystal structure of the μ -opioid receptor bound to a morphinan antagonist. *Nature* **485**, 321–6 (2012).
216. Huang, W. *et al.* Structural insights into μ -opioid receptor activation. *Nature* **524**, 315–321 (2015).
217. Navarro, G. *et al.* Quaternary structure of a G-protein-coupled receptor heterotetramer in complex with Gi and Gs. *BMC Biol.* **14**, 26 (2016).
218. Wu, H. *et al.* Structure of a Class C GPCR Metabotropic Glutamate Receptor 1 Bound to an Allosteric Modulator. *Science (80-.)*. **344**, 58–64 (2014).
219. Christopher, J. A. *et al.* Fragment and Structure-Based Drug Discovery for a Class C GPCR: Discovery of the mGlu₅ Negative Allosteric Modulator HTL14242 (3-Chloro-5-[6-(5-fluoropyridin-2-yl)pyrimidin-4-yl]benzotrile). *J. Med. Chem.* **58**, 6653–6664 (2015).
220. Hebert, T. E. *et al.* A Peptide Derived from a β 2-Adrenergic Receptor Transmembrane Domain Inhibits Both Receptor Dimerization and Activation. *J. Biol. Chem.* **271**, 16384–16392 (1996).
221. Granier, S. *et al.* A Cyclic Peptide Mimicking the Third Intracellular Loop of the V₂ Vasopressin Receptor Inhibits Signaling through Its Interaction with Receptor Dimer and G Protein. *J. Biol. Chem.* **279**, 50904–50914 (2004).
222. Jastrzebska, B. *et al.* Disruption of Rhodopsin Dimerization with Synthetic Peptides Targeting an Interaction Interface. *J. Biol. Chem.* **290**, 25728–25744 (2015).
223. Busnelli, M. *et al.* Design and Characterization of Superpotent Bivalent Ligands Targeting Oxytocin Receptor Dimers via a Channel-Like Structure. *J. Med. Chem.* **59**, 7152–7166 (2016).
224. He, S.-Q. *et al.* Facilitation of μ -Opioid Receptor Activity by Preventing δ -Opioid Receptor-Mediated Codegradation. *Neuron* **69**, 120–131 (2011).
225. Jonas, K. C., Fanelli, F., Huhtaniemi, I. T. & Hanyaloglu, A. C. Single molecule analysis of functionally asymmetric G protein-coupled receptor (GPCR) oligomers reveals diverse spatial and structural assemblies. *J. Biol. Chem.* **290**, 3875–92 (2015).
226. Ferré, S. *et al.* G Protein-Coupled Receptor Oligomerization Revisited: Functional and Pharmacological Perspectives. *Pharmacol. Rev.* **66**, 413–434 (2014).
227. Suzuki, Y., Moriyoshi, E., Tsuchiya, D. & Jingami, H. Negative Cooperativity of Glutamate Binding in the Dimeric Metabotropic Glutamate Receptor Subtype 1. *J. Biol. Chem.* **279**, 35526–35534 (2004).
228. Levitz, J. *et al.* Mechanism of Assembly and Cooperativity of Homomeric and Heteromeric Metabotropic Glutamate Receptors. *Neuron* **92**, 143–159 (2016).
229. Kammermeier, P. J. & Yun, J. Activation of Metabotropic Glutamate Receptor 1 Dimers Requires Glutamate Binding in Both Subunits. *J. Pharmacol. Exp. Ther.* **312**, 502–508 (2004).
230. Kniazeff, J. *et al.* Closed state of both binding domains of homodimeric mGlu receptors is required for full activity. *Nat. Struct. Mol. Biol.* **11**, 706–713 (2004).
231. Rondard, P. & Pin, J.-P. Dynamics and modulation of metabotropic glutamate receptors. *Curr. Opin. Pharmacol.* **20**, 95–101 (2015).

232. Bayburt, T. H., Leitz, A. J., Xie, G., Oprian, D. D. & Sligar, S. G. Transducin activation by nanoscale lipid bilayers containing one and two rhodopsins. *J. Biol. Chem.* **282**, 14875–81 (2007).
233. Whorton, M. R. *et al.* A monomeric G protein-coupled receptor isolated in a high-density lipoprotein particle efficiently activates its G protein. *Proc. Natl. Acad. Sci. U. S. A.* **104**, 7682–7687 (2007).
234. Kuszak, A. J. *et al.* Purification and functional reconstitution of monomeric mu-opioid receptors: allosteric modulation of agonist binding by Gi2. *J. Biol. Chem.* **284**, 26732–41 (2009).
235. Tsukamoto, H., Sinha, A., DeWitt, M. & Farrens, D. L. Monomeric rhodopsin is the minimal functional unit required for arrestin binding. *J. Mol. Biol.* **399**, 501–11 (2010).
236. Bayburt, T. H. *et al.* Monomeric rhodopsin is sufficient for normal rhodopsin kinase (GRK1) phosphorylation and arrestin-1 binding. *J. Biol. Chem.* **286**, 1420–8 (2011).
237. El Moustaine, D. *et al.* Distinct roles of metabotropic glutamate receptor dimerization in agonist activation and G-protein coupling. *Proc. Natl. Acad. Sci. U. S. A.* **109**, 16342–7 (2012).
238. Zhang, T. *et al.* Dimerization of visual pigments in vivo. *Proc. Natl. Acad. Sci. U. S. A.* **113**, 9093–8 (2016).
239. Fung, J. J. *et al.* Ligand-regulated oligomerization of β 2-adrenoceptors in a model lipid bilayer. *EMBO J.* **28**, 3315–3328 (2009).
240. Han, Y., Moreira, I. S., Urizar, E., Weinstein, H. & Javitch, J. A. Allosteric communication between protomers of dopamine class A GPCR dimers modulates activation. *Nat. Chem. Biol.* **5**, 688–95 (2009).
241. Silvano, E. *et al.* The Tetrahydroisoquinoline Derivative SB269,652 Is an Allosteric Antagonist at Dopamine D3 and D2 Receptors. *Mol. Pharmacol.* **78**, 925–934 (2010).
242. Lane, J. R. *et al.* A new mechanism of allostery in a G protein-coupled receptor dimer. *Nat. Chem. Biol.* **10**, 745–52 (2014).
243. Pin, J.-P., Galvez, T. & Prézeau, L. Evolution, structure, and activation mechanism of family 3/C G-protein-coupled receptors. *Pharmacol. Ther.* **98**, 325–54 (2003).
244. Pin, J.-P. & Bettler, B. Organization and functions of mGlu and GABAB receptor complexes. *Nature* **540**, 60–68 (2016).
245. Jonas, K. C., Rivero-Müller, A., Huhtaniemi, I. T. & Hanyaloglu, A. C. G Protein-Coupled Receptor Transactivation: From Molecules to Mice. *Methods Cell Biol.* **117**, 433–450 (2013).
246. Pascal, G. & Milligan, G. Functional complementation and the analysis of opioid receptor homodimerization. *Mol. Pharmacol.* **68**, 905–15 (2005).
247. Mesnier, D. & Banères, J.-L. Cooperative conformational changes in a G-protein-coupled receptor dimer, the leukotriene B(4) receptor BLT1. *J. Biol. Chem.* **279**, 49664–70 (2004).
248. Vilaradaga, J.-P. *et al.* Conformational cross-talk between α 2A-adrenergic and μ -opioid receptors controls cell signaling. *Nat. Chem. Biol.* **4**, 126–131 (2008).
249. McCormick, P. J. & Botta, J. in *G-Protein-Coupled Receptor Dimers* 467–475 (Springer International Publishing, 2017). doi:10.1007/978-3-319-60174-8_19
250. Avissar, S., Amitai, G. & Sokolovsky, M. Oligomeric structure of muscarinic receptors is shown by photoaffinity labeling: subunit assembly may explain high- and low-affinity agonist states. *Proc. Natl. Acad. Sci. U. S. A.* **80**, 156–9 (1983).
251. Guo, H. *et al.* Methods used to study the oligomeric structure of G-protein-coupled

References

- receptors. *Biosci. Rep.* **37**, (2017).
252. Szidonya, L., Cserzo, M. & Hunyady, L. Dimerization and oligomerization of G-protein-coupled receptors: debated structures with established and emerging functions. *J. Endocrinol.* **196**, 435–53 (2008).
253. Ciruela, F., Vilardaga, J.-P. & Fernández-Dueñas, V. Lighting up multiprotein complexes: lessons from GPCR oligomerization. *Trends Biotechnol.* **28**, 407–415 (2010).
254. Förster, T. Zwischenmolekulare Energiewanderung und Fluoreszenz. *Ann. Phys.* **437**, 55–75 (1948).
255. Hussain, S. A. Science Journal of Physics SJP. *Sci. J. Phys.* **2012**, (2012).
256. Stryer, L. Fluorescence Energy Transfer as a Spectroscopic Ruler. *Annu. Rev. Biochem.* **47**, 819–846 (1978).
257. Overton, M. C. & Blumer, K. J. G-protein-coupled receptors function as oligomers in vivo. *Curr. Biol.* **10**, 341–4 (2000).
258. Cottet, M. *et al.* Original Fluorescent Ligand-Based Assays Open New Perspectives in G-Protein Coupled Receptor Drug Screening. *Pharmaceuticals* **4**, 202–214 (2011).
259. Borroto-Escuela, D. O., Flajolet, M., Agnati, L. F., Greengard, P. & Fuxe, K. Bioluminescence resonance energy transfer methods to study G protein-coupled receptor-receptor tyrosine kinase heteroreceptor complexes. *Methods Cell Biol.* **117**, 141–64 (2013).
260. Kaczor, A. A. *et al.* Application of BRET for studying G protein-coupled receptors. *Mini Rev. Med. Chem.* **14**, 411–25 (2014).
261. Hall, M. P. *et al.* Engineered Luciferase Reporter from a Deep Sea Shrimp Utilizing a Novel Imidazopyrazinone Substrate. *ACS Chem. Biol.* **7**, 1848–1857 (2012).
262. Machleidt, T. *et al.* NanoBRET—A Novel BRET Platform for the Analysis of Protein–Protein Interactions. *ACS Chem. Biol.* **10**, 1797–1804 (2015).
263. James, J. R., Oliveira, M. I., Carmo, A. M., Iaboni, A. & Davis, S. J. A rigorous experimental framework for detecting protein oligomerization using bioluminescence resonance energy transfer. *Nat. Methods* **3**, 1001–1006 (2006).
264. Bouvier, M., Heveker, N., Jockers, R., Marullo, S. & Milligan, G. BRET analysis of GPCR oligomerization: newer does not mean better. *Nat. Methods* **4**, 3–4 (2007).
265. Degorce, F. *et al.* HTRF: A technology tailored for drug discovery - a review of theoretical aspects and recent applications. *Curr. Chem. Genomics* **3**, 22–32 (2009).
266. Cottet, M. *et al.* BRET and Time-resolved FRET strategy to study GPCR oligomerization: from cell lines toward native tissues. *Front. Endocrinol. (Lausanne)*. **3**, 92 (2012).
267. McVey, M. *et al.* Monitoring Receptor Oligomerization Using Time-resolved Fluorescence Resonance Energy Transfer and Bioluminescence Resonance Energy Transfer. *J. Biol. Chem.* **276**, 14092–14099 (2001).
268. Carrillo, J. J., López-Giménez, J. F. & Milligan, G. Multiple Interactions between Transmembrane Helices Generate the Oligomeric $\alpha 1b$ -Adrenoceptor. *Mol. Pharmacol.* **66**, 1123–1137 (2004).
269. Albizu, L. *et al.* Probing the existence of G protein-coupled receptor dimers by positive and negative ligand-dependent cooperative binding. *Mol. Pharmacol.* **70**, 1783–91 (2006).
270. Maurel, D. *et al.* Cell-surface protein-protein interaction analysis with time-resolved FRET and snap-tag technologies: application to GPCR oligomerization. *Nat. Methods*

- 5, 561–567 (2008).
271. Ward, R. J., Pediani, J. D. & Milligan, G. Heteromultimerization of Cannabinoid CB₁ Receptor and Orexin OX₁ Receptor Generates a Unique Complex in Which Both Protomers Are Regulated by Orexin A. *J. Biol. Chem.* **286**, 37414–37428 (2011).
272. Vidi, P.-A., Przybyla, J. A., Hu, C.-D. & Watts, V. J. Visualization of G protein-coupled receptor (GPCR) interactions in living cells using bimolecular fluorescence complementation (BiFC). *Curr. Protoc. Neurosci.* **Chapter 5**, Unit 5.29 (2010).
273. Kodama, Y. & Hu, C. D. Bimolecular fluorescence complementation (BiFC): A 5-year update and future perspectives. *BioTechniques* **53**, 285–298 (2012).
274. Miller, K. E., Kim, Y., Huh, W.-K. & Park, H.-O. Bimolecular Fluorescence Complementation (BiFC) Analysis: Advances and Recent Applications for Genome-Wide Interaction Studies. *J. Mol. Biol.* **427**, 2039–2055 (2015).
275. Shyu, Y. J., Liu, H., Deng, X. & Hu, C.-D. Identification of new fluorescent protein fragments for bimolecular fluorescence complementation analysis under physiological conditions. *Biotechniques* **40**, 61–6 (2006).
276. Miller, K. E., Kim, Y., Huh, W.-K. & Park, H.-O. Bimolecular Fluorescence Complementation (BiFC) Analysis: Advances and Recent Applications for Genome-Wide Interaction Studies. *J. Mol. Biol.* **427**, 2039–2055 (2015).
277. Shyu, Y. J. *et al.* Visualization of protein interactions in living *Caenorhabditis elegans* using bimolecular fluorescence complementation analysis. *Nat. Protoc.* **3**, 588–596 (2008).
278. Dixon, A. S. *et al.* NanoLuc Complementation Reporter Optimized for Accurate Measurement of Protein Interactions in Cells. *ACS Chem. Biol.* **11**, 400–408 (2016).
279. Ciruela, F., Vilardaga, J.-P. & Fernández-Dueñas, V. Lighting up multiprotein complexes: lessons from GPCR oligomerization. *Trends Biotechnol.* **28**, 407–15 (2010).
280. Carriba, P. *et al.* Detection of heteromerization of more than two proteins by sequential BRET-FRET. *Nat. Methods* **5**, 727–733 (2008).
281. Rebois, R. V. *et al.* Combining protein complementation assays with resonance energy transfer to detect multipartner protein complexes in living cells. *Methods* **45**, 214–218 (2008).
282. Raicu, V. & Singh, D. R. FRET spectrometry: a new tool for the determination of protein quaternary structure in living cells. *Biophys. J.* **105**, 1937–45 (2013).
283. Godin, A. G. *et al.* Revealing protein oligomerization and densities in situ using spatial intensity distribution analysis. *Proc. Natl. Acad. Sci. U. S. A.* **108**, 7010–5 (2011).
284. Kasai, R. S. & Kusumi, A. Single-molecule imaging revealed dynamic GPCR dimerization. *Curr. Opin. Cell Biol.* **27**, 78–86 (2014).
285. Hern, J. A. *et al.* Formation and dissociation of M1 muscarinic receptor dimers seen by total internal reflection fluorescence imaging of single molecules. *Proc. Natl. Acad. Sci.* **107**, 2693–2698 (2010).
286. Jonas, K. C., Huhtaniemi, I. & Hanyaloglu, A. C. in *Methods in cell biology* **132**, 55–72 (2016).
287. Scarselli, M., Annibale, P. & Radenovic, A. Cell type-specific β 2-adrenergic receptor clusters identified using photoactivated localization microscopy are not lipid raft related, but depend on actin cytoskeleton integrity. *J. Biol. Chem.* **287**, 16768–80 (2012).
288. Trifilieff, P. *et al.* Detection of antigen interactions ex vivo by proximity ligation assay: endogenous dopamine D2-adenosine A2A receptor complexes in the striatum.

References

- Biotechniques* **51**, 111–8 (2011).
289. Taura, J., Fernández-Dueñas, V. & Ciruela, F. Visualizing G protein-coupled receptor-receptor interactions in brain using proximity ligation in situ assay. *Curr. Protoc. Cell Biol.* **2015**, 17.17.1-17.17.16 (2015).
290. Gomes, I., Sierra, S. & Devi, L. A. in *Current Protocols in Pharmacology* **75**, 2.16.1-2.16.31 (John Wiley & Sons, Inc., 2016).
291. Fredriksson, S. *et al.* Protein detection using proximity-dependent DNA ligation assays. *Nat. Biotechnol.* **20**, 473–477 (2002).
292. Sierra, S. *et al.* Detection of cannabinoid receptors CB1 and CB2 within basal ganglia output neurons in macaques: changes following experimental parkinsonism. *Brain Struct. Funct.* **220**, 2721–2738 (2015).
293. Moreno, E. *et al.* Singular Location and Signaling Profile of Adenosine A2A-Cannabinoid CB1 Receptor Heteromers in the Dorsal Striatum. *Neuropsychopharmacology* **43**, 964–977 (2018).
294. Christopoulos, A. & Kenakin, T. G Protein-Coupled Receptor Allosterism and Complexing. *Pharmacol. Rev.* **54**, 323–374 (2002).
295. Kenakin, T. & Miller, L. J. Seven Transmembrane Receptors as Shapeshifting Proteins: The Impact of Allosteric Modulation and Functional Selectivity on New Drug Discovery. *Pharmacol. Rev.* **62**, 265–304 (2010).
296. Luttrell, L. M. & Kenakin, T. P. *Signal Transduction Protocols*. **756**, (Humana Press, Totowa, NJ, 2011).
297. Goupil, E. *et al.* A Novel Biased Allosteric Compound Inhibitor of Parturition Selectively Impedes the Prostaglandin F2 α -mediated Rho/ROCK Signaling Pathway. *J. Biol. Chem.* **285**, 25624–25636 (2010).
298. Ahn, K. H., Mahmoud, M. M., Shim, J.-Y. & Kendall, D. A. Distinct roles of β -arrestin 1 and β -arrestin 2 in ORG27569-induced biased signaling and internalization of the cannabinoid receptor 1 (CB1). *J. Biol. Chem.* **288**, 9790–800 (2013).
299. Ahn, K. H., Mahmoud, M. M. & Kendall, D. A. Allosteric modulator ORG27569 induces CB1 cannabinoid receptor high affinity agonist binding state, receptor internalization, and G α_i protein-independent ERK1/2 kinase activation. *J. Biol. Chem.* **287**, 12070–82 (2012).
300. Gomes, I., Ijzerman, A. P., Ye, K., Maillet, E. L. & Devi, L. A. G protein-coupled receptor heteromerization: a role in allosteric modulation of ligand binding. *Mol. Pharmacol.* **79**, 1044–52 (2011).
301. Ferré, S., von Euler, G., Johansson, B., Fredholm, B. B. & Fuxe, K. Stimulation of high-affinity adenosine A2 receptors decreases the affinity of dopamine D2 receptors in rat striatal membranes. *Proc. Natl. Acad. Sci. U. S. A.* **88**, 7238–7241 (1991).
302. Canals, M. *et al.* Adenosine A2A-dopamine D2receptor-receptor heteromerization: Qualitative and quantitative assessment by fluorescence and bioluminescence energy transfer. *J. Biol. Chem.* **278**, 46741–46749 (2003).
303. Ferré, S. *et al.* An update on adenosine A2A-dopamine D2 receptor interactions: implications for the function of G protein-coupled receptors. *Curr. Pharm. Des.* **14**, 1468–1474 (2008).
304. Orru, M. *et al.* Striatal Pre- and Postsynaptic Profile of Adenosine A2A Receptor Antagonists. *PLoS One* **6**, e16088 (2011).
305. Nussinov, R. & Tsai, C.-J. Allosteric in Disease and in Drug Discovery. *Cell* **153**, 293–305 (2013).
306. Changeux, J.-P. & Christopoulos, A. Allosteric Modulation as a Unifying Mechanism

- for Receptor Function and Regulation. *Cell* **166**, 1084–1102 (2016).
307. Gregorio, G. G. *et al.* Single-molecule analysis of ligand efficacy in β 2AR–G-protein activation. *Nature* **547**, 68–73 (2017).
 308. Li, Z., Zhou, X., Dai, Z. & Zou, X. Classification of G proteins and prediction of GPCRs-G proteins coupling specificity using continuous wavelet transform and information theory. *Amino Acids* **43**, 793–804 (2012).
 309. Ilyaskina, O. S., Lemoine, H. & Bünemann, M. Lifetime of muscarinic receptor-G-protein complexes determines coupling efficiency and G-protein subtype selectivity. *Proc. Natl. Acad. Sci. U. S. A.* **115**, 5016–5021 (2018).
 310. Fuxe, K. *et al.* Diversity and bias through receptor-receptor interactions in GPCR heteroreceptor complexes. Focus on examples from dopamine D2 receptor heteromerization. *Frontiers in Endocrinology* **5**, 71 (2014).
 311. Seeman, P. Atypical antipsychotics: mechanism of action. *Can. J. Psychiatry*. **47**, 27–38 (2002).
 312. Borroto-Escuela, D. O. *et al.* Dopamine D2 and 5-hydroxytryptamine 5-HT2A receptors assemble into functionally interacting heteromers. *Biochem. Biophys. Res. Commun.* **401**, 605–610 (2010).
 313. Albizu, L., Holloway, T., González-Maeso, J. & Sealfon, S. C. Functional crosstalk and heteromerization of serotonin 5-HT2A and dopamine D2 receptors. *Neuropharmacology* **61**, 770–777 (2011).
 314. Borroto-Escuela, D. O. *et al.* Hallucinogenic 5-HT2AR agonists LSD and DOI enhance dopamine D2R protomer recognition and signaling of D2-5-HT2A heteroreceptor complexes. *Biochem. Biophys. Res. Commun.* **443**, 278–284 (2014).
 315. Fox, M. A., French, H. T., Laporte, J. L., Blackler, A. R. & Murphy, D. L. The serotonin 5-HT2A receptor agonist TCB-2: A behavioral and neurophysiological analysis. *Psychopharmacology (Berl)*. **212**, 13–23 (2010).
 316. González-Maeso, J. *et al.* Identification of a serotonin/glutamate receptor complex implicated in psychosis. *Nature* **452**, 93–7 (2008).
 317. Fribourg, M. *et al.* Decoding the Signaling of a GPCR Heteromeric Complex Reveals a Unifying Mechanism of Action of Antipsychotic Drugs. *Cell* **147**, 1011–1023 (2011).
 318. Rozenfeld, R. & Devi, L. A. Receptor heterodimerization leads to a switch in signaling: beta-arrestin2-mediated ERK activation by mu-delta opioid receptor heterodimers. *FASEB J.* **21**, 2455–2465 (2007).
 319. Ciruela, F. *et al.* Presynaptic Control of Striatal Glutamatergic Neurotransmission by Adenosine A1-A2A Receptor Heteromers. *J. Neurosci.* **26**, 2080–2087 (2006).
 320. Vashist, S. & Ng, D. T. W. Misfolded proteins are sorted by a sequential checkpoint mechanism of ER quality control. *J. Cell Biol.* **165**, 41–52 (2004).
 321. Gent, J., van Kerkhof, P., Roza, M., Bu, G. & Strous, G. J. Ligand-independent growth hormone receptor dimerization occurs in the endoplasmic reticulum and is required for ubiquitin system-dependent endocytosis. *Proc. Natl. Acad. Sci. U. S. A.* **99**, 9858–63 (2002).
 322. Wu, J. J. & Guidotti, G. Proreceptor dimerization is required for insulin receptor post-translational processing. *J. Biol. Chem.* **279**, 25765–73 (2004).
 323. Bass, J., Chiu, G., Argon, Y. & Steiner, D. F. Folding of insulin receptor monomers is facilitated by the molecular chaperones calnexin and calreticulin and impaired by rapid dimerization. *J. Cell Biol.* **141**, 637–46 (1998).
 324. Zhao, G. Q. *et al.* The Receptors for Mammalian Sweet and Umami Taste. *Cell* **115**, 255–266 (2003).

References

325. Jones, K. A. *et al.* GABAB receptors function as a heteromeric assembly of the subunits GABABR1 and GABABR2. *Nature* **396**, 674–679 (1998).
326. Kaupmann, K. *et al.* GABAB-receptor subtypes assemble into functional heteromeric complexes. *Nature* **396**, 683–687 (1998).
327. Zhu, X. & Wess, J. Truncated V2 Vasopressin Receptors as Negative Regulators of Wild-Type V2 Receptor Function. *Biochemistry* **37**, 15773–15784 (1998).
328. Lee, S. P. *et al.* Inhibition of cell surface expression by mutant receptors demonstrates that D2 dopamine receptors exist as oligomers in the cell. *Mol. Pharmacol.* **58**, 120–8 (2000).
329. Wilson, S., Wilkinson, G. & Milligan, G. The CXCR1 and CXCR2 receptors form constitutive homo- and heterodimers selectively and with equal apparent affinities. *J. Biol. Chem.* **280**, 28663–74 (2005).
330. Hague, C., Uberti, M. A., Chen, Z., Hall, R. A. & Minneman, K. P. Cell Surface Expression of α 1D-Adrenergic Receptors Is Controlled by Heterodimerization with α 1B-Adrenergic Receptors. *J. Biol. Chem.* **279**, 15541–15549 (2004).
331. Hague, C. *et al.* Olfactory receptor surface expression is driven by association with the β 2-adrenergic receptor. *Proc. Natl. Acad. Sci. U. S. A.* **101**, 13672–13676 (2004).
332. Small, K. M. *et al.* Alpha2A- and alpha2C-adrenergic receptors form homo- and heterodimers: the heterodimeric state impairs agonist-promoted GRK phosphorylation and beta-arrestin recruitment. *Biochemistry* **45**, 4760–7 (2006).
333. Rajagopal, S. *et al.* Beta-arrestin- but not G protein-mediated signaling by the “decoy” receptor CXCR7. *Proc. Natl. Acad. Sci. U. S. A.* **107**, 628–32 (2010).
334. Levoye, A., Balabanian, K., Baleux, F., Bachelier, F. & Lagane, B. CXCR7 heterodimerizes with CXCR4 and regulates CXCL12-mediated G protein signaling. *Blood* **113**, (2009).
335. Bellot, M. *et al.* Dual agonist occupancy of AT1-R- α 2C-AR heterodimers results in atypical Gs-PKA signaling. *Nat. Chem. Biol.* **11**, 271–279 (2015).
336. Roed, S. N. *et al.* Functional consequences of glucagon-like peptide-1 receptor cross-talk and trafficking. *J. Biol. Chem.* **290**, 1233–43 (2015).
337. Liu, X.-Y. *et al.* Unidirectional Cross-Activation of GRPR by MOR1D Uncouples Itch and Analgesia Induced by Opioids. *Cell* **147**, 447–458 (2011).
338. Terrillon, S., Barberis, C. & Bouvier, M. Heterodimerization of V1a and V2 vasopressin receptors determines the interaction with beta-arrestin and their trafficking patterns. *Proc. Natl. Acad. Sci. U. S. A.* **101**, 1548–53 (2004).
339. Banères, J. L. & Parello, J. Structure-based analysis of GPCR function: Evidence for a novel pentameric assembly between the dimeric leukotriene B4 receptor BLT1 and the G-protein. *J. Mol. Biol.* **329**, 815–829 (2003).
340. Milligan, G. G protein-coupled receptor dimerisation: Molecular basis and relevance to function. *Biochim. Biophys. Acta - Biomembr.* **1768**, 825–835 (2007).
341. Fan, T. *et al.* A Role for the Distal Carboxyl Tails in Generating the Novel Pharmacology and G Protein Activation Profile of μ and δ Opioid Receptor Heterooligomers. *J. Biol. Chem.* **280**, 38478–38488 (2005).
342. Jarraghan, A., Watts, V. J. & Barker, E. L. D2 Dopamine Receptors Modulate G-Subunit Coupling of the CB1 Cannabinoid Receptor. *J. Pharmacol. Exp. Ther.* **308**, 880–886 (2003).
343. Kearn, C. S., Blake-Palmer, K., Daniel, E., Mackie, K. & Glass, M. Concurrent Stimulation of Cannabinoid CB1 and Dopamine D2 Receptors Enhances Heterodimer

- Formation: A Mechanism for Receptor Cross-Talk? *Mol. Pharmacol.* **67**, 1697–1704 (2005).
344. Ferrada, C. *et al.* Interactions between histamine H3 and dopamine D2 receptors and the implications for striatal function. *Neuropharmacology* **55**, 190–197 (2008).
345. Ferrada, C. *et al.* Marked changes in signal transduction upon heteromerization of dopamine D1 and histamine H3 receptors. *Br. J. Pharmacol.* **157**, 64–75 (2009).
346. Nichols, D. E. & Nichols, C. D. Serotonin Receptors. *Chem. Rev.* **108**, 1614–1641 (2008).
347. Grinde, E. & Herrick-Davis, K. in *G-Protein-Coupled Receptor Dimers* 129–172 (Springer International Publishing, 2017). doi:10.1007/978-3-319-60174-8_6
348. Hoyer, D. *et al.* International Union of Pharmacology classification of receptors for 5-hydroxytryptamine (Serotonin). *Pharmacol. Rev.* **46**, 157–203 (1994).
349. Alexander, S. P. *et al.* THE CONCISE GUIDE TO PHARMACOLOGY 2017/18: G protein-coupled receptors. *Br. J. Pharmacol.* **174**, S17–S129 (2017).
350. Hannon, J. & Hoyer, D. Molecular biology of 5-HT receptors. *Behav. Brain Res.* **195**, 198–213 (2008).
351. Hassaine, G. *et al.* X-ray structure of the mouse serotonin 5-HT₃ receptor. *Nature* **512**, 276–281 (2014).
352. Peng, Y. *et al.* 5-HT_{2C} Receptor Structures Reveal the Structural Basis of GPCR Polypharmacology. *Cell* **172**, 719–730.e14 (2018).
353. Shapiro, D. A., Kristiansen, K., Weiner, D. M., Kroeze, W. K. & Roth, B. L. Evidence for a Model of Agonist-induced Activation of 5-Hydroxytryptamine 2A Serotonin Receptors That Involves the Disruption of a Strong Ionic Interaction between Helices 3 and 6. *J. Biol. Chem.* **277**, 11441–11449 (2002).
354. Yun, H.-M. & Rhim, H. The Serotonin-6 Receptor as a Novel Therapeutic Target. *Exp. Neurobiol.* **20**, 159 (2011).
355. Jenkins, T. A., Nguyen, J. C. D., Polglaze, K. E. & Bertrand, P. P. Influence of Tryptophan and Serotonin on Mood and Cognition with a Possible Role of the Gut-Brain Axis. *Nutrients* **8**, (2016).
356. Walther, D. J. *et al.* Synthesis of serotonin by a second tryptophan hydroxylase isoform. *Science* **299**, 76 (2003).
357. Strüder, H. K. & Weicker, H. Physiology and Pathophysiology of the Serotonergic System and its Implications on Mental and Physical Performance. Part I. *Int. J. Sports Med.* **22**, 467–481 (2001).
358. Sangkuhl, K., Klein, T. E. & Altman, R. B. Selective serotonin reuptake inhibitors pathway. *Pharmacogenet. Genomics* **19**, 907–9 (2009).
359. Diaz, S. L. *et al.* 5-HT_{2B} receptors are required for serotonin-selective antidepressant actions. *Mol. Psychiatry* **17**, 154–63 (2012).
360. Ramírez, M. J. 5-HT₆ receptors and Alzheimer's disease. *Alzheimers. Res. Ther.* **5**, 15 (2013).
361. Barre, A. *et al.* Presynaptic serotonin 2A receptors modulate thalamocortical plasticity and associative learning. *Proc. Natl. Acad. Sci. U. S. A.* **113**, E1382-91 (2016).
362. Athar, S. in *Encyclopedia of Movement Disorders* 104–108 (Elsevier, 2010). doi:10.1016/B978-0-12-374105-9.00001-0
363. Hornung, J.-P. The human raphe nuclei and the serotonergic system. *J. Chem. Neuroanat.* **26**, 331–43 (2003).

References

364. Lesch, K.-P. & Waider, J. Serotonin in the Modulation of Neural Plasticity and Networks: Implications for Neurodevelopmental Disorders. *Neuron* **76**, 175–191 (2012).
365. Dahlström, A. & Fuxe, K. Localization of monoamines in the lower brain stem. *Experientia* **20**, 398–9 (1964).
366. Gaspar, P. & Lillesaar, C. Probing the diversity of serotonin neurons. *Philos. Trans. R. Soc. Lond. B. Biol. Sci.* **367**, 2382–94 (2012).
367. D’Addario, C. *et al.* A preliminary study of endocannabinoid system regulation in psychosis: Distinct alterations of CNR1 promoter DNA methylation in patients with schizophrenia. *Schizophr. Res.* **188**, 132–140 (2017).
368. Chevaleyre, V., Takahashi, K. A. & Castillo, P. E. Endocannabinoid-mediated synaptic plasticity in the CNS. *Annu. Rev. Neurosci.* **29**, 37–76 (2006).
369. Parsons, L. H. & Hurd, Y. L. Endocannabinoid signalling in reward and addiction. *Nat. Rev. Neurosci.* **16**, 579–94 (2015).
370. O’Sullivan, S. E. An update on PPAR activation by cannabinoids. *Br. J. Pharmacol.* **173**, 1899–910 (2016).
371. De Petrocellis, L. *et al.* Effects of cannabinoids and cannabinoid-enriched *Cannabis* extracts on TRP channels and endocannabinoid metabolic enzymes. *Br. J. Pharmacol.* **163**, 1479–1494 (2011).
372. Console-Bram, L., Brailoiu, E., Brailoiu, G. C., Sharir, H. & Abood, M. E. Activation of GPR18 by cannabinoid compounds: a tale of biased agonism. *Br. J. Pharmacol.* **171**, 3908–17 (2014).
373. Ryberg, E. *et al.* The orphan receptor GPR55 is a novel cannabinoid receptor. *Br. J. Pharmacol.* **152**, 1092–101 (2007).
374. Overton, H. A. *et al.* Deorphanization of a G protein-coupled receptor for oleylethanolamide and its use in the discovery of small-molecule hypophagic agents. *Cell Metab.* **3**, 167–175 (2006).
375. Pert, C. B. & Snyder, S. H. Opiate receptor: demonstration in nervous tissue. *Science* **179**, 1011–4 (1973).
376. Hughes, J. *et al.* Identification of two related pentapeptides from the brain with potent opiate agonist activity. *Nature* **258**, 577–579 (1975).
377. Gérard, C. M., Mollereau, C., Vassart, G. & Parmentier, M. Molecular cloning of a human cannabinoid receptor which is also expressed in testis. *Biochem. J.* **279** (Pt 1), 129–34 (1991).
378. Matsuda, L. A., Lolait, S. J., Brownstein, M. J., Young, A. C. & Bonner, T. I. Structure of a cannabinoid receptor and functional expression of the cloned cDNA. *Nature* **346**, 561–564 (1990).
379. Devane, W. A. *et al.* Isolation and structure of a brain constituent that binds to the cannabinoid receptor. *Science* **258**, 1946–9 (1992).
380. Mechoulam, R., Hanuš, L. O., Pertwee, R. & Howlett, A. C. Early phytocannabinoid chemistry to endocannabinoids and beyond. *Nat. Rev. Neurosci.* **15**, 757–764 (2014).
381. Di Marzo, V. in 1–24 (Springer, Berlin, Heidelberg, 2006). doi:10.1007/112_0505
382. van Esbroeck, A. C. M. *et al.* Activity-based protein profiling reveals off-target proteins of the FAAH inhibitor BIA 10-2474. *Science* **356**, 1084–1087 (2017).
383. Iannotti, F. A., Di Marzo, V. & Petrosino, S. Endocannabinoids and endocannabinoid-related mediators: Targets, metabolism and role in neurological disorders. *Prog. Lipid Res.* **62**, 107–128 (2016).

384. Pacher, P., Bátkai, S. & Kunos, G. The endocannabinoid system as an emerging target of pharmacotherapy. *Pharmacol. Rev.* **58**, 389–462 (2006).
385. Tibiriça, E. The multiple functions of the endocannabinoid system: a focus on the regulation of food intake. *Diabetol. Metab. Syndr.* **2**, 5 (2010).
386. Diana, M. A. & Marty, A. Endocannabinoid-mediated short-term synaptic plasticity: depolarization-induced suppression of inhibition (DSI) and depolarization-induced suppression of excitation (DSE). *Br. J. Pharmacol.* **142**, 9–19 (2004).
387. Lu, H.-C. & Mackie, K. An Introduction to the Endogenous Cannabinoid System. *Biol. Psychiatry* **79**, 516–525 (2016).
388. Castillo, P. E., Younts, T. J., Chávez, A. E. & Hashimotodani, Y. Endocannabinoid signaling and synaptic function. *Neuron* **76**, 70–81 (2012).
389. Kano, M., Ohno-Shosaku, T., Hashimotodani, Y., Uchigashima, M. & Watanabe, M. Endocannabinoid-Mediated Control of Synaptic Transmission. *Physiol. Rev.* **89**, 309–380 (2009).
390. Pertwee, R. G. *et al.* International Union of Basic and Clinical Pharmacology. LXXIX. Cannabinoid Receptors and Their Ligands: Beyond CB1 and CB2. *Pharmacol. Rev.* **62**, 588–631 (2010).
391. Ibsen, M. S., Connor, M. & Glass, M. Cannabinoid CB1 and CB2 Receptor Signaling and Bias. *Cannabis cannabinoid Res.* **2**, 48–60 (2017).
392. Tsou, K., Brown, S., Sañudo-Peña, M. C., Mackie, K. & Walker, J. M. Immunohistochemical distribution of cannabinoid CB1 receptors in the rat central nervous system. *Neuroscience* **83**, 393–411 (1998).
393. Herkenham, M. *et al.* Cannabinoid receptor localization in brain. *Proc. Natl. Acad. Sci. U. S. A.* **87**, 1932–6 (1990).
394. Galiègue, S. *et al.* Expression of central and peripheral cannabinoid receptors in human immune tissues and leukocyte subpopulations. *Eur. J. Biochem.* **232**, 54–61 (1995).
395. Buckley, N. E. The peripheral cannabinoid receptor knockout mice: an update. *Br. J. Pharmacol.* **153**, 309–18 (2008).
396. Basu, S. & Dittel, B. N. Unraveling the complexities of cannabinoid receptor 2 (CB2) immune regulation in health and disease. *Immunol. Res.* **51**, 26–38 (2011).
397. Hanson, M. A. *et al.* Crystal Structure of a Lipid G Protein-Coupled Receptor. *Science (80-.)*. **335**, 851–855 (2012).
398. Chrencik, J. E. *et al.* Crystal Structure of Antagonist Bound Human Lysophosphatidic Acid Receptor 1. *Cell* **161**, 1633–1643 (2015).
399. Hua, T. *et al.* Crystal Structure of the Human Cannabinoid Receptor CB1. *Cell* **167**, 750–762.e14 (2016).
400. Sansom, M. S. & Weinstein, H. Hinges, swivels and switches: the role of prolines in signalling via transmembrane alpha-helices. *Trends Pharmacol. Sci.* **21**, 445–51 (2000).
401. Arnam, E. B. Van, Lester, H. A. & Dougherty, D. A. Dissecting the Functions of Conserved Prolines within Transmembrane Helices of the D2 Dopamine Receptor. *ACS Chem. Biol* **6**, 1063–1068 (2011).
402. Lu, D. & Potter, D. E. in *Handbook of Cannabis and Related Pathologies: Biology, Pharmacology, Diagnosis, and Treatment* 553–563 (Elsevier, 2017). doi:10.1016/B978-0-12-800756-3.00068-5
403. Shao, Z. *et al.* High-resolution crystal structure of the human CB1 cannabinoid receptor. *Nature* **540**, 602–606 (2016).

References

404. Ward, R. J., Pediani, J. D., Godin, A. G. & Milligan, G. Regulation of Oligomeric Organization of the Serotonin 5-Hydroxytryptamine 2C (5-HT_{2C}) Receptor Observed by Spatial Intensity Distribution Analysis. *J. Biol. Chem.* **290**, 12844–12857 (2015).
405. Herrick-Davis, K., Grinde, E. & Weaver, B. A. Serotonin 5-HT_{2C} receptor homodimerization is not regulated by agonist or inverse agonist treatment. *Eur. J. Pharmacol.* **568**, 45–53 (2007).
406. Herrick-Davis, K., Grinde, E. & Mazurkiewicz, J. E. Biochemical and biophysical characterization of serotonin 5-HT_{2C} receptor homodimers on the plasma membrane of living cells. *Biochemistry* **43**, 13963–13971 (2004).
407. Salim, K. *et al.* Oligomerization of G-protein-coupled Receptors Shown by Selective Co-immunoprecipitation. *J. Biol. Chem.* **277**, 15482–15485 (2002).
408. Pasqualetti, M. *et al.* Distribution of the 5-HT_{5A} serotonin receptor mRNA in the human brain. *Brain Res. Mol. Brain Res.* **56**, 1–8 (1998).
409. Mackie, K. Cannabinoid receptor homo- and heterodimerization. *Life Sci.* **77**, 1667–1673 (2005).
410. Wager-Miller, J., Westenbroek, R. & Mackie, K. Dimerization of G protein-coupled receptors: CB1 cannabinoid receptors as an example. *Chem. Phys. Lipids* **121**, 83–9 (2002).
411. Zhang, Y. *et al.* Synthesis and Biological Evaluation of Bivalent Ligands for the Cannabinoid 1 Receptor. *J. Med. Chem.* **53**, 7048–7060 (2010).
412. Fernández-Fernández, C. *et al.* Description of a Bivalent Cannabinoid Ligand with Hypophagic Properties. *Arch. Pharm. (Weinheim)*. **346**, 171–179 (2013).
413. Zvonok, N. *et al.* Comprehensive Proteomic Mass Spectrometric Characterization of Human Cannabinoid CB2 Receptor. *J. Proteome Res.* **6**, 2068–2079 (2007).
414. Filppula, S. *et al.* Purification and mass spectroscopic analysis of human CB2 cannabinoid receptor expressed in the baculovirus system. *J. Pept. Res.* **64**, 225–236 (2004).
415. Bushlin, I., Rozenfeld, R. & Devi, L. A. Cannabinoid-opioid interactions during neuropathic pain and analgesia. *Curr. Opin. Pharmacol.* **10**, 80–6 (2010).
416. Coke, C. J. *et al.* Simultaneous Activation of Induced Heterodimerization between CXCR4 Chemokine Receptor and Cannabinoid Receptor 2 (CB2) Reveals a Mechanism for Regulation of Tumor Progression. *J. Biol. Chem.* **291**, 9991–10005 (2016).
417. Rozenfeld, R. *et al.* AT1R-CB₁R heteromerization reveals a new mechanism for the pathogenic properties of angiotensin II. *EMBO J.* **30**, 2350–63 (2011).
418. Darmani, N. A. Cannabinoids of diverse structure inhibit two DOI-induced 5-HT_{2A} receptor-mediated behaviors in mice. *Pharmacol. Biochem. Behav.* **68**, 311–7 (2001).
419. Cheer, J. F., Cadogan, A. K., Marsden, C. A., Fone, K. C. & Kendall, D. A. Modification of 5-HT₂ receptor mediated behaviour in the rat by oleamide and the role of cannabinoid receptors. *Neuropharmacology* **38**, 533–41 (1999).
420. Mato, S. *et al.* CB₁ knockout mice display impaired functionality of 5-HT_{1A} and 5-HT_{2A/C} receptors. *J. Neurochem.* **103**, 2111–2120 (2007).
421. Aso, E. *et al.* Lack of CB₁ receptor activity impairs serotonergic negative feedback. *J. Neurochem.* **109**, 935–944 (2009).
422. Weisstaub, N. V. *et al.* Cortical 5-HT_{2A} Receptor Signaling Modulates Anxiety-Like Behaviors in Mice. *Science (80-.)*. **313**, 536–540 (2006).
423. Porras, G. *et al.* 5-HT_{2A} and 5-HT_{2C/2B} Receptor Subtypes Modulate Dopamine

- Release Induced in Vivo by Amphetamine and Morphine in Both the Rat Nucleus Accumbens and Striatum. *Neuropsychopharmacology* **26**, 311–324 (2002).
424. López-Giménez, J. F., Mengod, G., Palacios, J. M. & Vilaró, M. T. Selective visualization of rat brain 5-HT_{2A} receptors by autoradiography with [3H]MDL 100,907. *Naunyn. Schmiedebergs. Arch. Pharmacol.* **356**, 446–54 (1997).
425. Kobayashi, K. Role of Catecholamine Signaling in Brain and Nervous System Functions: New Insights from Mouse Molecular Genetic Study. *J. Investig. Dermatology Symp. Proc.* **6**, 115–121 (2001).
426. Beaulieu, J.-M. & Gainetdinov, R. R. The physiology, signaling, and pharmacology of dopamine receptors. *Pharmacol. Rev.* **63**, 182–217 (2011).
427. Eisenhofer, G., Kopin, I. J. & Goldstein, D. S. Catecholamine metabolism: a contemporary view with implications for physiology and medicine. *Pharmacol. Rev.* **56**, 331–49 (2004).
428. Beaulieu, J.-M., Espinoza, S. & Gainetdinov, R. R. Dopamine receptors - IUPHAR Review 13. *Br. J. Pharmacol.* **172**, 1–23 (2015).
429. Monsma, F. J., McVittie, L. D., Gerfen, C. R., Mahan, L. C. & Sibley, D. R. Multiple D₂ dopamine receptors produced by alternative RNA splicing. *Nature* **342**, 926–929 (1989).
430. Peroutka, S. J. in *Molecular Neurology* 321–332 (Elsevier, 2007). doi:10.1016/B978-012369509-3.50023-8
431. Peterson, S. M. *et al.* Elucidation of G-protein and β -arrestin functional selectivity at the dopamine D₂ receptor. *Proc. Natl. Acad. Sci. U. S. A.* **112**, 7097–102 (2015).
432. Meiser, J., Weindl, D. & Hiller, K. Complexity of dopamine metabolism. *Cell Commun. Signal.* **11**, 34 (2013).
433. Ayano, G. Dopamine: Receptors, Functions, Synthesis, Pathways, Locations and Mental Disorders: Review of Literatures. *J. Ment. Disord. Treat.* **2**, 1–4 (2016).
434. Bromek, E., Haduch, A., Gołombiowska, K. & Daniel, W. A. Cytochrome P450 mediates dopamine formation in the brain in vivo. *J. Neurochem.* **118**, 806–815 (2011).
435. Hiroi, T., Imaoka, S. & Funae, Y. Dopamine Formation from Tyramine by CYP2D6. *Biochem. Biophys. Res. Commun.* **249**, 838–843 (1998).
436. Yaffe, D., Vergara-Jaque, A., Forrest, L. R. & Schuldiner, S. Emulating proton-induced conformational changes in the vesicular monoamine transporter VMAT2 by mutagenesis. *Proc. Natl. Acad. Sci. U. S. A.* **113**, E7390–E7398 (2016).
437. R.Gainetdinov, R. *et al.* Dopamine receptors. *IUPHAR/BPS Guide to PHARMACOLOGY* Available at: <http://www.guidetopharmacology.org/GRAC/FamilyDisplayForward?familyId=20>. (Accessed: 26th February 2018)
438. Wise, R. A. Dopamine, learning and motivation. *Nat. Rev. Neurosci.* **5**, 483–494 (2004).
439. Bowirrat, A. *et al.* Neuropsychopharmacology and neurogenetic aspects of executive functioning: should reward gene polymorphisms constitute a diagnostic tool to identify individuals at risk for impaired judgment? *Mol. Neurobiol.* **45**, 298–313 (2012).
440. Michel, P. P., Hirsch, E. C. & Hunot, S. Understanding Dopaminergic Cell Death Pathways in Parkinson Disease. *Neuron* **90**, 675–691 (2016).
441. Tang, T.-S., Chen, X., Liu, J. & Bezprozvanny, I. Dopaminergic signaling and striatal neurodegeneration in Huntington's disease. *J. Neurosci.* **27**, 7899–910 (2007).
442. Cepeda, C., Murphy, K. P. S., Parent, M. & Levine, M. S. The role of dopamine in

References

- Huntington's disease. *Prog. Brain Res.* **211**, 235–54 (2014).
443. DeLong, M. R. Primate models of movement disorders of basal ganglia origin. *Trends Neurosci.* **13**, 281–5 (1990).
444. Albin, R. L., Young, A. B. & Penney, J. B. The functional anatomy of basal ganglia disorders. *Trends Neurosci.* **12**, 366–75 (1989).
445. Hou, L., Chen, W., Liu, X., Qiao, D. & Zhou, F.-M. Exercise-Induced Neuroprotection of the Nigrostriatal Dopamine System in Parkinson's Disease. *Front. Aging Neurosci.* **9**, 358 (2017).
446. Calabresi, P., Picconi, B., Tozzi, A., Ghiglieri, V. & Di Filippo, M. Direct and indirect pathways of basal ganglia: a critical reappraisal. *Nat. Neurosci.* **17**, 1022–1030 (2014).
447. Bates, G. P. *et al.* Huntington disease. *Nat. Rev. Dis. Prim.* **1**, 15005 (2015).
448. Poewe, W. *et al.* Parkinson disease. *Nat. Rev. Dis. Prim.* **3**, 17013 (2017).
449. Tremblay, L., Worbe, Y., Thobois, S., Sgambato-Faure, V. & Féger, J. Selective dysfunction of basal ganglia subterritories: From movement to behavioral disorders. *Mov. Disord.* **30**, 1155–1170 (2015).
450. Arias-Carrión, O., Stamelou, M., Murillo-Rodríguez, E., Menéndez-González, M. & Pöppel, E. Dopaminergic reward system: a short integrative review. *Int. Arch. Med.* **3**, 24 (2010).
451. Wang, S. *et al.* D4 dopamine receptor high-resolution structures enable the discovery of selective agonists. *Science* **358**, 381–386 (2017).
452. Chien, E. Y. T. *et al.* Structure of the human dopamine D3 receptor in complex with a D2/D3 selective antagonist. *Science* **330**, 1091–5 (2010).
453. Wang, S. *et al.* Structure of the D2 dopamine receptor bound to the atypical antipsychotic drug risperidone. *Nature* **555**, 269–273 (2018).
454. Voss, T., Wallner, E., Czernilofsky, A. P. & Freissmuth, M. Amphipathic alpha-helical structure does not predict the ability of receptor-derived synthetic peptides to interact with guanine nucleotide-binding regulatory proteins. *J. Biol. Chem.* **268**, 4637–42 (1993).
455. Senogles, S. E., Heimert, T. L., Odife, E. R. & Quasney, M. W. A region of the third intracellular loop of the short form of the D2 dopamine receptor dictates Gi coupling specificity. *J. Biol. Chem.* **279**, 1601–6 (2004).
456. Nanoff, C. *et al.* The carboxyl terminus of the G α -subunit is the latch for triggered activation of heterotrimeric G proteins. *Mol. Pharmacol.* **69**, 397–405 (2006).
457. O'Mahony, L., Akdis, M. & Akdis, C. A. Regulation of the immune response and inflammation by histamine and histamine receptors. *J. Allergy Clin. Immunol.* **128**, 1153–1162 (2011).
458. Borriello, F., Iannone, R. & Marone, G. in *Handbook of experimental pharmacology* **241**, 121–139 (2017).
459. Panula, P. *et al.* International Union of Basic and Clinical Pharmacology. XCVIII. Histamine Receptors. *Pharmacol. Rev.* **67**, 601–55 (2015).
460. Leurs, R., Bakker, R. A., Timmerman, H. & de Esch, I. J. P. The histamine H3 receptor: from gene cloning to H3 receptor drugs. *Nat. Rev. Drug Discov.* **4**, 107–120 (2005).
461. Jones, A. W. Perspectives in Drug Development and Clinical Pharmacology: The Discovery of Histamine H₁ and H₂ Antagonists. *Clin. Pharmacol. Drug Dev.* **5**, 5–12 (2016).
462. Parsons, M. E. & Ganellin, C. R. Histamine and its receptors. *Br. J. Pharmacol.* **147** Suppl 1, S127-35 (2006).

463. Nakamura, T., Itadani, H., Hidaka, Y., Ohta, M. & Tanaka, K. Molecular Cloning and Characterization of a New Human Histamine Receptor, HH4R. *Biochem. Biophys. Res. Commun.* **279**, 615–620 (2000).
464. Arrang, J. M., Garbarg, M. & Schwartz, J. C. Auto-inhibition of brain histamine release mediated by a novel class (H₃) of histamine receptor. *Nature* **302**, 832–7 (1983).
465. Martinez-Mir, M. I. *et al.* Three histamine receptors (H₁, H₂ and H₃) visualized in the brain of human and non-human primates. *Brain Res.* **526**, 322–7 (1990).
466. Paul, C. *et al.* Histamine receptors. *IUPHAR/BPS Guide to PHARMACOLOGY* Available at: <http://www.guidetopharmacology.org/GRAC/FamilyDisplayForward?familyId=33>. (Accessed: 20th May 2018)
467. Celanire, S., Wijtmans, M., Talaga, P., Leurs, R. & de Esch, I. J. P. Keynote review: Histamine H₃ receptor antagonists reach out for the clinic. *Drug Discov. Today* **10**, 1613–1627 (2005).
468. Tiligada, E., Zampeli, E., Sander, K. & Stark, H. Histamine H₃ and H₄ receptors as novel drug targets. *Expert Opin. Investig. Drugs* **18**, 1519–1531 (2009).
469. Vohora, D. & Bhowmik, M. Histamine H₃ receptor antagonists/inverse agonists on cognitive and motor processes: relevance to Alzheimer's disease, ADHD, schizophrenia, and drug abuse. *Front. Syst. Neurosci.* **6**, 72 (2012).
470. Panula, P. & Nuutinen, S. The histaminergic network in the brain: basic organization and role in disease. *Nat. Rev. Neurosci.* **14**, 472–487 (2013).
471. Oda, T., Morikawa, N., Saito, Y., Masuho, Y. & Matsumoto, S. Molecular cloning and characterization of a novel type of histamine receptor preferentially expressed in leukocytes. *J. Biol. Chem.* **275**, 36781–6 (2000).
472. Thurmond, R. L., Gelfand, E. W. & Dunford, P. J. The role of histamine H₁ and H₄ receptors in allergic inflammation: the search for new antihistamines. *Nat. Rev. Drug Discov.* **7**, 41–53 (2008).
473. Thurmond, R. L. *et al.* A Potent and Selective Histamine H₄ Receptor Antagonist with Anti-Inflammatory Properties. *J. Pharmacol. Exp. Ther.* **309**, 404–413 (2004).
474. Jablonowski, J. A. *et al.* The First Potent and Selective Non-Imidazole Human Histamine H₄ Receptor Antagonists. *J. Med. Chem.* **46**, 3957–3960 (2003).
475. Thurmond, R. L. *et al.* Toreforant, A Histamine H₄ Receptor Antagonist, in Patients with Active Rheumatoid Arthritis Despite Methotrexate Therapy: Results of 2 Phase II Studies. *J. Rheumatol.* **43**, 1637–42 (2016).
476. Thurmond, R. L. *et al.* Clinical Development of Histamine H₄ Receptor Antagonists. *Handb. Exp. Pharmacol.* **241**, 301–320 (2017).
477. Thurmond, R. L. The histamine H₄ receptor: from orphan to the clinic. *Front. Pharmacol.* **6**, 65 (2015).
478. Nguyen, T. *et al.* Discovery of a novel member of the histamine receptor family. *Mol. Pharmacol.* **59**, 427–33 (2001).
479. Kim, S.-K., Fristrup, P., Abrol, R., Goddard, W. A. & III. Structure-based prediction of subtype selectivity of histamine H₃ receptor selective antagonists in clinical trials. *J. Chem. Inf. Model.* **51**, 3262–74 (2011).
480. Shimamura, T. *et al.* Structure of the human histamine H₁ receptor complex with doxepin. *Nature* **475**, 65–70 (2011).
481. Nieto-Alamilla, G., Márquez-Gómez, R., García-Gálvez, A.-M., Morales-Figueroa, G.-E. & Arias-Montaña, J.-A. The Histamine H₃ Receptor: Structure, Pharmacology, and Function. *Mol. Pharmacol.* **90**, 649–673 (2016).

References

482. Fukushima, Y. *et al.* Palmitoylation of the canine histamine H₂ receptor occurs at Cys(305) and is important for cell surface targeting. *Biochim. Biophys. Acta* **1539**, 181–91 (2001).
483. Kooistra, A. J., Kuhne, S., de Esch, I. J. P., Leurs, R. & de Graaf, C. A structural chemogenomics analysis of aminergic GPCRs: lessons for histamine receptor ligand design. *Br. J. Pharmacol.* **170**, 101–126 (2013).
484. Alraksinen, M. S. *et al.* Histamine neurons in human hypothalamus: Anatomy in normal and alzheimer diseased brains. *Neuroscience* **44**, 465–481 (1991).
485. Haas, H. L., Sergeeva, O. A. & Selbach, O. Histamine in the Nervous System. *Physiol. Rev.* **88**, 1183–1241 (2008).
486. Thakkar, M. M. Histamine in the regulation of wakefulness. *Sleep Med. Rev.* **15**, 65–74 (2011).
487. Maintz, L. & Novak, N. Histamine and histamine intolerance. *Am. J. Clin. Nutr.* **85**, 1185–1196 (2007).
488. Cumming, P. & Vincent, S. R. Inhibition of histamine-N-methyltransferase (HNMT) by fragments of 9-amino-1,2,3,4-tetrahydroacridine (tacrine) and by beta-carbolines. *Biochem. Pharmacol.* **44**, 989–92 (1992).
489. Bencharit, S. *et al.* Crystal structure of human carboxylesterase 1 complexed with the Alzheimer's drug tacrine: from binding promiscuity to selective inhibition. *Chem. Biol.* **10**, 341–9 (2003).
490. Haas, H. & Panula, P. The role of histamine and the tuberomamillary nucleus in the nervous system. *Nat. Rev. Neurosci.* **4**, 121–130 (2003).
491. Shan, L., Bao, A.-M. & Swaab, D. F. The human histaminergic system in neuropsychiatric disorders. *Trends Neurosci.* **38**, 167–177 (2015).
492. Masaki, T. *et al.* Involvement of hypothalamic histamine H₁ receptor in the regulation of feeding rhythm and obesity. *Diabetes* **53**, 2250–60 (2004).
493. Provensi, G., Blandina, P. & Passani, M. B. The histaminergic system as a target for the prevention of obesity and metabolic syndrome. *Neuropharmacology* **106**, 3–12 (2016).
494. Al-Anbari, H. H., Sahib, A. S. & Al-Mukhtar, A. O. Role of betahistine in glycemic control of obese subjects: a placebo- controlled clinical trial. *Int. J. Basic Clin. Pharmacol.* **6**, 167 (2016).
495. Barak, N., Greenway, F. L., Fujioka, K., Aronne, L. J. & Kushner, R. F. Effect of histaminergic manipulation on weight in obese adults: a randomized placebo controlled trial. *Int. J. Obes.* **32**, 1559–1565 (2008).
496. Sadek, B., Saad, A., Sadeq, A., Jalal, F. & Stark, H. Histamine H₃ receptor as a potential target for cognitive symptoms in neuropsychiatric diseases. *Behav. Brain Res.* **312**, 415–430 (2016).
497. Kubo, M., Kishi, T., Matsunaga, S. & Iwata, N. Histamine H₃ Receptor Antagonists for Alzheimer's Disease: A Systematic Review and Meta-Analysis of Randomized Placebo-Controlled Trials. *J. Alzheimer's Dis.* **48**, 667–671 (2015).
498. O'Dowd, B. F. *et al.* Dopamine Receptor Oligomerization Visualized in Living Cells. *J. Biol. Chem.* **280**, 37225–37235 (2005).
499. Marsango, S., Caltabiano, G., Pou, C., Varela Liste, M. J. & Milligan, G. Analysis of Human Dopamine D₃ Receptor Quaternary Structure. *J. Biol. Chem.* **290**, 15146–15162 (2015).
500. Gildea, J. J. *et al.* The cooperative roles of the dopamine receptors, D₁R and D₅R, on the regulation of renal sodium transport. *Kidney Int.* **86**, 118–26 (2014).

501. So, C. H. *et al.* Calcium Signaling by Dopamine D5 Receptor and D5-D2 Receptor Hetero-Oligomers Occurs by a Mechanism Distinct from That for Dopamine D1-D2 Receptor Hetero-Oligomers. *Mol. Pharmacol.* **75**, 843–854 (2009).
502. Scarselli, M. *et al.* D₂/D₃ Dopamine Receptor Heterodimers Exhibit Unique Functional Properties. *J. Biol. Chem.* **276**, 30308–30314 (2001).
503. Fiorentini, C. *et al.* Reciprocal Regulation of Dopamine D1 and D3 Receptor Function and Trafficking by Heterodimerization. *Mol. Pharmacol.* **74**, 59–69 (2008).
504. Borroto-Escuela, D. O. *et al.* Dopamine D2 and D4 receptor heteromerization and its allosteric receptor–receptor interactions. *Biochem. Biophys. Res. Commun.* **404**, 928–934 (2011).
505. Lee, S. P. *et al.* Dopamine D1 and D2 Receptor Co-activation Generates a Novel Phospholipase C-mediated Calcium Signal. *J. Biol. Chem.* **279**, 35671–35678 (2004).
506. Perreault, M. L., Hasbi, A., O’Dowd, B. F. & George, S. R. Heteromeric Dopamine Receptor Signaling Complexes: Emerging Neurobiology and Disease Relevance. *Neuropsychopharmacology* **39**, 156–168 (2014).
507. Asher, W. B. *et al.* in *G-Protein-Coupled Receptor Dimers* 99–127 (Springer International Publishing, 2017). doi:10.1007/978-3-319-60174-8_5
508. Flores-Hernández, J. *et al.* Dopamine Enhancement of NMDA Currents in Dissociated Medium-Sized Striatal Neurons: Role of D1 Receptors and DARPP-32. *J. Neurophysiol.* **88**, 3010–3020 (2002).
509. Fiorentini, C., Gardoni, F., Spano, P., Di Luca, M. & Missale, C. Regulation of Dopamine D₁ Receptor Trafficking and Desensitization by Oligomerization with Glutamate N-Methyl-D-aspartate Receptors. *J. Biol. Chem.* **278**, 20196–20202 (2003).
510. Navarro, G. *et al.* Direct involvement of α -1 receptors in the dopamine D1 receptor-mediated effects of cocaine. *Proc. Natl. Acad. Sci.* **107**, 18676–18681 (2010).
511. van Rijn, R. M. *et al.* Cloning and characterization of dominant negative splice variants of the human histamine H₄ receptor. *Biochem. J.* **414**, 121–131 (2008).
512. Zhu, Y. *et al.* Cloning, Expression, and Pharmacological Characterization of a Novel Human Histamine Receptor. *Mol. Pharmacol.* **59**, 434–441 (2001).
513. Fukushima, Y. *et al.* Oligomer formation of histamine H₂ receptors expressed in Sf9 and COS7 cells. *FEBS Lett.* **409**, 283–286 (1997).
514. Bakker, R. A. *et al.* Domain Swapping in the Human Histamine H₁ Receptor. *J. Pharmacol. Exp. Ther.* **311**, 131–138 (2004).
515. Shenton, F. C., Hann, V. & Chazot, P. L. Evidence for native and cloned H₃ Histamine receptor higher oligomers. *Inflamm. Res.* **54**, S48–S49 (2005).
516. Monczor, F. & Fernandez, N. Current Knowledge and Perspectives on Histamine H₁ and H₂ Receptor Pharmacology: Functional Selectivity, Receptor Crosstalk, and Repositioning of Classic Histaminergic Ligands. *Mol. Pharmacol.* **90**, 640–648 (2016).
517. Alonso, N. *et al.* Cross-desensitization and cointernalization of H₁ and H₂ histamine receptors reveal new insights into histamine signal integration. *Mol. Pharmacol.* **83**, 1087–98 (2013).
518. Morales-Figueroa, G.-E., Márquez-Gómez, R., González-Pantoja, R., Escamilla-Sánchez, J. & Arias-Montaña, J.-A. Histamine H₃ Receptor Activation Counteracts Adenosine A_{2A} Receptor-Mediated Enhancement of Depolarization-Evoked [³H]-GABA Release from Rat Globus Pallidus Synaptosomes. *ACS Chem. Neurosci.* **5**, 637–645 (2014).
519. Humbert-Claude, M., Morisset, S., Gbahou, F. & Arrang, J.-M. Histamine H₃ and

References

- dopamine D2 receptor-mediated [³⁵S]GTPγ[S] binding in rat striatum: Evidence for additive effects but lack of interactions. *Biochem. Pharmacol.* **73**, 1172–1181 (2007).
520. González-Sepúlveda, M. *et al.* Cellular distribution of the histamine H3 receptor in the basal ganglia: Functional modulation of dopamine and glutamate neurotransmission. *Basal Ganglia* **3**, 109–121 (2013).
521. Le Moine, C. & Bloch, B. D1 and D2 dopamine receptor gene expression in the rat striatum: Sensitive cRNA probes demonstrate prominent segregation of D1 and D2 mRNAs in distinct neuronal populations of the dorsal and ventral striatum. *J. Comp. Neurol.* **355**, 418–426 (1995).
522. Arias-Montaña, J.-A., Floran, B., Garcia, M., Aceves, J. & Young, J. M. Histamine H₃ receptor-mediated inhibition of depolarization-induced, dopamine D₁ receptor-dependent release of [³H]-γ-aminobutyric acid from rat striatal slices. *Br. J. Pharmacol.* **133**, 165–171 (2001).
523. Moreno, E. *et al.* Dopamine D1-histamine H3 receptor heteromers provide a selective link to MAPK signaling in GABAergic neurons of the direct striatal pathway. *J. Biol. Chem.* **286**, 5846–54 (2011).
524. Moreno, E. *et al.* Cocaine Disrupts Histamine H3 Receptor Modulation of Dopamine D1 Receptor Signaling: σ1-D1-H3 Receptor Complexes as Key Targets for Reducing Cocaine's Effects. *J. Neurosci.* **34**, 3545 (2014).
525. Rousseaux, C. G. & Greene, S. F. Sigma receptors [σRs]: biology in normal and diseased states. *J. Recept. Signal Transduct. Res.* **36**, 1–62 (2015).
526. Schmidt, H. R. *et al.* Crystal structure of the human σ1 receptor. *Nature* **532**, 527–530 (2016).
527. Rodríguez-Ruiz, M. *et al.* Heteroreceptor Complexes Formed by Dopamine D1, Histamine H3, and N-Methyl-D-Aspartate Glutamate Receptors as Targets to Prevent Neuronal Death in Alzheimer's Disease. *Mol. Neurobiol.* **54**, 4537–4550 (2017).
528. Paoletti, P. *et al.* Dopaminergic and Glutamatergic Signaling Crosstalk in Huntington's Disease Neurodegeneration: The Role of p25/Cyclin-Dependent Kinase 5. *J. Neurosci.* **28**, 10090–10101 (2008).
529. Liu, H. & Naismith, J. H. An efficient one-step site-directed deletion, insertion, single and multiple-site plasmid mutagenesis protocol. *BMC Biotechnol.* **8**, 91 (2008).
530. Gibson, D. G. *et al.* Enzymatic assembly of DNA molecules up to several hundred kilobases. *Nat. Methods* **6**, 343–345 (2009).
531. Trettel, F. *et al.* Dominant phenotypes produced by the HD mutation in STHdh(Q111) striatal cells. *Hum. Mol. Genet.* **9**, 2799–809 (2000).
532. Ke, N., Wang, X., Xu, X. & Abassi, Y. A. in 33–43 (Humana Press, 2011). doi:10.1007/978-1-61779-108-6_6
533. Lazar, J., Bondar, A., Timr, S. & Firestein, S. J. Two-photon polarization microscopy reveals protein structure and function. *Nat. Methods* **8**, 684–690 (2011).
534. Bondar, A. & Lazar, J. The G protein Gi1 exhibits basal coupling but not preassembly with G protein-coupled receptors. *J. Biol. Chem.* **292**, 9690–9698 (2017).
535. Ishchenko, A. *et al.* Structural insights into the extracellular recognition of the human serotonin 2B receptor by an antibody. *Proc. Natl. Acad. Sci.* **114**, 8223–8228 (2017).
536. Tesmer, J. J., Berman, D. M., Gilman, A. G. & Sprang, S. R. Structure of RGS4 bound to AIF4--activated G(i alpha1): stabilization of the transition state for GTP hydrolysis. *Cell* **89**, 251–61 (1997).
537. Martí-Renom, M. A. *et al.* Comparative Protein Structure Modeling of Genes and Genomes. *Annu. Rev. Biophys. Biomol. Struct.* **29**, 291–325 (2000).

538. Navarro, G. *et al.* Cross-communication between Gi and Gs in a G-protein-coupled receptor heterotetramer guided by a receptor C-terminal domain. *BMC Biol.* **16**, 24 (2018).
539. Glukhova, A. *et al.* Structure of the Adenosine A 1 Receptor Reveals the Basis for Subtype Selectivity. *Cell* **168**, 867–877.e13 (2017).
540. Pronk, S. *et al.* GROMACS 4.5: a high-throughput and highly parallel open source molecular simulation toolkit. *Bioinformatics* **29**, 845–854 (2013).
541. Cordini, A., Caltabiano, G. & Pardo, L. Membrane Protein Simulations Using AMBER Force Field and Berger Lipid Parameters. *J. Chem. Theory Comput.* **8**, 948–958 (2012).
542. Peng, Y. *et al.* 5-HT_{2C} Receptor Structures Reveal the Structural Basis of GPCR Polypharmacology. *Cell* **172**, 719–730.e14 (2018).
543. Inc., C. C. G. Molecular Operating Environment (MOE), 2013.08. (2017).
544. Manglik, A., Kobilka, B. K. & Steyaert, J. Nanobodies to Study G Protein–Coupled Receptor Structure and Function. *Annu. Rev. Pharmacol. Toxicol.* **57**, 19–37 (2017).
545. Mangiarini, L. *et al.* Exon 1 of the HD gene with an expanded CAG repeat is sufficient to cause a progressive neurological phenotype in transgenic mice. *Cell* **87**, 493–506 (1996).
546. Scott, D. E., Bayly, A. R., Abell, C. & Skidmore, J. Small molecules, big targets: drug discovery faces the protein–protein interaction challenge. *Nat. Rev. Drug Discov.* **15**, 533–550 (2016).
547. De Las Rivas, J. & Fontanillo, C. Protein–Protein Interactions Essentials: Key Concepts to Building and Analyzing Interactome Networks. *PLoS Comput. Biol.* **6**, e1000807 (2010).
548. Skwarczynska, M. & Ottmann, C. Protein–protein interactions as drug targets. *Future Med. Chem.* **7**, 2195–2219 (2015).
549. Milligan, G. A day in the life of a G protein-coupled receptor: The contribution to function of G protein-coupled receptor dimerization. in *British Journal of Pharmacology* **153**, S216-29 (2008).
550. Denis, C., Saulière, A., Galandrin, S., Sénard, J.-M. & Galés, C. Probing heterotrimeric G protein activation: applications to biased ligands. *Curr. Pharm. Des.* **18**, 128–44 (2012).
551. Kerppola, T. K. Design and implementation of bimolecular fluorescence complementation (BiFC) assays for the visualization of protein interactions in living cells. *Nat. Protoc.* **1**, 1278–86 (2006).
552. Brea, J. *et al.* Evidence for Distinct Antagonist-Revealed Functional States of 5HT_{2A} Homodimers. *Mol. Pharmacol.* **75**, 1380–1391 (2009).
553. DeWire, S. M., Ahn, S., Lefkowitz, R. J. & Shenoy, S. K. β -Arrestins and Cell Signaling. *Annu. Rev. Physiol.* **69**, 483–510 (2007).
554. Kenakin, T. The Effective Application of Biased Signaling to New Drug Discovery. *Mol. Pharmacol.* **88**, 1055–1061 (2015).
555. Zhang, R. & Xie, X. Tools for GPCR drug discovery. *Acta Pharmacol. Sin.* **33**, 372–84 (2012).
556. Wang, T. *et al.* Measurement of β -Arrestin Recruitment for GPCR Targets. *Assay Guid. Man.* 1–8 (2017).
557. Caninaert, A., Storme, J., Franz, F., Auwärter, V. & Stove, C. P. Detection and Activity Profiling of Synthetic Cannabinoids and Their Metabolites with a Newly Developed

References

- Bioassay. *Anal. Chem.* **88**, 11476–11485 (2016).
558. Nichols, D. E. Hallucinogens. *Pharmacol. Ther.* **101**, 131–181 (2004).
559. González-Maeso, J. *et al.* Hallucinogens Recruit Specific Cortical 5-HT_{2A} Receptor-Mediated Signaling Pathways to Affect Behavior. *Neuron* **53**, 439–452 (2007).
560. Schmid, C. L., Raehal, K. M. & Bohn, L. M. Agonist-directed signaling of the serotonin 2A receptor depends on beta-arrestin-2 interactions in vivo. *Proc. Natl. Acad. Sci. U. S. A.* **105**, 1079–84 (2008).
561. Oh-hashii, K., Hirata, Y. & Kiuchi, K. SOD1 dimerization monitoring using a novel split NanoLuc, NanoBit. *Cell Biochem. Funct.* **34**, 497–504 (2016).
562. Bodle, C. R., Hayes, M. P., O'Brien, J. B. & Roman, D. L. Development of a bimolecular luminescence complementation assay for RGS: G protein interactions in cells. *Anal. Biochem.* **522**, 10–17 (2017).
563. Dupuis, N. *et al.* Activation of the Orphan G Protein-Coupled Receptor GPR27 by Surrogate Ligands Promotes β -Arrestin 2 Recruitment. *Mol. Pharmacol.* **91**, 595–608 (2017).
564. Koushyar, S. *et al.* The prohibitin-repressive interaction with E2F1 is rapidly inhibited by androgen signalling in prostate cancer cells. *Oncogenesis* **6**, e333 (2017).
565. Raj, G. V *et al.* Estrogen receptor coregulator binding modulators (ERXs) effectively target estrogen receptor positive human breast cancers. *Elife* **6**, e26857 (2017).
566. Srisai, D. *et al.* MRAP2 regulates ghrelin receptor signaling and hunger sensing. *Nat. Commun.* **8**, 713 (2017).
567. Sungkaworn, T. *et al.* Single-molecule imaging reveals receptor–G protein interactions at cell surface hot spots. *Nature* **550**, 543–547 (2017).
568. Alves, I. D. *et al.* Direct Observation of G-protein Binding to the Human δ -Opioid Receptor Using Plasmon-Waveguide Resonance Spectroscopy. *J. Biol. Chem.* **278**, 48890–48897 (2003).
569. Galés, C. *et al.* Probing the activation-promoted structural rearrangements in preassembled receptor-G protein complexes. *Nat. Struct. Mol. Biol.* **13**, 778–786 (2006).
570. Barnes, N. M. *et al.* 5-Hydroxytryptamine receptors. *IUPHAR/BPS Guide to PHARMACOLOGY* Available at: <http://www.guidetopharmacology.org/GRAC/FamilyDisplayForward?familyId=1>. (Accessed: 20th May 2018)
571. Vidi, P.-A., Chemel, B. R., Hu, C.-D. & Watts, V. J. Ligand-dependent oligomerization of dopamine D(2) and adenosine A(2A) receptors in living neuronal cells. *Mol. Pharmacol.* **74**, 544–51 (2008).
572. Kilpatrick, L. E., Humphrys, L. J. & Holliday, N. D. A G protein-coupled receptor dimer imaging assay reveals selectively modified pharmacology of neuropeptide Y Y1/Y5 receptor heterodimers. *Mol. Pharmacol.* **87**, 718–32 (2015).
573. Kenakin, T. & Christopoulos, A. Signalling bias in new drug discovery: detection, quantification and therapeutic impact. *Nat. Rev. Drug Discov.* **12**, 205–16 (2013).
574. Ranjan, R., Dwivedi, H., Baidya, M., Kumar, M. & Shukla, A. K. Novel Structural Insights into GPCR- β -Arrestin Interaction and Signaling. *Trends Cell Biol.* **27**, 851–862 (2017).
575. Kang, Y. *et al.* Crystal structure of rhodopsin bound to arrestin by femtosecond X-ray laser. *Nature* **523**, 561–7 (2015).
576. Soethoudt, M. *et al.* Cannabinoid CB₂ receptor ligand profiling reveals biased

- signalling and off-target activity. *Nat. Commun.* **8**, 13958 (2017).
577. Thomas, B. F., Gilliam, A. F., Burch, D. F., Roche, M. J. & Seltzman, H. H. Comparative receptor binding analyses of cannabinoid agonists and antagonists. *J. Pharmacol. Exp. Ther.* **285**, 285–92 (1998).
578. Galés, C. *et al.* Real-time monitoring of receptor and G-protein interactions in living cells. *Nat. Methods* **2**, 177–184 (2005).
579. Yano, H. *et al.* Development of novel biosensors to study receptor-mediated activation of the G-protein α subunits Gs and Golf. *J. Biol. Chem.* **292**, 19989–19998 (2017).
580. Pertwee, R. G. *et al.* International Union of Basic and Clinical Pharmacology. LXXIX. Cannabinoid Receptors and Their Ligands: Beyond CB1 and CB2. *Pharmacol. Rev.* **62**, 588–631 (2010).
581. Blume, L. C., Eldeeb, K., Bass, C. E., Selley, D. E. & Howlett, A. C. Cannabinoid receptor interacting protein (CRIP1a) attenuates CB1R signaling in neuronal cells. *Cell. Signal.* **27**, 716–726 (2015).
582. Hughes, T. E., Zhang, H., Logothetis, D. E. & Berlot, C. H. Visualization of a Functional $G\alpha_q$ -Green Fluorescent Protein Fusion in Living Cells. *J. Biol. Chem.* **276**, 4227–4235 (2001).
583. Adjobo-Hermans, M. J. W. *et al.* Real-time visualization of heterotrimeric G protein Gq activation in living cells. *BMC Biol.* **9**, 32 (2011).
584. Wang, J., He, L., Combs, C. A., Roderiquez, G. & Norcross, M. A. Dimerization of CXCR4 in living malignant cells: control of cell migration by a synthetic peptide that reduces homologous CXCR4 interactions. *Mol. Cancer Ther.* **5**, 2474–2483 (2006).
585. Cai, X., Bai, B., Zhang, R., Wang, C. & Chen, J. Apelin receptor homodimer-oligomers revealed by single-molecule imaging and novel G protein-dependent signaling. *Sci. Rep.* **7**, 40335 (2017).
586. Lee, L. T. O. *et al.* Transmembrane peptides as unique tools to demonstrate the in vivo action of a cross-class GPCR heterocomplex. *FASEB J.* **28**, 2632–44 (2014).
587. Ziegler, A., Nervi, P., Dürrenberger, M. & Seelig, J. The cationic cell-penetrating peptide CPPTAT derived from the HIV-1 protein TAT is rapidly transported into living fibroblasts: Optical, biophysical, and metabolic evidence. *Biochemistry* **44**, 138–148 (2005).
588. Bird, G. H. *et al.* Hydrocarbon double-stapling remedies the proteolytic instability of a lengthy peptide therapeutic. *Proc. Natl. Acad. Sci. U. S. A.* **107**, 14093–8 (2010).
589. Pelay-Gimeno, M., Glas, A., Koch, O. & Grossmann, T. N. Structure-Based Design of Inhibitors of Protein-Protein Interactions: Mimicking Peptide Binding Epitopes. *Angew. Chemie Int. Ed.* **54**, 8896–8927 (2015).
590. Sclip, A. *et al.* c-Jun N-terminal kinase has a key role in Alzheimer disease synaptic dysfunction in vivo. *Cell Death Dis.* **5**, e1019 (2014).
591. Zou, L.-L., Ma, J.-L., Wang, T., Yang, T.-B. & Liu, C.-B. Cell-Penetrating Peptide-Mediated Therapeutic Molecule Delivery into the Central Nervous System. *Curr. Neuropharmacol.* **11**, 197–208 (2013).
592. Szalai, B. *et al.* Improved Methodical Approach for Quantitative BRET Analysis of G Protein Coupled Receptor Dimerization. *PLoS One* **9**, e109503 (2014).
593. Lan, T.-H. *et al.* BRET evidence that β_2 adrenergic receptors do not oligomerize in cells. *Sci. Rep.* **5**, 10166 (2015).
594. Kerppola, T. K. Visualization of molecular interactions by fluorescence complementation. *Nat. Rev. Mol. Cell Biol.* **7**, 449–456 (2006).

References

595. Kerppola, T. K. Bimolecular Fluorescence Complementation (BiFC) Analysis as a Probe of Protein Interactions in Living Cells. *Annu. Rev. Biophys.* **37**, 465–487 (2008).
596. Remy, I. & Michnick, S. W. A highly sensitive protein-protein interaction assay based on *Gussia* luciferase. *Nat. Methods* **3**, 977–979 (2006).
597. Stefan, E. *et al.* Quantification of dynamic protein complexes using Renilla luciferase fragment complementation applied to protein kinase A activities in vivo. *Proc. Natl. Acad. Sci. U. S. A.* **104**, 16916–21 (2007).
598. Armando, S. *et al.* The chemokine CXCR4 and CC2 receptors form homo- and heterooligomers that can engage their signaling G-protein effectors and β arrestin. *FASEB J.* **28**, 4509–23 (2014).
599. Brea, J. *et al.* Evidence for distinct antagonist-revealed functional states of 5-hydroxytryptamine(2A) receptor homodimers. *Mol. Pharmacol.* **75**, 1380–91 (2009).
600. Qin, J. Y. *et al.* Systematic Comparison of Constitutive Promoters and the Doxycycline-Inducible Promoter. *PLoS One* **5**, e10611 (2010).
601. Hasbi, A. *et al.* A peptide targeting an interaction interface disrupts the dopamine D1-D2 receptor heteromer to block signaling and function in vitro and in vivo: effective selective antagonism. *FASEB J.* **28**, 4806–4820 (2014).
602. Pei, L. *et al.* Uncoupling the dopamine D1-D2 receptor complex exerts antidepressant-like effects. *Nat. Med.* **16**, 1393–1395 (2010).
603. González-Maeso, J. Family A GPCR heteromers in animal models. *Front. Pharmacol.* **5**, 226 (2014).
604. Kuriyan, J. & Eisenberg, D. The origin of protein interactions and allostery in colocalization. *Nature* **450**, 983–990 (2007).
605. DeVree, B. T. *et al.* Allosteric coupling from G protein to the agonist-binding pocket in GPCRs. *Nature* **535**, 182–186 (2016).
606. Wreggett, K. A. & Wells, J. W. Cooperativity manifest in the binding properties of purified cardiac muscarinic receptors. *J. Biol. Chem.* **270**, 22488–99 (1995).
607. Armstrong, D. & Strange, P. G. Dopamine D2 receptor dimer formation: evidence from ligand binding. *J. Biol. Chem.* **276**, 22621–9 (2001).
608. Urizar, E. *et al.* Glycoprotein hormone receptors: link between receptor homodimerization and negative cooperativity. *EMBO J.* **24**, 1954–1964 (2005).
609. Springael, J.-Y. *et al.* Allosteric modulation of binding properties between units of chemokine receptor homo- and hetero-oligomers. *Mol. Pharmacol.* **69**, 1652–61 (2006).
610. Franco, R. *et al.* Evidence for Adenosine/Dopamine Receptor Interactions Indications for Heteromerization. *Neuropsychopharmacology* **23**, S50–S59 (2000).
611. Jordan, B. A., Gomes, I., Rios, C., Filipovska, J. & Devi, L. A. Functional interactions between mu opioid and alpha 2A-adrenergic receptors. *Mol. Pharmacol.* **64**, 1317–24 (2003).
612. Salahpour, A. *et al.* BRET biosensors to study GPCR biology, pharmacology, and signal transduction. *Frontiers in Endocrinology* **3**, 105 (2012).
613. Fiorentini, C. *et al.* Reciprocal regulation of dopamine D1 and D3 receptor function and trafficking by heterodimerization. *Mol. Pharmacol.* **74**, 59–69 (2008).
614. Marcellino, D. *et al.* Identification of dopamine D1-D3 receptor heteromers. Indications for a role of synergistic D1-D3 receptor interactions in the striatum. *J. Biol. Chem.* **283**, 26016–25 (2008).
615. Trehan, A., Jonas, K. C., Huhtaniemi, I., Hanyaloglu, A. C. & Rivero-Müller, A. in *G*

- Protein-Coupled Receptor Genetics* 239–255 (Humana Press, Totowa, NJ, 2014). doi:10.1007/978-1-62703-779-2_13
616. Scheerer, P. *et al.* Crystal structure of opsin in its G-protein-interacting conformation. *Nature* **455**, 497–502 (2008).
 617. Standfuss, J. *et al.* The structural basis of agonist-induced activation in constitutively active rhodopsin. *Nature* **471**, 656–60 (2011).
 618. Trzaskowski, B. *et al.* Action of molecular switches in GPCRs--theoretical and experimental studies. *Curr. Med. Chem.* **19**, 1090–109 (2012).
 619. Deupi, X. *et al.* Stabilized G protein binding site in the structure of constitutively active metarhodopsin-II. *Proc. Natl. Acad. Sci.* **109**, 119–124 (2012).
 620. Rasmussen, S. G. F. *et al.* Structure of a nanobody-stabilized active state of the $\beta(2)$ adrenoceptor. *Nature* **469**, 175–180 (2011).
 621. Day, M., Olson, P. A., Platzer, J., Striessnig, J. & Surmeier, D. J. Stimulation of 5-HT(2) receptors in prefrontal pyramidal neurons inhibits Ca(v)1.2 L type Ca(2+) currents via a PLCbeta/IP3/calcineurin signaling cascade. *J. Neurophysiol.* **87**, 2490–504 (2002).
 622. Sansuk, K. *et al.* A Structural Insight into the Reorientation of Transmembrane Domains 3 and 5 during Family A G Protein-Coupled Receptor Activation. *Mol. Pharmacol.* **79**, 262–269 (2011).
 623. Carrillo, J. J., Padiani, J. & Milligan, G. Dimers of Class A G Protein-coupled Receptors Function via Agonist-mediated Trans-activation of Associated G Proteins. *J. Biol. Chem.* **278**, 42578–42587 (2003).
 624. Howlett, A. C. & Fleming, R. M. Cannabinoid inhibition of adenylate cyclase. Pharmacology of the response in neuroblastoma cell membranes. *Mol. Pharmacol.* **26**, (1984).
 625. D'Antona, A. M., Ahn, K. H. & Kendall, D. A. Mutations of CB₁ T210 Produce Active and Inactive Receptor Forms: Correlations with Ligand Affinity, Receptor Stability, and Cellular Localization[†]. *Biochemistry* **45**, 5606–5617 (2006).
 626. Shim, J.-Y., Ahn, K. H. & Kendall, D. A. Molecular Basis of Cannabinoid CB1 Receptor Coupling to the G Protein Heterotrimer G $\alpha_i\beta\gamma$. *J. Biol. Chem.* **288**, 32449–32465 (2013).
 627. Rashid, A. J. *et al.* D1-D2 dopamine receptor heterooligomers with unique pharmacology are coupled to rapid activation of Gq/11 in the striatum. *Proc. Natl. Acad. Sci. U. S. A.* **104**, 654–9 (2007).
 628. Pertwee, R. G. The pharmacology of cannabinoid receptors and their ligands: an overview. *Int. J. Obes. (Lond)*. **30 Suppl 1**, S13-8 (2006).
 629. Raote, I., Bhattacharya, A. & Panicker, M. M. *Serotonin 2A (5-HT2A) Receptor Function: Ligand-Dependent Mechanisms and Pathways. Serotonin Receptors in Neurobiology* (CRC Press/Taylor & Francis, 2007).
 630. Eggan, S. M., Hashimoto, T. & Lewis, D. A. Reduced Cortical Cannabinoid 1 Receptor Messenger RNA and Protein Expression in Schizophrenia. *Arch. Gen. Psychiatry* **65**, 772 (2008).
 631. Molteni, R., Calabrese, F., Racagni, G., Fumagalli, F. & Riva, M. A. Antipsychotic drug actions on gene modulation and signaling mechanisms. *Pharmacol. Ther.* **124**, 74–85 (2009).
 632. Aringhieri, S. *et al.* Clozapine as the most efficacious antipsychotic for activating ERK 1/2 kinases: Role of 5-HT 2A receptor agonism. *Eur. Neuropsychopharmacol.* **27**, 383–398 (2017).

References

633. Borroto-Escuela, D. O. *et al.* Dopamine D2 receptor signaling dynamics of dopamine D2-neurotensin 1 receptor heteromers. *Biochem. Biophys. Res. Commun.* **435**, 140–146 (2013).
634. Bagher, A. M., Laprairie, R. B., Toguri, J. T., Kelly, M. E. M. & Denovan-Wright, E. M. Bidirectional allosteric interactions between cannabinoid receptor 1 (CB1) and dopamine receptor 2 long (D2L) heterotetramers. *Eur. J. Pharmacol.* **813**, 66–83 (2017).
635. Daigle, T. L., Kwok, M. L. & Mackie, K. Regulation of CB₁ cannabinoid receptor internalization by a promiscuous phosphorylation-dependent mechanism. *J. Neurochem.* **106**, 70–82 (2008).
636. Bellot, M. *et al.* Dual agonist occupancy of AT1-R- α 2C-AR heterodimers results in atypical Gs-PKA signaling. *Nat. Chem. Biol.* **11**, 271–9 (2015).
637. Navarro, G. *et al.* Cross-communication between Gi and Gs in a G-protein-coupled receptor heterotetramer guided by a receptor C-terminal domain. *BMC Biol.* **16**, 24 (2018).
638. Leterrier, C., Bonnard, D., Carrel, D., Rossier, J. & Lenkei, Z. Constitutive endocytic cycle of the CB1 cannabinoid receptor. *J. Biol. Chem.* **279**, 36013–21 (2004).
639. Carrillo, J. J., Pediani, J. & Milligan, G. Dimers of class A G protein-coupled receptors function via agonist-mediated trans-activation of associated G proteins. *J. Biol. Chem.* **278**, 42578–87 (2003).
640. Kang, Y. *et al.* Crystal structure of rhodopsin bound to arrestin by femtosecond X-ray laser. *Nature* **523**, 561–7 (2015).
641. Shukla, A. K. *et al.* Structure of active β -arrestin-1 bound to a G-protein-coupled receptor phosphopeptide. *Nature* **497**, 137–141 (2013).
642. Doumazane, E. *et al.* Illuminating the activation mechanisms and allosteric properties of metabotropic glutamate receptors. *Proc. Natl. Acad. Sci. U. S. A.* **110**, E1416-25 (2013).
643. Liu, J. *et al.* Allosteric control of an asymmetric transduction in a G protein-coupled receptor heterodimer. *Elife* **6**, (2017).
644. Navarro, G. *et al.* Orexin-corticotropin-releasing factor receptor heteromers in the ventral tegmental area as targets for cocaine. *J. Neurosci.* **35**, 6639–53 (2015).
645. Gupte, T. M., Malik, R. U., Sommese, R. F., Ritt, M. & Sivaramakrishnan, S. Priming GPCR signaling through the synergistic effect of two G proteins. *Proc. Natl. Acad. Sci. U. S. A.* **114**, 3756–3761 (2017).
646. García-Nafría, J., Nehmé, R., Edwards, P. C. & Tate, C. G. Cryo-EM structure of the serotonin 5-HT_{1B} receptor coupled to heterotrimeric Go. *Nature* **558**, 620–623 (2018).
647. Kang, Y. *et al.* Cryo-EM structure of human rhodopsin bound to an inhibitory G protein. *Nature* **558**, 553–558 (2018).
648. Draper-Joyce, C. J. *et al.* Structure of the adenosine-bound human adenosine A1 receptor–Gi complex. *Nature* **558**, 559–563 (2018).
649. Koehl, A. *et al.* Structure of the μ -opioid receptor–Gi protein complex. *Nature* **558**, 547–552 (2018).
650. Huntington, G. On Chorea. *Med. Surg. Report. A Wkly. J.* **25**, 317–321 (1872).
651. MacDonald, M. E. *et al.* A novel gene containing a trinucleotide repeat that is expanded and unstable on Huntington’s disease chromosomes. *Cell* **72**, 971–983 (1993).
652. Huntington’s disease: from molecular pathogenesis to clinical treatment. *Lancet*

- Neurol.* **10**, 83–98 (2011).
653. Ross, C. A. & Tabrizi, S. J. Huntington's disease: from molecular pathogenesis to clinical treatment. *Lancet Neurol.* **10**, 83–98 (2011).
654. Zuccato, C. & Cattaneo, E. in *Neurotrophic Factors* 357–409 (Springer, Berlin, Heidelberg, 2014). doi:10.1007/978-3-642-45106-5_14
655. Labbadia, J. & Morimoto, R. I. Huntington's disease: underlying molecular mechanisms and emerging concepts. *Trends Biochem. Sci.* **38**, 378–385 (2013).
656. Bäuerlein, F. J. B. *et al.* In Situ Architecture and Cellular Interactions of PolyQ Inclusions. *Cell* **171**, 179–187.e10 (2017).
657. Estrada Sánchez, A. M., Mejía-Toiber, J. & Massieu, L. Excitotoxic Neuronal Death and the Pathogenesis of Huntington's Disease. *Arch. Med. Res.* **39**, 265–276 (2008).
658. Shin, J.-Y. *et al.* Expression of mutant huntingtin in glial cells contributes to neuronal excitotoxicity. *J. Cell Biol.* **171**, 1001–1012 (2005).
659. Abdo, W. F., van de Warrenburg, B. P. C., Burn, D. J., Quinn, N. P. & Bloem, B. R. The clinical approach to movement disorders. *Nat. Rev. Neurol.* **6**, 29–37 (2010).
660. Chen, J. Y., Wang, E. A., Cepeda, C. & Levine, M. S. Dopamine imbalance in Huntington's disease: a mechanism for the lack of behavioral flexibility. *Front. Neurosci.* **7**, (2013).
661. Wersinger, C., Chen, J. & Sidhu, A. Bimodal induction of dopamine-mediated striatal neurotoxicity is mediated through both activation of D1 dopamine receptors and autoxidation. *Mol. Cell. Neurosci.* **25**, 124–137 (2004).
662. Frank, S. *et al.* Effect of Deutetrabenazine on Chorea Among Patients With Huntington Disease. *JAMA* **316**, 40 (2016).
663. Huntington Study Group. Tetrabenazine as antichorea therapy in Huntington disease: A randomized controlled trial. *Neurology* **66**, 366–372 (2006).
664. Tang, T.-S. *et al.* Modulation of type 1 inositol (1,4,5)-trisphosphate receptor function by protein kinase a and protein phosphatase 1alpha. *J. Neurosci.* **23**, 403–15 (2003).
665. Mestre, T., Ferreira, J., Coelho, M. M., Rosa, M. & Sampaio, C. Therapeutic interventions for symptomatic treatment in Huntington's disease. *Cochrane Database Syst. Rev.* CD006456 (2009). doi:10.1002/14651858.CD006456.pub2
666. Han, I., You, Y., Kordower, J. H., Brady, S. T. & Morfini, G. A. Differential vulnerability of neurons in Huntington's disease: the role of cell type-specific features. *J. Neurochem.* **113**, 1073–91 (2010).
667. Cepeda, C. *et al.* Differential electrophysiological properties of dopamine D1 and D2 receptor-containing striatal medium-sized spiny neurons. *Eur. J. Neurosci.* **27**, 671–682 (2008).
668. Spokes, E. G. S. The neurochemistry of Huntington's chorea. *Trends Neurosci.* **4**, 115–118 (1981).
669. André, V. M., Fisher, Y. E. & Levine, M. S. Altered Balance of Activity in the Striatal Direct and Indirect Pathways in Mouse Models of Huntington's Disease. *Front. Syst. Neurosci.* **5**, 46 (2011).
670. André, V. M. *et al.* Differential electrophysiological changes in striatal output neurons in Huntington's disease. *J. Neurosci.* **31**, 1170–82 (2011).
671. Giménez-Llort, L., Martínez, E. & Ferré, S. Different Effects of Dopamine Antagonists on Spontaneous and NMDA-Induced Motor Activity in Mice. *Pharmacol. Biochem. Behav.* **56**, 549–553 (1997).
672. Frank, S. *et al.* A study of chorea after tetrabenazine withdrawal in patients with

References

- Huntington disease. *Clin. Neuropharmacol.* **31**, 127–133 (2008).
673. Alfaro-Rodriguez, A. *et al.* Histamine H3 receptor activation prevents dopamine D1 receptor-mediated inhibition of dopamine release in the rat striatum: A microdialysis study. *Neurosci. Lett.* **552**, 5–9 (2013).
674. Swapna, I., Bondy, B. & Morikawa, H. Differential Dopamine Regulation of Ca²⁺ Signaling and Its Timing Dependence in the Nucleus Accumbens. *Cell Rep.* **15**, 563–573 (2016).
675. Guitart, X. *et al.* Functional Selectivity of Allosteric Interactions within G Protein–Coupled Receptor Oligomers: The Dopamine D₁-D₃ Receptor Heterotetramer. *Mol. Pharmacol. Mol Pharmacol* **86**, 417–429 (2014).
676. Tang, T.-S. *et al.* Disturbed Ca²⁺ signaling and apoptosis of medium spiny neurons in Huntington’s disease. *Proc. Natl. Acad. Sci. U. S. A.* **102**, 2602–7 (2005).
677. Shehadeh, J. *et al.* Striatal neuronal apoptosis is preferentially enhanced by NMDA receptor activation in YAC transgenic mouse model of Huntington disease. *Neurobiol. Dis.* **21**, 392–403 (2006).
678. Uto-Konomi, A. *et al.* CXCR7 agonists inhibit the function of CXCL12 by down-regulation of CXCR4. *Biochemical and Biophysical Research Communications* **431**, (2013).
679. Jocoy, E. L. *et al.* Dissecting the contribution of individual receptor subunits to the enhancement of N-methyl-d-aspartate currents by dopamine D1 receptor activation in striatum. *Front. Syst. Neurosci.* **5**, 28 (2011).
680. Fiorentini, C., Gardoni, F., Spano, P., Di Luca, M. & Missale, C. Regulation of Dopamine D₁ Receptor Trafficking and Desensitization by Oligomerization with Glutamate N-Methyl-D-aspartate Receptors. *J. Biol. Chem.* **278**, 20196–20202 (2003).
681. Rajagopal, S., Rajagopal, K. & Lefkowitz, R. J. Teaching old receptors new tricks: biasing seven-transmembrane receptors. *Nat. Rev. Drug Discov.* **9**, 373–386 (2010).
682. Kotowski, S. J., Hopf, F. W., Seif, T., Bonci, A. & von Zastrow, M. Endocytosis promotes rapid dopaminergic signaling. *Neuron* **71**, 278–290 (2011).
683. Joyce, J. N., Lexow, N., Bird, E. & Winokur, A. Organization of dopamine D1 and D2 receptors in human striatum: Receptor autoradiographic studies in Huntington’s disease and schizophrenia. *Synapse* **2**, 546–557 (1988).
684. Turjanski, N., Weeks, R., Dolan, R., Harding, A. E. & Brooks, D. J. Striatal D1 and D2 receptor binding in patients with Huntington’s disease and other choreas. A PET study. *Brain* **118 (Pt 3)**, 689–96 (1995).
685. Ariano, M. A. *et al.* Striatal neurochemical changes in transgenic models of Huntington’s disease. *J. Neurosci. Res.* **68**, 716–729 (2002).
686. André, V. M., Fisher, Y. E. & Levine, M. S. Altered Balance of Activity in the Striatal Direct and Indirect Pathways in Mouse Models of Huntington’s Disease. *Front. Syst. Neurosci.* **5**, 46 (2011).
687. Wheeler, V. C. *et al.* Length-dependent gametic CAG repeat instability in the Huntington’s disease knock-in mouse. *Hum. Mol. Genet.* **8**, 115–22 (1999).
688. Menalled, L. B. Knock-in mouse models of Huntington’s disease. *NeuroRx* **2**, 465–70 (2005).
689. Lloret, A. *et al.* Genetic background modifies nuclear mutant huntingtin accumulation and HD CAG repeat instability in Huntington’s disease knock-in mice. *Hum. Mol. Genet.* **15**, 2015–2024 (2006).
690. Lin, C. H. *et al.* Neurological abnormalities in a knock-in mouse model of Huntington’s disease. *Hum. Mol. Genet.* **10**, 137–44 (2001).

691. Dallérac, G. M., Cummings, D. M., Hirst, M. C., Milnerwood, A. J. & Murphy, K. P. S. J. Changes in Dopamine Signalling Do Not Underlie Aberrant Hippocampal Plasticity in a Mouse Model of Huntington's Disease. *NeuroMolecular Med.* **18**, 146–153 (2016).
692. Wang, Y. *et al.* Age-dependent decline of dopamine D1 receptors in human brain: A PET study. *Synapse* **30**, 56–61 (1998).
693. Amenta, F. *et al.* Age-related changes of dopamine receptors in the rat hippocampus: a light microscope autoradiography study. *Mech. Ageing Dev.* **122**, 2071–83 (2001).
694. Giralt, A. *et al.* Long-term memory deficits in Huntington's disease are associated with reduced CBP histone acetylase activity. *Hum. Mol. Genet.* **21**, 1203–1216 (2012).
695. Brito, V. *et al.* Neurotrophin receptor p75NTR mediates Huntington's disease-associated synaptic and memory dysfunction. *J. Clin. Invest.* **124**, 4411–4428 (2014).
696. Marco, S. *et al.* Suppressing aberrant GluN3A expression rescues synaptic and behavioral impairments in Huntington's disease models. *Nat. Med.* **19**, 1030–1038 (2013).
697. Charvin, D. *et al.* Unraveling a role for dopamine in Huntington's disease: The dual role of reactive oxygen species and D2 receptor stimulation. *Proc. Natl. Acad. Sci.* **102**, 12218–12223 (2005).
698. Brusa, L. *et al.* Treatment of the symptoms of Huntington's disease: Preliminary results comparing aripiprazole and tetrabenazine. *Mov. Disord.* **24**, 126–129 (2009).
699. Venuto, C. S., McGarry, A., Ma, Q. & Kiebertz, K. Pharmacologic approaches to the treatment of Huntington's disease. *Mov. Disord.* **27**, 31–41 (2012).
700. Bano, D. *et al.* Cleavage of the Plasma Membrane Na⁺/Ca²⁺ Exchanger in Excitotoxicity. *Cell* **120**, 275–285 (2005).
701. Spokes, E. G. S. The neurochemistry of Huntington's chorea. *Trends Neurosci.* **4**, 115–118 (1981).
702. Reiner, A., Dragatsis, I. & Dietrich, P. Genetics and neuropathology of Huntington's disease. *Int. Rev. Neurobiol.* **98**, 325–72 (2011).
703. Lemiere, J., Decruyenaere, M., Evers-Kiebooms, G., Vandenbussche, E. & Dom, R. Cognitive changes in patients with Huntington's disease (HD) and asymptomatic carriers of the HD mutation. *J. Neurol.* **251**, 935–42 (2004).
704. Begeti, F., Schwab, L. C., Mason, S. L. & Barker, R. A. Hippocampal dysfunction defines disease onset in Huntington's disease. *J. Neurol. Neurosurg. Psychiatry* **87**, 975–981 (2016).
705. Giralt, A., Saavedra, A., Alberch, J. & Pérez-Navarro, E. Cognitive Dysfunction in Huntington's Disease: Humans, Mouse Models and Molecular Mechanisms. *J. Huntingtons. Dis.* **1**, 155–73 (2012).
706. Luo, T., Wang, Y., Qin, J., Liu, Z. G. & Liu, M. Histamine H3 Receptor Antagonist Prevents Memory Deficits and Synaptic Plasticity Disruption Following Isoflurane Exposure. *CNS Neurosci. Ther.* **23**, 301–309 (2017).
707. Jay, T. M. Dopamine: a potential substrate for synaptic plasticity and memory mechanisms. *Prog. Neurobiol.* **69**, 375–90 (2003).
708. André, V. M., Cepeda, C. & Levine, M. S. Dopamine and glutamate in Huntington's disease: A balancing act. *CNS Neurosci. Ther.* **16**, 163–178 (2010).
709. Wiescholleck, V. & Manahan-Vaughan, D. Antagonism of D1/D5 receptors prevents long-term depression (LTD) and learning-facilitated LTD at the perforant path-dentate gyrus synapse in freely behaving rats. *Hippocampus* **24**, 1615–1622 (2014).

References

710. Vijayraghavan, S., Wang, M., Birnbaum, S. G., Williams, G. V & Arnsten, A. F. T. Inverted-U dopamine D1 receptor actions on prefrontal neurons engaged in working memory. *Nat. Neurosci.* **10**, 376–384 (2007).
711. Mattay, V. S. *et al.* Catechol O-methyltransferase val158-met genotype and individual variation in the brain response to amphetamine. *Proc. Natl. Acad. Sci.* **100**, 6186–6191 (2003).
712. Kern, A., Albarran-Zeckler, R., Walsh, H. E. & Smith, R. G. Apo-Ghrelin Receptor Forms Heteromers with DRD2 in Hypothalamic Neurons and Is Essential for Anorexigenic Effects of DRD2 Agonism. *Neuron* **73**, 317–332 (2012).
713. Baba, K. *et al.* Heteromeric MT1/MT2 Melatonin Receptors Modulate Photoreceptor Function. *Sci. Signal.* **6**, ra89-ra89 (2013).
714. WHO | Obesity and overweight. *WHO* (2018). Available at: <http://www.who.int/mediacentre/factsheets/fs311/en/>. (Accessed: 25th March 2018)
715. Di Cesare, M. *et al.* Trends in adult body-mass index in 200 countries from 1975 to 2014: A pooled analysis of 1698 population-based measurement studies with 19.2 million participants. *The Lancet* **387**, 1377–1396 (2016).
716. García-Cárceles, J. *et al.* A Positive Allosteric Modulator of the Serotonin 5-HT_{2C} Receptor for Obesity. *J. Med. Chem.* **60**, 9575–9584 (2017).
717. Deng, T., Lyon, C. J., Bergin, S., Caligiuri, M. A. & Hsueh, W. A. Obesity, Inflammation, and Cancer. *Annu. Rev. Pathol. Mech. Dis.* **11**, 421–449 (2016).
718. De Pergola, G. & Silvestris, F. Obesity as a major risk factor for cancer. *J. Obes.* **2013**, 291546 (2013).
719. Bocarsly, M. E. *et al.* Obesity diminishes synaptic markers, alters microglial morphology, and impairs cognitive function. *Proc. Natl. Acad. Sci.* **112**, 201511593 (2015).
720. Hruby, A. & Hu, F. B. The Epidemiology of Obesity: A Big Picture. *Pharmacoeconomics* **33**, 673–89 (2015).
721. Butryn, M. L., Webb, V. & Wadden, T. A. Behavioral treatment of obesity. *Psychiatr. Clin. North Am.* **34**, 841–59 (2011).
722. Onakpoya, I. J., Heneghan, C. J. & Aronson, J. K. Post-marketing withdrawal of anti-obesity medicinal products because of adverse drug reactions: a systematic review. *BMC Med.* **14**, 191 (2016).
723. Fidler, M. C. *et al.* A One-Year Randomized Trial of Lorcaserin for Weight Loss in Obese and Overweight Adults: The BLOSSOM Trial. *J. Clin. Endocrinol. Metab.* **96**, 3067–3077 (2011).
724. Smith, S. R. *et al.* Multicenter, Placebo-Controlled Trial of Lorcaserin for Weight Management. *N. Engl. J. Med.* **363**, 245–256 (2010).
725. Pompeiano, M., Palacios, J. M. & Mengod, G. Distribution of the serotonin 5-HT₂ receptor family mRNAs: comparison between 5-HT_{2A} and 5-HT_{2C} receptors. *Brain Res. Mol. Brain Res.* **23**, 163–78 (1994).
726. Garfield, A. S. & Heisler, L. K. Pharmacological targeting of the serotonergic system for the treatment of obesity. *J. Physiol.* **587**, 49–60 (2009).
727. Sargent, B. J. & Moore, N. A. New central targets for the treatment of obesity. *Br. J. Clin. Pharmacol.* **68**, 852–60 (2009).
728. Fisas, A. *et al.* Chronic 5-HT₆ receptor modulation by E-6837 induces hypophagia and sustained weight loss in diet-induced obese rats. *Br. J. Pharmacol.* **148**, 973–983 (2009).

729. Garfield, A. S., Burke, L. K., Shaw, J., Evans, M. L. & Heisler, L. K. Distribution of cells responsive to 5-HT₆ receptor antagonist-induced hypophagia. *Behav. Brain Res.* **266**, 201–206 (2014).
730. Iwamoto, K., Bundo, M. & Kato, T. Serotonin receptor 2C and mental disorders: genetic, expression and RNA editing studies. *RNA Biol.* **6**, 248–53 (2009).
731. Di Giovanni, G. & De Deurwaerdère, P. New therapeutic opportunities for 5-HT_{2C} receptor ligands in neuropsychiatric disorders. *Pharmacol. Ther.* **157**, 125–162 (2016).
732. Burke, L. K. & Heisler, L. K. 5-Hydroxytryptamine Medications for the Treatment of Obesity. *J. Neuroendocrinol.* **27**, 389–398 (2015).
733. Higgins, G. A., Zeeb, F. D. & Fletcher, P. J. Role of impulsivity and reward in the anti-obesity actions of 5-HT_{2C} receptor agonists. *J. Psychopharmacol.* **31**, 1403–1418 (2017).
734. Valencia-Torres, L. *et al.* Activation of Ventral Tegmental Area 5-HT_{2C} Receptors Reduces Incentive Motivation. *Neuropsychopharmacology* **42**, 1511–1521 (2017).
735. Shanahan, W. R., Rose, J. E., Glicklich, A., Stubbe, S. & Sanchez-Kam, M. Lorcaserin for Smoking Cessation and Associated Weight Gain: A Randomized 12-Week Clinical Trial. *Nicotine Tob. Res.* **19**, ntw301 (2016).
736. Rezvani, A. H., Cauley, M. C. & Levin, E. D. Lorcaserin, a selective 5-HT_{2C} receptor agonist, decreases alcohol intake in female alcohol preferring rats. *Pharmacol. Biochem. Behav.* **125**, 8–14 (2014).
737. Lorcaserin in the Treatment of Cocaine Use Disorder (NCT03007394). Available at: <https://clinicaltrials.gov/ct2/show/NCT03007394>. (Accessed: 26th August 2018)
738. Jaffre, F. *et al.* Involvement of the Serotonin 5-HT_{2B} Receptor in Cardiac Hypertrophy Linked to Sympathetic Stimulation: Control of Interleukin-6, Interleukin-1, and Tumor Necrosis Factor- Cytokine Production by Ventricular Fibroblasts. *Circulation* **110**, 969–974 (2004).
739. Miller, K. J. Serotonin 5-HT_{2C} receptor agonists: potential for the treatment of obesity. *Mol. Interv.* **5**, 282–291 (2005).
740. Rothman, R. B. *et al.* Evidence for possible involvement of 5-HT_{2B} receptors in the cardiac valvulopathy associated with fenfluramine and other serotonergic medications. *Circulation* **102**, 2836–41 (2000).
741. Foster, D. J. & Conn, P. J. Allosteric Modulation of GPCRs: New Insights and Potential Utility for Treatment of Schizophrenia and Other CNS Disorders. *Neuron* **94**, 431–446 (2017).
742. Jeffrey Conn, P., Christopoulos, A. & Lindsley, C. W. Allosteric modulators of GPCRs: a novel approach for the treatment of CNS disorders. *Nat. Rev. Drug Discov.* **8**, 41–54 (2009).
743. Im, W. B., Chio, C. L., Alberts, G. L. & Dinh, D. M. Positive Allosteric Modulator of the Human 5-HT_{2C} Receptor. *Mol. Pharmacol.* **64**, 78–84 (2003).
744. McAllister, C. E. *et al.* In vivo evaluation of novel serotonin 5-HT_{2C} receptor positive allosteric modulator CYD-1-79. *Drug Alcohol Depend.* **156**, e144 (2015).
745. Ding, C. *et al.* Exploration of Synthetic Approaches and Pharmacological Evaluation of PNU-69176E and Its Stereoisomer as 5-HT_{2C} Receptor Allosteric Modulators. *ACS Chem. Neurosci.* **3**, 538–545 (2012).
746. Wild, C. T. *et al.* Design, Synthesis, and Characterization of 4-Undecylpiperidine-2-carboxamides as Positive Allosteric Modulators of the Serotonin (5-HT) 5-HT_{2C} Receptor. *J. Med. Chem.* **acs.jmedchem.8b00401** (2018). doi:10.1021/acs.jmedchem.8b00401

References

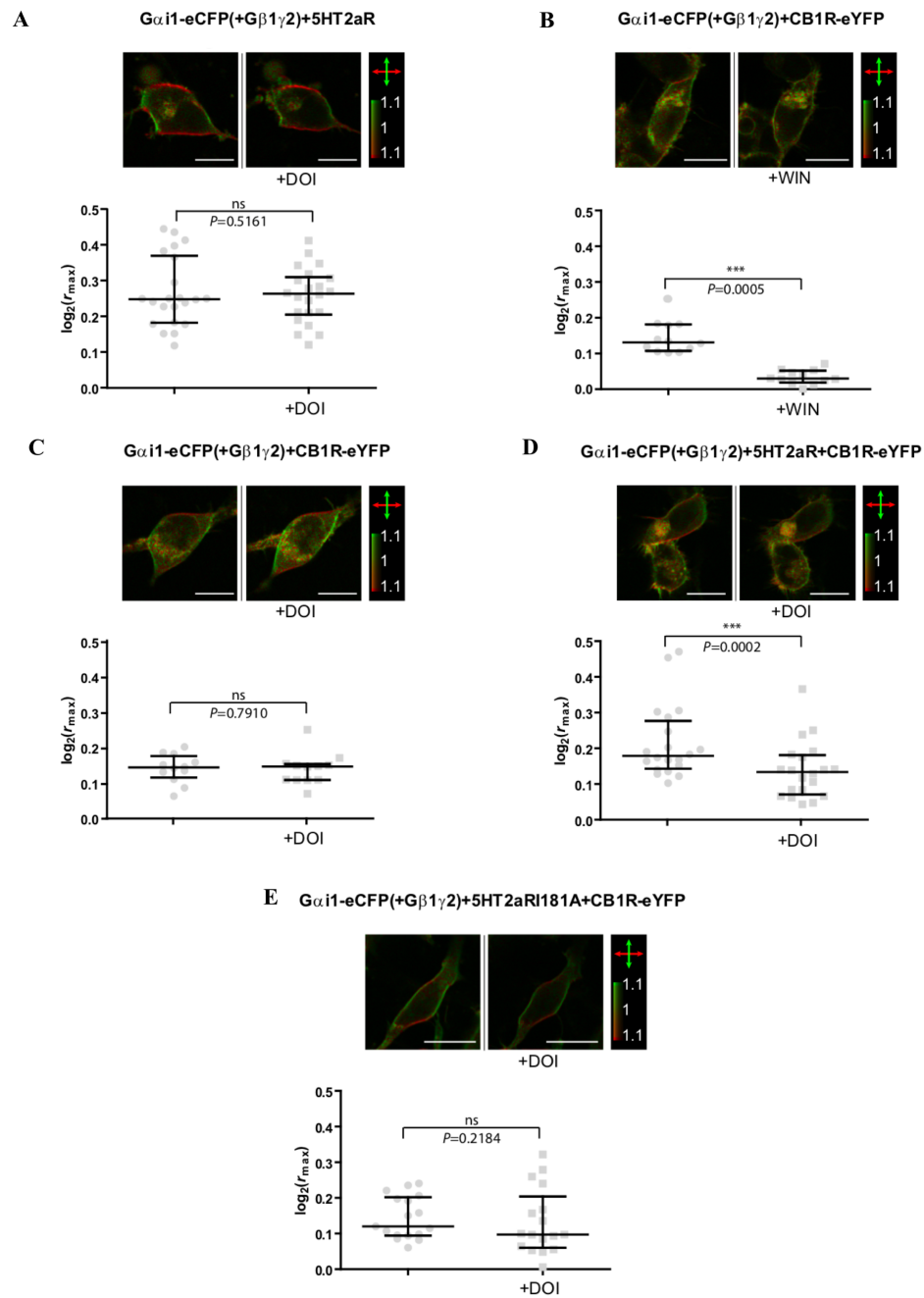
747. Hoyer, D., Hannon, J. P. & Martin, G. R. Molecular, pharmacological and functional diversity of 5-HT receptors. *Pharmacol. Biochem. Behav.* **71**, 533–54 (2002).
748. Chen, T.-W. *et al.* Ultrasensitive fluorescent proteins for imaging neuronal activity. *Nature* **499**, 295–300 (2013).
749. Korczynska, M. *et al.* Structure-based discovery of selective positive allosteric modulators of antagonists for the M2 muscarinic acetylcholine receptor. *Proc. Natl. Acad. Sci. U. S. A.* **115**, E2419–E2428 (2018).
750. Kruse, A. C. *et al.* Activation and allosteric modulation of a muscarinic acetylcholine receptor. *Nature* **504**, 101–106 (2013).
751. Roth, B. L. Drugs and Valvular Heart Disease. *N. Engl. J. Med.* **356**, 6–9 (2007).
752. Cheng, J. *et al.* Design and Discovery of Functionally Selective Serotonin 2C (5-HT_{2C}) Receptor Agonists. *J. Med. Chem.* **59**, 9866–9880 (2016).
753. Higgins, G. A., Sellers, E. M. & Fletcher, P. J. From obesity to substance abuse: therapeutic opportunities for 5-HT_{2C} receptor agonists. *Trends Pharmacol. Sci.* **34**, 560–70 (2013).
754. de Matos Feijó, F., Bertoluci, M. C. & Reis, C. Serotonin and hypothalamic control of hunger: a review. *Rev. da Assoc. Médica Bras. (English Ed.)* **57**, 74–77 (2011).
755. Halford, J. C. G., Harrold, J. A., Boyland, E. J., Lawton, C. L. & Blundell, J. E. Serotonergic drugs : effects on appetite expression and use for the treatment of obesity. *Drugs* **67**, 27–55 (2007).
756. Nonogaki, K. *et al.* Fluvoxamine, a selective serotonin reuptake inhibitor, and 5-HT_{2C} receptor inactivation induce appetite-suppressing effects in mice via 5-HT_{1B} receptors. *Int. J. Neuropsychopharmacol.* **10**, 675–81 (2007).
757. Nielsen, J. A., Chapin, D. S., Johnson, J. L. & Torgersen, L. K. Sertraline, a serotonin-uptake inhibitor, reduces food intake and body weight in lean rats and genetically obese mice. *Am. J. Clin. Nutr.* **55**, 185S–189S (1992).
758. Dawes, A. J. *et al.* Mental Health Conditions Among Patients Seeking and Undergoing Bariatric Surgery. *JAMA* **315**, 150 (2016).
759. Luppino, F. S. *et al.* Overweight, Obesity, and Depression. *Arch. Gen. Psychiatry* **67**, 220 (2010).
760. Gregory, K., Sexton, P. & Christopoulos, A. Allosteric Modulation of Muscarinic Acetylcholine Receptors. *Curr. Neuropharmacol.* **5**, 157–167 (2007).
761. Kruse, A. C. in *Multifaceted Roles of Crystallography in Modern Drug Discovery* 19–26 (2015). doi:10.1007/978-94-017-9719-1_2
762. Roth, B. L. Drugs and Valvular Heart Disease. *N. Engl. J. Med.* **356**, 6–9 (2007).
763. Schade, R., Andersohn, F., Suissa, S., Haverkamp, W. & Garbe, E. Dopamine Agonists and the Risk of Cardiac-Valve Regurgitation. *N. Engl. J. Med.* **356**, 29–38 (2007).
764. Zanettini, R. *et al.* Valvular Heart Disease and the Use of Dopamine Agonists for Parkinson's Disease. *N. Engl. J. Med.* **356**, 39–46 (2007).
765. DiNicolantonio, J. J., Chatterjee, S., O'Keefe, J. H. & Meier, P. Lorcaserin for the treatment of obesity? A closer look at its side effects. *Open Hear.* **1**, e000173 (2014).
766. Thomsen, W. J. *et al.* Lorcaserin, a novel selective human 5-hydroxytryptamine_{2C} agonist: in vitro and in vivo pharmacological characterization. *J. Pharmacol. Exp. Ther.* **325**, 577–87 (2008).
767. Gustafson, A., King, C. & Rey, J. A. Lorcaserin (Belviq): A Selective Serotonin 5-HT_{2C} Agonist In the Treatment of Obesity. *P T* **38**, 525–34 (2013).

768. Melancon, B. J. *et al.* Allosteric Modulation of Seven Transmembrane Spanning Receptors: Theory, Practice, and Opportunities for Central Nervous System Drug Discovery. *J. Med. Chem.* **55**, 1445–1464 (2012).
769. Conn, P. J., Kuduk, S. D. & Doller, D. Drug Design Strategies for GPCR Allosteric Modulators. *Annu. Rep. Med. Chem.* **47**, 441–457 (2012).
770. Beuming, T. *et al.* Docking and virtual screening strategies for GPCR drug discovery. *Methods Mol. Biol.* **1335**, 251–276 (2015).
771. Manglik, A. *et al.* Structure-based discovery of opioid analgesics with reduced side effects. *Nature* **537**, 185–190 (2016).
772. Zheng, Y. *et al.* Structure of CC chemokine receptor 2 with orthosteric and allosteric antagonists. *Nature* **540**, 458–461 (2016).
773. Zhang, D. *et al.* Two disparate ligand-binding sites in the human P2Y1 receptor. *Nature* **520**, 317–321 (2015).
774. Song, G. *et al.* Human GLP-1 receptor transmembrane domain structure in complex with allosteric modulators. *Nature* **546**, 312–315 (2017).
775. Jazayeri, A. *et al.* Extra-helical binding site of a glucagon receptor antagonist. *Nature* **533**, 274–277 (2016).
776. Liu, W. *et al.* Structural basis for allosteric regulation of GPCRs by sodium ions. *Science* **337**, 232–6 (2012).
777. Huang, X.-P. *et al.* Allosteric ligands for the pharmacologically dark receptors GPR68 and GPR65. *Nature* **527**, 477–483 (2015).
778. Parmentier-Batteur, S. *et al.* Mechanism based neurotoxicity of mGlu5 positive allosteric modulators – Development challenges for a promising novel antipsychotic target. *Neuropharmacology* **82**, 161–173 (2014).
779. Rook, J. M. *et al.* Biased mGlu5-Positive Allosteric Modulators Provide In Vivo Efficacy without Potentiating mGlu5 Modulation of NMDAR Currents. *Neuron* **86**, 1029–1040 (2015).
780. Laschet, C., Dupuis, N. & Hanson, J. A dynamic and screening-compatible nanoluciferase-based complementation assay enables profiling of individual GPCR-G protein interactions. *J. Biol. Chem.* jbc.RA118.006231 (2018). doi:10.1074/jbc.RA118.006231
781. Carpenter, B. & Tate, C. G. Engineering a minimal G protein to facilitate crystallisation of G protein-coupled receptors in their active conformation. *Protein Eng. Des. Sel.* **29**, 583–594 (2016).
782. Marquer, C. *et al.* Influence of MT7 toxin on the oligomerization state of the M1 muscarinic receptor1. *Biol. Cell* **102**, 409–420 (2010).
783. Bernal, F. *et al.* A Stapled p53 Helix Overcomes HDMX-Mediated Suppression of p53. *Cancer Cell* **18**, 411–422 (2010).
784. Ruan, H. *et al.* Stapled RGD Peptide Enables Glioma-Targeted Drug Delivery by Overcoming Multiple Barriers. *ACS Appl. Mater. Interfaces* **9**, 17745–17756 (2017).
785. Bird, G. H. *et al.* Stapled HIV-1 peptides recapitulate antigenic structures and engage broadly neutralizing antibodies. *Nat. Struct. Mol. Biol.* **21**, 1058–1067 (2014).
786. Kenakin, T. & Christopoulos, A. Signalling bias in new drug discovery: detection, quantification and therapeutic impact. *Nat. Rev. Drug Discov.* **12**, 205–216 (2012).
787. Calebiro, D. *et al.* Single-molecule analysis of fluorescently labeled G-protein-coupled receptors reveals complexes with distinct dynamics and organization. *Proc. Natl. Acad. Sci. U. S. A.* **110**, 743–8 (2013).

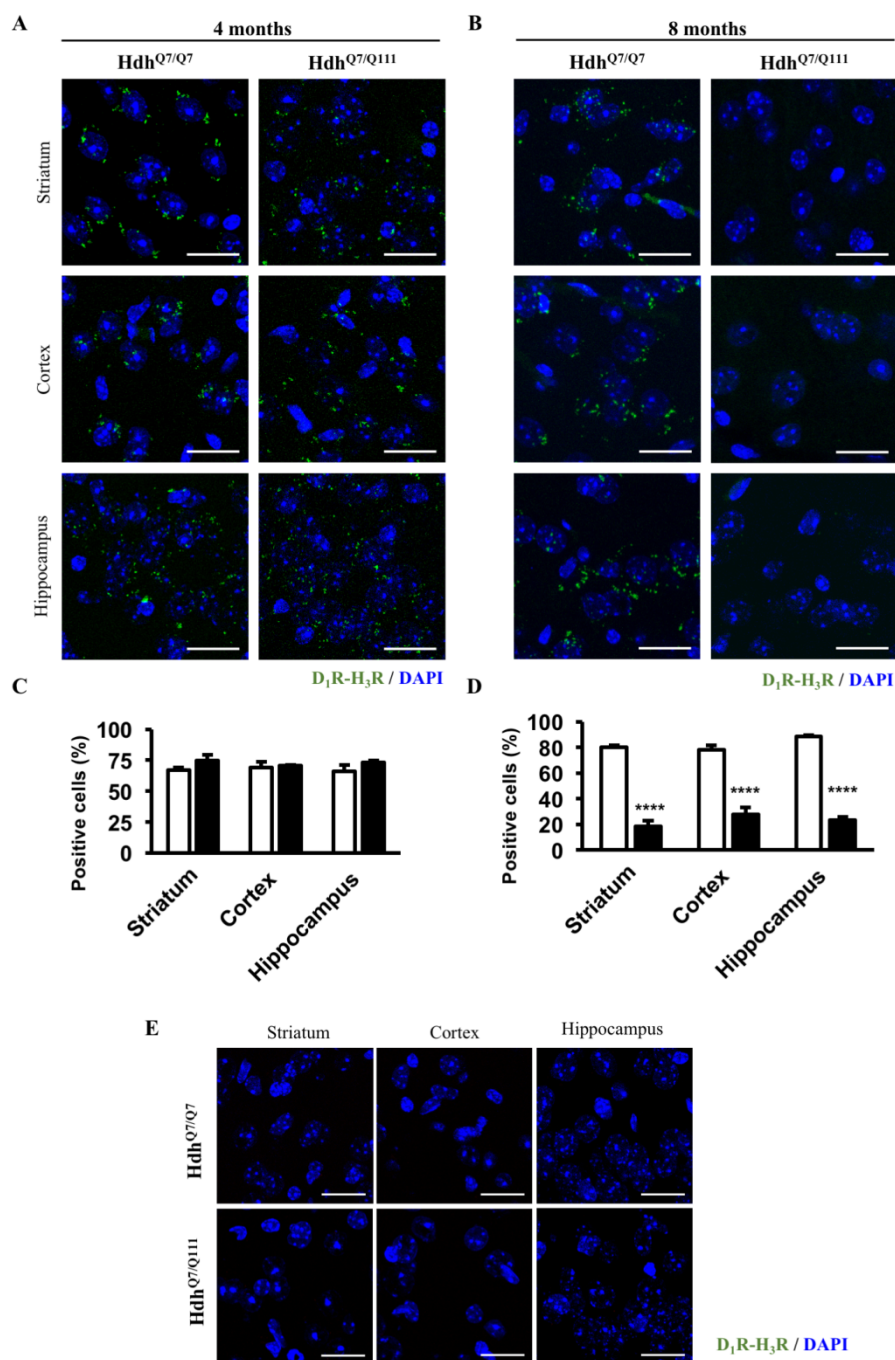
References

788. Tabor, A. *et al.* Visualization and ligand-induced modulation of dopamine receptor dimerization at the single molecule level. *Sci. Rep.* **6**, 33233 (2016).
789. Patel, R. C. *et al.* Ligand binding to somatostatin receptors induces receptor-specific oligomer formation in live cells. *Proc. Natl. Acad. Sci.* **99**, 3294–3299 (2002).
790. Felce, J. H., Davis, S. J. & Klenerman, D. Single-Molecule Analysis of G Protein-Coupled Receptor Stoichiometry: Approaches and Limitations. *Trends Pharmacol. Sci.* **39**, 96–108 (2018).
791. Milligan, G. G protein-coupled receptor hetero-dimerization: contribution to pharmacology and function. *Br. J. Pharmacol.* **158**, 5–14 (2009).
792. Kobilka, B. The structural basis of G-protein-coupled receptor signaling (Nobel Lecture). *Angew. Chem. Int. Ed. Engl.* **52**, 6380–8 (2013).
793. Lefkowitz, R. J. A Brief History of G-Protein Coupled Receptors (Nobel Lecture). *Angew. Chemie Int. Ed.* **52**, 6366–6378 (2013).
794. Boothe, T. *et al.* Inter-domain tagging implicates caveolin-1 in insulin receptor trafficking and Erk signaling bias in pancreatic beta-cells. *Mol. Metab.* **5**, 366–378 (2016).
795. Irwin, J. J. & Shoichet, B. K. ZINC--a free database of commercially available compounds for virtual screening. *J. Chem. Inf. Model.* **45**, 177–82
796. Mansouri, M. *et al.* Highly efficient baculovirus-mediated multigene delivery in primary cells. *Nat. Commun.* **7**, 11529 (2016).
797. Fitzgerald, D. J. *et al.* Protein complex expression by using multigene baculoviral vectors. *Nat. Methods* **3**, 1021–1032 (2006).

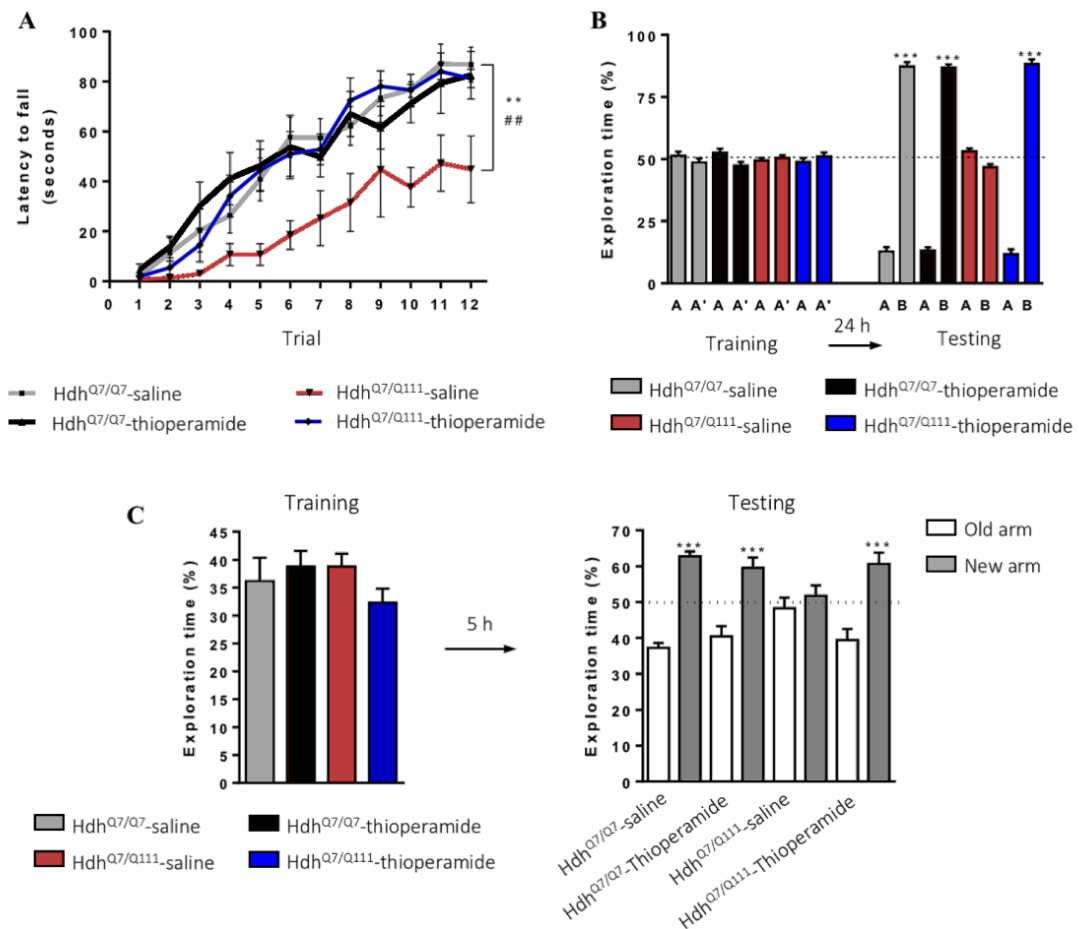
Annex I



Supplementary figure 1. 5-HT_{2A}R-CB₁R heteromers-driven G protein class switch occurs at the plasma membrane. HEK293 cells were transfected with GAP43-eCFP-Gai1, Gβ1 and Gγ2 subunits, as well as with 5-HT_{2A}R (A), CB₁R-eYFP (B and C), 5-HT_{2A}R and CB₁R-eYFP (D) or 5-HT_{2A}RI181A and CB₁R-eYFP (E). DOI or WIN was applied as indicated in the images and graphs. Images show representative cells before and after application of the appropriate agonist. Colour bars indicate the range of dichroic ratios shown in the images. Scale bars are 10 μm. Graphs show linear dichroism (values of $\log_2(r_{max})$) of individual cells (individual data points), along with the median and 25th and 75th percentiles. G protein activation was observed in B and D, as indicated by the significant decrease of $\log_2(r_{max})$ values upon agonist application. Statistical significance over treatments was evaluated by Wilcoxon signed rank test. (***)p < 0.001. ns: non-statistically significant.



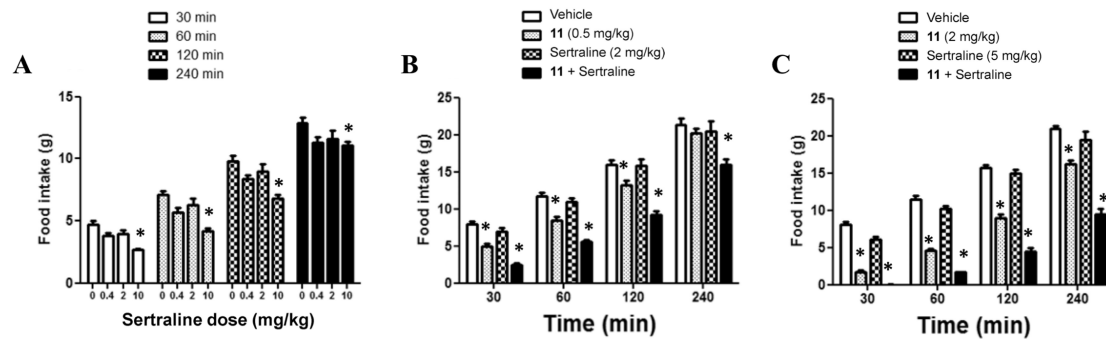
Supplementary figure 2. D₁R-H₃R heteromers are lost in 8-months old HdhQ^{7/111} HD mice. Representative striatal, cortical and hippocampal Proximity Ligation Assays (PLAs) confocal microscopy images of 4 months (**A**) and 8-months old (**B**) wild type Hdh^{Q7/7} and HD Hdh^{Q7/111} mice. D₁R-H₃R heteromers (green puncta) were visualised in 4-months old Hdh^{Q7/7} and Hdh^{Q7/111} and in 8-months old Hdh^{Q7/7} but not in 8-months old Hdh^{Q7/111} mice surrounding the blue nucleus stained with DAPI. Scale bars: 20 μ m. Quantification of the percentage of positive cells respect to the total number of cells (blue stained nucleus) in 4 months (**C**) and 8 months-old (**D**) mice. Data are mean \pm SEM percentage of positive cells (600-800 cells from 4-8 fields from 3 different animals). Statistical significance was evaluated by two-way ANOVA followed by Bonferroni post hoc tests showing significant differences (***p \leq 0.001) in heteromer expression between genotypes. In (**E**), negative PLA controls showing representative striatal, cortical and hippocampal confocal microscopy images of 4-months old Hdh^{Q7/7} and HD Hdh^{Q7/111} mice performed in the absence of the primary antibody against D₁R. Scale bars: 20 μ m.



Supplementary figure 3. Chronic administration of the H₃R antagonist Thioperamide prevents motor learning and long-term memory deficits in 6-months old Hdh^{Q7/111} HD mice. In (A), latency to fall in the accelerating rotarod task of 6-months old wild type Hdh^{Q7/Q7} and HD Hdh^{Q7/Q111} mice chronically treated with the H₃R antagonist Thioperamide since the 5th month of age. Data are mean \pm SEM of the latency to fall. Statistical significance was evaluated by two-way ANOVA with repeated measures of saline-treated Hdh^{Q7/Q7} versus Hdh^{Q7/Q111} (** $p \leq 0.01$) or between saline-treated Hdh^{Q7/111} versus Thioperamide-treated Hdh^{Q7/Q111} (## $p \leq 0.01$). In (B), the left panels illustrate the exploration time for saline and Thioperamide-treated Hdh^{Q7/Q7} and Hdh^{Q7/Q111} mice in the novel object recognition test (NORT) over the training session. 24 hours later (right panel), the NORT testing session was performed, showing long-term memory (LTM) deficits reversion in Thioperamide-treated Hdh^{Q7/Q111}. Data are mean \pm SEM percentage of exploration time. Statistical significance was evaluated by one-way ANOVA followed by Bonferroni post hoc tests showing significant differences between the time spent in the old versus the new object (** $p \leq 0.001$). In (C), the left panel illustrates the exploration time for saline and Thioperamide-treated Hdh^{Q7/Q7} and Hdh^{Q7/Q111} mice over the training session. 5 hours later, the T-maze spontaneous alternation task (T-SAT) was performed, showing reversion in the spatial LTM deficits in Thioperamide-treated Hdh^{Q7/Q111}. Data are mean \pm SEM percentage of exploration time. Statistical significance was evaluated by one-way ANOVA followed by Bonferroni post hoc tests showing significant differences between time spent in the old versus the new arm (** $p \leq 0.001$). These results correspond to 11 and 7 saline-treated

Annexes

Hdh^{Q7/Q7} and Hdh^{Q7/Q111} mice, respectively, and 10 and 9 Thioperamide-treated Hdh^{Q7/Q7} and Hdh^{Q7/Q111} mice, respectively.



Supplementary figure 4. Compound 11 displays *in vivo* positive allosteric modulation of 5-HT-induced feeding suppression. (A) Mild feeding suppression over time in rats administrated with increasing doses (see figure legends) of the selective serotonin reuptake inhibitor sertraline. (B and C) Compound 11 dose-dependently potentiates the anorectic effects of increasing 5-HT levels with sertraline. Data are mean \pm SEM food intake of at least 8 animals/group. Statistical significance between the treatments and the time of testing were evaluated by two-way analysis of variance (ANOVA) followed by Bonferroni post hoc tests indicating significant differences over control animals (* $p \leq 0.01$). Gaussian distribution ($p > 0.1$) of all data was validated beforehand using Kolmogorov–Smirnov normality tests.

Annex II

Table AII.1. Primer sequences for site-directed mutagenesis.

Mutant	Template	PRIMERS (5' → 3')	
5-HT _{2A} R I163A	3xHA-5-HT _{2A} R	FW	CTCCGCAATGCACCTCTGCGCCATCTC
		RV	GTGCATTGCGGAGGCCGTGGAGAAGAGCAC
5-HT _{2A} R I181A	3xHA-5-HT _{2A} R	FW	ATCCCCGCCACCACAGCCGCTTCAACTCC
		RV	GTGGGCGGGATTCTGGATGGCGACGTA
5-HT _{2A} R T257A	3xHA-5-HT _{2A} R	FW	CTACTTCTTAGCTATCAAGTCACTCCAGAAAGAAGCTAC
		RV	CTTGATAGCTAGAAAAGTAGGTGATCACCATGATGGTTAAGG
5-HT _{2A} R L325A	3xHA-5-HT _{2A} R	FW	GTGGCGGGCATCGTCTTCTCCTGTTTGTG
		RV	GCCCGCCACCTTGCATGCCTTTTGCTC
CB ₁ R V204A	3xHA-CB ₁ R	FW	CCGCAGGCAGCCTGTTCCTCACAGCC
		RV	CTGCCTGCGGAGGCAGTGAAGGAGGC
CB ₁ R T210A	3xHA-CB ₁ R	FW	GCAGCCTGTCTCGCAGCCATCGACAGG
		RV	CCTGTCGATGGCTGCGAGGAACAGGCTGC
CB ₁ R L222A	3xHA-CB ₁ R	FW	CCC GCGGCCTATAAGAGGATTGTCACCAGGC
		RV	GCCGCGGGCCTGTGAATGGATATGTACCT
CB ₁ R I297A	3xHA-CB ₁ R	FW	CATGTATGCTCTCTGGAAGGCTCACAGCCA
		RV	CAGAGAGCATAACATGTACGCATACAGATGAA
CB ₁ R L341A	3xHA-CB ₁ R	FW	AGGGCCGCCAAGACCCTGGTCTGATCCTG
		RV	CTTGGCGGCCCTAATGTCCATGCGGGCTTGGTC
CB ₁ R L345A	3xHA-CB ₁ R	FW	GACCGCAGTCCTGATCCTGGTGGTGTGAT
		RV	GGACTGCGGTCTTGGCTAACCTAATGTCCATG
CB ₁ R V204A/L222A	3xHA-CB ₁ R V204A	FW	CCC GCGGCCTATAAGAGGATTGTCACCAGGC
		RV	GCCGCGGGCCTGTGAATGGATATGTACCT
CB ₁ R V204A/L345A	3xHA-CB ₁ R V204A	FW	GACCGCAGTCCTGATCCTGGTGGTGTGAT
		RV	GGACTGCGGTCTTGGCTAACCTAATGTCCATG
CB ₁ R L222A/I297A	3xHA-CB ₁ R L222A	FW	CATGTATGCTCTCTGGAAGGCTCACAGCCA
		RV	CAGAGAGCATAACATGTACGCATACAGATGAA
CB ₁ R L222A/L345A	3xHA-CB ₁ R L222A	FW	GACCGCAGTCCTGATCCTGGTGGTGTGAT
		RV	GGACTGCGGTCTTGGCTAACCTAATGTCCATG
CMV-5-HT _{2A} R(I163A)-LgBiT	CMV-5-HT _{2A} R-LgBiT	FW	CTCCGCAATGCACCTCTGCGCCATCTC
		RV	GTGCATTGCGGAGGCCGTGGAGAAGAGCAC
CMV-5-HT _{2A} R(I181A)-LgBiT	CMV-5-HT _{2A} R-LgBiT	FW	ATCCCCGCCACCACAGCCGCTTCAACTCC
		RV	GTGGGCGGGATTCTGGATGGCGACGTA
CMV-CB ₁ R(L341A)-LgBiT	CMV-CB ₁ R-LgBiT	FW	AGGGCCGCCAAGACCCTGGTCTGATCCTG
		RV	CTTGGCGGCCCTAATGTCCATGCGGGCTTGGTC
CMV-CB ₁ R(L341A)-SmBiT	CMV-CB ₁ R-SmBiT	FW	AGGGCCGCCAAGACCCTGGTCTGATCCTG
		RV	CTTGGCGGCCCTAATGTCCATGCGGGCTTGGTC
CMV-CB ₁ R(L345A)-LgBiT	CMV-CB ₁ R-LgBiT	FW	GACCGCAGTCCTGATCCTGGTGGTGTGAT
		RV	GGACTGCGGTCTTGGCTAACCTAATGTCCATG
CMV-CB ₁ R(L345A)-SmBiT	CMV-CB ₁ R-SmBiT	FW	GACCGCAGTCCTGATCCTGGTGGTGTGAT
		RV	GGACTGCGGTCTTGGCTAACCTAATGTCCATG
pcDNA3.1-5-HT ₂ CR(V208A)	pcDNA3.1-5-HT ₂ CR	FW	CAACACGACGTGCGCGCTCAACGACCCAA
		RV	TTGGGTGCTTGAGCGCGCACGTCGTGTTG
pcDNA3.1-5-HT ₂ CR(L209A)	pcDNA3.1-5-HT ₂ CR	FW	ACAACACGACGTGCGTGGCCAACGACCCAAATTTCG
		RV	CGAAATTTGGGTGCTTGGCCACGCACGTCGTGTTGT
pcDNA3.1-5-HT ₂ CR(K348A)	pcDNA3.1-5-HT ₂ CR	FW	TCCTGTAACCAAAAAGCTCATGGAAAGCGCTTCTGAATGTGT TTGTTG
		RV	CAAACAAACACATTCAGAAGCGCTTCCATGAGCTTTTGGT TACAGGA
pcDNA3.1-5-HT ₂ CR(E347A)	pcDNA3.1-5-HT ₂ CR	FW	CTGTAACCAAAAAGCTCATGGCAAAGCTTCTGAATGTGTT G
		RV	CAAACACATTCAGAAGCTTTGCCATGAGCTTTTGGTTACA G

Annexes

pcDNA3.1-5-HT2CR(N331A)	pcDNA3.1-5-HT2CR	FW	CATTACCGCCATTCTGTCTGTTCTTTGTGAGAAGTCCTG
		RV	CAGAAT GG CGGTAATGAAAAATGGGCACCACATGATCAG
pcDNA3.1-5-HT2CR(S334A)	pcDNA3.1-5-HT2CR	FW	CATTCTGGCCGTTCTTTGTGAGAAGTCCTGTAACCAAAAG
		RV	AGAAC GG CCAGAATGGCGGTAATGAAAAATGGGCAC
pcDNA3.1-5-HT2CR(N351A)	pcDNA3.1-5-HT2CR	FW	AAAAGCTCATGGAAAAGCTTCTGGCTGTGTTTGGAT TGGCTATG
		RV	CATAGCCAATCCAAACAAACAC AG CCAGAAGCTTTCCAT GAGCTTT

Mutated alanine residues are indicated in bold.

Table AII.2. Primer sequences for cloning.

Plasmid name	Vector template	Vector template primers (5' 3')		Insert template	Insert template primers (5' 3')	
HSV-TK-5-HT_{2A}R-LgBiT	pBiT1.1-C [TK/LgBiT]	FW	CTGTGTGGGCTCGAG CGGTGGTGGC	pcDNA3.1-3xHA-5-HT _{2A} R	FW	GGAATTCTGGTACCACCA TGTACCCATACGA
		RV	GGTGGTACCAGAATT CCCCTGAGCTCC		RV	CTCGAGCCACACAGCTC ACCTTTCATTCACTCC
MYPYDVPDYAYPYDVPDYAYPYDVPDYADDILCEENTSLSSTTNSLMQLNDDTRLYSNDFNSEANTSDAFNWTVDSENRTNLSCEGCLSPSCLSLHLQEKNSALLTAVVILTIAGNILVIMAVSLEKKLQATNYFLMSLAIADMLLGF LVMVPVSMILTILYGYRWPLPSKLCVWVYLDVLFSTASIMHLCAISLDYVAIQNPIHHSRFSRRTKAFKIIAVWTIS VGISMPPIPVFGLQDDSKVFKEGSCLLADDNFVLIGSFVSFFIPLTIMVITYFLTIKSLQKEATLVCVSDLGTRAKLASFSF LPQSSLSSEKLFORSIHREPGSYTGRRTMQSISNEQKACKVLGIVFFLVVMWCPFFITNIMAVICKESCNEEDVIGALL NVFVWIGYLSAVNPLVYTLFNKTYRSAFSRYIQCYKQYKKNKPLQLLNTIPALAYKSSQLQMGQKKNKSKQDAKT TDNDCSMVVALGKQHSEASKDNSDGVNEKVCVSGSSGGGGSSGSSGVFTLEDFVGDWEQTAAYNLDQVLEQ GGVSSLLQNLAVSVTPIQIRIVRSGENALKIDIHVIIPYEGLSADQMAQIEEVFKVVPVDDHHFKVILPYGTLVIDGV TPNMLNYFGRPYEGIAVFDGKKITVTGTLWNGNKIIDERLITPDGSMFLFRVTINS*						
HSV-TK-5-HT_{2A}R-SmBiT	pBiT2.1-C [TK/SmBiT]	FW	CTGTGTGGGCTCGAG CGGTGGTGGC	pcDNA3.1-3xHA-5-HT _{2A} R	FW	GGAATTCTGGTACCACCA TGTACCCATACGA
		RV	GGTGGTACCAGAATT CCCCTGAGCTCC		RV	CTCGAGCCACACAGCTC ACCTTTCATTCACTCC
MYPYDVPDYAYPYDVPDYAYPYDVPDYADDILCEENTSLSSTTNSLMQLNDDTRLYSNDFNSEANTSDAFNWTVDSENRTNLSCEGCLSPSCLSLHLQEKNSALLTAVVILTIAGNILVIMAVSLEKKLQATNYFLMSLAIADMLLGF LVMVPVSMILTILYGYRWPLPSKLCVWVYLDVLFSTASIMHLCAISLDYVAIQNPIHHSRFSRRTKAFKIIAVWTIS VGISMPPIPVFGLQDDSKVFKEGSCLLADDNFVLIGSFVSFFIPLTIMVITYFLTIKSLQKEATLVCVSDLGTRAKLASFSF LPQSSLSSEKLFORSIHREPGSYTGRRTMQSISNEQKACKVLGIVFFLVVMWCPFFITNIMAVICKESCNEEDVIGALL NVFVWIGYLSAVNPLVYTLFNKTYRSAFSRYIQCYKQYKKNKPLQLLNTIPALAYKSSQLQMGQKKNKSKQDAKT TDNDCSMVVALGKQHSEASKDNSDGVNEKVCVSGSSGGGGSSGSSGVFTGYRLEFEIL*						
HSV-TK-CB1R-LgBiT	pBiT1.1-C [TK/LgBiT]	FW	TCTGCCGAGGCTCTG GGCTCGAGCGGTGGT	pcDNA3.1-3xHA-CB1R	FW	GCTCAGGGGAATTCTGGT ACCACCATGTACCC
		RV	GTACATGGTGGTACC AGAATTCCCCTGAGC TCC		RV	ACCACCGCTCGAGCCAG AGCCTCGGCAGA
MYPYDVPDYAYPYDVPDYAYPYDVPDYADKSIDGLADTFRITITDILLYVGSNDIQYEDIKGDMASKLGYFPQK FPLTSFRGSPFQEKMTAGDNPQLVPADQVNITEFYNKSLSSFKENEENIQCGENFMVLDIECFMVLNPSQQLAIAVLSLT LGTFTVLENLLVLCVILHSRSLRCRPSYHFIGSLAVADLLGSVIFVYSFIDFHVFRKDSRNVFLFKLGGVTAFTASV GSLFLTAIDRYISIHRLAYKRIVTRPKAVVAFCLMWTIAIVIAVPLLLGWNCLEKLSQVCSDFPHIDETYLMFWIGVT SVLLLFIYAYMYILWKAHSHAVRMIQRGTQKSIHHTSEDGKVVTRPDQARMDIRLAKTLVLILVLIICWGPLLA IMVYDVFVKMNKLIKTVFAFCMSMLCLLNSTVNPIIYALRSKDLRHAFRSMFSPCEGTAQPLDNSMGDSDCLHKHAN NAASVHRAAESICKSTVKIAKVTMSVSTDSAEALGSSGGGGSSGSSGVFTLEDFVGDWEQTAAYNLDQVLEQ GGVSSLLQNLAVSVTPIQIRIVRSGENALKIDIHVIIPYEGLSADQMAQIEEVFKVVPVDDHHFKVILPYGTLVIDGV TPNMLNYFGRPYEGIAVFDGKKITVTGTLWNGNKIIDERLITPDGSMFLFRVTINS*						
HSV-TK-CB1R-SmBiT	pBiT2.1-C [TK/SmBiT]	FW	TCTGCCGAGGCTCTG GGCTCGAGCGGTGGT	pcDNA3.1-3xHA-CB1R	FW	GCTCAGGGGAATTCTGGT ACCACCATGTACCC
		RV	GTACATGGTGGTACC AGAATTCCCCTGAGC TCC		RV	ACCACCGCTCGAGCCAG AGCCTCGGCAGA
MYPYDVPDYAYPYDVPDYAYPYDVPDYADKSIDGLADTFRITITDILLYVGSNDIQYEDIKGDMASKLGYFPQK FPLTSFRGSPFQEKMTAGDNPQLVPADQVNITEFYNKSLSSFKENEENIQCGENFMVLDIECFMVLNPSQQLAIAVLSLT LGTFTVLENLLVLCVILHSRSLRCRPSYHFIGSLAVADLLGSVIFVYSFIDFHVFRKDSRNVFLFKLGGVTAFTASV GSLFLTAIDRYISIHRLAYKRIVTRPKAVVAFCLMWTIAIVIAVPLLLGWNCLEKLSQVCSDFPHIDETYLMFWIGVT SVLLLFIYAYMYILWKAHSHAVRMIQRGTQKSIHHTSEDGKVVTRPDQARMDIRLAKTLVLILVLIICWGPLLA IMVYDVFVKMNKLIKTVFAFCMSMLCLLNSTVNPIIYALRSKDLRHAFRSMFSPCEGTAQPLDNSMGDSDCLHKHAN NAASVHRAAESICKSTVKIAKVTMSVSTDSAEALGSSGGGGSSGSSGVFTGYRLEFEIL*						
CMV-5-HT_{2A}R-LgBiT	pcDNA3.1-3xHA-5-HT _{2A} R	FW	GTAACCATCAACAGC TGACTCGAGTCTAGA GGG	pBiT1.1-C [TK/LgBiT]	FW	AAGGTGAGCTGTGTGGGC TCGAGCGGTGGT
		RV	ACCACCGCTCGAGCC CACACAGCTCACCTT TTC		RV	TCTAGACTCGAGTCAGCT GTTGATGGTTACTCGG
MYPYDVPDYAYPYDVPDYAYPYDVPDYADDILCEENTSLSSTTNSLMQLNDDTRLYSNDFNSEANTSDAFNWTVDSENRTNLSCEGCLSPSCLSLHLQEKNSALLTAVVILTIAGNILVIMAVSLEKKLQATNYFLMSLAIADMLLGF LVMVPVSMILTILYGYRWPLPSKLCVWVYLDVLFSTASIMHLCAISLDYVAIQNPIHHSRFSRRTKAFKIIAVWTIS VGISMPPIPVFGLQDDSKVFKEGSCLLADDNFVLIGSFVSFFIPLTIMVITYFLTIKSLQKEATLVCVSDLGTRAKLASFSF LPQSSLSSEKLFORSIHREPGSYTGRRTMQSISNEQKACKVLGIVFFLVVMWCPFFITNIMAVICKESCNEEDVIGALL NVFVWIGYLSAVNPLVYTLFNKTYRSAFSRYIQCYKQYKKNKPLQLLNTIPALAYKSSQLQMGQKKNKSKQDAKT TDNDCSMVVALGKQHSEASKDNSDGVNEKVCVSGSSGGGGSSGSSGVFTLEDFVGDWEQTAAYNLDQVLEQ						

Annexes

GGVSSLLQNLAVSVTPIQRIVRSGENALKIDIHVIIPYEGLSADQMAQIEEVFKVVYPVDDHHFKVILPYGTLVIDGV TPNMLNLYFGRPYEGIAVFDGKKITVTGTLWNGNKIIDERLITPDGSMLFRVTINS*						
CMV-5-HT_{2A}R-SmBiT	pcDNA3.1-3xHA-5-HT _{2A} R	FW	TTCGAGGAGATTCTG TGACTCGAGTCTAGA GGG	pBiT2.1-C [TK/SmBiT]	FW	AAGGTGAGCTGTGTGGGC TCGAGCGGTGGT
		RV	ACCACCGCTCGAGCC CACACAGCTCACCTT TTC		RV	TCTAGACTCGAGTCACAG AATCTCCTCGAACAGC
MYPYDVPDYAYPYDVPDYAYPYDVPDYADILCEENTSLSTTNSLMQLNDDTRLYSNDFNSEANTSDAFNWTVDSENRNLSCEGLSPCLSLHLQEKNSWALLTAVVILTIAGNILVIMAVSLEKKLQNAATNYFLMSLAIAADMLLGLF LVMPVSMILTILYGYRWPLPSKLCVWYLDVLFSTASIMHLCALSLDRYVAIQNPIHHSRFRSRTKAFKIIAVWTIS VGISMPIPVFGLQDDSKVFKEGSCLLADDNFVLIGSFVSFFIPLTIMVITYFLTIKSLQKEATLCVSDLGTRAKLASFSF LPQSSLSSEKLFQRSIHREPGSYTGRRTMQSISNEQKACKVLGIVFFLVVMMWCPFFITNIMAVICKESCNEVDIGALL NVFVWVGLSSAVNPLVYTLFNKTYRSAFSRYIQCYQKVENKPKLQLILVNTIPALAYKSSQLQMGQKNSKQDAKT TDNDCSMVALGKQHSEASKDNSDGVNEKVSVCVSSGGGGSSGGGGSSGVTGYRLFEEIL*						
CMV-5-HT_{2C}R-LgBiT	pcDNA3.1-5-HT _{2C} R	FW	ACCATCAACAGCTGA CTCGAGTCTAGAGGG C	CMV-5-HT _{2A} R-LgBiT	FW	AGGATTAGCAGTGTGGGC TCGAGCGGTGGT
		RV	ACCACCGCTCGAGCC CACACTGCTAATCCT TT		RV	CCCTCTAGACTCGAGTCA GCTGTTGATGGTTACTC
MVNLRNAVHSFLVHLIGLLVWQCDSVSPVAAIVTDIFNTSDGGRFKFPDGVQNWPAISIVIIIIMTIGGNILVIMAVS MEKKLHNAATNYFLMSLAIAADMLVGLLVMPLSLLAILYDYVWPLPRYLCPVWISLDVLFSTASIMHLCALSLDRYVA IRNPIEHSRFRSRTKAIMKIAIVWAISIGVSVPIVIGLRDEEKVFNNTTCLVNDPNFVLIGSFVAFFIPLTIMVITYCLT IYVLRQALMLLHGHTTEPPGLSLDFLKCCCKRNTAEENSANPNQDQARRRKKKERRPRGTMQAINNERKASKV LGIVFFVFLIMWCPFFITNILAVLCEKSCNQKLMKLLNVFVWIGYVCSGINPLVYTLFNKIYRRAFSNYLRCNYKVE KKPPVRQIPRVAATALSGRELNVNIYRHTNEPVIEKASDNEPGIEMQVENLELVPVNPSSVVSERISSVSSGGGGSSGG GGSSGVFTLEDFVGDWEQTAAYNLDQVLEQGGVSSLLQNLAVSVTPIQRIVRSGENALKIDIHVIIPYEGLSADQMA QIEEVFKVVYPVDDHHFKVILPYGTLVIDGVTPNMLNLYFGRPYEGIAVFDGKKITVTGTLWNGNKIIDERLITPDGS MLFRVTINS*						
CMV-5-HT_{2C}R-SmBiT	CMV-5-HT _{2A} R-SmBiT	FW	AGGATTAGCAGTGTG GGCTCGAGCGGTGGT	pcDNA3.1-5-HT _{2C} R	FW	AAGCTTGGTACCACCATG GTGAACCTGAGG
		RV	CCTCAGGTTACCAT GGTGGTACCAAGCTT AAGT		RV	ACCACCGCTCGAGCCAC ACTGCTAATCCTTT
MVNLRNAVHSFLVHLIGLLVWQCDSVSPVAAIVTDIFNTSDGGRFKFPDGVQNWPAISIVIIIIMTIGGNILVIMAVS MEKKLHNAATNYFLMSLAIAADMLVGLLVMPLSLLAILYDYVWPLPRYLCPVWISLDVLFSTASIMHLCALSLDRYVA IRNPIEHSRFRSRTKAIMKIAIVWAISIGVSVPIVIGLRDEEKVFNNTTCLVNDPNFVLIGSFVAFFIPLTIMVITYCLT IYVLRQALMLLHGHTTEPPGLSLDFLKCCCKRNTAEENSANPNQDQARRRKKKERRPRGTMQAINNERKASKV LGIVFFVFLIMWCPFFITNILAVLCEKSCNQKLMKLLNVFVWIGYVCSGINPLVYTLFNKIYRRAFSNYLRCNYKVE KKPPVRQIPRVAATALSGRELNVNIYRHTNEPVIEKASDNEPGIEMQVENLELVPVNPSSVVSERISSVSSGGGGSSGG GGSSGVFTLEDFVGDWEQTAAYNLDQVLEQGGVSSLLQNLAVSVTPIQRIVRSGENALKIDIHVIIPYEGLSADQMA QIEEVFKVVYPVDDHHFKVILPYGTLVIDGVTPNMLNLYFGRPYEGIAVFDGKKITVTGTLWNGNKIIDERLITPDGS MLFRVTINS*						
CMV-CB₁R^{A23}	pcDNA3.1-3xHA-CB ₁ R	FW	ATCGTATGGGTACAT GGTGGTACCAAGCTT	pcDNA3.1-3xHA-CB ₁ R	FW	TCTAGACTCGAGTCAGCA GCTTTCTGCGGC
		RV	ATCGTATGGGTACAT GGTGGTACCAAGCTT		RV	TCTAGACTCGAGTCAGCA GCTTTCTGCGGC
MYPYDVPDYAYPYDVPDYAYPYDVPDYADKSLDGLADTTFRTITDLLYVGSNDIQYEDIKGDMSKLGYPQK FPLTSFRGSPFQEKMTAGDNPQLVPADQVNITEFYNKSLSSFKENEENIQCGENFMDIECFMVLNPSQQLAIAVLSLT LGTFVLENLLVLCVILHSRSLRCRPSYHFIGSLAVADLLGSVIFVYSFIDFHVFRKDSRNVFLFKLGGVTAFTASV GSLFLTADRYISHRPLAYKRIVTRPKAVVAFCLMWTAIAVIAVPLLLGWNCLEKLSVCSDFPHIDETYLFWIGVT SVLLLFIVYAYMYLWKAHSHAVRMIQRGTQKSHIHTSEDGKVVTRPDQARMDIRLAKTLVLILVVLICWGPLLA IMVYDVFVKMKNLIKTVFAFCMLCLLNSTVNPIIYALRSKDLRHAFRSMFSPCEGTAQPLDNSMGSDCLHKHAN NAASVHRAAESC*						
CMV-CB₁R-LgBiT	pcDNA3.1-3xHA-CB ₁ R	FW	GTAACCATCAACAGC TGACTCGAGTCTAGA GGG	pBiT1.1-C [TK/LgBiT]	FW	TCTGCCGAGGCTCTGGGC TCGAGCGGTGGT
		RV	ACCACCGCTCGAGCC CAGAGCCTCGGCAG A		RV	TCTAGACTCGAGTCAGCT GTTGATGGTTACTCGG
MYPYDVPDYAYPYDVPDYAYPYDVPDYADKSLDGLADTTFRTITDLLYVGSNDIQYEDIKGDMSKLGYPQK FPLTSFRGSPFQEKMTAGDNPQLVPADQVNITEFYNKSLSSFKENEENIQCGENFMDIECFMVLNPSQQLAIAVLSLT LGTFVLENLLVLCVILHSRSLRCRPSYHFIGSLAVADLLGSVIFVYSFIDFHVFRKDSRNVFLFKLGGVTAFTASV GSLFLTADRYISHRPLAYKRIVTRPKAVVAFCLMWTAIAVIAVPLLLGWNCLEKLSVCSDFPHIDETYLFWIGVT SVLLLFIVYAYMYLWKAHSHAVRMIQRGTQKSHIHTSEDGKVVTRPDQARMDIRLAKTLVLILVVLICWGPLLA						

IMVYDVFGKMNKLIKTVFAFCSMCLLNSTVNPPIYALRSKDLRHAFRSMFSPCEGTAQPLDNSMGSDCLHKHAN NAASVHRAAESCKSTVKIAKVTMSVSTDTSAEALGSSGGGGSSGGSSGVFTLEDFVGDWEQTAAYNLDQVLEQ GGVSSLLQNLAVSVTPIQIRVRSGENALKIDIHVIIPYEGLSADQMAQIEEVFKVVPVDDHHFKVILPYGTLVIDGV TPNMLNYFGRPYEGIAVFDGKKITVTGTLWNGNKIIDERLITPDGSMLFRVTINS*						
CMV-CB₁R^{A23}- LgBiT	pcDNA3.1- 3xHA-CB ₁ R	FW	GTAACCATCAACAGC TGACTCGAGTCTAGA GGG	pBiT1.1-C [TK/LgBiT]	FW	GCCGCAGAAAGCTGCGGC TCGAGCGGTGGT
		RV	ACCACCGCTCGAGCC GCAGCTTTCTGCGGC		RV	TCTAGACTCGAGTCAGCT GTTGATGGTTACTCGG
MYPYDVPDYAYPYDVPDYAYPYDVPDYADKSILDGLADTFRITITDILLYVGSNDIQYEDIKGDMASKLGYFPQK FPLTSFRGSPFQEKMTAGDNPQLVPADQVNITEFYNKSLSSFKENEENIQCGENFMDIECFMVLNPSQQLAIAVLSLT LGTFTVLENLLVLCVILHSRSLRCRPSYHFIGSLAVADLLGSVIFVYSFIDFHVFRKDSRNVFLFKLGGVTASFTASV GSLFLTADRYISIHRLAYKRIVTRPKAVVAFCLMWTIAIVIAVLPPLGWNCEKLQSVCSDFPHIDETYLMFWIGVT SVLLLFIYVAYMYLWKAHSHAVRMIQRGTQKSIHHTSEDKVQVTRPDQARMDIRLAKTLVLILVLIICWGPLLA IMVYDVFGKMNKLIKTVFAFCSMCLLNSTVNPPIYALRSKDLRHAFRSMFSPCEGTAQPLDNSMGSDCLHKHAN NAASVHRAAESCGSSGGGGSSGGSSGVFTLEDFVGDWEQTAAYNLDQVLEQGGVSSLLQNLAVSVTPIQIRVRS GENALKIDIHVIIPYEGLSADQMAQIEEVFKVVPVDDHHFKVILPYGTLVIDGVTPNMLNYFGRPYEGIAVFDGKKI TVTGTWNGNKIIDERLITPDGSMLFRVTINS*						
CMV-CB₁R- SmBiT	pcDNA3.1- 3xHA-CB ₁ R	FW	TTCGAGGAGATTCTG TGACTCGAGTCTAGA GGG	pBiT2.1-C [TK/SmBiT]	FW	TCTGCCGAGGCTCTGGGC TCGAGCGGTGGT
		RV	ACCACCGCTCGAGCC CAGAGCCTCGGCAG A		RV	TCTAGACTCGAGTCACAG AATCTCCTCGAACAGC
MYPYDVPDYAYPYDVPDYAYPYDVPDYADKSILDGLADTFRITITDILLYVGSNDIQYEDIKGDMASKLGYFPQK FPLTSFRGSPFQEKMTAGDNPQLVPADQVNITEFYNKSLSSFKENEENIQCGENFMDIECFMVLNPSQQLAIAVLSLT LGTFTVLENLLVLCVILHSRSLRCRPSYHFIGSLAVADLLGSVIFVYSFIDFHVFRKDSRNVFLFKLGGVTASFTASV GSLFLTADRYISIHRLAYKRIVTRPKAVVAFCLMWTIAIVIAVLPPLGWNCEKLQSVCSDFPHIDETYLMFWIGVT SVLLLFIYVAYMYLWKAHSHAVRMIQRGTQKSIHHTSEDKVQVTRPDQARMDIRLAKTLVLILVLIICWGPLLA IMVYDVFGKMNKLIKTVFAFCSMCLLNSTVNPPIYALRSKDLRHAFRSMFSPCEGTAQPLDNSMGSDCLHKHAN NAASVHRAAESCKSTVKIAKVTMSVSTDTSAEALGSSGGGGSSGGSSGVFTLEDFVGDWEQTAAYNLDQVLEQGGV SSLLQNLAVSVTPIQIRVRSGENALKIDIHVIIPYEGLSADQMAQIEEVFKVVPVDDHHFKVILPYGTLVIDGVTPNMLNY FGRPYEGIAVFDGKKITVTGTLWNGNKIIDERLITPDGSMLFRVTINS*						
CMV-LgBiT- β-arrestin2	pcDNA3.1- ARRB2	FW	GGAGGCTCGAGCGG TATGGGGGAGAAAC CCG	pBiT1.1-N [TK/LgBiT]	FW	GAGCTCGGATCCACCATG GTCTTCACTCGAAG
		RV	GAGTGTGAAGACCAT GGTGGATCCGAGCTC G		RV	GGGTTTCTCCCCATACC GCTCGAGCTCC
MVFTLEDFVGDWEQTAAYNLDQVLEQGGVSSLLQNLAVSVTPIQIRVRSGENALKIDIHVIIPYEGLSADQMAQIEE VFKVVPVDDHHFKVILPYGTLVIDGVTPNMLNYFGRPYEGIAVFDGKKITVTGTLWNGNKIIDERLITPDGSMLFR VTINSGSSGGGGSSGGSSGMGEKPGTRVFKKSSPNCKLTVYLGKRDVFDHLDKVPDVGVLVDPDYDKDRKV FVTLTCAFYRGREDLDVGLSFRKDLFIATYQAFPPVNPVPPPTRLQDRLLRKLQHAHPFFFTIPQNLPCSVTLQP GPEDTGKACGVDFEIRAFCAKSLEEKSHKRNSVRLVIRKVFQFAPEKPGQPSAETTRHFLMSDRSLHLEASLDKELY YHGEPLNVNVHVTNNSKTVKKIKVSVRQYADICLFSTAQYKCPVAQLEQDDQVSPSSFTCKVYVITPLSDNREK RGLADGKCLKHEDTNLASSTIVKEGANKEVLGILVSVRVKLVVSRGGDVSVELPFVLMHPKPHDHIPLPRPQSA APETDVPVDTNLIEFDNTYATDDDIVFEDFARLRLKGMKDDDDYDDQLC*						
CMV-SmBiT- β-arrestin2	pcDNA3.1- ARRB2	FW	GGAGGCTCGAGCGG TATGGGGGAGAAAC CCG	pBiT2.1-N [TK/SmBiT]	FW	GAGCTCGGATCCACCATG GTGACCGGCTACC
		RV	GTAGCCGGTACCAT GGTGGATCCGAGCTC G		RV	GGGTTTCTCCCCATACC GCTCGAGCTCC
MVTGYRLFEEILGSSGGGGSSGGSSGMGEKPGTRVFKKSSPNCKLTVYLGKRDVFDHLDKVPDVGVLVDPD YLKDRKVFVTLTCAFYRGREDLDVGLSFRKDLFIATYQAFPPVNPVPPPTRLQDRLLRKLQHAHPFFFTIPQNL PQSVTLQPGPEDTGKACGVDFEIRAFCAKSLEEKSHKRNSVRLVIRKVFQFAPEKPGQPSAETTRHFLMSDRSLHLEA SLDKELYHGEPLNVNVHVTNNSKTVKKIKVSVRQYADICLFSTAQYKCPVAQLEQDDQVSPSSFTCKVYVITPL SDNREKRLALDGLKHKHEDTNLASSTIVKEGANKEVLGILVSVRVKLVVSRGGDVSVELPFVLMHPKPHDHIPL PRPQSAAPETDVPVDTNLIEFDNTYATDDDIVFEDFARLRLKGMKDDDDYDDQLC*						
CMV-CB₂R- LgBiT	pcDNA3.1- 3xHA-CB ₂ R	FW	GTAACCATCAACAGC TGACTCGAGTCTAGA GGG	pBiT1.1-C [TK/LgBiT]	FW	GACCTCTCTGATTGCGGC TCGAGCGGTGGT
		RV	GTAACCATCAACAGC TGACTCGAGTCTAGA GGG		RV	TCTAGACTCGAGTCAGCT GTTGATGGTTACTCGG
MYPYDVPDYAYPYDVPDYAYPYDVPDYADEECVWTEIANGSKDGLDSNPMKDYMILSGPQKTAVAVLCTLLGLL SALENVAVLYLILSSHQLRRKPSYLFIGSLAGADFLASVVFACSFVNFHVFHGVDSKAVFLKIGSVTMTFTASVGS LLTAIDRYLCLRYPPSYKALLTRGRALVTLGIMWVLSALVSYPLMGWTCPCPRCSELPLIPNDYLLSLLFI SGLIYTYGHVWKAHQHVASLSGHQDRQVPGMARMRLDVRLAKTLGLVLAVLLICWFPVLALMAHSLATLSDQ VKKAFACSMCLINSMVNPVIYALRSGEIRSSAHHLAHWKCCVRLGSEAKEAPRSSVTEADGKITPWPDS RDLDSLDCGSSGGGGSSGGSSGVFTLEDFVGDWEQTAAYNLDQVLEQGGVSSLLQNLAVSVTPIQIRVRS GENALKIDIHVIIPYEGLSADQMAQIEEVFKVVPVDDHHFKVILPYGTLVIDGVTPNMLNYFGRPYEGIAVFDGKKI TVTGTWNGNKIIDERLITPDGSMLFRVTINS*						

Annexes

CMV-CB₂R-SmBiT	pcDNA3.1-3xHA-CB ₂ R	FW	TTCGAGGAGATTCTG TGACTCGAGTCTAGA GGG	pBiT2.1-C [TK/SmBiT]	FW	GACCTCTCTGATTGCGGC TCGAGCGGTGGT
		RV	ACCACCGCTCGAGCC GCAATCAGAGAGGT CTAGAT		RV	TCTAGACTCGAGTCACAG AATCTCCTCGAACAGC
<p>MYPYDVPDYAYPYDVPDYAYPYDVPDYADEECWVTEIANGSKDGLDSNPMKDYMILSGPQKTAVAVLCTLLGLL SALENVAVLYLILSSHQLRRKPSYLFIGSLAGADFLASVVFACSFVNFHVFHGVDSKAVFLKIGSVMTTFASVGS LLTAIDRYLCLRYPPSYKALLTRGRALVTLGIMWVLSALVSYLPLMGWTCCPRPCSELPLIPNDYLLSWLLFIAFLF SGHIITYGHVWLKAAHQHVASLSGHQDRQVPGMARMRLDVR LAKTLGLVLA VLLICWFPVLALMAHSLATTLSDQ VKKAFAFCSMLCLINSMVNPVYALRSGEIRSSAHHCLAHWKCCVRLGSEAKEEAPRSSV TETEADGKITPWPDS RDLDSLDCGSSGGGGSSGGGGSSGGVTGYRLFEEIL*</p>						
CMV-LgBiT-5-HT_{2A}R	pcDNA3.1-3xHA-5-HT _{2A} R	FW	GGAGGCTCGAGCGG TGATATTCTTTGTGA AGAAAATACTT	pBiT1.1-N [TK/LgBiT]	FW	AAGCTTGGTACCACCATG GTCTTCACACTCGAAG
		RV	GAGTGTGAAGACCAT GGTGGTACCAAGCTT AAG		RV	TTCACAAAGAATATCACC GCTCGAGCCTCC
<p>MVFTLEDFVGDWEQTAAYNLDQVLEQGGVSSLLQNLAVSVTPIQIRIVRSGENALKIDIHVIIPYEGLSADQMAQIEE VFKVVYPVDDHHFKVILPYGTLVIDGVTNMLNYFGRPYEGIAVFDGKKITVTGTLWNGNKIIDERLITPDGSMLFR VTINSGSSGGGGSSGGGGSSGDILCEENTSLSTTNSLMQLNDDTRLYSNDFNSGEANTSDAFNWTVDSE GCLSPCLSLHLQEKNSALLTAVVILTIAGNILVIMAVSLEKKLQNA TNYFLMSLAIA DMMLLGFVMPVSM LTL YGYRWPLPSKLC AVWIYLDVLFSTASIMHLCAISLDRYVAIQNPIHHSRFSNRTKAFLKIIAVWTISV GISMPIV FGL QDDSKVFEKGSCLLADDFV LIGSFVFFIPLTIMVITYFLTIKSLQKEATLCVSDLGTRAKLASFSFLPQSSLSSEKLF QRSIHREPGSYTGRRTMQSISNEQKACKV LGIVFFLVVMWCPFFITNIMAVICKESCNE D VIGALLNVFVWIGY LSS AVNPLVYTLFNKTYRSAFSRYIQCYKENKKPLQLL VNTIPALAYKSSQLQMGQKKNKQDAKTTDNDCSMVAL GKQHSEEAASKDNSDGVNEKVCV*</p>						
CMV-SmBiT-5-HT_{2A}R	pcDNA3.1-3xHA-5-HT _{2A} R	FW	GGAGGCTCGAGCGG TGATATTCTTTGTGA AGAAAATACTT	pBiT2.1-N [TK/SmBiT]	FW	AAGCTTGGTACCACCATG GTGACCGGTACC
		RV	GTAGCCGGTCACCAT GGTGGTACCAAGCTT AAG		RV	TTCACAAAGAATATCACC GCTCGAGCCTCC
<p>MVTGYRLFEEILGSSGGGGSSGGGGSSGDILCEENTSLSTTNSLMQLNDDTRLYSNDFNSGEANTSDAFNWTVDSE NRTNLSCEGCLSPCLSLHLQEKNSALLTAVVILTIAGNILVIMAVSLEKKLQNA TNYFLMSLAIA DMMLLGFV MPVSM LTL YGYRWPLPSKLC AVWIYLDVLFSTASIMHLCAISLDRYVAIQNPIHHSRFSNRTKAFLKIIAVWTISV G SMPPIV FGLQDDSKVFEKGSCLLADDFV LIGSFVFFIPLTIMVITYFLTIKSLQKEATLCVSDLGTRAKLASFSFLPQ SSLSEKLFQRSIHREPGSYTGRRTMQSISNEQKACKV LGIVFFLVVMWCPFFITNIMAVICKESCNE D VIGALLNVF VWIGY LSSAVNPLVYTLFNKTYRSAFSRYIQCYKENKKPLQLL VNTIPALAYKSSQLQMGQKKNKQDAKTTDND DCSMVALGKQHSEEAASKDNSDGVNEKVCV*</p>						
CMV-LgBiT-CB₁R	pcDNA3.1-3xHA-CB ₁ R	FW	GGAGGCTCGAGCGG TAAGTCGATCCTAGA TGGCC	pBiT1.1-N [TK/LgBiT]	FW	AAGCTTGGTACCACCATG GTCTTCACACTCGAAG
		RV	GAGTGTGAAGACCAT GGTGGTACCAAGCTT AAGT		RV	ATCTAGGATCGACTTACC GCTCGAGCCTCC
<p>MVFTLEDFVGDWEQTAAYNLDQVLEQGGVSSLLQNLAVSVTPIQIRIVRSGENALKIDIHVIIPYEGLSADQMAQIEE VFKVVYPVDDHHFKVILPYGTLVIDGVTNMLNYFGRPYEGIAVFDGKKITVTGTLWNGNKIIDERLITPDGSMLFR VTINSGSSGGGGSSGGGGSSGKSILDGLADTTFRITITD LLYVGSNDIQYEDIKGD MASKLGYFPQKFP LTSFRGSPFQ EKMTAGDNPQLVPADQVNITEFYNKLS SSKENEENIQCGENFM D IECFMV LNPSQQLAIAVLSLTLGTFVLENLL VLCVILHSRSLRCRPSYHFIGSLA VADLLG SVIFVYSFIDFHV FHRKDSRNVFLFKLGGVTASFTASV GSLFLTAIDRY ISIHRLAYKRIVTRPKAVVAFCLMWTIAIVIAVLP LLGW NCEKLSVCS DIFPHIDETYLMFWIGVTSV LLLFIVYAY MYILWKAHSHAVRMIQRGTQKSIHHTSEDGKVQVTRPDQARMDIRLAKTLVLILVVLICWGPLLAIMVYDVF GK MNKLIKTVFAFC SMLCLLNSTVNP IYALRSKDLRHAFRSMFSPCEGTAQPLD NSMGDS DCLHKHANNAASVHRAA ESCIKSTVKIAKVTMSVSTDTSAEAL*</p>						
CMV-SmBiT-CB₁R	pcDNA3.1-3xHA-CB ₁ R	FW	GGAGGCTCGAGCGG TAAGTCGATCCTAGA TGGCC	pBiT2.1-N [TK/SmBiT]	FW	AAGCTTGGTACCACCATG GTGACCGGTACC
		RV	GTAGCCGGTCACCAT GGTGGTACCAAGCTT AAGT		RV	ATCTAGGATCGACTTACC GCTCGAGCCTCC
<p>MVTGYRLFEEILGSSGGGGSSGGGGSSGKSILDGLADTTFRITITD LLYVGSNDIQYEDIKGD MASKLGYFPQKFP LTS FRGSPFQEKMTAGDNPQLVPADQVNITEFYNKLS SSKENEENIQCGENFM D IECFMV LNPSQQLAIAVLSLTLGTF VLENLLVLCVILHSRSLRCRPSYHFIGSLA VADLLG SVIFVYSFIDFHV FHRKDSRNVFLFKLGGVTASFTASV GSLFL TAIDRYISIHRLAYKRIVTRPKAVVAFCLMWTIAIVIAVLP LLGW NCEKLSVCS DIFPHIDETYLMFWIGVTSV LLL FIVYAYMYILWKAHSHAVRMIQRGTQKSIHHTSEDGKVQVTRPDQARMDIRLAKTLVLILVVLICWGPLLAIMVY DVF GKMNKLIKTVFAFC SMLCLLNSTVNP IYALRSKDLRHAFRSMFSPCEGTAQPLD NSMGDS DCLHKHANNAAS VHRAAESCIKSTVKIAKVTMSVSTDTSAEAL*</p>						
CMV-HaloTag®-5-HT_{2A}R	CMV-SmBiT-5-HT _{2A} R	FW	ACCGATTTCTGCCAT GGTGGTACCAAGCTT AA	pFN21A HaloTag® CMV Flexi® Vector	FW	AAGCTTGGTACCACCATG GCAGAAATCGGT
		RV	ACCGATTTCTGCCAT GGTGGTACCAAGCTT AA		RV	ACCACCGGA ACTCCCGCC GGAAATCTCGAG

<p>MAEIGTGFPPDPHYVEVLGERMHYVDVGPDRDTPVLFHLHGNTSSYVWRNIIPHVAPTHRCIAPDLIGMGKSDKPD LGYFFDDHVRFMDFAEIALGLEEVVLVIHDWGSALGFHWAKRNPVERVKGIAMFIRPIPTWDEWPEFARETFQAF RTTDVGRKLIIDQNVFIEGTLPMGVVVRPLTEVEMDHYREPFLNPVDREPLWRFPNELPIAGEPANIVALVEEYMDWL HQSPVPKLLFWGTGPGVLIPPAEAAARLAKSLPNCKAVDIGPGLNLLQEDNPDIGSEIARWLSTLEISGGSSGGGGSSG GGSSGDILCEENTSLSSSTNSLMQLNDDTRLYSNDFNSGEANTSDAFNWTVDSENRTNLSCEGCLSPSCLSLHLQ KNWSALLTAVVILTIAGNILVIMAVSLEKKLQATNYFLMSLAIAADMLLGFVMPVSMILTILYGYRWPLPSKLC WIYLDVLFSTASIMHLCAISLDYVAIQNPIHHSRFSNRTKAFLKIIAVWTISVIGSMPPIPVFGLQDDSKVFK EGSCLLADDNFVLIGSFVFFIPLTIMVITYFLTIKSLQKEATLVCVSDLGTRAKLASFSFLPQSSLSSEKLFQ RSIHREPGSYTGRRTMQSISNEQKACKVGLVFFLVVVMWCPFFITNIMAVICKESCNEDEVIGALLNVFVW IGYLSSAVNPLVYTLFNKTYRSAFSRYIQCYKQKPLQLLILVNTIPALAYKSSQLQMGQKNSKQDAKT TDNDCSMVALGKQHSSEASKDNSDGVNEKVSCV*</p>						
CMV-HaloTag®-CB ₁ R	CMV-SmBiT-CB ₁ R	FW	ACCGATTCTGCCAT GGTGGTACCAAGCTT AA	pFN21A HaloTag® CMV Flexi® Vector	FW	AAGCTTGGTACCACCATG GCAGAAATCGGT
		RV	ACCGATTCTGCCAT GGTGGTACCAAGCTT AA		RV	ACCACCGGAACCTCCCGCC GGAAATCTCGAG
<p>MAEIGTGFPPDPHYVEVLGERMHYVDVGPDRDTPVLFHLHGNTSSYVWRNIIPHVAPTHRCIAPDLIGMGKSDKPD LGYFFDDHVRFMDFAEIALGLEEVVLVIHDWGSALGFHWAKRNPVERVKGIAMFIRPIPTWDEWPEFARETFQAF RTTDVGRKLIIDQNVFIEGTLPMGVVVRPLTEVEMDHYREPFLNPVDREPLWRFPNELPIAGEPANIVALVEEYMDWL HQSPVPKLLFWGTGPGVLIPPAEAAARLAKSLPNCKAVDIGPGLNLLQEDNPDIGSEIARWLSTLEISGGSSGGGGSSG GGSSGDILCEENTSLSSSTNSLMQLNDDTRLYSNDFNSGEANTSDAFNWTVDSENRTNLSCEGCLSPSCLSLHLQ KNWSALLTAVVILTIAGNILVIMAVSLEKKLQATNYFLMSLAIAADMLLGFVMPVSMILTILYGYRWPLPSKLC WIYLDVLFSTASIMHLCAISLDYVAIQNPIHHSRFSNRTKAFLKIIAVWTISVIGSMPPIPVFGLQDDSKVFK EGSCLLADDNFVLIGSFVFFIPLTIMVITYFLTIKSLQKEATLVCVSDLGTRAKLASFSFLPQSSLSSEKLFQ RSIHREPGSYTGRRTMQSISNEQKACKVGLVFFLVVVMWCPFFITNIMAVICKESCNEDEVIGALLNVFVW IGYLSSAVNPLVYTLFNKTYRSAFSRYIQCYKQKPLQLLILVNTIPALAYKSSQLQMGQKNSKQDAKT TDNDCSMVALGKQHSSEASKDNSDGVNEKVSCVGGSSGGGGSSGSMVSKGEELFTGVVPIVELDGDVNGH KFSVSGEGEDATYGKLTLLKLICTTGKLPVPWPVTLVTLGYLQCFARYPDHMKQHDFFKSAMPEGYVQERTIFFK DDGNYKTRAEVKFEGDTLVNRIELKIDFKEDGNILGHKLEYNNSHNVYITADKQKNGIKANFKIRHNIE*</p>						
CMV-5-HT _{2A} R-VN173	CMV-5-HT _{2A} R-SmBiT	FW	CACAACATCGAGTAG CTCGAGTCTAGAGGG CC	pBiFC- bJunVN173	FW	GGAGGGTCGTCAGGTATG GTGAGCAAGGGCG
		RV	GCCCTTGCTCACCAT ACCTGACGACCCTCC		RV	CCCTCTAGACTCGAGCTA CTCGATGTTGTGGCG
<p>MYPYDVPDYAYPYDVPDYAYPYDVPDYADDILCEENTSLSSSTNSLMQLNDDTRLYSNDFNSGEANTSDAFNWT VDSENRTNLSCEGCLSPSCLSLHLQKKNWSALLTAVVILTIAGNILVIMAVSLEKKLQATNYFLMSLAIAADMLLGF LVMPVSMILTILYGYRWPLPSKLCVWYLDVLFSTASIMHLCAISLDYVAIQNPIHHSRFSNRTKAFLKIIAVWTIS VIGSMPPIPVFGLQDDSKVFKEGSCLLADDNFVLIGSFVFFIPLTIMVITYFLTIKSLQKEATLVCVSDLGTRAK LASFSFLPQSSLSSEKLFQSIHREPGSYTGRRTMQSISNEQKACKVGLVFFLVVVMWCPFFITNIMAVICKESCNEDEVIGALL NVFVWIGYLSAVNPLVYTLFNKTYRSAFSRYIQCYKQKPLQLLILVNTIPALAYKSSQLQMGQKNSKQDAKT TDNDCSMVALGKQHSSEASKDNSDGVNEKVSCVGGSSGGGGSSGSMVSKGEELFTGVVPIVELDGDVNGH KFSVSGEGEDATYGKLTLLKLICTTGKLPVPWPVTLVTLGYLQCFARYPDHMKQHDFFKSAMPEGYVQERTIFFK DDGNYKTRAEVKFEGDTLVNRIELKIDFKEDGNILGHKLEYNNSHNVYITADKQKNGIKANFKIRHNIE*</p>						
CMV-5-HT _{2A} R-VC155	CMV-5-HT _{2A} R-SmBiT	FW	GAGCTGTACAAGTAA CTCGAGTCTAGAGGG CC	pBiFC- bFosVC155	FW	GGAGGGTCGTCAGGTGAC AAGCAGAAGAACGGC
		RV	GTTCTTCTGCTGTGTC ACCTGACGACCCTCC		RV	CCCTCTAGACTCGAGTTA CTGTACAGCTCGTCC
<p>MYPYDVPDYAYPYDVPDYAYPYDVPDYADKLSILDGLADTFRITITDLYVGSNDIQYEDIKGDMASKLGYFPQK FPLTSFRGSPFQEKMTAGDNPQLVPADQVNITEFYNKSLSSFKENEENIQCGENFMDIECFMVLNPSQQLAIAVLSLT LGTFTVLENLLVLCVILHSRSLRCRPSYHFIGSLAVADLLGSVIFVYFIDFHVFRKDSRNVFLKLGCVTASFTASV GSLFLTAIDRYISIHRLAYKRVTRPAVVAFLMWTIAIVIAVPLLLGWNCLEKLSQVCSDFPHIDETLMFWIGVT SVLLLFIYAYMYILWKAHSHAVRMIQRGTQKSIHHTSEDGKVQVTRPDQARMDIRLAKTLVLILVLIICWGPLLA IMVYDVFVKMKNLIKTVFAFCMSMLCLLNSTVNPIIYALRSKDLRHAFRSMFSPCEGTAQPLDMSMGDSCLHKKHAN NAASVHRAAESCISTVKIAKVTMSVSTDSAEALGSSGGGGSSGSMVSKGEELFTGVVPIVELDGDVNGH KFSVSGEGEDATYGKLTLLKLICTTGKLPVPWPVTLVTLGYLQCFARYPDHMKQHDFFKSAMPEGYVQERTIFFK DDGNYKTRAEVKFEGDTLVNRIELKIDFKEDGNILGHKLEYNNSHNVYITADKQKNGIKANFKIRHNIE*</p>						
CMV-CB ₁ R-VN173	CMV-CB ₁ R-SmBiT	FW	CACAACATCGAGTAG CTCGAGTCTAGAGGG CC	pBiFC- bJunVN173	FW	GGAGGGTCGTCAGGTATG GTGAGCAAGGGCG
		RV	GCCCTTGCTCACCAT ACCTGACGACCCTCC		RV	CCCTCTAGACTCGAGCTA CTCGATGTTGTGGCG
<p>MYPYDVPDYAYPYDVPDYAYPYDVPDYADKLSILDGLADTFRITITDLYVGSNDIQYEDIKGDMASKLGYFPQK FPLTSFRGSPFQEKMTAGDNPQLVPADQVNITEFYNKSLSSFKENEENIQCGENFMDIECFMVLNPSQQLAIAVLSLT LGTFTVLENLLVLCVILHSRSLRCRPSYHFIGSLAVADLLGSVIFVYFIDFHVFRKDSRNVFLKLGCVTASFTASV GSLFLTAIDRYISIHRLAYKRVTRPAVVAFLMWTIAIVIAVPLLLGWNCLEKLSQVCSDFPHIDETLMFWIGVT SVLLLFIYAYMYILWKAHSHAVRMIQRGTQKSIHHTSEDGKVQVTRPDQARMDIRLAKTLVLILVLIICWGPLLA IMVYDVFVKMKNLIKTVFAFCMSMLCLLNSTVNPIIYALRSKDLRHAFRSMFSPCEGTAQPLDMSMGDSCLHKKHAN NAASVHRAAESCISTVKIAKVTMSVSTDSAEALGSSGGGGSSGSMVSKGEELFTGVVPIVELDGDVNGH KFSVSGEGEDATYGKLTLLKLICTTGKLPVPWPVTLVTLGYLQCFARYPDHMKQHDFFKSAMPEGYVQERTIFFK DDGNYKTRAEVKFEGDTLVNRIELKIDFKEDGNILGHKLEYNNSHNVYITADKQKNGIKANFKIRHNIE*</p>						
CMV-CB ₁ R-VC155	CMV-CB ₁ R-SmBiT	FW	GAGCTGTACAAGTAA CTCGAGTCTAGAGGG CC	pBiFC- bFosVC155	FW	GGAGGGTCGTCAGGTGAC AAGCAGAAGAACGGC

Annexes

		RV	GTTCTTCTGCTTGTC ACCTGACGACCCTCC		RV	CCCTCTAGACTCGAGTTA CTGTGACAGCTCGTCC
<p>MYPYDVPDYAYPYDVPDYAYPYDVPDYADKSILDGLADTFFRITITDLDLYVGSNDIQYEDIKGDMASKLGYFPQK FPLTSFRGSPFQEKMTAGDNPQLVPADQVNITEFYNKLSSSFKENEENIQCGENFMDIECFMVLNPSQQLAIAVLSLT LGTFTVLENLLVLCVILHSRSLRCRPSYHFHIGSLAVADLLGVSIVFVYSFIDFHVHFRKDSRNVFLKLGVTASFTASV GSLFLTAIDRYISIHRLAYKRIVTRPKAVVAFCLMWTIAIVLPLLGNWCEKLSQVCSDFPHIDETYLMFWIGVT SVLLLFIVYAYMYLWKAHSHAVRMIQRGTQKSHIHTSEDGKVVQVTRPDQARMDIRLAKTLVLILVVLICWGPLLA IMVYDVFVKMNLKIKTVFAFCMLCLLNSTVNPIYALRSKDLRHAFRSMFSPCEGTAQPLDMSMGDSDLCHKHAN NAASVHRAAESCIKSTVKIAKVTMSVSTDTSAELGSSGGGGSSGGSSGDKQKNGIKANFKIRHNIEDGGVQLAD HYQQNTPIGDGPVLLPDNHVLSYQSKLSKDPNEKRDMVLEFVTAAGITLGMDEL^{YK*}</p>						
CMV-SmBiT-Gai1	CMV-SmBiT-β-arrestin2	FW	GATTGTGGTCTCTTT TAGGAATTCTGCAGA TATCCAG	pcDNA3.1- Galhai1	FW	GGAGGCTCGAGCGGTATG GGCTGCACGCTG
		RV	CAGCGTGCAGCCCAT ACCGCTCGAGCTCC		RV	TCTGCAGAATTCCTAAAA GAGACCACAATCTTTTAG ATT
<p>MVTGYRLFEEILGSSGGGGSSGGGGSSGMGCTLSAEDKAAVERSKMIDRNREDGEKAAREVKLLLLGAGESGKSTI VKQMKIIIEAGYSEEECKQYKAVVYSNTIQSHIIRAMGRLEKIDFGDSARADDARQLFVLAGAAEEGFMATAELAGV IKRLWKDSGVQACFNRSREYQLNDSAAYYLNDLDRIAQPNYIPTQQDVLTRVKTGIVETHFTFKDLHFKMFDVG GQRSEKRWIHC FEGVTAIIFCVALS DYDLVLAEDEEMNRMHESMKLFDSICNNKWFDTSTIILFLNKKDLFEKIK KSPLTICYPEYAGSNTYEEAAA YIQCFEDLNKRKDTKEIYTHFTCATDTKNVQVFDAVTDVVIKNNLKDCGLF[*]</p>						
CMV-SmBiT-Gai3	CMV-SmBiT-β-arrestin2	FW	GAATGTGGACTTTAT TAGGAATTCTGCAGA TATCCAG	pcDNA3.1- Galhai3	FW	GGAGGCTCGAGCGGTATG GGCTGCACGCTG
		RV	CAACGTGCAGCCCAT ACCGCTCGAGCTCC		RV	TCTGCAGAATTCCTAATA AAGTCCACATTCCTTTAA GTT
<p>MVTGYRLFEEILGSSGGGGSSGGGGSSGMGCTLSAEDKAAVERSKMIDRNREDGEKAAKEVKLLLLGAGESGKSTI VKQMKIIHEDGYSEDECKQYKVVVYSNTIQSHIIRAMGRLEKIDFGEAARADDARQLFVLAGSAEEGVMTPELAGV IKRLWRDGGVQACFRSREYQLNDSASYLNDLDRISQSNYIPTQQDVLTRVKTGIVETHFTFKDLYFKMFDVG GQRSEKRWIHC FEGVTAIIFCVALS DYDLVLAEDEEMNRMHESMKLFDSICNNKWFDTSTIILFLNKKDLFEKIK RSPLTICYPEYAGSNTYEEAAA YIQCFEDLNRRKDTKEIYTHFTCATDTKNVQVFDAVTDVVIKNNLKCEGLY[*]</p>						
CMV-SmBiT-Gaq	CMV-SmBiT-β-arrestin 2	FW	GAGTACAATCTGGTC TAGGAATTCTGCAGA TATCCAG	pcDNA3.1- Galphaq	FW	GGAGGCTCGAGCGGTATG ACTCTGGAGTCCATCA
		RV	GGACTCCAGAGTCAT ACCGCTCGAGCTCC		RV	TCTGCAGAATTCCTAGAC CAGATTGTACTCTCA
<p>MVTGYRLFEEILGSSGGGGSSGGGGSSGMTLESIMACCLSEEAKEARRINDEIERQLRRDKRDARRELKLLLLGTGES GKSTFIKQMRIHSGYSDEDEKRGFTKLVYQNIPTAMQAMIRAMDTLKIPYKYEHNKAAHAQLVREVDVEKVS AFEN PYVDAIKSLWNDPGIQECYDRRREYQLSDSTKYLLNDLDRVADPAYLPTQQDVLTRVVPPTGIIIEY PFDLQSVIFRM VDVGGQSRERRWIHC FENVT SIMFLValseyDQVLVESDNENRMEESKALFRITITYPWFQNSSVILFLNKKDLLEKI EKIMYSHLVDFPEYDGPQRDAQAAREFILKMFVDLNPDSKIIYSHFTCATDTENIRFVFAAVKDTILQLNLKEYN LV[*]</p>						
CMV-SmBiT124-Gaq	pcDNA3.1- Galphaq	FW	GCAATAAAGAGTTTA TGGAATGATCCTGGA ATCCA	Gblock (synthetic lineal dsDNA)	FW	AATAAGGCTCATGCACAATTAGTTCGAGAAGTT GATGTGGAGAAGGTGCTGCTTTTTCTGGTGGA GGTGGATCCGTGACCGGCTACCGGCTGTTGAG GAGATTCTGCTGGTGGAGGTGGATCCGAGAAT CCATATGTAGATGCAATAAAGAGTTTATGGAAT GATCCTGGAATCC
		RV	CTTCTCGAACTAATT GTGCATGAGCCTTAT TG		RV	
<p>MTLESIMACCLSEEAKEARRINDEIERQLRRDKRDARRELKLLLLGTGESGKSTFIKQMRIHSGYSDEDEKRGFTKLVYQNIPTAMQAMIRAMDTLKIPYKYEHNKAAHAQLVREVDVEKVS AFSGGGGSVTYRLFEEILSGGGGSENOPYD AIKSLWNDPGIQECYDRRREYQLSDSTKYLLNDLDRVADPAYLPTQQDVLTRVVPPTGIIIEY PFDLQSVIFRMVDV GGQSRERRWIHC FENVT SIMFLValseyDQVLVESDNENRMEESKALFRITITYPWFQNSSVILFLNKKDLLEEKI MYSHLVDFPEYDGPQRDAQAAREFILKMFVDLNPDSKIIYSHFTCATDTENIRFVFAAVKDTILQLNLKEYNLV[*]</p>						
CMV-5-HT_{2c}R-LgBiT	pcDNA3.1- 5-HT2CR	FW	ACCATCAACAGCTGA CTCGAGTCTAGAGGG C	CMV-5- HT2AR- LgBiT	FW	AGGATTAGCAGTGTGGGC TCGAGCGGTGGT
		RV	ACCACCGCTCGAGCC CACACTGTAATCT TT		RV	CCCTCTAGACTCGAGTCA GCTGTTGATGGTTACTC
<p>MVNLRNAVHSFLVHLIGLLVWQCDSVSPAIVTDFNTSDGGRFKFPDGVQNPALSIVIIIIMTIGGNILVIMAVS MEKLLHNATNYFLMSLAIAIDMLVGLLVMPLSLLAILDYVWPLPRYLCPVWISLDVLFSTASIMHLCAISLDRYVA IRNPIHSRFSRTKAIMKIAVWAISIGVSVPIVIGLRDEEKVFNNTTCVLDNPNFVLIGSFVAFIPLTIMVITYCLT IYVLRRLQALMLLHGHTTEPPGLSLDFLKCCCKRNTAEEENSANPNQDNARRRKKKERRPRGTMQAINNERKASKV LGIVFFVFLIMWCPFFITNILAVLCEKSCNQKLEKLLNVFVWIGYVCSGINPLVYTLFNKIYRRAFSNYLRNYKVE KKPPVRQIPRVAATALSGRELVNIYRHTNEPVIEKASDNPEGIEMQVENLELPVNPSSVVSERISSVSSGGGGSSGG GGSSGVFTLEDFVGDWEQTAAYNLNDQVLEQGGVSSLLQNLAVSVTPIQIRVRSGENALKIDHVIIPYEGLSADQMA QIEEVFKVVPVDDHHFKVILPYGTLVIDGVTPNMLNFGFRPYEGIAVFDGKKITVTGLWNGNKNIIDERLITPDGS MLFRVTINS[*]</p>						

CMV-5-HT _{2c} R-SmBiT	CMV-5-HT _{2AR} -SmBiT	FW	AGGATTAGCAGTGTG GGCTCGAGCGGTGGT	pcDNA3.1-5-HT _{2CR}	FW	AAGCTTGGTACCACCATG GTGAACCTGAGG
		RV	CCTCAGGTTCACCAT GGTGGTACCAAGCTT AAGT		RV	ACCACCGCTCGAGCCCAC ACTGCTAATCCTTT
MVNLRNAVHSFLVHLIGLLVWQCDSVSPVAAIVTDIFNTSDGGRFKFPDGVQNWPAISIVIIIIMTIGGNILVIMAVS MEKKLHNATNYFLMSLAIDMLVGLLVMP LSLAILYDYVWPLPRYLCPVWISLDVLFSTASIMHLCAISLDRYVA IRNPIEHSRFRNRTKAIMKIAIVWAISIGVSVPIPVIGLRDEEKVFNNTTCVLNDPNFVLIGSFVAFFIPLTIMVITYCLT IYVLRQALMLLHGHTTEPPGLSLDFLKCCRNTAEEENSANPNQDQNAARRRKKKERRRPRGTMQAINNERKASKV LGIVFFVFLIMWCPFFITNILAVLCEKSCNQKLEKLLNVFVWIGYVCSGINPLVYTLFNKIYRRAFSNYLRCNYKVE KKPPVRQIPRVAATALSGRELNVNIYRHTNEPVEIKASDNPEGIEMQVENLELPVNPSSVVSERISSVGS SGGGGSGG GGSSGVTGYRLEFEIL*						

The colour code corresponds to the translated sequences of the HA-Tag, GPCR, G/S flexible Linker, Sm/LgBiT, HaloTag®, N/C Venus YFP, Galpha subunit, β-arrestin2

PUBLICATIONS AND CONFERENCE PRESENTATIONS

Publications derived from the studies included in this thesis

McCormick, P. J* & **Botta, J***. Heteromers Form Novel Signaling Complexes. in *G-Protein-Coupled Receptor Dimers* 467–475 (Springer International Publishing, 2017). doi:10.1007/978-3-319-60174-8_19

García-Cárceles, J., Decara, J. M., Vázquez-Villa, H., Rodríguez, R., Codesido, E., Cruces, J., Brea, J. Loza, M. I., Alén, F., **Botta, J.**, McCormick, P. J., Ballesteros, J. A., Benhamú, B., Rodríguez de Fonseca, F., López-Rodríguez, M. L. A Positive Allosteric Modulator of the Serotonin 5-HT_{2C} Receptor for Obesity. *J. Med. Chem.* **60**, 9575–9584 (2017). doi:10.1021/acs.jmedchem.7b00994

Botta, J., Codomí, A., Bondar, A., D’augello, I. Howell, L., Lazar, J., Pardo, L., McCormick, P. J. Molecular basis underlying cross-talk in 5-HT_{2A}-CB₁ receptor heteromers (Manuscript in preparation).

Moreno-Delgado, D., Puigdel·livol, M., Rodríguez-Ruiz, M. Moreno, E., **Botta, J.**, Gasperini, P., Chiarlone, A., Howell, L., Scarselli, M., Casadó, V., Cortés, A., Ferré, S., Guzmán, M., Lluís, C., Alberch, J., Canela, E.I., Ginés, S., McCormick, P.J. Modulation of Dopamine D1 receptors via Histamine H3 receptors represent a novel therapeutic target for Huntington’s disease (Manuscript in submission).

Gonzalez, A*., **Botta, J***., McCormick, P.J., Pardo, L. Selective positive allosteric modulation of 5-HT_{2C} receptors. Structure-guided identification and validation of allosteric binding sites (Manuscript in preparation).

Botta, J., Darling, W., Howell, L. McCormick, P.J. Pharmacophore-based tailoring of novel neutral and biased 5-HT_{2C} receptor allosteric modulators of the (Manuscript in preparation).

Publications directly related to the studies included in this thesis

Moreno, E., Chiarlone, A., Medrano, M., Puigdel·livol, M., Bibic, L., Howell, L., Resel, E., Puente, N., Casarejos, M. J., Perucho, J., **Botta, J.**, Suelves, N., Ciruela, F., Ginés, S., Galve-Roperh, I., Casadó, V., Grandes, P., Lutz, B., Monory, K., Canela, E. I., Lluís, C., McCormick, P. J., Guzmán, M. Singular Location and Signaling Profile of Adenosine A_{2A}-Cannabinoid CB₁ Receptor Heteromers in the Dorsal Striatum. *Neuropsychopharmacology* **43**, 964–977 (2018). doi:10.1038/npp.2017.12

González-Vera, J. A., Medina, R. A., Martín-Fontecha, M., Gonzalez, A., de la Fuente, T., Vázquez-Villa, H., García-Cárceles, J., **Botta, J.**, McCormick, P. J., Benhamú, B., Pardo, L., López-Rodríguez, M. L. A new serotonin 5-HT₆ receptor antagonist with procognitive

activity–Importance of a halogen bond interaction to stabilize the binding. *Sci. Rep.* **7**, 41293 (2017). doi: 10.1038/srep41293.

* Denotes equal contribution

Conference presentations

How to separate THC's good from the bad? The molecular explaining how CB₁-5-HT_{2A} receptor heteromers control THC's cognitive effects. *7th Focused Meeting on Cell signalling, Nottingham, UK, 2018. (Poster presentation).*

How to separate THC's good from the bad? The molecular basis underlying cross-talk in CB₁-5-HT_{2A} receptors heteromers. *8th European Workshop on Cannabinoid Research, London, UK, 2018. (Poster presentation).*

The molecular basis behind separating trans- Δ^9 -tetrahydrocannabinol's (THC) analgesic and cognitive effects. *International Symposium on Neurobiology, Neuroscience Workshop in collaboration with the University of Milan-Bicocca, Milan, Italy, 2017. (Poster presentation).*

The molecular basis underlying cross-talk and cross-antagonism in CB₁-5-HT_{2A} receptors heteromers. *GLISTEN: GPCR-ligand interactions, structures and transmembrane signalling, Prague, Czech Republic, 2016. (Poster presentation).*

Cognitive impairment induced by delta9-tetrahydrocannabinol occurs through heteromers between cannabinoid CB₁ and serotonin 5-HT_{2A} receptors. *Pharmacology 2015. British Pharmacology Society, London, UK. (Poster presentation).*

Cognitive impairment induced by delta9-tetrahydrocannabinol occurs through heteromers between cannabinoid CB₁ and serotonin 5-HT_{2A} receptors. *GDR GPCR-Physio-Med 4th annual meeting, Toulouse, France. (Oral communication).*

Targeting dopamine D₁-histamine H₃ receptor heteromers reverts cognitive and motor deficits in a mouse model of Huntington's disease. *GDR GPCR-Physio-Med 3rd annual meeting, Montpellier, France. (Poster presentation).*